Oxidative Medicine and Cellular Longevity

Oxidative Stress-Mediated Reperfusion Injury: Mechanism and Therapies

Guest Editors: Zhengyuan Xia, Yanfang Chen, Qian Fan, and Mengzhou Xue

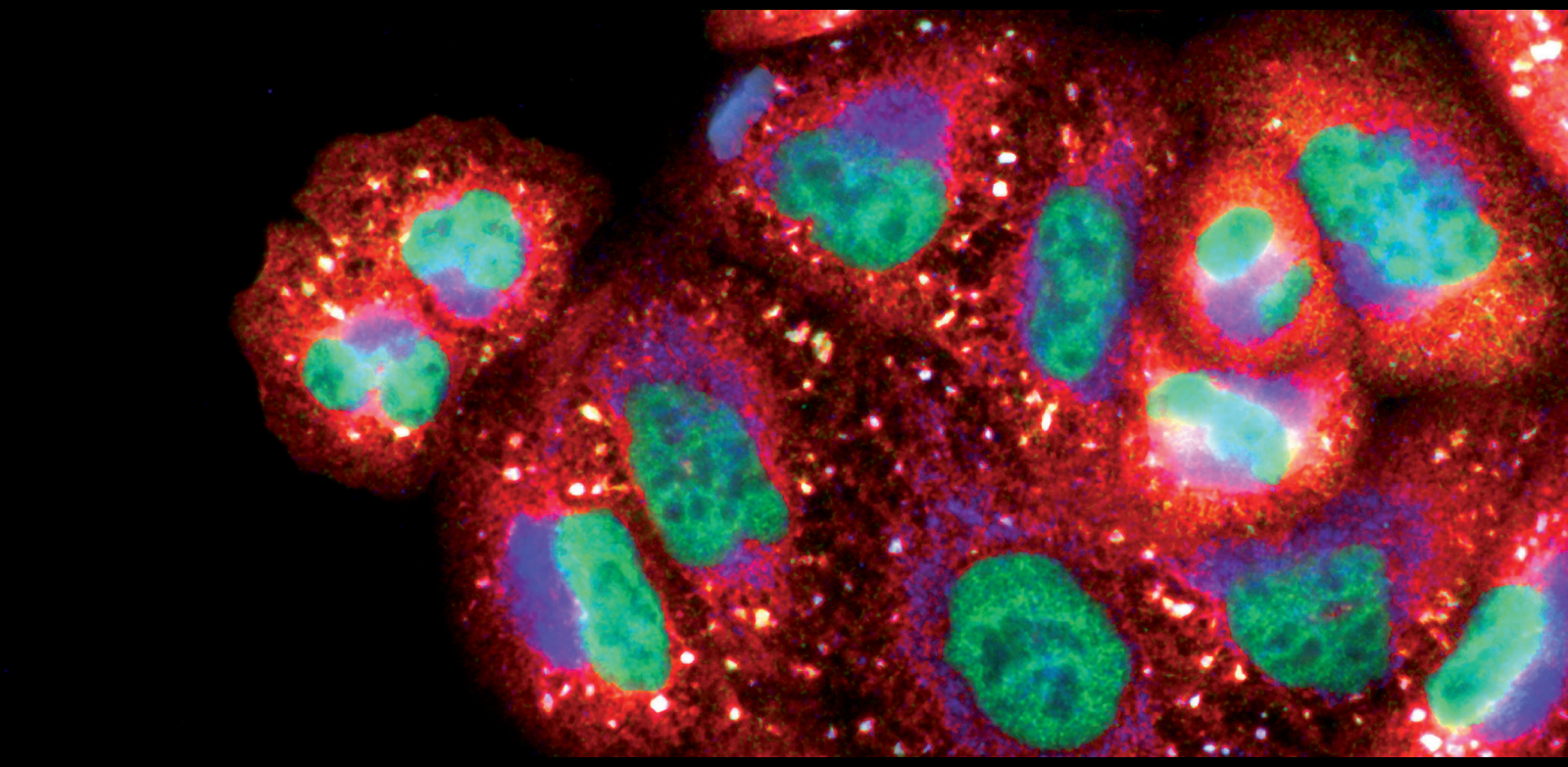

Oxidative Stress-Mediated Reperfusion Injury: Mechanism and Therapies

Oxidative Medicine and Cellular Longevity

Oxidative Stress-Mediated Reperfusion Injury: Mechanism and Therapies

Guest Editors: Zhengyuan Xia, Yanfang Chen, Qian Fan, and Mengzhou Xue

Editorial Board

Oxidative Stress-Mediated Reperfusion Injury: Mechanism and Therapies, Zhengyuan Xia, Yanfang Chen, Qian Fan, and Mengzhou Xue
Volume 2014, Article ID 373081, 2 pages

Global Consequences of Liver Ischemia/Reperfusion Injury, Constantinos Nastos, Konstantinos Kalimeris, Nikolaos Papoutsidakis, Marios-Konstantinos Tasoulis, Panagis M. Lykoudis, Kassiani Theodoraki, Despoina Nastou, Vassilios Smyrniotis, and Nikolaos Arkadopoulos
Volume 2014, Article ID 906965, 13 pages

Aging Aggravates Nitrate-Mediated ROS/RNS Changes, Qian Fan, Lifen Chen, Shujuan Cheng, Fang Li, Wayne Bond Lau, Le Feng Wang, and Jing Hua Liu
Volume 2014, Article ID 376515, 8 pages

BMP-2 Overexpression Augments Vascular Smooth Muscle Cell Motility by Upregulating Myosin Va via Erk Signaling, Ming Zhang, Min Yang, Li-ping Liu, Wayne Bond Lau, Hai Gao, Man-kun Xin, Li-Xiao Su, Jian Wang, Shu-Juan Cheng, Qian Fan, and Jing-Hua Liu
Volume 2014, Article ID 294150, 11 pages

NADPH Oxidase 1 and Its Derived Reactive Oxygen Species Mediated Tissue Injury and Repair, Xiu-Jun Fu, Ying-Bo Peng, Yi-Ping Hu, You-Zhen Shi, Min Yao, and Xiong Zhang
Volume 2014, Article ID 282854, 10 pages

Antiaging Properties of a Grape-Derived Antioxidant Are Regulated by Mitochondrial Balance of Fusion and Fission Leading to Mitophagy Triggered by a Signaling Network of Sirt1-Sirt3-Foxo3-PINK1-PARKIN, Somak Das, Goran Mitrovsky, Hannah R. Vasanthi, and Dipak K. Das
Volume 2014, Article ID 345105, 13 pages

Differential MicroRNA Profiling in a Cellular Hypoxia Reoxygenation Model upon Posthypoxic Propofol Treatment Reveals Alterations in Autophagy Signaling Network, Zhuo Chen, Zhe Hu, Zhiqi Lu, Shuyun Cai, Xiaoxia Gu, Haixia Zhuang, Zhihua Ruan, Zhengyuan Xia, Michael G. Irwin, Du Feng, and Liangqing Zhang
Volume 2013, Article ID 378484, 11 pages

The Protection of Salidroside of the Heart against Acute Exhaustive Injury and Molecular Mechanism in Rat, Yunru Wang, Peng Xu, Yang Wang, Haiyan Liu, Yuwen Zhou, and Xuebin Cao
Volume 2013, Article ID 507832, 8 pages

Astragalus Polysaccharide Suppresses Skeletal Muscle Myostatin Expression in Diabetes: Involvement of ROS-ERK and NF-κB Pathways, Min Liu, Jian Qin, Yarong Hao, Min Liu, Jun Luo, Tao Luo, and Lei Wei
Volume 2013, Article ID 782497, 10 pages

Nitroglycerine-Induced Nitrate Tolerance Compromises Propofol Protection of the Endothelial Cells against TNF-α: The Role of PKC-β_2 and NADPH Oxidase, Shaoqing Lei, Wating Su, Huimin Liu, Jinjin Xu, Zhong-yuan Xia, Qing-jun Yang, Xin Qiao, Yun Du, Liangqing Zhang, and Zhengyuan Xia
Volume 2013, Article ID 678484, 9 pages

Early Growth Response Protein 1 Promotes Restenosis by Upregulating Intercellular Adhesion Molecule-1 in Vein Graft, Kui Zhang, Jian Cao, Ran Dong, and Jie Du
Volume 2013, Article ID 432409, 9 pages

The Effect of Safflower Yellow on Spinal Cord Ischemia Reperfusion Injury in Rabbits, Daiwei Zhou, Bingbing Liu, Xiaoshan Xiao, Peng Dai, Songmei Ma, and Weihua Huang
Volume 2013, Article ID 692302, 9 pages

Contents

Resolvin D1 Reverts Lipopolysaccharide-Induced TJ Proteins Disruption and the Increase of Cellular Permeability by Regulating IκBα Signaling in Human Vascular Endothelial Cells, Xingcai Zhang, Tingting Wang, Ping Gui, Chengye Yao, Wei Sun, Linlin Wang, Huiqing Wang, Wanli Xie, Shanglong Yao, Yun Lin, and Qingping Wu
Volume 2013, Article ID 185715, 8 pages

Transient Limb Ischemia Alters Serum Protein Expression in Healthy Volunteers: Complement C3 and Vitronectin May Be Involved in Organ Protection Induced by Remote Ischemic Preconditioning, Ting Pang, Yang Zhao, Nan-Rong Zhang, San-Qing Jin, and San-Qiang Pan
Volume 2013, Article ID 859056, 9 pages

Aging Might Increase the Incidence of Infection from Permanent Pacemaker Implantation, Yun Lin, Zhi Zhong Li, Jingmei Zhang, Jinrong Zhang, Qian Fan, and Jie Du
Volume 2013, Article ID 943416, 6 pages

Acute Hyperglycemia Abolishes Ischemic Preconditioning by Inhibiting Akt Phosphorylation: Normalizing Blood Glucose before Ischemia Restores Ischemic Preconditioning, Zequan Yang, Yikui Tian, Yuan Liu, Sara Hennessy, Irving L. Kron, and Brent A. French
Volume 2013, Article ID 329183, 8 pages

***N*-n-Butyl Haloperidol Iodide Ameliorates Cardiomyocytes Hypoxia/Reoxygenation Injury by Extracellular Calcium-Dependent and -Independent Mechanisms**, Yanmei Zhang, Gaoyong Chen, Shuping Zhong, Fuchun Zheng, Fenfei Gao, Yicun Chen, Zhanqin Huang, Wenfeng Cai, Weiqiu Li, Xingping Liu, Yanshan Zheng, Han Xu, and Ganggang Shi
Volume 2013, Article ID 912310, 12 pages

Transient Acidosis during Early Reperfusion Attenuates Myocardium Ischemia Reperfusion Injury via PI3k-Akt-eNOS Signaling Pathway, Xin Qiao, Jinjin Xu, Qing-Jun Yang, Yun Du, Shaoqing Lei, Zhi-Hong Liu, Xinwei Liu, and Huimin Liu
Volume 2013, Article ID 126083, 6 pages

Protective Effects of Low-Frequency Magnetic Fields on Cardiomyocytes from Ischemia Reperfusion Injury *via* ROS and NO/ONOO$^-$, Sai Ma, Zhengxun Zhang, Fu Yi, Yabin Wang, Xiaotian Zhang, Xiujuan Li, Yuan Yuan, and Feng Cao
Volume 2013, Article ID 529173, 9 pages

Hyperglycemia-Induced Inhibition of DJ-1 Expression Compromised the Effectiveness of Ischemic Postconditioning Cardioprotection in Rats, Min Liu, Bin Zhou, Zhong-Yuan Xia, Bo Zhao, Shao-Qing Lei, Qing-Jun Yang, Rui Xue, Yan Leng, Jin-Jin Xu, and Zhengyuan Xia
Volume 2013, Article ID 564902, 8 pages

Effects of Endothelial Progenitor Cell-Derived Microvesicles on Hypoxia/Reoxygenation-Induced Endothelial Dysfunction and Apoptosis, Jinju Wang, Shuzhen Chen, Xiaotang Ma, Chuanfang Cheng, Xiang Xiao, Ji Chen, Shiming Liu, Bin Zhao, and Yanfang Chen
Volume 2013, Article ID 572729, 9 pages

Neuroprotective Effect of Ginkgolide B on Bupivacaine-Induced Apoptosis in SH-SY5Y Cells, Le Li, Qing-guo Zhang, Lu-ying Lai, Xian-jie Wen, Ting Zheng, Chi-wai Cheung, Shu-qin Zhou, and Shi-yuan Xu
Volume 2013, Article ID 159864, 11 pages

Hindawi Publishing Corporation
Oxidative Medicine and Cellular Longevity
Volume 2014, Article ID 373081, 2 pages
http://dx.doi.org/10.1155/2014/373081

Editorial

Oxidative Stress-Mediated Reperfusion Injury: Mechanism and Therapies

Zhengyuan Xia,[1,2] Yanfang Chen,[3,4] Qian Fan,[5] and Mengzhou Xue[6]

[1] *Department of Anesthesiology, The University of Hong Kong, 102 Pokfulam Road, Hong Kong*
[2] *Department of Anesthesiology, The Second Affiliated Hospital of Guangzhou Medical University, Guangzhou, China*
[3] *Department of Pharmacology & Toxicology, Boonshoft School of Medicine, Wright State University, 3640 Colonel Glenn Highway, Dayton, OH 45435, USA*
[4] *Cardiovascular Department, Guangzhou Institute of Cardiovascular Disease, The Second Affiliated Hospital of Guangzhou Medical University, Guangzhou 510000, China*
[5] *Department of Cardiology, Beijing Anzhen Hospital, Capital Medical University, Beijing 100029, China*
[6] *Department of Neurology, The First Affiliated Hospital, Henan University, 357 Ximen Street, Kaifeng 470010, China*

Correspondence should be addressed to Zhengyuan Xia; zyxia@hku.hk

Received 13 February 2014; Accepted 13 February 2014; Published 3 April 2014

Ischemia/reperfusion injury (IRI) and organ failure, especially IRI-induced remote and multiple organ failure, contribute significantly to postoperative mortality and morbidity, and reperfusion induced oxidative stress plays a critical role in this pathology. Postoperative mortality risk increases in aged patients and in patients with concomitant diseases like diabetes which itself is associated with increased oxidative stress. Given that people now live longer and are often with concomitant diseases, IRI in these population is more severe and prevention or treatment of IRI will be an increasing important area of intention.

Ischemic heart disease is a major complication of diabetes [1, 2]. Although expeditious percutaneous coronary intervention can restore coronary flow and limit myocardial infarction, reperfusion may also cause cardiac damage—"ischemia/reperfusion injury (IRI)" [3]. Diabetic heart is more vulnerable to IRI [4, 5] but less sensitive to percutaneous coronary intervention and ischemic pre- or postconditioning cardioprotection, and the underlying mechanism remains unclear. In this special issue, Y. Zhao et al. reported that acute hyperglycemia not only exacerbated myocardial IRI but completely abolished the cardioprotective effect of ischemic preconditioning by inhibiting Akt phosphorylation and disrupting signaling pathways downstream of adenosine A_1 receptor but not adenosine A_1 receptor activation itself. Interestingly, insulin treatment to normalize blood glucose levels could restore the cardioprotective effects of ischemic preconditioning, despite that insulin failed to counteract the detrimental effect of hyperglycemia. This is an interesting area that deserves further exploration. Further, M. Liu et al. reported that hyperglycemia-induced inhibition of myocardial DJ-1 protein expression may represent one of the major mechanisms why hearts of diabetic subjects are less or not responsive to ischemic postconditioning cardioprotection.

Remote ischemic preconditioning has recently been shown to effectively attenuate myocardial ischemia/ reperfusion injury in patients [6, 7], but the underlying mechanisms are incompletely understood. In this special issue, T. Pang et al. performed remote ischemic preconditioning in healthy volunteers and conducted comprehensive proteomic analysis in order to identify the mechanisms. Furthermore, X. Qiao et al. reported that transient acidosis during early reperfusion can mimic the cardioprotective effects of ischemic postconditioning in a rat model of myocardial IRI induced by coronary artery occlusion/reperfusion. These studies, among others, are significant advancement in the study of ischemic pre- and postconditioning cardioprotection.

Reactive oxygen species (ROS) induced vascular endothelial dysfunction plays an important role in the development of IRI in various organs. In this special

issue, J. Wang et al. reported that endothelial progenitor cell-derived microvesicles (EPC-MVs) can promote angiogenesis of endothelial cells and attenuate hypoxia/reoxygenation injury in human brain microvascular endothelial cells. Further, S. Ma et al. reported that the application of low frequency pulse magnetic fields can effectively reduce ROS generation and subsequently attenuate myocardial IRI. Their finding that low frequency pulse magnetic fields could protect the myocardium against IRI via regulating ROS generation and nitric oxide/peroxynitrite balance is a very novel finding that may have high potential to serve as a promising strategy for combating cardiac IRI. X. Zhang et al. reported that Resolvin D1 can effectively protect against impairment of endothelial barrier function induced by lipopolysaccharide in human vascular endothelial cells. This finding may be of significant clinical relevance given that during IRI the increased production of proinflammatory cytokines such as tumor necrosis factor-α (TNF-α) further increases oxidative stress and exacerbate reperfusion injury [8]. The paper by S. Lei et al. in this special issue reported that TNF-α stimulation in endothelial cells can induce oxidative stress primarily through protein kinase C (PKC)-β_2 dependent NADPH oxidase activation and reduce vascular endothelial cell viability.

The intravenous anesthetic propofol possesses antioxidant capacity and has been shown to attenuate IRI in patients undergoing cardiac surgery [9] and in animal models of IRI [10]. However, the mechanisms by which propofol confers protective effects against IRI has not been fully elucidated. In this special issue, Z. Chen et al. systematically analyzed the alterations in microRNA expression in human umbilical vein endothelial cells subjected to hypoxia/reoxygenation in the presence or absence of posthypoxic propofol treatment and provided genome-wide profiling of microRNAs assessed using microRNA microarray.

The experimental therapeutic studies regarding the neuroprotective effect and mechanisms of Ginkgolide B on cell injury reported by L. Li et al. and the effect of safflower yellow on spinal cord IRI reported by D. Zhou et al. are all of potential clinical implications.

The review article by C. Nastos et al. reviewed the existing literature regarding the proposed mechanisms of remote organ injury after liver ischemia and reperfusion. This review brings to our attention the important issue of liver IRI-induced remote organ injuries [11, 12].

We hope that the original and review articles presented in this special issue, representing the current advances in the oxidative stress-mediated ischemia-reperfusion injury, with respect to their potential impact in cellular survival pathways and therapeutic strategies, will stimulate further exploration of this important area.

Acknowledgments

This special issue would not be possible without the great efforts of the authors and the reviewers. In this regard, we would like to thank all these people that took part in the achievement of this issue.

Zhengyuan Xia
Yanfang Chen
Qian Fan
Mengzhou Xue

References

[1] S. M. Donahoe, G. C. Stewart, C. H. McCabe et al., "Diabetes and mortality following acute coronary syndromes," *The Journal of the American Medical Association*, vol. 298, no. 7, pp. 765–775, 2007.

[2] S. Boudina and E. D. Abel, "Diabetic cardiomyopathy revisited," *Circulation*, vol. 115, no. 25, pp. 3213–3223, 2007.

[3] H. R. Andersen, T. T. Nielsen, K. Rasmussen et al., "A comparison of coronary angioplasty with fibrinolytic therapy in acute myocardial infarction," *The New England Journal of Medicine*, vol. 349, no. 8, pp. 733–742, 2003.

[4] T. Miki, T. Itoh, D. Sunaga, and T. Miura, "Effects of diabetes on myocardial infarct size and cardioprotection by preconditioning and postconditioning," *Cardiovascular Diabetology*, vol. 11, article 67, 2012.

[5] H. Li, Z. Liu, J. Wang et al., "Susceptibility to myocardial ischemia reperfusion injury at early stage of type 1 diabetes in rats," *Cardiovascular Diabetology*, vol. 12, article 133, 2013.

[6] Q. Wu, P. Gui, J. Wu et al., "Effect of limb ischemic preconditioning on myocardial injury in patients undergoing mitral valve replacement surgery: a randomized controlled trial," *Circulation Journal*, vol. 75, no. 8, pp. 1885–1889, 2011.

[7] A. Stazi, G. Scalone, M. Laurito et al., "Effect of remote ischemic preconditioning on platelet activation and reactivity induced by ablation for atrial fibrillation," *Circulation*, vol. 129, no. 1, pp. 11–17, 2014.

[8] Y. Y. Yang, P. C. Lee, Y. T. Huang et al., "Involvement of the HIF-1alpha and Wnt/beta-catenin pathways in the protective effects of losartan on fatty liver graft with ischaemia/reperfusion injury," *Clinical Science*, vol. 126, no. 2, pp. 163–174, 2014.

[9] Z. Xia, Z. Huang, and D. M. Ansley, "Large-dose propofol during cardiopulmonary bypass decreases biochemical markers of myocardial injury in coronary surgery patients: a comparison with isoflurane," *Anesthesia and Analgesia*, vol. 103, no. 3, pp. 527–532, 2006.

[10] K.-X. Liu, T. Rinne, W. He, F. Wang, and Z. Xia, "Propofol attenuates intestinal mucosa injury induced by intestinal ischemia-reperfusion in the rat," *Canadian Journal of Anesthesia*, vol. 54, no. 5, pp. 366–374, 2007.

[11] A. Zhang, X. Chi, G. Luo et al., "Mast cell stabilization alleviates acute lung injury after orthotopic autologous liver transplantation in rats by downregulating inflammation," *PLoS ONE*, vol. 8, no. 10, Article ID e75262, 2013.

[12] Z.-Q. Hei, X.-Y. Li, N. Shen, H.-Y. Pang, S.-L. Zhou, and J.-Q. Guan, "Prognostic values of serum cystatin C and β2 microglobulin, urinary β2 microglobulin and N-acetyl-β-D-glucosaminidase in early acute renal failure after liver transplantation," *Chinese Medical Journal*, vol. 121, no. 14, pp. 1251–1256, 2008.

Hindawi Publishing Corporation
Oxidative Medicine and Cellular Longevity
Volume 2014, Article ID 906965, 13 pages
http://dx.doi.org/10.1155/2014/906965

Review Article

Global Consequences of Liver Ischemia/Reperfusion Injury

Constantinos Nastos,[1] Konstantinos Kalimeris,[2] Nikolaos Papoutsidakis,[2] Marios-Konstantinos Tasoulis,[1] Panagis M. Lykoudis,[3] Kassiani Theodoraki,[4] Despoina Nastou,[5] Vassilios Smyrniotis,[5] and Nikolaos Arkadopoulos[5]

[1] *Second Department of Surgery, School of Medicine, Aretaieion University Hospital, University of Athens, 76 Vassilisis Sofia's Avenue, 11528 Athens, Greece*
[2] *Second Department of Anesthesiology, School of Medicine, Attikon University Hospital, University of Athens, 1 Rimini Street, 12462 Athens, Greece*
[3] *Division of Surgery & Interventional Sciences, Royal Free Hospital Campus, University College London, 8 South Pond Street, Hampstead, London NW3 2QG, UK*
[4] *First Department of Anesthesiology, Aretaieion Hospital, University of Athens School of Medicine, Vassilissis Sofias 76, 11528 Athens, Greece*
[5] *Fourth Department of Surgery, School of Medicine, Attikon University Hospital, University of Athens, 1 Rimini Street, 12462 Athens, Greece*

Correspondence should be addressed to Constantinos Nastos; kosnastos@yahoo.gr

Received 21 August 2013; Revised 2 January 2014; Accepted 13 January 2014; Published 1 April 2014

Academic Editor: Mengzhou Xue

Liver ischemia/reperfusion injury has been extensively studied during the last decades and has been implicated in the pathophysiology of many clinical entities following hepatic surgery and transplantation. Apart from its pivotal role in the pathogenesis of the organ's post reperfusion injury, it has also been proposed as an underlying mechanism responsible for the dysfunction and injury of other organs as well. It seems that liver ischemia and reperfusion represent an event with "global" consequences that influence the function of many remote organs including the lung, kidney, intestine, pancreas, adrenals, and myocardium among others. The molecular and clinical manifestation of these remote organs injury may lead to the multiple organ dysfunction syndrome, frequently encountered in these patients. Remote organ injury seems to be in part the result of the oxidative burst and the inflammatory response following reperfusion. The present paper aims to review the existing literature regarding the proposed mechanisms of remote organ injury after liver ischemia and reperfusion.

1. Introduction

Liver ischemia and reperfusion has been the topic of intense study during the last decades since it is implicated in many clinical scenarios, including hemorrhagic shock and resuscitation, trauma [1], liver resections [2], and liver transplantation [3].

After the introduction of vascular control techniques during hepatic surgery, liver ischemia and reperfusion has been recognized as one of the key elements that contribute to postoperative morbidity and mortality [4]. Liver dysfunction and failure are serious postoperative complications which may ensue as a result of reperfusion injury. Although the liver has been studied in the aforementioned clinical scenario (i.e., hepatic surgery) and liver dysfunction is widely recognized as a consequence of hepatic reperfusion injury, many other remote organs seem to be influenced during this process as well [5–7].

The aim of this paper is to review the existing literature and summarize the proposed mechanisms of remote organ injury that are mediated by liver ischemia/reperfusion injury in hepatic surgery.

2. Liver Injury

The topic of liver reperfusion injury has been extensively investigated in the context of hepatic surgery and therefore it is not the aim of the present review to describe in detail the pathophysiology of this entity.

Briefly, liver ischemia/reperfusion injury can be divided into two distinct phases. Ischemia seems to be the initial insult to the organ, which, although tolerable from the liver, triggers the production of molecules that are essential for the induction of reperfusion injury. During this phase intracellular production of xanthine oxidase and NADPH oxidase from liver cells is promoted [3]. The early phase of reperfusion occurs from the first minutes after ischemia and up to 6 hours later. Immediately after reperfusion, cellular swelling takes place due to the disturbance of NA/K/ATPase function [8]. In addition, reactive oxidant species (ROS) can be found inducing oxidative stress to the liver as well as to distant organs [9, 10]. ROS activate Kuppfer cells, promoting even further ROS as well as cytokine production. In the meantime, NO levels are reduced and there is an imbalance between endothelin-1 and nitric oxide (NO) production from NO synthase (NOS), leading to vasoconstriction of the sinusoids [11]. The narrowing of the sinusoids leads to entrapment of platelets and neutrophils. Hepatocyte injury is promoted through hepatocellular necrosis and apoptosis, though distinct pathways [12–14].

An excessive inflammatory response is clearly recognized as a key mechanism of injury during reperfusion. Local production of cytokines (IL-1b and TNF-α) is the precursor of the late phase of reperfusion injury [3]. This is the cellular phase and is characterized by activation and migration of neutrophil, CD4+ T lymphocytes, and platelets into the liver. Cell-surface adhesion molecules (such as intracellular cell adhesion molecule, ICAM, and vascular cell adhesion molecule, VCAM) are expressed in the hepatocytes and endothelial cells and inflammatory cell adherence takes place [15]. These cells are trapped in the constricted and narrowed sinusoids and result in inflammatory injury and microvasculature failure. CD4+ T lymphocytes produce granulocyte-macrophage colony-stimulating factor, interferon gamma, and TNF-β, which amplify Kupffer cell activation and cytokine release [15].

Although intravascular coagulation during inflow occlusion can reduce or block blood flow in sinusoids and cause liver injury, active vasoconstriction and cell entrapment seems to be the major contributing factor to microcirculatory problems [15]. Microcirculatory failure leads to aggravated and prolonged ischemia, as parts of the liver remain hypoxic, aggravating necrosis, Kupffer cell activation, further cytokine and ROS release, and creating a vicious cycle of excessive inflammatory response, reactive oxygen and nitrogen species production, and further oxidative tissue injury [4, 15].

Although the many aspects of liver reperfusion injury remain to be elucidated, there is extensive literature on the mechanisms that mediate liver injury. However, only recently has there been research concerning the mechanisms involved in remote organ injury after the initial insult to the liver. Distant organs that have been implicated in the remote injury after hepatic ischemia/reperfusion are depicted in Figure 1.

3. Kidney Injury

Ischemia/reperfusion injury of the liver remnant or donor liver is a frequent cause of acute liver failure (ALF) during the perioperative period and is a common complication after major liver resection or liver transplantation [4, 16, 17]. Acute kidney injury (AKI) occurs frequently in patients with ALF and poses a serious clinical problem in the perioperative period [18, 19] increasing the associated morbidity and mortality. The reported incidence of AKI ranges from 40 to 85% [18, 20] and in the setting of liver transplantation can be as high as 95% [21]. Unfortunately, the pathophysiology of AKI associated with liver ischemia/reperfusion injury is not fully understood. However, there is emerging evidence suggesting multiple molecular mechanisms. The basic mechanisms are summarized in Figure 2.

The initiating event appears to be portal hypertension, which is the result of portal vein occlusion, incorporated in various techniques of vascular control of the liver used during hepatic surgery. This induces splanchnic vasodilation with subsequent intrarenal vasoconstriction [20, 22, 23]. Splanchnic vasodilation leads to hypotension [20] which in turn leads to activation of the renin-angiotensin system [20, 24]. Upregulation of renin-angiotensin system can cause severe reduction of glomerular filtration rate, urinary sodium excretion, and free water excretion. It has been proposed that intense intrarenal ischemia subsequent to renin-angiotensin activation leads to renal tubular necrosis and renal dysfunction.

However, other mechanisms may play an important role in the pathogenesis of renal dysfunction after liver ischemia/reperfusion injury. Systemic inflammatory response may induce renal injury [20, 25]. Circulating levels of proinflammatory cytokines and transcription factors, including interleukin (IL)-6, tumor necrosis factor-alpha (TNF-α), and high mobility group box (HMGB) 1, are increased and their release from the liver may promote inflammatory changes in the kidney after liver ischemia/reperfusion [25–28]. Kupffer cells activation plays the predominant role in the production and release of these cytokines. Recently, Park et al. reported the significant role of Paneth cell derived IL-17A in the aggravation of the observed systemic inflammatory syndrome and the exacerbation of renal injury [29]. These proinflammatory factors can upregulate endothelial adhesion molecules in distant organs including the kidney. Upregulation of renal endothelial adhesion molecules including E-selectin, P-selectin, and intercellular adhesion molecule (ICAM)-1 promotes leukocyte recruitment and extravasations to the renal interstitial space [30, 31]. Meyer et al. reported that liver ischemia/reperfusion results in significant ICAM-1 upregulation in remote tissues, including the kidney, and is likely mediated by cytokines such as TNF [32]. In addition, circulating bile acids and endotoxin and circulating immune complexes may contribute to the development of AKI [20].

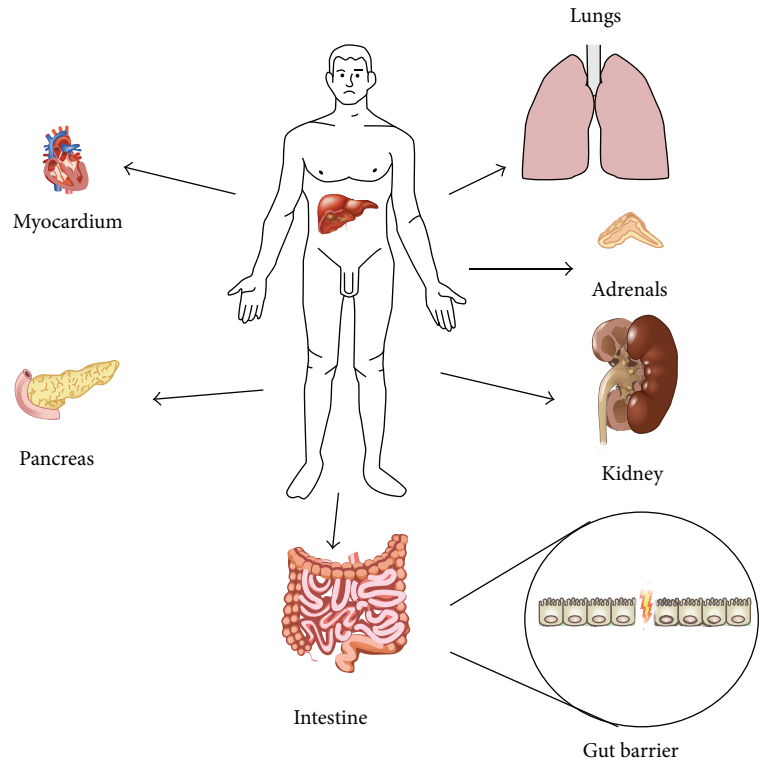

Figure 1: Distant organs that have been implicated in the remote injury after hepatic ischemia/reperfusion.

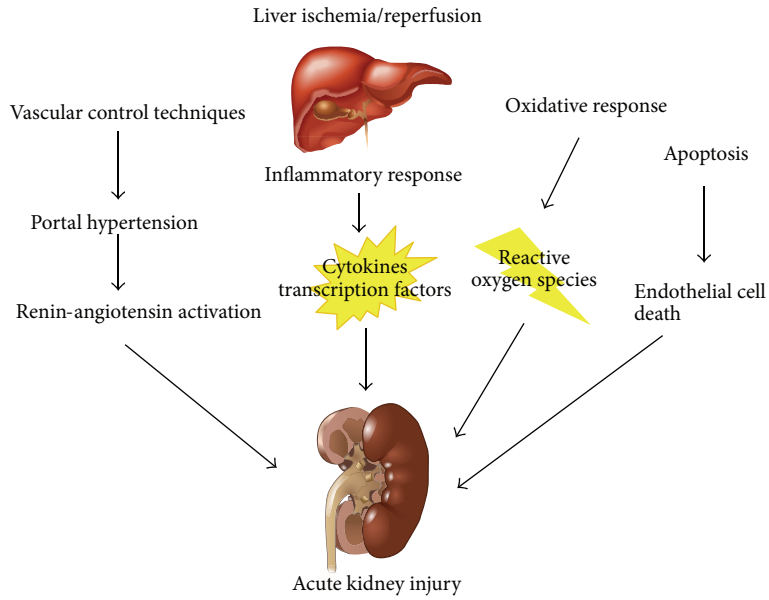

Figure 2: Mechanisms involved in remote injury to the kidney after liver ischemia/reperfusion.

The integrity of the endothelial barrier plays a pivotal role in the protection against AKI, by regulating leukocyte recruitment to the area of injury [25, 30]. Lee et al. reported that hepatic ischemia/reperfusion injury produces marked endothelial cell apoptosis in the kidney, which is more prominent in the interstitial capillary endothelial cells [33]. Endothelial cell death due to apoptosis would impair the regulation of leukocyte infiltration, further exacerbating renal injury. Apoptotic cell death represents the execution of an ATP-dependent process often initiated by death ligand/death receptor interactions, such as Fas ligand with Fas [34, 35].

Except from the aforementioned mechanisms, oxidative stress is also a major determinant of liver ischemia/reperfusion induced AKI. Activated neutrophils [33] aggregate in the subendothelial space, where they release reactive oxygen

species (ROS), enzymes, and cytokines, causing direct renal injury [36] and the recruitment of monocytes and macrophages leading to further aggravation of the oxidative injury. Kadkhodaee et al. reported that liver ischemia/reperfusion causes renal injury including oxidative status changes as shown by the increase in renal malondyaldehyde (MDA) levels and the decrease in superoxide dismutase (SOD) and catalase activity [28]. Similar results were reported in other studies showing that hepatic ischemia and reperfusion may cause oxidative stress to renal tissue and that administration of antioxidants seems to have a beneficial effect via the glutathione (GSH) system and the modulation of MDA levels [37, 38]. The pivotal role of reactive oxygen species in the development of AKI was also demonstrated by the beneficial effect of hepatic ischemic preconditioning and the administration of free radical scavengers [39]. However, although high concentrations of oxygen free radicals induce tissue injury during the reperfusion period after prolonged ischemia, moderate oxygen free radicals are an important prerequisite of ischemic preconditioning in renal cells [40]. Oxygen free radicals phosphorylate several important cytoprotective kinases, including extracellular signal-regulated kinase (ERK1/2), mitogen activated protein kinase (MAPK), and Akt, and are involved in the upregulation of several cytoprotective genes [41]. ROS are attractive signaling candidates to account for preconditioning in the kidney because renal cells are subject to obligatory bursts of oxidative stress during the reperfusion phase after each preconditioning stimulus. Therefore, distant renal exposure through the blood stream of moderate ROS caused by hepatic ischemic preconditioning may also initiate cytoprotective signaling to defend against subsequent and more severe free radical-mediated injury in renal tubule cells.

Damage of the actin cytoskeleton, which contributes to the development of AKI, is another proposed mechanism [42, 43]. Lee et al. have shown that liver ischemia/reperfusion promotes renal F-actin breakdown [33]. Additionally, F-actin disruption induces apoptosis in several cell lines [44]. Therefore, loss of actin cytoskeleton may contribute to the development of renal tubular and endothelial apoptosis.

At a molecular level, adenosine has been proposed to play a pivotal role. Adenosine release is increased after stress (e.g., hypoxia, ischemia/reperfusion) with subsequent activation of adenosine receptors (ARs), which protect against cell death in several cell types [45]. Endogenous adenosine production is crucial in protecting against ischemia-induced organ injury. Activation of cell surface Adenosine 1 (A1) ARs produces cytoprotective effects in many organ systems including the kidney [46]. A1AR activation produces several cellular effects that are suited to attenuate the multifaceted pathophysiology of AKI (endothelial and renal tubular cell apoptosis, inflammation, and necrosis). Acute renal protection after hepatic ischemia/reperfusion with A1AR activation is mediated by Akt activation [47]. In particular, Akt has diverse functions to counteract apoptosis including inhibition of mitochondrial cytochrome c and phosphorylation of several proapoptotic factors (e.g., caspase 9, glycogen synthase kinase 3) [48]. Akt can also increase the activity of heat shock protein 27 in certain cell types [49, 50] promoting F-actin stability. Better preserved F-actin cytoskeleton in the kidneys may contribute to reduced renal tubular necrosis and apoptosis [33].

Another suggested molecular pathway is the protease-activated receptor 1. As reported by Park et al. modulation of the receptor through the administration of activated protein C resulted in reduced expression of several proinflammatory genes, reduced kidney filamentous-actin degradation and neutrophil infiltration, and better preservation of vascular permeability of the kidney after liver ischemia/reperfusion [51]. Except from this receptor, the family of Sphingosine-1-phosphate (S1P) receptors have been shown to play a role either in the protection or the development of ischemia/reperfusion induced AKI. More specifically, S1P1 receptor activation via S1P provides a protective signaling cascade, whereas S1P3 activation can potentially initiate detrimental effects. The authors also showed that the protective effect of S1P activated S1P1 receptor was induced via pertussis toxin-sensitive G protein (Gi/o) ERK and Akt-mediated pathways [52] and included reduced necrosis, inflammation and apoptosis, enhanced preservation of F-actin cytoskeleton, improved vascular integrity, and reduced neutrophil infiltration [53].

Endogenous hydrogen sulphide has also been demonstrated to play a role as a modulator of key peroxidant and inflammatory events occurring after total hepatic ischemia and reperfusion, attenuating lipid peroxidation and inflammation reactions by reducing MDA, nuclear factor-κB (NF-κB), and ICAM-1 production [54]. Finally, Suzuki et al. have proposed a putative role for platelet activating factor (PAF) and endothelin (ET)-1 in the pathogenesis of renal injury after hepatic ischemia and reperfusion. Specifically, they reported that the pretreatment with a PAF receptor antagonist resulted in attenuation of renal injury [55].

4. Lung Injury

The impact of pulmonary complications on morbidity and mortality after hepatic ischemia/reperfusion was acknowledged more than 2 decades ago [56, 57]. It was soon realized that lung injury resulted from the reperfusion of the donor liver during transplantation, a condition that also ensues during extensive hepatectomies. One of the proposed mechanisms is the release of TNF-α from reperfused Kupffer cells, which interacts with pulmonary capillaries and elicits the expression of adhesion molecules, such as ICAM-1 and E-selectin, leading to migration of neutrophils and subsequent lung injury [58–60]. In combination with TNF-α, a variety of proinflammatory molecules, such as PAF, cytokine-induced neutrophil-chemoattractant protein [61], IL-6, and IL-18 [62, 63], as well as substance-P [64], are released from the reperfused liver and have been found to mediate lung injury after hepatic ischemia/reperfusion. On the contrary, IL-4 and IL-10 seem to exert a protective role [63, 65].

Cytokine production by the reperfused liver seems to provoke a sustained production of cytokines locally in the lung, such as TNF-α from alveolar macrophages, macrophage inflammatory protein (MIP)-2, and the pathway of interleukin-6/signal transducer and activator of

transcription-3 (STAT3) [60, 65, 66]. The importance of the locally sustained pulmonary inflammation was underlined by the suppression of pulmonary NF-κB through administration of IL-10, which was followed by cytokine suppression and prevention of hepatic ischemia/reperfusion-induced lung injury [65].

Another important mechanism is the translocation of endotoxin to the systemic circulation. Bacterial translocation is evident after liver resection under vascular control even after the creation of a portasystemic shunt [67]. In particular, insufficiency of Kupffer cells during reperfusion allows the spill-over of endotoxin in the pulmonary capillaries, stimulating TNF-α, IL-6, epithelial neutrophil activating protein-78, and MIP-2 production and subsequent neutrophil infiltration of the lungs [68, 69]. The protective action of inhibition of endotoxin against hepatic and pulmonary injury after hepatic ischemia/reperfusion alone or in combination with hepatectomy further strengthens the role of endotoxin in the pathophysiology of the syndrome [70].

Oxidative stress during hepatic ischemia/reperfusion has been consistently shown to play a crucial role in the development of lung injury. Although the lung resists oxidative stress by upregulating antioxidant enzymes, exogenous antioxidants offer significant benefits [7]. Xanthine oxidase (XO) has been shown to release hydroxyl and superoxide radicals during reperfusion. Its inhibition by allopurinol has been reported to ameliorate lung injury in this setting [71, 72]. Data from our laboratory have also marked nitrosylation of pulmonary proteins as a prominent feature in liver ischemia/reperfusion induced lung injury [60]. However, production of NO seems to protect the lung from injury [73–75]. In a recent work, we have also shown the role of oxidative reactions mediated by free iron in this setting, and the significant improvement of hepatic ischemia/reperfusion-induced lung injury by iron chelation [7]. Improvement has also been offered by other antioxidants, such as the general anesthetic propofol, methylene blue, and mannitol [76–78]. Recently, preconditioning of the lungs with isoflurane showed promising results, although the involved mechanisms remain poorly understood [79].

Lung injury and acute respiratory distress syndrome can severely complicate the postoperative course following liver transplantation [80]. Hepatic ischemia/reperfusion-induced lung injury may be implicated in these complications, due to the release of cytokines in the bloodstream, such as TNF-α and IL-6 and IL-8 [81, 82], as well as due to release of endotoxin, which seems to prolong ventilatory support [57, 83]. Whether this release of endotoxin and priming of neutrophils is responsible for the susceptibility of these patients to transfusion-related lung injury remains to be shown. Nevertheless, acute lung injury after liver transplantation has been repeatedly correlated to platelet transfusion [84–86].

5. Gut Injury

Gut barrier failure in the form of bacterial and/or endotoxin translocation has been reported following liver ischemia/reperfusion, either during hepatic resections with the use of the Pringle maneuver or after liver transplantation, both in the experimental and clinical setting [67, 87, 88]. However, liver ischemia/reperfusion injury has been implicated in other forms of intestinal dysfunction, including motility, transit time, and absorption function changes [89].

Multiple mechanisms have been proposed, but the exact pathophysiology remains to be elucidated. Experimental data suggest that intestinal mucosa oxidative injury results from the effect of liver-produced ROS, which are "spilled" in the systemic circulation. This is demonstrated in small animal model experimental studies. Okay et al. have reported decreased intestinal mucosal MDA concentration, attenuated intestinal mucosa injury, and bacterial translocation 24 hours after extensive hepatectomy in rats, following the administration of the antioxidant N-acetylcysteine [90]. Alexandris et al. have also reported decreased levels of protein carbonyls and decreased endotoxin translocation after antioxidant treatment, following extensive hepatectomy in rats [91]. The proposed mechanism of remote oxidative injury to the gut mucosa from liver derived ROS is damage of the tight junctions between enterocytes, which results in increased permeability and gut barrier failure.

Another suggested mechanism is congestion of the portal venous system. During the Pringle maneuver, blood from the intestine and pancreas is pooled in the portal venous system leading to portal hypertension. It has been demonstrated by Filos et al. that rats subjected to the Pringle maneuver for 30 minutes had immediate (30 minutes) and delayed (24 hours) gut barrier failure with increased bacterial and endotoxin translocation, which might be attributed to portal stasis leading to intestinal congestion. Bowel wall edema may lead to intra-abdominal hypertension resulting in further compromisation of intestinal perfusion [92] and gut barrier dysfunction [93]. In addition, sinusoidal microcirculatory failure during reperfusion decreases the total vascular bed of the liver, increasing intrahepatic portal resistance and leading to postoperative portal hypertension [94]. However, this scenario is only applicable in cases of liver ischemia/reperfusion injury following liver surgery, where vascular occlusion techniques are applied.

Postoperative liver failure seems to be one of the most serious complications after hepatic surgery, when liver ischemia and reperfusion occurs. Many of the factors which comprise gut barrier function seem to be compromised in postoperative liver failure [95]. Bile production and intestinal motility are decreased [89, 96, 97]. Bile has a trophic role for the intestinal mucosa. It binds to intraluminal endotoxin and bacteria creating nonabsorbable complexes and contains secretory IGA, which has antibacterial properties. The decreased intestinal motility results in increased intestinal bacterial load, which in turn has been shown to cause intestinal mucosal injury [97].

Apoptosis is implicated in gut mucosal injury following liver ischemia and reperfusion, since it is already known that extracellular free radicals can induce cell apoptosis [98–100]. It has been reported that oxidative stress can induce damage in enterocyte cell membranes and DNA, activating apoptotic pathways and thus disrupting the mucosal barrier [101, 102]. Ikeda et al. have shown that the typical intestinal oxidative

injury after ischemia and reperfusion is the "lifting" of the epithelial layer from the lamina propria and that apoptosis and necrosis are the main involved mechanisms [103]. During this process, enterocytes create subepithelial crypts and "blubs"—microscopically known as Gruenhagen's space [104]. Alterations in the expression of adhesion molecules between the cellular membrane and the matrix in the villi may be responsible. Beaulieu has implicated changes in the expression of B1 integrins [105], while Probstmeier et al. have reported changes in the expression and function of the complex molecule J1/tenascin in enterocytes located at the tip of the villi [106]. It is possible that oxygen free radicals damage these molecules leading to loss of interaction between enterocytes and matrix. It has been shown that loss of this interaction can lead to apoptotic cell death [107].

Remote intestinal injury has been reported by many authors in the setting of liver transplantation and liver ischemia and reperfusion protocols involving hepatectomy either under vascular control or not. Mochida et al. suggested that bacterial translocation, following liver transplantation in rats, is responsible for hypercoagulopathy in the graft's sinusoids, reversing it with oral antibiotic therapy [108]. Lemaire et al. described a porcine model of severe, extraintestinal tissue injury, consisting of prolonged hepatic ischemia and reperfusion, in combination with hemihepatectomy. Venous congestion of the gut during ischemia was prevented with a temporary portal-caval shunt. This prevented direct congestive damage to the gut, associating injury with remote ischemia/reperfusion. They reported bacterial translocation to the portal vain, lymph nodes, systemic circulation, and thoracic duct very early after liver reperfusion. In their model, gut injury can only be attributed to remote ischemia and reperfusion from the liver. Portal congestion was eliminated, while the extent of hepatectomy was too limited to cause liver failure, and barrier failure was evident very early during reperfusion [67]. Filos et al. reported immediate and delayed gut barrier failure increasing bacterial translocation and endotoxaemia after 30 minutes of liver ischemia in rats. In addition, they found increased apoptosis in the intestinal mucosa 30 min after reperfusion [88]. Bedurlu et al. reported increased levels of TNF-α, bacterial translocation, and endotoxaemia 48 hours after hepatectomy performed under liver ischemia and reperfusion [109]. Jiang et al. showed that remote injury of the intestinal mucosa takes place after 30 minutes of liver ischemia followed by reperfusion in a rat experimental model. Microscopic study revealed denuded villi, disintegration of the lamina propria, appearance of exposed capillaries, and infiltration of neutrophils and macrophages in the ileal mucosa. In addition, enterocyte apoptosis was found to be increased after liver ischemia and reperfusion. Splenectomy reversed these findings suggesting a role of the spleen in inflammatory and apoptotic pathways, through neutrophil activation and cytokine expression [110]. Leister et al. concluded that partial hepatic ischemia/reperfusion injury leads to significant alterations of small bowel microcirculation and mucosal injury, while vasoactive intestinal polypeptide and gastrin-releasing peptide attenuated the damage [111]. Ochiai et al. showed increased intestinal permeability, endotoxinemia, and morphologic changes in the intestinal mucosa after liver ischemia and reperfusion combined with hepatectomy. These findings were reversed in the group treated with I2 prostaglandin analogues [112]. Finally, Meyer et al. have shown that liver ischemia and reperfusion increases the expression of ICAM in various organs including the intestine, implicating a possible mechanism of multiple organ failure [32].

Most of the experimental studies have been done in small animal models and, as a result, vascular occlusion is accompanied by transient portal hypertension. This is a major confounding factor, as direct damage to the intestinal mucosa can take place during splanchnic congestion. Only when this factor has been eliminated can the injury be attributed to remote injury by spillage of toxic substances from the liver.

Our team has developed an experimental model of liver ischemia and reperfusion injury combined with major hepatectomy, as a clinical analogue to major hepatectomy under vascular control [2]. In this model we have demonstrated that liver ischemia and reperfusion produces reactive oxygen species that result in oxidative injury to the intestinal mucosa. Intestinal mucosa oxidative markers were increased, suggesting a causative association with intestinal mucosa injury, apoptosis of enterocytes, and bacterial and endotoxin translocation. These parameters were reversed when antioxidant therapy was administered [6].

Clinical data regarding remote intestinal injury after liver ischemia/reperfusion derive mostly from liver transplantation series, because in liver resection studies addressing gut dysfunction, vascular control is not always used and, as a result, liver ischemia/reperfusion injury is not always present. In a randomized clinical study from Abdala et al. increased endotoxin translocation from the gut was reported following liver transplantation. The patients were divided in two groups, undergoing liver transplantation with a venovenous shunt or with the "piggyback" method. No endotoxin clearance was documented through the grafts of either group 2 hours after reperfusion [87]. In another study from Ronholm et al. postreperfusion hypotension observed after reperfusion of the graft was attributed to complement cascade activation originating from the gut during the reperfusion phase of orthotopic liver transplantation [113]. Wu et al. also demonstrated bacterial translocation in a clinical study of cirrhotic patients undergoing liver transplantation [114]. However, in clinical studies, no direct measurements of intestinal tissue injury have been made and there is no direct proof if mucosal injury exists, if it is the result of liver vascular manipulations, or if it preexisted prior to transplantation as a result of liver parenchyma injury.

The above mechanisms are summarized in Figure 3.

6. Pancreatic Injury

Pancreatic dysfunction has been reported following major liver resections both in clinical trials [115] and in experimental studies [116]. The etiology of pancreatic dysfunction after these operations has not yet been clarified. However,

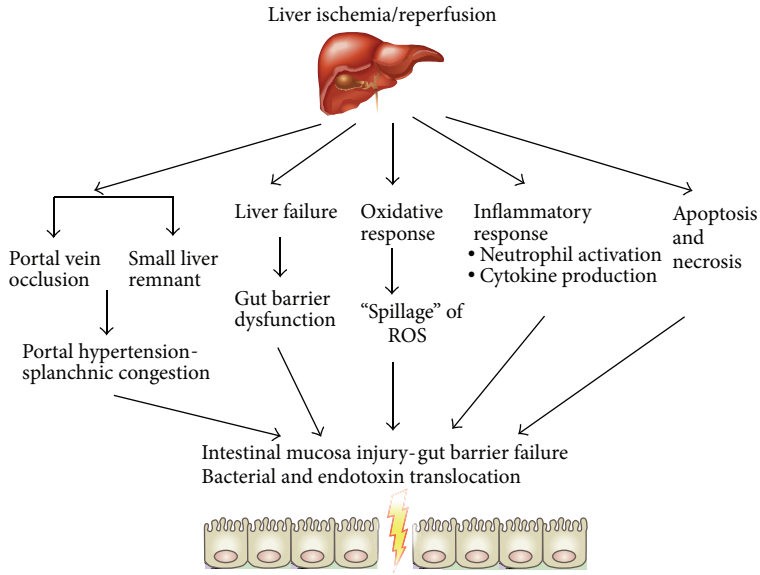

Figure 3: Mechanisms involved in remote injury to the gut mucosa leading to gut barrier failure after liver ischemia/reperfusion.

among the risk factors proposed to interpret hyperamylasemia following hepatectomy are chronic liver disease and extent of hepatectomy, as well as portal congestion caused by the vascular control of the liver during these surgical procedures [117]. In a clinical study, Miyagawa et al. reported that the use of the Pringle maneuver during liver resection increases the incidence of postoperative hyperamylasemia and that the severity of hyperamylasemia is increased as the vascular occlusion time is prolonged [118]. Hashimoto et al. described the same conclusion in their clinical study reporting attenuated pancreatic injury in patients who were subjected to selective vascular control techniques [119]. Although the fist assumption of pancreatic injury after hepatectomy proposed portal congestion during vascular control as being responsible, Kubota et al. carried out a series of hepatectomies, occluding the superior mesenteric artery as well, during hepatic vascular control and thus eliminating any increase in portal pressure [120]. There were no differences in amylase compared with patients with intraoperative portal hypertension, implying that the possible mechanism was remote ischemia/reperfusion injury of the liver. Meyer et al. have reported ICAM-1 upregulation in remote organs, after liver ischemia and reperfusion in rats, including the pancreas, intestine, kidney, and lung [121]. The proposed mechanism is oxidative damage, derived from ROS production during liver ischemia/reperfusion by the use of hepatic vascular control during surgery. Ochiai et al. have also demonstrated pancreatic tissue injury after partial hepatectomy combined with ischemia/reperfusion in rats. They demonstrated a peak of acinar cell necrosis at 24 hours postoperatively as well as increased apoptotic activity. These findings were attenuated after treatment with I2 prostaglandin analogues [122]. Yang et al. found increased pancreatic MDA content, decreased pancreatic SOD activity, and increased serum amylase after 6 hours of reperfusion in a rodent model of 45-minute hepatic ischemia and reperfusion [123].

Our team has studied the pathophysiology of pancreatic injury following hepatic ischemia/reperfusion combined with hepatectomy. The key factor of posthepatectomy pancreatitis is thought to be the production of ROS, resulting in remote organ injury. In our study we measured the MDA content of portal blood and pancreatic tissue samples as a marker of lipid peroxidation and oxidative damage. Portal blood and pancreatic tissue MDA content was increased during liver reperfusion. In addition, we found increased amylase and c-peptide levels during reperfusion and histological evidence of pancreatic necrosis [124]. These data support the hypothesis that ROS and oxidative stress, as assessed by lipid peroxidation and tissue necrosis, play a crucial role in pancreatitis following liver ischemia/reperfusion combined with hepatectomy. Further evidence from our team supports the aforementioned hypothesis. Antioxidant administration (desferrioxamine) attenuated pancreatic injury after major hepatectomy under vascular control in a porcine experimental model, possibly by preventing and reversing production and circulation of oxidative products [54].

Pancreatic injury, in the form of acute pancreatitis, is a rare but severe complication of liver transplantation in children and adults [125]. Although multiple factors have been implicated, it seems that remote oxidative burst plays a pivotal role. In a recent study in rodents from Li et al. pancreatic injury following liver transplantation was found to be oxidative stress dependant. They found increased MDA content in pancreatic tissue, increased amylase and lipase serum levels, and morphological changes. These were attenuated with antioxidant treatment [126].

7. Adrenal Injury

Adrenal function during liver ischemia/reperfusion has not been adequately studied to date. However, there are reports of macroscopic injury to the adrenals following hepatectomy

under vascular control and orthotopic liver transplantation [127, 128]. In addition, relative adrenal insufficiency has been reported in patients undergoing liver transplantation, even in steroid-free immunosuppressant protocols, in an incidence of up to 92% [129]. This has been described as the "hepatoadrenal" syndrome. A possible proposed mechanism is the decreased levels of high density lipoprotein (HDL) after liver transplantation and thus decreased cortisol synthesis. HDL levels have been shown to be a predictor of posttransplant relative adrenal insufficiency [130]. During the anhepatic phase, the liver does not produce apoA-1 (which is essential for the formation of HDL) for a number of hours. In addition, the transplanted liver suffers ischemia/reperfusion injury that is responsible for postoperative liver dysfunction. ApoA-1 has a relatively short half-life and, therefore, the HDL levels are decreased after transplantation.

Liver ischemia/reperfusion has been shown to increase the levels of endotoxin, as well as various cytokines, including TNF-α, IL-1β, and IL-6. Endotoxin and TNF-α have been shown to inhibit steroidogenesis. Endotoxin has been reported to bind to the HDL receptor, neutralizing it [131]. Increased levels of TNF-α, IL-1β, and IL-6, which are produced during hepatic ischemia/reperfusion, have been shown to decrease synthesis and secretion of apoA-1 [132]. In addition, TNF-α has been demonstrated to directly inhibit steroidogenesis and increase resistance to cortisol [130].

8. Myocardial Injury

Although indications about a connection between acute liver injury and myocardial damage had already been reported [133, 134], this was brought sharply into focus in a study by the US Acute Liver Failure Study Group which showed that elevation of serum troponin I (cTnI) levels is common (74% overall) in patients with ALF of various etiologies [135]. However, in both this and the previous studies, liver ischemia/reperfusion was absent as a mechanism of injury. Furthermore, these studies focused more on clinical aspects and less on pathophysiology. Tanaka et al. showed that liver ischemia/reperfusion is accompanied by myocardial cell necrosis (manifested by elevated troponin levels) and proposed ROS production as a putative mechanism of injury [25]. However, this study suffered from a major design limitation: to achieve liver ischemia/reperfusion, the portal vein was totally occluded, leading to intestinal congestion during liver ischemia, with unknown effects in the observed results. A similar follow-up study also documented myocardium injury after total hepatic ischemia and reperfusion and reversal with antioxidant treatment. However, this study had similar limitations, as the inferior vena cava was also occluded in the process, leading to certain hemodynamic instability and altered cardiac output, making pathophysiologic mechanisms unclear [54]. Recently, the same group published data showing attenuation of myocardium injury after total hepatic ischemia and reperfusion after the administration of tacrolimus, implicating inflammatory mechanisms in the pathophysiology as well [5].

Trying to overcome these limitations, our team designed a porcine model of liver ischemia/reperfusion that diverted portal blood flow during ischemia to the inferior vena cava and restored normal flow path during reperfusion. Our results showed a relatively subtle yet consistent injury to the myocardium early after liver ischemia/reperfusion, manifested mainly by increase in cardiac troponin I blood levels and confirmed histologically by myocardiocyte necrosis [136].

An unexpected result of this study was the early myocardial injury (prior to 6 hours after reperfusion), certainly before acute liver failure manifestations (e.g., increase in liver enzymes, intracranial hypertension, and hemodynamic instability). It is therefore speculated that myocardial injury was probably attributed to liver ischemia/reperfusion and not to the ensuing acute liver failure. A putative mechanism involves the generation of reactive oxygen and nitrogen species during liver ischemia/reperfusion. However, myocardial damage in this setting was subclinical and mostly evident under microscopic examination; therefore the heart might be one of the least clinically affected organs in liver ischemia/reperfusion. It must not be forgotten, however, that all experimental as well as most clinical observations are made in relatively healthy hearts and not those burdened with ischemia, cardiomyopathy, and/or systolic or diastolic dysfunction.

9. Comments

Liver ischemia/reperfusion injury has been shown to play a pivotal role in the pathogenesis of the frequently observed remote organ injury following a variety of clinical scenarios including hepatic surgery and transplantation. Multiple mechanisms have been implicated in the pathophysiology of this remote organ injury. Among them, the oxidative and the inflammatory pathway have been shown to play an important role. However, most of the available studies of remote organ injury after hepatic ischemia/reperfusion examine the liver and the respective organ *in vivo*. Therefore the employed therapeutic strategies could be hypothesized to ameliorate remote organ injury through attenuation of liver injury, without knowing their net effect on remote organ injury alone. A possible exception could be the experimental models of isolated perfused organs. Although the former strategy is clearly more applicable to the clinical scenario, the latter methodology could be more helpful in the elucidation and clarification of the underlying mechanisms implicated in the pathophysiology of hepatic ischemia/reperfusion-induced remote organ injury. One of course could argue that remote organ injury is dependent on cellular and molecular events following liver reperfusion and could be effectively attenuated with appropriate interventions to reduce hepatic ischemia/reperfusion injury. Such interventions can be targeted towards specific molecular mechanisms, as mentioned above, or towards more holistic methods such ischemic preconditioning or bioartificial liver devices. Finally, since most of the current knowledge on remote organ injury derives from experimental studies, the investigation of this

entity and the assessment of the efficacy of the various therapeutic strategies in the clinical setting are warranted.

Conflict of Interests

The authors declare that there is no conflict of interests regarding the publication of this paper.

References

[1] E. E. Douzinas, O. Livaditi, M.-K. Tasoulis et al., "Nitrosative and oxidative stresses contribute to post-ischemic liver injury following severe hemorrhagic shock: the role of hypoxemic resuscitation," *PLoS ONE*, vol. 7, no. 3, Article ID e32968, 2012.

[2] N. Arkadopoulos, G. Defterevos, C. Nastos et al., "Development of a porcine model of post-hepatectomy liver failure," *Journal of Surgical Research*, vol. 170, no. 2, pp. e233–e242, 2011.

[3] H. Jaeschke, "Molecular mechanisms of hepatic ischemia-reperfusion injury and preconditioning," *American Journal of Physiology—Gastrointestinal and Liver Physiology*, vol. 284, no. 1, pp. G15–G26, 2003.

[4] F. Serracino-Inglott, N. A. Habib, and R. T. Mathie, "Hepatic ischemia-reperfusion injury," *American Journal of Surgery*, vol. 181, no. 2, pp. 160–166, 2001.

[5] Y. Chen and X. Xie, "Tacrolimus attenuates myocardium damage to the total hepatic ischemia-reperfusion via regulation of the mitochondrial function," *Journal of Surgical Research*, vol. 172, no. 1, pp. e47–e54, 2012.

[6] C. Nastos, K. Kalimeris, N. Papoutsidakis et al., "Antioxidant treatment attenuates intestinal mucosal damage and gut barrier dysfunction after major hepatectomy. Study in a porcine model," *Journal of Gastrointestinal Surgery*, vol. 15, no. 5, pp. 809–817, 2011.

[7] K. Kalimeris, C. Nastos, N. Papoutsidakis et al., "Iron chelation prevents lung injury after major hepatectomy," *Hepatology Research*, vol. 40, no. 8, pp. 841–850, 2010.

[8] B. Vollmar, J. Glasz, R. Leiderer, S. Post, and M. D. Menger, "Hepatic microcirculatory perfusion failure is a determinant of liver dysfunction in warm ischemia-reperfusion," *American Journal of Pathology*, vol. 145, no. 6, pp. 1421–1431, 1994.

[9] V. Smyrniotis, C. Farantos, G. Kostopanagiotou, and N. Arkadopoulos, "Vascular control during hepatectomy: review of methods and results," *World Journal of Surgery*, vol. 29, no. 11, pp. 1384–1396, 2005.

[10] G. Garcea, A. Gescher, W. Steward, A. Dennison, and D. Berry, "Oxidative stress in humans following the Pringle manoeuvre," *Hepatobiliary and Pancreatic Diseases International*, vol. 5, no. 2, pp. 210–214, 2006.

[11] I. Marzi, Y. Takei, M. Rücker et al., "Endothelin-1 is involved in hepatic sinusoidal vasoconstriction after ischemia and reperfusion," *Transplant International*, vol. 7, supplement 1, pp. S503–S506, 1994.

[12] B. Vollmar and M. D. Menger, "The hepatic microcirculation: mechanistic contributions and therapeutic targets in liver injury and repair," *Physiological Reviews*, vol. 89, no. 4, pp. 1269–1339, 2009.

[13] D. Uhlmann, S. Glasser, G. Gaebel et al., "Improvement of postischemic hepatic microcirculation after endothelin A receptor blockade—endothelin antagonism influences platelet-endothelium interactions," *Journal of Gastrointestinal Surgery*, vol. 9, no. 2, pp. 187–197, 2005.

[14] C. D. Collard and S. Gelman, "Pathophysiology, clinical manifestations, and prevention of ischemia-reperfusion injury," *Anesthesiology*, vol. 94, no. 6, pp. 1133–1138, 2001.

[15] M. Mendes-Braz, M. Elias-Miro, M. B. Jimenez-Castro, A. Casillas-Ramirez, F. S. Ramalho, and C. Peralta, "The current state of knowledge of hepatic ischemia-reperfusion injury based on its study in experimental models," *Journal of Biomedicine and Biotechnology*, vol. 2012, Article ID 298657, 20 pages, 2012.

[16] N. C. Teoh and G. C. Farrell, "Hepatic ischemia reperfusion injury: pathogenic mechanisms and basis for hepatoprotection," *Journal of Gastroenterology and Hepatology*, vol. 18, no. 8, pp. 891–902, 2003.

[17] C. Fondevila, R. W. Busuttil, and J. W. Kupiec-Weglinski, "Hepatic ischemia/reperfusion injury—a fresh look," *Experimental and Molecular Pathology*, vol. 74, no. 2, pp. 86–93, 2003.

[18] A. P. Betrosian, B. Agarwal, and E. E. Douzinas, "Acute renal dysfunction in liver diseases," *World Journal of Gastroenterology*, vol. 13, no. 42, pp. 5552–5559, 2007.

[19] V. Arroyo, J. Fernandez, and P. Ginès, "Pathogenesis and treatment of hepatorenal syndrome," *Seminars in Liver Disease*, vol. 28, no. 1, pp. 81–95, 2008.

[20] C. L. Davis, T. A. Gonwa, and A. H. Wilkinson, "Pathophysiology of renal disease associated with liver disorders: implications for liver transplantation. Part I," *Liver Transplantation*, vol. 8, no. 2, pp. 91–109, 2002.

[21] Y. M. Barri, E. Q. Sanchez, L. W. Jennings et al., "Acute kidney injury following liver transplantation: definition and outcome," *Liver Transplantation*, vol. 15, no. 5, pp. 475–483, 2009.

[22] H. M. Wadei, M. L. Mai, N. Ahsan, and T. A. Gonwa, "Hepatorenal syndrome: pathophysiology and management," *Clinical Journal of the American Society of Nephrology*, vol. 1, no. 5, pp. 1066–1079, 2006.

[23] M. Schepke, "Hepatorenal syndrome: current diagnostic and therapeutic concepts," *Nephrology, Dialysis, Transplantation*, vol. 22, supplement 8, pp. viii2–viii4, 2007.

[24] S. Rivera-Huizar, A. R. Rincón-Sánchez, A. Covarrubias-Pinedo et al., "Renal dysfunction as a consequence of acute liver damage by bile duct ligation in cirrhotic rats," *Experimental and Toxicologic Pathology*, vol. 58, no. 2-3, pp. 185–195, 2006.

[25] Y. Tanaka, J. M. Maher, C. Chen, and C. D. Klaassen, "Hepatic ischemia-reperfusion induces renal heme oxygenase-1 via NF-E2-related factor 2 in rats and mice," *Molecular Pharmacology*, vol. 71, no. 3, pp. 817–825, 2007.

[26] A. Tsung, R. A. Hoffman, K. Izuishi et al., "Hepatic ischemia/reperfusion injury involves functional TLR4 signaling in nonparenchymal cells," *Journal of Immunology*, vol. 175, no. 11, pp. 7661–7668, 2005.

[27] R. M. Levy, K. P. Mollen, J. M. Prince et al., "Systemic inflammation and remote organ injury following trauma require HMGB1," *American Journal of Physiology—Regulatory Integrative and Comparative Physiology*, vol. 293, no. 4, pp. R1538–R1544, 2007.

[28] M. Kadkhodaee, S. Mikaeili, M. Zahmatkesh et al., "Alteration of renal functional, oxidative stress and inflammatory indices following hepatic ischemia-reperfusion," *General Physiology and Biophysics*, vol. 31, no. 2, pp. 195–202, 2012.

[29] S. W. Park, M. Kim, K. M. Brown, V. D. D'Agati, and H. T. Lee, "Paneth cell-derived interleukin-17A causes multiorgan dysfunction after hepatic ischemia and reperfusion injury," *Hepatology*, vol. 53, no. 5, pp. 1662–1675, 2011.

[30] T. A. Sutton, H. E. Mang, S. B. Campos, R. M. Sandoval, M. C. Yoder, and B. A. Molitoris, "Injury of the renal microvascular endothelium alters barrier function after ischemia," *American Journal of Physiology—Renal Physiology*, vol. 285, no. 2, pp. F191–F198, 2003.

[31] B. A. Molitoris, R. Sandoval, and T. A. Sutton, "Endothelial injury and dysfunction in ischemic acute renal failure," *Critical Care Medicine*, vol. 30, no. 5, supplement, pp. S235–S240, 2002.

[32] K. Meyer, M. F. Brown, G. Zibari et al., "ICAM-1 upregulation in distant tissues after hepatic ischemia/reperfusion: a clue to the mechanism of multiple organ failure," *Journal of Pediatric Surgery*, vol. 33, no. 2, pp. 350–353, 1998.

[33] H. T. Lee, S. W. Park, M. Kim, and V. D. D'Agati, "Acute kidney injury after hepatic ischemia and reperfusion injury in mice," *Laboratory Investigation*, vol. 89, no. 2, pp. 196–208, 2009.

[34] H. T. Lee, M. Kim, M. Jan, R. B. Penn, and C. W. Emala, "Renal tubule necrosis and apoptosis modulation by A1 adenosine receptor expression," *Kidney International*, vol. 71, no. 12, pp. 1249–1261, 2007.

[35] B. Li, B. Chen, G. Zhang, K. Wang, L. Zhou, and S. Hu, "Cell apoptosis and Fas gene expression in liver and renal tissues after ischemia-reperfusion injury in liver transplantation," *Transplantation Proceedings*, vol. 42, no. 5, pp. 1550–1556, 2010.

[36] L. E. C. Miranda, V. K. Capellini, G. S. Reis, A. C. Celotto, C. G. Carlotti Jr., and P. R. B. Evora, "Effects of partial liver ischemia followed by global liver reperfusion on the remote tissue expression of nitric oxide synthase: lungs and kidneys," *Transplantation Proceedings*, vol. 42, no. 5, pp. 1557–1562, 2010.

[37] C. Polat, Ç. Tokyol, A. Kahraman, B. Sabuncuoğlu, and S. Yilmaz, "The effects of desferrioxamine and quercetin on hepatic ischemia-reperfusion induced renal disturbance," *Prostaglandins Leukotrienes and Essential Fatty Acids*, vol. 74, no. 6, pp. 379–383, 2006.

[38] B. Seifi, M. Kadkhodaee, F. Delavari, S. Mikaeili, S. Shams, and S. N. Ostad, "Pretreatment with pentoxifylline and N-acetylcysteine in liver ischemia reperfusion-induced renal injury," *Renal Failure*, vol. 34, no. 5, pp. 610–615, 2012.

[39] J. A. Lee, J. W. Choi, J. H. In et al., "Hepatic ischemic preconditioning provides protection against distant renal ischemia and reperfusion injury in mice," *Journal of Korean Medical Science*, vol. 27, no. 5, pp. 547–552, 2012.

[40] J. D. Joo, M. Kim, V. D. D'Agati, and H. T. Lee, "Ischemic preconditioning provides both acute and delayed protection against renal ischemia and reperfusion injury in mice," *Journal of the American Society of Nephrology*, vol. 17, no. 11, pp. 3115–3123, 2006.

[41] M. Torres and H. J. Forman, "Redox signaling and the MAP kinase pathways," *BioFactors*, vol. 17, no. 1–4, pp. 287–296, 2003.

[42] P. S. Kellerman, S. L. Norenberg, and G. M. Jones, "Early recovery of the actin cytoskeleton during renal ischemic injury in vivo," *American Journal of Kidney Diseases*, vol. 27, no. 5, pp. 709–714, 1996.

[43] B. A. Molitoris, "Actin cytoskeleton in ischemic acute renal failure," *Kidney International*, vol. 66, no. 2, pp. 871–883, 2004.

[44] S. R. White, P. Williams, K. R. Wojcik et al., "Initiation of apoptosis by actin cytoskeletal derangement in human airway epithelial cells," *American Journal of Respiratory Cell and Molecular Biology*, vol. 24, no. 3, pp. 282–294, 2001.

[45] D. Dinour and M. Brezis, "Effects of adenosine on intrarenal oxygenation," *American Journal of Physiology—Renal Fluid and Electrolyte Physiology*, vol. 261, no. 5, part 2, pp. F787–F791, 1991.

[46] H. T. Lee, G. Gallos, S. H. Nasr, and C. W. Emala, "A1 adenosine receptor activation inhibits inflammation, necrosis, and apoptosis after renal ischemia-reperfusion injury in mice," *Journal of the American Society of Nephrology*, vol. 15, no. 1, pp. 102–111, 2004.

[47] S. W. Park, S. W. C. Chen, M. Kim, K. M. Brown, V. D. D'Agati, and H. T. Lee, "Protection against acute kidney injury via A1 adenosine receptor-mediated Akt activation reduces liver injury after liver ischemia and reperfusion in mice," *Journal of Pharmacology and Experimental Therapeutics*, vol. 333, no. 3, pp. 736–747, 2010.

[48] T. G. Cross, D. Scheel-Toellner, N. V. Henriquez, E. Deacon, M. Salmon, and J. M. Lord, "Serine/threonine protein kinases and apoptosis," *Experimental Cell Research*, vol. 256, no. 1, pp. 34–41, 2000.

[49] M. J. Rane, P. Y. Coxon, D. W. Powell et al., "p38 Kinase-dependent MAPKAPK-2 activation functions as 3-phosphoinositide-dependent kinase-2 for Akt in human neutrophils," *The Journal of Biological Chemistry*, vol. 276, no. 5, pp. 3517–3523, 2001.

[50] M. J. Rane, Y. Pan, S. Singh et al., "Heat shock protein 27 controls apoptosis by regulating Akt activation," *The Journal of Biological Chemistry*, vol. 278, no. 30, pp. 27828–27835, 2003.

[51] S. W. Park, S. W. C. Chen, M. Kim, V. D. D'Agati, and H. T. Lee, "Human activated protein C attenuates both hepatic and renal injury caused by hepatic ischemia and reperfusion injury in mice," *Kidney International*, vol. 76, no. 7, pp. 739–750, 2009.

[52] S. W. Park, M. Kim, S. W. C. Chen, K. M. Brown, V. D. D'Agati, and H. T. Lee, "Sphinganine-1-phosphate protects kidney and liver after hepatic ischemia and reperfusion in mice through S1P 1 receptor activation," *Laboratory Investigation*, vol. 90, no. 8, pp. 1209–1224, 2010.

[53] S. W. Park, M. Kim, S. W. C. Chen, V. D. D'Agati, and H. T. Lee, "Sphinganine-1-phosphate attenuates both hepatic and renal injury induced by hepatic ischemia and reperfusion in mice," *Shock*, vol. 33, no. 1, pp. 31–42, 2010.

[54] Y. Chen, Z. Liu, and X. Xie, "Hydrogen sulphide attenuates renal and cardiac injury after total hepatic ischemia and reperfusion," *Journal of Surgical Research*, vol. 164, no. 2, pp. e305–e313, 2010.

[55] S. Suzuki, A. Serizawa, T. Sakaguchi et al., "The roles of platelet-activating factor and endothelin-1 in renal damage after total hepatic ischemia and reperfusion," *Transplantation*, vol. 69, no. 11, pp. 2267–2273, 2000.

[56] D. J. Plevak, P. A. Southorn, B. J. Narr, and S. G. Peters, "Intensive-care unit experience in the Mayo liver transplantation program: the first 100 cases," *Mayo Clinic Proceedings*, vol. 64, no. 4, pp. 433–445, 1989.

[57] T. Miyata, I. Yokoyama, S. Todo, A. Tzakis, R. Selby, and T. E. Starzl, "Endotoxaemia, pulmonary complications, and thrombocytopenia in liver transplantation," *The Lancet*, vol. 2, no. 8656, pp. 189–191, 1989.

[58] L. M. Colletti, S. L. Kunkel, A. Walz et al., "Chemokine expression during hepatic ischemia/reperfusion-induced lung injury in the rat. The role of epithelial neutrophil activating protein," *The Journal of Clinical Investigation*, vol. 95, no. 1, pp. 134–141, 1995.

[59] L. M. Colletti, A. Cortis, N. Lukacs, S. L. Kunkel, M. Green, and R. M. Strieter, "Tumor necrosis factor up-regulates intercellular adhesion molecule 1, which is important in the neutrophil-dependent lung and liver injury associated with hepatic ischemia and reperfusion in the rat," *Shock*, vol. 10, no. 3, pp. 182–191, 1998.

[60] N. Arkadopoulos, K. Kalimeris, A. Papalois et al., "Treatment with bioartificial liver improves lung injury in a swine model of partial hepatectomy and ischemia/reperfusion," *International Journal of Artificial Organs*, vol. 33, no. 2, pp. 105–113, 2010.

[61] A. Serizawa, S. Nakamura, S. Suzuki, S. Baba, and M. Nakano, "Involvement of platelet-activating factor in cytokine production and neutrophil activation after hepatic ischemia-reperfusion," *Hepatology*, vol. 23, no. 6, pp. 1656–1663, 1996.

[62] G. A. Wanner, W. Ertel, P. Müller et al., "Liver ischemia and reperfusion induces a systemic inflammatory response through Kupffer cell activation," *Shock*, vol. 5, no. 1, pp. 34–40, 1996.

[63] D. Takeuchi, H. Yoshidome, H. Kurosawa et al., "Interleukin-18 exacerbates pulmonary injury after hepatic ischemia/reperfusion in mice," *Journal of Surgical Research*, vol. 158, no. 1, pp. 87–93, 2010.

[64] T. Okaya, R. Holthaus, A. Kato, and A. B. Lentsch, "Involvement of the neuropeptide substance P in lung inflammation induced by hepatic ischemia/reperfusion," *Inflammation Research*, vol. 53, no. 6, pp. 257–261, 2004.

[65] H. Yoshidome, A. Kato, M. J. Edwards, and A. B. Lentsch, "Interleukin-10 inhibits pulmonary NF-κB activation and lung injury induced by hepatic ischemia-reperfusion," *American Journal of Physiology—Lung Cellular and Molecular Physiology*, vol. 277, no. 5, part 1, pp. L919–L923, 1999.

[66] M. P. Callery, T. Kamei, M. J. Mangino, and M. W. Flye, "Organ interactions in sepsis: Host defense and the hepatic-pulmonary macrophage axis," *Archives of Surgery*, vol. 126, no. 1, pp. 28–32, 1991.

[67] L. C. J. M. Lemaire, B. A. van Wagensveld, T. M. van Gulik, J. Dankert, J. J. B. van Lanschot, and D. J. Gouma, "Bacterial translocation to the thoracic duct in a setting of ischemia, partial resection and reperfusion of the porcine liver," *Digestive Surgery*, vol. 16, no. 3, pp. 222–228, 1999.

[68] G. M. Matuschak, K. A. Henry, C. A. Johanns, and A. J. Lechner, "Liver-lung interactions following Escherichia coil bacteremic sepsis and secondary hepatic ischemia/reperfusion injury," *American Journal of Respiratory and Critical Care Medicine*, vol. 163, no. 4, pp. 1002–1009, 2001.

[69] L. M. Colletti and M. Green, "Lung and liver injury following hepatic ischemia/ reperfusion in the rat is increased by exogenous lipopolysaccharide which also increases hepatic tnf production in vivo and in vitro," *Shock*, vol. 16, no. 4, pp. 312–319, 2001.

[70] S. Q. van Veen, S. Dinant, A. K. van Vliet, and T. M. van Gulik, "Alkaline phosphatase reduces hepatic and pulmonary injury in liver ischaemia-reperfusion combined with partial resection," *British Journal of Surgery*, vol. 93, no. 4, pp. 448–456, 2006.

[71] A. Weinbroum, V. G. Nielsen, S. Tan et al., "Liver ischemia-reperfusion increases pulmonary permeability in rat: role of circulating xanthine oxidase," *American Journal of Physiology—Gastrointestinal and Liver Physiology*, vol. 268, no. 6, pp. G988–G996, 1995.

[72] V. G. Nielsen, S. Tan, A. Weinbroum et al., "Lung injury after hepatoenteric ischemia-reperfusion: role of xanthine oxidase," *American Journal of Respiratory and Critical Care Medicine*, vol. 154, no. 5, pp. 1364–1369, 1996.

[73] C. Peralta, N. Prats, C. Xaus, E. Gelpí, and J. Roselló-Catafau, "Protective effect of liver ischemic preconditioning on liver and lung injury induced by hepatic ischemia-reperfusion in the rat," *Hepatology*, vol. 30, no. 6, pp. 1481–1489, 1999.

[74] P. Liu, B. Xu, and C. E. Hock, "Inhibition of nitric oxide synthesis by L-name exacerbates acute lung injury induced by hepatic ischemia-reperfusion," *Shock*, vol. 16, no. 3, pp. 211–217, 2001.

[75] Y. Takamatsu, K. Shimada, K. Yamaguchi, S. Kuroki, K. Chijiiwa, and M. Tanaka, "Inhibition of inducible nitric oxide synthase prevents hepatic, but not pulmonary, injury following ischemia-reperfusion of rat liver," *Digestive Diseases and Sciences*, vol. 51, no. 3, pp. 571–579, 2006.

[76] A. A. Weinbroum, G. Paret, O. Szold, V. Rudick, and L. Krupitzky, "Selective attenuation of acute lung ventilatory injury by methylene blue after liver ischemia-reperfusion: a drug response study in an isolated perfused double organ model," *Transplantation*, vol. 72, no. 3, pp. 385–392, 2001.

[77] A. A. Weinbroum, I. Shapira, R. B. Abraham, and A. Szold, "Mannitol dose-dependently attenuates lung reperfusion injury following liver ischemia reperfusion: a dose-response study in an isolated perfused double-organ model," *Lung*, vol. 180, no. 6, pp. 327–338, 2002.

[78] K.-C. Chan, C.-J. Lin, P.-H. Lee et al., "Propofol attenuates the decrease of dynamic compliance and water content in the lung by decreasing oxidative radicals released from the reperfused liver," *Anesthesia and Analgesia*, vol. 107, no. 4, pp. 1284–1289, 2008.

[79] X. Lv, Z.-M. Wang, S.-D. Huang, S.-H. Song, F.-X. Wu, and W.-F. Yu, "Emulsified isoflurane preconditioning reduces lung injury induced by hepatic ischemia/reperfusion in rats," *International Journal of Medical Sciences*, vol. 8, no. 5, pp. 353–361, 2011.

[80] S. K. Hong, S. Hwang, S. G. Lee et al., "Pulmonary complications following adult liver transplantation," *Transplantation Proceedings*, vol. 38, no. 9, pp. 2979–2981, 2006.

[81] X.-H. Wen, H.-Y. Kong, S.-M. Zhu, J.-H. Xu, S.-Q. Huang, and Q.-L. Chen, "Plasma levels of tumor necrotic factor-alpha and interleukin-6, -8 during orthotopic liver transplantation and their relations to postoperative pulmonary complications," *Hepatobiliary and Pancreatic Diseases International*, vol. 3, no. 1, pp. 38–41, 2004.

[82] X.-J. Chi, J. Cai, C.-F. Luo et al., "Relationship between the expression of Toll-like receptor 2 and 4 in mononuclear cells and postoperative acute lung injury in orthotopic liver transplantation," *Chinese Medical Journal*, vol. 122, no. 8, pp. 895–899, 2009.

[83] M. Goto, Y. Takei, S. Kawano et al., "Tumor necrosis factor and endotoxin in the pathogenesis of liver and pulmonary injuries after orthotopic liver transplantation in the rat," *Hepatology*, vol. 16, no. 2, pp. 487–493, 1992.

[84] C. Spencer Yost, M. A. Matthay, and M. A. Gropper, "Etiology of acute pulmonary edema during liver transplantation: a series of cases with analysis of the edema fluid," *Chest*, vol. 119, no. 1, pp. 219–223, 2001.

[85] C. C. Silliman, L. K. Boshkov, Z. Mehdizadehkashi et al., "Transfusion-related acute lung injury: epidemiology and a prospective analysis of etiologic factors," *Blood*, vol. 101, no. 2, pp. 454–462, 2003.

[86] I. T. A. Pereboom, M. T. de Boer, E. B. Haagsma, H. G. D. Hendriks, T. Lisman, and R. J. Porte, "Platelet transfusion during liver transplantation is associated with increased postoperative mortality due to acute lung injury," *Anesthesia and Analgesia*, vol. 108, no. 4, pp. 1083–1091, 2009.

[87] E. Abdala, C. E. Sandoll Baía, S. Mies et al., "Bacterial translocation during liver transplantation: a randomized trial comparing conventional with venovenous bypass vs. piggyback methods," *Liver Transplantation*, vol. 13, no. 4, pp. 488–496, 2007.

[88] K. S. Filos, I. Kirkilesis, I. Spiliopoulou et al., "Bacterial translocation, endotoxaemia and apoptosis following Pringle manoeuvre in rats," *Injury*, vol. 35, no. 1, pp. 35–43, 2004.

[89] C. Zheyu and Y. Lunan, "Early changes of small intestine function in rats after liver transplantation," *Transplantation Proceedings*, vol. 38, no. 5, pp. 1564–1568, 2006.

[90] E. Okay, A. Karadenizli, B. Müezzinoglu, U. Zeybek, H. A. Ergen, and T. Isbir, "N-acetylcysteine attenuates bacterial translocation after partial hepatectomy in rats," *Journal of Surgical Research*, vol. 127, no. 2, pp. 164–170, 2005.

[91] I. H. Alexandris, S. F. Assimakopoulos, C. E. Vagianos et al., "Oxidative state in intestine and liver after partial hepatectomy in rats. Effect of bombesin and neurotensin," *Clinical Biochemistry*, vol. 37, no. 5, pp. 350–356, 2004.

[92] F. Bongard, N. Pianim, S. Dubecz et al., "Adverse consequences of increased intra-abdominal pressure on bowel tissue oxygen," *Journal of Trauma—Injury, Infection and Critical Care*, vol. 39, no. 3, pp. 519–525, 1995.

[93] S. Wattanasirichaigoon, M. J. Menconi, R. L. Delude, and M. P. Fink, "Effect of mesenteric ischemia and reperfusion or hemorrhagic shock on intestinal mucosal permeability and ATP content in rats," *Shock*, vol. 12, no. 2, pp. 127–133, 1999.

[94] D. G. Farmer, F. Amersi, J. Kupiec-Weglinski, and R. W. Busuttil, "Current status of ischemia and reperfusion injury in the liver," *Transplantation Reviews*, vol. 14, no. 2, pp. 106–126, 2000.

[95] X. D. Wang, H. Parsson, R. Andersson, V. Soltesz, K. Johansson, and S. Bengmark, "Bacterial translocation, intestinal ultrastructure and cell membrane permeability early after major liver resection in the rat," *British Journal of Surgery*, vol. 81, no. 4, pp. 579–584, 1994.

[96] B. A. van Wagensveld, T. M. van Gulik, E. E. E. Gabeler, A. J. van der Kleij, H. Obertop, and D. J. Gouma, "Intrahepatic tissue pO_2 during continuous or intermittent vascular inflow occlusion in a pig liver resection model," *European Surgical Research*, vol. 30, no. 1, pp. 13–25, 1998.

[97] X.-D. Wang, W.-D. Guo, Q. Wang et al., "The association between enteric bacterial overgrowth and gastrointestinal motility after subtotal liver resection or portal vein obstruction in rats," *European Journal of Surgery, Acta Chirurgica*, vol. 160, no. 3, pp. 153–160, 1994.

[98] S. Raha and B. H. Robinson, "Mitochondria, oxygen free radicals, and apoptosis," *American Journal of Medical Genetics—Seminars in Medical Genetics*, vol. 106, no. 1, pp. 62–70, 2001.

[99] I. Yokoyama, M. Negita, A. Hayakawa et al., "Free radicals and apoptosis of the endothelial cells," *Transplantation Proceedings*, vol. 32, no. 1, p. 26, 2000.

[100] I. Stoian, A. Oros, and E. Moldoveanu, "Apoptosis and free radicals," *Biochemical and Molecular Medicine*, vol. 59, no. 2, pp. 93–97, 1996.

[101] C. Zhang, Z.-Y. Sheng, S. Hu, J.-C. Gao, S. Yu, and Y. Liu, "The influence of apoptosis of mucosal epithelial cells on intestinal barrier integrity after scald in rats," *Burns*, vol. 28, no. 8, pp. 731–737, 2002.

[102] T. Noda, R. Iwakiri, K. Fujimoto, S. Matsuo, and T. Y. Aw, "Programmed cell death induced by ischemia-reperfusion in rat intestinal mucosa," *American Journal of Physiology—Gastrointestinal and Liver Physiology*, vol. 274, no. 2, part 1, pp. G270–G276, 1998.

[103] H. Ikeda, Y. Suzuki, M. Suzuki et al., "Apoptosis is a major mode of cell death caused by ischaemia and ischaemia/reperfusion injury to the rat intestinal epithelium," *Gut*, vol. 42, no. 4, pp. 530–537, 1998.

[104] K. A. Shah, S. Shurey, and C. J. Green, "Apoptosis after intestinal ischemia-reperfusion injury: a morphological study," *Transplantation*, vol. 64, no. 10, pp. 1393–1397, 1997.

[105] J.-F. Beaulieu, "Differential expression of the VLA family of integrins along the crypt-villus axis in the human small intestine," *Journal of Cell Science*, vol. 102, part 3, pp. 427–436, 1992.

[106] R. Probstmeier, R. Martini, and M. Schachner, "Expression of J1/tenascin in the crypt-villus unit of adult mouse small intestine: implications for its role in epithelial cell shedding," *Development*, vol. 109, no. 2, pp. 313–321, 1990.

[107] S. M. Frisch and H. Francis, "Disruption of epithelial cell-matrix interactions induces apoptosis," *Journal of Cell Biology*, vol. 124, no. 4, pp. 619–626, 1994.

[108] S. Mochida, M. Arai, A. Ohno, and K. Fujiwara, "Bacterial translocation from gut to portal blood in the recipient as a factor of hypercoagulopathy in hepatic sinusoids after orthotopic liver transplantation in rats," *Transplantation Proceedings*, vol. 29, no. 1-2, pp. 874–875, 1997.

[109] A. Bedurlu, S. Gokahmetoglu, K. C. Kucuk, I. Soyuer, L. Guler, and O. Sakrak, "Bacterial translocation after partial hepatic resection under ischemia and reperfusion in rats: incidence and time course," *Turkish Journal of Medical Sciences*, vol. 33, pp. 135–140, 2003.

[110] H. Jiang, F. Meng, W. Li, L. Tong, H. Qiao, and X. Sun, "Splenectomy ameliorates acute multiple organ damage induced by liver warm ischemia reperfusion in rats," *Surgery*, vol. 141, no. 1, pp. 32–40, 2007.

[111] I. Leister, J. Sydow, T. Stojanovic et al., "Impact of vasoactive intestinal polypeptide and gastrin-releasing peptide on small bowel microcirculation and mucosal injury after hepatic ischemia/reperfusion in rats," *International Journal of Colorectal Disease*, vol. 20, no. 1, pp. 42–48, 2005.

[112] H. Ochiai, S. Nakamura, S. Suzuki, S. Baba, and S. Baba, "Pancreatic damage resulting from temporary portal triad interruption during partial hepatectomy: protective effect of a prostaglandin I2 analogue," *Journal of Surgical Research*, vol. 73, no. 2, pp. 129–136, 1997.

[113] E. Ronholm, H. Tomasdottir, J. Runeborg et al., "Complement system activation during orthotopic liver transplantation in man: indications of peroperative complement system activation in the gut," *Transplantation*, vol. 57, no. 11, pp. 1594–1597, 1994.

[114] Z.-W. Wu, K.-J. Xu, L.-J. Li et al., "Investigation of intestinal bacterial translocation in 78 patients with cirrhosis after liver transplantation," *Zhonghua Wai Ke Za Zhi*, vol. 44, no. 21, pp. 1456–1459, 2006.

[115] T. Tsuzuki, S. Shimizu, S. Takahashi, and H. Iio, "Hyperamylasemia after hepatic resection," *American Journal of Gastroenterology*, vol. 88, no. 5, pp. 734–736, 1993.

[116] S. Sjovall, T. Holmin, A. Evander, and U. Stenram, "Splenic and gastro-duodenal vein occlusion-influence on the pancreatic gland and on the outcome of experimental pancreatitis," *International Journal of Pancreatology*, vol. 3, no. 2-3, pp. 143–149, 1988.

[117] S. Miyagawa, M. Makuuchi, S. Kawasaki, and T. Kakazu, "Changes in serum amylase level following hepatic resection in chronic liver disease," *Archives of Surgery*, vol. 129, no. 6, pp. 634–638, 1994.

[118] S. Miyagawa, M. Makuuchi, S. Kawasaki, T. Kakazu, K. Hayashi, and H. Kasai, "Serum amylase elevation following hepatic resection in patients with chronic liver disease," *American Journal of Surgery*, vol. 171, no. 2, pp. 235–238, 1996.

[119] N. Hashimoto, S. Haji, H. Nomura, and H. Ohyanagi, "Hyperamylasemia after hepatic resection," *Hepato-Gastroenterology*, vol. 50, no. 53, pp. 1472–1473, 2003.

[120] K. Kubota, M. Makuuchi, T. Noie et al., "Risk factors for hyperamylasemia after hepatectomy using the pringle maneuver: randomized analysis of surgical parameters," *Archives of Surgery*, vol. 133, no. 3, pp. 303–308, 1998.

[121] K. Meyer, M. F. Brown, G. Zibari et al., "ICAM-1 upregulation in distant tissues after hepatic ischemia/reperfusion: a clue to the mechanism of multiple organ failure," *Journal of Pediatric Surgery*, vol. 33, no. 2, pp. 350–353, 1998.

[122] H. Ochiai, S. Nakamura, S. Suzuki, S. Baba, and S. Baba, "Pancreatic damage resulting from temporary portal triad interruption during partial hepatectomy: protective effect of a prostaglandin I2 analogue," *Journal of Surgical Research*, vol. 73, no. 2, pp. 129–136, 1997.

[123] J.-C. Yang, Z.-W. Wang, C.-L. Li, J.-H. Lin, X.-G. Liu, and Q.-X. Ji, "Multiple organ injury at early stage of intestinal and hepatic ischemia-reperfusion in rats," *Di Yi Jun Yi da Xue Xue Bao*, vol. 24, no. 2, pp. 198–203, 2004.

[124] N. Arkadopoulos, C. Nastos, G. Defterevos et al., "Pancreatic injury after major hepatectomy: a study in a porcine model," *Surgery Today*, vol. 42, no. 4, pp. 368–375, 2012.

[125] C. A. Camargo Jr., P. D. Greig, G. A. Levy, and P.-A. Clavien, "Acute pancreatitis following liver transplantation," *Journal of the American College of Surgeons*, vol. 181, no. 3, pp. 249–256, 1995.

[126] Y. Li, P.-J. Zhang, C. Jin et al., "Protective effects of deferoxamine mesylate preconditioning on pancreatic tissue in orthotopic liver autotransplantation in rats," *Transplantation Proceedings*, vol. 43, no. 5, pp. 1450–1455, 2011.

[127] A. D. Gouliamos, A. Metafa, S. G. Ispanopoulou, F. Stamatelopoulou, L. J. Vlahos, and J. D. Papadimitriou, "Right adrenal hematoma following hepatectomy," *European Radiology*, vol. 10, no. 4, pp. 583–585, 2000.

[128] R. W. Prokesch, W. Schima, G. Berlakovich, and J. Zacherl, "Adrenal hemorrhage after orthotopic liver transplantation: MR appearance," *European Radiology*, vol. 11, no. 12, pp. 2484–2487, 2001.

[129] T. Iwasaki, M. Tominaga, T. Fukumoto et al., "Relative adrenal insufficiency manifested with multiple organ dysfunction in a liver transplant patient," *Liver Transplantation*, vol. 12, no. 12, pp. 1896–1899, 2006.

[130] P. E. Marik, T. Gayowski, and T. E. Starzl, "The hepatoadrenal syndrome: a common yet unrecognized clinical condition," *Critical Care Medicine*, vol. 33, no. 6, pp. 1254–1259, 2005.

[131] T. G. Vishnyakova, A. V. Bocharov, I. N. Baranova et al., "Binding and internalization of lipopolysaccharide by Cla-1, a human orthologue of rodent scavenger receptor B1," *The Journal of Biological Chemistry*, vol. 278, no. 25, pp. 22771–22780, 2003.

[132] W. H. Ettinger, V. K. Varma, M. Sorci-Thomas et al., "Cytokines decrease apolipoprotein accumulation in medium from Hep G2 cells," *Arteriosclerosis and Thrombosis*, vol. 14, no. 1, pp. 8–13, 1994.

[133] J. M. Mann, M. Pierre-Louis, P. J. Kragel, A. H. Kragel, and W. C. Roberts, "Cardiac consequences of massive acetaminophen overdose," *American Journal of Cardiology*, vol. 63, no. 13, pp. 1018–1021, 1989.

[134] R. A. Wakeel, H. T. Davies, and J. D. Williams, "Toxic myocarditis in paracetamol poisoning," *British Medical Journal*, vol. 295, no. 6606, p. 1097, 1987.

[135] N. K. Parekh, L. S. Hynan, J. De Lemos et al., "Elevated troponin I levels in acute liver failure: is myocardial injury an integral part of acute liver failure?" *Hepatology*, vol. 45, no. 6, pp. 1489–1495, 2007.

[136] N. Papoutsidakis, N. Arkadopoulos, V. Smyrniotis et al., "Early myocardial injury is an integral component of experimental acute liver failure—a study in two porcine models," *Archives of Medical Science*, vol. 7, no. 2, pp. 217–223, 2011.

Hindawi Publishing Corporation
Oxidative Medicine and Cellular Longevity
Volume 2014, Article ID 376515, 8 pages
http://dx.doi.org/10.1155/2014/376515

Clinical Study

Aging Aggravates Nitrate-Mediated ROS/RNS Changes

Qian Fan,[1] Lifen Chen,[2] Shujuan Cheng,[1] Fang Li,[1] Wayne Bond Lau,[3] Le Feng Wang,[4] and Jing Hua Liu[1]

[1] *Department of Cardiology, Beijing An Zhen Hospital, Capital Medical University, Beijing Institute of Heart, Lung and Blood Vessel Disease, Beijing 100029, China*
[2] *Department of Neurology, The Second Affiliated Hospital of Chong Qing Medical University, Chong Qing, China*
[3] *Department of Emergency Medicine, Thomas Jefferson University, Philadelphia, PA 19107, USA*
[4] *Heart Center, Beijing Chaoyang Hospital-Affiliate of Beijing Capital Medical University, 8 Gongtinan Road, Beijing 100020, China*

Correspondence should be addressed to Qian Fan; fanqian75@sina.com and Jing Hua Liu; liujinghua@vip.sina.com

Received 2 August 2013; Revised 17 August 2013; Accepted 18 August 2013; Published 23 March 2014

Academic Editor: Zhengyuan Xia

Nitrates are the most frequently prescribed and utilized drugs worldwide. The elderly are a major population receiving nitrate therapy. Both nitrates and aging can increase in vivo reactive oxygen species (ROS) and reactive nitrogen species (RNS). To date, the effects of aging upon nitrate-induced ROS/RNS alteration are unknown. The present study tested the effects of aging upon nitrate-induced ROS/RNS alteration in vivo. 32 adults and 43 elderly unstable angina (UA) patients were subjected to 48 hours of isosorbide dinitrate intravenous injection (50 μg/minutes) in this clinical study. Blood samples were obtained at baseline and conclusion. Outcome measures of oxidative stress included plasma malondialdehyde (MDA), myeloperoxidase (MPO), and reduced glutathione (GSH). Plasma concentrations of NOx and nitrotyrosine served as markers of RNS. Because of the significant differences in basic clinical characters between adults and the elderly, we designed an additional experiment determining ROS/RNS stress in rat cardiac tissue. Additionally, rat thoracic aortic NOS activity served as a marker indicating endothelial function. Our study demonstrated that nitrate therapy significantly increased in vivo ROS/RNS stress in the elderly compared to adult patients, confirmed by animal data. Decreased NOS activity was observed in old rats. Taken together, the present study's data suggests a synergism between nitrate treatment and the aging process.

1. Introduction

Rapid growth of the world's geriatric population has increased awareness of age-related cardiovascular diseases. Cardiovascular diseases are responsible for the majority of elderly mortality. 80 percent of patients with ischemic heart disease are ≥65 years old [1]. Organic nitrates have been employed in the treatment of ischemic heart disease for more than a century and remain the most frequently prescribed and utilized medications for treating the ischemic heart disease population worldwide, of which the elderly are a major constituent.

The process of aging is complex. Senescent pathophysiology arises from various factors through multiple mechanisms. Harman proposed the free radical theory of aging in the 1950s, expanding to implicate mitochondrial production of reactive oxygen species in the 1970s [2]. Per this theory, enhanced and unopposed metabolism-driven oxidative stress plays a major role in diverse chronic age-related disorders [3, 4]. In the free-radical theory of aging, organisms age because their cells accumulate free radical damage over time. In our previous study, aging resulted in significantly increased reactive oxygen species (ROS) and reactive nitrogen species (RNS) after myocardial infarction [5, 6]. Nitrate therapy also augments ROS and RNS production. In 1995, Munzel et al. [7] demonstrated that in vivo nitrate use was associated with an endothelial-dependent production of superoxide anion, an important mechanistic development in the understanding of nitrate tolerance. Munzel's work was further supported by the association of reduced superoxide anion production with inclusion of a nitrate-free period in vivo [8]. A randomized controlled trial (RCT) of patients undergoing elective coronary artery bypass grafting subjected to preoperative intravenous nitroglycerin (GTN) confirmed

increased superoxide generation in internal mammary artery samples after nitrate treatment [9].

Substantial evidence supports oxidative stress as one of the major etiologies of myocardial injury. Numerous experiments have demonstrated markedly increased superoxide (O_2^-) generation from ischemic/reperfused endothelial cells and increased neutrophil activation in postischemic myocardial tissue. O_2^- further dismutates to H_2O_2 and $^{\bullet}OH$, the latter highly toxic to biological tissues, causing significant myocardial necrosis and apoptosis. Additionally, accumulating evidence indicates RNS, such as peroxynitrite ($ONOO^-$), play vital roles in reperfusion-induced myocardial apoptosis [10]. The deleterious effects of RNS are further exacerbated by interaction with increased ambient ROS. Most studies investigating nitrate use have employed young animals. Although it is well known that both aging and nitrates increase in vivo ROS/RNS production; heretofore, the effects of nitrate administration in the aged population remain unknown.

The present study determined whether nitrates increase in vivo ROS/RNS concentrations in a clinical trial. Limitations of our study included clinical and demographic characteristic (blood pressure, diabetes, and past medical history) discrepancies between middle-aged and elderly patients and inability to obtain cardiac tissue samples from enrolled participants. A carefully controlled experiment upon rats was therefore included in the present study.

2. Materials and Methods

The clinical trial was carried out in accordance with the Declaration of Helsinki (2000) of the World Medical Association. The study protocol was approved by the institutional ethics committee of the Beijing Anzhen Hospital-Affiliate of Capital Medical University. After full disclosure of the study's purpose, nature, and inherent risks of participation, all subjects gave written informed consent prior to enrollment.

2.1. Inclusion and Exclusion Criteria of Acute Myocardial Infarction Patients. Unstable angina (UA) patients met inclusion criteria if the following conditions were true: (1) presence of typical angina, (2) presence of electrocardiographic S-T segment changes (representative of cardiac injury) during clinical chest pain, or (3) presence of the significant coronary stenosis (≥75%) diagnosed by either computed tomography coronary angiography (CTCA) or coronary angiography.

Exclusion criteria for this study included (1) increasing myocardial necrotic marker (cTnI or CKMB) levels; (2) cardiogenic shock; (3) occlusion or severe stenosis of the left main coronary artery; (4) previous myocardial infarction; (5) major infection or surgery within the past 2 weeks prior to presentation.

2.2. Coronary Angiography and Clinical Experimental Design. In present study, isosorbide dinitrate was used in the clinical trial and nitroglycerin was used in the animal experiment. Both of them are nitrates. Nitrates correct the imbalance between the flow of blood and oxygen to the heart and the work that the heart must do by dilating (expanding) the arteries and veins in the body. Dilation of the veins reduces the amount of blood that returns to the heart that must be pumped. Dilation of the arteries lowers the pressure in the arteries against which the heart must pump. As a consequence of both effects, the heart works less and requires less blood and oxygen.

All UA patients were given standard UA treatment protocol. Patients were divided into two groups: (1) adult patients (<65 years) and (2) elderly patients (≥65 years).

All patients received intravenous isosorbide dinitrate (50 μg/minute) treatment. Blood samples were obtained before and after 48 hours of nitrate treatment.

2.3. Animal Experiment Protocol. The study was approved by the institutional ethics committee and was in accordance with the United States National Institutes of Health guidelines. Male Sprague-Dawley rats were anesthetized with sodium pentobarbital. The rat model was described previously [5, 8, 11]. In brief, male Sprague-Dawley rats (aged either 8 weeks (young) or 24 months (old)) were anesthetized with sodium pentobarbital (50 mg/kg body weight) intravenously. An intratracheal tube was inserted via midline midline incision. All rats were given intermittent positive-pressure ventilation with oxygen-enriched room air via Harvard small animal respirator (Harvard Apparatus, South Natick, MA). A transfusion needle was inserted into the caudal vein for supplemental pentobarbital injection to maintain anesthesia and for drug administration. Rats (8 weeks or 24 months old) were divided into the following four groups: (1) sham young; (2) sham old; (3) young; and (4) old ($n = 12$ each). Vehicle (1 mL/kg/h) or nitroglycerin (60 μg/kg/h) [8] was continuously infused for 12 hours. Sham rats received vehicle solution only. After 12 hours of vehicle or nitroglycerin infusion, animals were sacrificed. Cardiectomies were performed.

2.4. Quantitative Evaluation of Reactive Oxygen Species (ROS) Level in Humans and Rats. To determine the effects of aging upon in vivo ROS, malondialdehyde (MDA), myeloperoxidase (MPO), and reduced glutathione (GSH) served as oxidative stress markers.

Blood samples were drawn from UA patients after 0 and 48 hours of injection. Blood samples were immediately centrifuged at 10000 RPM for 1 minute at 4°C. Supernatant was collected and stored at −80°C until measurement. Plasma malondialdehyde (MDA), myeloperoxidase (MPO), and reduced glutathione (GSH) concentrations were detected by commercially available kits, as reported previously [11].

Plasma MDA, MPO, and reduced GSH concentrations do not directly reflect oxidative stress within cardiac tissue. Therefore, MDA, MPO, and reduced GSH concentrations in rat cardiac tissue were measured. After 12 hours injection or either nitrate or vehicle, left ventricular samples were homogenized and centrifuged for 30 minutes at 10000 PRM at 4°C. Supernatant protein concentrations were measured by the bicinchoninic acid method. MDA, MPO, and reduced GSH concentrations were determined.

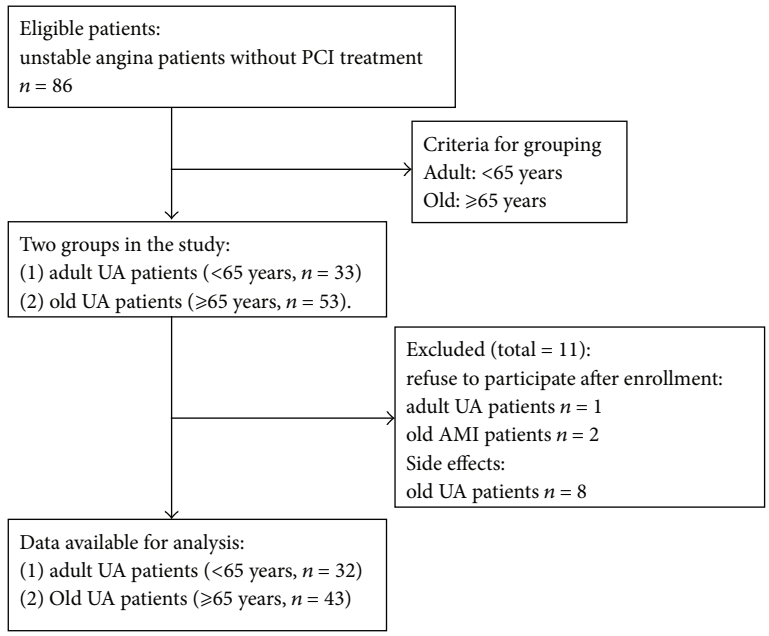

Figure 1: The grouping of clinical trial.

2.5. Quantitative Evaluation of Reactive Nitrogen Species (RNS) Level in Humans and Rats. NO*x* (nitrite and nitrate, the stable metabolites of NO) quantity in supernatants was determined via Griess reaction utilizing a NO*x* concentration assay kit (R and D Systems Inc., Minneapolis, MN). Rat cardiac tissues were harvested and similarly processed as described above.

Nitrotyrosine is the accepted footprint of in vivo $ONOO^-$ formation. Nitrotyrosine concentration of both rat cardiac tissue homogenate and patient plasma was determined via ELISA kit (Cell Sciences Inc., Canton, MA, USA), as previously described, reported as nanomoles of nitrotyrosine/gram of tissue protein homogenate or nanomoles of nitrotyrosine/liter plasma.

2.6. The Assay of NOS Activity in Rat Thoracic Aorta. Under physiological conditions, rat thoracic aortic NOS activity indirectly reflects vascular eNOS concentrations and endothelial function. Therefore, in the present study, NOS activity in rat thoracic aorta served as a marker of endothelial function. After 12 hours of nitrate administration, rat thoracic aortae were isolated and harvested. Samples were homogenized and centrifuged for 30 minutes at 12,000 g at 4°C. Supernatant protein concentrations were measured by the bicinchoninic acid method. Methods determining NOS activity have been described previously.

2.7. Statistical Analysis. All values are presented as means ± SEM. All biochemical assays were performed in duplicate and averaged. Data were subjected to ANOVA, followed by Bonferroni correction for post hoc Student's *t*-tests. All statistics were calculated utilizing Graphpad Prism 5.0. *P* values <0.05 were considered statistically significant.

3. Results

3.1. Patient Population Demographics and Characteristics. 33-adult UA patients and 53 elderly UA patients were enrolled in the clinical trial. Of 86 patients, 1 adult and 2 elderly patients refused participation after enrollment and 8 elderly patients discontinued participation due to side effects (Figure 1). Table 1 lists all demographic data, baseline statistics, cardiovascular risk profile, and medication profiles of patients. The major differences between the adult and elderly patient populations involved gender distribution and past medical history.

3.2. Aging Increased Oxidative Stress in Human Plasma after 48 Hours Nitrate Treatment. To determine the effects of aging upon plasma ROS levels after nitrate injection, plasma levels of MDA, MPO, and reduced GSH (markers reflecting myocardial oxidative stress) at two distinct time points (before and after 48 hours nitrate treatment) were determined. Plasma MDA and MPO concentration in elderly UA patients were significantly increased before and after nitrate administration compared to adult patients (Figures 2(a) and 2(b)). Nitrates increased plasma MDA by 140% in the elderly group. Nitrates increased plasma MDA by 60% in the adult group (Figure 2(a)). Nitrates increased plasma MPO by 50% in the elderly group, compared to 20% in the adult group.

Glutathione is one of the most important physiologic self-generating antioxidants. To indirectly evaluate in vivo oxidative stress burden, we determined the plasma concentrations of reduced-form GSH. In consistent trend with plasma MDA and MPO data, elderly patients manifested reduced GSH concentrations compared to adult patients, which further decreased after nitrate administration (Figure 2(c), 48%

Table 1: Baseline Characteristics of the Study Population (mean ± SD).

	MI adult (n = 34)	MI elderly (n = 45)	P
Age, y	50.1 ± 6.6	73.7 ± 4.8	<0.001
Sex, M/F	28/4	24/19	<0.01
HBP/total	23/32	35/43	NS
Dyslipidemia/total	21/32	34/43	NS
Diabetes/total	20/32	29/43	NS
Smoker/total	24/32	29/43	NS
Past drug treatment (n/total)			
Statins	17/32	30/43	NS
Calcium channel blocker	9/32	18/43	NS
ACEI	15/32	31/43	<0.05
ß-Adrenoceptor blocker	8/32	26/43	<0.01
Diuretic	5/32	20/43	<0.01
Drug treatment during the study (n/total)			
Statins	32/32	43/43	NS
Calcium channel blocker	19/32	32/43	NS
ACEI	17/32	27/43	NS
ß-Adrenoceptor blocker	21/32	27/43	NS
nitrates	32/32	43/43	NS
Mean dosage of nitrates (μg/min)	50	50	NS

HBP indicates high blood pressure; ACEI: angiotensin-converting enzyme inhibitor; y: year; M: male; F: female.

reduction of elderly plasma GSH after nitrates, compared to 9% reduction in adult patients).

3.3. Aging Increased Oxidative Stress in Rat Cardiac Tissue with 12-Hour Nitrate Treatment. Furthermore, in vivo study results confirm the results from clinical trial. Nitrate administration significantly increased rat myocardial MDA and MPO concentrations and decreased myocardial reduced-GSH level in the old group (Figures 2(d), 2(e), and 2(f)).

3.4. Aging Increased Plasma NOx or Nitrotyrosine Concentrations in Humans after 48-Hour Nitrate Treatment. RNS (reactive nitrogen species) play a critical pathogenic role in mediating myocardial injury. NO reacts with superoxide (whose production is increased with aging) to form the toxic molecule peroxynitrite ($ONOO^-$), a strongly nitrating and oxidizing agent. $ONOO^-$ substantially induces myocardial apoptosis. We determined both plasma NOx and nitrotyrosine concentrations in the present study. There were no significant differences in plasma NOx concentration between adult and elderly patients before nitrate administration. Baseline plasma nitrotyrosine concentration is significantly greater in the elderly than adult population. 48 hours of nitrate injection significantly increased plasma NOx (250% in the elderly compared to 150% in the adult patients) and nitrotyrosine (210% in the elderly compared to 105% in the adult patients) concentrations (Figures 3(a) and 3(c)).

3.5. Aging Increased Cardiac NOx and Nitrotyrosine Concentrations in Rats after 12-Hour Nitrate Treatment. To confirm the effects of aging upon RNS formation, we determined NOx and nitrotyrosine concentrations in a rat model after nitrate administration. As shown in Figures 3(b) and 3(d), 12 hours of nitrate infusion significantly increased cardiac NOx and nitrotyrosine concentrations in both the young and old rat groups. In the elderly group, NOx concentrations increased 255%, compared to 170% in the young group. Similarly, cardiac nitrotyrosine concentrations increased 78% in the old rats, compared to 22% in the young rats.

3.6. Aging Increased NOS Activity in Rat Thoracic Aorta after 12-Hour Nitrate Treatment. Both eNOS activity and nitric oxide bioavailability are vital markers indicating endothelial function. Rat thoracic aorta NOS activity served as an indirect index of eNOS activity and endothelial function. As shown in Figure 4, 12 hours of nitrate infusion significantly decreased NOS activity in both young and old rat thoracic aortae. 45% decreased NOS activity was observed in the elderly group, compared to 18% decrease in the young group, suggesting that nitrates induced more severe endothelial dysfunction in the elderly state.

4. Discussion

Several novel observations have been made in the present study. Firstly, we demonstrate for the first time with clinical data that nitrate treatment may increase oxidative/nitrative stress burden in the elderly. To our knowledge, previous investigations demonstrating nitrates increased ROS/RNS post I/R involved all young animals, heretofore unconfirmed in human studies. Secondly, although endothelial function depression has been observed after nitrate administration, our results suggest that aging exacerbated such effects.

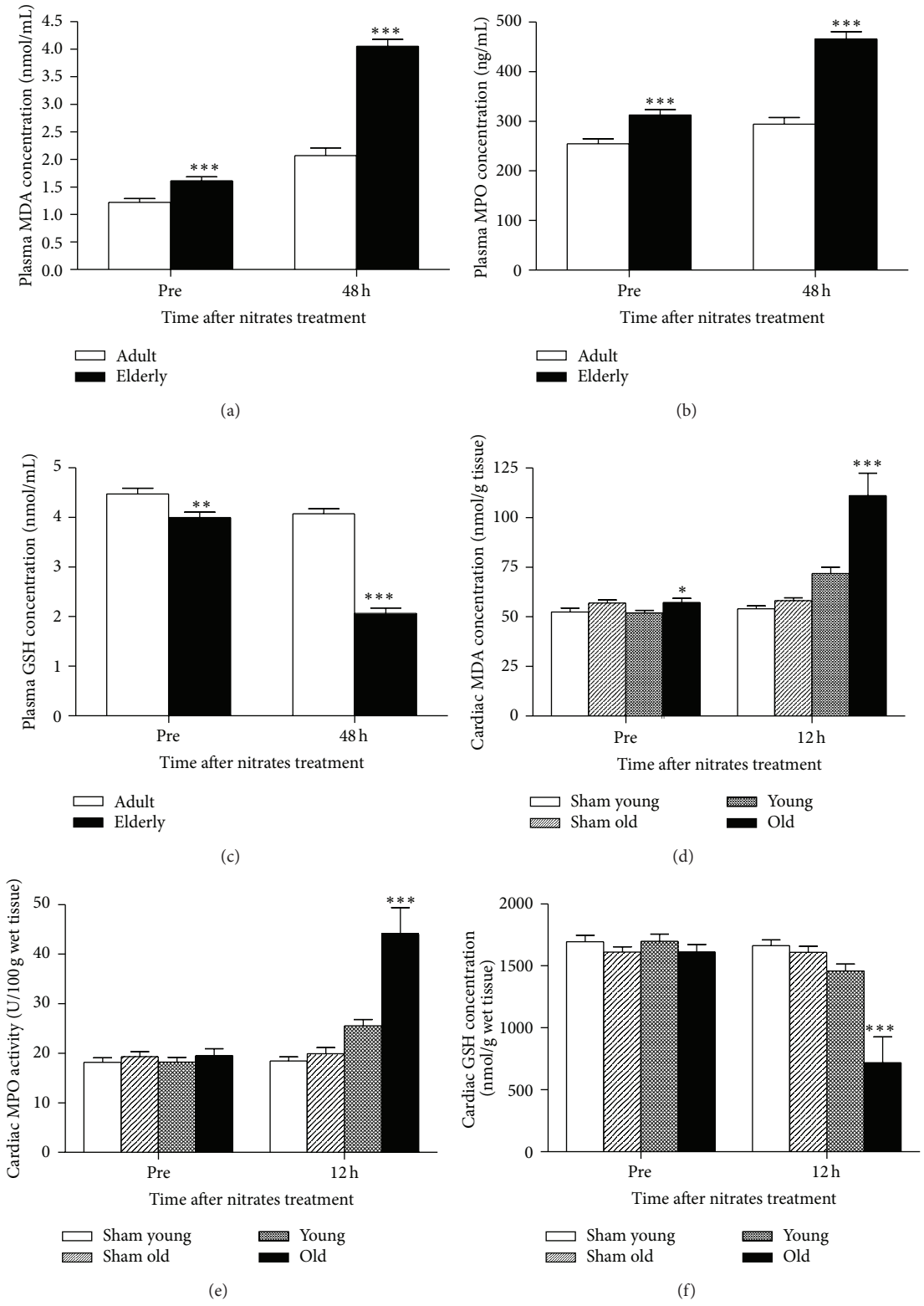

Figure 2: Aging was associated with increased ROS (MDA and MPO) and decreased reduced glutathione (GSH) after nitrates use. (a) Plasma malondialdehyde (MDA) concentration was higher in old patients than in adult patients; (b) plasma-reduced glutathione (GSH) concentration was lower in old patients than in adult patients; and (c) plasma myeloperoxidase (MPO) concentration was greater in elderly than adult patients. (d), (e), and (f) indicated aging was associated with increased ROS (MDA and MPO) and decreased reduced GSH in rat cardiac tissue after 12 hours nitrates use. Adult indicates adult group, and elderly indicates elderly group. Totals for the following groups: 32 adult patients; 43 elderly patients. Sham indicates sham group; young and old indicate rats receiving nitrates treatment. In animal experiment, $n = 12$ per group. Data are expressed as mean ± SEM. $^{***}P < 0.001$ versus adult group. $n = 12$ per group. Data are expressed as mean ± SEM. $^{*}P < 0.05$, $^{**}P < 0.001$ versus young group.

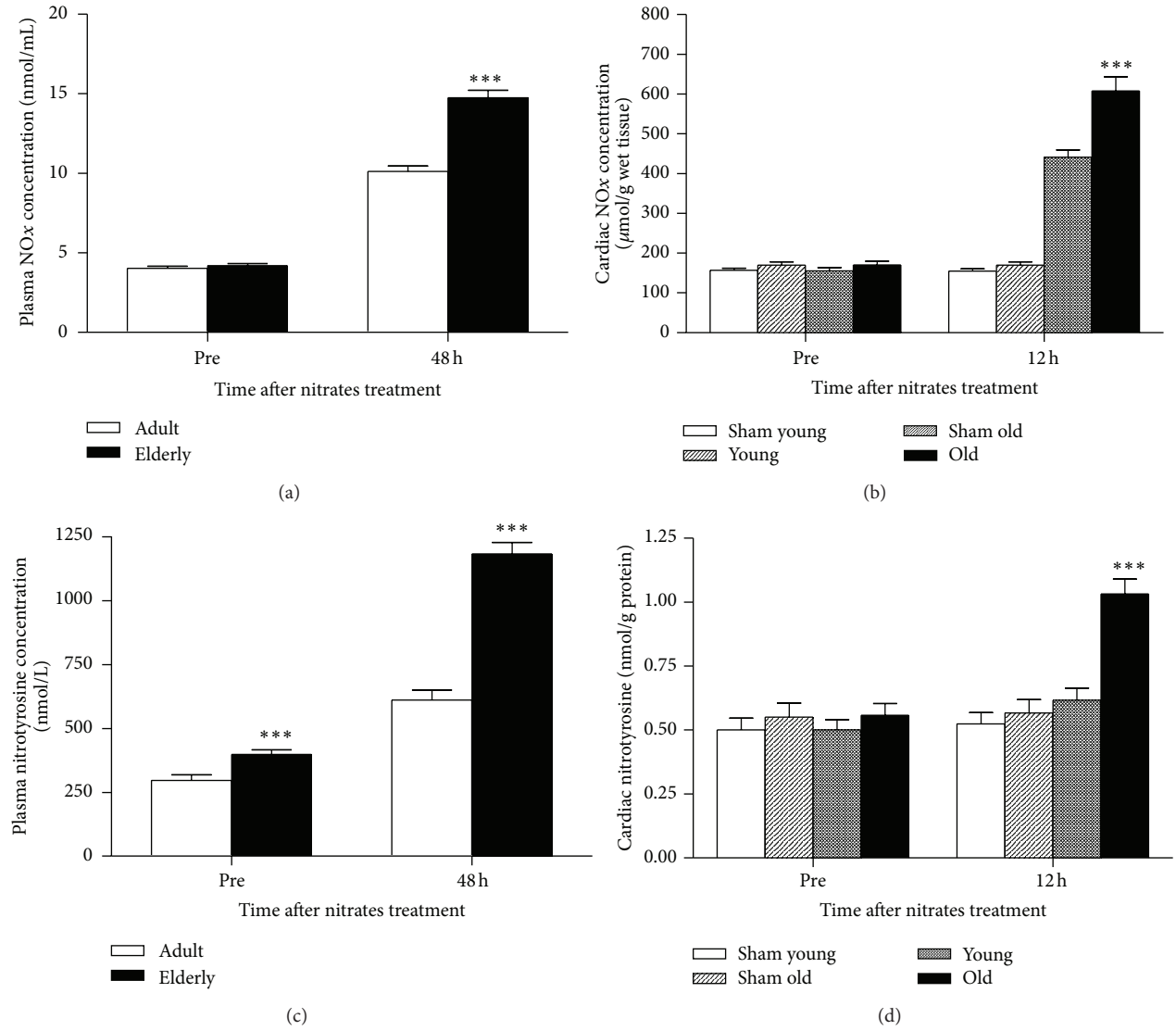

Figure 3: The effects of aging on nitrates-induced NO*x* and nitrotyrosine content change in patients plasma and rats cardiac tissue. (a) indicated the effects of aging on patients plasma NO*x* content; (b) rats cardiac tissue NO*x* content; (c) patients plasma nitrotyrosine concentration; and (d) rats cardiac tissue nitrotyrosine concentration. Nitrates were used in patients for 48 h and in rats for 12 h. Sham indicates sham group; young and old indicate rats receiving nitrates treatment. 32 adult patients and 43 elderly patients were included in the trial. In animal experiment, $n = 12$ per group. Data are expressed as mean ± SEM. $^{***}P < 0.001$ versus young/adult group.

Recent evidence suggests that the mitochondrial respiratory chain is the primary source of nitrate-induced vascular O_2^- overproduction, leading to subsequent activation of vascular nicotinamide adenine dinucleotide phosphate (NADPH) oxidase, and which mediates the majority of nitrate tolerance and endothelial dysfunction [12]. The superoxide anion is normally scavenged by various intracellular and extracellular mechanisms. Superoxide excess may overcome these compensatory mechanisms and rapidly react with NO (derived in nitrate-dependent fashion) to form toxic peroxynitrite [8, 13]. While the current study confirms the above principles, we provide data suggesting aging may augment nitrate-induced superoxide/peroxynitrite generation. Previously, we demonstrate that aging exacerbated reperfusion-induced myocardial injury [6], particularly apoptosis. It is widely accepted that superoxide anion/peroxynitrite exert severely deleterious myocardial effects. It is possible that nitrate-induced ROS/RNS alteration is an important cause of aging-related myocardial injury.

As a major predictor of cardiac events in patients with coronary artery disease and heart failure, endothelial dysfunction may be the pathologic sequelae of nitrate [14, 15]. Endothelial dysfunction generally reflects reduced nitric oxide bioavailability, due to increased oxidative/nitration stress. Aging is an independent risk factor of cardiovascular diseases such as myocardial infarction and heart failure. Nitrate administration increased in vivo RNS and ROS production, furthermore decreasing nitric oxide bioavailability. The present study indirectly demonstrated aging significantly exacerbated nitrate-induced endothelial dysfunction, both

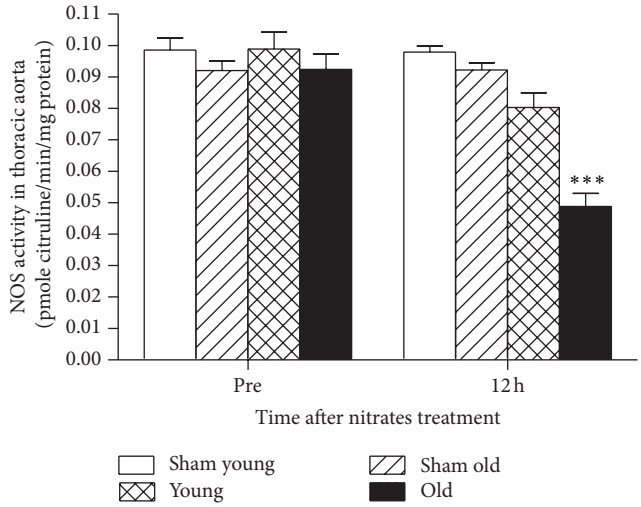

Figure 4: In rats experiment, 12 h nitroglycerin use resulted in the depressing of NOS activity in aorta. Sham indicates sham group; young and old indicate rats receiving nitrates treatment. Data are expressed as mean ± SEM. $^{***}P < 0.001$ versus young group.

in human and animals. Our results give insight to the contribution of aging to cardiovascular injury.

In summary, the elderly is a population treated extensively by nitrates. However, the effects of aging on nitrates use seem to be neglected. With supporting clinical human data and experimental animal data, the present study suggests a deleterious "synergism" between aging and nitrate treatment upon cardiovascular injury. Aging increases ROS/RNS after nitrate treatment, which may result in more severe myocardial injury. The current study's data warrants further studies investigating the use of nitrates in the elderly, with caveats regarding its judicious employment.

Conflict of Interests

The authors declare that there is no conflict of interests regarding the publication of this paper.

Authors' Contribution

Qian Fan and Lifen Chen contributed equally to the paper.

Acknowledgment

The research was supported by Chinese National Natural and Scientific Funding 81270434 to Qian Fan.

References

[1] W. Rosamond, K. Flegal, K. Furie et al., "Heart disease and stroke statistics—2008 update: a report from the American Heart Association Statistics Committee and Stroke Statistics Subcommittee," *Circulation*, vol. 117, no. 4, pp. e25–e146, 2008.

[2] B. Poljsak and I. Milisav, "The neglected significance of 'antioxidative stress'," *Oxidative Medicine and Cellular Longevity*, vol. 2012, Article ID 480895, 12 pages, 2012.

[3] D. Harman, "About 'origin and evolution of the free radical theory of aging: a brief personal history, 1954–2009'," *Biogerontology*, vol. 10, no. 6, p. 783, 2009.

[4] D. Harman, "Free radical theory of aging: an update—increasing the functional life span," *Annals of the New York Academy of Sciences*, vol. 1067, no. 1, pp. 10–21, 2006.

[5] Q. Fan, M. Chen, X. Fang et al., "Aging might augment reactive oxygen species (ROS) formation and affect reactive nitrogen species (RNS) level after myocardial ischemia/reperfusion in both humans and rats," *Age*, vol. 35, no. 4, pp. 1017–1026, 2013.

[6] M. Liu, P. Zhang, M. Chen et al., "Aging might increase myocardial ischemia/reperfusion-induced apoptosis in humans and rats," *Age*, vol. 34, no. 3, pp. 621–632, 2012.

[7] T. Munzel, H. Sayegh, B. A. Freeman, M. M. Tarpey, and D. G. Harrison, "Evidence for enhanced vascular superoxide anion production in nitrate tolerance. A novel mechanism underlying tolerance and cross-tolerance," *The Journal of Clinical Investigation*, vol. 95, no. 1, pp. 187–194, 1995.

[8] Q. Fan, F. Gao, L. Zhang, T. A. Christopher, B. L. Lopez, and X. L. Ma, "Nitrate tolerance aggravates postischemic myocardial apoptosis and impairs cardiac functional recovery after ischemia," *Apoptosis*, vol. 10, no. 6, pp. 1235–1242, 2005.

[9] P. R. Sage, I. S. de la Lande, I. Stafford et al., "Nitroglycerin tolerance in human vessels: evidence for impaired nitroglycerin bioconversion," *Circulation*, vol. 102, no. 23, pp. 2810–2815, 2000.

[10] M. M. Lalu, W. Wang, and R. Schulz, "Peroxynitrite in myocardial ischemia-reperfusion injury," *Heart Failure Reviews*, vol. 7, no. 4, pp. 359–369, 2002.

[11] Q. Fan, X.-C. Yang, Y. Liu et al., "Postconditioning attenuates myocardial injury by reducing nitro-oxidative stress in vivo in rats and in humans," *Clinical Science*, vol. 120, no. 6, pp. 251–261, 2011.

[12] E. Klemenska and A. Beresewicz, "Bioactivation of organic nitrates and the mechanism of nitrate tolerance," *Cardiology Journal*, vol. 16, no. 1, pp. 11–19, 2009.

[13] Z. Xia, T. Luo, H.-M. Liu et al., "L-arginine enhances nitrative stress and exacerbates tumor necrosis factor-α toxicity to human endothelial cells in culture: prevention by propofol," *Journal of Cardiovascular Pharmacology*, vol. 55, no. 4, pp. 358–367, 2010.

[14] P. R. A. Caramori, A. G. Adelman, E. R. Azevedo, G. E. Newton, A. B. Parker, and J. D. Parker, "Therapy with nitroglycerin increases coronary vasoconstriction in response to acetylcholine," *Journal of the American College of Cardiology*, vol. 32, no. 7, pp. 1969–1974, 1998.

[15] T. Gori, S. S. Mak, S. Kelly, and J. D. Parker, "Evidence supporting abnormalities in nitric oxide synthase function induced by nitroglycerin in humans," *Journal of the American College of Cardiology*, vol. 38, no. 4, pp. 1096–1101, 2001.

Hindawi Publishing Corporation
Oxidative Medicine and Cellular Longevity
Volume 2014, Article ID 294150, 11 pages
http://dx.doi.org/10.1155/2014/294150

Research Article

BMP-2 Overexpression Augments Vascular Smooth Muscle Cell Motility by Upregulating Myosin Va via Erk Signaling

Ming Zhang,[1] Min Yang,[2] Li-ping Liu,[3] Wayne Bond Lau,[4] Hai Gao,[1] Man-kun Xin,[1] Li-Xiao Su,[1] Jian Wang,[1] Shu-Juan Cheng,[1] Qian Fan,[1] and Jing-Hua Liu[1]

[1] *Department of Cardiology, Beijing An Zhen Hospital, Capital Medical University, and Beijing Institute of Heart, Lung and Blood Vessel Disease, Beijing 100029, China*
[2] *Department of Cardiology, Beijing Shijitan Hospital, Capital Medical University, Beijing 100038, China*
[3] *Department of Nephrology, First Hospital of Tsinghua University, Beijing 100016, China*
[4] *Department of Emergency Medicine, Thomas Jefferson University, Philadelphia, PA 19107, USA*

Correspondence should be addressed to Qian Fan; fanqian75@sina.com and Jing-Hua Liu; iujinghua@vip.sina.com

Received 8 August 2013; Revised 11 October 2013; Accepted 5 December 2013; Published 20 March 2014

Academic Editor: Mengzhou Xue

Background. The disruption of physiologic vascular smooth muscle cell (VSMC) migration initiates atherosclerosis development. The biochemical mechanisms leading to dysfunctional VSMC motility remain unknown. Recently, cytokine BMP-2 has been implicated in various vascular physiologic and pathologic processes. However, whether BMP-2 has any effect upon VSMC motility, or by what manner, has never been investigated. *Methods.* VSMCs were adenovirally transfected to genetically overexpress BMP-2. VSMC motility was detected by modified Boyden chamber assay, confocal time-lapse video assay, and a colony wounding assay. Gene chip array and RT-PCR were employed to identify genes potentially regulated by BMP-2. Western blot and real-time PCR detected the expression of myosin Va and the phosphorylation of extracellular signal-regulated kinases 1/2 (Erk1/2). Immunofluorescence analysis revealed myosin Va expression locale. Intracellular Ca^{2+} oscillations were recorded. *Results.* VSMC migration was augmented in VSMCs overexpressing BMP-2 in a dose-dependent manner. siRNA-mediated knockdown of myosin Va inhibited VSMC motility. Both myosin Va mRNA and protein expression significantly increased after BMP-2 administration and were inhibited by Erk1/2 inhibitor U0126. BMP-2 induced Ca^{2+} oscillations, generated largely by a "cytosolic oscillator". *Conclusion.* BMP-2 significantly increased VSMCs migration and myosin Va expression, via the Erk signaling pathway and intracellular Ca^{2+} oscillations. We provide additional insight into the pathophysiology of atherosclerosis, and inhibition of BMP-2-induced myosin Va expression may represent a potential therapeutic strategy.

1. Introduction

Recent studies demonstrate that BMP-2, a cytokine of the transforming growth factor-β superfamily, plays an important role in both physiological and pathophysiological vascular development [1, 2]. Genetically manipulated BMP-2 deficient mice die between days 7 and 10 of life from cardiac defects prior to bone formation, suggesting the significant cardiovascular importance of BMP-2 [3]. Vascular smooth muscle cells (VSMCs) are a significant source of BMP-2 [4]. VSMC migration from the vascular media to the intima is pivotal in atherosclerosis, playing a central role in the genesis of atherosclerotic plaques and restenotic lesions [5, 6].

VSMC migration is dependent upon cellular motility, driven by cycles of actin polymerization, cellular adhesion, and actin-myosin contraction. Myosins are a large family of structurally diverse actin-dependent molecular motors. All myosins utilize energy from ATP hydrolysis to generate force for unidirectional movement along actin filaments and are regarded as the most essential proteins driving cellular migration [7–9]. The myosin superfamily consists of both conventional and unconventional myosins [10, 11].

Found in various organelles, unconventional myosins are involved in RNA and protein transport, cellular movement, signal transduction, cellular morphology maintenance, and membrane trafficking [12].

The unconventional myosin Va is an actin-based motor protein that transports intracellular cargos and can bundle actin *in vitro*. The relationship and function of myosin Va pertaining to cytoskeletal aspects, cellular morphology, filopodia motility, and neurite extension have been reported [13–15]. Recently, myosin Va was implicated in human cancer dissemination [16, 17]. However, the function of myosin Va within cardiovascular disease remains unclear. Whether BMP-2 affects VSMCs migration via myosin Va, and if so, by what mechanism, has never been determined. We investigate the role of BMP-2 as a potential regulator of myosin Vain VSMCs and dissect the involved underlying mechanisms.

2. Material and Methods

The study was carried out in accordance with the institutional review board (IRB) approval. The study protocol was approved by the institutional ethics committee and IRB of the Beijing Anzhen Hospital, Affiliate of Capital Medical University.

2.1. Cell Culture. Rat vascular smooth muscle cells were primary-cultured via explant method and grown in RPMI-1640 supplemented with 10% FBS, 100 μg/mL penicillin, 100 μg/mL streptomycin, and 2 mM L-glutamine at 37°C in 5% CO_2 atmosphere. rVSMCs were utilized for experimentation at passage 4–8 [18].

2.2. Recombinant Ads. ViralpAV.EX1d-CMV constructs containing the rat BMP-2/myc/IRES/EGFP expression were from Cyagen Biosciences Inc. (Guangzhou, China). HEK293 cells were transfected by viruses via lipofectamine. The culture medium supernatant was collected and purified by double cesium chloride gradient ultracentrifugation [19]. The viruses were titrated by plaque assay in HEK293 cells. Physical viral particle concentration (vp/mL) was determined spectrophotometrically by wavelength (260 nm) absorbance [20]. Viruses were stored at −80°C until use.

2.3. Cell Motility. Cells were plated on 60 mm glass microwell dishes and cultured overnight in RPMI-1640 containing 10% FBS. Cellular movements were monitored by Leica SP5 inverted microscopy. Video images were collected by CCD camera (model 3000; Leica) at 15-minute intervals for 6 hours, digitized, and stored as image stacks via Image J 1.41 software (National Institutes of Health, http://rsb.info.nih.gov/ij/). Image stacks were converted to QuickTime movies. Nuclei positions were tracked to quantify cell motility, and velocities were calculated in μmat 15-minute intervals by the same software [21].

2.4. Boyden Chamber Assay. A 2×10^4 aliquot of each cell type was plated onto a 24-well BioCoat Invasion Chamber (BD Biosciences, USA) and cultured for 24 hours. Cells were fixed by methanol and stained by crystal violet. Five cell fields were counted at approximately 40-fold magnification [22].

2.5. Wounding Assay. Cells were seeded in 35 mm culture dishes (density 2×10^5 cells per well). An incision was made after 24 hours in the central region of confluence in the culture dish. After an additional 48 hours, the dish was carefully washed to remove detached cells. Fresh medium was added. Cultures were observed at the time of incision and after 48 hours. Phase-contrast microscopy pictures were taken of 6 separate fields of the incised region. The distance between two broad edges of cells was measured and analyzed by Leica LAF software.

2.6. RNA Extraction, cRNA Preparation, and Gene Chip Array. High quality rat RNA from BMP-2 infected VMSCs and control cells were obtained by gel electrophoresis (18S and 28S bands) and absorbance spectroscopy (240–320 nm). Briefly, 8 μg of total RNA was reverse-transcribed by oligo (dT) primer coupled to a T7 RNA polymerase binding site. Biotinylated complementary RNA (cRNA) was then synthesized from the resulting complementary DNA (cDNA) via T7 polymerase. 25 μg of biotinylated cRNA was randomly sheared and hybridized for 16 hours to Affymetrix gene chips.

The Affymetrix microarrays (Arabidopsis ATH1 genome array) contain 22,810 probe sets, representing approximately 80% of the gene sequences on a single array. Labeling and hybridization on the ATH1 microarrays (one sample per chip) were performed according to manufacturer's instructions (http://www.affymetrix.com/estore/). The probe arrays were scanned and further analyzed with Genespring software (ver 5.0; Silicon Genetics). Normalization per gene and per chip of the log2 values was performed to allow comparison of three independent replicates performed for each experiment set. Genes were considered to be up- or downregulated if the ratio between BMP-2 and control cells was, respectively, greater than 2 or less than 0.5.

2.7. RT-PCR. Gene expression was measured by reverse transcription kit (Promega, WI, USA). Briefly, after the RT of 3 μg of total RNA, cDNA was synthesized. The RT products were subjected to PCR with 2720 thermal cycles (abi) and qRT-PCR via real-time PCR system Fast 7500 (abi.) with the primer sets listed in Table 1(a). The cDNA of glyceraldehyde-3-phosphate dehydrogenase (GAPDH) served as internal control. The semiquantitative RT-PCR consisted of 30 cycles of 94°C, 57.5°C, and 72°C (each for 30 seconds).

2.8. Western Blot Analysis. Cellular pellets were lysed by RIPA buffer. 30 μg of total protein samples was separated by 10% SDS-PAGE and electrophoretically transferred to PVDF membranes. Membranes were blocked by 5% nonfat milk in TPBS and incubated for 1 hour at room temperature with primary antibody (see Table 1(b)). Secondary antibody HRP-IgG was applied for 1 hour. After three additional TPBS washes, signals were detected by enhanced chemiluminescence (Amersham Bioscience).

Table 1: (a) PCR primer sequences. (b) Information regarding antibodies employed in Western analysis.

(a)

Gene name	Sense	Antisense	Size (bp)
BMP-2	5′-TATATGCTCGACCTGTACCG-3′	5′-CTTCCTGCATTTGTTCCCGA-3′	247
Myosin Va	5′-CACCTACGGAACCCTGACAT-3′	5′-TGCAAAGATGTGAGGGTCCA-3′	243
Myosin Vb	5′-GGCTGAACTAACCAAGGACT-3′	5′-GGCAACAAGCACAATTCCAC-3′	256
Myosin Vc	5′-GAAGATGGAAGGAAAGCAGG-3′	5′-TCCTCAAGATCCCTGTTTTC-3′	255
SPP1	5′-TGGCTTACGGACTGAGGTCA-3′	5′-GACCTCAGAAGATGAACTC-3′	486
MGP	5′-ATCCTGGCTGCGCTGGCCGTG-3′	5′-GAAGTAGCGGTTGTAGGCGGC-3′	264
Sma22	5′-AAGCCAGTGAAGGTGCCTGAG-3′	5′-TTGAAGGCCAATCACGTGCTT-3′	311
Fstl1	5′-GTGGCAGTAATGGCAAGAC-3′	5′-GTACTTGTCTAGGATCTCAC-3′	260
GAPDH	5′-AAGAAGGTGGTGAAGCAGG-3′	5′-ACCCTGTTGCTGTAGCCATA-3′	197

(b)

Name	Vender	Cat. no.	Species	Dilution
BMP-2	Bioworld	BS3473	Rabbit monoclonal IgG	1 : 500
MYO5a	Sigma	Sab2501441	Goat polyclonal IgG	1 : 1000
Smad1	Cell Signaling	9516	Rabbit monoclonal IgG	1 : 1000
Sm22	Epitomics	S2112	Rabbit polyclonal IgG	1 : 1000
OPN	Bioworld	BS1264	Rabbit monoclonal IgG	1 : 1000
MGP	Abgent	Ap11953	Rabbit polyclonal IgG	1 : 200
FSTL1	Abcam	Ab71548	Rabbit polyclonal IgG	1 : 1000
Actin	Anbo	C0124	Rabbit polyclonal IgG	1 : 5000

2.9. Knockdown of Myosin Va, Expression by siRNA. Three specific sequences of small interfering RNA (siRNA) targeting different regions of rat MYO5a mRNA sequence were designed (RiboBio Co., Ltd, China. 124171130126): siRNA-1: 5′-GGAGAAAGACCACAGATTA-3′; siRNA-2: 5′-GAACCTGATTCTAGAACTA-3′; siRNA-3: 5′-GAAGCAATATAGTGGAGAA-3′. VSMCs were transfected after 48 hours of culture with BMP-2 factor (250 μg/mL). Lipofectamine in transfection reagent (8 μL) was added to 100 μL OptiMEM serum-free medium containing 2 nmol/L of each siRNA oligo, incubated for 10 minutes, and added to the 6 cm plate containing 2 mL medium. After 72 hours, the efficacy of myosin Va silencing (i.e., reduction of gene and protein expression) was determined.

2.10. Immunofluorescence Analysis. Cells were seeded upon cover slips at the bottom of culture dishes until subconfluence and were then fixed with 5% acetic acid/95% ethanol (v/v) for 20 minutes. To block nonspecific reactions, 5% nonfat milk was added for 30 minutes, and then anti-MYO5a polyclonal antibody (1 : 250 dilutions in PBS) was administered at room temperature for 1 hour. After washing, anti-goat IgG, FITC fluorescein (1 : 800, Jackson) was added at room temperature for 1 hour. DAPI (1 : 2000 in PBS; DABCO, Sigma) stained for total nuclei. Imaging was performed by Leica SP5 laser scanning confocal microscope.

2.11. $[Ca^{2+}]^i$ Determination Assay. Cells were treated with BMP-2 for 48 hours in dye-free media supplemented with 10% FBS, centrifuged prior to resuspension in calcium-free modified Tyrode buffer (145 mM NaCl, 5.6 mM KCl, 100 μM EGTA, 1.0 mM $MgCl_2$, 10 mM glucose, and 5.0 mM HEPES, pH 7.2), and incubated for an additional 15 minutes. Fluorescence was measured at room temperature via Leica SP5 confocal imaging system. Two-dimensional confocal images were taken at 1.5 second time intervals. Fluo-4 AM (Dojindo, Japan) was excited at wavelength 488 nm, and emission was detected at 515 nm. Changes in $[Ca^{2+}]^i$ were expressed as $R = F/F_0$, where R is resting fluorescence (F) divided by normalized fluorescence (F_0).

2.12. Statistical Analysis. All data are presented as mean ± SD. The student's two tailed t-test compared the difference between two groups. P values less than 0.05 were regarded as statistically significant.

3. Results

3.1. Successful BMP-2 Overexpression by Adenoviral Transfection Increases VSMC Motility. The adenoviral vector pAV.EX1d-CMV with cloned construct myc/IRES/EGFP was employed to overexpress BMP-2 in VSMCs. After purification, adenoviral titer was amplified in the recombinant adenoviral pAV-EX1d system, reaching 10^8 transducing units/mL (physical viral particle concentration vp/mL). AGFP protein detectable in coprimary culture of infected rat VSMCs confirmed an expression ratio exceeding 90% (Figure 1(a)). Single rat VSMC migration traced by time-lapse video microscopy revealed BMP-2 overexpressing VSMCs are faster

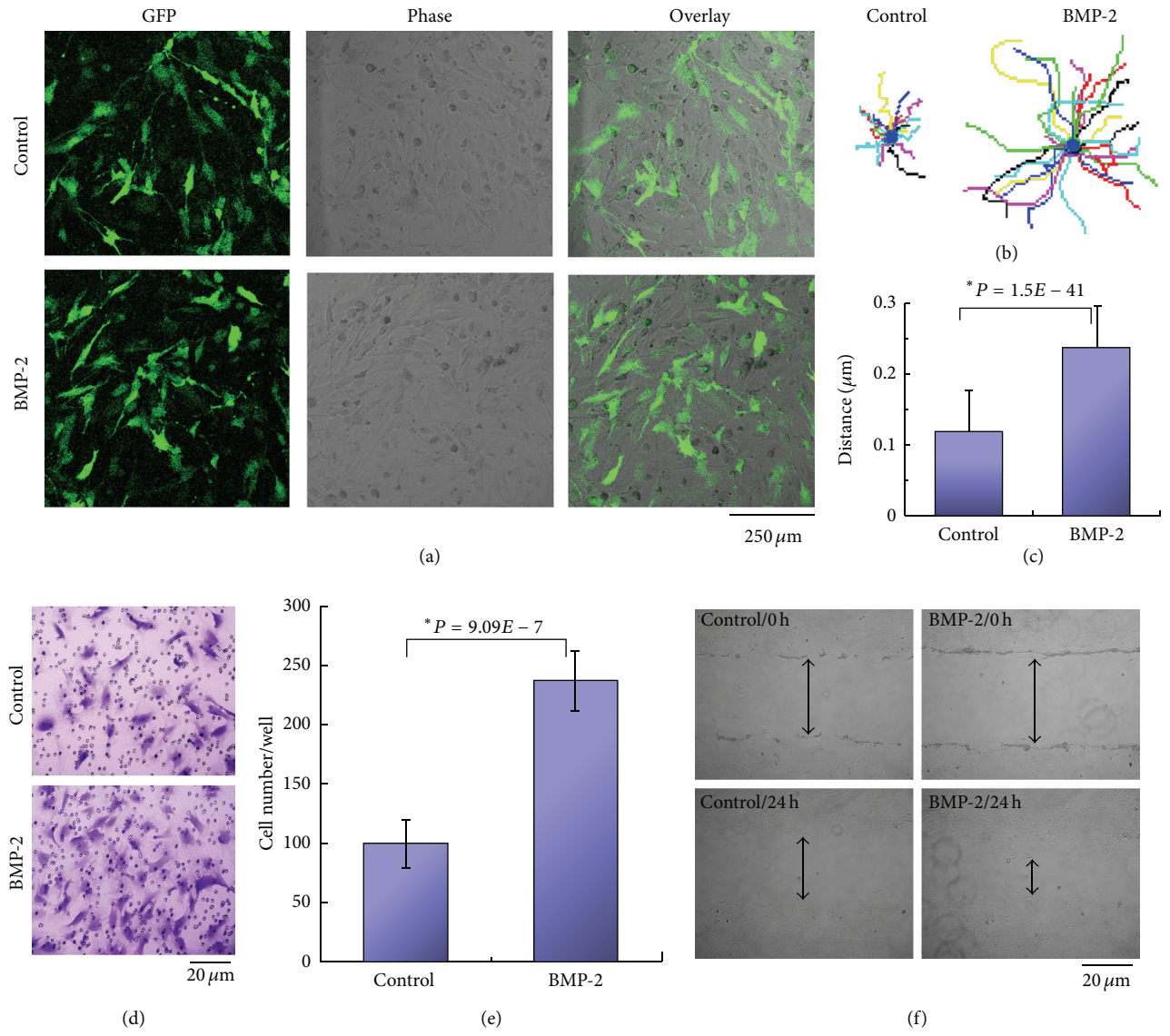

Figure 1: Adenoviral-mediated overexpression of BMP-2 and its effect upon cellular motility in both uni- and multicell populations. (a) GFP expression of adenoviral transfected rat VSMCs assessed by confocal microscopy. Infection efficiency exceeds 90%. (b) Rat VSMCs migration traced by time-lapse video microscopy. Sixteen representative paths for each treatment originated from a common point, in stellate fashion. Faster migration produced larger stars. Cellular motility was recorded on indicated substrates for 6 hours. (c) Movement assay: mean velocity determined by time-lapse recording via ImageJ software. Overexpression of BMP-2 approximately doubled migratory capacity. (d) Boyden chamber assay revealed increased cellular migration in adenoviral-transfected cells overexpressing BMP-2 compared to vector-only cells. (e) Quantification of migration of BMP-2 overexpressing transfected cells; values represent the mean ± SD of independent experiments. (f) Wounding assay, assessing motility, and spread potential of a cellular population. VSMCs cells were virally-transfected to overexpress BMP-2. Both at the time of cellular culture incision and 48 hours after, the state of wound closure was assessed by phase-contrast microscopy. Arrows indicate distance from incision edges. *Student's t-test: $P < 0.01$ versus control.

than those infected by vector alone. Swifter VSMC migration resulted in larger spanning stellate "star" formations (Figure 1(b)). The average distance travelled by a moving single cell in a six-hour observation period was confirmed every 15 minutes (BMP-2 travelled 0.24 ± 0.2 μm versus control: 0.12 ± 0.1 μm, Figure 1(c)). Migratory cell mounts of rat VSMCs overexpressing BMP-2 were compared to control cells in a Boyden chamber assay (Figure 1(d)). BMP-2 overexpression increased cellular intensity 130%, compared to vector alone ($P < 0.01$, Figure 1(e)). The wounding assay demonstrated BMP-2 influenced cellular population movement as well within 48 hours (BMP-2: 93.3 ± 17.8 μm versus control: 43.7 ± 16.7 μm, $P < 0.01$, Figure 1(f)).

3.2. BMP-2 Increases Motility of Both Unicellular and Multicellular VSMC Populations in Dose-Dependent Manner. VSMCs were treated with varying BMP-2 concentrations (ranging from 50 to 500 ng/mL) via Boyden chamber for

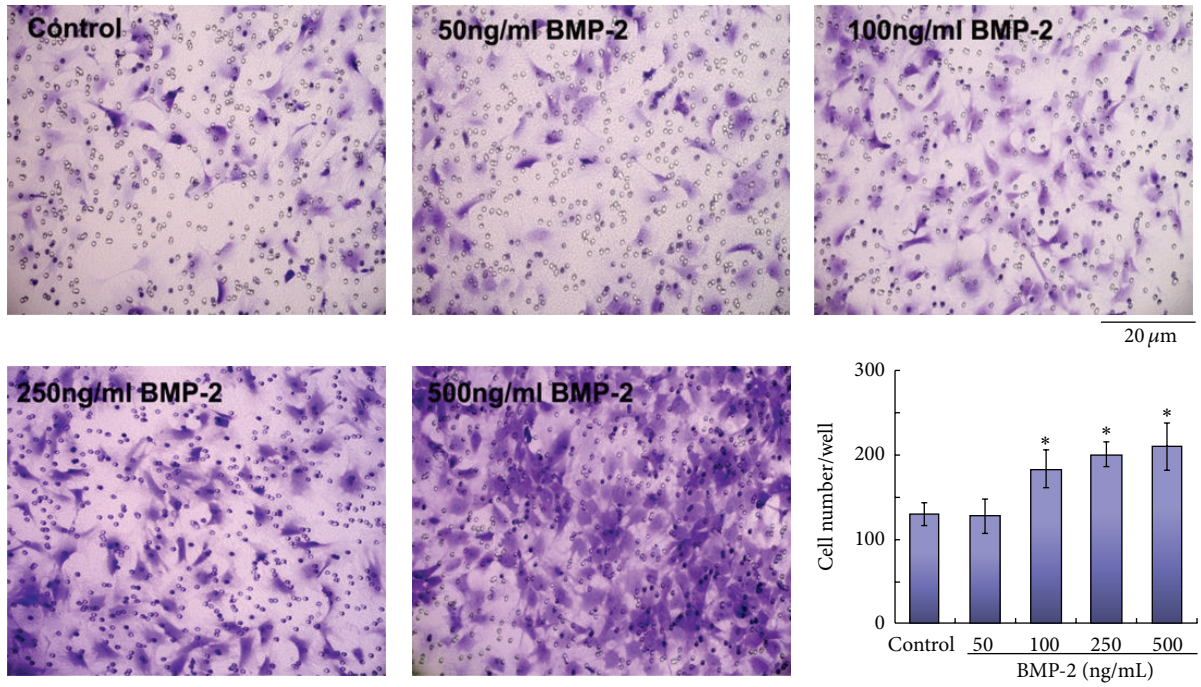

Figure 2: Dose-dependent effect of BMP-2 upon cellular motility. A Boyden chamber assay was performed upon rat VSMCs treated by exogenous BMP-2 concentrations. *Student's test: $P < 0.01$ versus control.

48 hours. Figure 2 demonstrates VSMCs exhibit a dose-dependent migratory effect in response to BMP-2 concentrations exceeding 100 ng/mL. Time-lapse video microscopy and wounding assay, respectively, demonstrated unicellular and multicellular VSMC populations responded in dose-dependent manner to BMP-2 (Table 2).

3.3. Identification of Genes Regulated by BMP-2 Overexpression. To gain mechanistic insight concerning BMP-2-mediated VSMC migration facilitation, microarray analyses were performed to determine global gene expression changes in BMP-2 overexpressing VSMCs. In VSMCs overexpressing BMP-2, 554 genes were downregulated, and 437 genes were upregulated. Not surprisingly, genes involved in the BMP signaling pathway (such as Fstl1, Fstl3, Smad1, and Msx1) were among those upregulated during BMP-2 overexpression. Although our gene chip array determined myosin Va was consistently upregulated during BMP-2 overexpression, myosin Vb and Vc were not detected. In addition, expression of smooth muscle alpha-actin, a characterizing marker of the systole phenotype, remained unchanged. The mRNA and protein levels of OPN and MGP, characterizing markers of the diastolic phenotype, were markedly altered (Figures 3(a) and 3(b)).

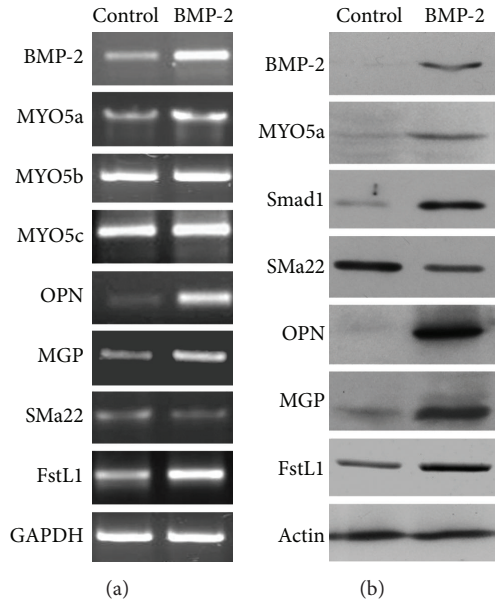

Figure 3: Gene chip array analysis demonstrating various gene and protein levels after gene array analysis. (a) Gene expression of myosin Va, myosin Vb, myosin Vc, OPN, MGP, SMa22, FSTL1, and GAPDH via RT-PCR. (b) Protein levels of BMP-2, myosin Va, Smad1, OPN, MGP, FSTL1, and pan-actin via Western analysis.

3.4. BMP-2 Overexpression Increases Myosin Va Expression. Via RT-PCR, we determined adenoviral-mediated BMP-2 overexpression significantly increased myosin Va mRNA sevenfold compared to control (Figure 4(a)), in a dose-dependent manner (Figure 4(b)). We then confirmed BMP-2 stimulation increased myosin Va protein expression by characterizing actin and myosin Va expressing VSMCs by immunofluorescence analysis. Representative photographs in Figure 4(c) display abundantly distributed myosin Va protein binding actin in the cytoplasm of VSMCs overexpressing

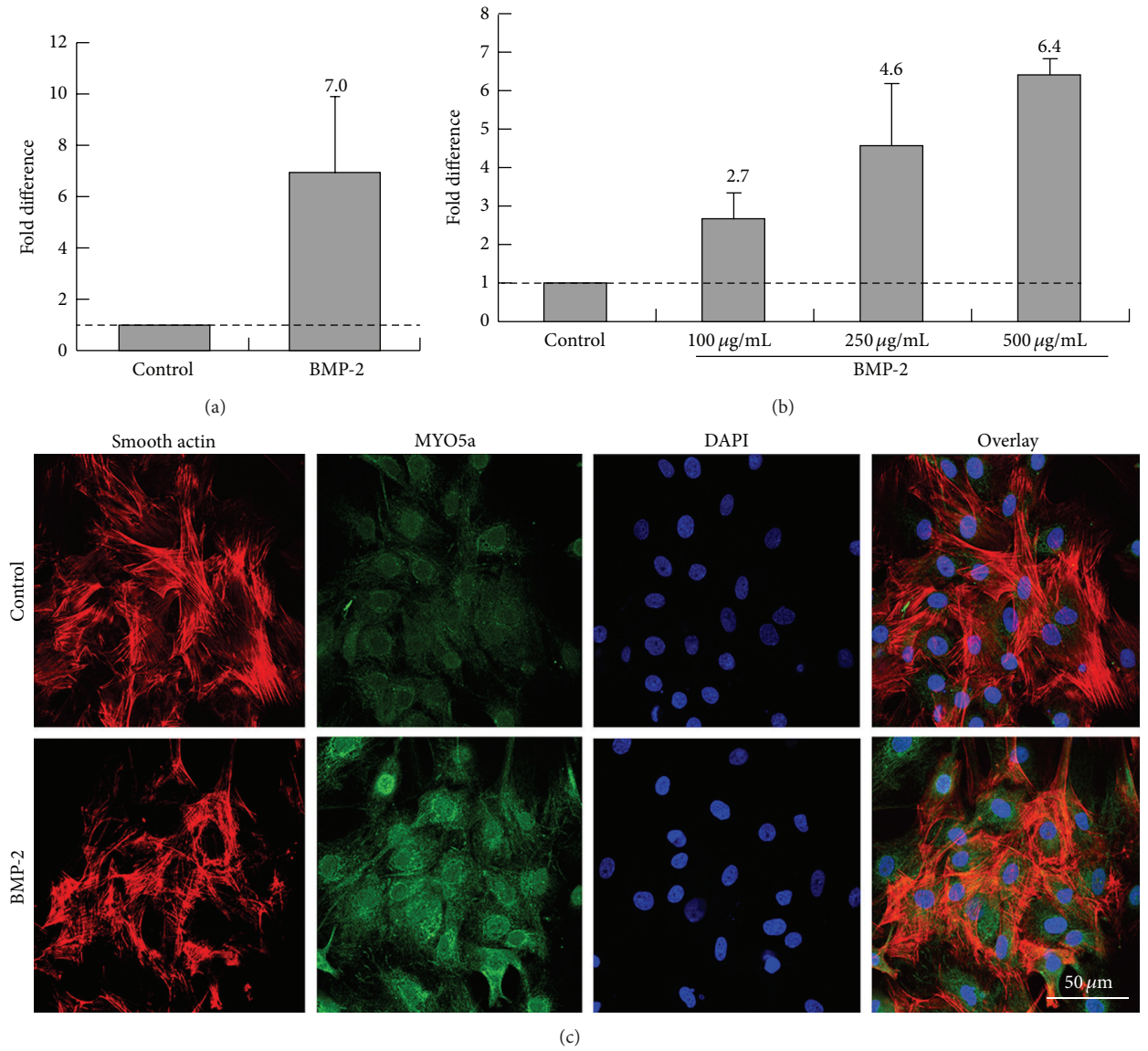

Figure 4: Myosin Va expression regulated by BMP-2. (a) qRT-PCR analysis revealed mRNA upregulation of the myosin Va gene associated with adenoviral-mediated BMP-2 overexpression in rat VSMCs. (b) Myosin Va expression reflects a dose-dependent response to BMP-2 administration. (c) Immunofluorescent assay characterizes actin and myosin Va expression. Myosin Va proteins were abundantly distributed in the cytoplasm of cells binding closed actin in BMP-2 overexpressing VSMCs, compared to control (which manifested only weakly positive signals).

BMP-2, compared to the weakly positive signals detected in control cells. Together, these results strongly support augmented myosin Va expression during BMP-2 overexpression.

3.5. siRNA-Mediated knockdown of VSMC Myosin Va Inhibits Migration. We generated three myosin Va-specific siRNA constructs. Compared to control or other generated siRNA constructs, siRNA-construct-3 (henceforth termed siRNA-3) significantly reduced the expression of both myosin Va mRNA (Figure 5(a)) and protein (Figure 5(b)). siRNA-mediated knockdown of myosin Va decreased its expression in locations known to be detectable by immunofluorescence assay in VSMCs simulated by BMP-2 (Figure 5(c)). We next determined the functional consequence of myosin Va knockdown in the setting of BMP-2 stimulation. VSMCs subjected to myosin Va-knockdown by siRNA-3migrate significantly slower compared to control or VSMCs subjected to siRNA constructs 1 or 2 (Figures 5(d) and 5(e)). These results suggest myosin Va may have significant role in BMP-2-mediated acceleration of VSMC migration.

3.6. Erk1/2 Modulates Myosin Va Expression by BMP-2. The signaling mechanisms responsible for the effects of BMP-2 overexpression upon VSMC migration are unclear. Software (IPA, Ingenuity Sys) analysis revealed the relationship and interaction between BMP-2, Erk1/2, myosin Va, and actin

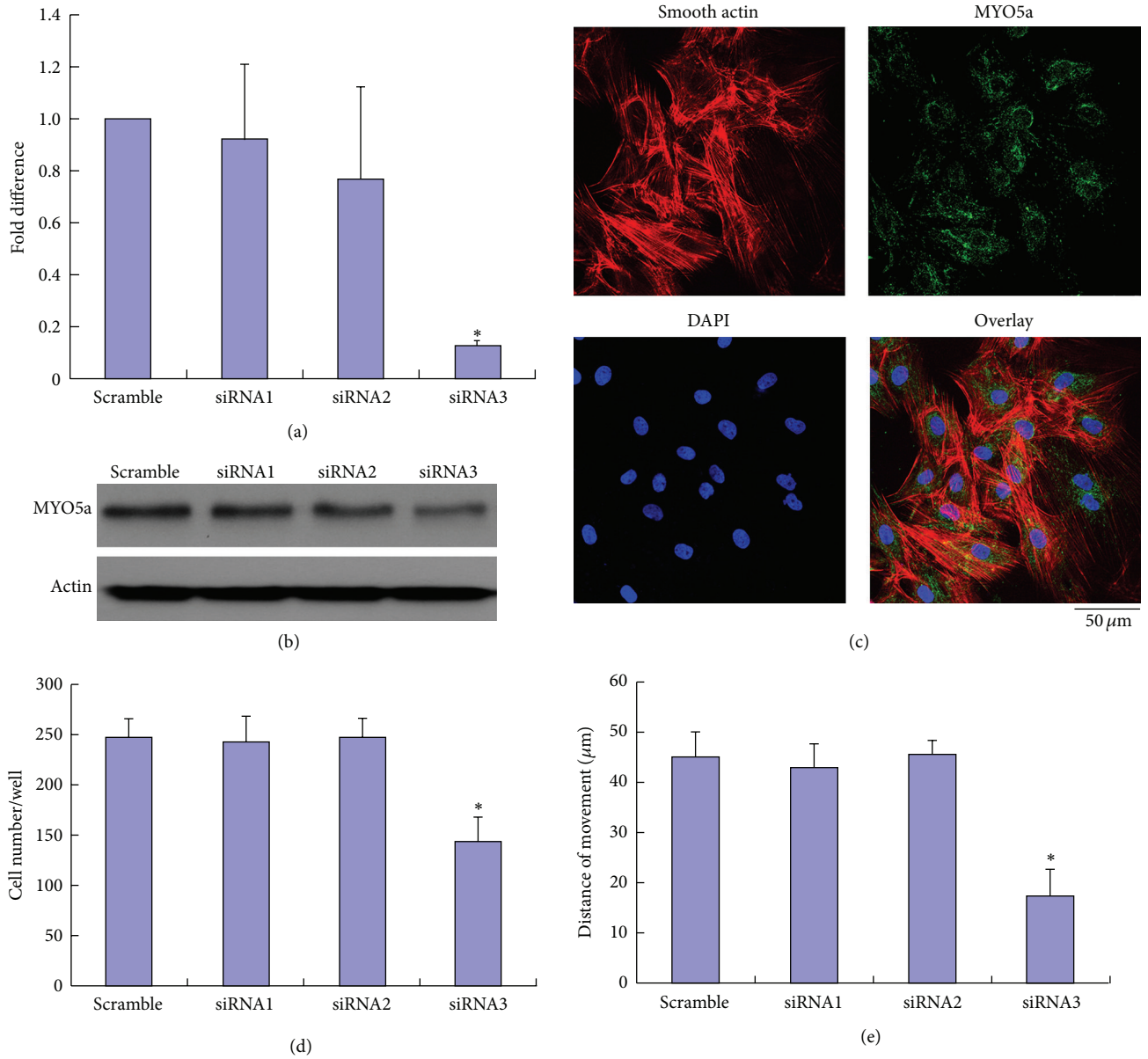

Figure 5: Effects of siRNA-mediated knockdown of myosin Vain rat VSMCs subjected to BMP-2 (250 ng/mL). (a) qRT-PCR analyses, demonstrating varying siRNA-mediated suppression of myosin Va mRNA expression. siRNA3 construct inhibited myosin Va mRNA expression to 0.13-fold of scramble levels. (b) Western blot demonstrating siRNA-3 construct inhibits the most myosin Va of all three generated siRNA constructs. (c) Myosin Va expression, determined by immunofluorescence, inhibited by siRNA-3. (d) Unicellular motility detected by Boyden chamber assay. (e) Multicellular population motility determined by wounding assay. Both (d) and (e) demonstrate that siRNA3 significantly inhibits migration compared to scramble control (unicellular motility 144 ± 25 versus 248 ± 20 cells/well, multicellular population 17.5 ± 5 μm versus 45.2 ± 4.8 μm). *Student's t-test: $P < 0.01$ versus control.

Table 2: BMP-2 increased uni- and multicellular population motility.

	Control	50 ng/mL	100 ng/mL	250 ng/mL	500 ng/mL
Signal cell movement distance (um/15 min)	0.112 + 0.01	0.134 + 0.01	0.165 + 0.02	0.202 + 0.05	0.221 + 0.028
P value with ctrl		0.08	0.0021*	0.0003*	0.00032*
Populations movement distance (um/24 h)	40.5 + 10.2	48.0 + 12.6	56.9 + 10.3	76.7 + 9.6	80.1 + 13.2
P value with ctrl		0.32	0.034*	0.0004*	0.0007*

Compared to control group, Student's test: *$P < 0.01$.

(Figure 6(a)). We investigated the degree of Erk1/2 stimulation in response to BMP-2 doses referenced in previous studies [23]. VSMCs were either treated with exogenous 250 ng/mL BMP-2 for 48 hours or adenovirally transfected to overexpress BMP-2. VSMCs were consequently exposed to Erk1/2 inhibitor U0126. Erk1/2 activation was determined by Western blot. Erk1/2 inhibitor significantly increased BAD protein production (typically downregulated by BMP-2) and significantly decreased Bcl-xl and myosin Va expression (typically upregulated by BMP-2) (Figure 6(b)). qRT-PCR demonstrated upregulation of myosin Va gene mRNA in rat VSMCs cells treated with 250 ng/mL BMP-2 for 48 hours, an effect blocked by 5 μM U0126 (Figure 6(c)). U0126 attenuated BMP-2 augmented VSMC motility (Figure 6(d)). Together, these results suggest Erk1/2 activity is essential for modulating myosin Va expression by BMP-2.

3.7. BMP-2 Increases Intracellular $[Ca^{2+}]^i$ *Oscillation.* Calcium (Ca^{2+}) plays a pivotal role in physiological biochemistry, acting as a second messenger in signal transduction pathways, involved with neurotransmitter release, all muscular cell type contraction, and fertilization [24, 25]. We investigate the potential involvement of Ca^{2+} in the signaling mechanism between BMP-2 and Erk1/2 by recording intracellular $[Ca^{2+}]^i$ oscillations within VSMCs. After loading the Ca^+-sensitive dye Fluo-4 AM, we monitored the time-dependent change of $[Ca^{2+}]^i$ within a colony's individual cells. Figure 6(e) demonstrates a representative VSMC colony, in which individual cells exhibit spontaneous Ca^{2+} oscillation. Without external Ca^{2+} supplementation, prolonged BMP-2 administration activated a large transient increase in Ca^{2+}, followed by a burst of Ca^{2+} spikes. The average amplitude of spontaneous oscillations increased intracellular Ca^{2+} concentration ($[Ca^{2+}]^i$) (Figure 6(f)). Individual cell fluorescence (F/F_0) plotted as a function of time demonstrates oscillatory changes in $[Ca^{2+}]^i$. Such $[Ca^{2+}]^i$ oscillations significantly increased in cells subjected to 250 ng/mL BMP-2 (Figure 6(g)). These data suggest BMP-2-induced Ca^{2+} oscillations are generated largely by a "cytosolic oscillator" in VSMCs. BMP-2-mediated regulation of myosin Va may be modulated by Erk signaling with Ca^{2+} involvement.

4. Discussion

We have made several important observations in the current study. Firstly, we demonstrated BMP-2 overexpression in VSMCs augments both unicellular and multicellular population motility. Secondly, we demonstrated BMP-2 overexpression increases the expression of myosin Va but not myosin Vb or Vc. Finally, we provide mechanistic evidence of ERK1/2 involvement in the modulation of myosin Va expression by BMP-2, with Ca^{2+} involvement.

Myosin Va directly assembles actin into antiparallel bundles [26, 27] localized at the leading edge of membrane ruffles [28]. A veritable actin-based motor protein, myosin Va, functions as an intracellular vesicle and organelle transporter and delivers cargo critical for maintaining cellular movement, thereby supporting cellular migration. Heretofore, whether myosin Va regulates VSMC migration was unknown. In this study, we demonstrate the abundant distribution of myosin Va binding actin in the cytoplasm of BMP-2 overexpressing VSMCs, compared to control cells. We also demonstrate knockdown of myosin Va inhibits VSMC motility, suggesting myosin Va is requisite for VSMC migration. More detailed analysis is required to elucidate how myosin Va specifically affects cellular motility, but it is plausible myosin Va participates in cell cytoskeleton reorganization, an essential event driving cellular movement [13, 29].

We clearly demonstrate BMP-2 overexpression stimulates cellular migration. We employed IPA software to analyze the relationships and interactions among BMP-2, Erk1/2, Myosin Va, and Ca^{2+}, but previous reports have not revealed any direct relationship between BMP-2 and myosin Va [30–32]. Erk1/2 inhibition not only blocked BMP-2-mediated downregulation of Bcl-xl protein production but also significantly decreased expression of both myosin Va and BAD. Myosin Va may mediate the functions of Bcl-xl by promoting islet cell migration and invasion [15]. We have demonstrated BMP-2 modulates myosin Va expression in VSMCs via Erk1/2 but cannot preclude the involvement of other contributory factors regulating the expression of myosin Va, such as gene regulatory elements like promoters and miRNAs. Further work is necessary to fully characterize the myosin Va promoter.

Spontaneous calcium oscillations occur in cells originating from excitable tissues of muscular, neuronal, and embryonic stem origin [33–35]. Calcium is an important second messenger regulating both intracellular and extracellular communications. The amplitude and duration of calcium transients can promote the expression of specific genes. Myosin Va is necessary for localization of IP3 receptors, which may connect with intracellular Ca^{2+} [24, 25]. In the current study, we observe the presence of spontaneous $[Ca^{2+}]^i$ oscillations in cultured VSMCs, further activated in the presence of BMP-2. The Erk signaling pathway can be stimulated by increased $[Ca^{2+}]^i$ oscillations, augmenting Erk1/2 phosphorylation [36, 37], supported by our results (Figure 6). Additional studies specifically defining the precise roles of Ca^{2+} as a second messenger in this system are ongoing.

VSMCs can change phenotype *in vivo* depending upon functional demands and can be contractile, proliferative, migratory, and/or synthetic [38, 39]. We demonstrate that BMP-2 overexpression increased expression of synthetic phenotypic markers OPN and MGP and decreased contractile phenotypic marker SM22α. The present study advances the notion BMP-2 may modulate SMC phenotype towards a synthetic state. Further studies are necessary to determine whether Ca^{2+} oscillations may have phenotypic implications.

In summary, our study demonstrates BMP-2 enhances VSMC migration via Erk1/2 signaling activation, which regulates myosin Va expression. Inhibition of BMP-2-induced myosin Va expression may represent a potential future therapeutic strategy attenuating atherosclerosis.

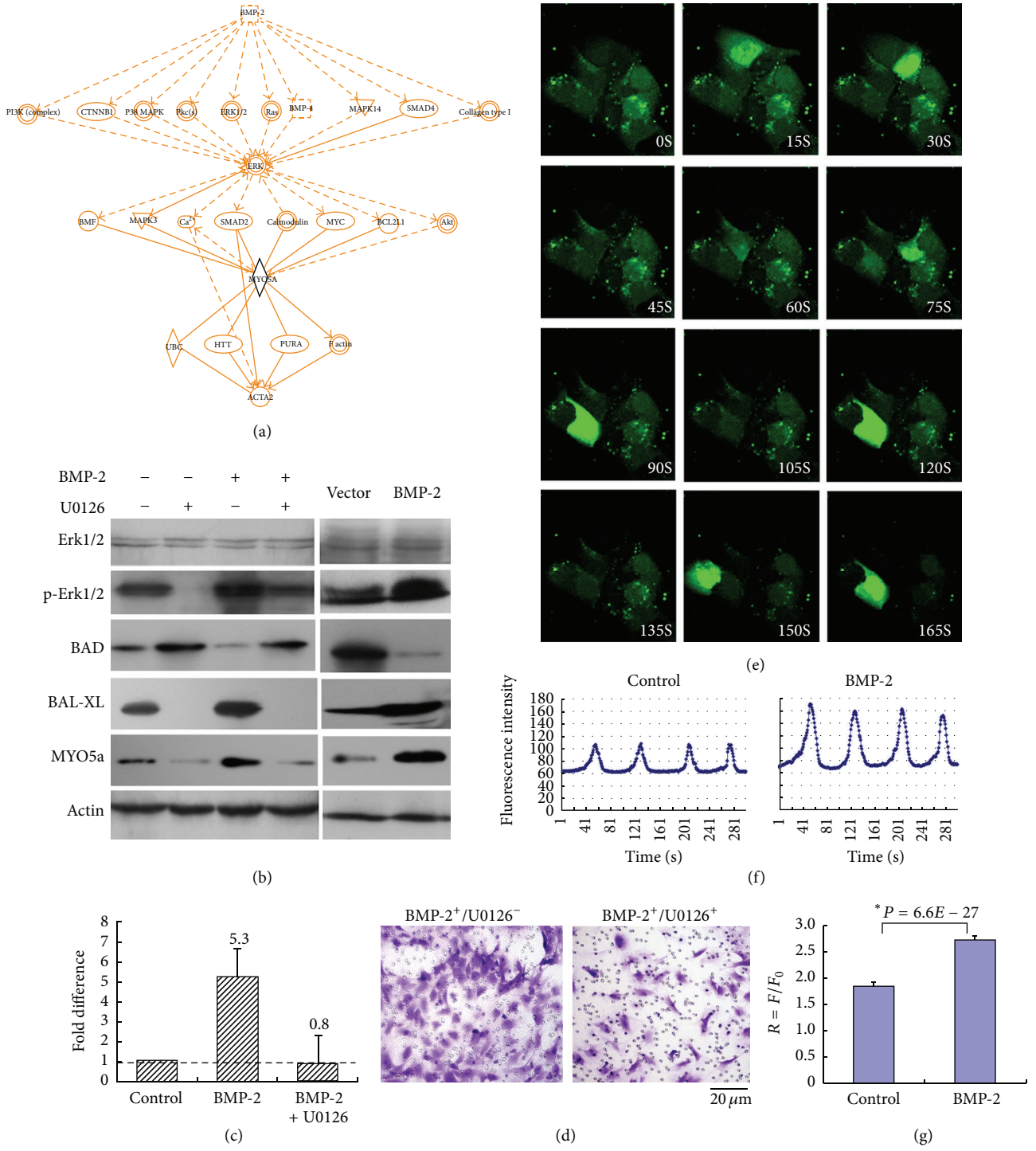

FIGURE 6: BMP-2-mediated regulation of myosin Va may be modulated by Erk signaling with Ca^{2+} involvement. (a) IPA software analysis of the relationships and interactions between BMP-2, Erk1/2, myosin Va, and actin. Although communication between the genes of these proteins genes has previously been reported, heretofore, a direct interaction between BMP-2 and myosin Va was not clarified. (b) Western demonstrates the presence of key proteins involved with myosin Va and Erk signaling in the lysates of rat VSMCs either adenovirally transfected to overexpress BMP-2 or treated with exogenous BMP-2 (250 ng/mL) for 48 hours. (c) qRT-PCR analysis demonstrating myosin Va gene mRNA was upregulated in VSMCs treated with 250 ng/mL BMP2 for 48 hours and downregulated in the presence of Erk1/2 inhibitor U0126 (dose 5 μM). (d) Migration of VSMCs subjected to identical conditions was detected by Boyden chamber assay (BMP-2^+ alone: 253 ± 29 versus BMP-2^+/U0126$^+$: 176 ± 11). (e) Oscillatory increase of intracellular Ca^{2+} concentration ($[Ca^{2+}]^i$) within individual cells of the colony. Chronological image sequence goes from left to right at 1.5-second intervals over 5 minutes. (f) Oscillations exhibited a mean interval of intracellular Ca^{2+} concentration (BMP-2 concentration 250 ng/mL, $n = 18$). (g) Fluorescence (F/F_0) of individual cells, values represent mean ± SD; *Student's t-test: $P < 0.01$).

Conflict of Interests

The authors declare that there is no conflict of interests regarding the publication of this paper.

Authors' Contribution

Ming Zhang and Min Yang contributed equally to the study.

Acknowledgment

This work was supported by the Beijing Novel Star Project on Science & Technology of China (no. 2009B38 to Ming Zhang).

References

[1] A. Csiszar, K. E. Smith, A. Koller, G. Kaley, J. G. Edwards, and Z. Ungvari, "Regulation of bone morphogenetic protein-2 expression in endothelial cells: role of nuclear factor-κB activation by tumor necrosis factor-α, H_2O_2, and high intravascular pressure," *Circulation*, vol. 111, no. 18, pp. 2364–2372, 2005.

[2] M. . Abedin, Y. Tintut, and L. L. Demer, "Vascular calcification: mechanisms and clinical ramifications," *Arteriosclerosis, Thrombosis, and Vascular Biology*, vol. 24, pp. 1161–1170, 2004.

[3] H. Zhang and A. Bradley, "Mice deficient for BMP2 are nonviable and have defects in amnion/chorion and cardiac development," *Development*, vol. 122, no. 10, pp. 2977–2986, 1996.

[4] C. M. Shanahan, N. R. B. Cary, J. C. Metcalfe, and P. L. Weissberg, "High expression of genes for calcification-regulating proteins in human atherosclerotic plaques," *Journal of Clinical Investigation*, vol. 93, no. 6, pp. 2393–2402, 1994.

[5] R. Ross, "Atherosclerosis: an inflammatory disease," *The New England Journal of Medicine*, vol. 340, no. 2, pp. 115–126, 1999.

[6] A. C. Newby, "Dual role of matrix metalloproteinases (matrixins) in intimal thickening and atherosclerotic plaque rupture," *Physiological Reviews*, vol. 85, no. 1, pp. 1–31, 2005.

[7] A. Mehta, "Myosin learns to walk," *Journal of Cell Science*, vol. 114, no. 11, pp. 1981–1998, 2001.

[8] J. M. A. Jbireal, C. Strell, B. Niggemann, K. Zänker, and F. Entschladen, "The selective role of myosin VI in lymphoid leukemia cell migration," *Leukemia Research*, vol. 34, no. 12, pp. 1656–1662, 2010.

[9] P. Bastian, K. Lang, B. Niggemann, K. S. Zaenker, and F. Entschladen, "Myosin regulation in the migration of tumor cells and leukocytes within a three-dimensional collagen matrix," *Cellular and Molecular Life Sciences*, vol. 62, no. 1, pp. 65–76, 2005.

[10] M. J. Tyska and M. S. Mooseker, "Myosin-V motility: these levers were made for walking," *Trends in Cell Biology*, vol. 13, no. 9, pp. 447–451, 2003.

[11] J. S. Berg, B. C. Powell, and R. E. Cheney, "A millennial myosin census," *Molecular Biology of the Cell*, vol. 12, no. 4, pp. 780–794, 2001.

[12] X. Wu, G. Jung, and J. A. Hammer III, "Functions of unconventional myosins," *Current Opinion in Cell Biology*, vol. 12, no. 1, pp. 42–51, 2000.

[13] F.-S. Wang, J. S. Wolenski, R. E. Cheney, M. S. Mooseker, and D. G. Jay, "Function of myosin-V in filopodial extension of neuronal growth cones," *Science*, vol. 273, no. 5275, pp. 660–663, 1996.

[14] T. T. Cao, W. Chang, S. E. Masters, and M. S. Mooseker, "Myosin-Va binds to and mechanochemically couples microtubules to actin filaments," *Molecular Biology of the Cell*, vol. 15, no. 1, pp. 151–161, 2004.

[15] Y. Takagishi, K. Hashimoto, T. Kayahara et al., "Diminished climbing fiber innervation of purkinje cells in the cerebellum of myosin Va mutant mice and rats," *Developmental Neurobiology*, vol. 67, no. 7, pp. 909–923, 2007.

[16] M. Miyata, Y. Kishimoto, M. Tanaka et al., "A role for myosin Va in cerebellar plasticity and motor learning: a possible mechanism underlying neurological disorder in myosin Va disease," *Journal of Neuroscience*, vol. 31, no. 16, pp. 6067–6078, 2011.

[17] H. Yoshida, W. Cheng, J. Hung et al., "Lessons from border cell migration in the Drosophila ovary: a role for myosin VI in dissemination of human ovarian cancer," *Proceedings of the National Academy of Sciences of the United States of America*, vol. 101, no. 21, pp. 8144–8149, 2004.

[18] C. Liu, T. Su, F. Li et al., "PI3K/Akt signaling transduction pathway is involved in rat vascular smooth muscle cell proliferation induced by apelin-13," *Acta Biochimica et Biophysica Sinica*, vol. 42, no. 6, pp. 396–402, 2010.

[19] G. Li, L. Xiang, W. Yang, Z. Wang, J. Wang, and K. Chen, "Efficient multicistronic co-expression of hNIS and hTPO in prostate cancer cells for nonthyroidal tumor radioiodine therapy," *The American Journal of Nuclear Medicine and Molecular Imaging*, vol. 2, pp. 483–498, 2012.

[20] S. Shiraso, Y. Katayose, K. Yamamoto et al., "Overexpression of adenovirus-mediated p27kip1 lacking the Jab1-binding region enhances cytotoxicity and inhibits xenografted human cholangiocarcinoma growth," *Anticancer Research*, vol. 29, no. 6, pp. 2015–2024, 2009.

[21] E. Cukierman, R. Pankov, D. R. Stevens, and K. M. Yamada, "Taking cell-matrix adhesions to the third dimension," *Science*, vol. 294, no. 5547, pp. 1708–1712, 2001.

[22] L. Lan, H. Han, H. Zuo et al., "Upregulation of myosin Va by snail is involved in cancer cell migration and metastasis," *International Journal of Cancer*, vol. 126, no. 1, pp. 53–64, 2010.

[23] Y.-C. N. Du, B. C. Lewis, D. Hanahan, and H. Varmus, "Assessing tumor progression factors by somatic gene transfer into a mouse model: Bcl-xL promotes islet tumor cell invasion," *PLoS Biology*, vol. 5, no. 10, pp. 2255–2269, 2007.

[24] J. R. Naranjo and B. Mellström, "Ca^{2+}-dependent transcriptional control of Ca^{2+} homeostasis," *Journal of Biological Chemistry*, vol. 287, pp. 31674–31680, 2012.

[25] M. J. Berridge, "Calcium signallingremodelling and disease," *Biochemical Society Transactions*, vol. 40, pp. 297–309, 2012.

[26] R. E. Cheney, M. K. O'Shea, J. E. Heuser et al., "Brain myosin-V is a two-headed unconventional myosin with motor activity," *Cell*, vol. 75, no. 1, pp. 13–23, 1993.

[27] S. B. F. Tauhata, D. V. Dos Santos, E. W. Taylor, M. S. Mooseker, and R. E. Larson, "High affinity binding of brain myosin-Va to F-actin induced by calcium in the presence of ATP," *Journal of Biological Chemistry*, vol. 276, no. 43, pp. 39812–39818, 2001.

[28] C. Lionne, F. Buss, T. Hodge, G. Ihrke, and J. Kendrick-Jones, "Localization of myosin Va is dependent on the cytoskeletal organization in the cell," *Biochemistry and Cell Biology*, vol. 79, no. 1, pp. 93–106, 2001.

[29] R. D. Eppinga, I.-F. Peng, J. L.-C. Lin, C.-F. Wu, and J. J.-C. Lin, "Opposite effects of overexpressed myosin Va or heavy meromyosin Va on vesicle distribution, cytoskeleton organization, and cell motility in nonmuscle cells," *Cell Motility and the Cytoskeleton*, vol. 65, no. 3, pp. 197–215, 2008.

[30] J. R. Sellers, K. Thirumurugan, T. Sakamoto, J. A. Hammer III, and P. J. Knight, "Calcium and cargoes as regulators of myosin 5a activity," *Biochemical and Biophysical Research Communications*, vol. 369, no. 1, pp. 176–181, 2008.

[31] X.-D. Li, K. Mabuchi, R. Ikebe, and M. Ikebe, "Ca^{2+}-induced activation of ATPase activity of myosin Va is accompanied with a large conformational change," *Biochemical and Biophysical Research Communications*, vol. 315, no. 3, pp. 538–545, 2004.

[32] D. N. Krementsov, E. B. Krementsova, and K. M. Trybus, "Myosin V: regulation by calcium, calmodulin, and the tail domain," *Journal of Cell Biology*, vol. 164, no. 6, pp. 877–886, 2004.

[33] N. Kapur, G. A. Mignery, and K. Banach, "Cell cycle-dependent calcium oscillations in mouse embryonic stem cells," *The American Journal of Physiology: Cell Physiology*, vol. 292, no. 4, pp. C1510–C1518, 2007.

[34] X. Liu, J. Zeng, Y. Zhao, Z. Xiao, C. Fang, and H. Ruan, "Inhibition of ATP-induced Ca^{2+} Influx by corticosterone in dorsal root ganglion neurons," *Neurochemical Research*, vol. 35, no. 5, pp. 804–810, 2010.

[35] M. Vukcevic, F. Zorzato, G. Spagnoli, and S. Treves, "Frequent calcium oscillations lead to NFAT activation in human immature dendritic cells," *Journal of Biological Chemistry*, vol. 285, no. 21, pp. 16003–16011, 2010.

[36] A. Pinsino, M. C. Roccheri, C. Costa, and V. Matranga, "Manganese interferes with calcium, perturbs ERK signaling, and produces embryos with no skeleton," *Toxicological Sciences*, vol. 123, no. 1, pp. 217–230, 2011.

[37] P. Vichi, A. Whelchel, H. Knot, M. Nelson, W. Kolch, and J. Posada, "Endothelin-stimulated ERK activation in airway smooth-muscle cells requires calcium influx and RaF activation," *The American Journal of Respiratory Cell and Molecular Biology*, vol. 20, no. 1, pp. 99–105, 1999.

[38] S. J. House, M. Potier, J. Bisaillon, H. A. Singer, and M. Trebak, "The non-excitable smooth muscle: calcium signaling and phenotypic switching during vascular disease," *Pflugers Archiv European Journal of Physiology*, vol. 456, no. 5, pp. 769–785, 2008.

[39] V. V. Matchkov, O. Kudryavtseva, and C. Aalkjaer, "Intracellular Ca^{2+} signalling and phenotype of vascular smooth muscle cells," *Basic and Clinical Pharmacology and Toxicology*, vol. 110, no. 1, pp. 42–48, 2012.

Hindawi Publishing Corporation
Oxidative Medicine and Cellular Longevity
Volume 2014, Article ID 282854, 10 pages
http://dx.doi.org/10.1155/2014/282854

Review Article

NADPH Oxidase 1 and Its Derived Reactive Oxygen Species Mediated Tissue Injury and Repair

Xiu-Jun Fu,[1] Ying-Bo Peng,[1] Yi-Ping Hu,[1,2] You-Zhen Shi,[1] Min Yao,[1,3] and Xiong Zhang[4]

[1] *Department of Burns and Plastic Surgery, No. 3 People's Hospital, Institute of Traumatic Medicine, School of Medicine, Shanghai Jiao Tong University, Shanghai 201900, China*
[2] *Department of Burns, The Fourth Hospital Affiliated to Jinan University, Guangzhou 51022, China*
[3] *Department of Dermatology, Wellman Center for Photomedicine, Harvard Medical School, Massachusetts General Hospital, Boston, MA 02114, USA*
[4] *Department of Burns and Plastic Surgery, Ruijin Hospital, School of Medicine, Shanghai Jiao Tong University, Shanghai 200025, China*

Correspondence should be addressed to Xiong Zhang; xiong@medmail.com.cn

Received 5 September 2013; Revised 11 December 2013; Accepted 17 December 2013; Published 19 January 2014

Academic Editor: Mengzhou Xue

Reactive oxygen species are mostly viewed to cause oxidative damage to various cells and induce organ dysfunction after ischemia-reperfusion injury. However, they are also considered as crucial molecules for cellular signal transduction in biology. NADPH oxidase, whose only function is reactive oxygen species production, has been extensively investigated in many cell types especially phagocytes. The deficiency of NADPH oxidase extends the process of inflammation and delays tissue repair, which causes chronic granulomatous disease in patients. NADPH oxidase 1, one member of the NADPH oxidase family, is not only constitutively expressed in a variety of tissues, but also induced to increase expression in both mRNA and protein levels under many circumstances. NADPH oxidase 1 and its derived reactive oxygen species are suggested to be able to regulate inflammation reaction, cell proliferation and migration, and extracellular matrix synthesis, which contribute to the processes of tissue injury and repair.

1. Introduction

The general view of the primary role of reactive oxygen species (ROS) in biology is to cause oxidative damage to organs and tissues suffering ischemia-reperfusion injury [1–3] and inactivate and clear microorganisms through respiratory burst of phagocytic cells [4]. High concentration of hydrogen peroxide is used clinically for wound disinfection, which might not be beneficial for overall wound healing because of the oxidative damage to host tissue in addition to bacteria [5, 6]. However, low concentration of ROS regulates intracellular signal transduction pathways by redox-dependent mechanisms, which facilitates the process of tissue repair [6]. As signal transduction molecules, ROS are controlling a large array of biological processes including the regulation of organ development and cell growth and the response to environmental stimuli [4]. In the process of tissue injury and repair, ROS has both detrimental and beneficial roles through regulating cell damages and promoting cell proliferation and migration.

One of the most important sources of intracellular ROS is the enzyme NADPH oxidase (Nox), which is the only mammalian enzyme dedicated to ROS generation. NADPH oxidase enzyme complex, formed by Nox and other cytosolic subunits, catalyzes the production of ROS from molecular oxygen. The Nox family has been extensively investigated in many cell types especially phagocytes [7]. The ROS and their oxidants are critical for bacteria and necrotic tissue purging by phagocytes. And the deficiency of Nox extends the process of inflammation and delays tissue repair, which causes chronic granulomatous disease (CGD) in patients [8]. NADPH oxidase was further found in extensive cell types such as epithelial cells, fibroblasts, and vascular endothelial cells [9]. A large number of evidence suggest that NADPH

oxidase contributes to the initiation and development of many physiological and pathophysiological events, including thyroid hormone production in the thyroid gland, ischemia-reperfusion injury in multiple organs, septic shock, obesity, cancer, neuronal degeneration, and cardiovascular diseases, as well as vascular diseases [10–12]. Based on these, Nox and its derived ROS are suggested to play an essential role in wound repair and regeneration, through modulating inflammation reaction, cell proliferation and migration, and extracellular matrix synthesis and deposition [13, 14].

Nox1 as the first discovered homologue of the catalytic subunit of the superoxide-generating NADPH oxidase of phagocytes is expressed in multiple organs and various cell types, especially in colon epithelial cells and vascular smooth muscle cells [15]. In addition to its constitutive expression in a variety of tissues, Nox1 is induced to increase expression in both mRNA and protein levels under many circumstances such as proinflammatory factors and growth factors stimulation, ultraviolet (UV) radiation, hypoxia, and mechanical injury [16–19]. This review will focus on the possible roles Nox1 plays in the process of tissue injury and repair mainly through regulating the function of repair cells, namely epithelial cells, fibroblast cells, and endothelial cells and smooth muscle cells.

2. Nox Family and Nox1

In mammalian, the Nox enzymes can be divided into three subfamilies: one containing Nox1–Nox4 (the Nox1–Nox4 subgroup), which form a heterodimer with $p22^{phox}$; the Nox5 subfamily; and the Duox subfamily (Figure 1). All Nox family members are transmembrane proteins that transport electrons across biological membranes to reduce oxygen to superoxide. In accordance with this preserved function, there are conserved structural properties of Nox enzymes that are common to all family members. Starting from the COOH terminus, these conserved structural features include an NADPH-binding site at the cytoplasmic COOH terminus, a FAD-binding region in proximity of the NADPH-binding site, six conserved transmembrane domains, and four highly conserved heme-binding histidines in the third and fifth transmembrane domains [7, 20]. A long intracellular NH_2 terminus containing a Ca^{2+}-binding EF hand domain is present in Nox5 and Duox proteins, distinguishing them from Nox1–4. And given the additional NH_2-terminal transmembrane domain, the histidines are in the fourth and sixth transmembrane domains in Duox proteins [7].

Nox1 was the first homolog of Nox2 to be described. The number and the length of the exons of the Nox1 genes are virtually identical to Nox2. And at the protein level, similarly, there is a high degree of sequence identity (57%) between Nox1 and Nox2 [15]. Like Nox2, Nox1 is broadly expressed in a variety of cell types, including vascular smooth muscle cells, endothelial cells, uterus, placenta, prostate, osteoclasts, and retinal pericytes, as well as in several cell lines such as the colon tumor cell lines Caco2 and HT29 and the pulmonary epithelial cell line A549 [7, 9, 15]. However, it is most highly expressed in colon epithelium. Two cytosolic subunits are necessary for Nox1 to generate superoxide. One is Nox Organizer 1 (NoxO1) having the same role as $p47^{phox}$, while the other is Nox Activator 1 (NoxA1), which is similar to $p67^{phox}$. In addition to these two cytosolic subunits, Nox1 as well as Nox2 depends on the membrane subunit $p22^{phox}$ [21, 22]. However, the dependence of Nox1 on subunit $p22^{phox}$ is not so strict as its analogues Nox2 and Nox3. Like Nox2, the activation of Nox1 also depends on the Rac1, which provides a major trigger for Nox1-dependent ROS generation [23].

ROS from Nox1 and other Nox isoforms can achieve the regulation of cell proliferation, differentiation, survival, apoptosis, metabolism, and migration through redox-sensitive cysteine residues. A very common targeted molecule by ROS inside cell is protein tyrosine phosphorylations (PTPs), which controls the phosphorylation of tremendous proteins involving cellular signal transduction [24]. Although the precise mechanism is presently unknown, the mitogen-activated protein kinase (MAPK) system and phosphoinositide 3-kinase (PI3K) activated by the Nox family including Nox1 are shown in numerous studies (Figure 2) [24, 25]. Nox isoforms derived ROS has also been suggested to regulate some ion channels such as potassium channel and membrane and intracellular calcium channels. And these might happen through the ROS-sensitive signaling systems. Interestingly, Nox enzymes may reversibly be activated by the changing of intracellular calcium [26]. In addition, abundant evidences indicate that Nox-dependent ROS influence the expression of multiple genes, including chemotactic factors, inflammatory factors, and growth factors [27, 28].

3. The Activation of Nox1 in Epithelial Cells and Wound Repair

The process of reepithelialization is critical for completing wound healing. The epithelial cells from wound edges and dermal appendages proliferate and migrate across the wound and finally form a barrier between the wound and environment. Emerging evidence indicates that ROS from Nox and other resources regulate epithelial cells proliferation. In physiological condition, Nox1 is mainly present in large intestine epithelial cells, with much lower expression in the small intestine (jejunum, ileum) and the uterine and prostate [29]. However, constitutively expression of Nox1 and cytosolic proteins Rac1, $p40^{phox}$, and $p67^{phox}$ was identified as a source of superoxide in human immortalized skin (HaCaT) and gingival mucosal (GM16) keratinocyte cell lines [22]. Although Nox2 and Nox4 mRNA levels were also detected in both cell lines, Nox1 but not Nox4 protein was detected in HaCaT and GM16 cells, indicating that Nox1 may play a vital role in redox-mediated signaling which is associated with wound healing after tissue injury and epithelial tumorigenesis in human keratinocytes [22].

Rapidly increased NADPH oxidase activity and intracellular ROS were also found on human keratinocytes after treatment with a nontoxic dose of UVA radiation, which is a major environmental stress on skin [17]. Depleting the Nox1 isoform of the catalytic subunit of NADPH oxidase using small interfering RNA (siRNA) blocked the UVA-induced

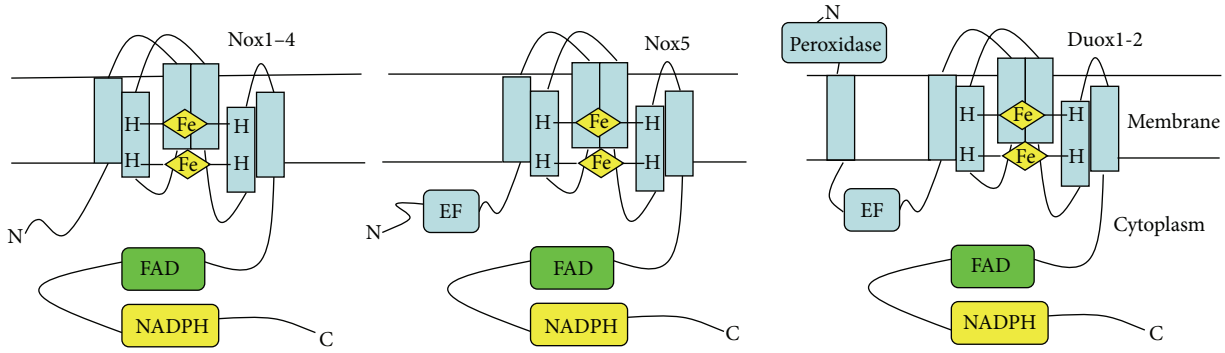

Figure 1: Structural differences among mammalian Nox homologues. Nox1–5 share six highly conserved transmembrane domains, while Duox1 and Duox2 have an additional N-terminal transmembrane domain. Four conserved histidines that bind two hemes between the third and fifth (fourth and sixth in Duox) of the transmembrane domains provide an oxygen binding site. The cytoplasmic C-terminus contains domans for binding of the substrate NADPH and the cofactor FAD. An additional N-terminal extension containing Ca^{2+}-binding EF hands exists in both Nox5 and Duox, allowing for Ca^{2+} activation. Duox also has an extracellular peroxidase homology domain at the N-terminus.

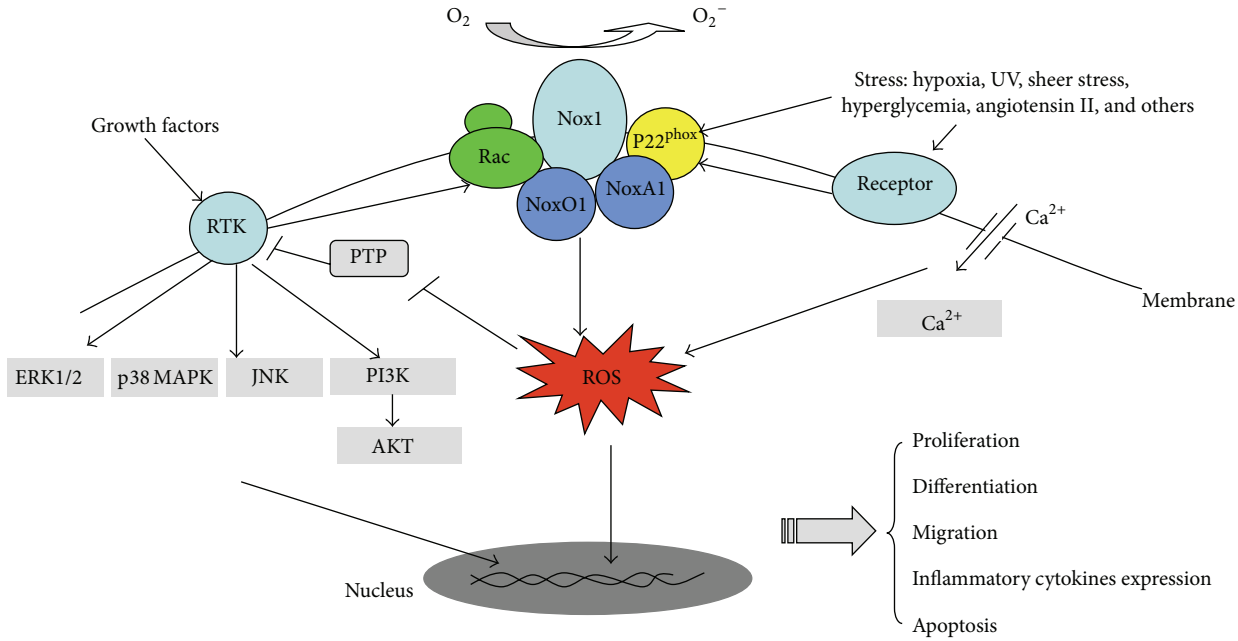

Figure 2: Nox1 modulates intracellular signaling. Nox1 can be activated by a diverse array of stimuli, such as the binding of growth factors to their receptor tyrosine kinases (RTK) and the stimulation by agonists such as angiotensin II. ROS produced by activated Nox1 oxidize the cysteine residue of protein tyrosine phosphatases (PTP), inactivate these enzymes, and lead to enhanced activation of MAPK system and PI3 K. ROS may also interact with intracellular Ca^{2+} by enhancing the entry of Ca^{2+} through cell membrane. The activated intracellular signals may further activate Nox1 or other Nox homologues, causing additional increasing of ROS. All these mechanisms may be involved in regulating cell proliferation, differentiation, apoptosis, and migration, and angiogenesis, which are crucial components of tissue injury and repair.

ROS increase and UVA-initiated prostaglandin E_2 (PGE_2) synthesis [17]. The increase in intracellular calcium was suggested to induce the activation of Nox1 [17]. Nox1 subunit of NADPH oxidase was also demonstrated to be of importance for UVA-induced ROS and PGE_2 production, which might cause photosensitivity to UVA in patients with Smith-Lemli-Opitz syndrome (SLOS) [30]. These results indicate that UVA activates Nox1-based NADPH oxidase to produce ROS that stimulate PGE_2 synthesis and that Nox1 may be an appropriate target for agents designed to block UVA-induced skin injury and tumor promotion. And another in vitro experiment indicated that Nox1 lies downstream of BLT2 and mediates UVB-induced ROS production and apoptosis of HaCaT [31]. This was further testified by in vivo BLT2-blocking and -overexpressing animal models, which concluded that "BLT2-Nox1"-linked pathway plays a crucial role in UVB-induced ROS generation and mediates apoptosis in human keratinocytes [31].

Using scratch wound motility assay, Nox1 and Nox4 isozymes of NADPH oxidase involved in enhanced ROS production and migration of HaCaT cells with cotreatment of hepatocyte growth factor (HGF) and transforming growth factor-β1 (TGF-β1) [19]. Reepithelialization by means of proliferation and migration of keratinocytes from the margin is one of the principal events in the process of wound healing. HGF and TGF-β1 as well as other various growth factors accelerate tissue repair by enhancing proliferation and migration of keratinocytes, fibroblasts, and endothelial cells and promoting the formation of granulation tissue [32, 33]. Another study testified that growth factor neuregulin, a member of the epidermal growth factor family (EGF), could also activate ROS generation through Nox1 and Nox2 and further increase cofilin dephosphorylation and activation in HaCaT keratinocytes to promote cell migration [34]. Thus, Nox1 might be beneficial in the process of tissue repair by participating in growth factor induced enhancement of reepithelialization. However, Nox1-generated ROS was found to mediate EGF-induced inhibition of the Rho activity in human colon cancer Caco2 cells that may be required for cell migration [35].

Like growth factor, other cytokines such as inflammatory factor signal transduction also have Nox1 and ROS involved in epithelial cells. Nox1 is responsible for the rapid production of ROS in response to IL-13 and Interferon-γ stimulation in human intestinal epithelial cells [36, 37]. Nox1 and ROS respond to IL-13 treatment, regulate phosphorylation of ERK1/2 and STAT6, and further increase the expression of intestinal trefoil factor 3 (TFF3) and antiapoptosis factor Bcl-xl, which contributes to the epithelial restitution and wound healing [36]. Interestingly, Nox1 may also induce the increased expression of the homologues Nox4 and Duox2 in IL-13 treated intestinal epithelial cells [36].

Nox1 was demonstrated to render immortalized human gingival mucosal keratinocytes resistant against Ca^{2+}/serum induced differentiation [38]. Nox1-transfected cells produced fast dividing resistant cells and contained varying amounts of vimentin and K8/K18, which are associated with malignant progression in different types of human epithelial tumors [38]. And Nox1 was measured to be expressed in colon cancer samples and cancer cell lines Caco2, HT29, and T84 and human melanoma cell lines, which may likely be able to facilitate cancer cell migration and invasion [29, 39, 40]. This makes us concerned about the fact that Nox1 may be one of the crucial signal sources triggering the formation of epithelial tumor in people experiencing too much UV radiation exposure and patients suffering chronic wounds. However, evidence was also presented that Nox1 is not a mitogenic oxidase and suggests that Nox1 functions as a specialized phox-like enzyme in differentiated colon epithelium [29].

Beside intestinal epithelial cells and skin keratinocytes, Nox1 is likely to be the key source of ROS in lung epithelial cells after hypoxia injury and influenza virus infection [18, 41]. All of these confirm the crucial role of Nox1 in physiological homeostasis and pathological development of epithelial tissue, including defense bacterial invasion and radiation injury of intestinal and skin epithelium, promoting cell proliferation and migration in wound healing and tumorigenesis.

4. The Effects of Nox1 and ROS on ECM Deposition and Fibrosis

Fibroblast and myofibroblast cells, the main sources of extracellular matrix (ECM), especially collagen fibers, are indispensable in wound repair. Nox1 as well as Nox4 and Nox5 are constitutively expressed in human corneal stromal fibroblasts in mRNA level, contributing to the main source of superoxide [42]. The transcription of Nox1 mRNA in mouse embryonic fibroblasts (MEFs) could be elevated by calcium ionophore ionomycin in a dose-dependent manner [43]. Constitutively expressed or induced expressed Nox1 in fibroblast cells and Nox1-dependent superoxide may be potential for regulating gene expression and participating in the processes of inflammation and wound repair, as second signal messengers.

NIH3T3 cells overexpression of mox1 (also known as Nox1) was shown to increase superoxide generation and cell growth [15]. The transfected cells also had a transformed appearance, showed anchorage-independent growth, and produced tumors in athymic mice [15]. In another study, Nox1-generated oxidants were shown to downregulate the Rho activity through inactivation of the low molecular weight protein-tyrosine phosphatase in K-Ras-transformed normal rat kidney fibroblast cells, which leads to disruption of both actin stress fibers and focal adhesions [35]. In addition, fibroblast Nox1 was also demonstrated to form a complex with TRADD, RIP1 and Rac1, and be responsible for TNF-induced superoxide generation in murine fibrosarcoma L929 cells and MEF cells [44]. The large number of superoxides caused by adding TNF to these cells induced prolonged c-jun N-terminal kinase (JNK) activation and finally led cells to die, while knockdown of Nox1 using siRNA inhibited cell necrosis [44].

The fibrotic factors TGF-β and fibronectin were induced to express much more in diabetes milieu through the interaction of Nox1 and iNOS (inducible nitric oxide synthase) [45]. The increased expression of fibrotic factors is suggested to be one of key mechanisms for kidney fibrogenesis of diabetes patients. The NADPH oxidase inhibitor and antioxidant reduced the expression of profibrotic factor TGF-β and collagen accumulation in cultured glomerular mesangial cells [46, 47]. And in vivo studies suggested that interventions with various antioxidants or NADPH oxidase inhibitor apocynin have beneficial effects on renal fibrosis [48, 49]. However, there is no direct or indirect evidence indicating that Nox1 rather than other Nox family members plays crucial role in renal fibrosis.

The matricellular protein CCN1 (also known as CYR61: cysteine-rich protein 61), which regulates diverse cellular functions, including cell adhesion, migration, differentiation, and survival in a cell-type and context-dependent manner, is dynamically expressed at sites of wound repair [50]. CCN1, highly expressed in granulation tissues during cutaneous wound healing, drives fibroblasts into senescence and upregulates the expression of antifibrotic genes to restrict fibrosis during tissue wound repair [51, 52]. It could induce fibroblast senescence by binding to integrin $\alpha 6\beta 1$ and the heparan sulphate proteoglycans, which further induces DNA damage

response pathways and activates p53 and the Rac1-Nox1 complex. CCN1 is unique among ECM proteins as a cell-adhesive substrate in triggering a robust and sustained accumulation of ROS necessary for senescence. The activated Nox1 results in the ROS-dependent activation of the $p16^{INK4a}$/pRb pathway, leading to senescence and concomitant expression of antifibrotic genes [52]. Therefore, CCN1-Nox1 dependent fibroblast senescence response in cutaneous injury functions to curb fibrosis during wound healing.

5. Nox1 Regulates Vessel Damage and New Vessel Formation

Endothelial cells and smooth muscle cells of vascular system play a central role in angiogenesis and vascular remodeling during tissue injury, and repair, including ischemic heart disease, peripheral artery disease, acute lung injury, and wound healing. Angiogenesis, the process of new blood vessel growth, is dependent on cell proliferation, migration, and capillary tube formation, which is partially regulated by the redox system. The effects of ROS on vascular cells are tightly regulated and dependent on the amount and site of production as well as the intracellular balance of prooxidant and antioxidant enzyme activity. Low levels of ROS appear to be physiological and beneficial cellular signal in reparative angiogenesis in response to ischemia and wound healing [6, 53], while excess amount of ROS contributes to endothelial cells and smooth muscle cells injury and dysfunction [54]. In the vascular system, Nox1 mRNA has been detected mainly in vascular smooth muscle cells but not in adventitial cells, whereas Nox2 is localized primarily in endothelial and adventitial cells, and Nox4 is abundantly expressed in all of the vessel constituents [55–57]. And more recently, all Nox isoforms (Nox1–5) were shown to exist in human cardiovascular cells, and the whole-cell and nuclear levels of Nox1 were reported to be similar in human vascular endothelial cells and smooth muscle cells [58]. Nox1 was suggested to be strongly related to vascular physiopathological changes, such as angiotensin II-induced hypertension and aortic dissection [59, 60] and atherosclerosis development in diabetic apolipoprotein E-deficient mice [61].

Vascular endothelial growth factor (VEGF) and its receptor VEGFR play an indispensable role in angiogenesis after tissue injury. VEGF, a potent angiogenic growth factor, primarily through VEGFR2 (KDR/Flk1), stimulates proliferation, migration, cytoskeletal reorganization, and tube formation of endothelial cells. VEGFR is activated through dimerization and autophosphorylation of tyrosine residues in the cytoplasmic kinase domain [62]. The receptor activation is followed by activation of downstream signaling pathways such as mitogen-activated protein kinases, PI3 kinase, Src, Akt, and eNOS, which are essential to induce endothelial cell migration and proliferation and contribute to angiogenesis [54, 62, 63]. NADPH oxidase is one of the major sources of ROS in endothelial cells. VEGF can activate NADPH oxidase and induce the production of ROS, which in turn can increase the expression of VEGF and VEGFR and be involved in VEGFR phosphorylation, cell proliferation, and migration [64, 65]. The major producers of ROS in endothelial cells have been thought to be Nox2 and Nox4, as well as xanthine oxidase and eNOS, rather than Nox1 [66]. However, Nox1 was found to be expressed in activated sinusoidal endothelial cells (NP31). The expression of Nox1 mRNA was increased by approximately sixfold in NP31/kinase cells (transformed by the introduction of a constitutively activated form of the VEGFR1 kinase) by Northern blotting [67]. Neither Nox2 expression in NP31 cells nor induced expression of Nox2 in transformed Np31/kinase cells was detected [67]. Anti-Nox1 siRNA treatment failed to inhibit tubulogenesis in vitro, indicating that Nox1 together with Ras and other molecules participated in the VEGFR1 kinase-derived tubulogenic pathway through ROS [67].

The overexpression of Nox1 and hydrogen peroxide from NIH 3T3 cells as well as DU-145 cells was demonstrated to trigger the conversion of previous dormant tumors to the angiogenic phenotype, which indicates the progress of dormant tumors to active tumors. Nox1 led to a nearly 10-fold increase in hydrogen peroxide levels, 4-fold induction of VEGF mRNA in NIH 3T3 cells, and high-level expression of VEGFR1 and VEGFR2 in the newly growing blood vessels [65]. Zymographic analysis also showed that Nox1 expression induced increment of matrix metalloproteinase MMP-9 bioactivity [65]. The balance of protease and antiprotease activity in the vascular tissue is thought to play an important role in pathogenesis of aortic dissection and aneurysm as well as the process of angiogenesis. Matrix metalloproteinases are thought to favor the pathogenesis of vascular disease and promote new blood vessels formation, whereas the specific inhibitor tissue inhibitor of metalloproteinases (TIMPs) is thought to be preventive. In a hypertension animal model, angiotensin II increased TIMP-1 mRNA level in both Nox1 deficient mice and wild type mice but increased TIMP-1 mRNA protein levels much more tremendously in Nox1 deficient mice than wild type mice [60]. This indicated that Nox1 might be able to alter the protease and antiprotease equilibrium, which is critical for vascular tissue injury and wound healing.

Besides endothelial cells, vascular smooth muscle cells participate in new vessel development through cell migration, proliferation, and extracellular matrix production after tissue injury. Nox1 and its oxidant were shown in vitro to contribute to vascular smooth muscle cell proliferation and neointima formation induced by urokinase plasminogen activator (uPA) [68]. Basic fibroblast growth factor (bFGF) induced migration of vascular smooth muscle cells is mediated by Nox1 rather than Nox4, through phosphorylation of the adaptor protein paxillin, which is essential for migration and secretion of MMPs [16]. And an in vivo animal study demonstrated that Nox1 and Nox2 from medial and neointimal smooth muscle cells and adventitial fibroblasts contributed to the increased superoxide production 3 to 15 days after balloon injury of the rat carotid artery [69]. The activated Nox1 and oxidative stress may be critical to smooth muscle phenotypic modulation in restenosis. Furthermore, wire injury-induced neointima formation in the femoral artery, along with proliferation and apoptosis, was reduced in Nox1 knock out mice [70]. Compared to wild type

cells, in vitro cultured Nox1 knock out smooth muscle cells exhibited more phosphorylated cofilin (a regulator of actin depolymerization) both basally and after PDGF stimulation, without alteration of cofilin expression [70]. Phosphorylation of cofilin at Ser3 inhibits its activity, which is responsible for reduced migration of Nox1 deficient cells [70].

Nevertheless, it seems that Nox1 also can inhibit endothelial cell proliferation. Chronic treatment primary human umbilical vein endothelial cells with resveratrol (10 μM) elevated ROS levels (mainly from Nox1 and Nox4) that were linked to an accumulation of cells in S phase [71]. This indicates that Nox1 and other Nox proteins in vascular system have a complex regulation mechanism under different conditions, which needs specific research for targeting therapy.

6. Nox1 and ROS from Other Cells Involving Cell Damage and Dysfunction

As mentioned above Nox1 is broadly expressed in various cell types besides epithelial cell, endothelial cell, and vascular smooth muscle cell. Nox1 is expressed in BeWo choriocarcinoma cells, which can be activated by EGF [72]. This is further confirmed by the evidence that in placental tissues Nox1 was localized in syncytiotrophoblasts, in villous vascular endothelium, and in some stromal cells, which is increased in patients with preeclampsia [72]. Additionally, expression of Nox1 protein and ROS is increased in pancreatic beta cells in response to proinflammatory cytokines stimulation, which might lead to cell dysfunction and death [73]. Moreover, Nox1 is suggested to play critical roles in spermatogonial stem cells self-renewal via the activation of the p38 MAPK and JNK [74].

7. Nox1 and Inflammation

Inflammation following injury is the essential process for tissue repair. Inflammatory cells such as neutrophils and macrophages are major source of ROS, which are needed for scavenging bacteria and necrotic tissue. As mentioned above, the activation of Nox1 and rapid production of ROS could be induced by inflammatory cytokines like IL-13 and interferon-γ [36, 37]. Nox1 and its derived ROS further participate in intracellular signaling processes regulating gene expression, which contributes to cell proliferation, differentiation, and tissue repair.

ROS may serve as the primary signal inducing the migration of inflammatory cells directly after tissue injury. In a study performed on zebrafish larvae, a rapid and sustained increase of hydrogen peroxide at the wound margin was detected upon local injury of the tail fin, which occurred before the recruitment of leukocytes, suggesting that the source of hydrogen peroxide was the tail fin epithelium, not leukocytes [13]. This finding contrasts with the prevailing view that the ROS molecules found at the wound site are mainly produced by oxidative bursts of inflammatory cells. Furthermore, Duox1 in epithelium was shown to be the Nox isoform responsible for the early ROS production after epithelial injury [13]. As of now, there is no evidence indicating that local Nox1 can be activated upon tissue injury and form a ROS gradient activating migration of inflammatory cells, as its homologue Duox1 did in zebrafish. However, Nox1 and its derived ROS can indirectly affect inflammation by regulating inflammatory cytokines such as PGE_2, CCL2, CCL3, CXCL2, IL-1β, GM-CSF, and TNF-α [17, 30, 41].

8. Conclusion and Future Perspectives

NADPH oxidase, whose only function is ROS production, has been extensively investigated in many cell types of both mammalian and plant. Nox1, one member of the NADPH oxidase family, is not only constitutively expressed in a variety of tissues, but also induced to increase expression in both mRNA and protein levels under many circumstances. Nox1 is most expressed by intestinal epithelium and participates in the maintenance of epithelial barrier and mucosal homeostasis, including promoting intestinal mucosa wound healing by activation of focal cell matrix adhesion proteins and cell motility. It could also be induced and activated by growth factors, inflammatory cytokines, and UV injury in skin and mucosal keratinocytes in vitro, regulating cell proliferation, differentiation, and migration. In addition, Nox1 and ROS have been suggested to regulate cellular differentiation, ECM deposition, and fibrosis formation both in vitro and in vivo. As for in the processes of blood vessel damage and regeneration, Nox1 from smooth muscle cell and endothelial cell, together with some of its homologues (Nox2 and Nox4), is critical for vascular injury response and pathology. Nox1 and its derived ROS are also involved in inflammatory response caused by injury or infection through interaction with inflammatory cells. In short, Nox1 and its derived reactive oxygen species are crucial intracellular signaling regulators involving cell proliferation, differentiation, migration, extracellular matrix production and deposition, and inflammatory process after tissue injury, which contribute to the processes of tissue repair (Table 1).

Although a large number of evidence indicates that Nox1 has critical effect upon the process of tissue repair, there are many open questions regarding the complex mechanisms of Nox1. Nox1, as well as some of its homologues, has broad tissue and cellular distribution and is either constitutively expressed or stimulatively upregulated. One tissue or cell may express various NADPH oxidase molecules, and the same cell type in different tissues may have different dominant Nox isoforms at mRNA and protein levels [7, 15, 55–57]. Nox molecules are activated by different stimuli and present the function of proinjuring or protection [41, 75]. Cross talk exists between Nox homologues so that the activation of one Nox might further activate other Nox molecules in the same cell through the production and regulation of ROS [36, 76]. Additionally, Nox1 accomplishes its functions through complicated and unique intracellular signaling pathways upon disparate stimuli. Therefore, in order to get improved understanding of the roles of Nox1 in the process of tissue repair, the specificity of cell and tissue, the type of injury and severity of injury, the specific intracellular signaling, and the

Table 1: Nox1 expression, intracellular signaling, and function.

Cells involved	Intracellular signaling	Function	References
Intestinal epithelial cell; colon carcinoma cells (Caco2 and HT29)	IL13-Nox1-ERK/STAT6-TFF3/Bcl-xl; Nox1-RhoA-alpha3 integrin	Proliferation and differentiation; migration	[29, 36, 37, 40]
HaCaT; GM16	Ca^{2+}-Nox1-PGE_2; Ca^{2+}/serum-Nox1-vimentin/K8/K18	Proliferation and host defense; skin injury; apoptosis; migration	[17, 19, 22, 30, 31, 34, 38]
Lung epithelial cell	Nox1-JNK/ERK/Caspase-3	Cell death and protection	[18, 41]
Corneal stromal fibroblast		May participate in inflammation	[42]
Mouse embryonic fibroblast		Ischemia-reperfusion injury	[43]
NIH 3T3 fibroblast; rat kidney fibroblast	Ras-Nox1-Rho-actin stress fibers and focal adhesions	Tumorigenic conversion	[15, 35]
Fibrosarcoma L929 cells	TNF-TRADD/RIP1/Rac1/Nox1	Necrosis	[44]
Human BJ foreskin fibroblast and IMR-90 lung fibroblast	CCN1-Nox1/Rac-ERK/p38 MAPK-$p16^{INK4a}$ /pRb	Senescence and expression of antifibrotic genes	[52]
Mouse vessel	Angiotensin II-Nox1-nitric oxide	Hypertension	[59]
Mouse aorta	Angiotensin II-Nox1-tissue inhibitor of metalloproteinase 1	Aortic dissection	[60]
Human aortic endothelial cell	Hyperglycemia-Nox1-proinflammatory and profibrotic markers	Atherosclerosis	[61]
Rat kidney cell; tumor cells and vessel; sinusoidal endothelial cell	K-Ras-Nox1-ERK-sp1-VEGF; Nox1-VEGF/VEGFR/MMP	Upregulate VEFG expression; increase tumorigenicity and upregulate VEGF/VEGFR and MMP; tubulogenic	[64, 65, 67]
Vascular smooth muscle cell	uPA-Nox1/Nox4; PDGF-Nox1-cofilin	Migration; proliferation and necrosis	[68–70]

potential cross talk between various Nox homologues remain to be elucidated.

Conflict of Interests

The authors declare that there is no conflict of interests regarding the publication of this paper.

Acknowledgments

This study was supported partially by a Grant from Ph.D. Programs Foundation of Ministry of Education of China (20120073110088), a Grant from the Doctoral Innovative Fund at the School of Medicine, Shanghai Jiao Tong University (BXJ201238), and the Project of Shanghai "PU JIANG REN CAI" (10PJ1407000).

References

[1] M. Sasaki and T. Joh, "Oxidative stress and ischemia-reperfusion injury in gastrointestinal tract and antioxidant, protective agents," *Journal of Clinical Biochemistry and Nutrition*, vol. 40, no. 1, pp. 1–12, 2007.

[2] M. Elias-Miro, M. B. Jimenez-Castro, J. Rodes et al., "Current knowledge on oxidative stress in hepatic ischemia/reperfusion," *Free Radical Research*, vol. 47, no. 8, pp. 555–568, 2013.

[3] K. M. Venardos, A. Perkins, J. Headrick, and D. M. Kaye, "Myocardial ischemia-reperfusion injury, antioxidant enzyme systems, and selenium: a review," *Current Medicinal Chemistry*, vol. 14, no. 27, p. 2944, 2007.

[4] N. Suzuki, G. Miller, J. Morales, V. Shulaev, M. A. Torres, and R. Mittler, "Respiratory burst oxidases: the engines of ROS signaling," *Current Opinion in Plant Biology*, vol. 14, no. 6, pp. 691–699, 2011.

[5] C. K. Sen, "The general case for redox control of wound repair," *Wound Repair and Regeneration*, vol. 11, no. 6, pp. 431–438, 2003.

[6] S. Roy, S. Khanna, K. Nallu, T. K. Hunt, and C. K. Sen, "Dermal wound healing is subject to redox control," *Molecular Therapy*, vol. 13, no. 1, pp. 211–220, 2006.

[7] K. Bedard and K.-H. Krause, "The NOX family of ROS-generating NADPH oxidases: physiology and pathophysiology," *Physiological Reviews*, vol. 87, no. 1, pp. 245–313, 2007.

[8] J. Bylund, K. L. Brown, C. Movitz, C. Dahlgren, and A. Karlsson, "Intracellular generation of superoxide by the phagocyte NADPH oxidase: how, where, and what for?" *Free Radical Biology and Medicine*, vol. 49, no. 12, pp. 1834–1845, 2010.

[9] K.-H. Krause, "Tissue distribution and putative physiological function of NOX family NADPH oxidases," *Japanese Journal of Infectious Diseases*, vol. 57, no. 5, pp. S28–S29, 2004.

[10] B. Caillou, C. Dupuy, L. Lacroix et al., "Expression of reduced nicotinamide adenine dinucleotide phosphate oxidase (*Thox, LNOX, Duox*) genes and proteins in human thyroid tissues," *Journal of Clinical Endocrinology & Metabolism*, vol. 86, no. 7, pp. 3351–3358, 2001.

[11] P. W. Kleikers, K. Wingler, J. J. Hermans et al., "NADPH oxidases as a source of oxidative stress and molecular target in ischemia/reperfusion injury," *Journal of Molecular Medicine*, vol. 90, no. 12, pp. 1391–1406, 2012.

[12] I. Andreadou, E. K. Iliodromitis, D. Farmakis, and D. T. Kremastinos, "To prevent, protect and save the ischemic heart: antioxidants revisited," *Expert Opinion on Therapeutic Targets*, vol. 13, no. 8, pp. 945–956, 2009.

[13] P. Niethammer, C. Grabher, A. T. Look, and T. J. Mitchison, "A tissue-scale gradient of hydrogen peroxide mediates rapid wound detection in zebrafish," *Nature*, vol. 459, no. 7249, pp. 996–999, 2009.

[14] E. C. Chan, F. Jiang, H. M. Peshavariya, and G. J. Dusting, "Regulation of cell proliferation by NADPH oxidase-mediated signaling: potential roles in tissue repair, regenerative medicine and tissue engineering," *Pharmacology & Therapeutics*, vol. 122, no. 2, pp. 97–108, 2009.

[15] Y.-A. Suh, R. S. Arnold, B. Lassegue et al., "Cell transformation by the superoxide-generating oxidase Mox1," *Nature*, vol. 401, no. 6748, pp. 79–82, 1999.

[16] K. Schröder, I. Helmcke, K. Palfi, K.-H. Krause, R. Busse, and R. P. Brandes, "Nox1 mediates basic fibroblast growth factor-induced migration of vascular smooth muscle cells," *Arteriosclerosis, Thrombosis, and Vascular Biology*, vol. 27, no. 8, pp. 1736–1743, 2007.

[17] A. Valencia and I. E. Kochevar, "Nox1-based NADPH oxidase is the major source of UVA-induced reactive oxygen species in human keratinocytes," *Journal of Investigative Dermatology*, vol. 128, no. 1, pp. 214–222, 2008.

[18] S. Carnesecchi, C. Deffert, A. Pagano et al., "NADPH oxidase-1 plays a crucial role in hyperoxia-induced acute lung injury in mice," *American Journal of Respiratory and Critical Care Medicine*, vol. 180, no. 10, pp. 972–981, 2009.

[19] H.-J. Nam, Y.-Y. Park, G. Yoon, H. Cho, and J.-H. Lee, "Co-treatment with hepatocyte growth factor and TGF-β1 enhances migration of HaCaT cells through NADPH oxidase-dependent ROS generation," *Experimental & Molecular Medicine*, vol. 42, no. 4, pp. 270–279, 2010.

[20] H. Sumimoto, K. Miyano, and R. Takeya, "Molecular composition and regulation of the Nox family NAD(P)H oxidases," *Biochemical and Biophysical Research Communications*, vol. 338, no. 1, pp. 677–686, 2005.

[21] T. Kawahara, D. Ritsick, G. Cheng, and J. D. Lambeth, "Point mutations in the proline-rich region of $p22^{phox}$ are dominant inhibitors of Nox1- and Nox2-dependent reactive oxygen generation," *The Journal of Biological Chemistry*, vol. 280, no. 36, pp. 31859–31869, 2005.

[22] W. Chamulitrat, W. Stremmel, T. Kawahara et al., "A constitutive NADPH oxidase-like system containing $gp91^{phox}$ homologs in human keratinocytes," *Journal of Investigative Dermatology*, vol. 122, no. 4, pp. 1000–1009, 2004.

[23] G. Cheng, B. A. Diebold, Y. Hughes, and J. D. Lambeth, "Nox1-dependent reactive oxygen generation is regulated by Rac1," *The Journal of Biological Chemistry*, vol. 281, no. 26, pp. 17718–17726, 2006.

[24] F. Jiang, Y. Zhang, and G. J. Dusting, "NADPH oxidase-mediated redox signaling: roles in cellular stress response, stress tolerance, and tissue repair," *Pharmacological Reviews*, vol. 63, no. 1, pp. 218–242, 2011.

[25] B. Lassègue, D. Sorescu, K. Szöcs et al., "Novel $gp91^{phox}$ homologues in vascular smooth muscle cells: Nox1 mediates angiotensin II-induced superoxide formation and redox-sensitive signaling pathways," *Circulation Research*, vol. 88, no. 9, pp. 888–894, 2001.

[26] Y. Ge, W. Jiang, L. Gan et al., "Mouse embryonic fibroblasts from CD38 knockout mice are resistant to oxidative stresses through inhibition of reactive oxygen species production and Ca^{2+} overload," *Biochemical and Biophysical Research Communications*, vol. 399, no. 2, pp. 167–172, 2010.

[27] S. Teshima, H. Kutsumi, T. Kawahara, K. Kishi, and K. Rokutan, "Regulation of growth and apoptosis of cultured guinea pig gastric mucosal cells by mitogenic oxidase 1," *American Journal of Physiology—Gastrointestinal and Liver Physiology*, vol. 279, no. 6, pp. G1169–G1176, 2000.

[28] F. J. Miller Jr., M. Filali, G. J. Huss et al., "Cytokine activation of nuclear factor κB in vascular smooth muscle cells requires signaling endosomes containing Nox1 and ClC-3," *Circulation Research*, vol. 101, no. 7, pp. 663–671, 2007.

[29] M. Geiszt, K. Lekstrom, S. Brenner et al., "NAD(P)H oxidase 1, a product of differentiated colon epithelial cells, can partially replace glycoprotein 91^{phox} in the regulated production of superoxide by phagocytes," *Journal of Immunology*, vol. 171, no. 1, pp. 299–306, 2003.

[30] A. Valencia, A. Rajadurai, A. B. Carle, and I. E. Kochevar, "7-Dehydrocholesterol enhances ultraviolet A-induced oxidative stress in keratinocytes: roles of NADPH oxidase, mitochondria, and lipid rafts," *Free Radical Biology and Medicine*, vol. 41, no. 11, pp. 1704–1718, 2006.

[31] H.-C. Ryu, C. Kim, J.-Y. Kim, J.-H. Chung, and J.-H. Kim, "UVB radiation induces apoptosis in keratinocytes by activating a pathway linked to 'BLT2-reactive oxygen species'," *Journal of Investigative Dermatology*, vol. 130, no. 4, pp. 1095–1106, 2010.

[32] K. Carter, "Growth factors: the wound healing therapy of the future," *British Journal of Community Nursing*, vol. 8, no. 9, pp. S15–S30, 2003.

[33] X. J. Wang, G. Han, P. Owens et al., "Role of TGF β-mediated inflammation in cutaneous wound healing," *Journal of Investigative Dermatology*, vol. 11, no. 1, pp. 112–117, 2006.

[34] J.-S. Kim, E.-J. Bak, B.-C. Lee, Y.-S. Kim, J.-B. Park, and I.-G. Choi, "Neuregulin induces HaCaT keratinocyte migration via Rac1-mediated NADPH-oxidase activation," *Journal of Cellular Physiology*, vol. 226, no. 11, pp. 3014–3021, 2011.

[35] M. Shinohara, W.-H. Shang, M. Kubodera et al., "Nox1 redox signaling mediates oncogenic Ras-induced disruption of stress fibers and focal adhesions by down-regulating Rho," *The Journal of Biological Chemistry*, vol. 282, no. 24, pp. 17640–17648, 2007.

[36] D. Mandal, P. Fu, and A. D. Levine, "REDOX regulation of IL-13 signaling in intestinal epithelial cells: usage of alternate pathways mediates distinct gene expression patterns," *Cellular Signalling*, vol. 22, no. 10, pp. 1485–1494, 2010.

[37] Y. Kuwano, T. Kawahara, H. Yamamoto et al., "Interferon-γ activates transcription of NADPH oxidase 1 gene and upregulates production of superoxide anion by human large intestinal epithelial cells," *American Journal of Physiology—Cell Physiology*, vol. 290, no. 2, pp. C433–C443, 2006.

[38] W. Chamulitrat, A. Huber, H.-D. Riedel, and W. Stremmel, "Nox1 induces differentiation resistance in immortalized human keratinocytes generating cells that express simple epithelial keratins," *Journal of Investigative Dermatology*, vol. 127, no. 9, pp. 2171–2183, 2007.

[39] F. Liu, A. M. Gomez Garcia, and F. L. Meyskens Jr., "NADPH oxidase 1 overexpression enhances invasion via matrix metalloproteinase-2 and epithelial-mesenchymal transition in melanoma cells," *Journal of Investigative Dermatology*, vol. 132, no. 8, pp. 2033–2041, 2012.

[40] A. Sadok, A. Pierres, L. Dahan, C. Prévôt, M. Lehmann, and H. Kovacic, "NADPH oxidase 1 controls the persistence of directed cell migration by a Rho-dependent switch of $\alpha 2/\alpha 3$ integrins," *Molecular and Cellular Biology*, vol. 29, no. 14, pp. 3915–3928, 2009.

[41] S. Selemidis, H. J. Seow, B. R. Broughton et al., "Nox1 oxidase suppresses influenza A virus-induced lung inflammation and oxidative stress," *PLoS ONE*, vol. 8, no. 4, Article ID e60792, 2013.

[42] W. J. O'Brien, T. Heimann, and F. Rizvi, "NADPH oxidase expression and production of superoxide by human corneal stromal cells," *Molecular vision*, vol. 15, pp. 2535–2543, 2009.

[43] Y. Ge, W. Jiang, L. Gan et al., "Mouse embryonic fibroblasts from CD38 knockout mice are resistant to oxidative stresses through inhibition of reactive oxygen species production and Ca^{2+} overload," *Biochemical and Biophysical Research Communications*, vol. 399, no. 2, pp. 167–172, 2010.

[44] Y.-S. Kim, M. J. Morgan, S. Choksi, and Z.-G. Liu, "TNF-induced activation of the Nox1 NADPH Oxidase and its role in the induction of necrotic cell death," *Molecular Cell*, vol. 26, no. 5, pp. 675–687, 2007.

[45] L. Gao, W. Huang, and J. Li, "NOX1 abet mesangial fibrogenesis via iNOS induction in diabetes," *Molecular and Cellular Biochemistr*, vol. 381, no. 1-2, pp. 185–191, 2013.

[46] J. S. Grewal, Y. V. Mukhin, M. N. Garnovskaya, J. R. Raymond, and E. L. Greene, "Serotonin 5-HT_{2A} receptor induces TGF-β1 expression in mesangial cells via ERK: proliferative and fibrotic signals," *American Journal of Physiology—Renal Physiology*, vol. 276, no. 6, part 2, pp. F922–F930, 1999.

[47] P. A. Craven, S. L. Phillips, M. F. Melhem, J. Liachenko, and F. R. DeRubertis, "Overexpression of manganese superoxide dismutase suppresses increases in collagen accumulation induced by culture of mesangial cells in high-media glucose," *Metabolism*, vol. 50, no. 9, pp. 1043–1048, 2001.

[48] W. Zhao, S. S. Chen, Y. Chen, R. A. Ahokas, and Y. Sun, "Kidney fibrosis in hypertensive rats: role of oxidative stress," *American Journal of Nephrology*, vol. 28, no. 4, pp. 548–554, 2008.

[49] A. R. Chade, M. Rodriguez-Porcel, J. Herrmann et al., "Beneficial effects of antioxidant vitamins on the stenotic kidney," *Hypertension*, vol. 42, no. 4, pp. 605–612, 2003.

[50] C.-C. Chen and L. F. Lau, "Functions and mechanisms of action of CCN matricellular proteins," *International Journal of Biochemistry & Cell Biology*, vol. 41, no. 4, pp. 771–783, 2009.

[51] C.-C. Chen, F.-E. Mo, and L. F. Lau, "The angiogenic factor Cyr61 activates a genetic program for wound healing in human skin fibroblasts," *The Journal of Biological Chemistry*, vol. 276, no. 50, pp. 47329–47337, 2001.

[52] J.-I. Jun and L. F. Lau, "The matricellular protein CCN1 induces fibroblast senescence and restricts fibrosis in cutaneous wound healing," *Nature Cell Biology*, vol. 12, no. 7, pp. 676–685, 2010.

[53] T. Tojo, M. Ushio-Fukai, M. Yamaoka-Tojo, S. Ikeda, N. Patrushev, and R. W. Alexander, "Role of $gp91^{phox}$ (Nox2)-containing NAD(P)H oxidase in angiogenesis in response to hindlimb ischemia," *Circulation*, vol. 111, no. 18, pp. 2347–2355, 2005.

[54] M. Ushio-Fukai, "Redox signaling in angiogenesis: role of NADPH oxidase," *Cardiovascular Research*, vol. 71, no. 2, pp. 226–235, 2006.

[55] R. P. Brandes and K. Schröder, "Composition and functions of vascular nicotinamide adenine dinucleotide phosphate oxidases," *Trends in Cardiovascular Medicine*, vol. 18, no. 1, pp. 15–19, 2008.

[56] B. Lassègue and R. E. Clempus, "Vascular NAD(P)H oxidases: specific features, expression, and regulation," *American Journal of Physiology—Regulatory Integrative and Comparative Physiology*, vol. 285, no. 2, pp. R277–R297, 2003.

[57] I. Takac, K. Schröder, and R. P. Brandes, "The Nox family of NADPH oxidases: friend or foe of the vascular system?" *Current Hypertension Reports*, vol. 14, no. 1, pp. 70–78, 2012.

[58] L. Ahmarani, L. Avedanian, J. Al-Khoury et al., "Whole-cell and nuclear NADPH oxidases levels and distribution in human endocardial endothelial, vascular smooth muscle, and vascular endothelial cells," *Canadian Journal of Physiology and Pharmacology*, vol. 91, no. 1, pp. 71–79, 2013.

[59] K. Matsuno, H. Yamada, K. Iwata et al., "Nox1 is involved in angiotensin II-mediated hypertension: a study in Nox1-deficient mice," *Circulation*, vol. 112, no. 17, pp. 2677–2685, 2005.

[60] G. Gavazzi, C. Deffert, C. Trocme, M. Schäppi, F. R. Herrmann, and K.-H. Krause, "NOX1 deficiency protects from aortic dissection in response to angiotensin II," *Hypertension*, vol. 50, no. 1, pp. 189–196, 2007.

[61] S. P. Gray, E. Di Marco, J. Okabe et al., "NADPH oxidase 1 plays a key role in diabetes mellitus-accelerated atherosclerosis," *Circulation*, vol. 127, no. 18, pp. 1888–1902, 2013.

[62] T. Matsumoto and L. Claesson-Welsh, "VEGF receptor signal transduction," *Science's STKE*, vol. 2001, no. 112, article re21, 2001.

[63] M. Ushio-Fukai, "VEGF signaling through NADPH oxidase-derived ROS," *Antioxidants & Redox Signaling*, vol. 9, no. 6, pp. 731–739, 2007.

[64] D. Komatsu, M. Kato, J. Nakayama, S. Miyagawa, and T. Kamata, "NADPH oxidase 1 plays a critical mediating role in oncogenic Ras-induced vascular endothelial growth factor expression," *Oncogene*, vol. 27, no. 34, pp. 4724–4732, 2008.

[65] J. L. Arbiser, J. Petros, R. Klafter et al., "Reactive oxygen generated by Nox1 triggers the angiogenic switch," *Proceedings of the National Academy of Sciences of the United States of America*, vol. 99, no. 2, pp. 715–720, 2002.

[66] A. Görlach, R. P. Brandes, K. Nguyen, M. Amidi, F. Dehghani, and R. Busse, "A $gp91^{phox}$ containing NADPH oxidase selectively expressed in endothelial cells is a major source of oxygen radical generation in the arterial wall," *Circulation Research*, vol. 87, no. 1, pp. 26–32, 2000.

[67] S. Kobayashi, Y. Nojima, M. Shibuya, and Y. Maru, "Nox1 regulates apoptosis and potentially stimulates branching morphogenesis in sinusoidal endothelial cells," *Experimental Cell Research*, vol. 300, no. 2, pp. 455–462, 2004.

[68] M. Menshikov, O. Plekhanova, H. Cai et al., "Urokinase plasminogen activator stimulates vascular smooth muscle cell proliferation via redox-dependent pathways," *Arteriosclerosis, Thrombosis, and Vascular Biology*, vol. 26, no. 4, pp. 801–807, 2006.

[69] K. Szocs, B. Lassegue, D. Sorescu et al., "Upregulation of Nox-based NAD(P)H oxidases in restenosis after carotid injury,"

Arteriosclerosis, Thrombosis, and Vascular Biology, vol. 22, no. 1, pp. 21–27, 2002.

[70] M. Y. Lee, A. S. Martin, P. K. Mehta et al., "Mechanisms of vascular smooth muscle NADPH oxidase 1 (Nox1) contribution to injury-induced neointimal formation," *Arteriosclerosis, Thrombosis, and Vascular Biology*, vol. 29, no. 4, pp. 480–487, 2009.

[71] Y. D. C. Schilder, E. H. Heiss, D. Schachner et al., "NADPH oxidases 1 and 4 mediate cellular senescence induced by resveratrol in human endothelial cells," *Free Radical Biology and Medicine*, vol. 46, no. 12, pp. 1598–1606, 2009.

[72] X.-L. Cui, D. Brockman, B. Campos, and L. Myatt, "Expression of NADPH oxidase isoform 1 (Nox1) in human placenta: involvement in preeclampsia," *Placenta*, vol. 27, no. 4-5, pp. 422–431, 2006.

[73] J. R. Weaver and D. A. Taylor-Fishwick, "Regulation of NOX-1 expression in beta cells: a positive feedback loop involving the Src-kinase signaling pathway," *Molecular and Cellular Endocrinology*, vol. 369, no. 1-2, pp. 35–41, 2013.

[74] H. Morimoto, K. Iwata, N. Ogonuki et al., "ROS are required for mouse spermatogonial stem cell self-renewal," *Cell Stem Cell*, vol. 12, no. 6, pp. 774–786, 2013.

[75] P. Fu, V. Mohan, S. Mansoor et al., "Role of nicotinamide adenine dinucleotide phosphate-reduced oxidase proteins in *Pseudomonas aeruginosa*-induced lung inflammation and permeability," *American Journal of Respiratory Cell and Molecular Biology*, vol. 48, no. 4, pp. 477–488, 2013.

[76] D. P. O'Leary, L. Bhatt, J. F. Woolley et al., "TLR-4 signalling accelerates colon cancer cell adhesion via NF-κB mediated transcriptional up-regulation of Nox-1," *PLoS ONE*, vol. 7, no. 10, Article ID e44176, 2012.

Hindawi Publishing Corporation
Oxidative Medicine and Cellular Longevity
Volume 2014, Article ID 345105, 13 pages
http://dx.doi.org/10.1155/2014/345105

Research Article

Antiaging Properties of a Grape-Derived Antioxidant Are Regulated by Mitochondrial Balance of Fusion and Fission Leading to Mitophagy Triggered by a Signaling Network of Sirt1-Sirt3-Foxo3-PINK1-PARKIN

Somak Das,[1] Goran Mitrovsky,[2] Hannah R. Vasanthi,[3] and Dipak K. Das[1,4]

[1] *Cardiovascular Research Center, University of Connecticut School of Medicine, Farmington, CT, USA*
[2] *Laboratory of Physiologic Studies, Department of Molecular Biology and Biochemistry, Debrecen University, Debrecen, Hungary*
[3] *Department of Biotechnology, School of Life Sciences, Pondicherry University, Pondicherry, India*
[4] *Center for Medicinal Food and Applied Nutrition, Jadavpur University, Jadavpur, Kolkata, India*

Correspondence should be addressed to Dipak K. Das; ddas054@gmail.com

Received 14 August 2013; Revised 17 October 2013; Accepted 18 October 2013; Published 12 January 2014

Academic Editor: Yanfang Chen

It was proposed that resveratrol, a polyphenolic antioxidant and a calorie restriction mimetic could promote longevity but subsequent studies could not prove this. The original proposal was based on the fact that a grape-derived antioxidant could activate the antiaging gene Sirt1. Most studies agree that indeed grape activates Sirt1, but a question remains whether Sirt1 is the cause or consequence of resveratrol treatment. Subsequently, mitochondrial Sirt3 was found to be activated. The present study on ischemic reperfusion (I/R) in rat hearts demonstrates that Foxo3a is activated subsequent to Sirt3 activation, which then activates PINK1. PINK1 potentiates activation of PARKIN leading to the activation of mitochondrial fission and mitophagy. Confocal microscopy conclusively shows the coexistence of Sirt3 with Foxo3a and Foxo3a with PINK1 and PARKIN. Mitophagy was demonstrated both by confocal microscopy and transmission electron microscopy. Western blot analyses data are consistent with the results of confocal microscopy. It appears that the grape-derived antioxidant modifies the intracellular environment by changing the oxidizing milieu into a reducing milieu and upregulating intracellular glutathione, potentiates a signal transduction cascade consisting of Sirt1/Sirt3-Foxo3a-PINK1-PARKIN-mitochondrial fusion fission-mitophagy that leads to cardioprotection, and paves the way to an anti-aging environment.

1. Introduction

A growing body of evidence supports the crucial role of mitochondrial dynamics in aging process. Mitochondrial dysfunctions caused by morphological alterations and mitochondrial mtDNA mutations are intimately involved in aging [1]. Mitochondrion is continuously remodeled by two opposite processes, fusion and fission, contributing to mitochondrial dynamics. Fusion causes mixing of the intact mitochondria with slightly dysfunctional mitochondrial dynamics thereby replacing damaged mitochondrial DNA and restoring mitochondrial integrity [2]. Fission, on the other hand, sequesters irreversibly damaged mitochondria that are eliminated by the process involving autophagy of mitochondria (mitophagy) [3].

Mutations of PTEN-induced kinase 1 (PINK-1), a mitochondrial Ser/Thr kinase, regulate the oxidative phosphorylation machinery through mitochondrial fission [4]. PINK-1 activity is crucial for the development of heart through its role in maintaining mitochondrial function and redox homeostasis in cardiomyocytes [5]. PINK-1 in turn activates PARKIN, which translocates to depolarized mitochondria and promotes their degradation by mitophagy [6]. Thus, PINK-1 and PARKIN, with PARKIN acting downstream

of PINK-1, act to maintain mitochondrial homeostasis. It appears that PINK-1/PARKIN pathway may act synergistically to promote fission by blocking fusion thereby promoting mitophagy.

A recent study has demonstrated that a member of the Forkhead box, subgroup O (FoxO) transcription factors FoxO3, controls PINK-1 transcription in both mouse and human cells subjected to growth factor deprivation through evolutionary conserved FoxO binding elements [7]. The authors of this study identified Foxo3a as a key transcription factor directing the expression of PINK-1 in cells deprived of growth factors. Interestingly, it has been known that mitochondrial sirtuin, Sirt3, interacts and regulates the activity of Foxo3a in mitochondria [8]. In this study, the authors showed that overexpression of Sirt3 gene increases Foxo3a DNA binding activity as well as Foxo3a dependent gene expression.

It has long been known that calorie restriction promotes longevity, and several recent studies have indicated that resveratrol, a polyphenolic antioxidant, a calorie restriction mimetic could promote longevity [9, 10]. The antiaging effects of resveratrol are believed to be mediated by the activation of Sirt1 and reduced oxidative stress [11]. Unfortunately, subsequent studies could not confirm antiaging effects of resveratrol nor the role of Sirt1 in promoting antiaging effects [12]. Recently, several studies determined the importance of Sirt3 along with FoxO3 in addition to Sirt1, in promoting antiaging function of resveratrol [13]. This study was designed to determine if Sirt3 and Foxo3a comprise the initial mitochondrial signaling response to activate PINK-1/PARKIN thereby promoting mitophagy through the activation of mitochondrial fission. The results of our study demonstrated that Sirt3 in cooperation with Sirt1 indeed activates FoxO3 thereby promoting the activation of PINK-1/PARKIN pathway leading to mitochondrial fission and mitophagy. It is tempting to speculate that resveratrol promotes antiaging functions through this signaling pathway comprising Sirt3-Foxo3a-PINK1-PARKIN-mitochondrial fusion/fission-mitophagy.

2. Materials and Methods

2.1. Chemicals. Resveratrol was of analytical grade and obtained from Sigma-Aldrich chemical company (St. Louis, MO, USA). Longevinex (modified resveratrol) was a gift from Bill Sardi, Longevinex LLC (San Dimas, CA, USA). All other chemicals were of analytical grade and were obtained from Sigma-Aldrich chemical company, unless otherwise specified. Antibodies of Sirt1, Sirt3, Foxo3a, PINK1, PARKIN, and TOM 20 were obtained from either Cell Signaling, Boston, MA, USA, or Santa Cruz Biotechnology, CA, USA.

2.2. Animals. All animals used in this study received humane care in compliance with the principles of the laboratory animal care formulated by the National Society for Medical Research and Guide for the Care and Use of Laboratory Animals prepared by the National Academy of Sciences and published by the National Institute of Health (Publication Number NIH 85-23, revised 1996). Sprague-Dawley male rats weighing between 250 and 300 g were fed *ad libitum* regular rat chow (Harlan Teklad, Madison, WI, USA) with free access to water until the start of the experimental procedure that is, ischemic reperfusion (I/R) injury. The rats were randomly assigned to one of the following groups: control I/R, resveratrol treated-I/R, and longevinex treated-I/R. A total of 2.5 mg/kg/day resveratrol or longevinex was gavaged to the animals for 15 days. Previous studies from our laboratory established the appropriate dose and time periods for each compound used in this experiment both on normal and I/R treated [14, 15].

2.3. Isolated Working Heart Preparation. After completing the feeding protocol, the animals were anaesthetized with sodium pentobarbital (80 mg/kg, i.p.) (Abbott Laboratories, North Chicago, IL, USA) intraperitoneally and heparin sodium (500 IU/kg., i.v.) (Elkins-Sinn Inc., Cherry Hill, NJ, USA) was used as an anticoagulant. After deep anaesthesia was conformed, hearts were excised, the aorta was cannulated, and the hearts were perfused through the aorta in a Langendorff mode at a constant (100 cm of water) perfusion pressure at 37°C with the KHB for a 5-min washout period as described previously [14]. The perfusion medium consisted of a modified Krebs-Henseleit bicarbonate buffer (millimolar concentration: sodium chloride 118, potassium chloride 4.7, calcium chloride 1.7, sodium bicarbonate 25, potassium dihydrogenphosphate 0.36, magnesium sulphate 1.2, and glucose 10), and after its oxygenation, pH was 7.4 at 37°C. During the washout period, left atria was cannulated, and the Langendorff preparation was switched to the working mode for 10 min with a left atrial filling pressure of 17 cm H_2O; aortic afterload pressure was set to 100 cm of water. At the end of 10 min, baseline cardiac functions like heart rate (HR, beats/min), aortic flow (AF, mL/min), coronary flow (CF, mL/min), left ventricular developed pressure (LVDP, mmHg), and first derivative of developed pressure (LVdp/dt, mmHg/sec.) were recorded. After that, 30 min of global ischemia was initiated by clamping the left atrial inflow and aortic outflow lines at a point close to their origins. At the end of 30 min of ischemia, reperfusion was initiated for 120 min by unclamping the atrial inflow and aortic outflow lines. The first 10 min reperfusion was in Langendorff mode to avoid the ventricular fibrillations, after the hearts were switched to antigrade working mode [16].

2.4. Cardiac Function Assessment. After 10 min of working mode perfusion, baseline parameters were recorded. To monitor the recovery of the heart, the left ventricular cardiac function was recorded after 60 and 120 min of reperfusion [16, 17]. A calibrated flow-meter (Gilmont Instrument Inc., Barrington, IL, USA) was used to measure the aortic flow (AF). Coronary flow (CF) was measured by timed collection of the coronary effluent dripping from the heart. During the entire experiment, aortic pressure was monitored using a Gould P23XL pressure transducer (Gould Instrument Systems Inc., Valley View, OH, USA) connected to a side arm of the aortic cannula; the signal was amplified using a Gould 6600 series signal conditioner, 0.8 CORDAT II real-time data

acquisition and analysis system (Triton Technologies, San Diego, CA, USA) [17]. Heart rate (HR), left ventricular developed pressure (LVDP), and the first derivative of developed pressure (LVdp/dt) were all calculated from the continuously generated pressure signal.

2.5. Infarct Size Estimation. Infarct size was measured according to the triphenyl tetrazolium chloride (TTC) method. After 2 hrs of reperfusion, 40 mL of 1% (w/v) solution of TTC in phosphate buffer was infused into aortic cannula, and the heart samples were stored at −70°C for subsequent analysis. Sections of frozen heart were fixed in 2% paraformaldehyde, placed between two cover slips, and digitally imaged using a Microtek ScanMaker 600z. To quantitate the areas of infarct in pixels, standard NIH image program was used. The infarct size was quantified and expressed in pixels [16].

2.6. Assessment of Apoptotic Cell Death. Immunohistochemical detection of apoptotic cells was carried out using the Tdt-mediated dUTP-biotin nick end labeling (TUNEL) method (Promega, Madison, WI, USA) [17]. Briefly, after the isolated heart experiments, the heart tissues were immediately put in 10% formalin and fixed in an automatic tissue fixing machine. The tissues were carefully embedded in the molten paraffin in metallic blocks. Prior to analysis of tissues for apoptosis, the samples were sectioned and placed on a glass slide. The tissue sections were deparaffinized with xylene, washed and rehydrated by sequential washing with different concentrations of ethanol (absolute, 95%, 85%, 70%, and 50%). Then the TUNEL staining was performed according to the manufacturer's instructions. The fluorescence staining was viewed with a fluorescence microscope (AXIOPLAN2 IMAGING, Carl Zeiss Microimaging Inc., NY, USA) at 520 nm for green fluorescence of fluorescein and at 620 nm for red fluorescence of propidium iodide. The number of apoptotic cells was counted and expressed as a percent of total myocyte population.

2.7. Assessment of Intracellular Reactive Oxygen Species (ROS) with CM-H_2DCFDA. Since resveratrol functions by changing ischemia/reperfusion-mediated harmful oxidative environment into a reducing environment, intracellular ROS concentration was determined with CMH_2DCFDA [5-(and -6)-chloromethyl-2′,7′-dichlorodihydrofluorescein diacetate, acetyl ester] [10 μM; Molecular Probes, Eugene, OR] [18]. A derivative of DCF-DA, with an additional thiol reactive chloromethyl group, enhances the ability of the compound to bind to intracellular components, thereby prolonging the dye's cellular retention. The dye was injected intravenously, prior to induction of ischemia/reperfusion, and at the end of the experiments, the level of fluorescence was determined for the generation of ROS by measuring the fluorescent oxidation product CM-DCF in the cytosol, at an excitation wavelength of 480 nm, and an emission wavelength of 520 nm.

2.8. Determination of Intracellular Glutathione Level (GSH). Since activation of FoxO3-PINK1 pathway is directly linked with (GSH) level of the tissue, we determined the intracellular GSH activity of the heart [19]. Total GSH level was determined with a GSH assay kit obtained from Oxford Biomedical Research, Oxford, MI, USA.

2.9. Western Blot Analysis. Left ventricles from the hearts were homogenized in 1 mL of buffer (25 mM Tris-HCl, 25 mM NaCl, 1 mM orthovanadate, 10 mM NaF, 10 mM pyrophosphate, 10 mM okadaic acid, 0.5 mM EDTA, 1 mM PMSF, and 1_protease inhibitor cocktail). The homogenates were centrifuged at 2000 rpm at 4°C for 10 min The supernatant was centrifuged at 10,000 rpm at 4°C for 20 min The resultant supernatant was the cytosolic fraction. The cytosolic extracts were aliquoted, snap frozen, and stored at 80°C until use. Total protein concentrations in the cytosolic extracts were determined using a BCA Protein Assay Kit (Pierce, Rockford, IL, USA) [20]. Proteins were separated in SDS-PAGE and transferred to nitrocellulose membranes. The membranes were blocked in 5% nonfat dry milk and probed with primary antibody 1 : 1000 dilution overnight. The following primary antibodies were obtained from Cell Signaling Technology (Boston, MA, USA): Sirt1, Sirt3, and Foxo3a. Whereas, PINK1, PARKIN, and TOM20 were obtained from Santa Cruz Biotechnology (Santa Cruz, CA, USA). The protein bands were detected using horseradish peroxidase conjugated secondary antibody (1 : 2000 dilution) and Western blot luminol reagent (Santa Cruz Biotechnology). GAPDH was used for the cytosolic loading control. The bands were digitized, subjected to densitometric scanning using a standard NIH image program, and normalized against the loading control.

2.10. Transmission Electron Microscopy. A small sample of myocardium from control, IR resveratrol, and longevinex treated hearts was fixed in 4% glutaraldehyde. For the correct identification of autophagosomes by transmission electron microscopy (TEM), we have used the helpful notes detailed in two articles [21, 22]. Membrane contrast was enhanced using an osmium-ferrocyanide mixture in 0.1 M cacodylate buffer in the postfixation step. Subsequently, the samples were dehydrated, infiltrated, and embedded in Epon 812 at 60°C for 48 hrs. Light microscopy was performed on 1 μm semithin section stained with 1% toluidine blue and digital images were recorded using a CCD Axiocam HRcZeiss camera with AxioVision software (Carl Zeiss Imaging solution GmbH, Germany) on Nikon Eclipse E600 microscope (Nikon Instruments, Inc.). Routine 60 nm ultrathin sections were cut with a diamond knife, mounted on formwar-coated grids, and stained with 1% uranyl acetate and Reynolds's lead citrate. Ultrathin sections were examined using a Morgagni 286 TEM (FEI Company, Eindhoven, The Netherlands) at 60 kV. Digital electron micrographs were recorded with a MegaView III CCD using iTEM-SIS software (Olympus, Soft Imaging System GmbH, Germany).

2.11. Confocal Microscopy Imaging Techniques and Image Analysis. Heart tissue samples were collected at the end of experiments, fixed in 2% buffered paraformaldehyde (pH 7.4), embedded and frozen in O.C.T. compound, and subjected to cryosectioning. The obtained specimens (5-μm cuts) were processed for immunofluorescence analysis as described previously [23]. Primary antibodies against Sirt3 (rabbit IgG from Santa Cruz Biotechnology, Inc), PARKIN (rabbit IgG from Abcam), Foxo3a (goat IgG from Abcam), PINK1 (goat IgG from Abcam), Tom20 (mouse IgG from Abcam), and LC3 (rabbit and goat IgG from Santa Cruz Biotechnology, Inc) were used with optimal dilution of 1 : 250. This was followed by incubation with secondary fluorochrome-conjugated antibody and nuclei counterstaining with Hoechst 33342 (Molecular Probes, Inc., Eugene OR) diluted 1 : 3000. The secondary antibodies used were donkey IgG raised against goat, rabbit, and mouse immunoglobulins and were conjugated with the Alexa Fluor 488, Alexa Fluor 594, and Alexa Fluor 647 dyes. Negative controls for nonspecific binding included normal donkey serum without primary antibody or with secondary antibody alone. The labeled specimens were rinsed, mounted in Gelvatol (Monsanto Corp., St. Louis, MO), and placed under a cover slip for fluorescence microscopy. The background fluorescence was determined for each of the analyzed images of the immunolabeled proteins using images from specimens labeled with secondary antibodies only. Confocal fluorescence was captured with a Zeiss LSM 7100 microscope. Processing and analysis of digital images were conducted using Simple PCI High Performance Imaging software (Compix Inc., Hamamatsu Co., http://www.cimaging.net/) and Image software (http://rsb.info.nih.gov/).

3. Results

3.1. Effects of Resveratrol and Longevinex on the ROS Content and Intracellular Glutathione Concentration of the Heart. Intracellular ROS activity determined by monitoring the level of fluorescence by measuring the fluorescent oxidation product CM-DCF in the cytosol is shown in Figure 1(a). Both resveratrol and longevinex lowered intracellular ROS concentration to the same extent, without any significant difference. Intracellular glutathione concentration is shown in Figure 1(b).

3.2. Effects of Resveratrol and Longevinex on Postischemic Ventricular Recovery, Reduction of Infarct Size, and Cardiomyocyte Apoptosis. Table 1 shows the recovery of postischemic ventricular function such as CF, AF, LVDP, and LVdp/dt of isolated hearts subjected to 30 min global ischemia followed by 120 min of reperfusion. As expected, both resveratrol and longevinex treatment protected the hearts against ischemia/reperfusion injury as evidenced by improved postischemic AF, LVDP, and LVdp/dt in comparison with the vehicle treated group (Table 1). However, there were no significant differences between the resveratrol or longevinex treated groups.

Both resveratrol and longevinex treatments significantly reduced I/R-induced infarct size compared to the drug-free control (Table 1). There were no statistically significant differences between resveratrol and longevinex treated groups. As the infarct size is contributed from both necrosis and apoptosis, we estimated the apoptosis by employing TUNEL assay. In consonance with the infarct size, both resveratrol and longevinex significantly decreased the percentage of apoptotic cells.

3.3. Assessment of Arrangements of Mitophagy-Related Proteins with Confocal Microscopy. The stress-response and autophagy proteins Sirt3, PINK1, PARKIN, Foxo3a, and LC3 were suggested recently to mediate remodeling of the mitochondrial network in a variety of adaptive responses [2, 3, 5–11, 15, 21]. The progress of this area is closely associated with development of confocal fluorescence imaging techniques that provides a great deal of reliable data compared to results of immunoblot assessment of nuclear fraction of the same proteins [2, 18]. In a previous study, we reported increase in Sirtuins and Foxo3a proteins in the hearts of animals fed with resveratrol or longevinex that was determined using immunoblot analysis of tissue specimens [15]. Therefore, in this work we employed confocal fluorescence imaging to assess spatial localization of Sirt3, PINK1, PARKIN, Foxo3a, and LC3 in the infarcted regions of interest (ROI).

In the first set of experiments, cardiac specimens were analyzed for the status of Sirt3 and Foxo3a in nuclei and mitochondria. The data presented in Figure 2 shows elevated immunoreactivity of Sirt3 (green channel) in the specimens treated with resveratrol or longevinex and I/R (Figure 2, Panels b2 and c2) as compared to I/R treatment only (Figure 2, Panel a2). The results of the analysis showed presence of Foxo3a immunofluorescence (red channel) in nuclei (fluorescence in blue channel) in the infracted ROI (Figure 2, panels a3, a4, b3, b4, c3, c4). However, the Foxo3a immunofluorescence in the specimens from the groups treated with resveratrol or longevinex displayed higher colocalization with the Sirt3 immunofluorescence (appearing in yellow in Figure 2, panels b4 and c4). This effect suggested a possibility of involvement of Sirt3 in upregulation of Foxo3a in mitochondria, since the Sirt3 is situated in both cytoplasm and mitochondria [11, 21]. The spatial colocalization of Sirt3 and Foxo3a in these tissue sections was closely associated with the sites of mitochondrial disorder as determined by confocal analysis (Figure 2).

In the next set of experiments we conducted image analysis of mitochondrial fission, the PINK1/PARKIN mitophagy signaling proteins in conjunction with upregulation of autophagosome formation determined by confocal imaging of LC3, an autophagy marker. The images presented in Figure 3 (panels a1-a2, b1-b2, and c1-c2) showed increase in the expression of mitochondrial PINK1/PARKIN in the infarcted areas of hearts treated with resveratrol or longevinex followed by I/R as compared to hearts of the untreated I/R group. Projections of mitochondrial PINK1/PARKIN were spatially colocalized with projections of the Foxo3a factor (Figure 3, panels a1, b1, and c1). Further, TOMO20 also

Table 1: Effect of resveratrol and longevinex on myocardial function.

	Control	Resveratrol	Longevinex
Coronary flow (mL/min)			
Baseline	24 ± 2.1	25 ± 3.0	24 ± 2.4
60 min rep.	22 ± 2.3	24 ± 2.5	23 ± 3.1
120 min rep.	23 ± 2.0	24 ± 2.8	25 ± 1.9
Aortic flow (mL/min)			
Baseline	51 ± 2.3	53 ± 4.0	52 ± 3.8
60 min rep.	25 ± 3.2	35 ± 3.7	38 ± 2.7
120 min rep.	8.5 ± 2.7	24 ± 3.2	26 ± 3.5
LVDP (mm Hg)			
Baseline	116 ± 6	117 ± 7	119 ± 9
60 min rep.	80 ± 5	98 ± 5	101 ± 6
120 min rep.	54 ± 7	84 ± 7	86 ± 5
LVmaxdp/dt (mm Hg/sec)			
Baseline	3056 ± 48	1845 ± 45	1028 ± 56
60 min rep.	1689 ± 65	2356 ± 33	1754 ± 39
120 min rep.	1206 ± 38	1877 ± 62	2012 ± 32
Infarct size (infarct area/area of risk)			
Baseline	3 ± 2	2.8 ± 1.2	2.1 ± 0.8
120 min rep.	36 ± 4	19 ± 3	17 ± 2
Apoptosis (%)			
Baseline	1 ± 1	1 ± 0.8	1 ± 0.7
120 min rep.	22 ± 3	9 ± 2	8 ± 2

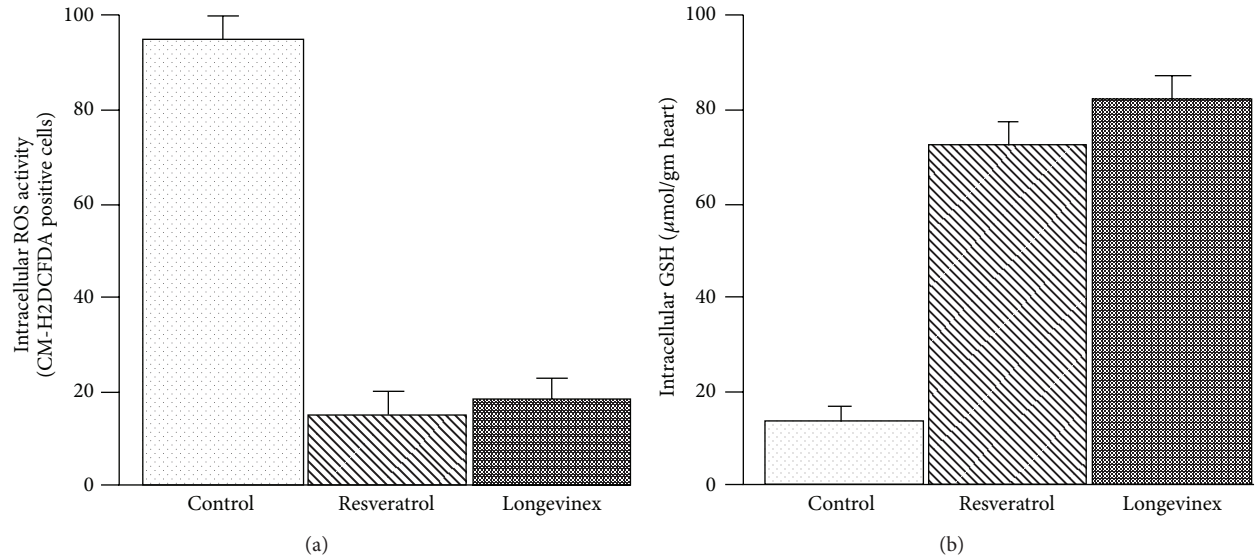

Figure 1: (a) Intracellular quantification of ROS by DCFDA in the samples. (b) Intracellular concentration of glutathione (GSH).

colocalized in mitochondria with PARKIN (Figure 3, panels b2 and c2), where PARKIN, a multifunctional E3 ubiquitin ligase, could mediate interaction of the autophagic adaptor protein p62/SQSTM1/sequestosome-1 with the disordered mitochondria and further with LC3-II on autophagosomes as proposed recently [5, 9, 10]. Overlay of the immunofluorescence images of Sirt3 (green), TOM20 (red), and nuclei (blue) shown in panels (a), (b), and (c) of Figure 4 reveals the mitochondrial fission indicated with white arrows in panels (b) and (c). Likewise, overlay of the immunofluorescence images of LC3 (green), TOM20 (red), and nuclei (blue) shown in panels (d–g) of Figure 4 also reveals mitochondrial fission shown by white arrows.

To confirm the implication of LC3-mediated mitophagy mechanism in the sequence of events following activation, PINK1/PARKIN cascade, and mitochondrial fission in the

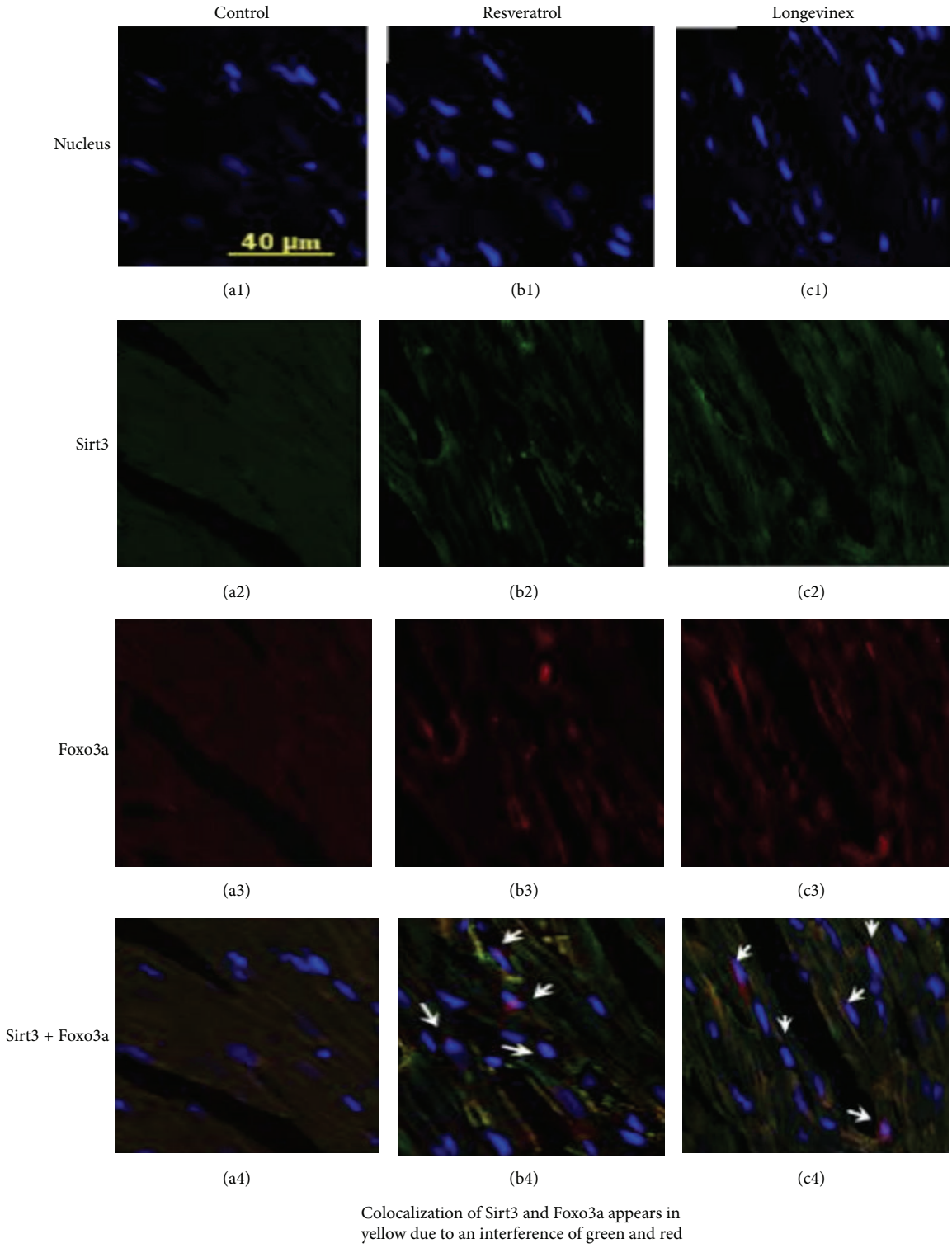

Figure 2: Immunofluorescence multichromatic projections of mitochondrial Sirt3 and the nuclear factor Foxo3a in the ischaemic (IR) cardiac specimens after treatments with resveratrol or longevinex. Panels (a1–a4) are administration of vehicle only; panels (b1–b4) are administration of resveratrol; panels (c1–c4) are administration of longevinex, where (1) is counterstaining of nuclei with Hoechst 33342 (blue), (2) is the immunofluorescence images of Sirt3 (green), (3) is the immunofluorescence images of Foxo3a (red), and (4) is overlay of (1–3) images. Nuclear localization of Foxo3a is indicated with white arrows. The confocal images were taken with optical Z-step of 0.5 μm.

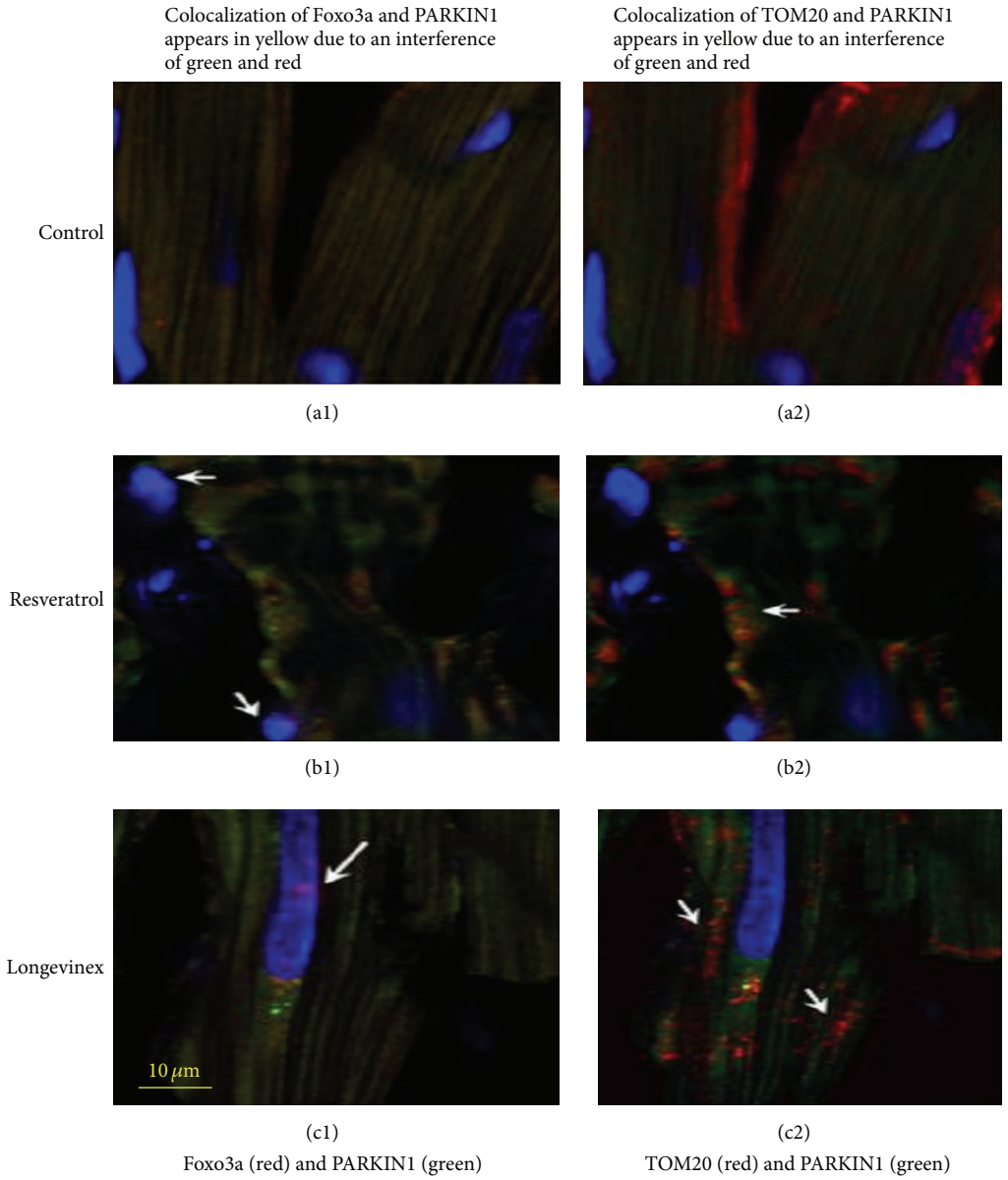

Figure 3: Immunofluorescence multichromatic projections of PARKIN1, the nuclear factor Foxo3a, and the mitochondrial marker TOM20 in the ischaemic (IR) cardiac specimens after treatments with resveratrol or longevinex. Panels (a1) and (a2) are administration of vehicle only; panels (b1) and (b2) are administration of resveratrol; panels (c1) and (c2) are administration of longevinex, where: (1) are projections of PARKIN1 (green), Foxo3a (red), and nuclei (blue); nuclear localization of Foxo3a is indicated with white arrows in panels (b1) and (c1); (2) are projections of PARKIN1 (green), TOM20 (red), and nuclei (blue); and mitochondrial fission is indicated with white arrows in panels (b2) and (c2). The confocal images were taken with optical Z-step of 0.5 μm.

experimental groups we analyzed colocalization of LC3 with TOM20 and PINK1. The results of these analyses are shown in Figure 5. The presented data indicate that treatment with resveratrol and longevinex upregulates the mitophagy pathway following I/R that can facilitate remodeling of damaged mitochondria. The data obtained using immunfluorescence confocal imaging were corroborated by the results of (i) immunoblotting confirming increase in expression of Sirt1, Sirt3, Foxo3a, PINK1, and PARKIN proteins in the resveratrol- and longevinex-treated experimental groups (Figure 7) and (ii) the transmission electron microscopy indicating the presence of extensive mitophagy in the resveratrol-treated specimens (see next section).

3.4. Transmission Electron Microscopy. Electron microscopy examination of resveratrol and longevinex-treated samples showed almost normal ultrastructural appearance and presence of numerous autophagosomes at different stages of maturation. Early autophagic vacuoles contained still identifiable organelles. In general, the autophagosomes enclosed single

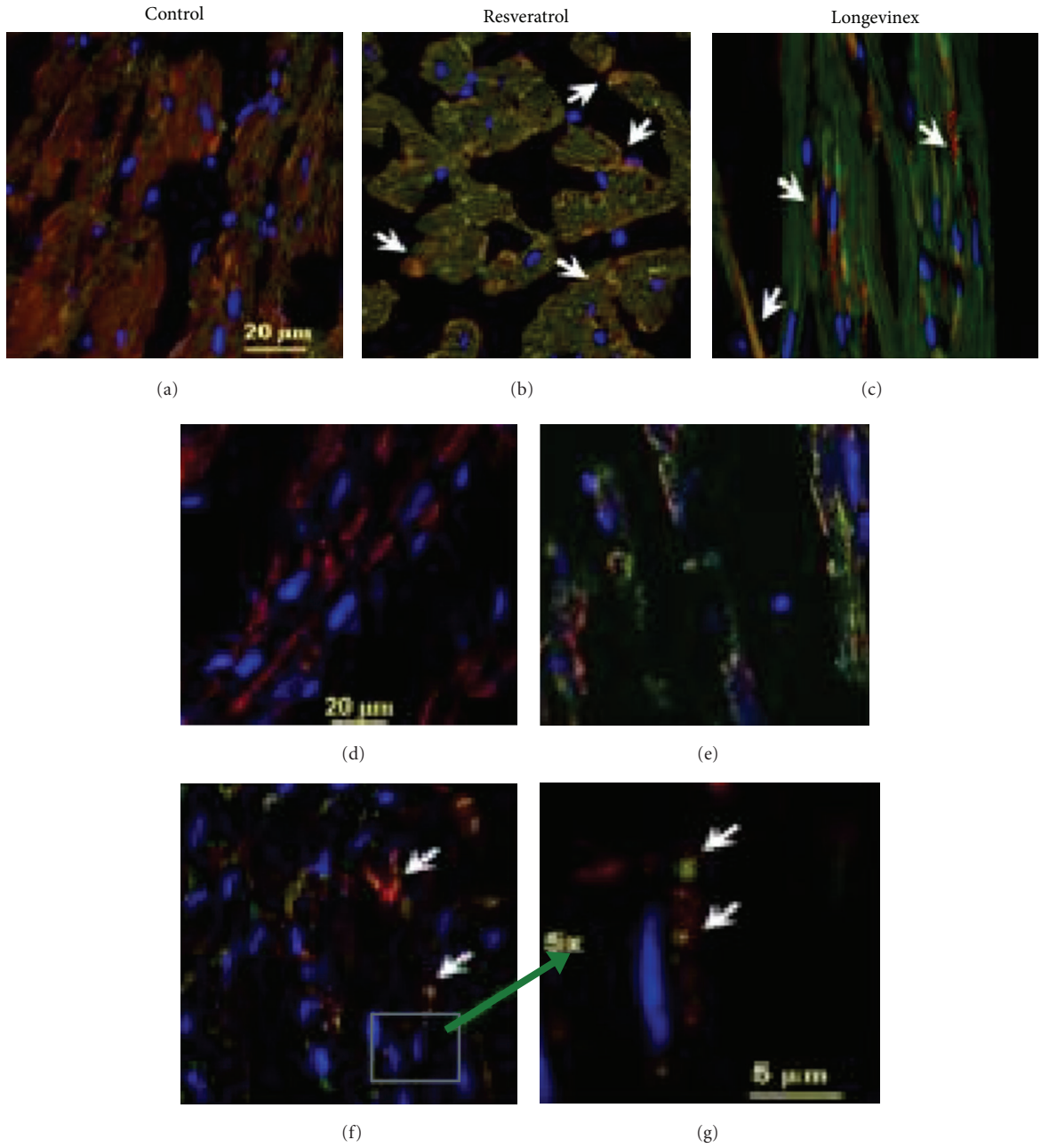

Figure 4: Immunofluorescence multichromatic projections of mitochondrial Sirt3 and TOM20 along with LC3 protein, a marker of autophagosome formation, in the ischaemic (IR) cardiac specimens after treatments with resveratrol or longevinex. Panels (a) and (d) are administration of vehicle only; panels (b) and (e) are administration of resveratrol; panels (c) and (f) are administration of longevinex. Panel (g) is 5x magnification of the selected area indicated in panel (f) where mitochondrial fission and mitophagy are indicated with white arrows. Overlay of the immunofluorescence images of Sirt3 (green), TOM20 (red), and nuclei (blue) is shown in panels (a), (b), and (c); mitochondrial fission is indicated in panels (b) and (c) with white arrows. Overlay of the immunofluorescence images of LC3 (green), TOM20 (red), and nuclei (blue) is shown in panels (d–g); mitochondrial fission is shown in panel (f) with white arrows. The confocal images were taken with optical Z-step of 0.5 μm.

or grouped mitochondria lamellar structures and cytoplasmic content (Figure 6). Electron microscopy examination of resveratrol- and longevinex-treated samples showed an almost normal ultrastructure and their presence of numerous autophagosomes in different stages of maturation. Early autophagic vacuoles contain still identifiable organelles. The autophagosomes enclose single or grouped mitochondria, lamellar structure, and cytoplasmic content (Figure 6).

3.5. Western Blot. We then performed Western blot on the biopsies obtained after each experiment to demonstrate the expression of SirTs, FoxOs, PARKIN, and Pink. As shown

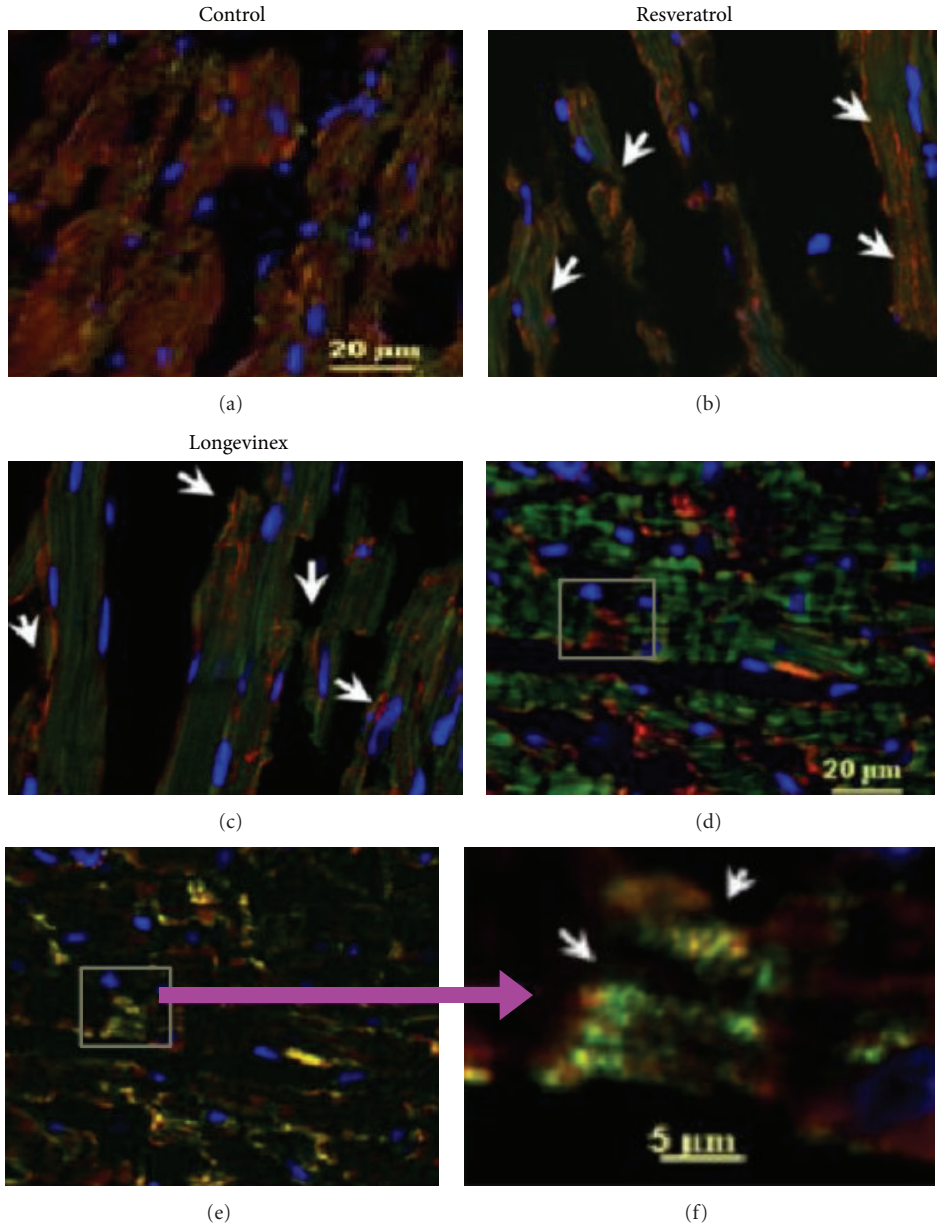

FIGURE 5: Immunofluorescence multichromatic projections of PINK1, LC3 protein, a marker of autophagosome formation, and the mitochondrial TOM20 in the ischaemic (IR) cardiac specimens after treatments with resveratrol or longevinex. Panel (a) is administration of vehicle only; panel (b) is administration of resveratrol; panels (c–e) are administration of longevinex. Panel (f) is 5x magnification of the selected area indicated in panel (e) where mitochondrial fission and mitophagy are indicated with white arrows. Overlay of the immunofluorescence images of LC3 (green), PINK1 (red), and nuclei (blue) is shown in panels (a), (b), and (c); autophagy activation is indicated in panels (b) and (c) with white arrows. Overlay of the immunofluorescence images of PINK1 (green), TOM20 (red), and nuclei (blue) is shown in panel (d). Overlay of the immunofluorescence images of LC3 (green), TOM20 (red), and nuclei (blue) is shown in panel (e); mitochondrial fission is shown in panel (f) with white arrows. The confocal images were taken with optical Z-step of 0.5 μm.

in Figure 7, both resveratrol and longevinex induced the expression of Sirt1, Sirt3, Foxo3a, PINK1, and PARKIN to the same extent.

3.6. Statistical Analysis. The values of myocardial functional parameters, total and infarct volumes, and infarct sizes are all expressed as the mean standard error of the mean (SEM). Analysis of variance test followed by Bonferroni's correction was first carried out to test for any differences between the mean values of all groups. If differences between groups were established, the values of the treated groups were compared with those of the control group by a modified t-test. The results were considered to be significant if $P < 0.05$.

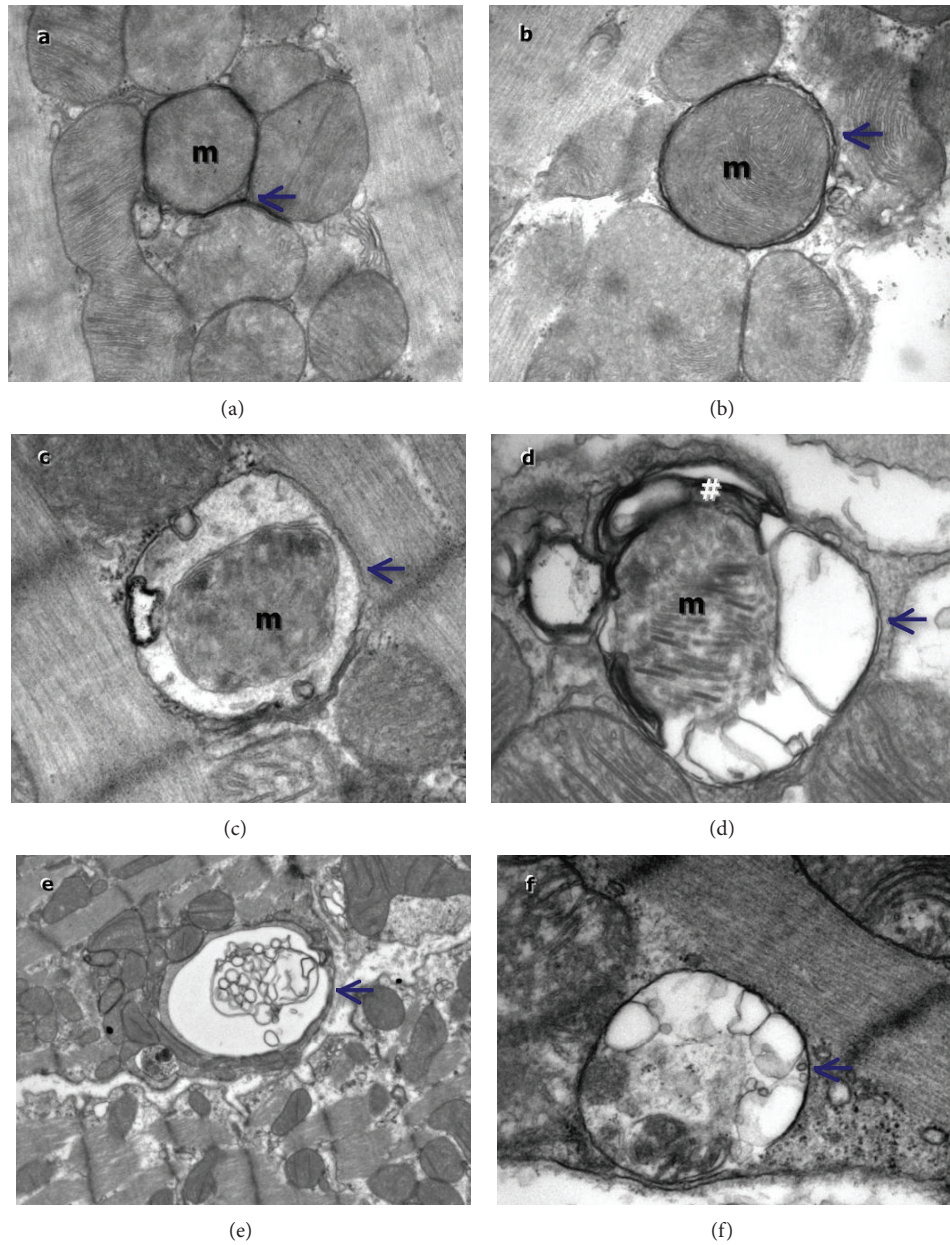

Figure 6: Transmission electron microscopy images showing the ultrastructure findings in control and resveratrol treated hearts. Cardiomyocytes from control show normal ultrastructure and resveratrol treated hearts show mitophagy. Autophagosomes in resveratrol treated samples TEM images show early autophagic vacuoles containing still identifiable organelles (a–c) and late autophagosomes containing lamellar and vesicular structures (d–f). Autophagosomes preferentially contain mitochondria (m) enclosed by distinctive double membrane (arrows).

4. Discussion

The results of our study demonstrated that resveratrol and modified resveratrol longevinex both acetylate Sirt3, which then activates FoxO3 leading to the activation of PINK-1/PARKIN pathway potentiating mitochondrial fission and mitophagy. We compared pure resveratrol against longevinex, because in certain cases longevinex was found superior to resveratrol. For example, unlike resveratrol, longevinex (modified resveratrol) exhibited no toxic effects (hormesis) even at higher concentrations.

Confocal microscopy reveals colocalization of Sirt3 with Foxo3a, and further Foxo3a with PARKIN. Mitochondrial fission occurs subsequently followed by mitophagy. It is interesting to note that mitophagy is associated with PINK1. Western blot results are also in agreement with the results of confocal microscopy. Both resveratrol and longevinex lead to a similar degree of cardioprotection.

Sirtuins, a family of NAD+-dependent proteins deacetylases, regulate biological function through deacetylation of many target proteins including antiaging genes. Sirt1 and Sirt3 are two important sirtuins that are localized within two

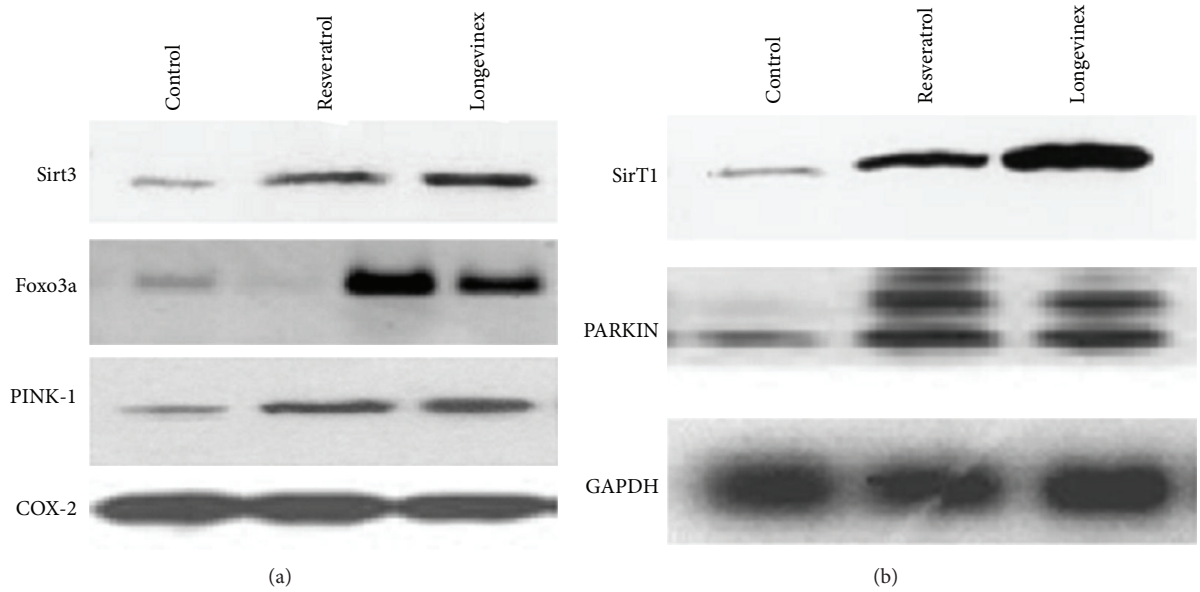

Figure 7: Western blot analysis of Sirt3, Foxo3a, and PINK-19 (a) and Sirt1 and PARKIN (b). Mitochondrial marker and cytosolic marker GAPDH are shown below.

different subcellular compartments, nucleus and mitochondria, respectively, Our previous studies indicated that Sirt 1 and Sirt3 are the two interacting partners [24], being activated by resveratrol or red wine [25]. The role of resveratrol has been speculated for some time because resveratrol could activate Sirt1, but the role of Sirt1 in aging is not fully defined [26]. A recent study showed that Sirt1 and Sirt3 have a common molecular target HSP70, wherein their molecular chaperone is playing a protective role against various adverse conditions [27]. HSP70 is an aging related protein, and the reduction of HSP70 leads to aging in various biological systems and aging related diseases [28]. In addition Sirt1 and Sirt3 are involved in autophagy, an aging related process [29].

A recent study has demonstrated that Sirt3 interacts with the daf-16 homolog Foxo3a in the mitochondria as well as increases Foxo3a dependent gene expression [30]. It is well known that Sirtuins, especially Sirt1, interact with the FoxO gene family proteins [31]. FoxO family of transcription factors including Foxo3a are the human homologs of the daf-16 C. elegans gene, a master regulator of dauer formation and contributer to the regulation of lifespan in nematodes [32]. Our confocal microscopy picture clearly shows that Sirt3 physically interacts with Foxo3a, suggesting that Sirt3 may be a mitochondrial surveillance factor that detects metabolic imbalances, since Foxo3a controls mitochondrial metabolism and redox balance [33]. Many recent studies indicate that Foxo3a gene is associated with human longevity since aging phenotypes are associated with Foxo3a genotype and long-lived men and women exhibit several biological markers indicative of greater insulin sensitivity and homozygosity for the Foxo3a GG genotype [34]. The same study shows that analysis of five candidate genes revealed that Foxo3a is undoubtedly the major longevity gene. Indeed, variants of the Foxo3a gene are a common characteristic for many people who live past 100 years [35].

Interestingly, Foxo3a-dependent regulation of PINK1 mediates survival signaling in certain cases such as cytokine deprivation [36]. PINK1 is an essential prosurvival factor that is induced in response to oxidative stress [37]. This study demonstrated that Foxo3a controls PINK1 transcription in both mouse and human cells subjected to growth factor deprivation and that this regulation is exerted through evolutionarily conserved FoxO binding elements. The above study [38] suggests that induction of prosurvival factor like PINK1 by Foxo3a may allow protection of cells. Indeed our results demonstrate myocardial protection by resveratrol/longevinex, which readily change ischemia/reperfusion-mediated oxidative environment into a reducing environment and increase GSH. Indeed loss of PINK1 causes mitochondrial functional defects and increased sensitivity to oxidative stress [39]. A recent study demonstrated that PINK1 is indispensable for normal heart function and possesses a distinct nonredundant function in the surveillance and maintenance of cardiac tissue homeostasis [40]. This study has shown that PINK1$^{-/-}$ mice develop cardiac hypertrophy and LV dysfunction by 2 months of age associated with increased oxidative stress and mitochondrial dysfunction. It has long been known that PINK1, a highly conserved Parkinson's disease susceptibility gene [41], provides the link between mitochondrial dysfunction and oxidative stress in Parkinson's disease [42].

Mitochondrial dynamics is regulated by a common pathway involving PINK1-PARKIN. Recent studies have suggested a role for the PINK1-PARKIN pathway in mitochondrial quality control through promotion of mitophagy [43]. PINK1 is stabilized on damaged mitochondria, which

then recruits PARKIN to mitochondrial outer membrane leading to the removal of damaged mitochondria through mitophagy [44]. Previous studies also revealed a functional relationship between PINK1-PARKIN and the mitochondrial fusion-fission pathway implicating defective mitochondrial dynamics [45]. Our studies demonstrate that resveratrol activates PINK1-PARKIN pathway subsequent to the activation of Sirt3-Foxo3a pathway and such activation of PINK1-PARKIN pathway runs parallel to mitochondrial fission leading to mitophagy. An elegant study by Geisler and coworkers showed that PARKIN is translocated to mitochondria prior to inducing mitophagy [46]. It is not clear, however, how PINK1-PARKIN pathway cooperates with mitochondrial fusion-fission pathway leading to the induction of mitophagy. Mitophagy is a cell-repair mechanism that is intimately linked with aging [47].

In conclusion, the results of the present study demonstrates that both resveratrol and a modified resveratrol longevinex reduce ROS and preserve GSH and can induce a signaling pathway involving Sirt3-Foxo3a-PINK1-PARKIN-Mitochondrial fusion-fission-mitophagy. All the members in this pathway are intimately linked with aging process. The results further indicate that resveratrol and longevinex trigger an antiaging pathway in the mitochondria involving Sirt3-Foxo3a-PINK1-PARKIN-Mitochondrial fusion-fission-mitophagy.

Conflict of Interests

The authors declare that there is no conflict of interests regarding the publication of this paper.

Acknowledgments

This study was supported in part by NIH HL 33889, HL 22559, and HL 34360. Gift sample of longevinex from Resveratrol Partners, USA, is acknowledged.

References

[1] R. Scherz-Shouval and Z. Elazar, "ROS, mitochondria and the regulation of autophagy," *Trends in Cell Biology*, vol. 17, no. 9, pp. 422–427, 2007.

[2] D. C. Chan, "Mitochondrial fusion and fission in mammals," *Annual Review of Cell and Developmental Biology*, vol. 22, pp. 79–99, 2006.

[3] H. Chen and D. C. Chan, "Mitochondrial dynamics—fusion, fission, movement, and mitophagy—in neurodegenerative diseases," *Human molecular genetics*, vol. 18, no. 2, pp. R169–176, 2009.

[4] W. Liu, R. Acín-Peréz, K. D. Geghman, G. Manfredi, B. Lu, and C. Li, "Pink1 regulates the oxidative phosphorylation machinery via mitochondrial fission," *Proceedings of the National Academy of Sciences of the United States of America*, vol. 108, no. 31, pp. 12920–12924, 2011.

[5] F. Billia, L. Hauck, F. Konecny, V. Rao, J. Shen, and T. W. Mak, "PTEN-inducible kinase 1 (PINK1)/Park6 is indispensable for normal heart function," *Proceedings of the National Academy of Sciences of the United States of America*, vol. 108, no. 23, pp. 9572–9577, 2011.

[6] C. A. Gautier, T. Kitada, and J. Shen, "Loss of PINK1 causes mitochondrial functional defects and increased sensitivity to oxidative stress," *Proceedings of the National Academy of Sciences of the United States of America*, vol. 105, no. 32, pp. 11364–11369, 2008.

[7] Y. Mei, Y. Zhang, K. Yamamoto, W. Xie, T. W. Mak, and H. You, "FOXO3a-dependent regulation of Pink1 (Park6) mediates survival signaling in response to cytokine deprivation," *Proceedings of the National Academy of Sciences of the United States of America*, vol. 106, no. 13, pp. 5153–5158, 2009.

[8] K. M. Jacobs, J. D. Pennington, K. S. Bisht et al., "SIRT3 interacts with the daf-16 homolog FOXO3a in the mitochondria, as well as increases FOXO3a dependent gene expression," *International Journal of Biological Sciences*, vol. 4, no. 5, pp. 291–299, 2008.

[9] K. T. Howitz, K. J. Bitterman, H. Y. Cohen et al., "Small molecule activators of sirtuins extend Saccharomyces cerevisiae lifespan," *Nature*, vol. 425, no. 6954, pp. 191–196, 2003.

[10] D. K. Das, S. Mukherjee, and D. Ray, "Resveratrol and red wine, healthy heart and longevity," *Heart Failure Reviews*, vol. 16, no. 4, pp. 425–435, 2011.

[11] Y. Shi, G. G. Camici, and T. F. Lüscher, "Cardiovascular determinants of life span," *Pflügers Archiv*, vol. 459, no. 2, pp. 315–324, 2010.

[12] G. Petrovski and D. K. Das, "Does autophagy take a front seat in lifespan extension?" *Journal of Cellular and Molecular Medicine*, vol. 14, no. 11, pp. 2543–2551, 2010.

[13] S. Mukherjee, I. Lekli, N. Gurusamy, A. A. A. Bertelli, and D. K. Das, "Expression of the longevity proteins by both red and white wines and their cardioprotective components, resveratrol, tyrosol, and hydroxytyrosol," *Free Radical Biology and Medicine*, vol. 46, no. 5, pp. 573–578, 2009.

[14] B. Juhasz, S. Mukherjee, and D. K. Das, "Hormetic response of resveratrol against cardioprotection," *Experimental and Clinical Cardiology*, vol. 15, no. 4, pp. e134–e138, 2010.

[15] S. Mukherjee, D. Ray, I. Lekli, I. Bak, A. Tosaki, and D. K. Das, "Effects of longevinex (modified resveratrol) on cardioprotection and its mechanisms of action," *Canadian Journal of Physiology and Pharmacology*, vol. 88, no. 11, pp. 1017–1025, 2010.

[16] I. Lekli, D. Ray, S. Mukherjee et al., "Co-ordinated autophagy with resveratrol and γ-tocotrienol confers synergetic cardioprotection," *Journal of Cellular and Molecular Medicine*, vol. 14, no. 10, pp. 2506–2518, 2010.

[17] S. Mukherjee, D. Ray, I. Lekli, I. Bak, A. Tosaki, and D. K. Das, "Effects of longevinex (modified resveratrol) on cardioprotection and its mechanisms of action," *Canadian Journal of Physiology and Pharmacology*, vol. 88, no. 11, pp. 1017–1025, 2010.

[18] E. C. Ferber, B. Peck, O. Delpuech, G. P. Bell, P. East, and A. Schulze, "FOXO3a regulates reactive oxygen metabolism by inhibiting mitochondrial gene expression," *Cell Death and Differentiation*, vol. 19, no. 6, pp. 968–979, 2012.

[19] J. Benner, H. Daniel, and B. Spanier, "A glutathione peroxidase, intracellular peptidases and the tor complexes regulate peptide transporter PEPT-1 in C. elegans," *PLoS ONE*, vol. 6, no. 9, Article ID e25624, 2011.

[20] S. Mukherjee, H. Gangopadhyay, and D. K. Das, "Broccoli: a unique vegetable that protects mammalian hearts through the redox cycling of the thioredoxin superfamily," *Journal of Agricultural and Food Chemistry*, vol. 56, no. 2, pp. 609–617, 2008.

[21] E. L. Eskelinen, "To be or not to be? Examples of incorrect identification of autophagic compartments in conventional transmission electron microscopy of mammalian cells," *Autophagy*, vol. 4, no. 2, pp. 257–260, 2008.

[22] D. J. Klionsky, H. Abeliovich, P. Agostinis et al., "Guidelines for the use and interpretation of assays for monitoring autophagy in higher eukaryotes," *Autophagy*, vol. 4, no. 2, pp. 151–175, 2008.

[23] N. Gurusamy, I. Lekli, N. V. Gorbunov, M. Gherghiceanu, L. M. Popescu, and D. K. Das, "Cardioprotection by adaptation to ischaemia augments autophagy in association with BAG-1 protein," *Journal of Cellular and Molecular Medicine*, vol. 13, no. 2, pp. 373–387, 2009.

[24] I. K. M. Law, L. Liu, A. Xu et al., "Identification and characterization of proteins interacting with SIRT1 and SIRT3: implications in the antiaging and metabolic effects of sirtuins," *Proteomics*, vol. 9, no. 9, pp. 2444–2456, 2009.

[25] S. Mukherjee, I. Lekli, N. Gurusamy, A. A. A. Bertelli, and D. K. Das, "Expression of the longevity proteins by both red and white wines and their cardioprotective components, resveratrol, tyrosol, and hydroxytyrosol," *Free Radical Biology and Medicine*, vol. 46, no. 5, pp. 573–578, 2009.

[26] C. Mannari, A. A. E. Bertelli, G. Stiaccini, and L. Giovannini, "Wine, sirtuins and nephroprotection: not only resveratrol," *Medical Hypotheses*, vol. 75, no. 6, pp. 636–638, 2010.

[27] S. D. Westerheide, J. Anckar, S. M. Stevens Jr., L. Sistonen, and R. I. Morimoto, "Stress-inducible regulation of heat shock factor 1 by the deacetylase SIRT," *Science*, vol. 323, no. 5917, pp. 1063–1066, 2009.

[28] V. Calabrese, C. Cornelius, A. T. Dinkova-Kostova et al., "Cellular stress responses, hormetic phytochemicals and vitagenes in aging and longevity," *Biochimica et Biophysica Acta*, vol. 1822, no. 5, pp. 753–783, 2012.

[29] M. Das and D. K. Das, "Resveratrol and cardiovascular health," *Molecular Aspects of Medicine*, vol. 31, no. 6, pp. 503–512, 2010.

[30] K. M. Jacobs, J. D. Pennington, K. S. Bisht et al., "SIRT3 interacts with the daf-16 homolog FOXO3a in the mitochondria, as well as increases FOXO3a dependent gene expression," *International Journal of Biological Sciences*, vol. 4, no. 5, pp. 291–299, 2008.

[31] F. Wang, C. H. Chan, K. Chen, X. Guan, H. K. Lin, and Q. Tong, "Deacetylation of FOXO3 by SIRT1 or SIRT2 leads to Skp2-mediated FOXO3 ubiquitination and degradation," *Oncogene*, vol. 31, no. 12, pp. 1546–1557, 2012.

[32] G. Rizki, T. N. Iwata, J. Li et al., "The evolutionarily conserved longevity determinants HCF-1 and SIR-2.1/SIRT1 collaborate to regulate DAF-16/FOXO," *PLoS Genetics*, vol. 7, no. 9, Article ID e1002235, 2011.

[33] D. Frescas, L. Valenti, and D. Accili, "Nuclear trapping of the forkhead transcription factor FoxO1 via sirt-dependent deacetylation promotes expression of glucogenetic genes," *Journal of Biological Chemistry*, vol. 280, no. 21, pp. 20589–20595, 2005.

[34] Y. Zeng, L. Cheng, H. Chen et al., "Effects of FOXO genotypes on longevity: a biodemographic analysis," *Journals of Gerontology A*, vol. 65, no. 12, pp. 1285–1299, 2010.

[35] M. Soerensen, S. Dato, K. Christensen et al., "Replication of an association of variation in the FOXO3A gene with human longevity using both case-control and longitudinal data," *Aging Cell*, vol. 9, no. 6, pp. 1010–1017, 2010.

[36] Y. Mei, Y. Zhang, K. Yamamoto, W. Xie, T. W. Mak, and H. You, "FOXO3a-dependent regulation of Pink1 (Park6) mediates survival signaling in response to cytokine deprivation," *Proceedings of the National Academy of Sciences of the United States of America*, vol. 106, no. 13, pp. 5153–5158, 2009.

[37] J. Sämann, J. Hegermann, E. von Gromoff, S. Eimer, R. Baumeister, and E. Schmidt, "Caenorhabditits elegans LRK-1 and PINK-1 act antagonistically in stress response and neurite outgrowth," *Journal of Biological Chemistry*, vol. 284, no. 24, pp. 16482–16491, 2009.

[38] D. Wang, L. Qian, H. Xiong et al., "Antioxidants protect PINK1-dependent dopaminergic neurons in Drosophila," *Proceedings of the National Academy of Sciences of the United States of America*, vol. 103, no. 36, pp. 13520–13525, 2006.

[39] W. Liu, R. Acín-Peréz, K. D. Geghman, G. Manfredi, B. Lu, and C. Li, "Pink1 regulates the oxidative phosphorylation machinery via mitochondrial fission," *Proceedings of the National Academy of Sciences of the United States of America*, vol. 108, no. 31, pp. 12920–12924, 2011.

[40] C. Vassalle, A. Mercuri, and S. Maffei, "Oxidative status and cardiovascular risk in women: keeping pink at heart," *World Journal of Cardiology*, vol. 1, no. 1, pp. 26–30, 2009.

[41] C. A. Gautier, T. Kitada, and J. Shen, "Loss of PINK1 causes mitochondrial functional defects and increased sensitivity to oxidative stress," *Proceedings of the National Academy of Sciences of the United States of America*, vol. 105, no. 32, pp. 11364–11369, 2008.

[42] E. Ziviani and A. J. Whitworth, "How could Parkin-mediated ubiquitination of mitofusin promote mitophagy?" *Autophagy*, vol. 6, no. 5, pp. 660–662, 2010.

[43] L. A. Kane and R. J. Youle, "PINK1 and Parkin flag miro to direct mitochondrial traffic," *Cell*, vol. 147, no. 4, pp. 721–723, 2011.

[44] A. S. Rambold and J. Lippincott-Schwartz, "Mechanisms of mitochondria and autophagy crosstalk," *Cell Cycle*, vol. 10, no. 23, pp. 4032–4038, 2011.

[45] A. Rakovic, A. Grünewald, J. Kottwitz et al., "Mutations in PINK1 and Parkin impair ubiquitination of Mitofusins in human fibroblasts," *PLoS ONE*, vol. 6, no. 3, Article ID e16746, 2011.

[46] S. Geisler, K. M. Holmström, D. Skujat et al., "PINK1/Parkin-mediated mitophagy is dependent on VDAC1 and p62/SQSTM1," *Nature Cell Biology*, vol. 12, no. 2, pp. 119–131, 2010.

[47] D. R. Green, L. Galluzzi, and G. Kroemer, "Mitochondria and the autophagy-inflammation-cell death axis in organismal aging," *Science*, vol. 333, no. 6046, pp. 1109–1112, 2011.

Hindawi Publishing Corporation
Oxidative Medicine and Cellular Longevity
Volume 2013, Article ID 378484, 11 pages
http://dx.doi.org/10.1155/2013/378484

Research Article

Differential MicroRNA Profiling in a Cellular Hypoxia Reoxygenation Model upon Posthypoxic Propofol Treatment Reveals Alterations in Autophagy Signaling Network

Zhuo Chen,[1] Zhe Hu,[1] Zhiqi Lu,[1] Shuyun Cai,[1] Xiaoxia Gu,[1] Haixia Zhuang,[1] Zhihua Ruan,[1] Zhengyuan Xia,[2] Michael G. Irwin,[2] Du Feng,[3] and Liangqing Zhang[1]

[1] *Department of Anesthesiology, Affiliated Hospital of Guangdong Medical College, Zhanjiang 524001, China*
[2] *Anesthesiology Research Laboratory, Department of Anesthesiology, University of Hong Kong, Hong Kong*
[3] *Key Laboratory of Age-Associated Cardiac-Cerebral Vascular Disease of Guangdong Province, Department of Neurology, Affiliated Hospital of Guangdong Medical College, Zhanjiang 524001, China*

Correspondence should be addressed to Du Feng; feng_du@foxmail.com and Liangqing Zhang; zhanglq1970@163.com

Received 10 September 2013; Revised 16 November 2013; Accepted 22 November 2013

Academic Editor: Mengzhou Xue

Recent studies indicate that propofol may protect cells via suppressing autophagic cell death caused by excessive reactive oxygen species induced by hypoxia reoxygenation (H/R). It is established that gene expression patterns including autophagy-related genes changed significantly during the process of H/R in the presence or absence of propofol posthypoxia treatment (P-PostH). The reasons for such differences, however, remain largely unknown. MicroRNAs provide a novel mechanism for gene regulation. In the present study, we systematically analyzed the alterations in microRNA expression using human umbilical vein endothelial cells (HUVECs) subjected to H/R in the presence or absence of posthypoxic propofol treatment. Genome-wide profiling of microRNAs was then conducted using microRNA microarray. Fourteen miRNAs are differentially expressed and six of them were validated by the quantitative real-time PCR (Q-PCR) of which three were substantially increased, whereas one was decreased. To gain an unbiased global perspective on subsequent regulation by altered miRNAs, predicted targets of ten miRNAs were analyzed using the Gene Ontology (GO) analysis to build signaling networks. Interestingly, six of the identified microRNAs are known to target autophagy-related genes. In conclusion, our results revealed that different miRNA expression patterns are induced by propofol posthypoxia treatment in H/R and the alterations in miRNA expression patterns are implicated in regulating distinctive autophagy-related gene expression.

1. Introduction

As a result of increased oxidative stress, reperfusion of ischemic tissues or cells leads to a systemic inflammatory response which in turn may cause widespread microvascular dysfunction and tissue/cell injury [1–3]. Studies have shown that the vascular endothelium is a crucial site that is affected by ischemia/reperfusion (I/R) injury [4–6]. Due to the instability of the current overall animal model of I/R injury which is largely affected by multifaceted factors *in vivo* and *in vitro*, animal models thus cannot reflect the exact protective mechanisms of drugs on the tissue/cell damage. *In vitro* cultured endothelial cells, however, are simple and controllable system that can create useful I/R injury model [7, 8].

Propofol is a widely used intravenous anesthetic with antioxidant capacity. It shows protective roles on the hydrogen peroxide (H_2O_2)-induced apoptosis in cardiac cells and myocardial ischemia and reperfusion (I/R) injury in rats [9, 10]. Recent evidences have shown that propofol may suppress the I/R activated autophagic cell death through affecting the expressions of autophagy-related genes [11–14]. But the mechanisms of the protective effects of propofol on HUVECs I/R injury have not been well studied.

MicroRNAs (miRNAs) are an evolutionarily conserved family of short noncoding RNAs, that negatively regulate

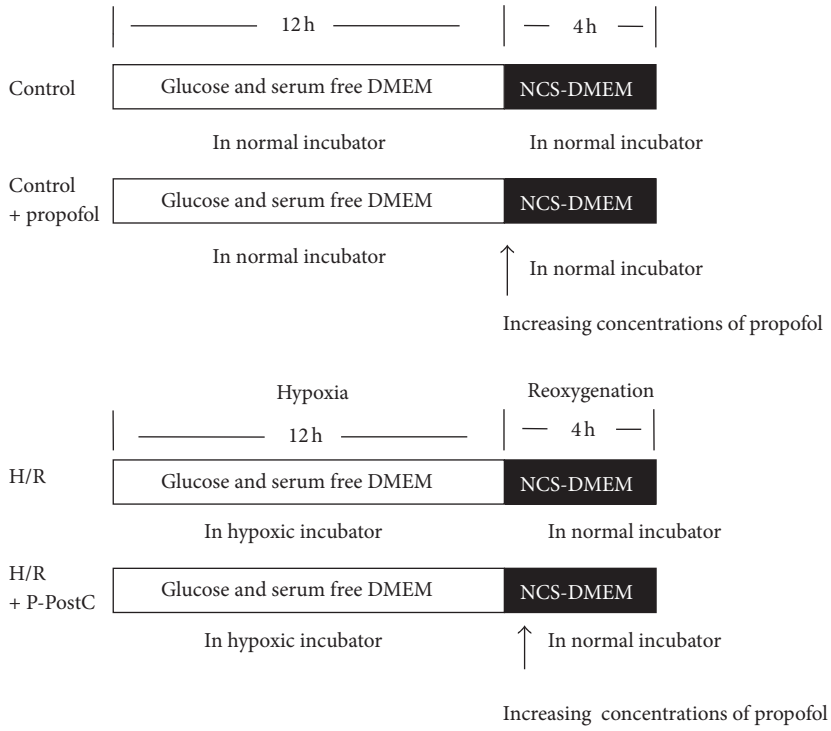

FIGURE 1: Build the H/R and P-PostH model. The culture media were replaced by glucose and serum free DMEM balanced in normal incubator in 30 minutes, and these HUVEC cells were then placed in hypoxic conditions which were created by a small enclosed humidified plexiglass chamber filled with 94% N_2, 5% CO_2, and 1% O_2 at 37°C for 12 h. After hypoxia, the medium was immediately washed off, and the HUVECs were returned to the maintenance medium (NCS-DMEM) in normal incubator for 4 h. At the same time, prepared propofol was added to the medium to different concentrations (25 μmol/L–150 μmol/L).

genes in a cell via degradation or translation inhibition of their target mRNAs [15]. In recent years, many associations between disease mechanisms and specific miRNAs have been identified and confirmed using large-scale microarrary profiling and genetic approaches [16]. Studies provide an overview of the role of miRNAs in the development of I/R injury in the heart and kidney [17]. However, miRNAs that are associated with the protective effect of propofol on I/R injury remain largely unknown.

In the present study, we constructed an *in vitro* cellular hypoxia/reperfusion (H/R) model and found that propofol effectively reduced H/R injury. We performed systemic analysis of the alterations in miRNA expression using miRNA microarray in human umbilical vein endothelial cells (HUVECs) treated with H/R in the presence or absence of propofol posthypoxia treatment. Fourteen miRNAs were shown to be differentially expressed of which eight were substantially increased, whereas six were decreased and six of them were picked and further validated by qRT-PCR. Then, the Gene Ontology (GO) analysis was conducted to build signaling networks of predicted targets of ten miRNAs. Interestingly, six of the identified microRNAs are found to target autophagy-related genes. Our results revealed that different autophagy-associated miRNA expression patterns are induced by propofol posthypoxia treatment in H/R, which implicates that differential autophagy-related gene-expression regulated by miRNAs may play a role in propofol posthypoxia treatment in H/R.

2. Results

2.1. Protective Effects of Propofol Posthypoxia Treatment against H/R Injury on Cell Viability. The construction of the cellular H/R P-PostH model is shown in Figure 1. The cells in the control group were considered 100% viable. As shown in Figure 2(a), there was no marked alteration in propofol-treated cells compared with control cells under normal conditions. CCK-8 assay showed that propofol treatment for 4 h at concentrations up to 150 μmol/L did not influence cell viability ($P > 0.05$). Exposure of cells to H/R resulted in reduction of cell viability (Figure 2(b)). The viabilities of cells in the H/R groups were 55.9 ± 1.8% ($P < 0.01$ versus control). In all the groups of H/R+P-PostH, the viability of cells increased compared with the H/R only group ($P < 0.05$) except 150 μmol/L (68.1 ± 5.3, 69.4 ± 3.6, 72.2 ± 5.7, and 62.5 ± 6.7%, resp.) indicating that administration of excessive propofol has no protective effects. The results did not show significant dose-dependent manner compared with previous reports. This discrepancy may be due to different experimental condition (e.g., the concentration of oxygen in hypoxic chamber, the H/R time and different cell lines that we used).

2.2. Inhibitory Effect of Posthypoxia Treatment with Propofol on Apoptosis and Autophagy Induced by H/R. To confirm the inhibitory effect of P-PostH on cell apoptosis, HUVECs were stained with Annexin V-FITC and propidium iodide,

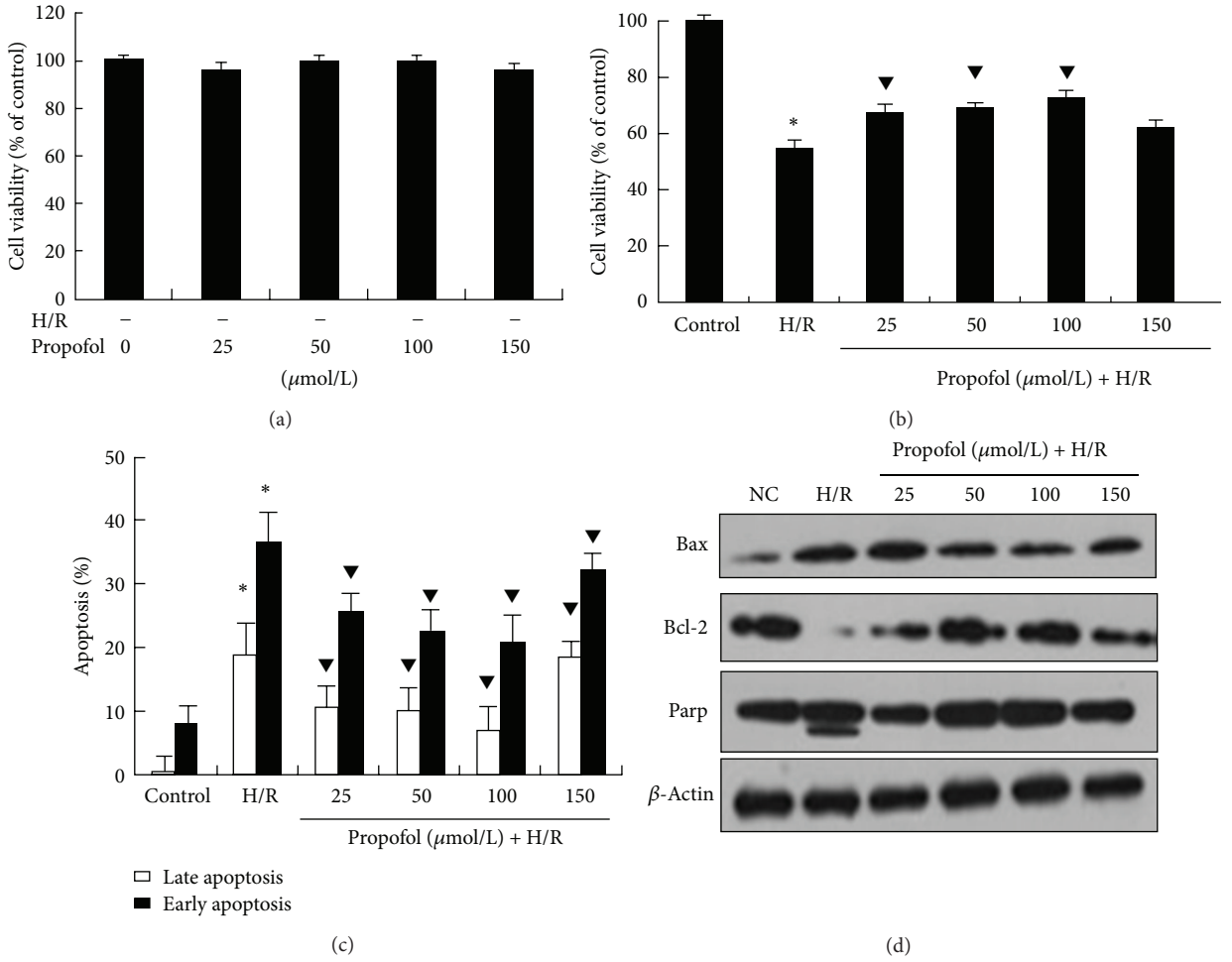

Figure 2: Propofol increased the viability and reduced the apoptosis of the H/R induced injury in HUVECs. (a) The normal HUVECs were treated with different concentrations (0–150 μmol/L) of propofol for 4 h. (b) The cells were postconditioned with increasing concentrations of propofol (0–150 μmol/L) after 12 h of hypoxia and 4 h of reperfusion. Cell viability was determined by CCK-8 assay, as previously described. Values are represented as the percentage of viable cells; vehicle-treated cells were considered as 100% viable. The data represented are mean percentage of viable cells + SD of three independent experiments. $^{*}P < 0.001$, compared with control group, $^{\blacktriangledown}P < 0.05$, compared with the H/R group. (c) Detection of apoptosis with Annexin V-FITC and propidium iodide staining. Every group of cells with Annexin V and propidium iodide staining was measured by flow cytometry. Histogram representing the percentage of early apoptotic cells and late apoptotic cells. The data represent the mean + SD of three independent experiments. $^{*}P < 0.01$, compared with the control group, and $^{\blacktriangledown}P < 0.05$ with H/R group. (d) Expression of apoptosis-related proteins in normal group, H/R injury group, and propofol posthypoxia treatment groups. Data are representative WB from 3 independent experiments ($n = 2$).

and then analyzed by flow cytometry. The percentage of early apoptosis in the control and H/R groups was 8 + 4.4% and 36.6 + 2.4%, respectively ($P < 0.01$ versus control). There was an obvious reduction in the number of early apoptotic cells, (25.6 + 2.8, 22.6 + 2.6, 21 + 3.2, 32.2 + 2.5%) when cells were treated with different concentrations of propofol (25, 50, 100, 150 μmol/L) respectively, compared with the H/R group ($P < 0.05$ versus H/R group) in Figure 2(c). We then examined the apoptosis-related proteins by using Western blotting (WB). Apoptotic protein Bax is upregulated and PARP is cleaved while anti-apoptotic protein Bcl-2 is downregulated upon H/R treatment (Figure 2(d)). However, the expression of these proteins is reversed and PARP cleavage is prevented upon adding propofol after hypoxia treatment in a dose-dependent manner except 150 μmol/L, which is in agreement with the results from the viability assay and Annexin V-FITC and PI staining (Figure 2(d)).

Next, we investigated whether H/R-induced autophagy in HUVECs can be regulated by propofol. H/R promoted effective transition of LC3-I to LC3-II, which was prevented by propofol treatment except 150 μmol/L, compared with control cells subjected to DMSO during the course of H/R injury or normoxia (Figures 3(a), 3(b), and 3(c)). The immunofluorescence observation strengthened the WB results. HR induced a significant number of LC3 puncta and irregular shape of mitochondria (indicative apoptosis) while cells can be recovered to normal state upon propofol treatment (Figure 3(d)).

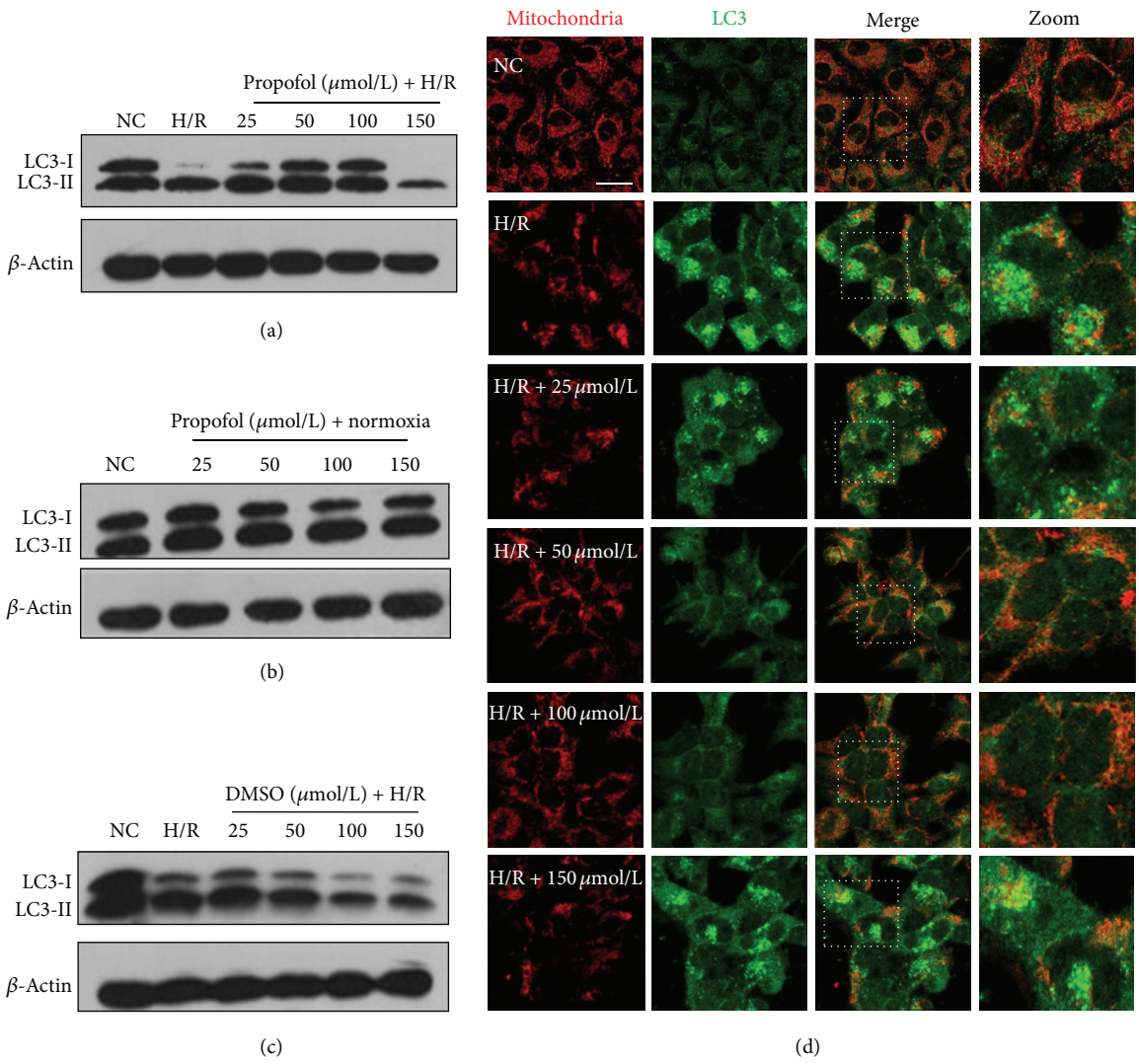

Figure 3: Propofol suppresses the H/R-induced autophagy. (a) The expression of LC3 was determined in normal cells, H/R injury cells, and propofol posthypoxia treatment cells (25–150 μmol/L). (b) The expression of LC3 was determined in control cells and cells treated by normoxia with propofol (25–150 μmol/L). (c) The expression of LC3 was determined in normal cells group, H/R injury cells group, and DMSO posthypoxia treatment groups (25–150 μmol/L). Data are representative WB from 3 independent experiments ($n = 3$). (d) Autophagosomes and mitochondria were probed by anti-LC3 and anti-Tim23 in normal cells, H/R injury cells, and propofol posthypoxia treated cells. Bar, 20 μm.

Together, these data indicate that Propofol could effectively suppress the apoptosis and autophagy induced by the H/R in HUVECs.

2.3. miRNA Are Differently Expressed in P-Post+H/R Compared with H/R Alone. To study the potential miRNAs that may function in the protective effect on H/R injury in HUVECs, we determined the miRNA expression profile in HUVECs through miRNA microarray analysis. We first assessed the miRNA expression profiles in the P-PostH and H/R groups. The expression profiles of hundreds of miRNAs determined to be regulated between P-Post and H/R separate samples into biologically interpretable groups. Among these, 8 miRNAs were identified to be upregulated more than two fold in P-PostH group compared with the same 8 miRNAs in H/R group, while 6 miRNAs were downregulated more than twofold ($P < 0.01$) (Figure 4). 6 miRNAs among these filtered ones were selected for qRT-PCR verification, four of which were validated to be significantly different between the propofol and HR groups ($P < 0.05$). The other two show the expression tendency consistent with the array result but without statistical significance. As is shows in Figure 5, the levels of hsa-miR-30b, hsa-miR-20b, hsa-miR-196a, hsa-miR-374b were upregulated in propofol-treated group with the HR only group, while hsa-let-7e and hsa-miR-15b showed an opposite expression pattern, which was in agreement with the result of microarray hybridization.

2.4. Potential Autophagy-Related Targets of the Differentially Expressed miRNAs Are Revealed. Computational algorithms

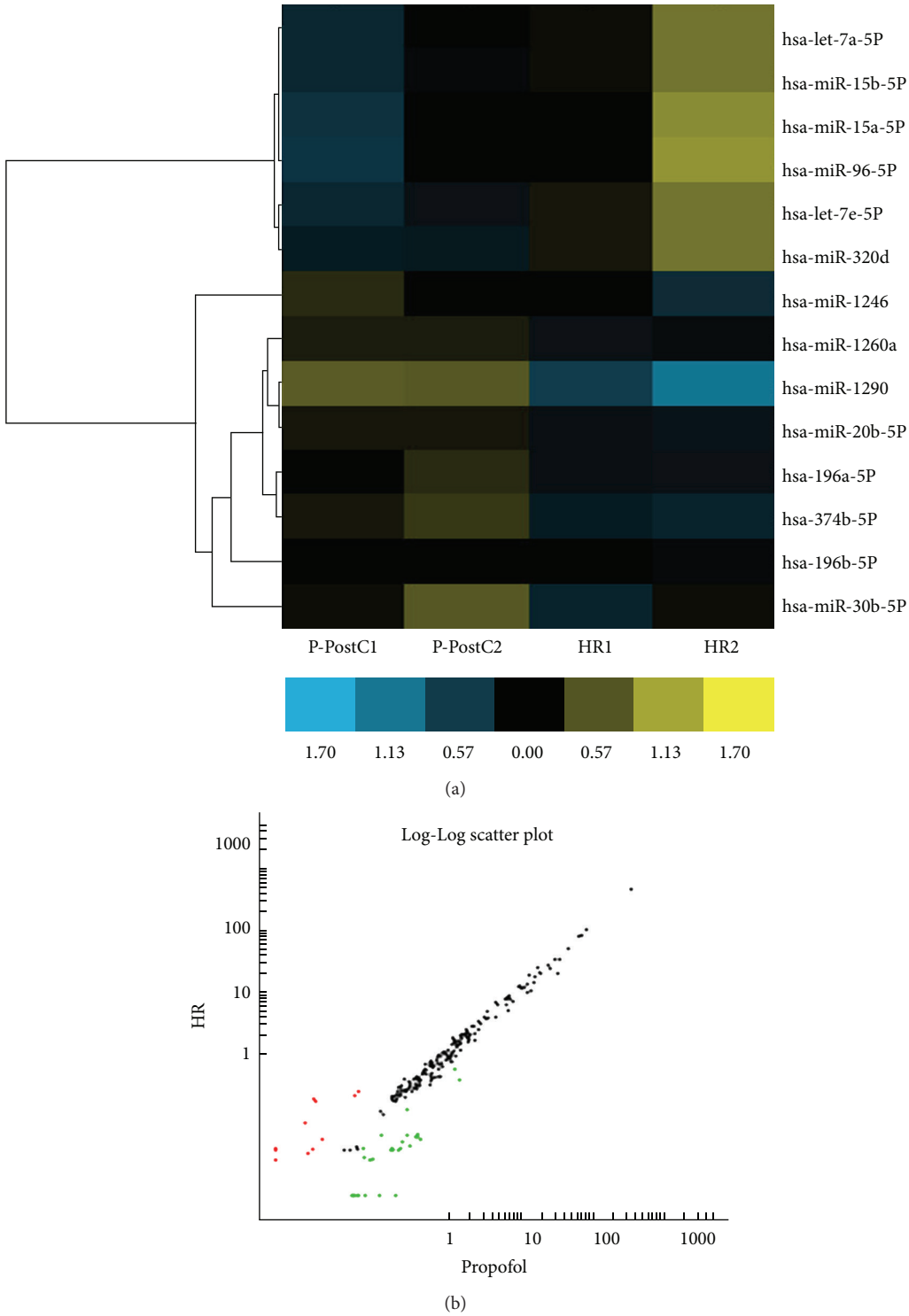

Figure 4: miRNA profiles differentiate the propofol group from the H/R group. (a) Hierarchical clustering of 14 miRNAs whose expression was significantly altered (fold change >2, $P < 0.01$, FDR > 0.05) in the propofol and HR groups. The color stands for the intensity of the signal ($n = 3$). (b) In the scatter diagram, red spots stand for the miRNAs expressed higher in the HR group, the green ones stand for the ones higher in the propofol groups, and the black ones with no significant changes.

Table 1: The targets and the expression levels of microRNAs.

miRNA	Target symbol	Target common name	Miranda	TargetScan	HR expression level miRNA
hsa-miR-30b	BECN1	Beclin 1, autophagy related	Yes	Yes	↓
hsa-miR-30b	ATG5	Autophagy related 5	Yes	Yes	↓
hsa-miR-20b	ULK1	unc-51 like autophagy activating kinase 1	Yes	Yes	↓
hsa-miR-20b	MAP3K14	mitogen-activated protein kinase kinase kinase 14	Yes	Yes	↓
hsa-miR-196a	RICTOR	RPTOR independent companion of MTOR	Yes	Yes	↓
hsa-miR-96	ATG7	Autophagy related 7	Yes	Yes	↑
hsa-miR-15b	BCL2	B-cell CLL/lymphoma 2	Yes	Yes	↑
hsa-miR-374b	VEGFA	Vascular endothelial growth factor A	Yes	Yes	↓
hsa-let-7e	ATP2A2	ATPase, Ca++ transporting, cardiac muscle, and slow twitch 2	Yes	Yes	↑

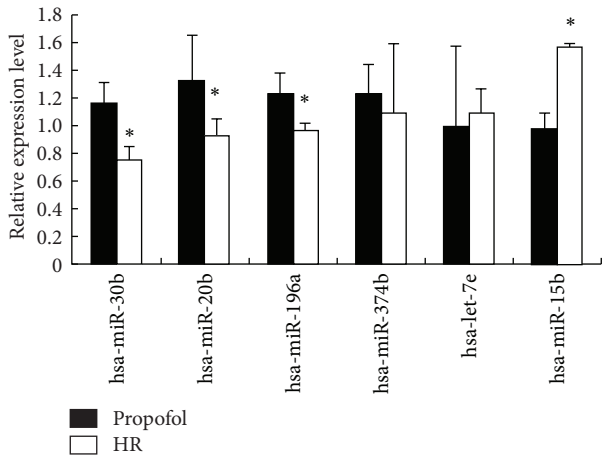

Figure 5: Validation of selected microarray data by qRT-PCR. Statistically significant difference between propofol and H/R is indicated by $^{*}P < 0.05$ ($n = 4$).

showed that hsa-miR-20b, hsa-miR-30b, hsa-miR-96, and hsa-miR-196a may target autophagy-associated genes ULK1, Becline-1, ATG7 and Rictor respectively. Hsa-miR-15b or hsa-miR-374b may target anti-apoptosis- or proliferation-related genes. Hsa-miR-7e may target mitochondria-associated gene (Table 1). All of the reciprocally expressed miRNAs and proteins were predicted by two of the algorithms (Table 1). MTOR inhibition is directly involved in autophagy induction [18, 19]. We found that Hsa-miR-20b, hsa-miR-196 and hsa-miR-15b might be the key regulators of autophagy, mTOR and anti-apoptosis pathway in the protective effects of propofol on H/R injury, respectively. The miRNA-target gene interaction networks related to the autophagy and mTOR pathway which we predicted previously are shown in Figure 6. The upregulated miRNAs hsa-miR-20b showed the 10 target mRNAs when autophagy pathway is concerned, while hsa-miR-30b is also importantly related to autophagy pathway. Hsa-miR-96 and hsa-miR-196a were predicted to target mTOR pathway related genes (Figure 6).

3. Discussion

H/R-associated cell injury may involve oxidative stress-induced damage, through formation of reactive oxygen species (ROS). As potent oxidizing and reducing agents, ROS directly damage the endothelium cellular membrane through lipid peroxidation and reductase inhibition [20]. ROS also upregulate the expression of cell adhesion molecules, induce transcription of cytokines, and subsequently stimulate the activation and chemotaxis of neutrophils, which can lead to the death of the endothelial cells [21].

Propofol is structurally similar to the endogenous antioxidant vitamin E and exhibits antioxidant activities [22]. It has a protective effect against oxidative stress-mediated cell injuries [23]. Propofol prevents reactive oxygen species (ROS) such as hydrogen peroxide (H_2O_2)-induced cellular damages in cultured endothelial cells and cardiac cells *in vitro* [24, 25] and in hearts with ischemia/reperfusion injury *in vivo* [10].

To date, only a few studies concerning regulation of propofol-mediated cellular protection by microRNA have been reported. Large scale and systemic profiling of key node microRNAs in H/R treated with P-PostH have not been conducted. Consistent with previous results, our study also found the protective effect of propofol against the H/R injury in HUVECs. In order to reveal critical microRNAs involved in this process, we firstly evaluated the miRNA expression profile in the propofol-postconditioned H/R injury of HUVEC cells to reveal the potential role of miRNAs in the protective effect. We found a set of differently expressed miRNAs, with 6 downregulated and 8 upregulated miRNAs in Propofol-postconditioned groups when compared to H/R groups. qRT-PCR of hsa-miR-30b, hsa-miR-20b, hsa-miR-15b, hsa-let-7e, hsa-miR-374b, and hsa-miR-196a further validated the reliability of the microarray result.

In order to gain insight into the function of miRNAs, GO term and KEGG pathway annotation were applied to their target gene pool. KEGG annotation showed a significant change with the autophagy and mTOR signaling pathway in the P-PostH group compared with the H/R group. Further investigation of the miRNA-gene network of these two pathways shows that hsa-miR-20, hsa-miR-30b, and hsa-miR-196a might be the key regulators of autophagy and mTOR pathway, respectively.

Autophagy is an evolutionary conserved process involved in degradation of long-lived or damaged proteins and organelles [26–28]. A previous study showed that propofol

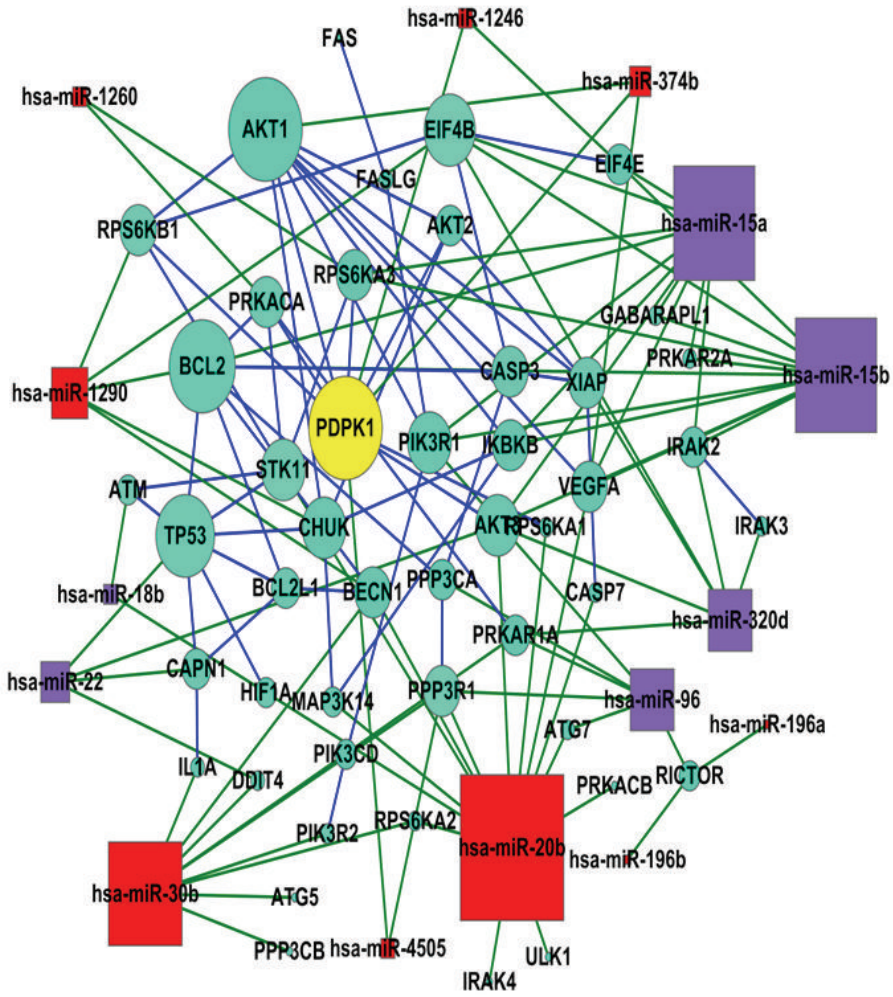

Figure 6: miRNA-gene interaction networks of autophagy and mTOR pathway. Red box nodes represent miRNA that are upregulated in propofol group. Blue represent downregulated ones and green cycle nodes represent mRNA. Edges show the inhibitory effect of miRNA on mRNA.

protects the autophagic cell death induced by the myocardial I/R injury [14]. Beclin-1 and ATG5 were also shown to be target genes of hsa-miR-30b [29], which were confirmed by our study. Further experiments are needed to probe the detailed mechanism. We also revealed other differentially expressed miRNAs in P-PostH when compared with H/R group which may regulate the MAPK signaling pathway and apoptosis, such as hsa-miR-20b and hsa-miR-15b [30–33].

In conclusion, our study, for the first time, systematically studied the microRNA profiling in P-PostH-treated H/R HUVEC cells and revealed some miRNAs that differentially expressed in P-PostH H/R induced cell injury. Their regulatory roles in the autophagy and anti-apoptosis pathways may be involved in the protective effects of the propofol against H/R injury. The low expression of hsa-miR-30b and hsa-miR-20b may lead to the abnormal upregulation of autophagy-related proteins, induce excessive autophagy, and contribute to the cell death. Confirmation and elucidation of this mechanism requires further study. Present results also point to several exciting directions for future research. Each possible miRNA-gene pair we identified is a strong candidate for a major study to definitively confirm the presence of specific miRNA-gene interactions, thus creating a more detailed picture of the effects of propofol.

4. Materials and Methods

4.1. Reagents and Antibodies. Propofol was purchased from Sigma Chemical to exclude the influence of lipid emulsion. Regents include Dulbecco's modified Eagle's medium (DMEM), newborn calf serum (NCS), penicillin, streptomycin, trypsin-EDTA (GIBCO Laboratories, Grand Island, New York, USA), dimethylsulfoxide (DMSO), Annexin V-FITC apoptosis detection kit, and CCK-8 cell counting kit. Propofol was dissolved in DMSO and further diluted in phosphate buffered saline (PBS). The final DMSO concentration was 0.1%, which did not affect either cell function or the assay system. The following primary antibodies were used in this study: anti-beta-Actin antibody (Santa Cruz, sc-47778), anti-LC3B polyclonal antibody (Sigma, L7543), anti-LC3

polyclonal antibody (MBL, PM036), anti-TOM20 (FL-145) (Santa Cruz, sc-11415).

4.2. HUVEC Cell Culture. HUVECs were isolated from fresh human umbilical cord veins by collagenase digestion according to a modified technique described by Jaffe et al. [34]. Briefly, HUVECs were cultured at 37°C in a 95% O_2 and 5% CO_2 humidified atmosphere in DMEM supplemented with 20% fetal bovine serum, 100 μg/mL streptomycin, and 100 IU/mL penicillin. The HUVECs were subcultured nine to ten days later.

4.3. Construction of an In Vitro Cellular Propofol Posthypoxia Treatment H/R Model. For hypoxia, the culture media was replaced by glucose and serum free DMEM balanced in normal incubator in 30 minutes and the HUVEC cells were then placed in hypoxic conditions which were created by a small enclosed humidified plexiglass chamber filled with 94% N_2, 5% CO_2, and 1% O_2 at 37°C for 12 h. After hypoxia, the medium was washed off, and the HUVECs were returned to the maintenance medium (NCS-DMEM) in normal incubator with 5% CO_2 and 95% N_2 for 4 h. At the same time, prepared propofol was added to the medium to different concentrations (25 μmol/L–150 μmol/L). Clinically relevant blood concentration of propofol is approximately 17–62 μmol/L for the maintenance of satisfactory anaesthesia [11]. The blood concentration of bolus injection of propofol can reach 56 μmol/L. Therefore, we consider 25–100 μmol/L as the range of clinically relevant concentrations and increasing propofol concentrations were designed as 25, 50, 100, and 150 μmol/L, respectively (Figure 1).

4.4. Cell Viability Assay. The cellular viability was evaluated using a CCK-8 kit. Cells were plated at $1 * 10^4$ cells per well in 96-well plates and treated with H/R and various concentrations of propofol posthypoxia treatment. Each concentration of propofol (0–150 μmol/L) was repeated in 6 wells. Meanwhile, increasing concentrations of propofol were given to non-H/R cells for 4 h. After the radiation exposure, the cells were washed twice with PBS and incubated with 1 mL culture medium, which contained 10% CCK-8 solution, for 2 h at 37°C. The absorbance was measured by a multimode microplate reader at 450 nm. The cellular viability (%) was calculated using the formula $[(As - Ab)/(Ac - Ab)] * 100\%$. As: the absorbance of the well containing supernatant from exposure or sham-exposure dishes; Ac: the absorbance of the well containing supernatant from the normal control; Ab: the absorbance of the well containing culture medium with 10% CCK-8 solution.

4.5. Detection of Apoptosis. To quantify apoptosis, HUVECs were stained with Annexin V-FITC and propidium iodide. Prepared cells were washed twice with cold PBS and resuspended in 500 mL binding buffer. Five microlitres of Annexin V-FITC and 5 mL of propidium iodide (1 mg/mL) were then added to these cells, which were analysed with a FACSCalibur flow cytometer. Early apoptotic cells were positive for Annexin V and negative for propidium iodide, whereas late apoptotic dead cells displayed both high Annexin V and propidium iodide labelling.

4.6. Western Blotting. The expressions of apoptosis related proteins and LC3 were determined by Western blot analysis. The whole cell lysates were prepared in RIPA buffer (50 mM Tris HCl, pH 8, 150 mM NaCl, 1% Nonidet P-40, 0.1% SDS, and 1% Triton X-100 plus proteinase inhibitors; Sigma). Protein concentration was determined by Bradford assay, and samples containing 30 ug were separated by 12% SDS-PAGE. Proteins were transferred to nitrocellulose membranes. After membranes were blocked in 5% nonfat milk in 20 mM Tris-HCl, 150 mM NaCl, and 0.05% Tween 20 for 1 hr at room temperature, the membranes were incubated overnight at 4°C with different primary monoclonal antibodies; β-actin antibody was used as a loading control. The membranes were then incubated with secondary antibody conjugated to horseradish peroxide for 1 hr at room temperature and were exposed to enhanced chemiluminescence reagents. Densitometric analysis was performed to quantify the signal intensity.

4.7. Immunofluorescence. Cells were grown to 70% confluence on a coverslip. After treatment, cells were washed twice with PBS (Shanghai Sangon Biotech) and fixed with freshly prepared 4% paraformaldehyde at 37°C for 15 min. Antigen accessibility was increased by treatment with 0.1% Triton X-100 (Shanghai Sangon Biotech). After blocking with 1% BSA, cells were incubated with primary antibodies for 1 h at room temperature, and, after washing with PBS, stained with a secondary antibody for a further 50 min at room temperature. Cell images were captured with a TCS SPF5 II Leica confocal microscope.

4.8. RNA Extraction and miRNA Microarray Analysis. Total RNA containing small RNA was extracted from H/R groups and P-PostH groups in HUVECs by using the Trizol reagent (Invitrogen) and purified with mirVana miRNA Isolation Kit (Ambion, Austin, TX, USA) according to manufacture's protocol. The purity and concentration of RNA were determined from OD260/280 readings using spectrophotometer (NanoDrop ND-1000). RNA integrity was determined by 1% formaldehyde denaturing gel electrophoresis. The miRNA profiling was performed using Agilent miRNA array. The Agilent array was designed with eight identical arrays per slide (8×60 K format), with each array containing probes interrogating 1887 human mature miRNAs and 121 human virus related miRNAs, both from miRBase R18.0. Each miRNA was detected by probes repeat for 30 times.

Microarray experiments were conducted according to the manufacturer's instructions. Briefly, the miRNAs were labeled using the Agilent miRNA labeling reagent. Total RNA (100 ng) was dephosphorylated and ligated with pCp-Cy3, the labeled RNA was purified and hybridized to miRNA arrays. Images were scanned with the Agilent microarray scanner (Agilent), gridded, and analyzed using Agilent feature extraction software version 10.10.

4.9. Validation of Selected Microarray Data by qRT-PCR. The differentially expressed miRNAs between H/R and P-PostH

Table 2: Primers used in qRT-PCR.

Gene	Annealing temperature °C	Number of gene primer (5′ → 3′)	Accession number
U6	60	F: 5′CTCGCTTCGGCAGCACATATACT3′ R: 5′CGAATTTGCGTGTCATCCTTGCG3′	NR_004394.1
hsa-miR-30b	60	F: 5′CGCTGTAAACATCCTACACTCA3′ R: 5′GCAGGGTCCGAGGTATTC3′	MIMAT0000420
Hsa-miR-15b-5P	60	F: 5′ATGGTTCGTGGGTAGCAGCACATCATGGTTTACA3′ R: 5′GCAGGGTCCGAGGTATTC3′	MIMAT0000417
Has-miR-196a-5p	60	F: 5′ATGGTTCGTGGGTAGGTAGTTTCATGTTGTTGG3′ R: 5′GCAGGGTCCGAGGTATTC3′	MIMAT0000226
Hsa-miR-374b-5P	60	F: 5′CGTGGGATATAATACAACCTGCTAAGTG3′ R: 5′CTCAACTGGTGTCGTGGA3′	MIMAT0004955
Hsa-miR-20b-5P	60	F: 5′ATGGTTCGTGGGCAAAGTGCTCATAGTGCAGGTAG3′ R: 5′CTCAACTGGTGTCGTGGA3′	MIMAT0001413
Hsa-let-7e	60	F: 5′CGCTGAGGTAGGAGGTTGTA3′ R: 5′GCAGGGTCCGAGGTATTC3′	MIMAT0000066

F: forward primer; R: reverse primer.
miRNA number and sequence of a specific miRNA can be obtained from miRBase sequence.

levels were determined by qRT-PCR as described [35, 36]. Briefly, RNAs from HUVECs were isolated with mirVana miRNA Isolation Kit (Ambion). QRT-PCR for miRNAs was performed on cDNA generated from 50 ng of total RNA using the protocol of the mirVana quantitative real-time polymerase chain reaction miRNA detection kit (Ambion). As an internal control, U6 was used for miRNAs template normalization. Fluorescent signals were normalized to an internal reference, and the threshold cycle (Ct) was set within the exponential phase of the polymerase chain reaction. The relative gene expression was calculated by comparing cycle times for each target polymerase chain reaction. The target polymerase chain reaction Ct values were normalized by subtracting the U6 Ct value, which provided the ΔCt value. The relative expression level between treatments was then calculated using the following equation: relative gene using the ΔΔCt method with normalization to U6 rRNA endogenous control. The primers used for RT-PCR are shown in Table 2.

4.10. Target Gene Prediction. Prediction of miRNA target prediction can be performed by computational algorithms due to their base-pairing rules between miRNA and mRNA target sites, location of binding sequences within the target's 3′UTR, and conservation of target binding sequences within related genomes. In our study, genes that were predicted by TargetScan v5.1 (http://www.targetscan.org/) and Miranda v5 (http://www.mirbase.org/) were regarded as potential targets of a certain miRNA.

4.11. Bioinformatic Analysis of Differentially Expressed miRNAs. Gene Ontology (GO) analysis was applied in order to organize genes into hierarchical categories and uncover the miRNA gene regulatory network on the basis of biological process, cellular component, and molecular function. We divided the differentially expressed miRNAs into two groups (H/R upregulated and H/R downregulated) and mapped these two groups to each node of the GO database. The miRNAs corresponding to every node were counted by GSEABase package on the R statistic platform (http://www.r-project.org/). We also analyzed the potential target gene related pathways using GenMAPP v2.1 based on Kyoto Encyclopedia of Genes and Genomes (KEGG) pathway database. The enrichment *P*-value of the target genes involved in every pathway was calculated. Afterward, we integrated the regulatory interactions between the genes and miRNAs. We analyzed two different interactions simultaneously: (1) data from KEGG database describing the relationship between genes, including enzyme-enzyme relation, protein-protein interaction, and gene expression interaction (KEGGSOAP software package (http://www.bioconductor.org/packages/2.4/bioc/html/KEGGSOAP.html)) and (2) protein-protein interactions verified by high-flux experiments (the MIPS mammalian protein-protein interaction database: http://mips.helmholtz-muenchen.de/proj/ppi/). Then, we integrated the results into the gene network, and displayed the figure with the software Medusa 21 (data not shown). Finally, we built certain pathway-related networks using predicted targets for the miRNAs to identify critical miRNAs that might modulate the pathways according to the miRNA degree.

Conflict of Interests

The authors declare that they have no conflict of interests.

Acknowledgments

This work is supported by the National Natural Science Foundation of China (81270916, 31301104) and also by the Scientific Research Start-up grant from Guangdong Medical College (XB1342, 701B01206).

References

[1] H. K. Eltzschig and C. D. Collard, "Vascular ischaemia and reperfusion injury," *British Medical Bulletin*, vol. 70, pp. 71–86, 2004.

[2] Z. Huang, X. Zhong, M. G. Irwin et al., "Synergy of isoflurane preconditioning and propofol postconditioning reduces myocardial reperfusion injury in patients," *Clinical Science*, vol. 121, no. 2, pp. 57–69, 2011.

[3] G. Tan and M. G. Irwin, "Recent advances in using propofol by non-anesthesiologists," *F1000 Medicine Reports*, vol. 2, no. 1, article 79, 2010.

[4] S. F. Hughes, M. J. Cotter, S. A. Evans, K. P. Jones, and R. A. Adams, "Role of leucocytes in damage to the vascular endothelium during ischaemia-reperfusion injury," *British Journal of Biomedical Science*, vol. 63, no. 4, pp. 166–170, 2006.

[5] V. V. Shuvaev and V. R. Muzykantov, "Targeted modulation of reactive oxygen species in the vascular endothelium," *Journal of Controlled Release*, vol. 153, no. 1, pp. 56–63, 2011.

[6] Z. Xia, Z. Huang, and D. M. Ansley, "Large-dose propofol during cardiopulmonary bypass decreases biochemical markers of myocardial injury in coronary surgery patients: a comparison with isoflurane," *Anesthesia and Analgesia*, vol. 103, no. 3, pp. 527–532, 2006.

[7] T. Radovits, J. Zotkina, L. N. Lin, M. Karck, and G. Szabó, "Endothelial dysfunction after hypoxia-reoxygenation: do in vitro models work?" *Vascular Pharmacology*, vol. 51, no. 1, pp. 37–43, 2009.

[8] S. Dohgu, T. Nishioku, N. Sumi et al., "Adverse effect of cyclosporin A on barrier functions of cerebral microvascular endothelial cells after hypoxia-reoxygenation damage in vitro," *Cellular and Molecular Neurobiology*, vol. 27, no. 7, pp. 889–899, 2007.

[9] B. Wang, J. Shravah, H. Luo, K. Raedschelders, D. D. Y. Chen, and D. M. Ansley, "Propofol protects against hydrogen peroxide-induced injury in cardiac H9c2 cells via Akt activation and Bcl-2 up-regulation," *Biochemical and Biophysical Research Communications*, vol. 389, no. 1, pp. 105–111, 2009.

[10] Y. C. Jin, W. Kim, Y. M. Ha et al., "Propofol limits rat myocardial ischemia and reperfusion injury with an associated reduction in apoptotic cell death in vivo," *Vascular Pharmacology*, vol. 50, no. 1-2, pp. 71–77, 2009.

[11] D. R. Cui, L. Wang, W. Jiang, A. H. Qi, Q. H. Zhou, and X. L. Zhang, "Propofol prevents cerebral ischemia-triggered autophagy activation and cell death in the rat hippocampus through the NF-kappaB/p53 signaling pathway," *Neuroscience*, vol. 246, pp. 117–132, 2013.

[12] D. Cui, L. Wang, A. Qi, Q. Zhou, X. Zhang, and W. Jiang, "Propofol prevents autophagic cell death following oxygen and glucose deprivation in PC12 cells and cerebral ischemia-reperfusion injury in rats," *PLoS ONE*, vol. 7, no. 4, Article ID e35324, 2012.

[13] S. Lee, K. Kim, Y. H. Kim et al., "Preventive role of propofol in hypoxia/reoxygenation-induced apoptotic H9c2 rat cardiac myoblast cell death," *Molecular Medicine Reports*, vol. 4, no. 2, pp. 351–356, 2011.

[14] H. S. Noh, I. W. Shin, J. H. Ha, Y. S. Hah, S. M. Baek, and D. R. Kim, "Propofol protects the autophagic cell death induced by the ischemia/reperfusion injury in rats," *Molecules and Cells*, vol. 30, no. 5, pp. 455–460, 2010.

[15] V. Ambros, "MicroRNA pathways in flies and worms: growth, death, fat, stress, and timing," *Cell*, vol. 113, no. 6, pp. 673–676, 2003.

[16] K. K. H. Farh, A. Grimson, C. Jan et al., "Biochemistry: the widespread impact of mammalian microRNAs on mRNA repression and evolution," *Science*, vol. 310, no. 5755, pp. 1817–1821, 2005.

[17] C. Yin, X. Wang, and R. C. Kukreja, "Endogenous microRNAs induced by heat-shock reduce myocardial infarction following ischemia-reperfusion in mice," *FEBS Letters*, vol. 582, no. 30, pp. 4137–4142, 2008.

[18] J. J. Jaboin, E. T. Shinohara, L. Moretti, E. S. Yang, J. M. Kaminski, and B. Lu, "The role of mTOR inhibition in augmenting radiation induced autophagy," *Technology in Cancer Research and Treatment*, vol. 6, no. 5, pp. 443–447, 2007.

[19] B. Ravikumar, C. Vacher, Z. Berger et al., "Inhibition of mTOR induces autophagy and reduces toxicity of polyglutamine expansions in fly and mouse models of Huntington disease," *Nature Genetics*, vol. 36, no. 6, pp. 585–595, 2004.

[20] H. Y. Sun, N. P. Wang, F. Kerendi et al., "Hypoxic postconditioning reduces cardiomyocyte loss by inhibiting ROS generation and intracellular Ca2+ overload," *American Journal of Physiology—Heart and Circulatory Physiology*, vol. 288, no. 4, pp. H1900–H1908, 2005.

[21] S. Grotti and T. Gori, "Endothelium, ischemia and the good side of oxygen free radicals," *Clinical Hemorheology and Microcirculation*, vol. 39, no. 1–4, pp. 197–203, 2008.

[22] I. Gülçin, H. A. Alici, and M. Cesur, "Determination of in vitro antioxidant and radical scavenging activities of propofol," *Chemical and Pharmaceutical Bulletin*, vol. 53, no. 3, pp. 281–285, 2005.

[23] I. Vasileiou, T. Xanthos, E. Koudouna et al., "Propofol: a review of its non-anaesthetic effects," *European Journal of Pharmacology*, vol. 605, no. 1-3, pp. 1–8, 2009.

[24] J. J. Xu and Y. L. Wang, "Propofol attenuation of hydrogen peroxide-mediated oxidative stress and apoptosis in cultured cardiomyocytes involves haeme oxygenase-1," *European Journal of Anaesthesiology*, vol. 25, no. 5, pp. 395–402, 2008.

[25] B. Wang, T. Luo, D. Chen, and D. M. Ansley, "Propofol reduces apoptosis and up-regulates endothelial nitric oxide synthase protein expression in hydrogen peroxide-stimulated human umbilical vein endothelial cells," *Anesthesia and Analgesia*, vol. 105, no. 4, pp. 1027–1033, 2007.

[26] N. Mizushima, "Physiological functions of autophagy," *Current Topics in Microbiology and Immunology*, vol. 335, no. 1, pp. 71–84, 2009.

[27] L. Liu, D. Feng, G. Chen et al., "Mitochondrial outer-membrane protein FUNDC1 mediates hypoxia-induced mitophagy in mammalian cells," *Nature Cell Biology*, vol. 14, no. 2, pp. 177–185, 2012.

[28] D. Feng, L. Liu, Y. Zhu, and Q. Chen, "Molecular signaling toward mitophagy and its physiological significance," *Experimental Cell Research*, vol. 319, pp. 1697–1705, 2013.

[29] W. Pan, Y. Zhong, C. Cheng et al., "MiR-30-regulated autophagy mediates angiotensin II-induced myocardial hypertrophy," *PLoS ONE*, vol. 8, Article ID e53950, 2013.

[30] S. Cascio, A. D'Andrea, R. Ferla et al., "miR-20b modulates VEGF expression by targeting HIF-1α and STAT3 in MCF-7 breast cancer cells," *Journal of Cellular Physiology*, vol. 224, no. 1, pp. 242–249, 2010.

[31] Z. Lei, B. Li, Z. Yang et al., "Regulation of HIF-1α and VEGF by miR-20b tunes tumor cells to adapt to the alteration of oxygen concentration," *PLoS ONE*, vol. 4, no. 10, Article ID e7629, 2009.

[32] F. An, B. Gong, H. Wang et al., "miR-15b and miR-16 regulate TNF mediated hepatocyte apoptosis via BCL2 in acute liver failure," *Apoptosis*, vol. 17, no. 7, pp. 702–716, 2012.

[33] L. Xia, D. Zhang, R. Du et al., "miR-15b and miR-16 modulate multidrug resistance by targeting BCL2 in human gastric cancer cells," *International Journal of Cancer*, vol. 123, no. 2, pp. 372–379, 2008.

[34] E. A. Jaffe, R. L. Nachman, C. G. Becker, and C. R. Minick, "Culture of human endothelial cells derived from umbilical veins. Identification by morphologic and immunologic criteria," *Journal of Clinical Investigation*, vol. 52, no. 11, pp. 2745–2756, 1973.

[35] R. Ji, Y. Cheng, J. Yue et al., "MicroRNA expression signature and antisense-mediated depletion reveal an essential role of MicroRNA in vascular neointimal lesion formation," *Circulation Research*, vol. 100, no. 11, pp. 1579–1588, 2007.

[36] Y. Lin, X. Liu, Y. Cheng, J. Yang, Y. Huo, and C. Zhang, "Involvement of MicroRNAs in hydrogen peroxide-mediated gene regulation and cellular injury response in vascular smooth muscle cells," *Journal of Biological Chemistry*, vol. 284, no. 12, pp. 7903–7913, 2009.

Hindawi Publishing Corporation
Oxidative Medicine and Cellular Longevity
Volume 2013, Article ID 507832, 8 pages
http://dx.doi.org/10.1155/2013/507832

Research Article

The Protection of Salidroside of the Heart against Acute Exhaustive Injury and Molecular Mechanism in Rat

Yunru Wang, Peng Xu, Yang Wang, Haiyan Liu, Yuwen Zhou, and Xuebin Cao

Department of Cardiology, Geriatric Cardiovascular Disease Research and Treatment Center, No. 252 Hospital of PLA, Baoding 071000, China

Correspondence should be addressed to Xuebin Cao; caoxb252@163.com

Received 6 August 2013; Accepted 4 October 2013

Academic Editor: Qian Fan

Objective. To investigate the protection of salidroside of the heart against acute exhaustive injury and its mechanism of antioxidative stress and MAPKs signal transduction. *Method*. Adult male SD rats were divided into four groups randomly. Cardiomyocytes ultrastructure was observed by optical microscopy and transmission electron microscopy. The contents of CK, CK-MB, LDH, MDA, and SOD were determined by ELISA method, and the phosphorylation degrees of ERK and p38 MAPK were assayed by Western blotting. Cardiac function of isolated rat heart ischemia/reperfusion was detected by Langendorff technique. *Results*. Salidroside reduced the myocardium ultrastructure injury caused by exhaustive swimming, decreased the contents of CK, CK-MB, and LDH, improved the LVDP, $\pm$LV dp/dt_{max} under the basic condition, reduced the content of MDA and the phosphorylation degree of p38 MAPK, and increased the content of SOD and the phosphorylation degree of ERK in acute exhaustive rats. *Conclusion*. Salidroside has the protection of the heart against acute exhaustive injury. The cardioprotection is mainly mediated by antioxidative stress and MAPKs signal transduction through reducing the content of MDA, increasing the content of SOD, and increasing p-ERK and decreasing p-p38 protein expressions in rat myocardium, which might be the mechanisms of the cardioprotective effect of salidroside.

1. Introduction

Exhaustive exercise is a pathological state of multiple organ dysfunction due to the strong and durable exercise load which is beyond the bearing ability of the body. It will increase the oxygen consumption of cardiomyocytes, which may produce an imbalance between reactive oxygen species (ROS) and antioxidants, inducing oxidative stress as a result of increased ROS production [1–3] and damage to cardiac structure, metabolism, and function [4, 5]. More specifically, oxidative stress is the imbalance between oxidation and antioxidation system. Superoxide dismutase (SOD) is one of the important enzymes to eliminate ROS and malondialdehyde (MDA) is the terminal product of the membrane lipid peroxidation; the changes of their contents can reflect the degree of oxidative stress of cardiomyocytes.

Exhaustive exercise can destroy the balance of antagonism between atrial natriuretic peptide and endothelin, which will cause sustained contraction of coronary artery, making the blood supply of coronary artery unable to satisfy the demand of cardiomyocytes for blood and oxygen and then induce continuous ischemia-hypoxia of myocardium and the damage factor will increase at the same time; both of them are deleterious to myocardium [6, 7]. Mitogen-activated protein kinases (MAPKs) are one of the important signal transduction systems in cell, including the ways of extra cellular signal-regulated kinase (ERK) and p38 MAPK. Research shows that the activation of ERK can inhibit the apoptosis of myocardial cell and p38 MAPK might promote the apoptosis of cardiomyocytes [8–11]. As an important second messenger in the cell, ROS also can mediate cell survival and death by influencing the ways of ERK and p38 MAPK.

Salidroside (SAL) as one of the effective components of *Rhodiola rosea* L. has the protection against the liver and kidney injury of rat, and it is related to the function of antioxidative stress and antiapoptosis [12, 13]. In addition,

salidroside has good protection against acute myocardial ischemia injury and isolated heart ischemia/reperfusion injury of normal rats. It can increase myocardial contraction force, improve myocardial ischemia, and reduce myocardial ischemia infarction area [14, 15]. However, there is no research regarding whether salidroside is protective against acute myocardial ischemia injury caused by exhaustion exercise and exhaustive heart ischemia-reperfusion injury at present. Thus, in this study, we established the model of isolated rat heart ischemia/reperfusion by Langendorff technique to investigate the effect of salidroside on cardiac function of acute exhaustion rat and its changes after ischemia/reperfusion and discussed whether the protection mechanisms are antioxidation stress and MAPKs signal transduction.

2. Method

2.1. Material. 99% salidroside powder (Lot: 080901-1) was purchased from Ying Xuan Biochemicals Co. Ltd. (Shanghai, China); ELISA kits were obtained from BD Co. (New York, USA); antibodies used were as follows: total p38 MAPK (D13E1) 1 : 1000, phospho-p38 MAPK (Thr180/Tyr182) (D3F9) 1 : 1000, total SAPK/JNK 1 : 1000, phospho-SAPK/JNK (Thr183/Tyr185) 1 : 1000, total p44/42 MAPK (Erk1/2) (137F5) 1 : 2000, and phosphor-p44/42 MAPK (Erk1/2) (Thr202/Tyr204) 1 : 2000 were all purchased from CST Co. (USA). Horseradish peroxidase labeling goat anti-mouse IgG was obtained from CWBIO Co. Ltd. (Beijing, China). All of the chemicals were of analytical reagent grade.

Forty adult male Sprague Dawley (SD) rats of pathogen-free were provided by Laboratory Animal Center of the Academy of Military Medical Sciences (Beijing), certification number SCXK (Beijing): 2003-1-003. The animal experimental procedures were approved by the university committee for animal experiments and in accordance with the principles outlined in the NIH Guide for the Care and Use of Laboratory Animals.

A rat isolated perfusion system (120102EZ-220, Radnoti Co., USA), a rat physiological recorder system (ML880/P16, AD Co. USA), a microplate reader (Thermo fisher SC, FI), a biochemical analyzer (7600-02, HITACHI, Japan), a transmission electron microscope (TEM) (H-7500, HITACHI, Japan), and an ultramicrotome (Leica instrument Co. Ltd., GER) were used in the experiments.

2.2. The Establishment of Exhaustive Animal Model. The classical Thomas method [16] was used to establish the model of acute exhaustive cardiac injury through exhaustive swimming. The rats were divided into control group (Con), salidroside group (Sal), salidroside-acute exhaustive swimming group (SE), and acute exhaustive swimming group (EE) randomly and averagely. The rats of Con group and SE group were given 0.9% NaCl ($12\,mL{\cdot}kg^{-1}{\cdot}d^{-1}$) by intraperitoneal injection for fourteen days; meanwhile the rats of Sal group and SE group were given salidroside ($24\,mg{\cdot}kg^{-1}{\cdot}d^{-1}$) in the same way. Then the rats of SE group and EE group submitted to one-time exhaustive swimming, stopped the exhaustive exercise when met the Thomas standard of exhaustion and dried the fur to avoid the rats sick.

2.3. The Collection of Serum. Blood was collected from abdominal aorta by plain tube within 2 h after exhausted exercise and centrifuged (3000 g/min) for twenty minutes. The serum was preserved at −80°C.

2.4. The Protein Extraction of Myocardium. Freeze the rat heart immediately after the heart was taken out and washed in PSB solution. Then cut the left ventricular myocardial into small pieces, weighed 0.05 g, and put them into the extraction reagent, which consisted of 3.6 mL of lysis buffer, 400 μL of PMSF, homogenized and lysed for thirty minutes and then centrifuged (10000 g/min) for five minutes at 4°C. The supernatant was preserved at −20°C until needed.

2.5. The Preparation of Myocardial Specimen. The rat heart was fixed in 10% formaldehyde and preserved at normal temperature. Then observe it by optical microscope after HE coloration.

A small piece (2 mm × 1 mm × 1 mm) of subendocardial myocardium from the root of left ventricular papillary muscle was taken and fixed in 0.1 mmol/L phosphate buffer (pH = 7.2) which included 3% glutaraldehyde and 1.5% paraformaldehyde at 4°C. Then cut it into small pieces of $1\,mm^3$ and continue fixed in the above solution for 4 h. Fixed in 1% osmic acid again at 4°C for 1.5 h after rinsed by phosphate buffer. Afterwards, the tissue was dehydrated by alcohol and acetone in order, embedded by epoxy resin 618, located by semithin sectioning, and sliced into ultrathin sections in a thickness of 60 nm. The sections were dyed with uranium acetate and lead citrate, and observed by transmission electron microscopy (TEM).

2.6. Heart Isolation and Perfusion. Rats were anesthetized with sodium pentobarbital (40 mg/kg, i.p.), and hearts were quickly removed out and mounted on a Langendorff apparatus via aorta for retrograde perfusion with Krebs-Henseleit (K-H) buffer at constant pressure (10 KPa) and constant temperature (37°C). K-H buffer (in mmol/L) was composed of NaCl 118, KCl 4.7, $MgSO_4$ 1.2, $CaCl_2$ 2.5, KH_2PO_4 1.2, $NaHCO_3$ 25, and glucose 11. The buffer was saturated with 95% O_2/5% CO_2 (pH 7.4). A water-filled latex balloon-tipped catheter was placed into the left ventricle through the left atrium and adjusted to a left ventricular end diastolic pressure (LVEDP) of 5–10 mmHg during the initial equilibration. The distal end of the catheter was connected to a PowerLab system via a pressure transducer (model Gould P23Db, AD Instrument Ltd., Australia). After 20 min stabilization with K-H buffer, the hearts were subjected to 30 min no-flow global ischemia followed by 60 min reperfusion. Left ventricular developed pressure (LVDP), LVEDP, and the maximal differentials of LVDP ($\pm LV dp/dt_{max}$) were continuously recorded with PowerLab system. The data were analyzed by Chart software.

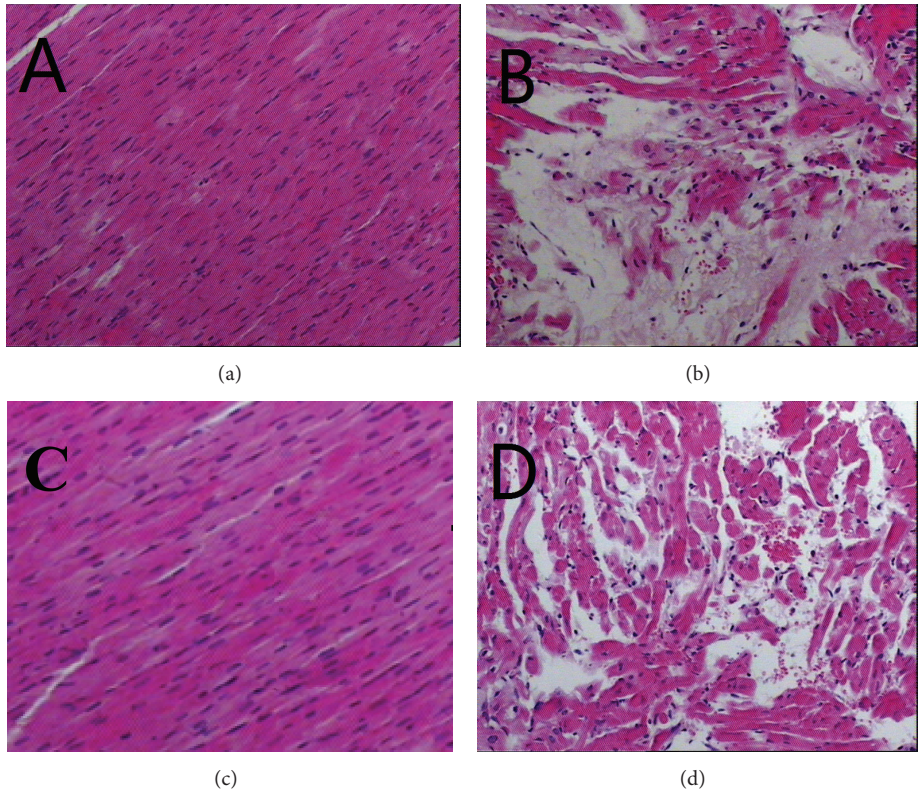

Figure 1: Effects of SAL on the cell morphology. Hematoxylin and eosin (HE) stain (×400). (a) Control group; (b) acute exhaustive swimming group; (c) salidroside group; (d) salidroside-acute exhaustive swimming group.

2.7. Measurement of the Contents of CK, CK-MB, LDH, MDA, and SOD. Enzyme linked immunosorbent assay (ELISA) kits were used to determinate the contents of Mitogen-activated protein kinases (CK), creatine kinase isoenzyme (CK-MB) and lactate dehydrogenase (LDH) in rats serum and MDA, SOD in rats left ventricular myocardium. All assays were performed according to the manufacturer's instructions. All samples and standards were prepared in triplicate.

2.8. Determination of Phosphorylation Degree of ERK and p38 MAPK. Western blot method was used to detect the phosphorylation degree of ERK and p38 MAPK in rats left ventricular myocardium. The protein concentration was assayed using bicinchoninic acid (BCA) method with bovine serum albumin as the standard. Then the protein was diluted to the same volume and heated at 100°C for 5 min after being added in loading buffer in proportion. The denatured protein samples were separated by SDS/polyacrylamide gel electrophoresis (SDS-PAGE) at 100 V for 2 h and transferred to polyvinylidene fluoride (PVDF) membranes. The membranes were blocked in 5% skimmed milk blocking buffer at room temperature for 1 h and then incubated overnight at 4°C with primary antibodies. After being washed with tris-buffered saline (TBS) tween for three times, the membranes were incubated with secondary antibody of horseradish peroxidase labeling goat anti-mouse IgG for 1 h at room temperature and ECL detection was used to color for 1 to 2 min. Automatically, imaging system was used for imaging and quantitative analysis; grey value which had been deducted background was obtained at last. All tests were repeated three times.

2.9. Statistical Analysis. Data were expressed as means ± SD. *t*-test was used to compare the data between two groups, and one-way analysis of variance (ANOVA) was used to data among multi groups. $P<0.05$ was considered significant.

3. Results

3.1. The Effect of Salidroside on the Myocardial Structure of Acute Exhaustive Rat. Figure 1 shows the optical microscopy of rat myocardial structure. From Figures 1(a) and 1(c) we can find that the myocardial structures of Con group and Sal group rats are as follows: muscle fibers arrange neatly, interstitial substance has no edema, muscle membrane has no damage, and muscle fibers have no fracture, degeneration, and necrosis; Figure 1(b) shows the myocardial structure of EE group rats: muscle fibers arrange irregularly, interstitial substance has edema, muscle membrane is damaged, and muscle fibers have fracture, degeneration, and necrosis. As Figure 1(d) shows, the myocardial structure of SE group rats is as follows: muscle fiber direction changes, interstitial substance has slight edema, muscle membrane has no damage, and pathological change of degeneration is visible.

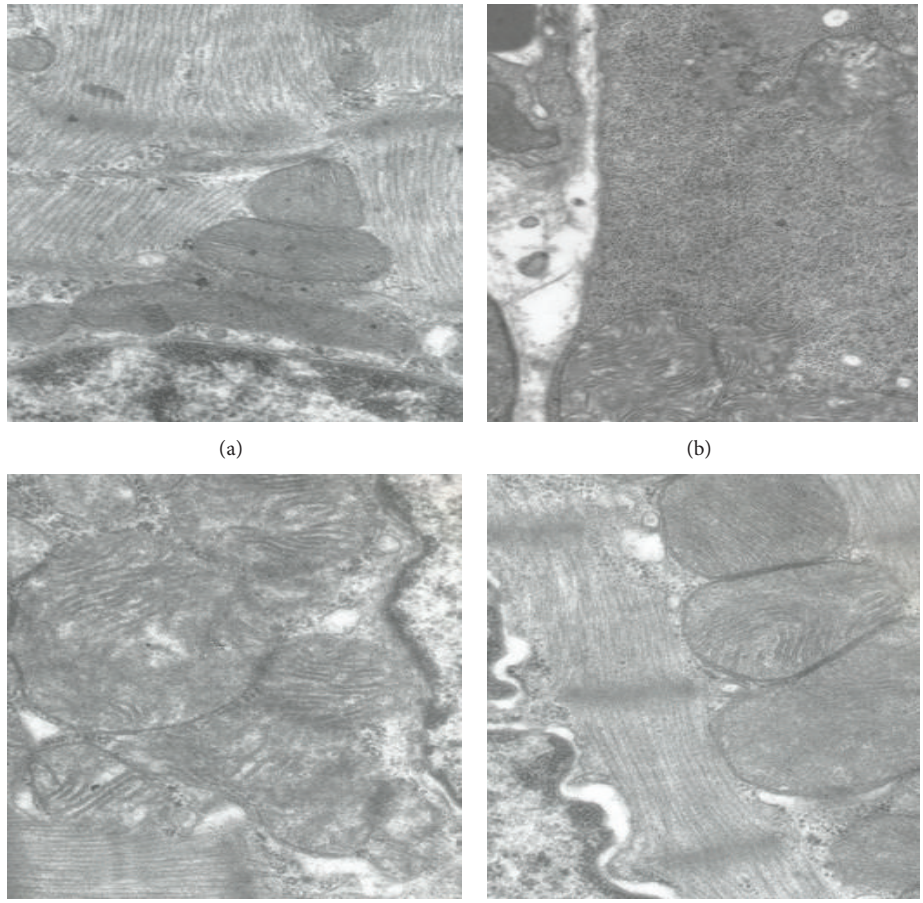

Figure 2: Effects of SAL on the ultrastructure of cardiomyocytes (×20,000). (a) Control group; (b) acute exhaustive swimming group; (c) salidroside group; (d) salidroside-acute exhaustive swimming group.

Figure 2 shows the transmission electron microscopy (TEM) of rat myocardial structure. Figures 2(a) and 2(c) show the myocardial structures of Con group and Sal group rats: sarcomeres arrange neatly, the density is uniform, organelles have no edema, and the membrane and crest of mitochondria are normal; Figure 2(b) shows the myocardial structures of EE group rats: myocardial nuclear matrix has edema, nuclear gap widens, the number of mitochondria and glycogen decreases significantly, the membrane and crest of mitochondria fuse partly and become blurry or missing, a small amount of muscle fiber is necrotize. As Figure 2(d) shows, the myocardial structure of SE group rats is as follows: myocardial cell matrix has edema and the membrane and crest of mitochondria fuse partly and become blurry or missing.

3.2. The Effect of Salidroside on the Contents of CK, CK-MB, and LDH of Acute Exhaustion Rats. The content of serum CK (ng/mL): compared to Con group (27.990 ± 2.279), the content of serum CK in SE group (34.642 ± 2.374) and EE group (38.671 ± 1.374) increased significantly ($P < 0.05$), and in EE group it was significantly higher than in SE group ($P < 0.05$) while Sal group (27.911 ± 1.911) and Con group had no significant difference ($P > 0.05$) (Figure 3(a)).

The content of serum CK-MB (ng/mL): compared to Con group (12.104 ± 0.473), the content of serum CK-MB in SE group (12.758 ± 0.359) and EE group (13.289 ± 0.348) increased significantly ($P < 0.05$), and in EE group it was significantly higher than in SE group ($P < 0.05$) while Sal group (12.230 ± 0.637) and Con group had no significant difference ($P > 0.05$) (Figure 3(b)).

The content of serum LDH (U/L): compared to Con group (4.066 ± 0.068), the content of serum LDH in SE group (4.191 ± 0.094) and in EE group (4.474 ± 0.146) increased significantly ($P < 0.05$), and in EE group it was significantly higher than in SE group ($P < 0.05$) while Sal group (4.043 ± 0.084) and Con group had no significant difference ($P > 0.05$) (Figure 3(c)).

3.3. The Effect of Salidroside on the Cardiac Function of Isolated Rat Heart. Under the basic condition, compared with Con group, $\pm$LV dp/dt_{max} values of EE group significantly fell and HR sped up prominently there was significant difference between the two groups ($P < 0.05$). LVDP of EE group and LVDP of SE group were both significantly lower than that of

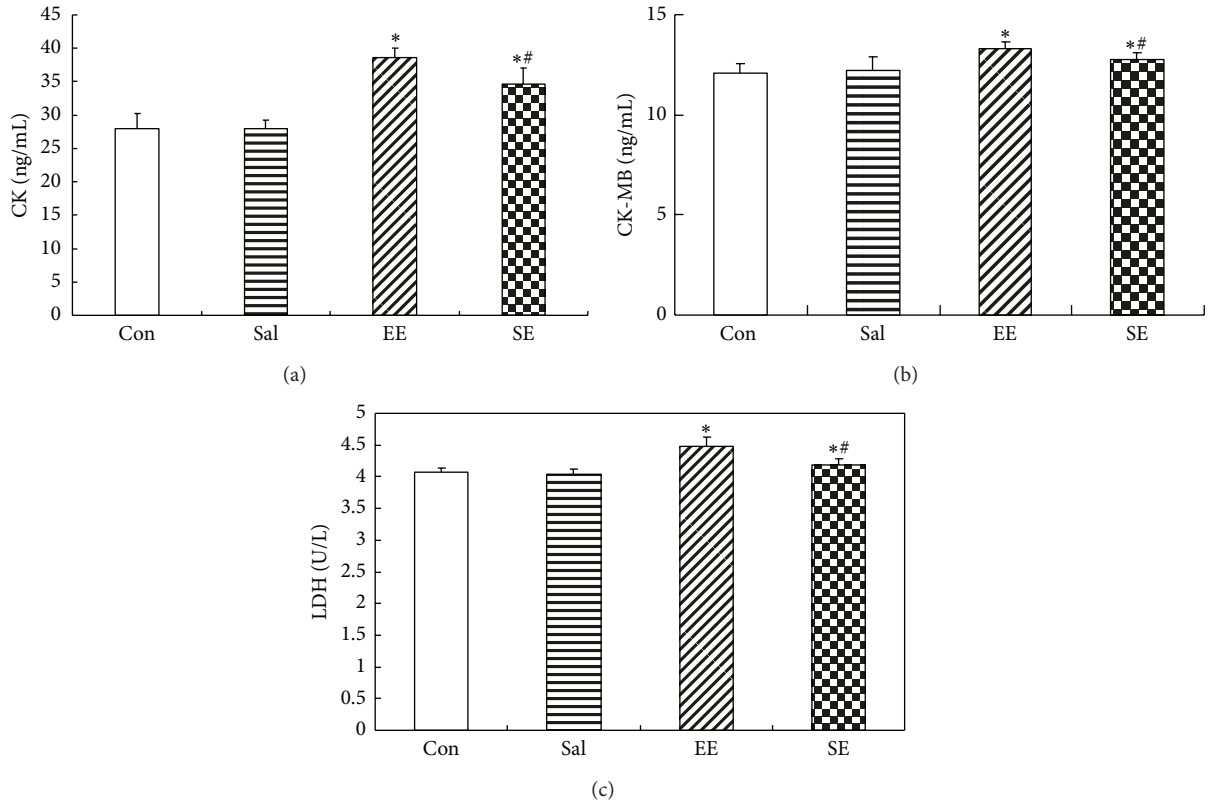

Figure 3: The effect of salidroside on the contents of CK (a), CK-MB (b), and LDH (c) of acute exhaustion rats in serum. $^{*}P < 0.05$ versus control group; $^{\#}P < 0.05$ versus EE group. Con: control group; Sal: salidroside group; EE: acute exhaustive swimming group; SE: salidroside-acute exhaustive swimming group.

Con group ($P < 0.01$, $P < 0.05$), and LVDP of EE group was also lower than that of SE group ($P < 0.05$). Other groups had no significant difference compared to Con group.

Ischemia/reperfusion after reperfusion for 60 minutes, the recovery of LVDP, +LV dp/dt_{max} and − LV dp/dt_{max} in Con group rats was 74%, 69% and 68%, respectively; in the Sal group rats, LVDP, $+dp/dt_{max}$ and $-dp/dt_{max}$ were recovered to 71%, 75% and 75%; the recovery of LVDP, $+dp/dt_{max}$ and $-dp/dt_{max}$ in SE group rats was 92%, 86% and 84%. And the recovery of EE group could reach to 97%, 97% and 95%. There was no significant difference between Con group and Sal group ($P > 0.05$), while the recovery of EE group and SE group was better than that of the rest of the two groups (Figure 4).

3.4. The Effect of Salidroside on the Contents of MDA and SOD of Acute Exhaustion Rats. The content of MDA (mmol/mg): compare with Con group (2.97 ± 0.16), the content of MDA in EE group increased significantly ($P < 0.05$). The content of SOD (ng/mg): compare with Con group (2.63 ± 0.06), the content of SOD in EE group (2.27 ± 0.13) and SE group (2.48±0.08) decreased significantly ($P < 0.05$). Regarding the contents of SOD and MDA, there was significant difference between SE group and EE group ($P < 0.05$), but no significant difference between Sal group and Con group ($P > 0.05$) (Table 1).

3.5. The Effect of Salidroside on the Phosphorylation Degree of ERK and p38 of Acute Exhaustion Rats. The gray value ratio of p-ERK to ERK: compared to Con group (0.201 ± 0.037), the gray value ratio of p-ERK to ERK in SE group (0.967 ± 0.0788) and EE group (0.633 ± 0.087) increased significantly ($P < 0.05$), and in SE group it was significantly higher than in EE group ($P < 0.05$) while Sal group (0.229 ± 0.047) and Con group had no significant difference ($P > 0.05$).

The gray value ratio of p-p38 to p38 MAPK: compared to Con group (0.316 ± 0.041), the gray value ratio of p-p38 to p38 MAPK in SE group (0.770 ± 0.070) and EE group (1.050 ± 0.091) increased significantly ($P < 0.05$), and in EE group was significant higher than SE group ($P < 0.05$) while Sal group (0.389 ± 0.074) and Con group had no significant difference ($P > 0.05$) (Figure 5).

4. Discussion

In this study, we mainly investigated the effect of salidroside on cardiac structure, serum myocardial enzyme, antioxidant stress, and MAPKs signal transduction of acute exhaustive exercise rats. In addition, we also observed the changes of cardiac function, heart rate, and coronary flow of isolated heart ischemia/reperfusion of acute exhaustive exercise rats.

Myocardium is one of the organizations which are sensitive to hypoxia and have high oxygen uptake. Hypoxia not

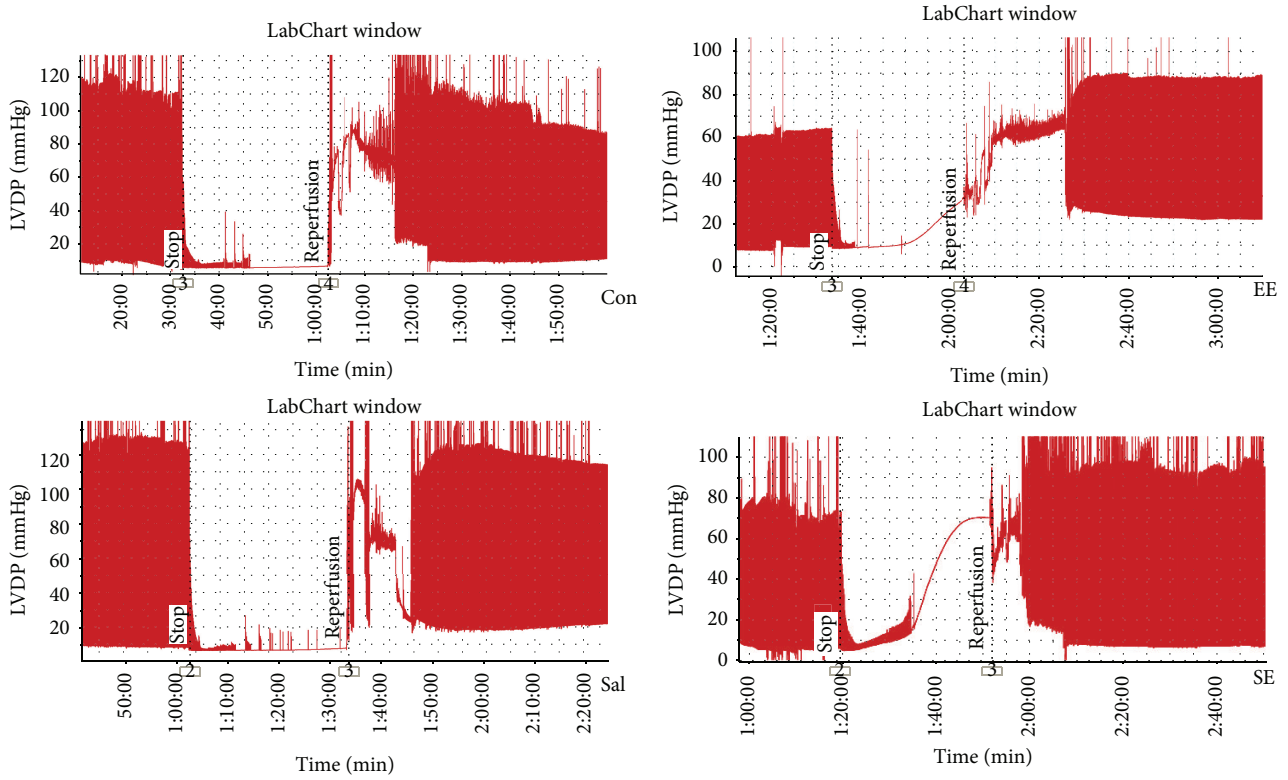

(a)

	Con	EE	Sal	SE
Preischemia LVDP (mmHg)	129.77 ± 12.91	74.15 ± 11.86$^{**\#}$	129.58 ± 15.02$^{\#}$	99.48 ± 12.19*
+LV$dp/dt_{max}$ (mmHg·s^{-1})	2707.09 ± 278.98	2033.43 ± 436.93*	2876.47 ± 391.56	2411.83 ± 400.99
−LV$dp/dt_{max}$ (mmHg·s^{-1})	−2120.79 ± 322.29	−1301.01 ± 320.85**	−1999.21 ± 368.70	−1713.21 ± 292.99
HR (beats·min^{-1})	241 ± 22	287 ± 18*	257 ± 33	269 ± 36
CF (mL·min^{-1})	12.2 ± 3.6	13.1 ± 2.8	12.8 ± 3.2	12.0 ± 3.1
Reperfusion LVDP (mmHg)	94.99 ± 9.28	87.40 ± 8.02	90.42 ± 20.98	91.11 ± 13.82
+LV$dp/dt_{max}$ (mmHg·s^{-1})	1877.17 ± 498.29	1879.51 ± 194.08	2150.19 ± 421.32	2078.43 ± 386.01
−LV$dp/dt_{max}$ (mmHg·s^{-1})	−1441.60 ± 356.93	−1178.77 ± 270.37	−1461.49 ± 188.31	−1419.55 ± 173.21
HR (beats·min^{-1})	214 ± 45	240 ± 68	248 ± 21	229 ± 14
CF (mL·min^{-1})	7.4 ± 2.3	7.4 ± 3.3	8.9 ± 2.3	7.8 ± 1.0

(b)

Figure 4: Cardiac performance in isolated rat hearts submitted to 30 min ischemia and 60 min reperfusion. (a) Original recording. (b) Cardiac functional parameters. Con: control group; EE: acute exhaustive swimming group; Sal: salidroside group; SE: salidroside-acute exhaustive swimming group. LVDP: left ventricular developped pressure; LVEDP: left ventricular end-diastolic pressure; ±LV dp/dt_{max}: maximum change rate of left ventricular pressure; HR: heart rate; CF: coronary flow. Data were expressed as mean ± SE, $n = 6$ for each group. $^{*}P < 0.05$, $^{**}P < 0.01$ versus control group; $^{\#}P < 0.05$ versus SE.

only affects the ultrastructure of cardiomyocytes but also influences the metabolism and function of myocardium [17].

The TEM figures showed that the characteristics of EE group rats myocardium were myocardial nuclear matrix edema, nuclear gap widened, the number of mitochondria and glycogen decreased significantly, the membrane and crest of mitochondria were fused partly and became blurry or missing, and a small amount of muscle fiber necrosis. Acute exhaustive exercise damaged the structure of cardiomyocytes, and amounts of CK, CK-MB, and LDH were released into blood, so the contents of these enzymes in rat serum increased significantly.

The results of isolated heart ischemia/reperfusion showed, in basal state, compared with Con group, the LVESP, LVDP, $+dp/dt_{max}$, and $-dp/dt_{max}$ of EE group, that HR sped up and CF decreased. This indicated that the function of cardiac systole and diastole weakened, and exhaustive exercise had damaged the cardiac function. After ischemia/reperfusion, it caused myocardial reversible or irreversible damage; myocardial systole and diastole

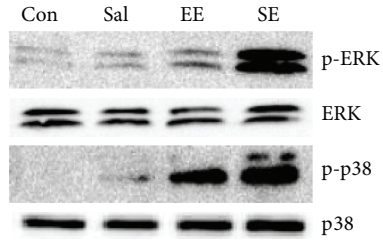

	Con	Sal	EE	SE
p-ERK/ERK	0.201 ± 0.037	0.229 ± 0.047	0.633 ± 0.087*	0.967 ± 0.079*#
p-p38/p38	0.316 ± 0.041	0.389 ± 0.074	1.050 ± 0.091*	0.770 ± 0.070*#

Figure 5: The effect of salidroside on the phosphorylation degree of p-ERK and p-p38 of acute exhaustion rats. Data were expressed as mean ± SE, $n = 7$ for each group. $^{*}P < 0.05$ versus control; $^{\#}P < 0.05$ versus the acute exhaustive group. Con: control group; EE: acute exhaustive swimming group; Sal: salidroside group; SE: salidroside-acute exhaustive swimming group.

Table 1: The effect of salidroside on the contents of MDA and SOD of acute exhaustion rats.

	Con	Sal	EE	SE
SOD (ng/mg)	2.63 ± 0.06	2.54 ± 0.06	2.27 ± 0.13**	2.48 ± 0.08*#
MDA (nmol/mg)	2.97 ± 0.16	2.91 ± 0.19	3.34 ± 0.06**	3.17 ± 0.12#

Data were expressed as mean ± SE, $n = 7$ for each group. $^{*}P < 0.05$ versus control group, $^{**}P < 0.01$ versus control group, and $^{\#}P < 0.05$ versus the acute exhaustive group. Con: control group; EE: acute exhaustive swimming group; Sal: salidroside group; SE: salidroside-acute exhaustive swimming group.

functions reduced further, LVEDP rose, $+dp/dt_{\max}$ and $-dp/dt_{\max}$ reduced, and CF decreased. This might be owed to a large number of oxygen free radicals and other products [18]. From the analysis of cardiac function, after reperfusion for 60 min, the recovery data of EE group had no significant differences with other groups, but the recovery rates of LVDP, +LV $dp/dt_{\max}$, and −LV $dp/dt_{\max}$ were significantly higher than those of Con group, and the recovery rates of SE group were also significantly higher than those of Con group. This might be associated with the adaption of ischemia caused by exhaustive exercise and still need further research.

Acute exhaustive exercise stimulated cardiomyocytes and caused oxidative stress; amount of ROS was produced and caused lipid peroxidation with unsaturated fatty acids on cell membrane, so a large number of MDA were generated. Moreover, the content of SOD decreased obviously because of the massive consumption of the superfluous ROS. Oxidative stress destroyed the stability of cell membrane. The liquidity is changed. The permeability is enhanced. The structure and activity of the protein are destroyed, so the structure and function of cardiomyocytes are damaged at last.

Salidroside could reduce the content of MDA and increase the content of SOD significantly. It enhanced the antioxidant system and improved the function of endogenous clearing system, which sped up the elimination of ROS, reduced the lipid peroxidation with membrane lipid, reduced the damage of ROS to cardiomyocytes, and improved the myocardium ultrastructure and cardiac function of acute exhaustive exercise to a certain extent. Furthermore, salidroside also increased the coronary flow, improved the blood and oxygen supply of ischemia area, ameliorated myocardial systole and diastole functions, and bettered the recovery of cardiac function of acute exhaustive exercise rats after ischemia/reperfusion; all of these indicated that salidroside could evidently protect the myocardium against ischemia/reperfusion injury. So, salidroside could protect the heart of acute exhaustive rats through the way of antioxidative stress.

ERK and p38 MAPK were both activated significantly in acute exhaustive rats. This might be because the ROS generated from oxidative stress caused by acute exhaustive exercise activated the access of MAPKs signaling transduction, while salidroside could inhibit the activation of p38 MAPK and promote the activation of ERK of acute exhaustive rats, which prompted that the heart protection might be related to the inhibition of cardiomyocytes apoptosis signal, the delay of cell apoptosis induced by stress. So, salidroside could protect the heart of acute exhaustive rats through the way of MAPKs signal transduction.

In conclusion, salidroside could effectively inhibit the cardiac function decreasing of acute exhaustive rats and reduce the cardiac function injury caused by acute exhaustive exercise. The protection mechanism might be associated with antioxidative stress and MAPKs signal transduction. However, we could not ensure whether salidroside has the protection against ischemia/reperfusion injury of exhaustive heart; it might be the same as the protection against myocardial ischemia caused by exhaustion and did not superimpose.

Conflict of Interests

The authors declare that there is no conflict of interests regarding the publication of this paper.

Authors' Contribution

Yunru Wang and Peng Xu contributed equally to this work.

Acknowledgments

This study was supported by Medical Science Research Program of Chinese Army (no. CWS12J064) and Medical Technology Project of Chinese Army (no. BWS11J058).

References

[1] J. Xu and Y. Li, "Effects of salidroside on exhaustive exercise induced oxidative stress in rats," *Molecular Medicine Reports*, vol. 6, no. 5, pp. 1195–1198, 2012.

[2] F. B. Ortega, J. R. Ruiz, A. Gutiérrez, and M. J. Castillo, "Extreme mountain bike challenges may induce sub-clinical myocardial damage," *Journal of Sports Medicine and Physical Fitness*, vol. 46, no. 3, pp. 489–493, 2006.

[3] G. L. Wu, Y. S. Chen, X. D. Huang, and L. X. Zhang, "Exhaustive swimming exercise related kidney injury in rats—protective effects of acetylbritannilactone," *International Journal of Sports Medicine*, vol. 33, no. 1, pp. 1–7, 2012.

[4] W. Aoi, Y. Naito, K. Sakuma et al., "Astaxanthin limits exercise-induced skeletal and cardiac muscle damage in mice," *Antioxidants and Redox Signaling*, vol. 5, no. 1, pp. 139–144, 2003.

[5] L. L. Ji, M.-C. Gomez-Cabrera, N. Steinhafel, and J. Vina, "Acute exercise activates nuclear factor (NF)-κB signaling pathway in rat skeletal muscle," *The FASEB Journal*, vol. 18, no. 13, pp. 1499–1506, 2004.

[6] S. Maeda, T. Miyauchi, K. Goto, and M. Matsuda, "Differences in the change in the time course of plasma endothelin-1 and endothelin-3 levels after exercise in humans. The response to exercise of endothelin-3 is more rapid than that of endothelin-1," *Life Sciences*, vol. 61, no. 4, pp. 419–425, 1997.

[7] Z. Li, O. H. L. Bing, X. Long, K. G. Robinson, and E. G. Lakatta, "Increased cardiomyocyte apoptosis during the transition to heart failure in the spontaneously hypertensive rat," *American Journal of Physiology—Heart and Circulatory Physiology*, vol. 272, no. 5, pp. H2313–H2319, 1997.

[8] A. Matsuzawa and H. Ichijo, "Stress-responsive protein kinases in redox-regulated apoptosis signaling," *Antioxidants and Redox Signaling*, vol. 7, no. 3-4, pp. 472–481, 2005.

[9] R. A. Kaiser, O. F. Bueno, D. J. Lips et al., "Targeted inhibition of p38 mitogen-activated protein kinase antagonizes cardiac injury and cell death following ischemia-reperfusion in vivo," *Journal of Biological Chemistry*, vol. 279, no. 15, pp. 15524–15530, 2004.

[10] T.-L. Yue, C. Wang, J.-L. Gu et al., "Inhibition of extracellular signal-regulated kinase enhances ischemia/reoxygenation-induced apoptosis in cultured cardiac myocytes and exaggerates reperfusion injury in isolated perfused heart," *Circulation Research*, vol. 86, no. 6, pp. 692–699, 2000.

[11] Z. Liu, "The role of ERK molecules in the cardiovascular system," *Molecular Cardiology of China*, vol. 5, pp. 818–820, 2005.

[12] J. Xu and Y. Li, "Effects of salidroside on exhaustive exercise induced oxidative stress in rats," *Molecular Medicine Reports*, vol. 6, no. 5, pp. 1195–1198, 2012.

[13] S.-C. Huang, F.-T. Lee, T.-Y. Kuo, J.-H. Yang, and C.-T. Chien, "Attenuation of long-term Rhodiola rosea supplementation on exhaustive swimming-evoked oxidative stress in the rat," *Chinese Journal of Physiology*, vol. 52, no. 5, pp. 316–324, 2009.

[14] T.-H. Yan, B.-S. Du, W. Yang, Y. Ma, J. Xu, and Q.-J. Wang, "Effects of salidroside on hemorheology and myocardial ischemic reperfusion injury in isolated heart of rats," *Chinese Journal of Natural Medicines*, vol. 6, no. 3, pp. 219–222, 2008.

[15] T. H. Yan, Y. Ma, W. Yang, Q. Wang, Y. Jia, and Z. Pan, "Protective effects of salidroside on acute myocardial ischemia of rats and neonatal rat cardiocytes," *Lishizhen Medicine and Materia Medica Research*, vol. 20, no. 3, pp. 693–695, 2009.

[16] D. P. Thomas, "Effects of acute and chronic exercise on myocardial ultrastructure," *Medicine and Science in Sports and Exercise*, vol. 17, no. 5, pp. 546–553, 1985.

[17] V. A. Browne, V. M. Stiffel, W. J. Pearce, L. D. Longo, and R. D. Gilbert, "Activator calcium and myocardial contractility in fetal sheep exposed to long-term high-altitude hypoxia," *American Journal of Physiology—Heart and Circulatory Physiology*, vol. 272, no. 3, pp. H1196–H1204, 1997.

[18] J.-G. Zhuang and Z.-N. Zhou, "Protective effects of intermittent hypoxic adaptation on myocardium and its mechanisms," *Biological Signals and Receptors*, vol. 8, no. 4-5, pp. 316–322, 1999.

Hindawi Publishing Corporation
Oxidative Medicine and Cellular Longevity
Volume 2013, Article ID 782497, 10 pages
http://dx.doi.org/10.1155/2013/782497

Research Article

Astragalus Polysaccharide Suppresses Skeletal Muscle Myostatin Expression in Diabetes: Involvement of ROS-ERK and NF-κB Pathways

Min Liu,[1,2] Jian Qin,[2] Yarong Hao,[3] Min Liu,[4] Jun Luo,[5] Tao Luo,[4] and Lei Wei[1]

[1] *Department of Pathology and Pathophysiology, School of Medicine, Wuhan University, Wuhan 430071, China*
[2] *Central Laboratory, Renmin Hospital of Wuhan University, Wuhan 430060, China*
[3] *Department of Cardiology, Renmin Hospital of Wuhan University, Wuhan 430060, China*
[4] *Department of Anesthesiology, Renmin Hospital of Wuhan University, Wuhan 430060, China*
[5] *Department of Pathology, Zhongnan Hospital of Wuhan University, Wuhan 430071, China*

Correspondence should be addressed to Lei Wei; leiweifr@hotmail.com

Received 7 August 2013; Revised 24 October 2013; Accepted 27 October 2013

Academic Editor: Zhengyuan Xia

Objective. The antidiabetes drug astragalus polysaccharide (APS) is capable of increasing insulin sensitivity in skeletal muscle and improving whole-body glucose homeostasis. Recent studies suggest that skeletal muscle secreted growth factor myostatin plays an important role in regulating insulin signaling and insulin resistance. We hypothesized that regulation of skeletal muscle myostatin expression may be involved in the improvement of insulin sensitivity by APS. *Methods*. APS was administered to 13-week-old diabetic KKAy and nondiabetic C57BL/6J mice for 8 weeks. Complementary studies examined APS effects on the saturated acid palmitate-induced insulin resistance and myostatin expression in C2C12 cells. *Results*. APS treatment ameliorated hyperglycemia, hyperlipidemia, and insulin resistance and decreased the elevation of myostatin expression and malondialdehyde production in skeletal muscle of noninsulin-dependent diabetic KKAy mice. In C2C12 cells in vitro, saturated acid palmitate-induced impaired glucose uptake, overproduction of ROS, activation of extracellular regulated protein kinases (ERK), and NF-κB were partially restored by APS treatment. The protective effects of APS were mimicked by ERK and NF-κB inhibitors, respectively. *Conclusion*. Our study demonstrates elevated myostatin expression in skeletal muscle of type 2 diabetic KKAy mice and in cultured C2C12 cells exposed to palmitate. APS is capable of improving insulin sensitivity and decreasing myostatin expression in skeletal muscle through downregulating ROS-ERK-NF-κB pathway.

1. Introduction

Skeletal muscle comprises 40% to 50% of the total body mass and is the major tissue responsible for insulin-dependent glucose utilization [1]. Impaired insulin-stimulated muscle glycogen synthesis plays a significant role in insulin resistance and noninsulin-dependent diabetes mellitus [2]. Several factors including elevated oxidative stress, inflammation, and free fatty acids have been implicated as the major defects responsible for causing muscle insulin resistance in patients with type 2 diabetes.

Myostatin is a growth factor produced by skeletal muscle and secreted into the circulation that negatively regulates muscle mass [3]. Recent studies suggest that myostatin plays a major role in regulating insulin signaling and insulin resistance [4]. Patients with type 2 diabetes had higher levels of muscle myostatin mRNA content than the control subjects [5]. A loss-of-function mutation in either one or both alleles of the myostatin gene was able to protect mice against obesity-induced insulin resistance [6]. Therefore, myostatin could be a potent target for the treatment of diabetes and insulin resistance.

The dry roots of *Astragalus membranaceus* (Fisch.) Bge. (Leguminosae), also known as Huang Qi in China, have long been used as an important component of herbal prescriptions to treat diabetes in traditional Chinese medicine

[7–9]. Studies from our group and others have previously shown that astragalus polysaccharide (APS), the extracts of *Astragalus membranaceus*, can effectively alleviate diabetes and diabetes related complications such as cardiovascular and kidney disease [10–12]. One of the mechanisms of the APS's antidiabetic effect is to improve whole-body glucose homeostasis and increase insulin sensitivity in skeletal muscle [13]. We hypothesized that regulation of skeletal muscle myostatin expression may be involved in the improvement of insulin sensitivity by APS. In the current study, we investigated the effects of APS on myostatin expression in skeletal muscle of type 2 diabetic KKAy mice in vivo and culture skeletal muscle myocyte in vitro.

2. Materials and Methods

2.1. Chemicals and Reagents. *Astragalus membranaceus* (Fisch) Bunge var. mongholicus (Bunge) Hsiao was purchased from Shanghai Medicinal Materials (Shanghai, China). Identification was carried out by the Department of Authentication of Chinese Medicine, Hubei University of Chinese Traditional Medicine (Wuhan, China). APSs were extracted with optimized techniques using direct water decoction, as previously described [10]. C2C12 myoblast cell line was obtained from CCTCC (Wuhan, China). Insulin, 2-deoxyglucose, fatty acid-free bovine serum albumin (BSA), palmitate (PA), PD98059, and parthenolide were purchased from Sigma-Aldrich (Shanghai, China). High glucose-DMEM, fetal bovine serum (FBS), and horse serum were from GIBCO (Shanghai, China). NF-κBp65, IκBα, ERK (42/44), phospho-ERK (42/44), p38, phospho-p38, SAPK/JNK, phospho-SAPK/JNK, and GAPDH antibodies were purchased from Cell Signal Technology (USA). Myostatin (GDF-8) antibody was purchased from Santa Cruz. Fluorescent-conjugated secondary antibodies were from LI-COR Biosciences.

2.2. In Vivo Experiments. The experimental procedures and protocols used in this investigation were approved by the Ethical Committee for the Experimental Use of Animals at Renmin Hospital of Wuhan University (Wuhan, China). Eight-week-old KKAy male mice and age-matched C57BL/6J male mice were purchased from Beijing HFK Bioscience Co. Ltd. (Beijing, China). Mice were housed under a 12 h light-dark cycle and an ambient temperature of 22°C. The KKAy mice were fed with a purified high-fat diet consisting of a percentage of total kcal of 41% fat, 41% carbohydrates, and 18% protein. The C57BL/6J mice were fed with a normal chow diet consisting of 12% fat, 60% carbohydrates, and 28% protein. KKAy mice were treated with either vehicle (KKAy, $n = 8$) or APS (KKAy + APS, $n = 8$), starting at 13 weeks of age. Age-matched C57BL/6J mice were also dosed with vehicle (C57BL/6J, $n = 8$) or APS (C57BL/6J + APS, $n = 8$) as healthy nondiabetic control animals. The APS was delivered slowly into the animal stomach through a stainless steel ball-tipped gavage needle at a dose of 700 mg kg^{-1} day^{-1} for 8 weeks. The control groups received an equal volume of vehicle (saline).

2.3. Blood Chemistry Assay. Blood glucose and insulin levels were determined before (age of 12 weeks) and after APS treatment (age of 20 weeks). Blood glucose levels were assessed using blood collected from the tail vein with a One-Touch Ultra blood glucose meter (LifeScan, Milpitas, CA, USA). Plasma insulin concentrations were determined using blood collected from the orbita of anesthetized animal following a 12 h overnight fasting period, with mouse high range insulin ELISA kit (ALPCO Diagnostics, USA). The index of homeostasis model assessment of insulin resistance (HOMA) was calculated as fasting plasma glucose [mmol/L] × fasting plasma insulin [mU/L]/22.5. Blood plasma FFAs were measured using the spectrophotometric NEFA C kit (Wako Chemicals, Neuss, Germany).

2.4. Malondialdehyde (MDA) Analysis in Skeletal Muscle. MDA level in the skeletal muscle was determined by the thiobarbituric acid (TBA) method with an assay kit according to manufactory guidance (Jiancheng Bioengineering Institute, Nanjing, China). Briefly, samples were incubated with TBA and SDS at 95°C for 1 h, followed by a centrifugation at 800 ×g for 10 min. Supernatants were transferred to a 96-well plate and the absorbance was measured at 532 nm. The MDA level after the calculation was further corrected by sample protein concentration (mmol/mg protein).

2.5. Cell Culture and Treatment. C2C12 myoblasts were cultured in Dulbecco's modified Eagle's medium (DMEM) supplemented with 10% FBS, 2 mM glutamine, 100 unit/mL penicillin, and 100 μg/mL streptomycin. Cells were maintained at 37°C under 5% CO_2 in a humidified incubator. Differentiation of myoblasts into myotubes was induced when the cells had achieved 70% confluence by replacing the media with DMEM containing 2% horse serum. Six days later, the differentiated C2C12 cells had fused into myotubes and were used for the experiments.

Palmitate (C16:0; Sigma) stock solutions of 20 mmol/L were dissolved in ethanol. Before application to the cells, palmitate was conjugated to bovine serum albumin (BSA) by diluting the palmitate solution with differentiation medium containing 5% (w/v) palmitate-free BSA (Sigma). Myotubes were incubated for 24 h in DMEM containing 5% BSA in either the presence (palmitate-treated cells) or absence (control cells) of 0.5 mmol/L palmitate. Cells treated with APS were incubated with additional APS at the final concentration of 200 μg/mL.

2.6. In Vitro Glucose Uptake Assay. Glucose uptake was assayed using [3H]2-deoxyglucose according to previous report. After 24 h of treatment, cells were incubated in the presence or in the absence of 100 nm insulin for 30 min and then washed two times with wash buffer [20 mm HEPES (pH 7.4), 140 mm NaCl, 5 mm KCl, 2.5 mm $MgSO_4$, and 1 mm $CaCl_2$]. Cells were then incubated in buffer transport solution (wash buffer containing 10 μM of unlabeled 2-deoxy-D-glucose and 0.5 μCi/mL [3H]2-deoxy-D-glucose) for 10 min. Nonspecific uptake was determined incubating the cells in the presence or in the absence of 5 μM cytochalasin B. Uptake

was terminated by aspiration of the solution. Cells were then washed three times, and radioactivity associated with the cells was determined by cell lysis in 0.05 m NaOH, followed by scintillation counting.

2.7. Measurement of ROS Production. C2C12 cells (2×10^5 cells/well) in a 96-well plate were treated with or without APS for 1 h, followed by incubation with palmitate for 24 h. ROS generation was measured by incubation of the cells with 10 mM DCFH2-DA for 45 min. The fluorescence, corresponding to intracellular ROS, was measured on a Victor3 1420 Multilabel Counter (PerkinElmer, Turku, Finland) at 485 nm excitation and 530 nm emission wavelengths.

2.8. Measurements of mRNA. Total RNA was extracted from soleus muscle biopsies of both KKAy and C57BL/6J mice using TRIZOL reagent (Invitrogen) following the manufacture's instruction. Levels of myostatin mRNA were examined using semiquantitative reverse transcriptase (RT) PCR. One microgram of total RNA was reverse-transcribed with First Strand cDNA Synthesis Kit (Thermo Scientific). The sequences of primers used for amplification were 5′-GGTCTGCTGAGTTAGGAGGGT-3′ and 5′-TGTGTGTGTGGAGATGCACCT-3′. Amplification of gene yielded a single band of the expected size 339 bp. Thermal amplifications were carried out with PCR Master Mix (Thermo Scientific). PCR was performed within a linear range of amplification, which was determined in a preliminary experiment. All PCR data were normalized to beta-actin gene expression.

2.9. Western Blot Analysis. For the preparation of total protein extract, frozen tissues (50 mg) from soleus muscles or cells (1×10^6) were homogenized in 0.5 mL or 0.2 mL ice-cold lysis buffer (50 mM Tris-HCl, pH 7.4, 1% NP-40, 0.25% sodium deoxycholate, 150 mM NaCl, 1 mM EGTA) containing protease inhibitor cocktail (1 mM phenylmethylsulfonyl fluoride, 1 μg/mL aprotinin, 5 μg/mL leupeptin, 1 mM Na_3VO_4, and 1 mM NaF). Tissue or cell lysates were centrifuged at 12,000 ×g for 15 min at 4°C. The supernatant was collected and stored at −70°C as total protein samples. The preparation of cytoplasmic and nuclear extracts was performed using a commercial kit (Pierce, USA) according to the manufacturer's instructions. Protein concentration was then determined using BCA protein assay kit. Samples of the lysates were separated by 10% SDS-PAGE and then transferred onto PVDF membranes. After being placed in blocking buffer, the membranes were incubated with the following primary antibodies (1 : 1,000 dilutions): anti-GDF-8, anti-NF-κBp65, anti-IκBα, anti-p-P38, anti-P38, anti-p-ERK, and anti-ERK, anti-p-SARP/JNK, anti-SARP/JNK and GAPDH. Then, secondary antibody was conjugated to a fluorescent entity: IRDye 800-conjugated goat anti-rabbit IgG and/or Alexa Fluor 680-conjugated goat anti-mouse IgG (dilution 1 : 10000) in 10 mL LI-COR blocking buffer with gentle agitation for 1 h at room temperature. The membrane was scanned and analyzed on the Odyssey Infrared Imaging System (LI-COR Biosciences).

2.10. Statistical Analysis. Data are expressed as means ± SD. Statistical significance was determined using analysis of variance (ANOVA) followed by Tukey's test. A P value of less than 0.05 was considered statistically significant.

3. Results

3.1. Effect of APS on Body Weight, Blood Glucose, HOMA Score, and Plasma FFAs. To test whether APS improves glucose metabolism and lowers insulin resistance in KKAy mice, APS was administered for 8 weeks starting at 13 weeks of age. During this period, blood was collected from the tail vein weekly and plasma glucose levels were measured. Consistent with our previous finding, plasma glucose was significantly reduced in the APS + KKAy group compared with the KKAy group. In particular, at the end of 8 weeks of APS treatment, the glucose level was 30 ± 3.63 mM in the KKAy group and approximately 17.05 ± 3.69 mM in the APS + KKAy group ($P < 0.001$, $n = 8$, Figure 1(a)).

At the beginning of APS treatment, the index of homeostasis model assessment of insulin resistance (HOMA Score) was not different between the APS + KKAy group and the KKAy group (data not shown). However, after 8 weeks treatment, the HOMA score (Figure 1(b)) was significantly lower in the APS + KKAy (8.41 ± 2.12) group than in the KKAy group (13.72 ± 3.84, $P < 0.001$, $n = 8$). Similarly, APS treatment resulted in a significant decrease in plasma FFA levels (Figure 1(c)) and weight gain (Figure 1(d)) for the KKAy mice ($P < 0.05$, KKAy + APS versus KKAy at the age of 20 weeks), whereas APS by itself had no effect on body weight and glucose metabolism in nondiabetic C57BL/6J mice.

3.2. Effect of APS on MDA Production and Myostatin Expression in KKAy Mice. Oxidative stress plays a causal role in the development of insulin resistance. We tested whether APS treatment alters skeletal muscle redox balance by assessing MDA levels, a stable indicator of oxidative stress. As shown in Figure 2(a), MDA level in the skeletal muscle of KKAy mice was increased approximately 2-fold when compared with that in the C57BL/6C mice ($P < 0.001$, $n = 6$, KKAy versus C57BL/6J). APS administration significantly decreased muscular MDA content ($P < 0.01$, $n = 6$, KKAy + APS versus KKAy).

Since myostatin is expressed predominantly in skeletal muscle, we therefore set out to determine the effects of the APS on both protein and mRNA levels of myostatin in the skeletal muscle tissues of KKAy mice. Immunoblotting assay showed that there was a 3.3-fold increase in the levels of myostatin in KKAy mice ($P < 0.001$, $n = 6$, KKAy versus C57BL/6J). APS administration for 8 weeks resulted in 37% decrease in myostatin as compared to vehicle treated KKAy group ($P < 0.001$, $n = 6$, KKAy + APS versus KKAy) (Figure 2(b)).

The decreased levels of myostatin could be due to the decrease in generation or increase in degradation of myostatin. We then assessed the effects of the APS on the mRNA levels of myostatin (Figure 2(c)). Compared with normal C57BL/6J mice, diabetic KKAy mice exhibited prominent

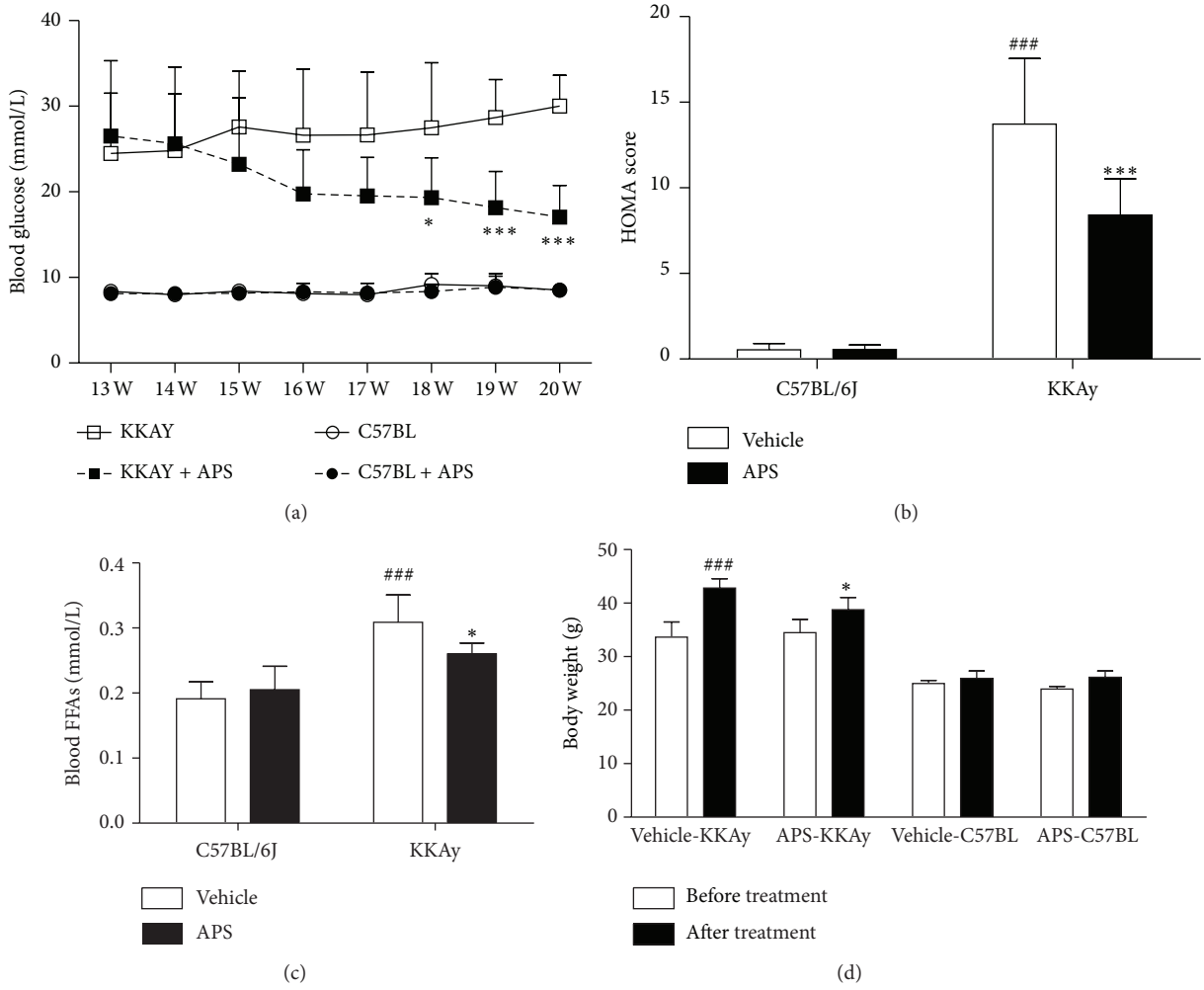

Figure 1: Effect of APS on blood glucose level (a), insulin resistance index HOMA score (b), plasma FFAs level (c), and body weight (d). Changes in blood glucose and body weight were evaluated before and after APS treatment for 8 weeks. Insulin resistance HOMA score and plasma FFAs were examined at the end of 8-week APS administration. Results are expressed as means ± SD for 8 animals in each group. $^{###}P < 0.001$ versus C57BL/6J at the same age, $^{*}P < 0.05$, $^{***}P < 0.01$ versus KKAy at the same age. HOMA: homeostasis model assessment; FFA: free fatty acids.

upregulated myostatin gene expression ($P < 0.001$, $n = 6$, KKAy versus C57BL/6J) in the skeletal muscle tissues. The increases in myostatin mRNA were significantly attenuated by APS treatment ($P < 0.001$, $n = 6$, KKAy + APS versus KKAy).

3.3. APS Attenuates Insulin Resistance in C2C12 Cells In Vitro. Elevated lipids can cause insulin resistance, and exposure of C2C12 skeletal muscle cells to the FFA palmitate has been widely used as an in vitro model of insulin resistance. To extend these observations from KKAy mice to a cellular model of insulin resistance, C2C12 cells were treated with palmitate to induce insulin resistance, as assessed by their decreased intracellular glucose uptake. C2C12 cells exposed to 0.5 mmol/L palmitate showed a 23% ($P < 0.05$) reduction in insulin-stimulated deoxyglucose uptake compared with untreated control skeletal muscle cells (Figure 3(a)). This palmitate-induced insulin resistance coincided with a 3.3-fold increase in myostatin accumulation (Figure 3(b)). As expected, APS administration resulted in significant reduction of myostatin expression and improvement in insulin-stimulated deoxyglucose uptake.

3.4. APS Attenuates Palmitate-Induced Generation of ROS in C2C12 Cells. Oxidative stress has been implicated in the pathogenesis of insulin resistance. It is suggested that increased ROS levels are an important trigger for insulin resistance. We next investigated whether ROS levels were altered by palmitate and APS treatment. As shown in Figure 4, ROS levels were increased in C2C12 cells by exposure to palmitate (0.5 mmol/L, 24 h). APS treatment significantly inhibited generation of ROS in response to palmitate.

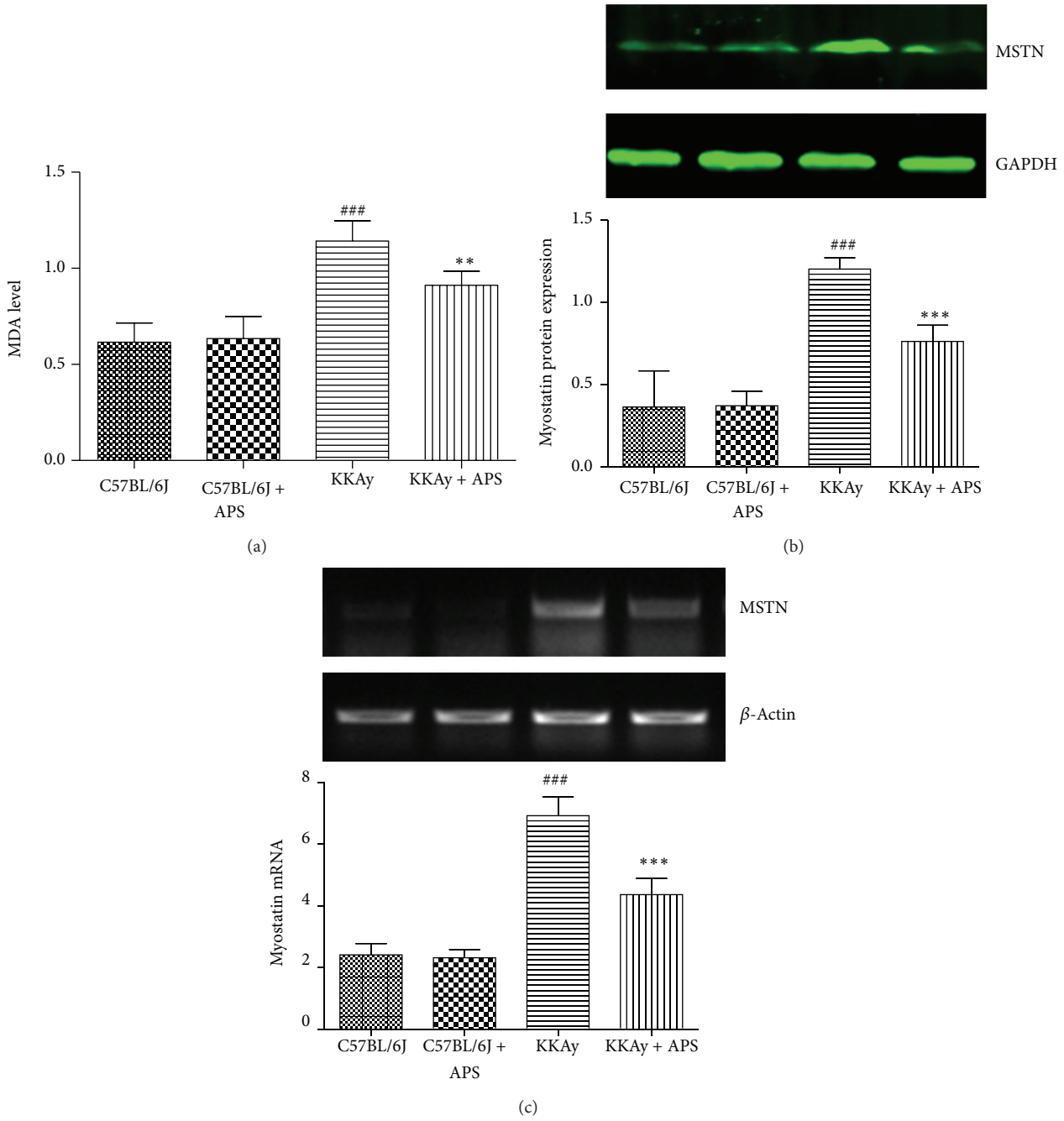

Figure 2: Effect of APS on MDA production and myostatin expression in skeletal muscle. At the end of 8-week APS administration, skeletal muscle MDA level (a), myostatin protein (b), and mRNA expression (c) were assessed, respectively. Results are expressed as means ± SD for 6 animals in each group. $^{###}P < 0.001$ versus C57BL/6J, $^{**}P < 0.01$, $^{***}P < 0.001$ versus KKAy. MDA: malondialdehyde; MSTN: myostatin.

3.5. APS Inhibits ERK/NF-κB Pathway in C2C12 Cells. ROS have been shown to induce various signaling pathways, including the p38 MAPK, ERK, and JNK pathways. We then investigated the downstream pathways involved in the upregulation of myostatin following palmitate exposure. Immunoblotting detection of total and phosphorylated ERK1/2 (Figure 5(a)) revealed that palmitate treatment induced activation of phosphorylated ERK1/2 (3.4-fold induction, $P < 0.001$). The upregulation of phosphorylated ERK1/2 levels achieved by palmitate was abrogated when the cells were coincubated with APS ($P < 0.001$ versus palmitate-treated cells, Figure 5(a)). Although palmitate treatment also induced phosphorylation of P38 and JNK, APS showed no significant effect on P38 and JNK activation. (Figures 5(b)-5(c)). These results indicate that inhibition of the MAPK-ERK cascade might

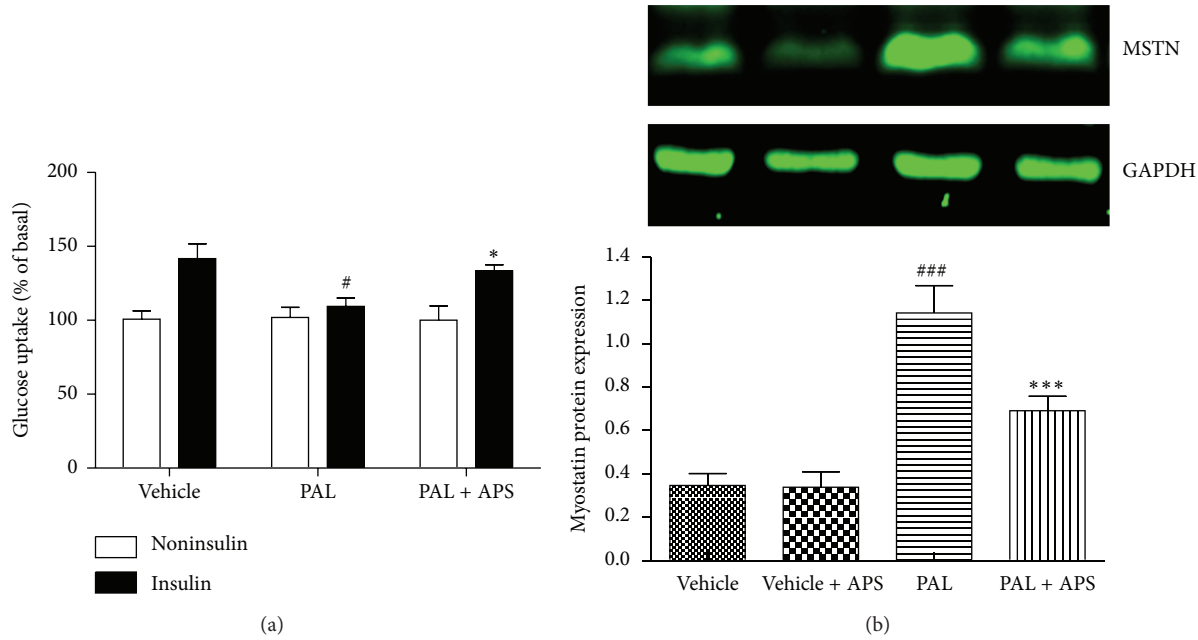

Figure 3: Effect of APS on glucose uptake and myostatin expression in C2C12 cells exposure to palmitate. C2C12 cells were incubated for 24 h in DMEM containing 5% BSA in either the presence (FFA-treated cells) or absence (control cells) of 0.5 mmol/L FFAs. Cells treated with APS were incubated with additional APS at the final concentration of 200 μg/mL. (a) Glucose uptake was assayed using [3H]2-deoxyglucose in the presence or in the absence of 100 nM insulin. $^{\#}P < 0.05$ versus vehicle, $^{*}P < 0.05$ versus palmitate. (b) Myostatin protein expression was assessed by western blot. Data are expressed as means ± SD of 6 different experiments. $^{\#\#\#}P < 0.001$ versus vehicle, $^{***}P < 0.001$ versus palmitate; PAL: palmitate; MSTN: myostatin.

be involved in the decrease of myostatin following APS treatment.

It is reported that C2C12 exposure to palmitate activates NF-κB and activation of the MAPK-ERK cascade may influence NF-κB activation in skeletal muscle. We next determined whether activation of this transcription factor was involved in palmitate-mediated myostatin upregulation. Palmitate treatment resulted in a 1.9-fold increase in nuclear NF-κBp65 protein, whereas this activation was prevented in cells coincubated with palmitate and APS (Figure 6(a)). Since NF-κB is located in the cytosol bound to the inhibitor IκB, we next assessed whether palmitate resulted in changes in the content of IκBa (Figure 6(b)). Palmitate addition to cells caused a 51% decrease ($P < 0.001$) in the abundance of IκBa, whereas APS significantly blocked the palmitate-induced IκBa degradation (Figure 6(b)), thereby inhibiting activation and translocation of NF-κB.

To clearly demonstrate whether ERK1/2/NF-κB pathway was involved in APS downregulating palmitate-induced myostatin expression, we used pharmacological inhibitors PD98059 and parthenolide to block ERK and NF-κB, respectively. Coincubation of the cells with palmitate, in either the presence of PD98059 or parthenolide, prevented the upregulation of myostatin (Figure 7). Overall, these results suggest that myostatin downregulation in skeletal muscle cells following APS exposure is regulated by the ERK-MAPK-NF-κB pathway.

4. Discussion

We showed that APS treatment ameliorated hyperglycemia, hyperlipidemia, and insulin resistance, which were associated with the decreased MDA and myostatin level in the skeletal muscle of KKAy mice. Myostatin is an important negative regulator of skeletal muscle growth. In our study, increased myostatin expression is inversely related to insulin sensitivity in diabetes. The finding suggests the concept that myostatin may play a role in the development of insulin resistance [14]. Previous report by Palsgaard et al. performed a gene chip analysis of skeletal muscle biopsies from human subject and demonstrated that the levels of myostatin mRNA were increased in type 2 diabetics [5]. The elevation of muscle and plasma myostatin protein contents in insulin-resistant patients can be decreased by aerobic exercise training [15]. Notably, preclinical study showed that administration of a neutralizing antibody to myostatin for six weeks can effectively reduce the blood glucose level in ob/ob mice [16], while injection of recombinant myostatin decreased insulin sensitivity in healthy male mice [15]. The mechanisms by which myostatin achieves this suppression of insulin sensitivity have not been clearly defined. Myostatin is known to increase glucose uptake and glycolysis and inhibit glycogen synthesis in cultured skeletal muscle cells in vitro via an AMP kinase-dependent mechanism [17]. Myostatin may also affect glucose uptake indirectly through its effects on TNF-α

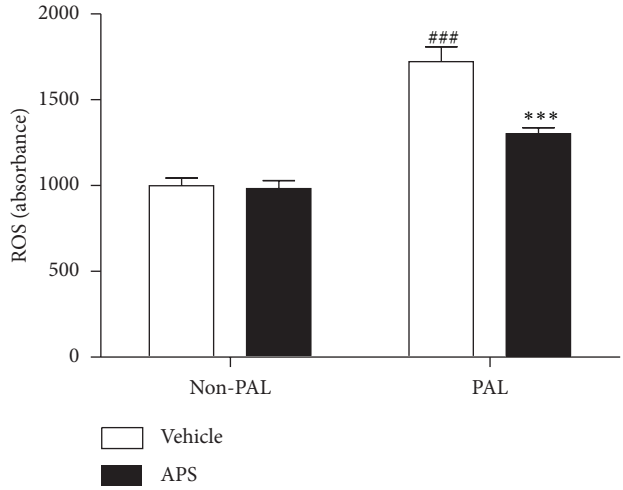

Figure 4: Effects of APS on the production of ROS in palmitate-stimulated C2C12 cells. C2C12 cells were incubated for 24 h in DMEM containing 5% BSA in either the presence (FFA-treated cells) or absence (control cells) of 0.5 mmol/L FFAs. Cells treated with APS were incubated with additional APS at the final concentration of 200 μg/mL. The intracellular levels of ROS were determined by fluorescence using a fluorescence microplate reader with excitation/emission set to 485/530 nm. Cells were plated at 1×10^6 cells/mL and pretreated with APS for 0.5 h, followed by incubation with palmitate for 24 h. Data are expressed as means ± SD of 6 different experiments. $^{###}P < 0.001$ versus vehicle, $^{***}P < 0.001$ versus palmitate. ROS: reactive oxygen species. PAL: palmitate.

expression, which can antagonize the effects of insulin on glucose uptake [18].

Since elevated plasma FFA is a major cause of insulin resistance in type 2 diabetes [19], we therefore used an in vitro FFA-induced insulin resistance cell culture model to further characterize the mechanisms by which APS attenuating myostatin expression. In this in vitro model, FFA palmitate inhibited insulin-stimulated glucose uptake, accompanied with a strong induction of the myostatin expression protein in skeletal muscle C2C12 cells, which was significantly attenuated by APS. Because an inverse relationship between the insulin resistance and muscle myostatin has been reported [14], we hypothesized that reducing skeletal muscle myostatin expression might be one of the mechanisms by which APS enables insulinsensitizing and hypoglycemic activity.

Oxidative stress, which may be precipitated by hyperglycemia and hyperlipidemia, plays a pivotal role in the development of diabetes [20]. ROS overproduction can lead to impairment of intracellular signaling pathways and development of insulin resistance [21]. Oxidative stress has been proposed as a link between FFA and skeletal muscle insulin resistance [22]. Consequently, reducing oxidative stress by lowering ROS production is crucial in the management of insulin resistance. We showed that palmitate stimulates ROS formation and APS presented effective suppression on palmitate-induced ROS overproduction and facilitated insulin action on the C2C12 cells, well demonstrating its antioxidant potency against FFA insult. Consistent with our in vitro finding, the decreased MDA level in skeletal muscle of KKAy mice after APS treatment also supported an antioxidant action of APS. There are several pathways involved in ROS production under the conditions of insulin resistance, including NADPH oxidase, xanthine oxidase, and mitochondria-mediated pathways [23]. APS is reported to protect mitochondria by scavenging ROS, inhibiting mitochondrial permeability transition, and increasing the activities of antioxidases [24]. Future research will therefore involve investigations of the mechanisms behind the antioxidant effect of APS in response to palmitate stimulation and other pathophysiological conditions.

We studied several different signal transduction pathways known to be activated by ROS. MAPKs are important mediators involved in a variety of cell signalling functions, including insulin resistance. The MAPK family includes p38, ERK, and JNK [25]. Our data indicate that palmitate induced marked phosphorylation of ERK in C2C12 cells, while APS downregulated the expression of the phospho-ERK following palmitate stimulation. The transcription factor NF-κB has been proposed as a critical mediator between oxidant stress and gene expression. Activation of the NF-κB has been suggested to participate in diabetes and its complications [26]. We therefore explored whether NF-κB participates in APS attenuating palmitate-induced myostatin expression and insulin resistance. Exposure of C2C12 cells to palmitate resulted in degradation of IκBα and the subsequent release and translocation of NF-κB into the nucleus. APS administration, however, leads to the upregulation of IκBα and decreased NF-κB translocation. We propose that APS may reduce FFA palmitate-stimulated myostatin expression in skeletal muscle cells through a mechanism involving activation of the ROS-ERK-NF-κB pathway, since the ERK inhibitor PD98059, as well as NF-κB inhibitor parthenolide, partially reversed the effect of palmitate-stimulated myostatin expression.

Several other lines of evidences also suggest an effect of APS on ROS-ERK/NF-κB signaling pathway. For example, *Astragalus membranaceus* can inhibit inflammation via phospho-P38 MAPK and NF-κB pathways in advanced glycation end product-stimulated macrophages [18]. *Astragalus membranaceus* has been shown to inhibit mRNA expressions of NF-κB and IκB in renal cortex of streptozotoxin-induced diabetic rats [27]. Similar to our finding, a recent study suggests that astragalus polysaccharide inhibits palmitate-induced insulin resistance in C2C12 myotubes by inhibiting expression of PTP1B and regulating NF-κB [28]. In previous studies from our colleagues, APS has been shown to increase insulin-induced tyrosine phosphorylation of the insulin receptor and IRS-1 in the skeletal muscles of fat-fed diabetic rats, with parallel reduces in protein levels and activity of protein tyrosine phosphatase-1B [10]. Furthermore, our recent finding indicated that the antihyperglycemic activity of APS is mediated by insulin sensitivity improvement related to GSK3 inhibition in the liver [11]. All these results suggest that APS might regulate insulin sensitivity at multiple sites in various diabetic animal models.

In conclusion, the present study demonstrated elevated myostatin expression in skeletal muscle of type 2 diabetic

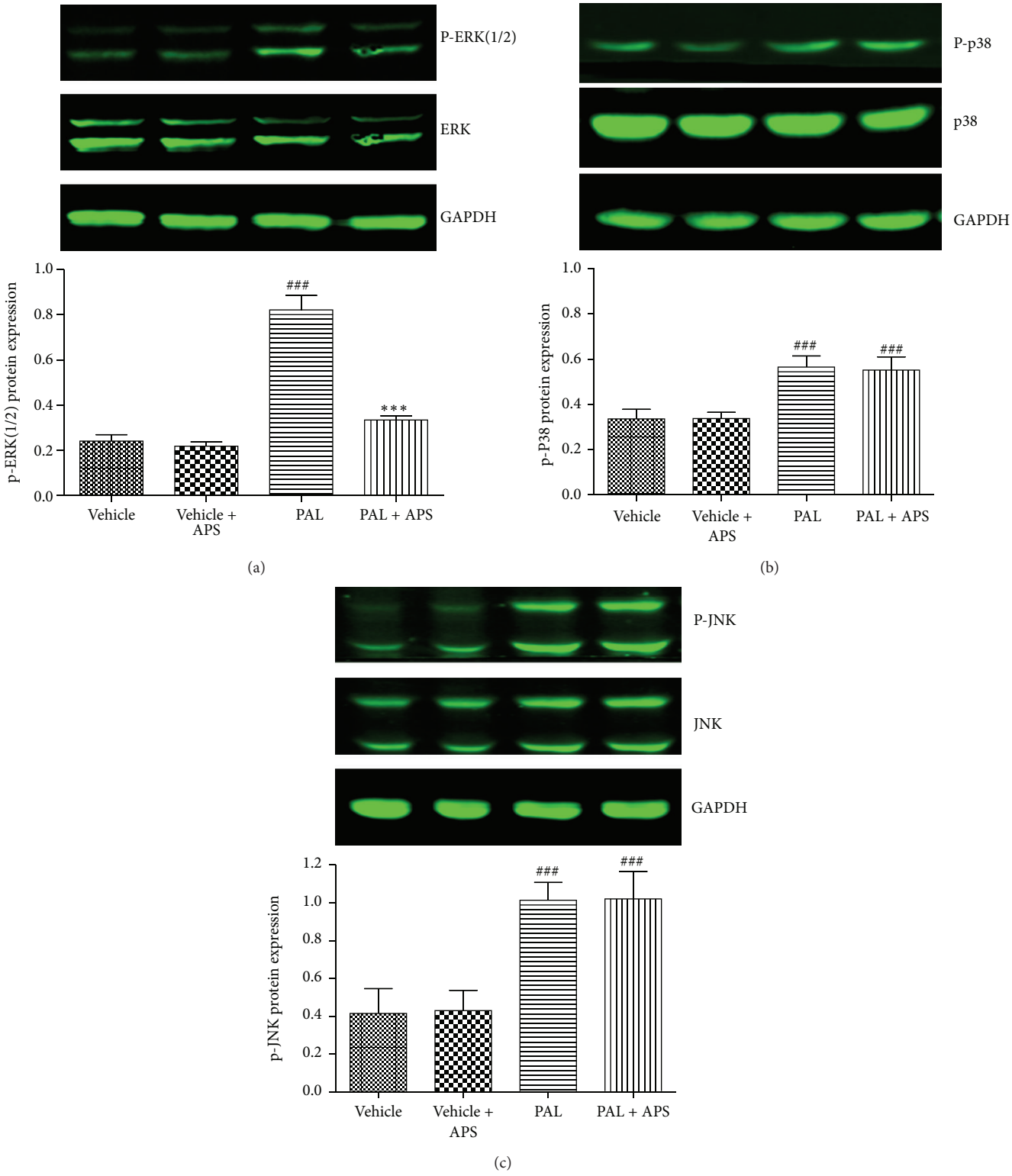

Figure 5: Effects of APS on the MAPK expression in palmitate-stimulated C2C12 cells. C2C12 cells were incubated for 24 h in DMEM containing 5% BSA in either the presence (FFA-treated cells) or absence (control cells) of 0.5 mmol/L FFAs. Cells treated with APS were incubated with additional APS at the final concentration of 200 μg/mL. The expression of ERK, p38, and JNK and phosphorylated ERK, p38, and JNK were determined by western blot. Data are expressed as means ± SD of 6 different experiments. $^{###}P < 0.001$ versus vehicle, $^{***}P < 0.001$ versus palmitate. ERK: extracellular signal-regulated kinase; JNK: c-Jun amino-terminal kinases.

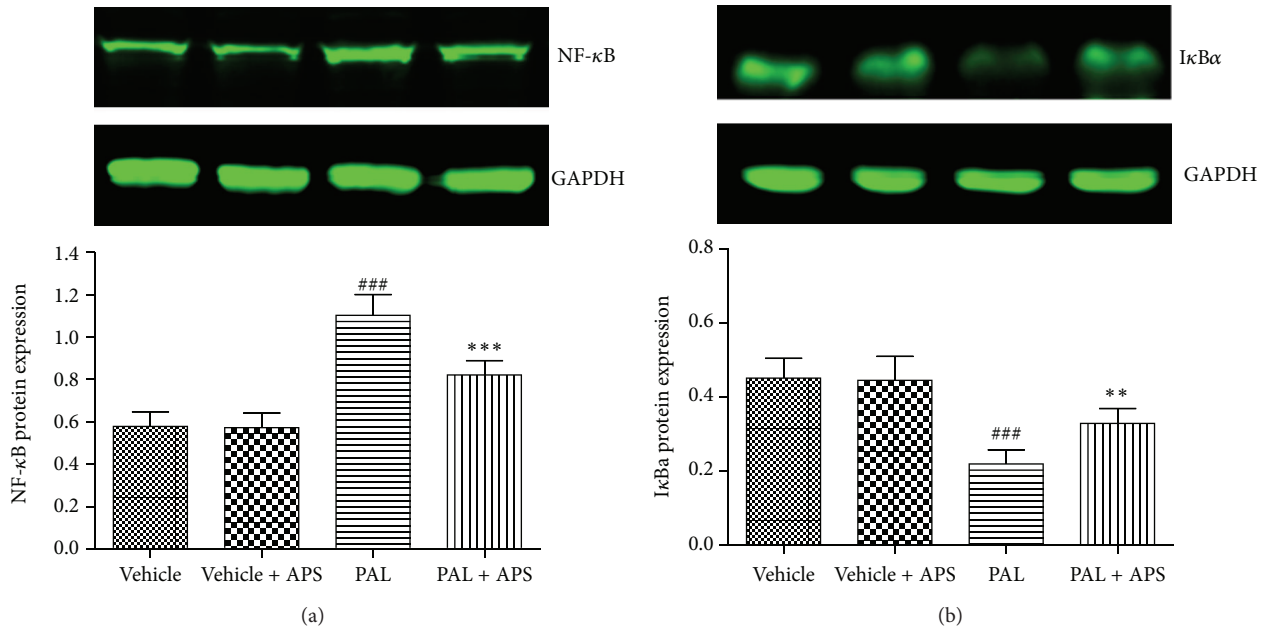

Figure 6: Effects of APS on NF-κB activation in palmitate-stimulated C2C12 cells. C2C12 cells were incubated for 24 h in DMEM containing 5% BSA in either the presence (FFA-treated cells) or absence (control cells) of 0.5 mmol/L FFAs. Cells treated with APS were incubated with additional APS at the final concentration of 200 μg/mL. The expression of nuclear NF-κB and cytoplasmic IκBa was determined by western blot. Data are expressed as means ± SD of 6 different experiments. $^{###}P < 0.001$ versus vehicle, $^{**}P < 0.01$, $^{***}P < 0.001$ versus palmitate. NF-κB: nuclear factor-kappa B.

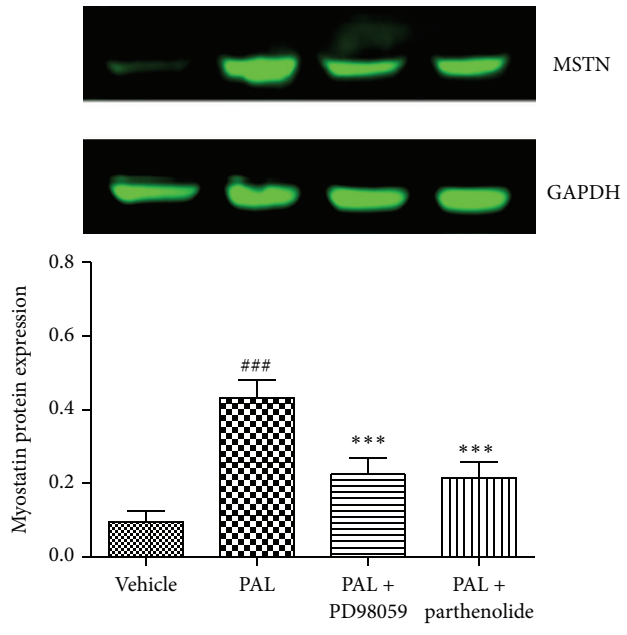

Figure 7: The ERK-MAPK cascade is involved in palmitate-induced myostatin expression in skeletal muscle cells. C2C12 myotubes were incubated with either 0.5 mM palmitate in the presence or in the absence of 100 μM PD98059 or with 10 μM parthenolide. Analysis of the protein levels of myostatin was analyzed by western blot assay. Data are expressed as means ± SD of 6 different experiments. $^{###}P < 0.001$ versus vehicle, $^{***}P < 0.001$ versus palmitate. MSTN: myostatin.

KKAy mice and in cultured C2C12 cells exposed to palmitate. APS is capable of improving insulin sensitivity and decreasing myostatin expression in skeletal muscle through downregulating ROS-ERK-NF-κB pathway. This study provides new insight into the molecular mechanisms of antidiabetes action of APS.

Acknowledgment

This work is supported by NSFC Grant nos. 81102863, 81271205, and 81172043.

References

[1] D. R. Sinacore and E. A. Gulve, "The role of skeletal muscle in glucose transport, glucose homeostasis, and insulin resistance: implications for physical therapy," *Physical Therapy*, vol. 73, no. 12, pp. 878–891, 1993.

[2] K. Eckardt, A. Taube, and J. Eckel, "Obesity-associated insulin resistance in skeletal muscle: role of lipid accumulation and physical inactivity," *Reviews in Endocrine and Metabolic Disorders*, vol. 12, no. 3, pp. 163–172, 2011.

[3] B. Elliott, D. Renshaw, S. Getting, and R. Mackenzie, "The central role of myostatin in skeletal muscle and whole body homeostasis," *Acta Physiologica*, vol. 205, no. 3, pp. 324–340, 2012.

[4] T. Guo, W. Jou, T. Chanturiya, J. Portas, O. Gavrilova, and A. C. McPherron, "Myostatin inhibition in muscle, but not adipose tissue, decreases fat mass and improves insulin sensitivity," *PLoS ONE*, vol. 4, no. 3, Article ID e4937, 2009.

[5] C. Brandt, A. R. Nielsen, C. P. Fischer, J. Hansen, B. K. Pedersen, and P. Plomgaard, "Plasma and muscle myostatin in relation to type 2 diabetes," *PLoS ONE*, vol. 7, no. 5, Article ID e37236, 2012.

[6] J. J. Wilkes, D. J. Lloyd, and N. Gekakis, "Loss-of-function mutation in myostatin reduces tumor necrosis factor a production and protects liver against obesity-induced insulin resistance," *Diabetes*, vol. 58, no. 5, pp. 1133–1143, 2009.

[7] Y. Tong and H. Hou, "Effects of Huangqi Guizhi Wuwu Tang on diabetic peripheral neuropathy," *Journal of Alternative and Complementary Medicine*, vol. 12, no. 6, pp. 506–509, 2006.

[8] Z. Sang, L. Zhou, X. Fan, and R. J. McCrimmon, "Radixz astragali (Huangqi) as a treatment for defective hypoglycemia counterregulation in diabetes," *The American Journal of Chinese Medicine*, vol. 38, no. 6, pp. 1027–1038, 2010.

[9] Y. W. Zhang, D. Xie, B. Xia, R. T. Zhen, I. M. Liu, and J. T. Cheng, "Suppression of transforming growth factor-β1 gene expression by danggui buxue tang, a traditional Chinese herbal preparation, in retarding the progress of renal damage in streptozotocin-induced diabetic rats," *Hormone and Metabolic Research*, vol. 38, no. 2, pp. 82–88, 2006.

[10] Y. Wu, J. P. Ou-Yang, K. Wu, Y. Wang, Y. F. Zhou, and C. Y. Wen, "Hypoglycemic effect of Astragalus polysaccharide and its effect on PTP1B," *Acta Pharmacologica Sinica*, vol. 26, no. 3, pp. 345–352, 2005.

[11] X. Q. Mao, Y. Wu, K. Wu et al., "Astragalus polysaccharide reduces hepatic endoplasmic reticulum stress and restores glucose homeostasis in a diabetic KKAy mouse model," *Acta Pharmacologica Sinica*, vol. 28, no. 12, pp. 1947–1956, 2007.

[12] Y. X. Chen, Q. Y. Zhang, and J. Wang, "Changes of peripheral blood dendritic cell functions in children with Henoch-Schonlein purpura and in vitro effect of Astragalus membranaceus," *Zhonghua Er Ke Za Zhi*, vol. 46, no. 9, pp. 708–709, 2008 (Chinese).

[13] M. Liu, K. Wu, X. Mao, Y. Wu, and J. Ouyang, "Astragalus polysaccharide improves insulin sensitivity in KKAy mice: regulation of PKB/GLUT4 signaling in skeletal muscle," *Journal of Ethnopharmacology*, vol. 127, no. 1, pp. 32–37, 2010.

[14] D. L. Allen, D. S. Hittel, and A. C. McPherron, "Expression and function of myostatin in obesity, diabetes, and exercise adaptation," *Medicine and Science in Sports and Exercise*, vol. 43, no. 10, pp. 1828–1835, 2011.

[15] D. S. Hittel, M. Axelson, N. Sarna, J. Shearer, K. M. Huffman, and W. E. Kraus, "Myostatin decreases with aerobic exercise and associates with insulin resistance," *Medicine and Science in Sports and Exercise*, vol. 42, no. 11, pp. 2023–2029, 2010.

[16] B. L. Bernardo, T. S. Wachtmann, P. G. Cosgrove et al., "Postnatal PPARdelta activation and myostatin inhibition exert distinct yet complimentary effects on the metabolic profile of obese insulin-resistant mice," *PLoS ONE*, vol. 5, no. 6, Article ID e11307, 2010.

[17] C. Zhang, C. McFarlane, S. Lokireddy et al., "Myostatin-deficient mice exhibit reduced insulin resistance through activating the AMP-activated protein kinase signalling pathway," *Diabetologia*, vol. 54, no. 6, pp. 1491–1501, 2011.

[18] Q. Qin, J. Niu, Z. Wang, W. Xu, Z. Qiao, and Y. Gu, "Astragalus membranaceus inhibits inflammation via phospho-P38 mitogen-activated protein kinase (MAPK) and nuclear factor (NF)-κB pathways in advanced glycation end product-stimulated macrophages," *International Journal of Molecular Sciences*, vol. 13, no. 7, pp. 8379–8387, 2012.

[19] G. Boden, "Effects of free fatty acids (FFA) on glucose metabolism: significance for insulin resistance and type 2 diabetes," *Experimental and Clinical Endocrinology and Diabetes*, vol. 111, no. 3, pp. 121–124, 2003.

[20] K. Stadler, "Oxidative stress in diabetes," *Advances in Experimental Medicine and Biology*, vol. 771, pp. 272–287, 2012.

[21] F. Giacco and M. Brownlee, "Oxidative stress and diabetic complications," *Circulation Research*, vol. 107, no. 9, pp. 1058–1070, 2010.

[22] A. R. Martins, R. T. Nachbar, R. Gorjao et al., "Mechanisms underlying skeletal muscle insulin resistance induced by fatty acids: importance of the mitochondrial function," *Lipids in Health and Disease*, vol. 11, article 30, 2012.

[23] D. H. Endemann and E. L. Schiffrin, "Nitric oxide, oxidative excess, and vascular complications of diabetes mellitus," *Current Hypertension Reports*, vol. 6, no. 2, pp. 85–89, 2004.

[24] X. T. Li, Y. K. Zhang, H. X. Kuang et al., "Mitochondrial protection and anti-aging activity of Astragalus polysaccharides and their potential mechanism," *International Journal of Molecular Sciences*, vol. 13, no. 2, pp. 1747–1761, 2012.

[25] E. K. Kim and E. J. Choi, "Pathological roles of MAPK signaling pathways in human diseases," *Biochimica et Biophysica Acta*, vol. 1802, no. 4, pp. 396–405, 2010.

[26] A. Bierhaus, S. Schiekofer, M. Schwaninger et al., "Diabetes-associated sustained activation of the transcription factor nuclear factor-κB," *Diabetes*, vol. 50, no. 12, pp. 2792–2808, 2001.

[27] Y. W. Zhang, C. Y. Wu, and J. T. Cheng, "Merit of Astragalus polysaccharide in the improvement of early diabetic nephropathy with an effect on mRNA expressions of NF-κB and IκB in renal cortex of streptozotoxin-induced diabetic rats," *Journal of Ethnopharmacology*, vol. 114, no. 3, pp. 387–392, 2007.

[28] M. Zhao, Z. F. Zhang, Y. Ding, J. B. Wang, and Y. Li, "Astragalus polysaccharide improves palmitate-induced insulin resistance by inhibiting PTP1B and NF-κB in C2C12 myotubes," *Molecules*, vol. 17, no. 6, pp. 7083–7092, 2012.

Hindawi Publishing Corporation
Oxidative Medicine and Cellular Longevity
Volume 2013, Article ID 678484, 9 pages
http://dx.doi.org/10.1155/2013/678484

Research Article

Nitroglycerine-Induced Nitrate Tolerance Compromises Propofol Protection of the Endothelial Cells against TNF-α: The Role of PKC-β_2 and NADPH Oxidase

Shaoqing Lei,[1,2] Wating Su,[1] Huimin Liu,[1,2] Jinjin Xu,[1] Zhong-yuan Xia,[1] Qing-jun Yang,[3] Xin Qiao,[4] Yun Du,[4] Liangqing Zhang,[5] and Zhengyuan Xia[2,5]

[1] *Department of Anesthesiology, Renmin Hospital of Wuhan University, Wuhan, Hubei 430060, China*
[2] *Department of Anesthesiology, University of Hong Kong, Hong Kong*
[3] *Department of Cardiac Surgery, Chongqing Zhongshan Hospital, Chongqing 400013, China*
[4] *Department of Anesthesia, Chongqing Zhongshan Hospital, Chongqing 400013, China*
[5] *Department of Anesthesiology, Affiliated Hospital of Guangdong Medical College, Zhanjiang, Guangdong 524001, China*

Correspondence should be addressed to Huimin Liu; huimin_liu2006@126.com and Qing-jun Yang; peter.yangqin@gmail.com

Received 10 September 2013; Accepted 18 October 2013

Academic Editor: Yanfang Chen

Continuous treatment with organic nitrates causes nitrate tolerance and endothelial dysfunction, which is involved with protein kinase C (PKC) signal pathway and NADPH oxidase activation. We determined whether chronic administration with nitroglycerine compromises the protective effects of propofol against tumor necrosis factor (TNF-) induced toxicity in endothelial cells by PKC-β_2 dependent NADPH oxidase activation. Primary cultured human umbilical vein endothelial cells were either treated or untreated with TNF-α (40 ng/mL) alone or in the presence of the specific PKC-β_2 inhibitor CGP53353 (1 μM)), nitroglycerine (10 μM), propofol (100 μM), propofol plus nitroglycerin, or CGP53353 plus nitroglycerine, respectively, for 24 hours. TNF-α increased the levels of superoxide, Nox (nitrate and nitrite), malondialdehyde, and nitrotyrosine production, accompanied by increased protein expression of p-PKC-β_2, gP91phox, and endothelial cell apoptosis, whereas all these changes were further enhanced by nitroglycerine. CGP53353 and propofol, respectively, reduced TNF-α induced oxidative stress and cell toxicity. CGP53353 completely prevented TNF-α induced oxidative stress and cell toxicity in the presence or absence of nitroglycerine, while the protective effects of propofol were neutralized by nitroglycerine. It is concluded that nitroglycerine comprises the protective effects of propofol against TNF-α stimulation in endothelial cells, primarily through PKC-β_2 dependent NADPH oxidase activation.

1. Introduction

Ischemic heart disease is a leading cause of death in many regions. The mortality of myocardial infarction remains significant despite advancement in surgical techniques and pharmacological therapies. Organic nitrates (such as nitroglycerin, L-arginine) are still useful drugs and have been widely used for the prevention and treatment of ischemic heart disease for more than 100 years [1, 2]. However, these drugs are also known to induce nitrate tolerance after prolonged, continuous, or high dose administration, which leads to the abolishment of clinical or hemodynamic response to organic nitrates [3] and subsequently induces endothelial dysfunction [4]. It has been reported that nitrate tolerance and endothelial dysfunction are associated with increased vascular production of reactive oxygen species (ROS) via mechanisms that involve increased protein kinase C (PKC) and NADPH oxidase activation, eNOS uncoupling in the vascular endothelium [4–6]. Interestingly, circulatory proapoptotic inflammatory cytokines (such as tumor necrosis factor (TNF-)α), which are increased during myocardial infraction and atherosclerosis, may promote the production of ROS subsequent to the induction of cardiomyocyte apoptosis and endothelial cells apoptosis [7]. A further study had shown TNF-α induced human endothelial cell apoptosis which involved the activation of PKC [8]. Despite these

observations, whether or not organic nitrates aggravate TNF-α induced endothelial cell apoptosis and the underlying mechanisms by which PKC isoforms exert adverse effects in this pathology remain unclear.

Propofol, an anesthetic with demonstrated antioxidant properties [9], has shown protective effects in various models against ischemia-reperfusion injury [10–12]. We previously reported that propofol dose-dependently reduced TNF-α induced apoptosis in primary cultured human umbilical vein endothelial cells (HUVECs) [13]. Our further study showed that the supplementation of L-arginine exacerbated TNF-α induced cellular toxicity by enhancing oxidative stress and nitrative stress, which was neutralized by propofol treatment [14]. It is unknown, however, whether or not propofol achieves these effects via inhibition of PKC-β_2, a PKC isoform that may play a major role in TNF-α induced human endothelial cell apoptosis [15]. Of interest, propofol has been shown to activate PKC-α, PKC-δ, PKC-ε, and PKC-ξ in cardiomyocytes [16–18], which may represent an important cellular mechanism of propofol-induced myocardial protection in the setting of ischemia-reperfusion injury. However, in all these studies, the effect of propofol on PKC-β_2 has not been reported, nor has it been investigated in endothelial cells in the condition of nitrate tolerance. In the present study, we hypothesize that nitrate tolerance induced by organic nitrates comprises the protective effects of propofol against TNF-α induced toxicity in endothelial cells. Our data suggests that nitroglycerine supplementation promoted PKC-β_2 activation in HUVECs subjected to TNF-α stimulation, which subsequently increased the activation of NADPH oxidase and compromised the protective effects of propofol against TNF-α induced damage.

2. Materials and Methods

2.1. Cell Culture. Primary cultured HUVECs will be prepared using established procedures as previously described [13]. Briefly, cells were digested from the umbilical vein with 0.1% collagenase I (w/v) at 37°C for 20 min, after which they were cultured in 0.1% (w/v) gelatin-coated flasks in Medium 199 supplemented with 10% fetal bovine serum, 15 mg/L ECGS, 2 mM glutamine, 100 units/mL penicillin, and 100 μg/mL streptomycin in an atmosphere of 5% CO_2 at 37°C. The medium was changed every 2-3 days until the ECs reached confluence. Cultured cells were identified as ECs by their morphology and the presence of the Factor VIII-related antigen was detected using an indirect immunocytochemistry method as described [19]. The purity of HUVECs in culture was higher than 95% and passages 2–4 were used in the research.

2.2. Experimental Conditions. When the cells were at 70% confluence, the cultured cells were then randomly divided into the following groups: cells were either not treated (control group, Con.) or treated with 40 ng/mL TNF-α (TNF-α group, T) alone or TNF-α in the presence of 1 μM CGP53353 (CGP) (TNF-α + CGP group, T + C), 10 μM nitroglycerine (NTG) (TNF-α + NTG group, T + N), 100 μM propofol (TNF-α + propofol group, T + P), or NTG plus propofol (TNF-α + NTG + propofol group, T + N + P), and NTG plus CGP53353 (TNF-α + NTG + CGP53353 group, T + N + C), respectively, for 24 hours. In specific groups, cultured cells were pretreated with propofol for 30 min before other treatments. The concentration of TNF-α used to induce apoptosis in the present study was chosen on the basis of our previous studies [13], which demonstrated that TNF-α at the dose of 40 ng/mL could significantly induce ECs apoptosis. The concentration of NTG adopted is according to the studies [20, 21], which demonstrated that NTG at the dose of 10 μM could induce nitrate tolerance. The choice of concentration of PKC-β_2 inhibitor was based on that 1 μM CGP53353 could selectively inhibit PKC-β_2 activation in our previous study [22]. In our preliminary study, propofol at the dose of 100 μM reversed TNF-α (40 ng/mL) induced cell injury but propofol at the dose of 100 μM per se did not cause apparent apoptosis under the present experimental condition in the absence of TNF-α stimulation. Therefore, we chose the concentration of 100 μM as the treatment dose of propofol for the further mechanistic study.

2.3. Determination of Cytotoxicity. Cytotoxicity will be assessed by measuring lactate dehydrogenase (LDH) (Jiancheng Co., Nanjing, China) release in the medium in addition to the measurement of cell viability using the 3-(4,5-Dimethylthiazol-2-yl)-2,5-diphenyltetrazolium bromide (MTT) (Sigma, St. Louis, MO, USA) assay according to the manufacturer's instructions.

2.4. Determination of Lipid Peroxidation. The content of malondialdehyde (MDA), which is a marker of lipid peroxidation, was measured to evaluate the oxidative injury of ECs. After homogenizing on ice in normal saline, the MDA levels of the supernatants of cell samples was determined by the thiobarbituric acid colorimetric method using MDA assay kit (Jiancheng Co., Nanjing, China) as described [23, 24]. The results were expressed as nanomole per milligram protein (nmol/mg protein).

2.5. Determination of the Levels of NOx, O_2^-, and Nitrotyrosine. Cultured cells were homogenized in ice-cold PBS and centrifuged at 3,000 g for 15 minutes at 4°C for supernatant collection. The supernatant protein concentration was determined via a Lowry assay kit (Bio-Rad, CA, USA). Concentrations of nitrites (NO_2^-) and nitrates (NO_3^-), the stable end products of nitric oxide (NO), were determined by the Griess reaction as previously described [13]. NOx levels were expressed as μmol/L protein. Myocardial O_2^- production was determined via lucigenin chemiluminescence method [25, 26]. The supernatant samples were loaded with dark-adapted lucigenin (5 μM) and read in 96-well microplates by luminometer (GloMax, Promega). Light emission, expressed as mean light units (MLU)/min/100 μg protein, was recorded for 5 minutes. Myocardial nitrotyrosine levels (μg/mg protein) in the collected supernatant were determined by chemiluminescence detection via the Nitrotyrosine Assay Kit per manufacturer's protocol (Millipore, USA).

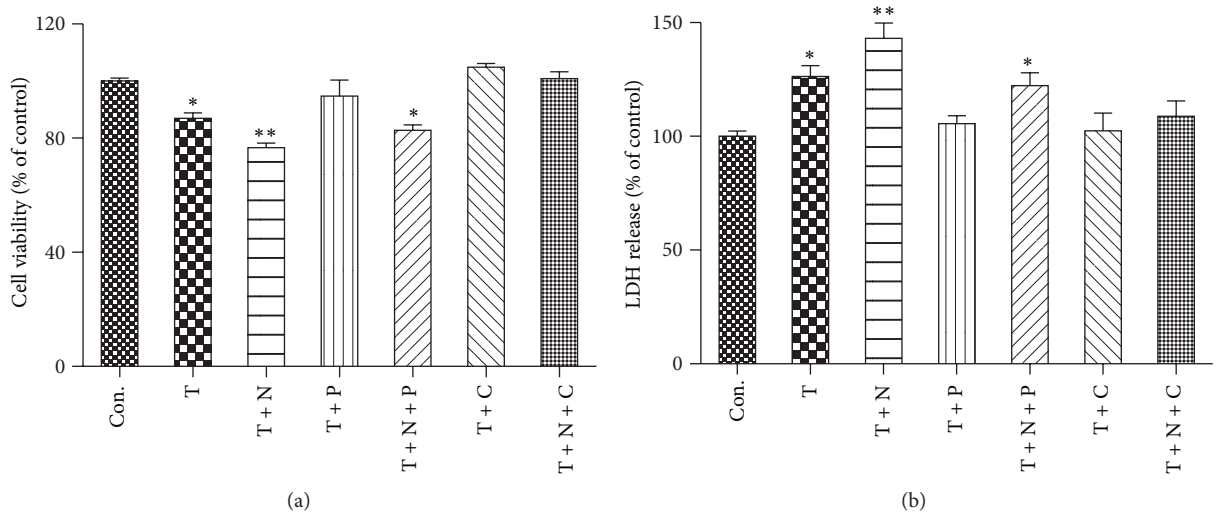

Figure 1: Cell viability (a) and LDH release (b). Primary cultured human umbilical vein endothelial cells (HUVECs) were either not treated (control, Con.) or treated with TNF-α (40 ng/mL) alone (T) or with TNF-α in the presence of nitroglycerine (10 μM) (T + N), propofol (100 μM) (T + P), CGP53353 (1 μM) (T + C), propofol plus nitroglycerin (T + N + P), or CGP53353 plus nitroglycerine (T + N + C), respectively, for 24 h. All results are expressed as mean ± S.E.M., $n = 7$, $^{*}P < 0.05$ compared with Con., T + N, T + P, T + C and T + N + C, $^{**}P < 0.01$ compared with Con., T + P, T + C and T + N + C.

2.6. Detection of Apoptosis by Flow Cytometry. DNA fragments which are lost from apoptotic nuclei and nuclear DNA content can be easily measured by flow cytometry after nucleic acid staining with specific fluorochromes. Briefly, cells (1×10^6) were harvested and processed as described [14]. Then the cells were performed to Annexin-V-fluos Staining and analyzed using a flow cytometer (Beckman Coulter, Brea, CA) according to manufacturer's protocol. Electronic compensation of the instrument is required to exclude overlapping of the two emission spectra. All measurements were performed in the same instrumental settings.

2.7. Western Blot Analysis. Cultured cells were homogenized in cell lysis buffer containing Tris-HCl (20 mM, pH 7.4), NaCl (150 mM), EDTA (l mM), EGTA (l mM), β-glycerolphosphate (1 mM), sodium pyrophosphate (2.5 mM), Triton X-100 (1%), PMSF (1 mM), DTT (l mM), leupeptin (1 μg/mL), aprotinin (1 μg/mL), and pepstatin (1 μg/mL). The homogenate was centrifuged at 1,000 g for 10 min at 4°C to collect the supernatant as total protein preparations. Equal amounts of protein were combined with 5×SDS loading buffer, boiled for 5 min, then separated via 10% SDS-PAGE, and subsequently transferred to PVDF membrane for immunoblot analysis. The membranes were blocked in 5% no fat milk for 2 hours at room temperature and then incubated overnight at 4°C with primary antibodies against p-PKC-β_2 (ser660) (1 : 1000, Cell Signaling Technology), PKC-β2 (1 : 1000, Cell Signaling Technology), and gP91phox (1 : 500, Santa Cruz Biotechnology). After being washed with TBST, the membranes were incubated with proper secondary horseradish peroxidase (HRP-)conjugated antibodies (1 : 5,000–1 : 10,000, Cell Signaling Technology) and developed with enhanced chemiluminescence reagent (GE Healthcare, USA). The membranes were subsequently reblotted for GAPDH (1 : 2,000, Cell Signaling Technology), and the results were normalized to GAPDH to correct for loading.

2.8. Statistical Analysis. All the data are expressed as mean ± S.E.M. Significance was evaluated by analysis of one-way variance (ANOVA) followed by Tukey's test. GraphPad Prism software program (GraphPad Software Inc., San Diego, CA, USA) was used for statistical analysis. $P < 0.05$ was considered statistically significant.

3. Results

3.1. Cell Viability and LDH Release. The cytotoxicity of the cultured endothelial cells was assessed by MTT assay and LDH release. As shown in Figure 1(a), cell viability was significantly reduced after TNF-α stimulation as compared with control, which was reversed by propofol treatment. The supplementation of nitroglycerine further exacerbated TNF-α induced reduction in cell viability. The treatment of propofol improved but not restored the viability of the cells subjected to TNF-α stimulation in the presence of nitroglycerine. By contrast, CGP53353, a selective inhibitor of PKC-β_2, reversed the reduced cell viability induced by TNF-α with or without the presence of nitroglycerine.

Stimulation with TNF-α resulted in a significant increase in LDH release in the medium of cultured HUVECs (Figure 1(b)). Addition of nitroglycerine further increased TNF-α induced LDH release. Both propofol and CGP53353 significantly restored the TNF-α induced LDH release. By contrast, propofol reduced but not reversed the levels of LDH release in the presence of nitroglycerine.

3.2. Endothelial Cell Apoptosis. Stimulation of HUVECs with TNF-α resulted in a marked significant increase in apoptotic

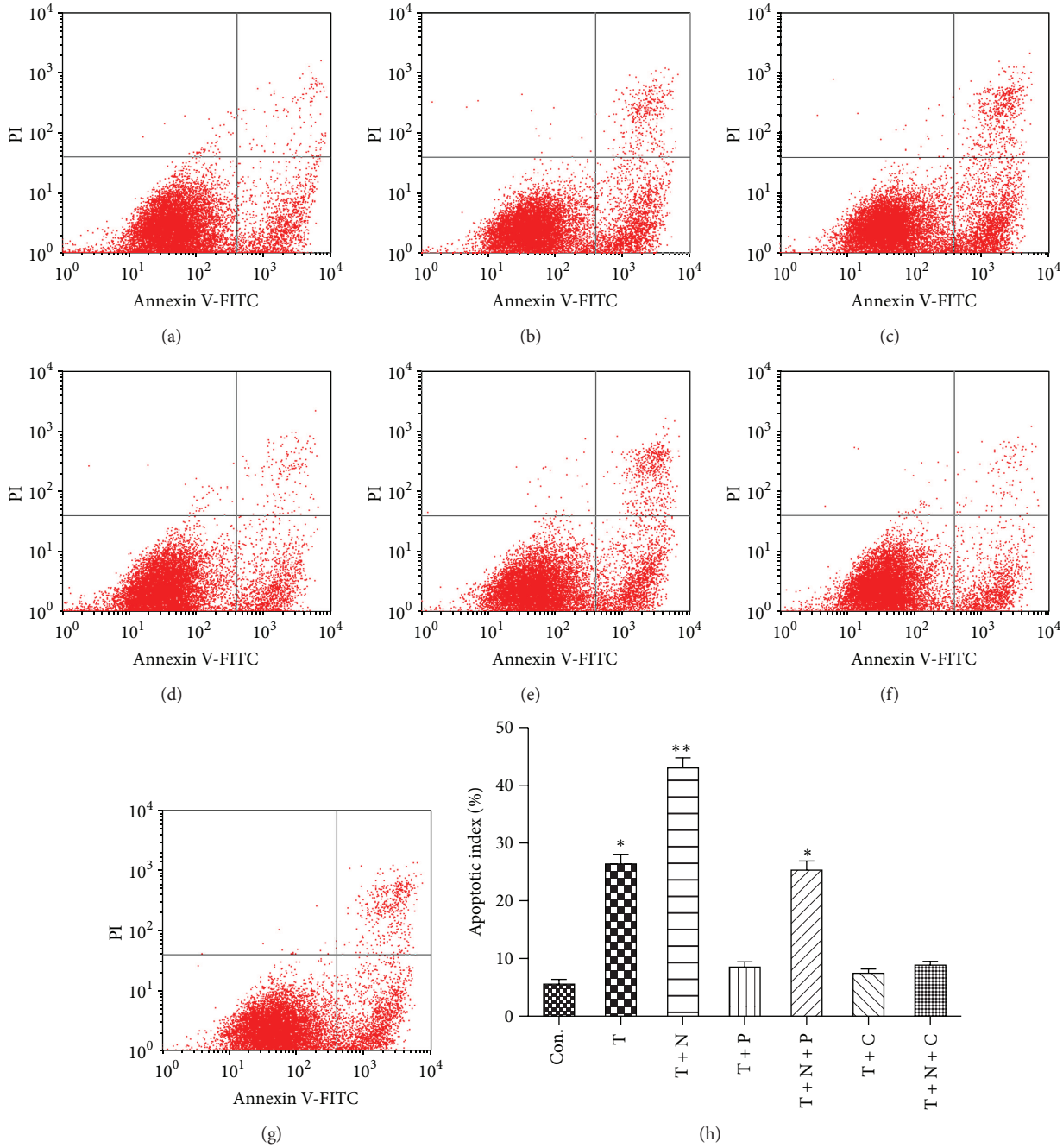

Figure 2: Representative figures of flow cytometry results (a)–(g) and rate of apoptotic cells measured by flow cytometry (h). Flow cytometric analysis was carried out as described in methods. Primary cultured human umbilical vein endothelial cells (HUVECs) were either not treated (control, Con.) or treated with TNF-α (40 ng/mL) alone (T) or with TNF-α in the presence of nitroglycerine (10 μM) (T + N), propofol (100 μM) (T + P), CGP53353 (1 μM) (T + C), propofol plus nitroglycerin (T + N + P), or CGP53353 plus nitroglycerine (T + N + C), respectively, for 24 h. (a)–(g) Representatives of the C, T, T + N, T + P, T + N + P, T + C and T + N + C, respectively. All results are expressed as mean ± S.E.M., $n = 7$, $^{*}P < 0.05$ compared with Con., T + N, T + P, T + C and T + N + C, $^{**}P < 0.01$ compared with Con., T + P, T + C and T + N + C.

index (Figure 2). Nitroglycerine further increased TNF-α induced cell apoptotic death. On the other hand, CGP53353 and propofol significantly attenuated cell apoptosis induced by TNF-α. Propofol attenuated but not prevented the combination of nitroglycerine and TNF-α induced cell apoptotic death, which was profoundly decreased by the treatment of CGP53353. The patterns of apoptotic index results obtained from TUNEL staining were similar to those obtained by flow cytometry (data not shown).

3.3. Superoxide and MDA Production. As the production of ROS plays an important role in the development and

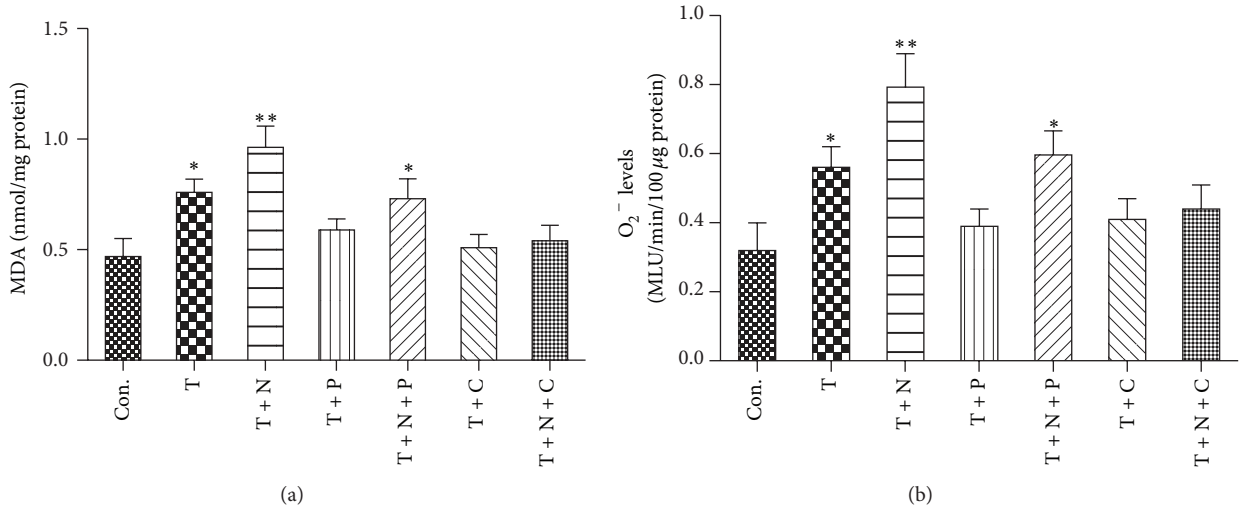

Figure 3: Effects of TNF-α, nitroglycerine, and CGP53353 on MDA (a) and superoxide production (b). Primary cultured human umbilical vein endothelial cells (HUVECs) were either not treated (control, Con.) or treated with TNF-α (40 ng/mL) alone (T) or with TNF-α in the presence of nitroglycerine (10 μM) (T + N), propofol (100 μM) (T + P), CGP53353 (1 μM) (T + C), propofol plus nitroglycerin (T + N + P), or CGP53353 plus nitroglycerine (T + N + C), respectively, for 24 h. All results are expressed as mean ± S.E.M., $n = 7$, $^*P < 0.05$ compared with Con., T + N, T + P, T + C and T + N + C, $^{**}P < 0.01$ compared with Con., T + P, T + C and T + N + C.

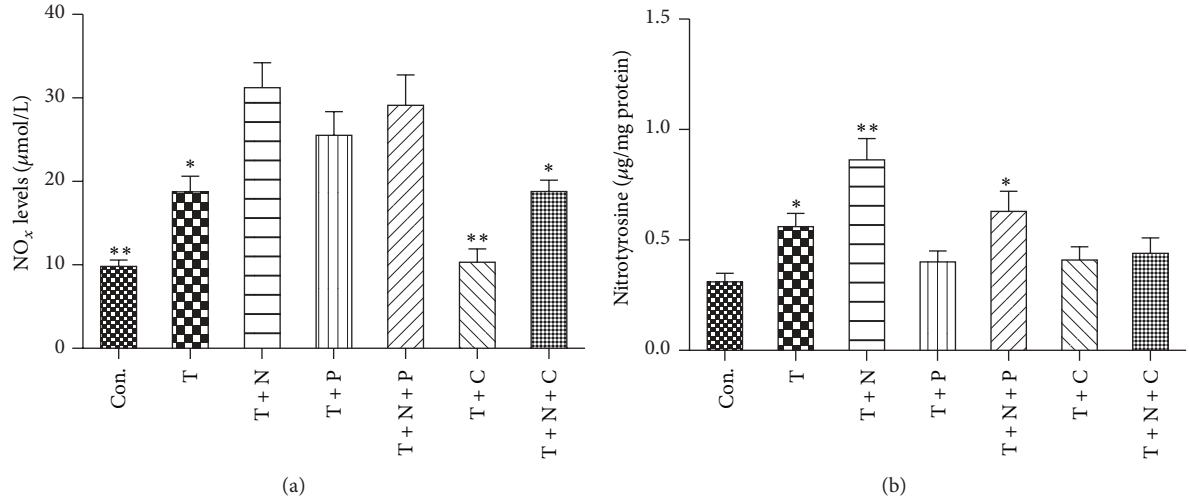

Figure 4: Effects of TNF-α, nitroglycerine and CGP53353 on NOx (a) and nitrotyrosine production (b). Primary cultured human umbilical vein endothelial cells (HUVECs) were either not treated (control, Con.) or treated with TNF-α (40 ng/mL) alone (T) or with TNF-α in the presence of nitroglycerine (10 μM) (T + N), propofol (100 μM) (T + P), CGP53353 (1 μM) (T + C), propofol plus nitroglycerin (T + N + P), or CGP53353 plus nitroglycerine (T + N + C), respectively, for 24 h. All results are expressed as mean ± S.E.M., $n = 7$, (a) $^*P < 0.05$ compared with Con., T + N, T + P, T + N + P and T + C, $^{**}P < 0.01$ compared with T + N, T + P and T + N + P; (b) $^*P < 0.05$ compared with Con., T + N, T + P, T + C and T + N + C, $^{**}P < 0.01$ compared with Con., T + P, T + C and T + N + C.

progress of nitrate tolerance and endothelial dysfunction [4], we measured superoxide and MDA production, which is a marker of lipid peroxidation. As shown in Figure 3, the levels of superoxide and MDA were significantly increased in HUVECs subjected to TNF-α stimulation as compared to control group, which were prevented by the treatment of propofol or CGP53353. Addition of nitroglycerine further promoted the production of superoxide and MDA, which was neutralized by propofol treatment but reversed by CGP53353 treatment.

3.4. NO_x and Nitrotyrosine Production. We next determined the production of NOx and nitrotyrosine in HUVECs. Stimulation of TNF-α increased the levels of NOx and nitrotyrosine production, and nitroglycerine further increased their levels (Figure 4). Propofol treatment had no effects on NOx production in the cells subjected to TNF-α or combination with nitroglycerine stimulation, but significantly decreased TNF-α induced production of nitrotyrosine. By contrast, CGP53353 prevented TNF-α induced NOx production and nitroglycerine-mediated increase of NOx production and

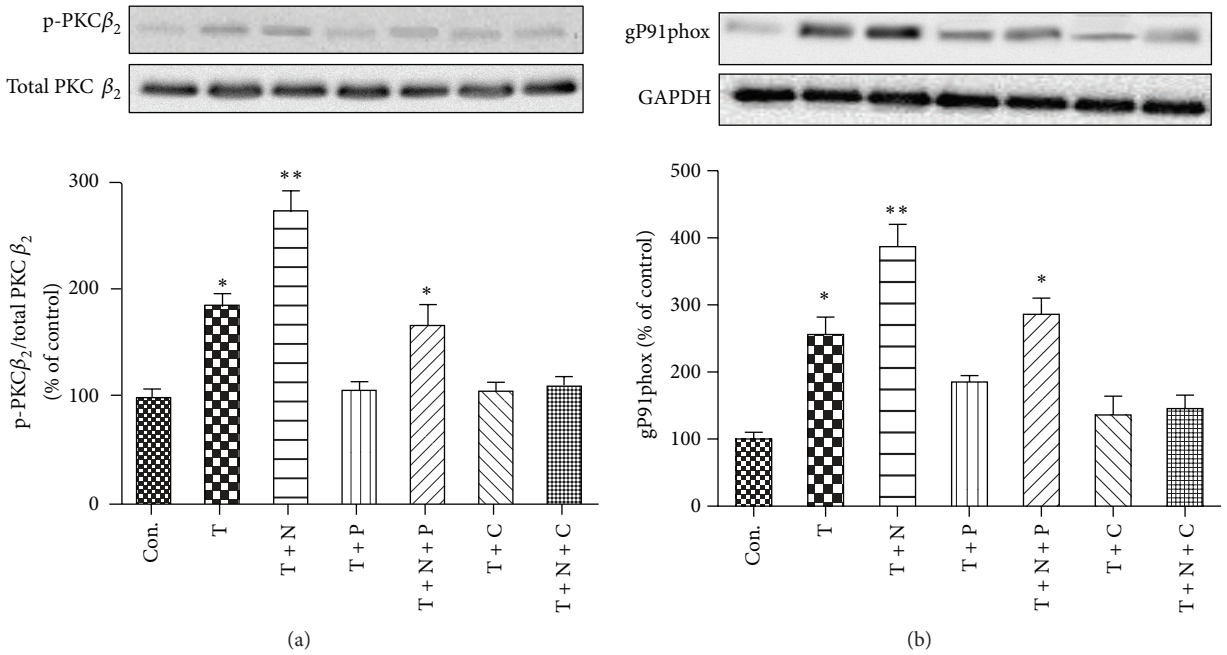

Figure 5: Effects of TNF-α, nitroglycerine, and CGP53353 on the protein expression of p-PKC-β_2 (a) and gP91phox (b). Primary cultured human umbilical vein endothelial cells (HUVECs) were either not treated (control, Con.) or treated with TNF-α (40 ng/mL) alone (T) or with TNF-α in the presence of nitroglycerine (10 μM) (T + N), propofol (100 μM) (T + P), CGP53353 (1 μM) (T + C), propofol plus nitroglycerin (T + N + P), or CGP53353 plus nitroglycerine (T + N + C), respectively, for 24 h. All results are expressed as mean ± S.E.M., $n = 7$, $^*P < 0.05$ compared with Con., T + N, T + P, T + C and T + N + C, $P < 0.01$ compared with Con., T + P, T + C and T + N + C.

reversed TNF-α induced production of nitrotyrosine whether or not in the presence of nitroglycerine.

3.5. Protein Expression of p-PKC-β_2 and gP91phox. We previously found that PKC-β_2 activation played a critical role in TNF-α induced oxidative stress in endothelial cells [27], and further study have shown that gP91phox but not p22phox played an important role in TNF-α induced ROS production and HUVECs apoptosis [15]. Therefore, our present study measured the protein expression of p-PKC-β_2 and gP91phox, one of the membrane subunits of NADPH oxidase, which catalyzes the generation of superoxide and is the major source of ROS in cardiovascular system [28]. As shown in Figure 5, the protein expressions of p-PKC-β_2 and gP91phox were significantly increased in HUVECs subjected to TNF-α stimulation as compared to those of control group, which were prevented by the treatment of propofol or CGP53353. Addition of nitroglycerine further increased the protein expression of p-PKC-β_2 and gP91phox, which was neutralized by propofol treatment but reversed by CGP53353 treatment.

4. Discussion

In the present study, we examined the protective effects of propofol against TNF-α induced toxicity in human umbilical vein endothelial cells in the presence or absence of nitrate tolerance. We demonstrated that propofol inhibited or prevented the adverse effects of TNF-α stimulation in the cultured endothelial cells. Furthermore, our results demonstrated that chronic treatment with nitroglycerine further exacerbated TNF-α induced cell toxicity by promoting PKC-β_2 activation, with subsequently increased activation of NADPH oxidase, and ultimately neutralized the protective effects of propofol. This is the first study showing the role of PKC-β_2 activation in nitroglycerin induced nitrate tolerance, which compromises the protective effects of propofol in endothelial cells subjected to TNF-α stimulation.

Endothelial dysfunction is implicated in a variety of cardiovascular diseases, such as hypercholesterolemia, atherosclerosis, hypertension, diabetes, and heart failure (see for review [29]). A relationship has been suggested to exist between inflammation and endothelial dysfunction [30]. TNF-α, one of the most important proinflammatory cytokines, is well known to increase ROS production in the endothelium and subsequently induce endothelial dysfunction [31]. This is well demonstrated by our present study showing that TNF-α resulted in a significant increase of LDH release and cell apoptosis, accompanied with increased superoxide and NOx production, elevated levels of the lipid peroxidation product MDA, and increased production of nitrotyrosine, a nitration product formed by peroxynitrite-mediated nitration of protein tyrosine residues. All these changes except NOx production were suppressed or prevented by propofol, an anesthetic with demonstrated antioxidant properties [9]. However, the precise mechanisms by which propofol attenuates TNF-α induced oxidative stress and endothelial dysfunction are not clear.

Endothelial NADPH oxidase is a major source of superoxide in blood vessels and is implicated in the oxidative stress

accompanying various vascular diseases [32, 33]. NADPH oxidase contains two membrane-bound subunits gp91phox (Nox2) and p22phox and cytoplasmic subunits such as p47phox, p67phox, and a low-molecular-weight G protein (rac 1 and rac 2) [34]. Many protein kinase pathways have been involved in the regulation of NADPH oxidase activation, among which the PKC family seems to play an important role in this process [35]. PKC-β activation has been shown to play important or critical roles in NADPH oxidase activation [36, 37]. PKC-β_2 is preferably upregulated in failing human hearts [38], which is accompanied with increased levels of TNF-α production [39] and NADPH oxidase activation [40]. Therefore, PKC-β_2 and NADPH oxidase interplay may play critical roles in mediating cellular damage in situations associated with increased TNF-α production, such as AMI, heart failure, and diabetes, as well as during cardiac surgery using cardiopulmonary bypass. In the present study, propofol prevented TNF-α induced overexpression of p-PKC-β_2 and gP91phox in endothelial cells. Of interest, the selective inhibitor of PKC-β_2 CGP53353 has the similar effects as propofol. Therefore, we assumed that propofol preserves endothelial cells though inhibits PKC-β_2 activation signal pathway, including inhibition of NADPH oxidase.

Although there are reports on PKC involvement upon NADPH oxidase activation after TNF-α stimulation in cultured HUVECs [8], especially in nitrate tolerance condition, the major or specific PKC isoform that is involved and the precise regulation mechanism remain unknown. Our previous study has demonstrated that PKC-β_2 but not PKC-δ isoform pathway activation played dominant role in ROS production in this context [15]. However, a new finding in the present study showed that PKC-β_2 activation was involved in NADPH oxidase activation in the condition of nitrate tolerance, a well known phenomenon that the clinical or hemodynamic response to organic nitrates (such as nitroglycerin, L-arginine) is attenuated or abolished after prolonged, continuous, or high dose nitrate treatment (see for review [2]). In the present study, supplementation of nitroglycerine further increased the apoptosis of endothelial cells and the activation of PKC-β_2 induced by TNF-α stimulation, accompanied with enhanced levels of gP91phox and ROS production, which were reversed by the selective inhibition of PKC-β_2 with CGP53353. This suggests that excessive activation of PKC-β_2 and subsequent activation of NADPH oxidase paly a critical role in nitrate tolerance induced adverse effects. Of interest, propofol treatment reversed the increased levels of superoxide, MDA, nitrotyrosine, and the elevated protein expression of PKC-β_2 and gP91phox, as well as LDH release and cell apoptosis in the endothelial cells after TNF-α stimulation. In the presence of nitroglycerine administration, however, propofol attenuated but not completely prevented these changes induced by TNF-α stimulation. This means that chronic treatment with nitroglycerin neutralized the protective effects of propofol.

In summary, the results from the present study indicate that nitrate tolerance further exacerbated TNF-α induced human vascular endothelial cell injury, as well as increased ROS production by PKC-β_2 dependent activation of endothelial NADPH oxidase, and that the protective effects of propofol were compromised by nitroglycerine administration in experimental settings that are associated with persistent TNF-α stimulation. Further studies need to be performed in endothelial cell with deficit of the targeted kinase enzyme derived from gene knockout animals or gene silenced with specific antisenses to confirm the findings of the current study.

Authors' Contribution

Shaoqing Lei and Wating Su wrote the paper. Shaoqing Lei, Wating Su, Jinjin Xu, Zhengyuan Xia, Zhong-yuan Xia, Huimin Liu, Qing-jun Yang, Yun Du, and Xin Qiao performed the studies. Shaoqing Lei, Wating Su, Zhengyuan Xia, Zhong-yuan Xia, and Huimin Liu contributed to discussion and reviewed/edited the manuscript. Huimin Liu, Qing-jun Yang, and Zhengyuan Xia designed the study, reviewed the data, and revised the manuscript. Shaoqing Lei and Wating Su contributed equally to this work.

Conflict of Interests

The authors declare that they have no conflict of interests.

Acknowledgments

This study was supported by grants from the National Natural Science Foundation of China (NSFC 81270899, 81270196) and in part by a Society of Cardiovascular Anesthesiologist (SCA) Research Starter grant.

References

[1] V. E. Nossaman, B. D. Nossaman, and P. J. Kadowitz, "Nitrates and nitrites in the treatment of ischemic cardiac disease," *Cardiology in Review*, vol. 18, no. 4, pp. 190–197, 2010.

[2] T. Munzel, A. Daiber, and T. Gori, "More answers to the still unresolved question of nitrate tolerance," *European Heart Journal*, vol. 34, no. 34, pp. 2666–2673, 2013.

[3] T. Münzel, A. Daiber, and A. Mülsch, "Explaining the phenomenon of nitrate tolerance," *Circulation Research*, vol. 97, no. 7, pp. 618–628, 2005.

[4] M. Knorr, M. Hausding, S. Kröller-Schuhmacher et al., "Nitroglycerin-induced endothelial dysfunction and tolerance involve adverse phosphorylation and S-glutathionylation of endothelial nitric oxide synthase: beneficial effects of therapy with the AT1 receptor blocker telmisartan," *Arteriosclerosis, Thrombosis, and Vascular Biology*, vol. 31, no. 10, pp. 2223–2231, 2011.

[5] J. D. Parker, "Nitrate tolerance, oxidative stress, and mitochondrial function: another worrisome chapter on the effects of organic nitrates," *The Journal of Clinical Investigation*, vol. 113, no. 3, pp. 352–354, 2004.

[6] A. Daiber, P. Wenzel, M. Oelze, and T. Münzel, "New insights into bioactivation of organic nitrates, nitrate tolerance and cross-tolerance," *Clinical Research in Cardiology*, vol. 97, no. 1, pp. 12–20, 2008.

[7] T. Scarabelli, A. Stephanou, N. Rayment et al., "Apoptosis of endothelial cells precedes myocyte cell apoptosis in ischemia/reperfusion injury," *Circulation*, vol. 104, no. 3, pp. 253–256, 2001.

[8] D. Li, B. Yang, and J. L. Mehta, "Tumor necrosis factor-α enhances hypoxia-reoxygenation-mediated apoptosis in cultured human coronary artery endothelial cells: critical role of protein kinase C," *Cardiovascular Research*, vol. 42, no. 3, pp. 805–813, 1999.

[9] I. Vasileiou, T. Xanthos, E. Koudouna et al., "Propofol: a review of its non-anaesthetic effects," *European Journal of Pharmacology*, vol. 605, no. 1–3, pp. 1–8, 2009.

[10] D. Ozkan, T. Akkaya, A. Yalcindag et al., "Propofol sedation in total knee replacement : effects on oxidative stress and ischemia-reperfusion damage," *Der Anaesthesist*, vol. 62, no. 7, pp. 537–542, 2013.

[11] Z. Huang, X. Zhong, M. G. Irwin et al., "Synergy of isoflurane preconditioning and propofol postconditioning reduces myocardial reperfusion injury in patients," *Clinical Science*, vol. 121, no. 2, pp. 57–69, 2011.

[12] K.-X. Liu, S.-Q. Chen, W.-Q. Huang, Y.-S. Li, M. G. Irwin, and Z. Xia, "Propofol pretreatment reduces ceramide production and attenuates intestinal mucosal apoptosis induced by intestinal ischemia/reperfusion in rats," *Anesthesia and Analgesia*, vol. 107, no. 6, pp. 1884–1891, 2008.

[13] T. Luo, Z. Xia, D. M. Ansley et al., "Propofol dose-dependently reduces tumor necrosis factor-α-induced human umbilical vein endothelial cell apoptosis: effects on Bcl-2 and bax expression and nitric oxide generation," *Anesthesia and Analgesia*, vol. 100, no. 6, pp. 1653–1659, 2005.

[14] Z. Xia, T. Luo, H.-M. Liu et al., "L-arginine enhances nitrative stress and exacerbates tumor necrosis factor-α toxicity to human endothelial cells in culture: prevention by propofol," *Journal of Cardiovascular Pharmacology*, vol. 55, no. 4, pp. 358–367, 2010.

[15] B. Deng, S. Xie, J. Wang, Z. Xia, and R. Nie, "Inhibition of protein kinase C β(2) prevents tumor necrosis factor-α-induced apoptosis and oxidative stress in endothelial cells: the role of NADPH oxidase subunits," *Journal of Vascular Research*, vol. 49, no. 2, pp. 144–159, 2012.

[16] P. J. Wickley, T. Shiga, P. A. Murray, and D. S. Damron, "Propofol decreases myofilament Ca2+ sensitivity via a protein kinase C-, nitric oxide synthase-dependent pathway in diabetic cardiomyocytes," *Anesthesiology*, vol. 104, no. 5, pp. 978–987, 2006.

[17] P. J. Wickley, X. Ding, P. A. Murray, and D. S. Damron, "Propofol-induced activation of protein kinase C isoforms in adult rat ventricular myocytes," *Anesthesiology*, vol. 104, no. 5, pp. 970–977, 2006.

[18] J. Yu, T. Kakutani, K. Mizumoto, A. Hasegawa, and Y. Hatano, "Propofol inhibits phorbol 12, 13-dibutyrate-induced, protein kinase C-mediated contraction of rat aortic smooth muscle," *Acta Anaesthesiologica Scandinavica*, vol. 50, no. 9, pp. 1131–1138, 2006.

[19] S. Kakiuchi-Kiyota, T. A. Crabbs, L. L. Arnold et al., "Evaluation of expression profiles of hematopoietic stem cell, endothelial cell, and myeloid cell antigens in spontaneous and chemically induced hemangiosarcomas and hemangiomas in mice," *Toxicologic Pathology*, vol. 41, no. 5, pp. 709–721, 2013.

[20] G.-G. Zhang, R.-Z. Shi, D.-J. Jiang et al., "Involvement of the endothelial DDAH/ADMA pathway in nitroglycerin tolerance: the role of ALDH-2," *Life Sciences*, vol. 82, no. 13-14, pp. 699–707, 2008.

[21] W. H. Kaesemeyer, A. A. Ogonowski, L. Jin, R. B. Caldwell, and R. W. Caldwell, "Endothelial nitric oxide synthase is a site of superoxide synthesis in endothelial cells treated with glyceryl trinitrate," *British Journal of Pharmacology*, vol. 131, no. 5, pp. 1019–1023, 2000.

[22] S. Lei, H. Li, J. Xu et al., "Hyperglycemia-induced PKCbeta2 activation induces diastolic cardiac dysfunction in diabetic rats by impairing caveolin-3 expression and Akt/eNOS signaling," *Diabetes*, vol. 62, no. 7, pp. 2318–2328, 2013.

[23] Z.-Y. Xia, J. Gao, A. K. Ancharaz, K.-X. Liu, Z. Xia, and T. Luo, "Ischaemic post-conditioning protects lung from ischaemia-reperfusion injury by up-regulation of haeme oxygenase-1," *Injury*, vol. 41, no. 5, pp. 510–516, 2010.

[24] B. Xu, X. Gao, J. Xu et al., "Ischemic postconditioning attenuates lung reperfusion injury and reduces systemic proinflammatory cytokine release via heme oxygenase 1," *Journal of Surgical Research*, vol. 166, no. 2, pp. e157–e164, 2011.

[25] Y.-L. Li, L. Gao, I. H. Zucker, and H. D. Schultz, "NADPH oxidase-derived superoxide anion mediates angiotensin II-enhanced carotid body chemoreceptor sensitivity in heart failure rabbits," *Cardiovascular Research*, vol. 75, no. 3, pp. 546–554, 2007.

[26] J.-M. Li and A. M. Shah, "Mechanism of endothelial cell NADPH oxidase activation by angiotensin II. Role of the $p47^{phox}$ subunit," *The Journal of Biological Chemistry*, vol. 278, no. 14, pp. 12094–12100, 2003.

[27] F. Wang, H.-M. Liu, M. G. Irwin et al., "Role of protein kinase C β2 activation in TNF-α-induced human vascular endothelial cell apoptosis," *Canadian Journal of Physiology and Pharmacology*, vol. 87, no. 3, pp. 221–229, 2009.

[28] S. Lei, Y. Liu, H. Liu, H. Yu, H. Wang, and Z. Xia, "Effects of N-acetylcysteine on nicotinamide dinucleotide phosphate oxidase activation and antioxidant status in heart, lung, liver and kidney in streptozotocin-induced diabetic rats," *Yonsei Medical Journal*, vol. 53, no. 2, pp. 294–303, 2012.

[29] H. Cai and D. G. Harrison, "Endothelial dysfunction in cardiovascular diseases: the role of oxidant stress," *Circulation Research*, vol. 87, no. 10, pp. 840–844, 2000.

[30] A. Halaris, "Inflammation, heart disease, and depression," *Current Psychiatry Reports*, vol. 15, no. 10, article 400, 2013.

[31] J.-M. Li, A. M. Mullen, S. Yun et al., "Essential role of the NADPH oxidase subunit $p47^{phox}$ in endothelial cell superoxide production in response to phorbol ester and tumor necrosis factor-α," *Circulation Research*, vol. 90, no. 2, pp. 143–150, 2002.

[32] T. J. Guzik, N. E. West, E. Black et al., "Vascular superoxide production by NAD(P)H oxidase: association with endothelial dysfunction and clinical risk factors," *Circulation Research*, vol. 86, no. 9, pp. E85–E90, 2000.

[33] S. Selemidis, G. J. Dusting, H. Peshavariya, B. K. Kemp-Harper, and G. R. Drummond, "Nitric oxide suppresses NADPH oxidase-dependent superoxide production by S-nitrosylation in human endothelial cells," *Cardiovascular Research*, vol. 75, no. 2, pp. 349–358, 2007.

[34] A. N. Lyle and K. K. Griendling, "Modulation of vascular smooth muscle signaling by reactive oxygen species," *Physiology*, vol. 21, no. 4, pp. 269–280, 2006.

[35] T. Inoguchi and H. Nawata, "NAD(P)H oxidase activation: a potential target mechanism for diabetic vascular complications, progressive β-cell dysfunction and metabolic syndrome," *Current Drug Targets*, vol. 6, no. 4, pp. 495–501, 2005.

[36] M. Kitada, D. Koya, T. Sugimoto et al., "Translocation of glomerular $p47^{phox}$ and $p67^{phox}$ by protein kinase C-β activation is required for oxidative stress in diabetic nephropathy," *Diabetes*, vol. 52, no. 10, pp. 2603–2614, 2003.

[37] L. V. Dekker, M. Leitges, G. Altschuler et al., "Protein kinase C-β contributes to NADPH oxidase activation in neutrophils," *Biochemical Journal*, vol. 347, pp. 285–289, 2000.

[38] T. Noguchi, M. Hünlich, P. C. Camp et al., "Thin filament-based modulation of contractile performance in human heart failure," *Circulation*, vol. 110, no. 8, pp. 982–987, 2004.

[39] M. Satoh, Y. Ishikawa, T. Itoh, Y. Minami, Y. Takahashi, and M. Nakamura, "The expression of TNF-α converting enzyme at the site of ruptured plaques in patients with acute myocardial infarction," *European Journal of Clinical Investigation*, vol. 38, no. 2, pp. 97–105, 2008.

[40] C. Nediani, E. Borchi, C. Giordano et al., "NADPH oxidase-dependent redox signaling in human heart failure: relationship between the left and right ventricle," *Journal of Molecular and Cellular Cardiology*, vol. 42, no. 4, pp. 826–834, 2007.

Hindawi Publishing Corporation
Oxidative Medicine and Cellular Longevity
Volume 2013, Article ID 432409, 9 pages
http://dx.doi.org/10.1155/2013/432409

Research Article

Early Growth Response Protein 1 Promotes Restenosis by Upregulating Intercellular Adhesion Molecule-1 in Vein Graft

Kui Zhang,[1] Jian Cao,[1] Ran Dong,[1] and Jie Du[2]

[1] *Cardiac Surgery, Beijing Institute of Heart, Lung and Blood Vessel Diseases, Beijing Anzhen Hospital Affiliated with Capital Medical University, Beijing 100029, China*
[2] *Vessel Biology, Beijing Institute of Heart, Lung and Blood Vessel Diseases, Beijing Anzhen Hospital Affiliated with Capital Medical University, Beijing 100029, China*

Correspondence should be addressed to Ran Dong; dongran6618@hotmail.com and Jie Du; jiedubj@126.com

Received 1 August 2013; Accepted 12 October 2013

Academic Editor: Qian Fan

Objectives. To verify the relationship between Egr-1 and vein graft restenosis and investigate the related mechanisms. *Methods*. Mouse vein graft models were established in Egr-1 knockout (KO) and wild-type (WT) mice. The vein grafts in the mice were taken for pathological examination and immunohistochemical analysis. The endothelial cells (ECs) were stimulated by using a computer-controlled cyclic stress unit. BrdU staining and PCR were used to detect ECs proliferation activity and Egr-1 and ICAM-1 mRNA expression, respectively. Western-blot analysis was also used to detect expression of Egr-1 and intercellular adhesion molecule-1 (ICAM-1) proteins. *Results*. The lumens of vein grafts in Egr-1 KO mice were wider than in WT mice. ECs proliferation after mechanical stretch stimulation was suppressed by Egr-1 knockout ($P < 0.05$). Both in vein grafts and ECs from WT mice after mechanical stretch stimulation, mRNA expression and protein of Egr-1 and ICAM-1 showed increases ($P < 0.05$). However, ICAM-1 expression was significantly suppressed in ECs from Egr-1 knockout mice ($P < 0.05$). *Conclusions*. Egr-1 may promote ECs proliferation and result in vein graft restenosis by upregulating the expression of ICAM-1. As a key factor of vein graft restenosis, it could be a target for the prevention of restenosis after CABG surgery.

1. Introduction

Coronary artery bypass graft (CABG) is one of the most effective therapies for coronary artery diseases (CAD). However, some studies revealed that about 10% of vein grafts occluded within one month after CABG and that only 50% of vein grafts remained unobstructed 10 years after CABG [1]. Thus, how to improve the efficiency of vein grafts over time is a challenge in cardiac surgery. Some of the mechanisms involved in the occlusion of vein grafts have been identified.

Normal vascular endothelial cells (ECs) play a central role in regulating intimal growth [2, 3]. After CABG, vein grafts walls sustain a blood pressure that is much higher than the usual venous pressure, and the walls of the vein graft are often injured by pulsatile stretching [4–6]. These stresses lead to endothelial dysfunction, which is the initial factor inducing the proliferative thickening of the intima [7]. These injuries induce changes in ECs proliferation, cytokines secretion, platelet aggregation, and leukocyte adherence, which are involved in the onset of acute thrombosis [7, 8]. This impairment in the function of ECs then activates vascular smooth muscle cells (VSMCs) migration to the intima, where they transform into a proliferative phenotype. Synthesis and accumulation of an extracellular matrix by these activated SMCs form a matrix for atherosclerosis development [9, 10]. Finally, activated ECs and SMCs produce a number of attracting chemokines, recruiting and retaining monocytes into the endothelium and the extracellular matrix, where they transform into macrophages participating to atherosclerotic plaque development [9, 10]. Together, these three mechanisms are involved in the proliferative thickening of the intima and, ultimately, in CABG failure [11, 12].

Recent studies suggested that three families of adhesion factors are involved in restenosis: (1) the immunoglobulin

superfamily (including the intercellular adhesion molecule-1 (ICAM-1) and the vascular cell adhesion molecule-1 (VCAM-1), [13–15]) (2) the integrin family (including the macrophage 1 antigen (MAC-1) and the lymphocyte function associated antigen-1 (LFA-1)) [16, 17], (3) the selectin family (including E-selectin) [18]. Increases in ICAM-1 expression are characteristic of early endothelial dysfunction induced by blood flow mechanical shear stress [19, 20]. ICAM-1 and VCAM-1 participate to lymphocyte attraction and retention, in VSMCs migration and proliferation and in formation of the atherosclerotic plaque [21, 22]. sICAM-1 levels are inversely correlated with endothelial dysfunction [23]. Recently, some studies suggested that sICAM-1 could be used as a biomarker predicting secondary cardiovascular disease in patients with CAD [24, 25].

Early growth response protein 1 (Egr-1) is a member of the immediate early gene family and is also an important transcription factor. Recent studies show that Egr-1 is involved in the regulation of intracellular signaling and multiple genes including growth factor, signal transduction genes, transcription factor, and oncogenes. Other studies also revealed that Egr-1 plays an important role in cell growth, development, differentiation and wound healing [26–28]. Our preliminary study showed that Egr-1 is closely related with restenosis, and the degree of vein graft stenosis in Egr-1 knockout (KO) mice was significantly lower than that in wild-type (WT) mice, indicating that Egr-1 could promote vein graft stenosis. However, the mechanisms involved in this effect of Egr-1 on vein graft stenosis were unclear. To our knowledge, no such information has been reported. Therefore, this study further verified the effect of Egr-1 on vein graft restenosis and investigated the related mechanisms. We hoped that this study would provide valuable information for prevention and treatment of vein graft restenosis.

2. Materials and Methods

2.1. Animals. We used male Egr-1 KO mice as described [29] and WT C57BL/6J mice (Vital River Company, Beijing, China), aged between 8 and 12 weeks. All animals were managed according to the guidelines of Beijing An Zhen Hospital, Capital Medical University. Experimental protocols were approved by Cardiac Surgery of Beijing An Zhen Hospital, Capital Medical University. Before experiments, mice were kept for one week at 24°C, on a 12-hour light/dark cycle and received a normal diet. In the experimental group, Egr-1 KO mice were used as donors, and littermate Egr-1 KO mice were used as recipients. In the control group, WT C57BL/6J mice were used as donors, and littermate WT C57BL/6J mice were used as recipients. Egr-1 KO mice originated from a C57BL/6J × 129 background and were backcrossed with the C57BL/6J strain for at least 10 generations. Animal experiments were approved by the Beijing Institute of Heart, Lung and Blood Vessel Diseases.

2.2. Mouse Vein Graft Model. We used a vein graft model as previously described by Zou et al. [30]. In brief, mice were anesthetized using an intraperitoneal injection of 1% pentobarbital sodium. The right common carotid artery was dissected from surrounding tissue as far (distally and proximally) as possible. We ligatured the right common carotid artery at midpoint with sutures and divided it. Distal and proximal segments were combined inside a cuff, and we controlled the arterial inflow and outflow using clamps placed at the cuffs' handles. Sutures were removed; distal and proximal arteries were everted over the cuffs' tubular body and fixed using sutures. Consequently, a sleeved vein segment (inferior vena cava from donor mice) was grafted over the cuffs and secured into position with sutures. Finally, incision was closed using 3-0 Dacron (Hangzhou AiPu Medical Products Co., Zhejiang, China).

We tested the patency of vein graft after the operation. If the grafted vessel pulsed vigorously and there was no bleeding, we considered that the surgery was a success. If there was no pulsation within a few minutes of blood flow restoration or if clot formation was suspected, the surgery was considered a surgical failure [30]. We harvested the vein grafts at 3 h, 1 day, 1 week, 2 weeks, and 4 weeks after surgery.

Mice in the sham surgery group (sham) were anesthetized and their neck was incised, but no surgery was performed on the carotid arteries.

2.3. Mechanical Stretch Stimulation. ECs isolated from the inferior vena cava endothelial cells (IVCECs) and vena cava of Egr-1 KO and WT mice were kept in Dulbecco's modified Eagle medium (DMEM) with 10% fetal bovine serum (FBS) at 37°C with 95% air and 5% CO_2. We then plated ECs on silicone elastomer-bottomed and collagen-coated plates (Flexcell, McKeesport, PA, USA). A computer-controlled cyclic stress unit (Flexcell, McKeesport, PA, USA) was used to subject ECs to mechanical stretch (cyclic deformation was 60 cycles/min, elongation was 15%) [31, 32].

2.4. Measure of ECs Proliferation. We performed BrdU immunostaining according to the manufacturer's protocol (Roche Molecular Systems, Pleasanton, CA, USA). In brief, ECs were cultured for 12 hours in medium containing 0.4% FBS to synchronize them, then cultured in DMEM with 10% FBS, and stimulated with mechanical stretch for 24 hours. In the last 4 hours of cell culture at 37°C, BrdU was added. After being washed three times with PBS, cells were fixed using 4% paraformaldehyde for 10 min, washed three times with PBS, exposed to 0.3% Triton X-100 for 5 min, and washed three times with PBS again. Cells were treated with 2 M HCl at 37°C for 30 min, then with 0.1 M sodium tetraborate for 10 min, and washed three times with PBS. Cells were incubated in 10% fetal calf serum for 30 min before being incubated overnight at 4°C with antimouse BrdU monoclonal antibody. Finally, the cells were treated with fluorescence-labeled goat antimouse IgG at room temperature for 1 h. PBS was used as a negative control. DAPI was used for staining nuclei specifically. The mean percentage of cells positive for BrdU was determined in 4 or 5 different fields using a Leica DMI4000B fluorescence microscope (Leica, Wetzlar, Germany) under 100× magnification. Count was repeated 4 times.

2.5. Real-Time RT-PCR. Total RNA was extracted from ECs stimulated with mechanical stretch, using Trizol reagent (Sigma, Saint Louis, MO, USA). RNA purity was determined using absorbance at 260 and 280 nm (A260/280). After assessing RNA concentration, total RNA was reverse-transcribed into complementary DNA (cDNAs) using a first strand cDNA synthesis kit (Fermentas Life Sciences). For mouse Egr-1 amplification, primers were forward, 5′-CAG CAG CCT TCG CTA ACC-3′, and reverse, 5′-CCA CTG GGC AAG CGT AA-3′. For mouse ICAM-1 amplification, primers were forward, 5′-AGG TGT GAT ATC CGG TAG AT-3′ and reverse, 5′-CCT TCT AAG TGG TTG GAA CA-3′. were forward, 5′-TGA CTT CAA CAG CGA CAC CCA-3′, Primers for mouse GAPDH and reverse, 5′-CAC CCT GTT GCT GTA GCC AAA-3′. All reactions involved initial denaturation at 95°C for 15 s, followed by 45 cycles of 95°C for 5 s and 60°C for 30 s. Specific mRNA quantification was performed by real-time PCR using SYBR Premix Ex Taq II (TaKaRa Bio, Dalian, China) in a TP800 real-time PCR System (TaKaRa Bio, Dalian, China), according to the guidelines provided by the manufacturer. Results were analyzed using the comparative threshold cycle, as previously described [33].

2.6. Western-Blot Analysis. ECs from the vena cava of Egr-1 KO and WT mice were stimulated with mechanical stretch, then lysed in RIPA buffer (50 mmol/L Tris, 150 mmol/L NaCl, 5 mmol/L EDTA, 1% NP-40, 1% sodium deoxycholate, 0.1% SDS, 1 mmol/L Phenylmethanesulfonyl fluoride (PMSF), 10 ug/mL aprotinin, 1 mmol/L $NaVO_4$), and centrifuged 15 min at 4°C (12000 rpm). After protein concentration was measured using the BCA protein assay kit (HyClone-Pierce, Utah, CA, USA), equal amounts of protein (40 μg) were separated on 8% SDS-polyacrylamide gels and transferred onto PVDF membranes (Millipore, Massachusetts, CA, USA). The nonspecific sites on each blot were blocked with 5% nonfat milk powder diluted in TBS with 0.05% Tween 20 (TBST). Membranes were incubated overnight with primary antibodies against IL-1, IL-4, TGF-β, and TNF-α (Abcam, Cambridge, UK) at 4°C. After washing by TBST, proteins were revealed with HRP-labeled IgG (Pierce antibodies, Thermo Fisher Scientific, Waltham, MA, USA) at room temperature for 1 hour. Membranes were developed using the ECL system (Amersham) and analyzed using the Biological electrophoresis image analysis system (Furi Science & Technology Company, Shanghai, China).

2.7. Immunohistochemistry. Immunohistochemistry was performed on 4 μm thick formalin-fixed, paraffin-embedded tissue sections. Deparaffinized sections were treated with 3% hydrogen peroxide for 30 min at 30°C and boiled in 1% citric acid solution for 20 min after washing in PBS. After blocking with 10% sheep serum (Vector Laboratories, Burlingame, CA, USA) for 30 min, sections were incubated with the primary antibody against Egr-1 (Epitomic, San Francisco, CA, USA) and ICAM-1 (Abcam, Cambridge, UK) overnight. After washing with PBS, sections were incubated with the secondary antibody (goat antirabbit, Vector Laboratories, Burlingame, CA, USA) for 40 min at 30°C, and finally with avidin-biotin complex (Vector Laboratories, Burlingame, CA, USA) for 10 min. Immunogenicity was visualized using 3,3′-diaminobenzidine (Vector Laboratory, Burlingame, CA, USA) for 2 min. Sections were counterstained with hematoxylin, dehydrated in alcohol, and cleared with Histoclear. For negative control, the same protocol was used with antigen dilution reagent instead of the primary antibodies. Stained slides were viewed with light microscope, images were captured, and the percentages of positive cells in vein grafts were analyzed using the NIS Elements BR software (Nikon Instruments Inc., Japan).

2.8. Statistical Analysis. Results are presented as mean ± SEM. Comparisons between groups were analyzed by one-way ANOVA followed by the Bonferroni/Dunn post hoc analysis. All statistical analyses were performed using SPSS 17.0 (SPSS Inc., Chicago, IL, USA). A P value <0.05 was considered statistically significant.

3. Results

3.1. Egr-1 KO Decreases Stenosis in Vein Grafts. To demonstrate the pathophysiological importance of mechanical stretch-activated Egr-1, we construct mouse vein graft model in Egr-1 KO mice and WT mice. We harvested the vein grafts and analyzed them by HE staining at 4 weeks after surgery. As shown in Figure 1, the lumens of vein grafts in WT and Egr-1 KO mice were both narrower, compared with the lumen of inferior vena cava in WT mice (71.85 ± 8.36 μm versus 205.25 ± 13.12 μm, 138.73 ± 11.24 μm versus 205.25 ± 13.12 μm; $P < 0.05$). However, the lumen of vein grafts in Egr-1 KO mice was wider almost two fold, compared with that in WT mice (138.73 ± 11.24 μm versus 71.85 ± 8.36 μm; $P < 0.05$).

3.2. Egr-1 KO Inhibits ECs Proliferation Induced by Mechanical Stretch Stimulation. To study the link between Egr-1 KO and mechanical stretch-induced ECs proliferation, we isolated ECs from veins of WT and Egr-1 KO mice. As shown in Figure 2, after mechanical stretch stimulation for 24 h, BrdU-positive cells in WT/ST ECs were increased by 7.6-fold compared with WT. However, the proliferation was suppressed in Egr-1 KO cells (50.9 ± 7.9% of WT/ST; $P < 0.05$).

3.3. Mechanical Stretch Increases Egr-1 Expression. Vein grafts were harvested to measure Egr-1 mRNA levels. Three-h after being placed into carotid artery in WT mice, ECs isolated from veins showed significantly increased Egr-1 mRNA levels, compared with that in the sham surgery group (5.7 ± 1.6 fold; $P < 0.05$) (Figure 3(a)). The time course of Egr-1 mRNA expression in ECs from WT mice with mechanical stretch stimulation was assessed. As early as 10 min after being stimulated, Egr-1 mRNA levels increased and reached a peak at 60 min (5.9 ± 0.6 fold versus 0 min; $P < 0.05$). Egr-1 mRNA returned to baseline after 90 min (Figure 4(b)). Egr-1 protein reached a peak at 90 min (5.5±0.5 fold versus 0 min; $P < 0.05$) (Figure 4(c)).

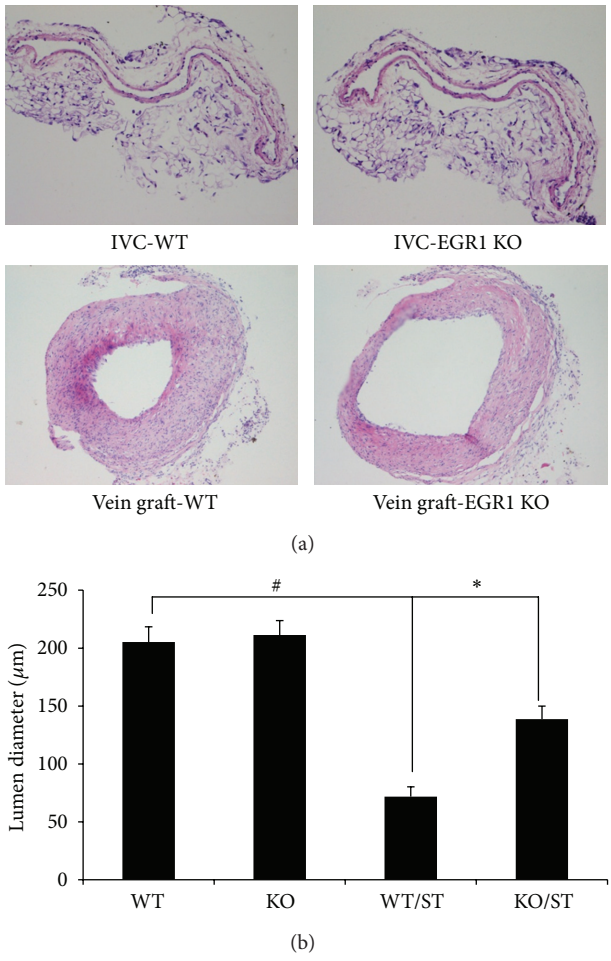

Figure 1: Egr-1 KO decreases lumen stenosis in vein grafts at 4 weeks after surgery. (a) Vein grafts from Egr-1 KO mice and WT mice were stained with hematoxylin and eosin (×100). (b) Quantitative analysis of lumen of vein grafts stenosis using NIS Elements BR software (NIKON, Japan). Data are expressed as mean ± SEM. $^{*}P < 0.05$ versus WT/ST group; $^{\#}P < 0.05$ versus WT group. WT: inferior vena cava (IVC) in wild-type mice; WT/ST: vein graft from WT mice; Egr-1 KO: IVC in Egr-1 knockout mice; Egr-1 KO/ST: vein graft from Egr-1 knockout mice.

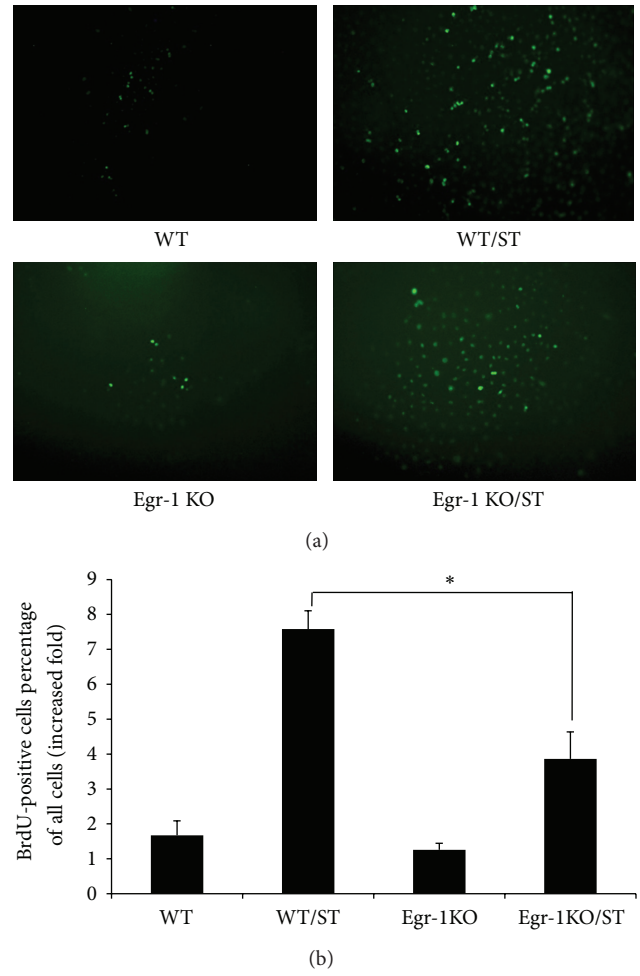

Figure 2: Egr-1 KO inhibits ECs proliferation induced by mechanical stretch stimulation. ECs were isolated from WT (above) and Egr-1 KO (below) mice. The ECs were submitted or not to mechanical stretch for 24 h, and BrdU staining was performed 24 h later. Cells were counted in 4 or 5 different views (×100) under fluorescence microscope and repeated 4 times. Data are expressed as mean ± SEM. $^{*}P < 0.05$ versus WT/ST group. WT: wild-type mice; WT/ST: venous ECs from WT mice stimulated with mechanical stretch; Egr-1 KO: Egr-1 knockout mice; Egr-1 KO/ST: venous ECs from Egr-1 knockout mice stimulated with mechanical stretch.

3.4. Egr-1 KO Suppressed ICAM-1 Expression. ICAM-1 plays an important role in inflammation after vascular injury [13]. We studied the role of Egr-1 in ICAM-1 expression. Venous ECs from WT and Egr-1 KO mice were isolated and stimulated with mechanical stretch from 0 to 3 h. After 3 h, mechanical stretch increased ICAM-1 mRNA expression in WT ECs and was significantly suppressed in ECs from Egr-1 KO mice (68.2 ± 8.2% of WT/ST; $P < 0.05$) (Figure 4(a)). ICAM-1 protein levels in ECs from Egr-1 KO mice were significantly reduced, compared with that in ECs from WT mice, after mechanical stretch stimulation for 24 h (54.3 ± 9.1% of WT/ST; $P < 0.05$) (Figure 4(b)). Subsequently, we explored whether Egr-1 regulate ICAM-1 in mouse vein graft model. We harvested vein grafts from WT and Egr-1 KO mice 3 h after surgery. In vein grafts from WT mice, ICAM-1 mRNA was significantly increased, compared to WT mice in the sham surgery group (2.9 ± 0.9 fold; $P < 0.05$). Egr-1 KO significantly decreased ICAM-1 expression (61.0 ± 10.3% of vein grafts from WT mice 3 h after surgery; $P < 0.05$) (Figure 4(c)). Immunohistochemistry showed that the percentages of Egr-1- and ICAM-1- positive cells both reduced in vein grafts from Egr-1 KO mice at 4 weeks after surgery, compared to that from WT mice (4.3±1.0% versus 59.4±7.2%, 20.7 ± 1.7% versus 66.7 ± 4.2%; $P < 0.05$) (Figure 5).

4. Discussion

In this study, we found that the expression of Egr-1 in endothelial cells stimulated by mechanical stretch was significantly increased and the ECs proliferation activity was significantly improved. We also found that Egr-1 mRNA expression

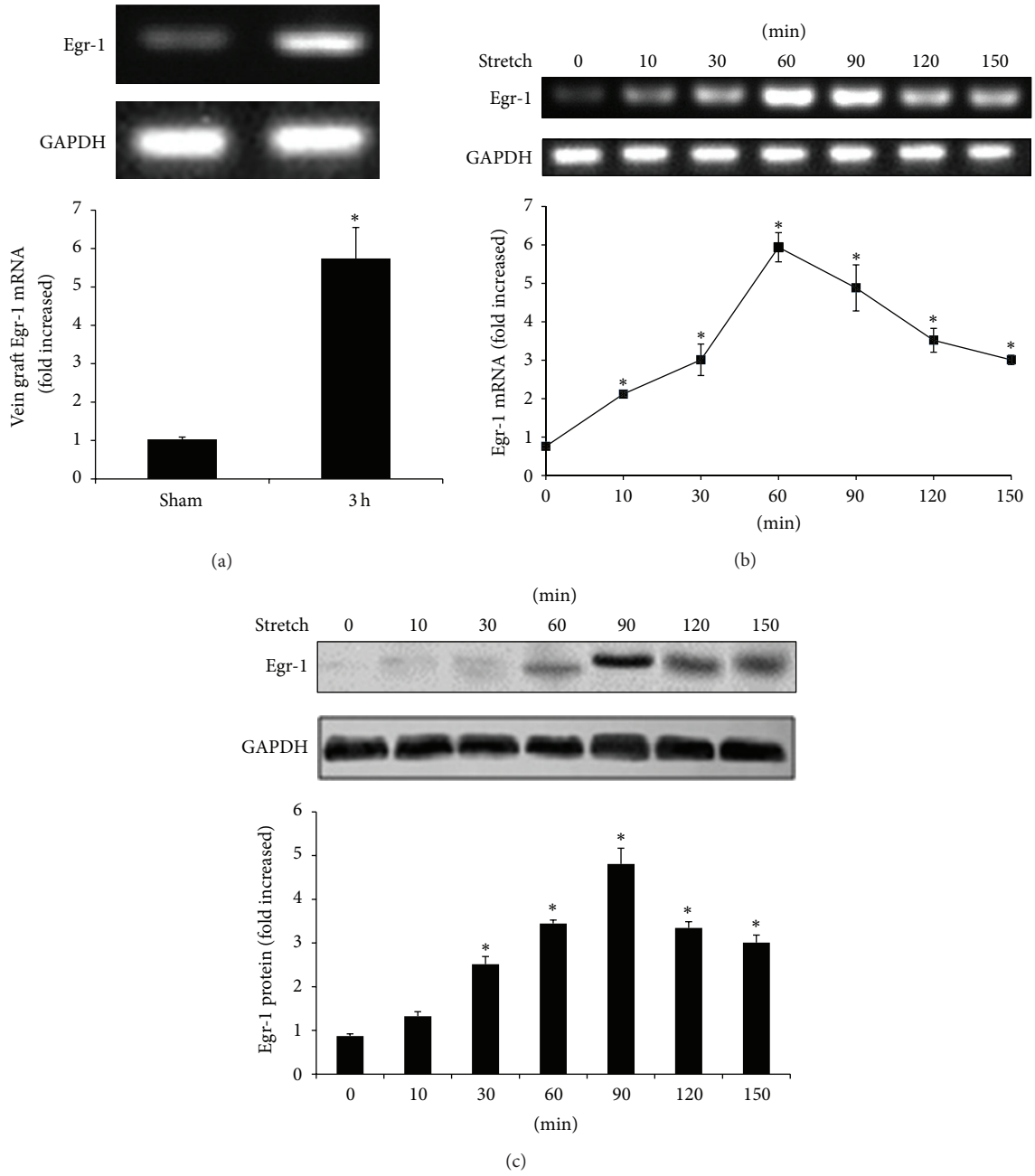

Figure 3: Mechanical stretch increased Egr-1 expression in wild-type (WT) mice. (a) Egr-1 mRNA levels in endothelial cells (ECs) increased 3 h after grafting the vein in WT mice ($n = 5$). $^*P < 0.05$ versus sham group. Time course of Egr-1 mRNA (b) and protein (c) expression in ECs from WT mice after mechanical stretch (60 cycles/min and 15% elongation) for 0 to 150 min ($n = 5$). GAPDH was used as an internal control. Data are expressed as mean ± SEM. $^*P < 0.05$ versus 0 min.

changed over time; it increased after mechanical stretch stimulation for ten minutes, reached a peak after stimulation for 60 min, and then gradually declined. In the early stage after CABG surgery, the vein graft was under high arterial blood pressure; then the sudden hemodynamic change and mechanical stretch stimulation could damage endothelial cells. The increase of Egr-1 mRNA expression after stimulation for ten minutes indicated that Egr-1 was expressed in endothelial cells immediately after the cells were damaged, which subsequently induced a series of pathophysiological changes. Egr-1 belongs to the immediate early gene rather than the long-term gene. Apparently, its expression was not sustained as opposed to long-term gene expression. Hence, Egr-1 mRNA expression declined after reaching a peak. It was reported that the duration of Egr-1 expression varied with different stimulations [34–36]. When Egr-1 expression

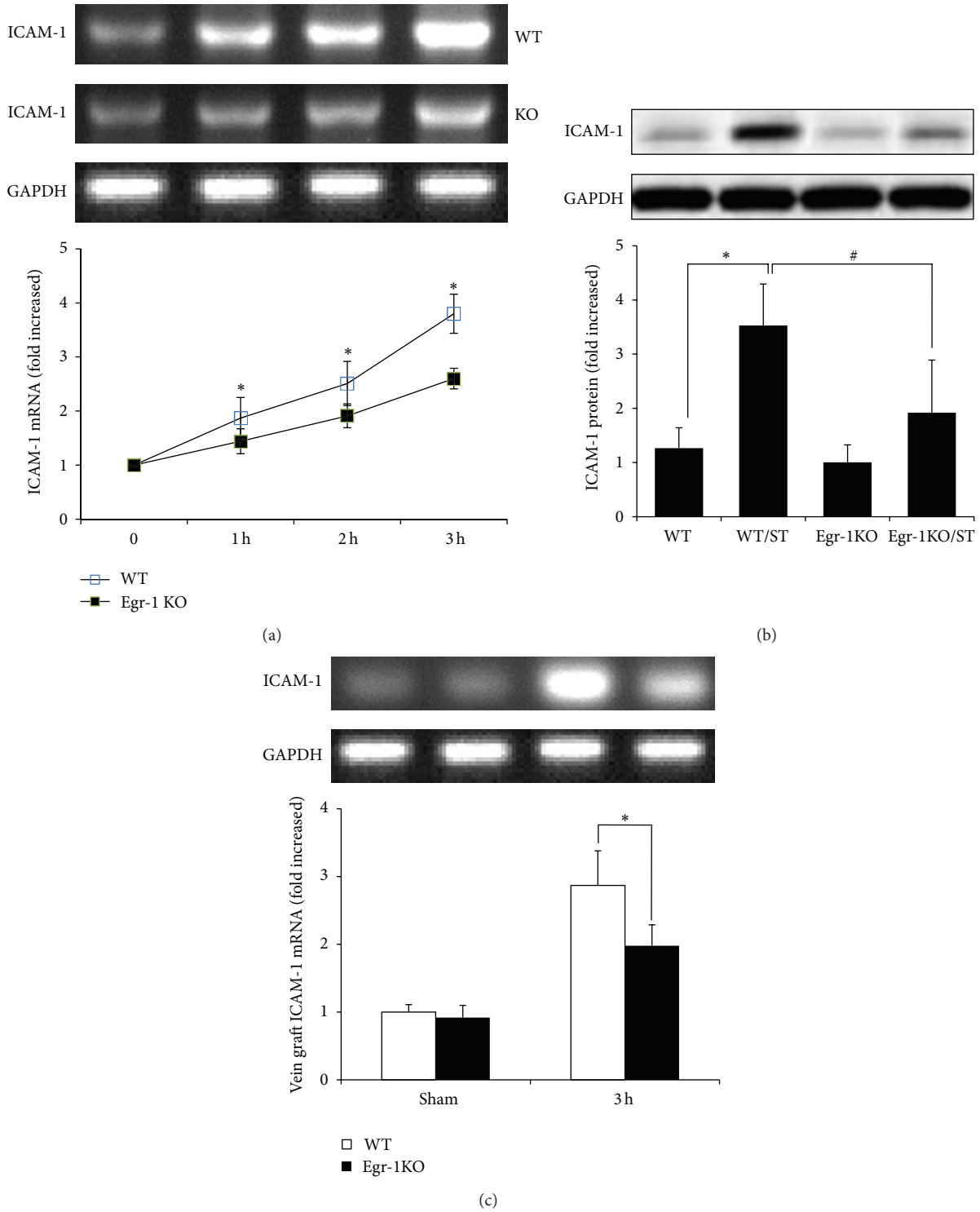

Figure 4: Egr-1 knockout (KO) decreased ICAM-1 expression. (a) Venous ECs from WT and Egr-1 KO mice were isolated and stimulated with mechanical stretch from 0 to 3 h ($n = 5$). ICAM-1 mRNA expression was determined by real-time RT-PCR. (b) Egr-1 KO decreased ICAM-1 protein levels after mechanical stretch stimulation for 24 h ($n = 5$). Data are expressed as mean ± SEM. $^{*}P < 0.05$ versus WT group; $^{\#}P < 0.05$ versus WT/ST group. (c) Egr-1 KO decreased ICAM-1 mRNA expression in mouse vein graft model ($n = 5$). Data are expressed as mean ± SEM. $^{*}P < 0.05$ versus WT group. WT: wild-type mice; WT/ST: venous ECs from WT mice stimulated with mechanical stretch; Egr-1 KO: Egr-1 knockout mice; Egr-1 KO/ST: venous ECs from Egr-1 knockout mice stimulated with mechanical stretch.

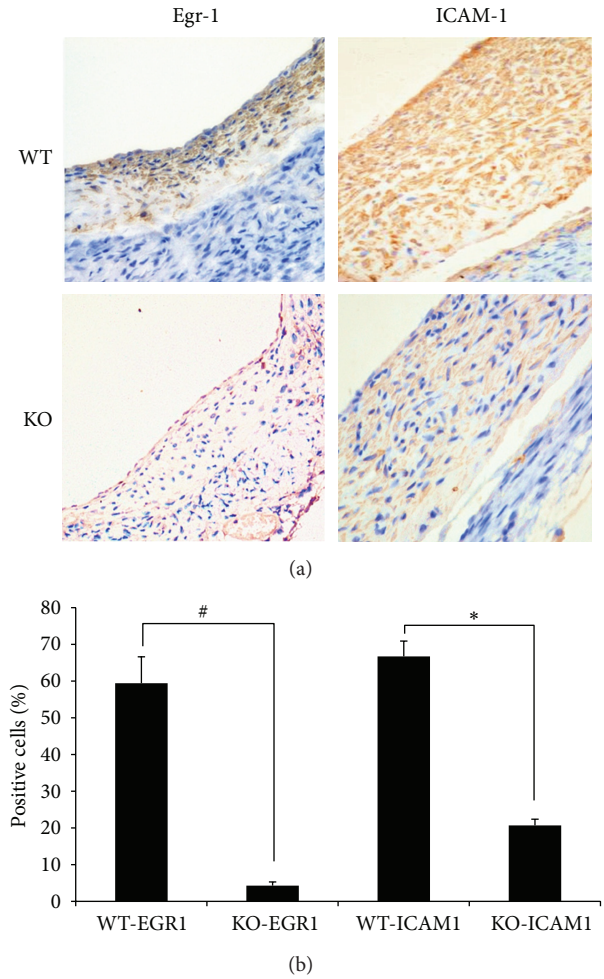

Figure 5: Immunohistochemistry of Egr-1 and ICAM-1 was performed in vein grafts from Egr-1 KO mice and WT mice at 4 weeks after surgery. (a) Vein grafts from Egr-1 KO mice and WT mice were stained with Egr-1 and ICAM-1 monoclonal antibody (×200). Brown colour indicates positive staining for all primary antibodies. (b) Quantitative analysis of the percentages of Egr-1 or ICAM-1 positive cells in vein grafts using NIS Elements BR software (NIKON, Japan). Data are expressed as mean ± SEM. $^{\#}P < 0.05$ WT-EGR1 versus KO-EGR1 group; $^{*}P < 0.05$ WT-ICAM1 versus KO-ICAM1 group. WT-EGR1: vein grafts from WT mice were stained with Egr-1 monoclonal antibody; KO-EGR1: vein grafts from Egr-1 KO mice were stained with Egr-1 monoclonal antibody; WT-ICAM1: Vein grafts from WT mice were stained with ICAM-1 monoclonal antibody; KO-ICAM1: Vein grafts from Egr-1 KO mice were stained with ICAM-1 monoclonal antibody.

was upregulated, it could be regulated by negative feedback regulators such as c-fos [37], phosphatase inhibitors [38], and free radical scavengers [39].

After mechanical stretch stimulation, the expression of Egr-1 and ICAM-1 in ECs cells of WT mice was significantly increased, whereas expression of ICAM-1 in ECs cells or vein graft of Egr-1 KO mice was significantly inhibited in this study. Meanwhile, the intimal hyperplasia was greatly reduced in the vein graft of Egr-1 KO mice. It suggested that Egr-1 expression could upregulate ICAM-1 expression, increase inflammatory cell adhesion, aggravate vascular inflammation, and result in vein graft restenosis. However, Egr-1 knockout did not completely inhibit inner cortex thickening and intimal hyperplasia indicating that other factors may be involved in the process of intimal hyperplasia. It was reported that mechanical strain can enhance NF-κB activity and NF-κB can increase intimal hyperplasia and result in restenosis by regulating IGF-1R transcription [29].

In addition to mechanical strain stimulation, vein graft was also subjected to oxidative stress injury. Oxidative stress-induced apoptosis was a key to a variety of cardiovascular diseases and it was found throughout intimal hyperplasia after vascular injury was induced by a variety of damaging factors [40]. After CABG surgery, the vein graft, especially the anastomosis, was infiltrated by macrophages and covered with lipid deposition [41]. The macrophages activated by inflammation could produce excessive reactive oxygen species (ROS), and increase interleukin-8 (IL-8) and monocyte chemotactic protein-1 (MCP-1), which aggravated inflammation again [42]. The ischemia-reperfusion reaction during surgery not only produced excessive ROS, resulting in oxidative damage for the vascular wall cells, but also upregulated Egr-1 expression directly [43]. ROS could upregulate Egr-1 expression by activating families of protein kinase K isoenzymes and the mitogen-activated protein kinases/extracellular signal-regulated kinases (MEK/ERK) pathway [44], and increase lipid deposition in the blood vessel wall. The deposited low-density lipoprotein (LDL) in the ROS could form oxidized LDL (ox-LDL) protein, stimulate VSMC proliferation by activating caspase family proteins and mediating the NF-κB signaling pathway, and eventually lead to intimal hyperplasia and stenosis [45].

In summary, Egr-1 played an important role in vein graft restenosis. It could lead to vein graft restenosis probably by upregulating ICAM-1, aggravating vascular inflammation, and promoting endothelial cell proliferation. As a key factor of vein graft restenosis, Egr-1 may be used for an effective target for gene prevention and treatment.

5. Conclusion

Our results suggest that Egr-1 plays a role in restenosis by upregulating ICAM-1 in ECs in vein graft, which may provide new clues for the prevention of vein grafts restenosis in CABG, leading to new strategies to improve patients' prognosis after CABG. However, the specific mechanisms still need to be elucidated, as well as the exact relations between ECs and SMCs during restenosis.

Conflict of Interests

The authors declare that they have no conflict of interests.

Acknowledgment

This study was supported by the National Natural Science Foundation of China (81070202).

References

[1] P. Parang and R. Arora, "Coronary vein graft disease: pathogenesis and prevention," *Canadian Journal of Cardiology*, vol. 25, no. 2, pp. e57–e62, 2009.

[2] E. Allaire and A. W. Clowes, "Endothelial cell injury in cardiovascular surgery: the intimal hyperplastic response," *Annals of Thoracic Surgery*, vol. 63, no. 2, pp. 582–591, 1997.

[3] E. D. Verrier and E. M. Boyle Jr., "Endothelial cell injury in cardiovascular surgery," *Annals of Thoracic Surgery*, vol. 62, no. 3, pp. 915–922, 1996.

[4] R. Stigler, C. Steger, T. Schachner et al., "The impact of distension pressure on acute endothelial cell loss and neointimal proliferation in saphenous vein grafts," *European Journal Cardio-Thoracic Surgery*, vol. 42, no. 4, pp. e74–e79, 2012.

[5] K. Hinokiyama, G. Valen, S. Tokuno, J. B. Vedin, and J. Vaage, "Vein graft harvesting induces inflammation and impairs vessel reactivity," *Annals of Thoracic Surgery*, vol. 82, no. 4, pp. 1458–1464, 2006.

[6] A. A. Soyombo, G. D. Angelini, and A. C. Newby, "Neointima formation is promoted by surgical preparation and inhibited by cyclic nucleotides in human saphenous vein organ cultures," *Journal of Thoracic and Cardiovascular Surgery*, vol. 109, no. 1, pp. 2–12, 1995.

[7] F. D. Li, K. W. Sexton, K. M. Hocking et al., "Intimal thickness associated with endothelial dysfunction in human vein grafts," *Journal of Surgical Research*, vol. 180, no. 1, pp. e55–e62, 2013.

[8] J. Roquer, T. Segura, J. Serena, and J. Castillo, "Endothelial dysfunction, vascular disease and stroke: the ARTICO study," *Cerebrovascular Diseases*, vol. 27, supplement 1, pp. 25–37, 2009.

[9] A. K. Mitra, D. M. Gangahar, and D. K. Agrawal, "Cellular, molecular and immunological mechanisms in the pathophysiology of vein graft intimal hyperplasia," *Immunology and Cell Biology*, vol. 84, no. 2, pp. 115–124, 2006.

[10] J. Bonatti, A. Oberhuber, T. Schachner et al., "Neointimal hyperplasia in coronary vein grafts: pathophysiology and prevention of a significant clinical problem," *Heart Surgery Forum*, vol. 7, no. 1, pp. 72–87, 2004.

[11] C. Lawson and S. Wolf, "ICAM-1 signaling in endothelial cells," *Pharmacological Reports*, vol. 61, no. 1, pp. 22–32, 2009.

[12] E. Corrado, M. Rizzo, G. Coppola, I. Muratori, M. Carella, and S. Novo, "Endothelial dysfunction and carotid lesions are strong predictors of clinical events in patients with early stages of atherosclerosis: a 24-month follow-up study," *Coronary Artery Disease*, vol. 19, no. 3, pp. 139–144, 2008.

[13] C. V. Carman and T. A. Springer, "A transmigratory cup in leukocyte diapedesis both through individual vascular endothelial cells and between them," *Journal of Cell Biology*, vol. 167, no. 2, pp. 377–388, 2004.

[14] S. Yoshimura, Y. Kaku, J. Kokuzawa, K. Hayashi, and N. Sakai, "Strategy for prevention of restenosis after PTA. Clinical and basic approaches," *Interventional Neuroradiology*, vol. 10, no. 1, pp. 63–66, 2004.

[15] E. F. Plow and S. E. D'Souza, "A role for intercellular adhesion molecule-1 in restenosis," *Circulation*, vol. 95, no. 6, pp. 1355–1356, 1997.

[16] G. Li, J. M. Sanders, M. H. Bevard et al., "CD40 ligand promotes Mac-1 expression, leukocyte recruitment, and neointima formation after vascular injury," *American Journal of Pathology*, vol. 172, no. 4, pp. 1141–1152, 2008.

[17] K. Rahimi, H. K. Maerz, R. J. Zotz, and A. Tárnok, "Preprocedural expression of Mac-1 and LFA-1 on leukocytes for orediction of late Restenosis and their possible correlation with advanced coronary artery disease," *Cytometry Part B*, vol. 53, no. 1, pp. 63–69, 2003.

[18] G. S. Sainani and V. G. Maru, "The endothelial leukocyte adhesion molecule. Role in coronary artery disease," *Acta Cardiologica*, vol. 60, no. 5, pp. 501–507, 2005.

[19] J.-J. Chiu, P.-L. Lee, S.-F. Chang et al., "Shear stress regulates gene expression in vascular endothelial cells in response to tumor necrosis factor-α: a study of the transcription profile with complementary DNA microarray," *Journal of Biomedical Science*, vol. 12, no. 3, pp. 481–502, 2005.

[20] P. L. Walpola, A. I. Gotlieb, M. I. Cybulsky, and B. L. Langille, "Erratum: expression of ICAM-1 and VCAM-1 and monocyte adherence in arteries exposed to altered shear stress," *Arteriosclerosis, Thrombosis, and Vascular Biology*, vol. 15, no. 1, pp. 2–10, 1995.

[21] K. Kitagawa, M. Matsumoto, T. Sasaki et al., "Involvement of ICAM-1 in the progression of atherosclerosis in APOE-knockout mice," *Atherosclerosis*, vol. 160, no. 2, pp. 305–310, 2002.

[22] Y. Nakashima, E. W. Raines, A. S. Plump, J. L. Breslow, and R. Ross, "Upregulation of VCAM-1 and ICAM-1 at atherosclerosis-prone sites on the endothelium in the apoE-deficient mouse," *Arteriosclerosis, Thrombosis, and Vascular Biology*, vol. 18, no. 5, pp. 842–851, 1998.

[23] O. Eschen, J. H. Christensen, C. Dethlefsen, and E. B. Schmidt, "Cellular adhesion molecules in healthy subjects: short term variations and relations to flow mediated dilation," *Biomarker Insights*, vol. 2008, no. 3, pp. 57–62, 2008.

[24] L. Badimon, J. C. Romero, J. Cubedo, and M. Borrell-Pagès, "Circulating biomarkers," *Heart Surgery Forum*, vol. 130, supplement 1, pp. S12–S15, 2012.

[25] N. M. Mordwinkin, J. G. Ouzounian, L. Yedigarova, M. N. Montoro, S. G. Louie, and K. E. Rodgers, "Alteration of endothelial function markers in women with gestational diabetes and their fetuses," *Journal of Maternal-Fetal and Neonatal Medicine*, vol. 26, no. 5, pp. 507–512, 2013.

[26] L. M. Khachigian, "Early growth response-1 in cardiovascular pathobiology," *Circulation Research*, vol. 98, no. 2, pp. 186–191, 2006.

[27] F. Blaschke, D. Bruemmer, and R. E. Law, "Egr-1 is a major vascular pathogenic transcription factor in atherosclerosis and restenosis," *Reviews in Endocrine and Metabolic Disorders*, vol. 5, no. 3, pp. 249–254, 2004.

[28] T. A. McCaffrey, C. Fu, B. Du et al., "High-level expression of Egr-1 and Egr-1-inducible genes in mouse and human atherosclerosis," *Journal of Clinical Investigation*, vol. 105, no. 5, pp. 653–662, 2000.

[29] X. Wu, J. Cheng, P. Li et al., "Mechano-sensitive transcriptional factor egr-1 regulates insulin-like growth factor-1 receptor expression and contributes to neointima formation in vein grafts," *Arteriosclerosis, Thrombosis, and Vascular Biology*, vol. 30, no. 3, pp. 471–476, 2010.

[30] Y. Zou, H. Dietrich, Y. Hu, B. Metzler, G. Wick, and Q. Xu, "Mouse model of venous bypass graft arteriosclerosis," *American Journal of Pathology*, vol. 153, no. 4, pp. 1301–1310, 1998.

[31] J. Cheng, Y. Wang, Y. Ma et al., "The mechanical stress-activated serum-, glucocorticoid-regulated kinase 1 contributes to neointima formation in vein grafts," *Circulation Research*, vol. 107, no. 10, pp. 1265–1274, 2010.

[32] W. Zheng, L. P. Christensen, and R. J. Tomanek, "Stretch induces upregulation of key tyrosine kinase receptors in microvascular

endothelial cells," *American Journal of Physiology—Heart and Circulatory Physiology*, vol. 287, no. 6, pp. H2739–H2745, 2004.

[33] N. A. Abdel-Malak, R. Harfouche, and S. N. A. Hussain, "Transcriptome of angiopoietin 1-activated human umbilical vein endothelial cells," *Endothelium*, vol. 14, no. 6, pp. 285–302, 2007.

[34] A. D. Kondratyev, K.-N. Chung, and M. O. Jung, "Identification and characterization of a radiation-inducible glycosylated human early-response gene," *Cancer Research*, vol. 56, no. 7, pp. 1498–1502, 1996.

[35] B. G. Bruneau, L. A. Piazza, and A. J. De Bold, "α1-Adrenergic stimulation of isolated rat atria results in discoordinate increases in natriuretic peptide secretion and gene expression and enhances Egr-1 and c-Myc expression," *Endocrinology*, vol. 137, no. 1, pp. 137–143, 1996.

[36] F. R. Sharp, S. M. Sagar, and R. A. Swanson, "Metabolic mapping with cellular resolution: c-fos vs. 2-deoxyglucose," *Critical Reviews in Neurobiology*, vol. 7, no. 3-4, pp. 205–228, 1993.

[37] D. Gius, X. Cao, F. J. Rauscher III, D. R. Cohen, T. Curran, and V. P. Sukhatme, "Transcriptional activation and repression by Fos are independent functions: the C terminus represses immediate-early gene expression via CArG elements," *Molecular and Cellular Biology*, vol. 10, no. 8, pp. 4243–4255, 1990.

[38] D. Chauhan, S. M. Kharbanda, H. Uchiyama, V. P. Sukhatme, D. W. Kufe, and K. C. Anderson, "Involvement of serum response element in okadaic acid-induced EGR-1 transcription in human T-cells," *Cancer Research*, vol. 54, no. 8, pp. 2234–2239, 1994.

[39] M. Ohba, M. Shibanuma, T. Kuroki, and K. Nose, "Production of hydrogen peroxide by transforming growth factor-β1 and its involvement in induction of egr-1 in mouse osteoblastic cells," *Journal of Cell Biology*, vol. 126, no. 4, pp. 1079–1088, 1994.

[40] D. X. Zhang and D. D. Gutterman, "Mitochondrial reactive oxygen species-mediated signaling in endothelial cells," *American Journal of Physiology—Heart and Circulatory Physiology*, vol. 292, no. 5, pp. H2023–H2031, 2007.

[41] E.-H. Yao, Y. Yu, and N. Fukuda, "Oxidative stress on progenitor and stem cells in cardiovascular diseases," *Current Pharmaceutical Biotechnology*, vol. 7, no. 2, pp. 101–108, 2006.

[42] Y. Kayanoki, S. Higashiyama, K. Suzuki et al., "The requirement of both intracellular reactive oxygen species and intracellular calcium elevation for the induction of heparin-binding EGF-like growth factor in vascular endothelial cells and smooth muscle cells," *Biochemical and Biophysical Research Communications*, vol. 259, no. 1, pp. 50–55, 1999.

[43] H. Wu, S. Lei, J. Yuan et al., "Ischemic postconditioning down-regulates Egr-1 expression and attenuates postischemic pulmonary inflammatory cytokine release and tissue injury in rats," *Journal of Surgical Research*, vol. 181, no. 2, pp. 204–212, 2013.

[44] K.-S. Heo, D.-U. Kim, L. Kim et al., "Activation of PKCβII and PKCθ is essential for LDL-induced cell proliferation of human aortic smooth muscle cells via Gi-mediated Erk1/2 activation and Egr-1 upregulation," *Biochemical and Biophysical Research Communications*, vol. 368, no. 1, pp. 126–131, 2008.

[45] J. A. Van Aalst, D.-M. Zhang, K. Miyazaki, S. M. Colles, P. L. Fox, and L. M. Graham, "Role of reactive oxygen species in inhibition of endothelial cell migration by oxidized low-density lipoprotein," *Journal of Vascular Surgery*, vol. 40, no. 6, pp. 1208–1215, 2004.

Hindawi Publishing Corporation
Oxidative Medicine and Cellular Longevity
Volume 2013, Article ID 692302, 9 pages
http://dx.doi.org/10.1155/2013/692302

Research Article

The Effect of Safflower Yellow on Spinal Cord Ischemia Reperfusion Injury in Rabbits

Daiwei Zhou,[1] Bingbing Liu,[1] Xiaoshan Xiao,[1] Peng Dai,[2] Songmei Ma,[1] and Weihua Huang[1]

[1] *Department of Anesthesiology, Guangdong No. 2 Provincial People's Hospital, Guangdong Provincial Emergency Hospital, Guangzhou, Guangdong Province 0086 510317, China*
[2] *Department of Anesthesiology, Foshan First People's Hospital, Guangdong Province 0086 510317, China*

Correspondence should be addressed to Xiaoshan Xiao; mzkgd177@126.com

Received 10 August 2013; Revised 30 October 2013; Accepted 30 October 2013

Academic Editor: Zhengyuan Xia

Safflower yellow (SY) is the safflower extract and is the one of traditional Chinese medicine. The aim of the present work was to investigate the effect of SY on spinal cord ischemia reperfusion injury (SCIRI) in rabbits. The models of spinal cord ischemia reperfusion (SI/R) were constructed, and the degree of the post-ischemic injury was assessed by means of the neurological deficit scores and plasma levels of lipid peroxidation reactioin and neuronal morphologic changes. SCIRI remarkably affected the functional activities of the hind limbs and activated lipid peroxidation reaction. SY could attenuate apoptosis and SCIRI by enhancing Bcl-2 expression and inhibiting Bax and caspase-3 activation.

1. Introduction

According to the pathophysiologic features, spinal cord injury is mainly categorized into primary injury and secondary injury. Primary injury mainly includes direct injury and ischemic injury, and it often occurs in a relatively short period of time after injury (generally considered as early as 4 h after injury), with the irreversible nerve damage [1]. The perfusion after spinal cord ischemia may further aggravate the damage and cause spinal cord ischemia reperfusion injury (SCIRI). SCIRI is one of the most frequent types of secondary spinal cord injury and it aggravates the neuro functional impairment of the limbs. Secondary injury generally lasts longer time, up to 7 days or longer, and the secondary nerve damage can be reversed by means of appropriate interventions [2]. Spinal cord ischemia reperfusion injury (SCIRI) is defined as follows: after removing the factors that cause spinal cord ischemia and the recovery of spinal cord blood supply, its neuronal function cannot be improved and its ischemia injury is more intense than its original level, or even present in the irreversible tardive dead phenomenon on spinal cord neurons [3]. It was generally considered that the reasons for SCIRI included oxygen free radical-induced lipid peroxidation, leukocyte activation, and inflammatory and neuronal apoptosis. In recent years, although there have been many clinical treatments of spinal cord injury, the results were not satisfactory.

Safflower yellow (SY) is extracted from the flowers of the plant safflower (*Carthamus tinctorius*) and as the traditional Chinese medicine it has been extensively used for the treatment of cardio cerebrovascular diseases. SY can promote blood circulation, remove blood stasis, and thereby improve capillary circulation at the site of tissue injury [2]. SY is mixtures of a water-soluble chalcone component, in which both hydroxyl safflower yellow A (HSYA) and safflower yellow B (SYB) are the main components. It has been shown that safflower injection excellently protected the heart by way of improving functions of cardiac contraction and dilation, increasing coronary blood flow, and strengthening the bcl-2 (anti apoptosis gene) protein expression [4]. Additionally, our previous study indicated that SY alleviated the injured tendon adhesion and inflammatory reaction and promoted the repair of injured tendon [2]. However, it is still unknown whether SY can effectively protect against SCIRI. Therefore,

this study constructed SCIRI models with New Zealand rabbits to determine the degree of spinal cord injury and the protective effect of SY on SCIRI.

2. Materials and Methods

2.1. Animals. The adult male New Zealand rabbits (body weight 2.0–2.5 kg), obtained from the Animal Experimental Center of Southern Medical University, were used in this study. All procedures are in strict accordance with the protocols approved by the Chinese institutional ethics committee. The rabbits were housed in individual cages in a temperature-controlled room (22–25°C) and acclimated for 1 week before experiments. Food was removed 8 h prior to the study, but all animals had free access to water.

2.2. Model Establishment. After being anesthetized with ketamine (10 mg/kg body weight, intramuscularly), the airway was maintained by endotracheal intubation (ID = 3.5 mm, depth 10–12 cm) and mechanical ventilation was performed with a 35–45 mmHg $P_{ET}CO2$. The polyethylene catheter was inserted into the right femoral artery for monitoring the mean arterial pressure (MAP) and drawing blood samples, and the one was did into the right femoral vein for solution infusion. The abdominal aorta was exteriorized by midline laparotomy. The SCIRI model was established by occluding the abdominal aorta under the left renal artery for 40 min (when the abdominal aorta was occluded MAP decreased to 0 mmHg) followed by reperfusion as described [5].

2.3. Experimental Protocol. Twenty-four rabbits were randomly divided into three groups ($n = 6$ per group): sham-operated control (Cont), spinal cord ischemia reperfusion (SI/R), and SI/R treated with safflower yellow (SI/R + SY). The control group only executed anesthesia and surgical procedures, except for occluding the abdominal aorta. The SI/R + SY group was intravenously injected with 2 mL/kg of a solution of 16% (wt/vol) SY (1 mL, containing 1.6 mg SY, Z20050146; Yongning Pharma, Zhejiang Province, China), followed by continuous infusion of a total of 5 mL/kg through the right femoral vein at the moment of reperfusion beginning after 40 minutes of the abdominal aorta occlusion. The same volumes of 0.9% saline solution were administrated in control and SI/R groups. Blood samples were obtained at the end of 0 hour ($T0$), 4 hours ($T1$), 12 hours ($T2$), 24 hours ($T3$), and 48 hours ($T4$) after reperfusion, and the plasma was separated and stored at −80°C for further analysis. All animals were sacrificed 48 hours after reperfusion and were rapidly perfused with 0.9% sodium chloride, and the L2-5 segments of the spinal cord were quickly removed. The L2-3 segment in each animal was used for western blot, and the other segment (L4-5) was immersed into 10% neutral formaldehyde for 2-3 days and was used for morphology analysis.

2.4. Neurological Deficit Scores for Hind Limbs. At the end of 4 hours (h), 12 h, 24 h, and 48 h after reperfusion, neurological deficit scores of hind limbs were recorded according to the criterion as follows [6].

0: hind limbs are absolutely paralysed and cannot move.

1: hind limbs move slightly but cannot move against gravity.

2: hind limbs can move but cannot walk or jump.

3: hind limbs can walk and jump with obvious ataxia.

4: hind limbs can jump normally.

2.5. Measurement of MDA, SOD, and IL-8 with ELISA. Plasma levels of MDA, SOD, and IL-8 were determined by using the commercially available rabbit ELISA kit (BenderMed, Vienna, Austria). Plasma samples (in PBS) were purified using Affinity Sorbent and Affinity Column (Cayman chemical, Ann Arbor, MI) and then processed for analysis, according to the instructions provided by the manufacturer (Quantikine; R&D, Minneapolis, MN). The optical density (OD) value was measured at 490 nm wavelength. The OD values of the blank control were subtracted from those of every standard sample, and then the standard curves were drafted. The levels of MDA, SOD, and IL-8 were calculated according to the standard curve as the methods described in our prior study [2].

2.6. Western Blot Assay for Caspase-3. Frozen spinal cord tissues were homogenized using lysis buffer and then were centrifuged at 15000 g for 40 min at 4°C, and protein concentrations were determined using the Bradford assay (Bio-Rad, USA). 50 μg total protein was separated by sodium dodecyl sulfate-polyacrylamide gel electrophoresis (10% SDS-PAGE) and transferred to PVDF membranes (Millipore). Membranes were incubated in blocking buffer (5% skim milk in TBST), then with rabbit anticaspase-3 (1 : 800, Abcam, USA), and GAPDH (1 : 2000, Cell Signaling Technology, Beverly, MA) in TBST overnight at 4°C [7]. Incubated membranes were then treated with secondary antibody conjugated with horseradish peroxidase in TBST for 2 h at 37°C. Blots were developed by enhanced chemiluminescence and digitally scanned. The optical density of each resulting labeled band was measured in an image analysis program.

2.7. HE Staining. After immersing in 10% neutral formaldehyde for 2-3 d, the spinal cord samples (L4-5 segments) were fixed and dehydrated through a graded ethanol series, embedded, and sectioned at 5 mm on a frozen microtome and then mounted and covered. The sections were routinely dewaxed and hydrated, and as our previous study described [2] they were stained by HE and dehydrated, cleared, and covered.

According to neuronal morphological criteria [8], the anterior horn neurons were observed at the magnification of 200 times. Five high-powered visual fields were randomly selected on every section and eight sections were randomly selected in each animal. The anterior horn motor neurons were counted and the normal neurons to total neurons ratios were calculated.

2.8. TUNEL Immunohistochemical Staining. TUNEL staining was used to detect the expression of apoptosis protein in the spinal cord anterior horn neurons in rabbits. The sections were stained with TUNEL (In Situ Cell Death Detection Kit, POD; Roche, Basel) according to the manufacturer's instructions. Five dark visual fields were randomly selected on every section, and the TUNEL-positive neurons and the total numbers of neurons in the selective visual fields were counted. TUNEL-positive index (the TUNEL-positive to whole neurons ratio) was calculated. Eight sections of each animal from all groups were used for measurement, and five high-powered visuals from every section were randomly selected to measure the TUNEL-positive indexes.

2.9. Immunohistochemical Staining for Bax and Bcl-2. To detect the expression of proapoptotic protein and antiapoptotic protein, the spinal cord sections were, respectively, stained with Bax and Bcl-2 (Santa Cruz, CA, USA) according to the manufacturer's instructions. Five high-powered visual fields were randomly selected on every section, and eight sections were selected in each animal. OD values of Bax and Bcl-2 positive neurons were, respectively, measured with Image-Pro plus 6.0 software. The OD value was the sum of all positive neurons pixel OD values divided by the areas of the spinal cord anterior horn regions.

Statistical Analysis. All experimental data were expressed as means ± SD. The statistical significance of the results was evaluated by one-way ANOVA with SPSS 17.0 software, and $P < 0.05$ was considered significant.

3. Results

3.1. Basic Data. No animal died during the experimental period. Five cases of postoperative urinary retention were improved after bladder massage. Basic vital signs of all animals including heart rate (HR) and MAP were stable and there were no significant differences between groups (Table 1). Postoperative abdominal incisions grew well without flare and purulent secretion.

3.2. Neurological Deficit Scores of Hind Limbs. Animal hind limbs appeared at different degrees of functional activity limitation in SI/R and SI/R + SY groups. Statistical results showed that the scores of SI/R + SY group were all higher than those of SI/R group at $T1$, $T2$, $T3$, and $T4$ time points ($P < 0.05$, Figure 1). In SI/R group, the scores were obviously lower at $T4$ than those at $T1$, $T2$, and $T3$ ($P < 0.05$). Animal functional activities of SI/R + SY group were better at $T3$ and $T4$ than at $T1$ and $T2$, but the comparison between $T1$ and $T2$ had no statistical significance ($P > 0.05$), and also no significant difference was seen between $T3$ and $T4$ ($P > 0.05$).

3.3. Levels of MDA and the Activities of SOD. The result showed that MDA levels at the different time points in the Control group were not obviously changed ($P > 0.05$, Figure 2). Plasma levels of MDA in the SI/R group were gradually increased from $T1$ to $T4$ ($P < 0.05$), and similar trend of progressive increase in MDA was also seen in the SI/R + SY group ($P < 0.05$). At $T0$ time point, the levels of MDA between SI/R and SI/R + SY groups did not show statistical significance ($P > 0.05$), but they were higher than those in the control group ($P < 0.05$). Beyond the $T0$ time point, at the same time point from $T1$ to $T4$, MDA levels were markedly lower in SI/R + SY group than in SI/R group ($P < 0.05$).

Table 1: Basic vital signs of all animals at the different time points.

Item	Cont. group	SI/R group	SI/R + SY group
HR (order/rate)			
$T0$	213 ± 8.5	218 ± 10.6	224 ± 7.5
$T1$	213 ± 17.4	207 ± 15.2	216 ± 12.3
$T2$	215 ± 9.1	212 ± 14.8	205 ± 10.0
$T3$	204 ± 15.0	213 ± 7.9	213 ± 14.6
$T4$	213 ± 11.9	215 ± 16.7	213 ± 9.7
MAP (mmHg)			
$T0$	90 ± 7.1	93 ± 7.6	92 ± 4.9
$T1$	89 ± 5.8	88 ± 5.4	91 ± 5.6
$T2$	91 ± 6.5	87 ± 6.2	88 ± 8.1
$T3$	88 ± 6.2	90 ± 4.3	90 ± 4.9
$T4$	95 ± 3.7	91 ± 4.8	93 ± 7.3

HR: heart rate; MAP: mean arterial pressure; $T1$: 4 h after reperfusion; $T2$: 12 h after reperfusion; $T3$: 24 h after reperfusion; $T4$: 48 h after reperfusion.

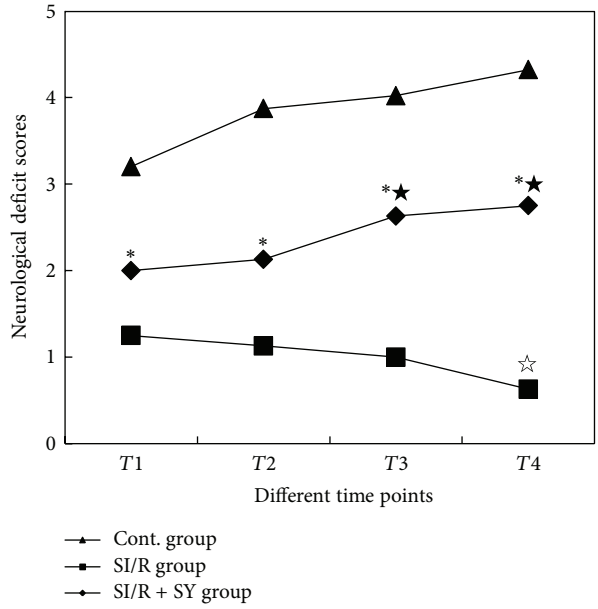

Figure 1: Neurological deficit scores of hind limbs at the different time points. ∗ indicates comparison with control (Cont) group and SI/R group in SI/R + SY group at the same time point, $P < 0.0$; ★ indicates comparison with $T1$ and $T2$ at $T3$ or $T4$ in SI/R+SY group, $P < 0.05$; ☆ indicates comparison with $T1$–$T3$ at $T4$ in SI/R group, $P < 0.05$. $T1$: 4 h after reperfusion; $T2$: 12 h after reperfusion; $T3$: 24 h after reperfusion; $T4$: 48 h after reperfusion.

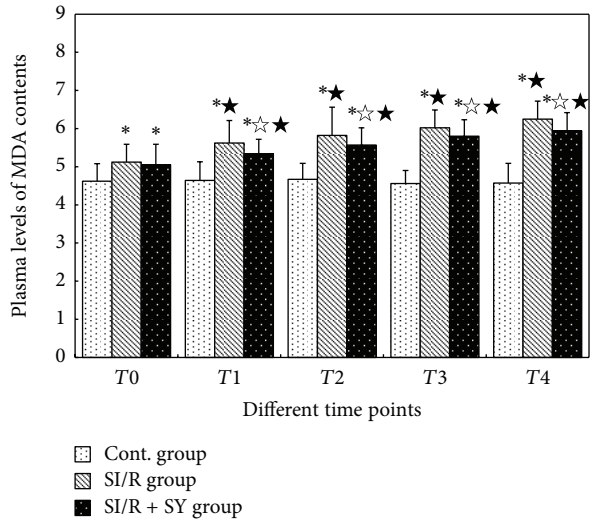

Figure 2: Changes of MDA levels at the different time points. ∗ indicates comparison with control (Cont) group at the same time point, $P < 0.05$; ☆ indicates comparison with SI/R group at the same time point, $P < 0.05$; ★ indicates comparison with $T0$ in the same group, $P < 0.05$. $T0$: 0 h after reperfusion; $T1$: 4 h after reperfusion; $T2$: 12 h after reperfusion; $T3$: 24 h after reperfusion; $T4$: 48 h after reperfusion.

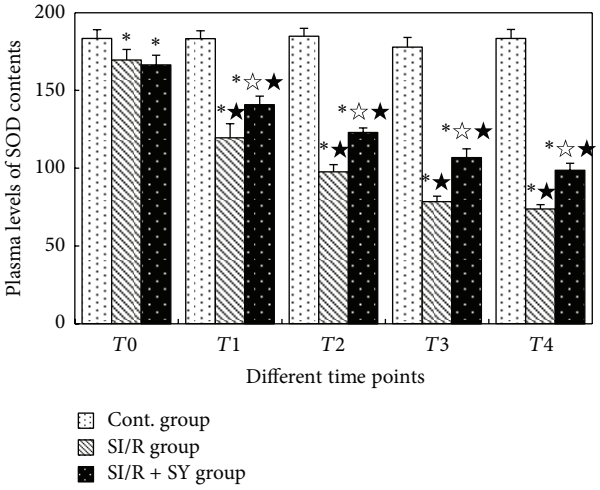

Figure 3: Changes of SOD activities at the different time points. $T1$: 4 h after reperfusion; $T2$: 12 h after reperfusion; $T3$: 24 h after reperfusion; $T4$: 48 h after reperfusion. ∗ indicates comparison with Cont. group at the same time point, $P < 0.05$; ☆ indicates comparison with SI/R group at the same time point, $P < 0.05$; ★ indicates comparison with $T0$ in the same group, $P < 0.05$.

Changes of SOD activities in Cont. group had no statistical significance at the different points ($P > 0.05$, Figure 3). At $T0$ time point, SOD activities of SI/R group and SI/R + SY group were markedly lower than those of Control group ($P < 0.05$), but the comparison between SI/R group and SI/R + SY group has no statistical significance ($P > 0.05$). From $T1$ to $T4$, SOD activities of the SI/R group decreased gradually, and they were all lower than those at $T0$ ($P < 0.05$); additionally, they were all lower than those at the same time points of Control group ($P < 0.05$). Compared with SI/R group, SOD activities of SI/R + SY group were higher at the same time point ($P < 0.05$), but they were all lower than those of the control group ($P < 0.05$).

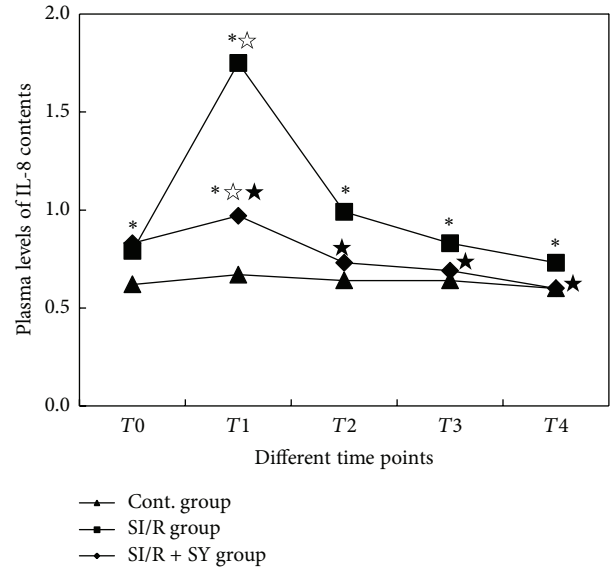

Figure 4: Changes of plasma IL-8 levels at the different time points. $T1$: 4 h after reperfusion; $T2$: 12 h after reperfusion; $T3$: 24 h after reperfusion; $T4$: 48 h after reperfusion; Cont, sham control. ∗ indicates comparison with the sham control group at the same time point, $P < 0.05$; ☆ indicates comparison with SI/R group at the same time point, $P < 0.05$; ★ indicates comparison with $T0$ in the same group, $P < 0.05$.

3.4. Changes of the Serum Levels of IL-8. Similar to the changes of MDA and SOD in the Control group, the expression levels of IL-8 did not show significant difference over time ($P > 0.05$, Figure 4), but it was higher in the SI/R group ($P < 0.05$ versus control) and was significantly reduced in the SI/R + SY group.

3.5. Caspase-3 Protein Expression. Western blotting (Figure 5) revealed that caspase-3 protein expression in the SI/R group was significantly increased as compared to the control group ($P < 0.05$), which was significantly attenuated in the SI/R + SY group ($P < 0.05$ versus SI/R, Figure 5(b)).

3.6. Morphological Changes of the Anterior Horn Neurons

Histopathological Changes. The sections with HE staining were observed at the light microscopic level by an investigator who was initially blinded in terms of group assignment. The results showed that the spinal cord motoneurons in the sham control group (Figure 6(a)) were morphologically normal with clear profile, polygonal perikaryon, and round nucleus. There were no vacuoles present surrounding these neurons. By contrast, in the SI/R group, the number of normal motoneurons was apparently reduced (Figure 6(b)).

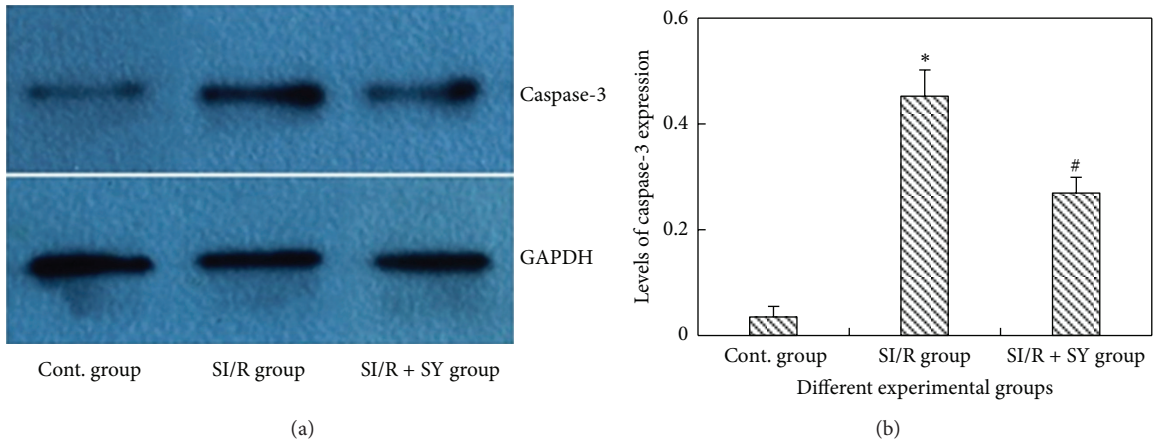

(a) (b)

Figure 5: Western blot assay of caspase-3 apoptosis protein in three groups (a). Cont: sham control. Levels of caspase-3 expression were measured (b), and ∗ indicates comparison with the other two groups, $P < 0.05$; # indicates comparison with SI/R group, $P < 0.05$.

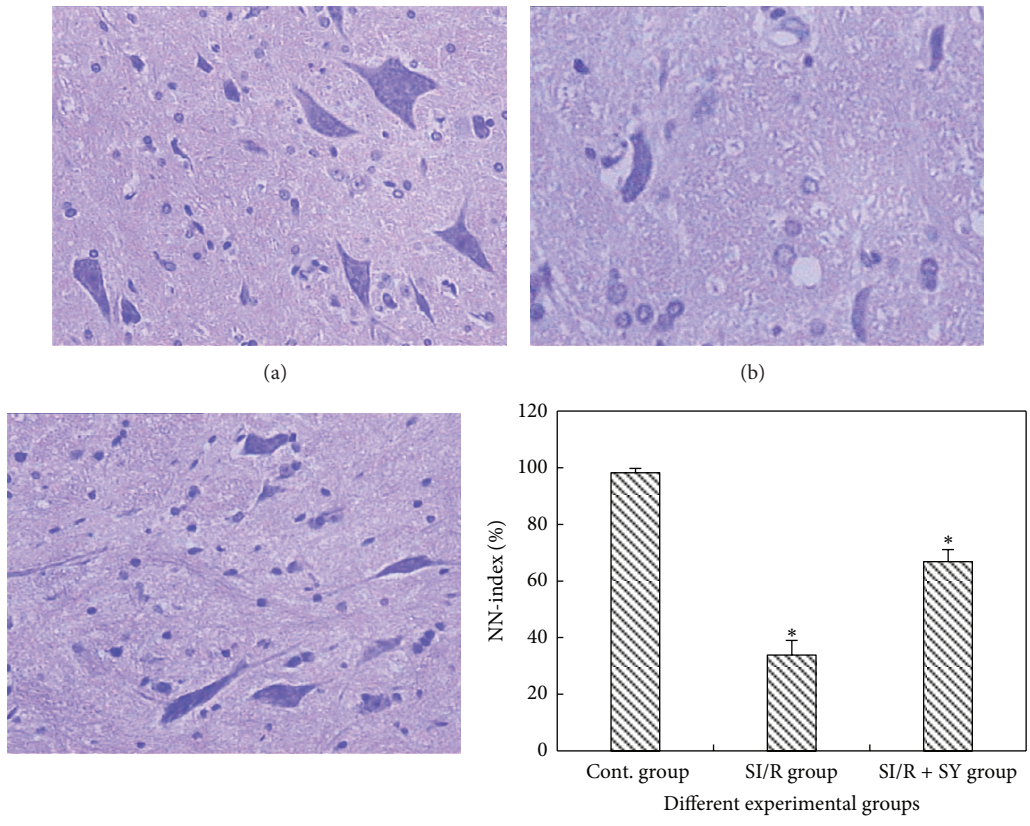

(a) (b) (c) (d)

Figure 6: The neurons of spinal cord anterior horn were assessed by HE staining and viewed at the magnification of 200 times. There were numerous normal neurons without morphological change in the control (Cont.) group (a). Neuronal structural changes appeared in SI/R group (b), such as neuronal pyknosis, light staining tigroid body, and nucleus atrophy. The percentage of normal neurons was higher in the SI/R + SY group (c) as compared to that in the SI/R group, and only slight edema was observed in SI/R + SY group. Bar graph (d) showed the comparison for the ratio of normal motoneurons in spinal cord anterior horn between SI/R group and SI/R + SY group, and ∗ indicated comparison with the other groups, $P < 0.05$. NN-index: normal to total neuron number ratio.

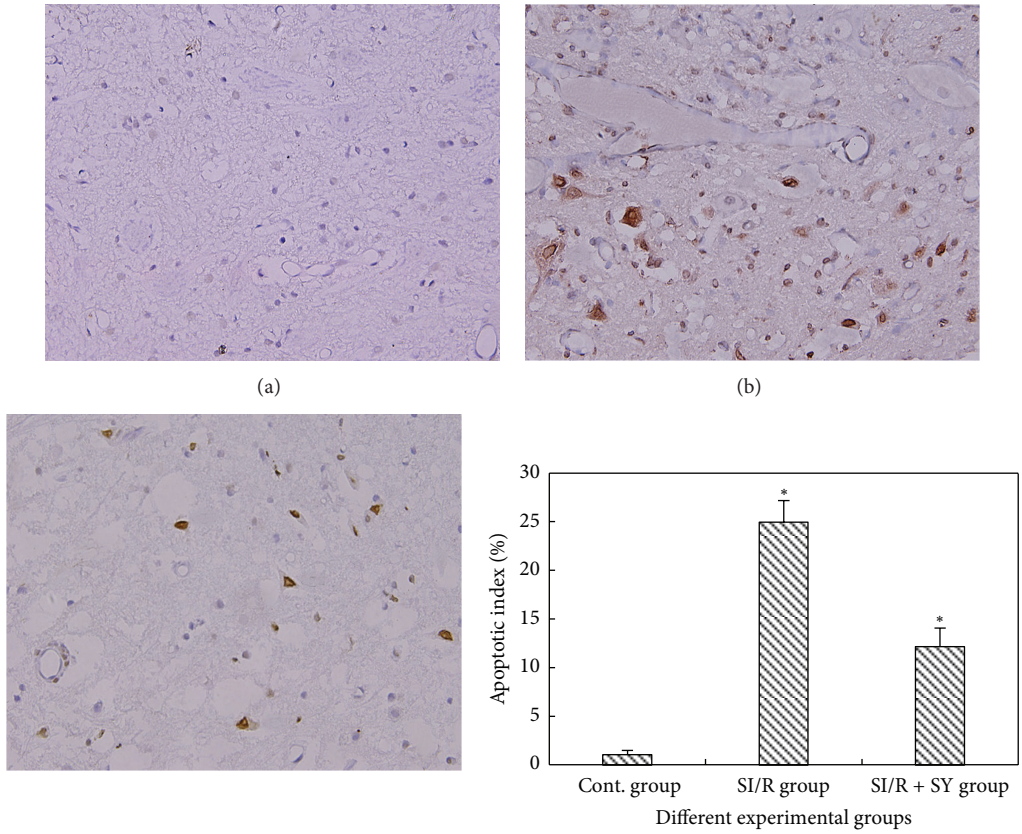

Figure 7: ((a)–(d)) TUNEL immunohistochemical staining in the spinal cord anterior horn at the same magnification of 200 times. TUNEL-positive neurons were observed in SI/R group (b) and SI/R + SY group (c), but in the control group they were almost not detected (a). (d) The apoptotic index (TUNEL-positive to total neuron ratio) of anterior horn neurons, and ∗ indicates comparison with the two other groups, $P < 0.05$.

In addition, neuronal structural changes were observed, which included neuronal pyknosis, light staining tigroid body, nucleus atrophy and nucleolus disappearance, and so on. Furthermore, hemorrhagic macules were scattered into tissue structures and vacuolar changes were observed in the cytoplasm. Morphologic structures of neurons in SI/R + SY group were basically normal, except for slight edema (Figure 6(c)). Statistical analysis showed that the percentage of normal motoneurons was larger in the SI/R + SY group (66.75% ± 4.37% of all neurons) than that in the SI/R group (33.74% ± 5.31% of all neurons, $P < 0.05$; Figure 6(d)).

Light Microscopic (LM) Observation of Apoptotic TUNEL-Positive Cells. Spinal cord sections were stained with TUNEL and were observed at the high light microscopic level (200 times magnification, Figure 7). The results showed that neuronal structures in spinal cord anterior horn in the sham control group were basically normal with rare detectable TUNEL-positive staining (Figure 7(a)). In the spinal cord anterior horn of the SI/R group, amount of vacuoles appeared and a large number of TUNEL-positive neurons were observed (Figure 7(b)). By contrary, apoptosis neurons marked by TUNEL in the SI/R + SY group were obviously decreased (Figure 7(c)). Apoptotic indexes were calculated (the ratios of TUNEL-positive neurons to whole neurons) which showed that the apoptotic index was smaller in the SI/R + SY group than that in the SI/R group ($P < 0.05$, Figure 7(d)), despite the fact that the apoptotic indexes in the two injury groups were all higher than that in the control group.

LM Observation of Bax and Bcl-2 Protein Expression. Spinal cord sections were, respectively, stained with Bax and Bcl-2 and were observed at the high LM level (200 times magnification, Figures 8 and 9). The results showed that Bax protein was more intensely expressed in the SI/R group than in the other groups ($P < 0.05$, Figure 8(d)), but Bcl-2 expression of SI/R + SY group was obviously intense (Figures 9(a)–9(c)), and its OD value was also higher than that of the Control group and SI/R group ($P < 0.05$, Figure 9(d)).

4. Discussion

Spinal cord blood supply is significantly segmental, and its collateral circulation is relatively poor, so that it is easy to suffer from ischemia damage [5]. Due to constant and seldom variation of vascular distribution in the lumbar region, the degree of spinal cord injury is stable with higher repeatability and less complications. Therefore, we constructed spinal cord

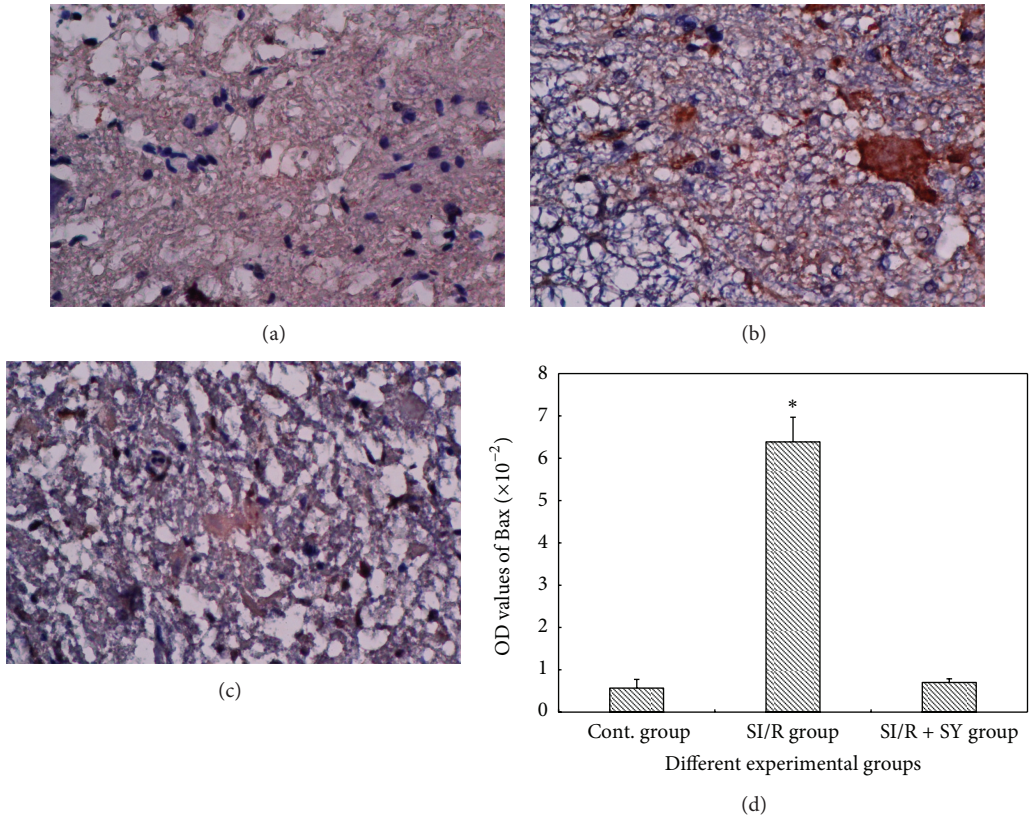

Figure 8: Images (a)–(c) showed Bax protein expression in the spinal cord anterior horn at the same magnification of 200 times, and OD values of Bax protein staining were measured and analyzed in image (d); ∗ indicate comparison with the two other groups, $P < 0.05$.

ischemia reperfusion model in rabbits as Zivin's description [5].

The cell membranes of spinal cord neurons are rich in lipid content and large amounts of catecholamines and unsaturated fatty acids, so that they are more susceptible to oxygen free radical attack [9]. Reactive oxygen species-mediated lipid peroxidation plays an important role in ischemia reperfusion injuries in various organs [10–12]. After spinal cord suffered the injury, the lipid peroxidation reaction was extensively activated and MDA was largely produced, but SOD activities markedly decreased. Increasing SOD activity has been shown to evidently attenuate spinal cord injury [2].

Many traditional Chinese medicines are used as the natural oxygen free radical scavenger and have the advantage of lowering toxic adverse actions of the nonnatural products, which have protective effects against ischemia reperfusion injury [13]. Safflower and its extracts play an important role of inhibiting lipid peroxidation and clearing oxygen free radical. Safflower injection can significantly increase the activities of glutathione peroxidase (SE-GSHPX) and SOD and decrease MDA contents in ischemia reperfusion injury myocardium. The present study showed that increase in MDA and decrease in SOD were part of the reaction of the entire body in response to SCIRI, and they were closely correlative with the degree of injury. Immediately after reperfusion (reperfusion 0 hour), the lipid peroxidation of spinal cord neurons in the reperfusion groups (including SY treatment group) began to intensify as observed from changes in MDA contents, and at 4 hours after reperfusion the plasma level of MDA production in the SI/R group was further increased and SOD activity was further decreased. These results indicated that lipid peroxidation had been triggered in the ischemia stage, and then in the reperfusion stage it further increased and aggravated ischemia reperfusion injury in the spinal cord. However, lipid peroxidation in the SI/R + SY group was attenuated (which means lower MDA content and higher SOD activity) at the different time points after reperfusion. These results indicated that SY played an important role in the spinal cord protection by relieving lipid peroxidation.

The study has confirmed that IL-8 is an important type of cytokine, which takes part in inflammation reaction [14]. It primarily plays a role through the cytomembrane surface receptors. Compared with the other cells, neutrophil granulocyte surfaces significantly raise expressed IL-8 receptors, so that IL-8 mainly induces chemotaxis of neutrophil chemotactic and may be an important chemotactic factor in mediating neutrophil aggregation [15]. The present results showed that, compared with sham-cont group, IL-8 contents in the reperfusion group without SY treatment obviously increased. Moreover, with the progression of reperfusion, IL-8 level gradually increased and reached the peak after reperfusion 12 h before it started to decrease. In the SI/R + SY group its change had the same tendency, but it was lower than that in the SI/R group at various time points. This

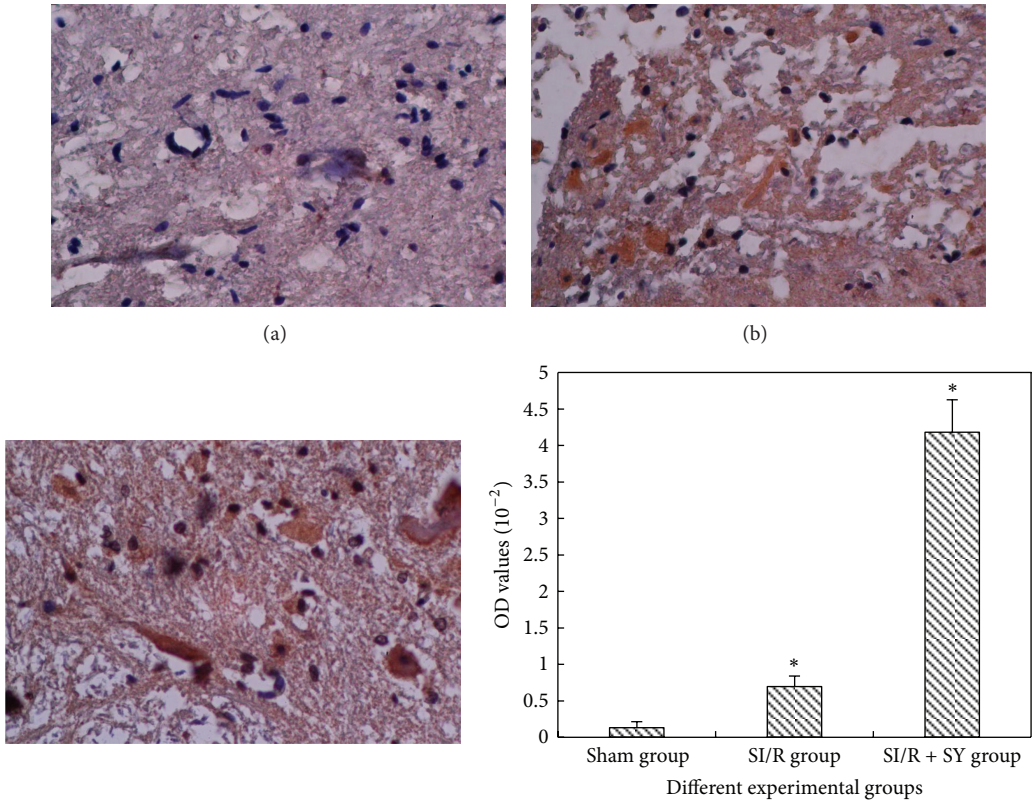

Figure 9: ((a)–(c)) Bcl-2 protein expression in the spinal cord anterior horn at the same magnification of 200 times, and OD values of Bcl-2 protein staining were measured and analyzed in image (d); ∗ indicate comparison with the two other groups, $P < 0.05$.

result indicated that SY might inhibit IL-8 expression and inflammatory reaction induced by SCIRI.

The mechanism of cell apoptosis is very complicated and is influenced by many factors, especially by gene regulation. caspase family, a type of calcium-dependent Cysteine protease, is the key protease triggering cell apoptosis and is present in the whole process of apoptosis [16]. The current study confirmed that the changes of caspase-3 expression were in line with the changes in cell apoptosis after SCIRI, suggesting that caspase-3 could be used as biochemical index in assessing post-ischemic spinal cord injury. The present result showed that the expression level of caspase-3 in SI/R + SY group was obviously lower than that in SI/R group, which suggests that inhibiting caspase-3 expression may represent a mechanism by which SY confers protection against SCIRI. The process of apoptosis is regulated by a complex interaction of proapoptotic (Bax group of proteins) and antiapoptotic (Bcl-2 family of proteins) mitochondrial membrane proteins and the activation of effector caspase [17]. The findings from studying the neurons in animal models of spinal cord injury should help to enhance our understanding of the morphologic features of damaged neurons, to identify the mechanism of neuronal damage, and, therefore, to develop more effective therapies against SCIRI.

5. Conclusions

SI/R remarkably affected the neurological function of hind limbs and activated the lipid peroxidation reaction and promoted the inflammatory cytokine release. SY can reduce postischemic lipid peroxidation and inflammatory response and effectively attenuate SCIRI in rabbits.

Authors' Contribution

Daiwei Zhou and Bingbing Liu contributed equally to this paper.

Acknowledgments

This study was supported by grants from the National Science Foundations of Guangdong Province (no. 9151031701000002).

References

[1] C. B-Rao and J. Stewart, "Inverse analysis of empirical matrices of idiotypic network interactions," *Bulletin of Mathematical Biology*, vol. 58, no. 6, pp. 1123–1153, 1996.

[2] B. S. Uydes-Dogan, M. Nebigil, S. Aslamaci, E. Onuk, I. Kanzik, and F. Akar, "The comparison of vascular reactivities of arterial and venous grafts to vasodilators: management of graft spasm," *International Journal of Cardiology*, vol. 53, no. 2, pp. 137–145, 1996.

[3] E. Kieffer, L. Chiche, E. Cormier, and H. Guegan, "Recurrent spinal cord ischemia after endovascular stent grafting for chronic traumatic aneurysm of the aortic isthmus," *Journal of Vascular Surgery*, vol. 45, no. 4, pp. 831–833, 2007.

[4] S.-Q. Zhang and L.-D. Jiang, "Effect of safflower injection on cardiac energy charge and anti-apoptosis gene bcl-2 in rats' heart," *Chinese Journal of Integrated Traditional and Western Medicine*, vol. 24, no. 5, pp. 442–444, 2004.

[5] M. P. Bowes, E. Masliah, D. A. C. Otero, J. A. Zivin, and T. Saitoh, "Reduction of neurological damage bye peptide segment of the amyloid β/A4 protein precursor in a rabbit spinal cord ischemia model," *Experimental Neurology*, vol. 129, no. 1, pp. 112–119, 1994.

[6] T. P. Jacobs, O. Kempski, D. McKinley, A. J. Dutka, J. M. Hallenbeck, and G. Feuerstein, "Blood flow and vascular permeability during motor dysfunction in a rabbit model of spinal cord ischemia," *Stroke*, vol. 23, no. 3, pp. 367–373, 1992.

[7] S. Mu, L. Ouyang, B. Liu et al., "Protective effect of melatonin on 3-NP induced striatal interneuron injury in rats," *Neurochemistry International*, vol. 59, no. 2, pp. 224–234, 2011.

[8] W. I. Rosenblum, "Histopathologic clues to the pathways of neuronal death following ischemia/hypoxia," *Journal of Neurotrauma*, vol. 14, no. 5, pp. 313–326, 1997.

[9] B. Halliwell, "Oxidative stress and neurodegeneration: where are we now?" *Journal of Neurochemistry*, vol. 97, no. 6, pp. 1634–1658, 2006.

[10] H. Li, Z. Liu, J. Wang et al., "Susceptibility to myocardial ischemia reperfusion injury at early stage of type 1 diabetes in rats," *Cardiovascular Diabetology*, vol. 12, no. 1, p. 133, 2013.

[11] X. Chi, A. Zhang, G. Luo et al., "Knockdown of myeloid differentiation protein-2 reduces acute lung injury following orthotopic autologous liver transplantation in a rat model," *Pulmonary Pharmacology & Therapeutics*, vol. 26, no. 3, pp. 380–387, 2013.

[12] K. Ohno, M. Ito, M. Ichihara, and M. Ito, "Molecular hydrogen as an emerging therapeutic medical gas for neurodegenerative and other diseases," *Oxidative Medicine and Cellular Longevity*, vol. 2012, Article ID 353152, 11 pages, 2012.

[13] L.-H. Wan, J. Chen, L. Li, W.-B. Xiong, and L.-M. Zhou, "Protective effects of Carthamus tinctorius injection on isoprenaline-induced myocardial injury in rats," *Pharmaceutical Biology*, vol. 49, no. 11, pp. 1204–1209, 2011.

[14] T. Kunihara, S. Sasaki, N. Shiiya et al., "Lazaroid reduces production of IL-8 and IL-1 receptor antagonist in ischemic spinal cord injury," *Annals of Thoracic Surgery*, vol. 69, no. 3, pp. 792–798, 2000.

[15] E. M. Boyle Jr., T. H. Pohlman, C. J. Cornejo, and E. D. Verrier, "Endothelial cell injury in cardiovascular surgery: ischemia-reperfusion," *Annals of Thoracic Surgery*, vol. 62, no. 6, pp. 1868–1875, 1996.

[16] N. A. Thornberry and Y. Lazebnik, "Caspases: enemies within," *Science*, vol. 281, no. 5381, pp. 1312–1316, 1998.

[17] N. H. Bishopric, P. Andreka, T. Slepak, and K. A. Webster, "Molecular mechanisms of apoptosis in the cardiac myocyte," *Current Opinion in Pharmacology*, vol. 1, no. 2, pp. 141–150, 2001.

Hindawi Publishing Corporation
Oxidative Medicine and Cellular Longevity
Volume 2013, Article ID 185715, 8 pages
http://dx.doi.org/10.1155/2013/185715

Research Article

Resolvin D1 Reverts Lipopolysaccharide-Induced TJ Proteins Disruption and the Increase of Cellular Permeability by Regulating IκBα Signaling in Human Vascular Endothelial Cells

Xingcai Zhang,[1,2] Tingting Wang,[1] Ping Gui,[1] Chengye Yao,[1] Wei Sun,[1] Linlin Wang,[1] Huiqing Wang,[1] Wanli Xie,[1] Shanglong Yao,[1] Yun Lin,[1] and Qingping Wu[1]

[1] *Department of Anesthesiology, Union Hospital, Tongji Medical College, Huazhong University of Science and Technology, Wuhan 430022, China*
[2] *Department of Anesthesiology, Ningbo First Hospital, Ningbo 315010, China*

Correspondence should be addressed to Yun Lin; linyun7801@yahoo.com.cn and Qingping Wu; wqp1968@126.com

Received 2 August 2013; Revised 29 September 2013; Accepted 30 September 2013

Academic Editor: Zhengyuan Xia

Tight Junctions (TJ) are important components of paracellular pathways, and their destruction enhances vascular permeability. Resolvin D1 (RvD1) is a novel lipid mediator that has treatment effects on inflammatory diseases, but its effect on inflammation induced increase in vascular permeability is unclear. To understand whether RvD1 counteracts the lipopolysaccharide (LPS) induced increase in vascular cell permeability, we investigated the effects of RvD1 on endothelial barrier permeability and tight junction reorganization and expression in the presence or absence of LPS stimulation in cultured Human Vascular Endothelial Cells (HUVECs). Our results showed that RvD1 decreased LPS-induced increased in cellular permeability and inhibited the LPS-induced redistribution of zo-1, occludin, and F-actin in HUVECs. Moreover, RvD1 attenuated the expression of IκBα in LPS-induced HUVECs. The NF-κB inhibitor PDTC enhanced the protective effects of RvD1 on restoration of occludin rather than zo-1 expression in LPS-stimulated HUVECs. By contrast, the ERK1/2 inhibitor PD98059 had no effect on LPS-induced alterations in zo-1 and occludin protein expressions in HUVECs. Our data indicate that RvD1 protects against impairment of endothelial barrier function induced by LPS through upregulating the expression of TJ proteins in HUVECs, which involves the IκBα pathway but not the ERK1/2 signaling.

1. Introduction

Endothelial cells form a selective barrier that dynamically controls the transport of bioactive molecules between the circulating blood and the interstitial fluid [1, 2]. The disruption of this barrier induces a direct increase in vascular permeability. Vascular permeability is determined by a combination of transcellular and paracellular pathways, with the latter being a major contributor to inflammation-induced barrier disruption [3]. Studies have shown that lipopolysaccharide (LPS), by eliciting a variety of inflammatory response, can induce the breakdown of endothelial barrier functions. However, the underlying mechanism is unclear, and the potential interventions are required to reverse the inflammation-induced barrier disruption.

Tight junctions (TJ) are important components of paracellular pathways, and their destruction causes barrier hyperpermeability. TJ proteins are located at the apical-most portion of the lateral interendothelial membrane. Occludin is a major transmembrane protein localizing at the TJ [4]. Zonula occludens 1 (zo-1) is considered as a scaffolding protein, linking TJ transmembrane proteins to cytoskeletal filaments. Studies have shown that zo-1 is required for occludin to be localized at TJ. Disrupting either the expression or the distribution of zo-1 leads to disruption of TJ assembly [5–7]. It has also been shown that zo-1 limits solute transport,

by depleting zo-1 in MDCK cells [5]. These investigations suggest that TJ proteins occludin and zo-1 play active roles in regulating paracellular permeability of endothelia [8].

Resolvin D1 (RvD1) is a novel lipid mediator that has been identified to possess the property in resolving inflammatory exudates. It is enzymatically derived from docosahexaenoic acid (DHA) [9, 10]. RvD1 has important beneficial effects in the treatment of many inflammatory diseases. It markedly reduces the levels of IL-1β and IL-6 and increases the levels of IL-10 and IFN-γ [11]. Pretreatment with RvD1 reduces lung edema and inhibits the activation of ERK1/2 in an acute lung injury model of mice [12]. Moreover, some studies show that activation of the MAPK extracellular signal-regulated kinase (ERK) 1/2 (p44/p42, resp.) is associated with the disruption of TJ proteins [13, 14]. Interestingly, RvD1 significantly reduces tumor necrosis factor (TNF)-α induced phosphorylation of IκB, a critical regulator of NF-κB activation and nuclear translocation in human monocytes [15].

Therefore, in the present study, we tested the hypothesis that RvD1 could counteract the LPS-induced increase in permeability, primarily through reversing LPS-induced TJ proteins disruption and expression in human umbilical vein endothelial cells (HUVECs).

2. Materials and Methods

2.1. Cell Cultures and Treatments. HUVECs were obtained from ATCC. Cells were cultured in M199 media with 10% fetal bovine serum (FBS), 100 U/mL penicillin, and 100 μg/mL streptomycin. HUVECs were incubated at 37°C in a humidified atmosphere of 5% CO2. After 2-3 days, cells reached 80–90% confluence in all experiments.

HUVECs were randomly divided into four groups: (1) control group: cells without treatment; (2) LPS group: cells were treated with LPS (400 ng/mL) for 6 hours (h); (3) RvD1 group: cells were treated with RvD1 (100 ng/mL) for 6 h; (4) RvD1 + LPS group: cells were pretreated with RvD1 (100 ng/mL) for 30 min and then treated with LPS (400 ng/mL) for 6 h. In some experiments, cells were pretreated with PD98059 (20 μM) or PDTC (20 μM) for 30 minutes, before being treated with RvD1 and LPS as described.

2.2. Permeability Assay. HUVECs (1×10^5) were seeded on transwell filters (0.4-um pore size, Costar) in 24-well dishes and grown until they reached confluence. After treatment, the medium was replaced with serum-free medium. Fluorescein isothiocyanate (FITC)-dextran (Mr 40 000; Sigma) was then added to the upper chamber at a final concentration of 1 mg/mL. After 1 hour of incubation at 37°C, 100 μL samples were taken from the lower chamber for fluorescence measurements. The fluorescent content of the samples were measured by using a spectrofluorimeter (λEX 480 nm, λEM 520 nm; Bio-Tek Synergy 2).

2.3. Immunofluorescence. After treatment, cells grown on coverslips were washed with PBS and fixed with 4% paraformaldehyde. Then, cells were washed twice with 1% PBS and permeabilized with 0.1% Triton X-100 for 5 min. The cells were blocked with 1% BSA in PBS for 30 min. For the staining of F-actin, cells were incubated with FITC-phalloidin (1 : 50; Enzo Life Sciences) for 60 min at room temperature. For zo-1 and occludin staining, cells were fixed with 4% paraformaldehyde and permeabilized with 0.05% Triton X-100 for 3 min. The cells were blocked with 1% BSA in PBS for 30 min and then incubated overnight at 4°C with the zo-1 antibody (1 : 50; Zymed, San Francisco, CA) or the occludin antibody (1 : 60; Zymed, San Francisco, CA) in a solution of 0.05% Tween-20 in TBS-goat serum (1 : 1). On the next day, the cell were washed with 0.05% Tween-20 in TBS and incubated with Dylight 594 AffiniPure Goat Anti-Rabbit IgG (1 : 400; EarthOx LLC San Francisco, CA) for 30 min at RT. The slides were incubated with antifade medium with DAPI for nuclear staining, and cell images were taken with the Olympus IX71 microscope.

2.4. Western Blotting. Proteins were extracted from scraped cells with RIPA buffer containing protease and phosphatase inhibitor cocktail tablets. Protein concentrations were assessed using the BCA protein assay kit. Samples were boiled in a 99°C heat block for 10 min and stored at −20°C until being used for immunoblotting. The samples (40 μg) were separated by 8% SDS/PAGE, and the separated proteins were electrically transferred to PVDF membranes. The membranes were blocked for 1 hour with 5% nonfat dry milk in TBST (0.1% Tween-20 in TBS) at room temperature and then incubated overnight at 4°C with the following antibodies: polyclonal rabbit anti-zo-1 (1 : 400, Zymed, San Francisco, CA), occludin (1 : 500; Zymed, San Francisco, CA), ERK1/2 (1 : 1000; Cell Signal Technology), P-ERK1/2 (1 : 1000; Cell Signal Technology), IκBα (1 : 1000; Cell Signal Technology), or rabbit anti-GAPDH (1 : 1000; Proteintech Group, Inc.). The membranes were washed 3 times with TBS-T and incubated with goat anti-rabbit IgG (1 : 5000; Proteintech Group, Inc) for 1 hour at RT. Protein bands were revealed by fluorography using ECL (enhanced chemiluminescence) reagents and quantified by the Image Lab image acquisition and analysis software (Bio-Rad).

2.5. Statistical Analyses. All data were expressed as the means ± s.e.m. and were analyzed with one-way analysis of variance followed by Newman-Keuls Multiple Comparison Test (GraphPad Prism (version 5 for Windows, San Diego, CA) software). Statistical significance was defined at $P < 0.05$.

3. Results

3.1. RvD1 Counteracted the LPS-Induced Increase in Endothelial Cell Permeability. The effects of LPS and RvD1 on endothelial TJ permeability in HUVECs were examined, as shown in Figure 1. LPS disrupted the permeability barrier in HUVECs ($P < 0.01$ Control versus LPS group) and the result is consistent with previous study [16]. RvD1 reduced the LPS-induced increase in permeability to a level comparable to that in the control group in HUVECs ($P < 0.01$ LPS group versus RvD1 + LPS group; Figure 1).

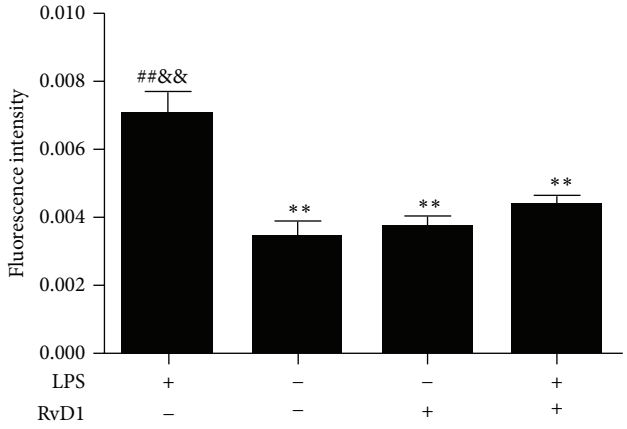

Figure 1: Effects of LPS and RvD1 on endothelial permeability measured by fluorescence intensity in HUVECs. Permeability was measured by determining the flux of FITC-dextran from the upper to the lower chamber. Data were expressed as mean ± s.e.m. ($n = 3$ per group). $^{**}P < 0.01$ versus LPS group; $^{\#\#}P < 0.01$ versus control group; $^{\&\&}P < 0.01$ versus RvD1 + LPS group.

3.2. RvD1 Reversed the LPS-Induced Reorganization of the Actin Cytoskeleton and Tight Junctions and Increases zo-1 and Occludin Expression in HUVECs. LPS has been shown to induce the redistribution of occludin and zo-1 from intercellular junctions [17, 18]. To study the effect of RvD1 on the reorganization and expression of zo-1, occludin and F-actin in LPS-induced endothelial cells, we treated HUVECs with RvD1 prior to LPS induction. As demonstrated in Figure 2, LPS induced a vast assembly of stress fibers and fragmentation of the occludin and zo-1 signals. Gaps were detected between cells, and the expression of zo-1 and occludin decreased significantly ($P < 0.01$ control versus LPS group; Figure 2(d)). Interestingly, RvD1 counteracted the LPS-induced formation of stress fibers (Figure 2(a)). The linear structure of the zo-1 and occludin signals appeared at the cell margins upon pretreatment with RvD1 (Figures 2(b) and 2(c)). In addition the expressions of zo-1 and occludin were increased ($P < 0.01$ LPS group versus RvD1 + LPS group; Figure 2(d)). The formation of stress fibers and the changes in tight junctions induced by LPS correlated with a decrease in endothelial barrier function, as measured by passage of FITC-dextran through HUVEC monolayers grown on Transwell filters.

3.3. Effects of RvD1 on ERK1/2 and IκBα Signaling Pathways in LPS-Treated Endothelial Cells. Our findings demonstrated that pretreatment with RvD1 increased IκBα expression in LPS-induced HUVECs (Figure 3). There was no significant difference in ERK1/2 phosphorylation among the different groups of HUVECs (Figure 3(a)). Compared with the control group, the expression of IκBα was reduced in the LPS-stimulated group ($P < 0.01$; Figure 3(b)). Compared with the LPS-treated group, the expression of IκBα was significantly higher in RvD1 + LPS group ($P < 0.05$; Figure 3(b)). ERK inhibitor PD98059 significantly decreased ERK1/2 phosphorylation in RvD1 + LPS group ($P < 0.05$; Figure 3(c)). The NF-κB inhibitor PDTC significantly increased IκBα expression ($P < 0.05$; Figure 3(d)), which was consistent with the notion that PDTC can suppress the transfer of NF-κB from the cytoplasm into the nucleus by inhibition of the IκBα degradation.

3.4. RvD1 Prevented LPS-Induced Disruption of TJ by a Mechanism Dependent on IκBα rather than ERK1/2. As shown in Figure 4, RvD1 restored the expression of zo-1 and occludin in LPS-stimulated HUVECs. The NF-κB inhibitor PDTC further enhanced the protective effects of RvD1 on restoration of occludin but not zo-1 expression in LPS-stimulated HUVECs ($P < 0.05$ RvD1 + LPS group versus RvD1 + LPS + PDTC group). However, ERK inhibitor PD98059 had no effect on the expression of TJ proteins in RvD1 + LPS group in HUVECs.

4. Discussion

Rapid changes in local blood vessel perfusion and permeability increase extravasation of circulating leucocytes and plasma proteins, which is the early phase of an acute inflammatory response [19]. Endothelial hyperpermeability plays a crucial role in vascular inflammation diseases, such as ischemia-reperfusion injury, thrombosis, cancer, and adult respiratory distress syndrome [20]. Increase in endothelial cell permeability can be caused by stimulation from a variety of inflammatory mediators including LPS, an endotoxin in the outer membrane of Gram-negative bacteria that stimulates mononuclear cells and neutrophils to produce immunoregulatory and proinflammatory cytokines [21]. Our results demonstrated that LPS induced an increase in endothelial cell permeability, which was in agreement with previous reports showing that LPS disrupts the permeability barrier of HUVECs [16]. RvD1, generated through sequential oxygenation of DHA, can reduce human polymorphonuclear leukocyte (PMN) transendothelial migration and inflammatory pain [22]. Interestingly, RvD1 reduces the levels of proinflammatory cytokines and increases the levels of antnflammatory cytokines [11]. RvD1 treatment leads to a significant reduction in the inflammatory cytokines IL-1α, IL-1β, and TNF-α [23]. We therefore examined whether RvD1 could protect cells from permeability barrier disruption induced by LPS. Our results showed that RvD1 indeed counteracted the LPS-induced increase in endothelial cell permeability. The reversal of LPS-induced barrier disruption by RvD1 seemed to be partly associated with the inhibition of inflammatory signaling pathway.

Inflammation leads to the loss of endothelial cell (EC) functional integrity and the formation of small gaps between ECs, which are a major cause of vascular leakage [24]. There is increasing evidence showing that zo-1 plays a crucial role in regulating TJ assembly. Studies have shown that TJ assembly is disrupted in cells with disrupted zo-1 expression [5–7]. Occludin is a 65-kDa protein located at the TJ and is the first transmembrane TJ protein identified [25]. Occludin also

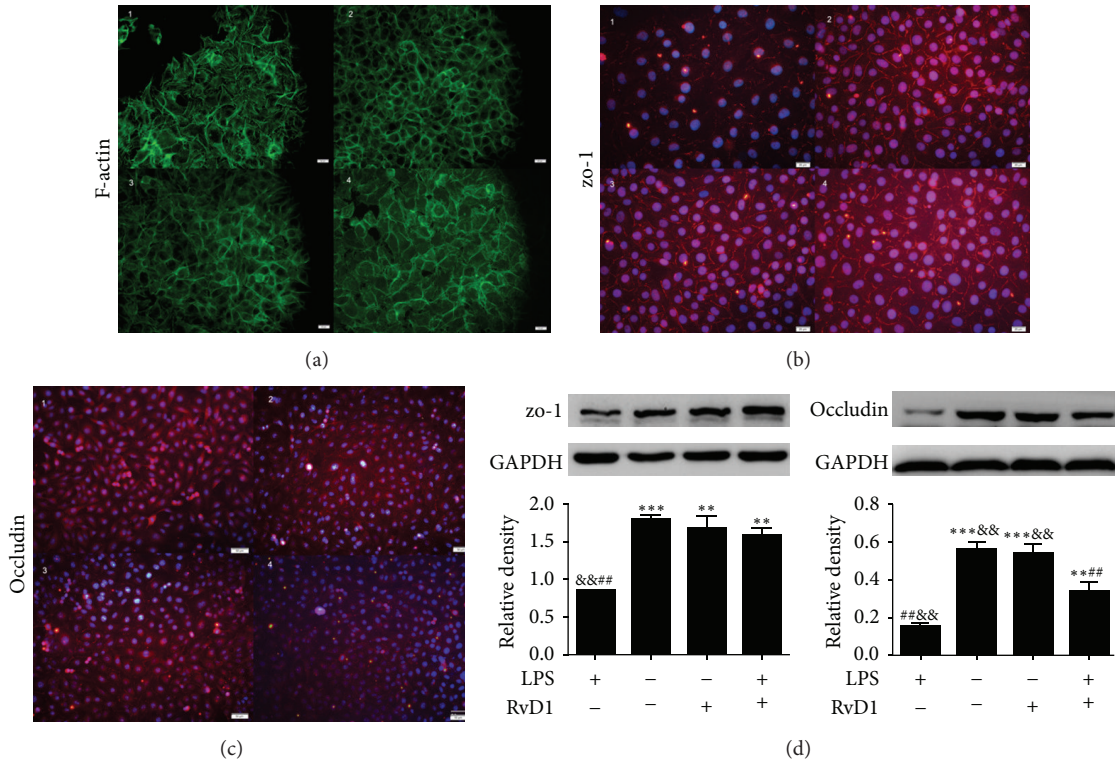

Figure 2: Effects of RvD1 and LPS on the junctional localization of zo-1, occludin, and F-actin as well as the expression of zo-1 and occludin in HUVECs. The locations of F-actin (a), zo-1 (b), and occludin (c) were detected by immunofluorescence. The protein expressions of zo-1 and occludin (d) were detected by western blotting. Data were expressed as mean ± s.e.m. ($n = 3$ per group). $^{**}P < 0.01$, $^{***}P < 0.001$ versus LPS group; $^{\#\#}P < 0.01$ versus control group; $^{\&\&}P < 0.01$ versus RvD1 + LPS group.

plays an important role in the paracellular barrier which mediates the flux of large macromolecules [26]. The main function of occludin involves TJ regulation [27, 28], although one study using occludin knockout mice and embryonic stem cells [29] has shown opposite results. Zo-1 and occludin are key molecules in paracellular permeability. Our results demonstrated that RvD1 protected the endothelial cells from barrier dysfunction, as measured by passage of FITC-dextran through HUVEC monolayers grown on Transwell filters after LPS stimulation. We also showed that RvD1 inhibited the redistribution of zo-1 and occludin and increases their expression in LPS-stimulated HUVECs. Exposure of HUEVCs to LPS significantly reduced zo-1 and occludin protein expressions, and this effect was reversed by pretreatment with RvD1. We next addressed the mechanism regarding how RvD1 influenced protein expression at TJ.

As a tight junction-associated cytoskeletal protein, zo-1 is involved in signal transduction and provides a link between occludin and the actin cytoskeleton [30]. The F-actin cytoskeleton determines cell shape and participates in the regulation of TJ proteins, which plays a major role in TJ barrier function and the regulation of paracellular pathways in different physiological and pathological states [31, 32]. It is thus not surprising that the disruption of this F-actin pool is associated with increased paracellular permeability. Recent research shows that incubation of human polymorphonuclears (PMNs) with RvD1 results in a decrease in actin polymerization [33]. Therefore, we examined whether RvD1 was able to reduce LPS-induced actin polymerization and reduce LPS-induced increase of permeability in HUVECs. Our findings revealed that LPS increased actin reorganization, which was consistent with the findings [34]. In addition, RvD1 indeed reduced LPS-induced actin polymerization. We thus concluded that RvD1 reversed the LPS-induced permeability of HUVEC by reducing actin polymerization.

Many inflammatory mediators are known to disrupt interendothelial junction assembly, thereby causing endothelial hyperpermeability. LPS, the interleukins IL-1, IL-3, and IL-4, tumor necrosis factor alpha (TNF-α), and interferon gamma (IFN-γ) are shown to influence TJ barrier function in epithelia and endothelia [35–37]. It is known that RvD1 significantly reduces the levels of IL-1β and IL-6 and increases the levels of IL-10 [11]. Moreover, the regulation of cytokines by RvD1 involves an increase in IκBα expression, suggesting reduced NF-κB activation in the lung [38]. It is well known that the activation of NF-κB is regulated mainly by its subcellular localization, which is determined by the level of expression and the nucleocytoplasmic distribution of the IκB proteins [39]. Although there are a number of IκB proteins, IκBα is the main regulator of NF-κB activation, through

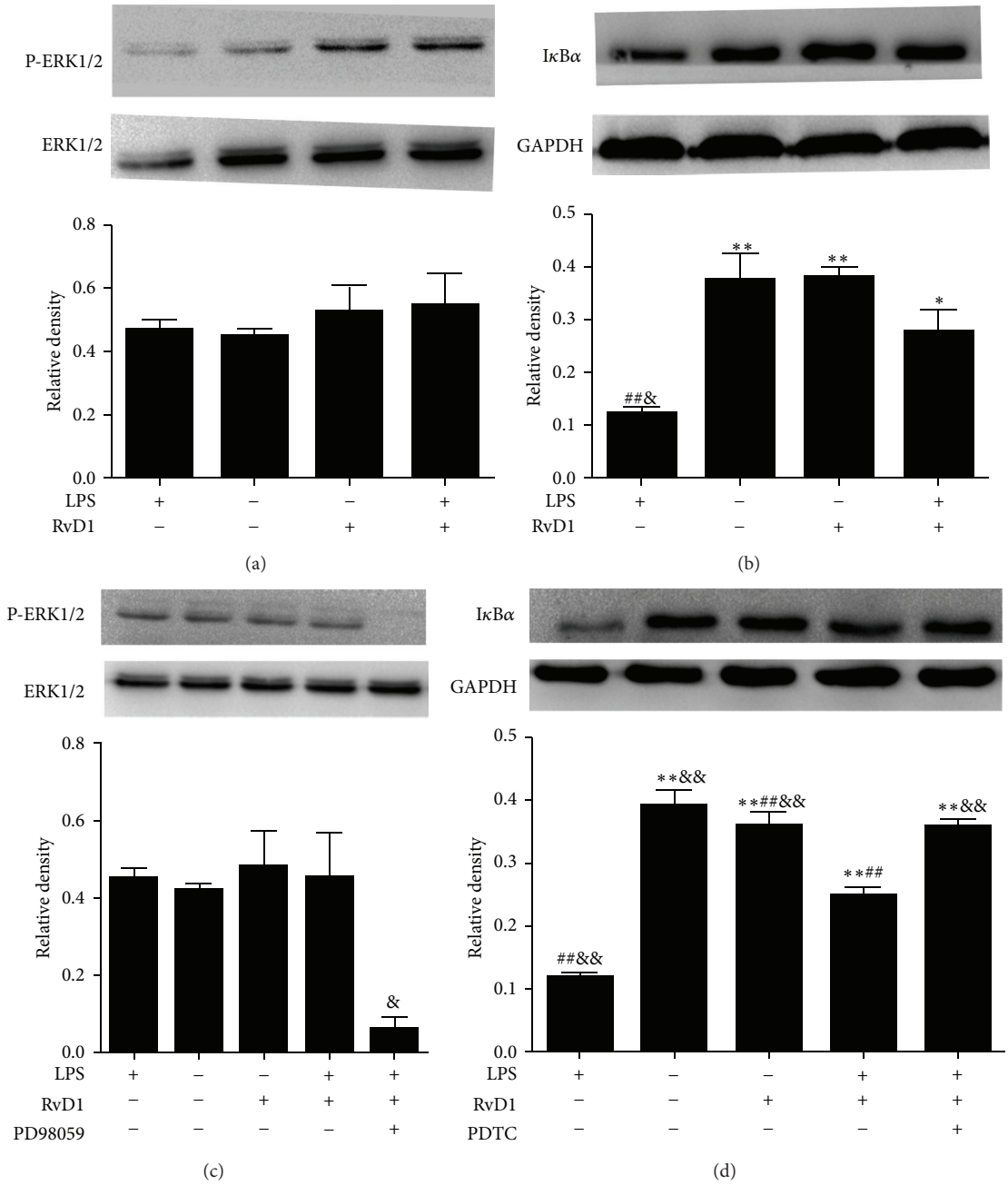

Figure 3: Effects of RvD1 and LPS on the ERK1/2 and IκBα signaling pathways in HUVECs. (a) Effect of RvD1 and LPS on ERK1/2 phosphorylation. (b) Effect of RvD1 and LPS on IκBα protein expression. (c) Effect of ERK inhibitor PD98059 on ERK1/2 phosphorylation in RvD1 + LPS group. (d) Effect of NF-κB inhibitor PDTC on IκBα protein expression in RvD1 + LPS group. Densitometric analysis of the protein levels of zo-1 and occludin were shown ($n = 3$). Data were expressed as mean ± s.e.m. $^{**}P < 0.01$, $^{*}P < 0.05$ versus LPS; $^{\#\#}P < 0.01$ versus control; $^{\&\&}P < 0.01$, $^{\&}P < 0.05$ versus LPS + RvD1.

a mechanism involving IκBα degradation. LPS binds to Toll-like receptor 4 (TLR4) to activate NF-κB and thus induces the transcription of proinflammatory mediators, leading to endothelial hyperpermeability [40, 41]. The activation of NF-κB can inhibit the expression of TJ proteins [42]. Previous studies show that the absence of IκBα increased NF-κB activity after stimulation with LPS [43]. We therefore speculated that RvD1 might increase the expression of IκBα, causing an increase in TJ protein expression. Our results showed that LPS reduced the expression of IκBα, which was consistent with the report [44]. Importantly, when we pretreated cells with RvD1 before LPS stimulation, the expression of IκBα was enhanced. The NF-κB inhibitor PDTC further enhanced the protective effect of RvD1 on restoration of occludin but not zo-1 expression in LPS-stimulated HUVECs. From the above results, we concluded that RvD1 inhibited the LPS-induced

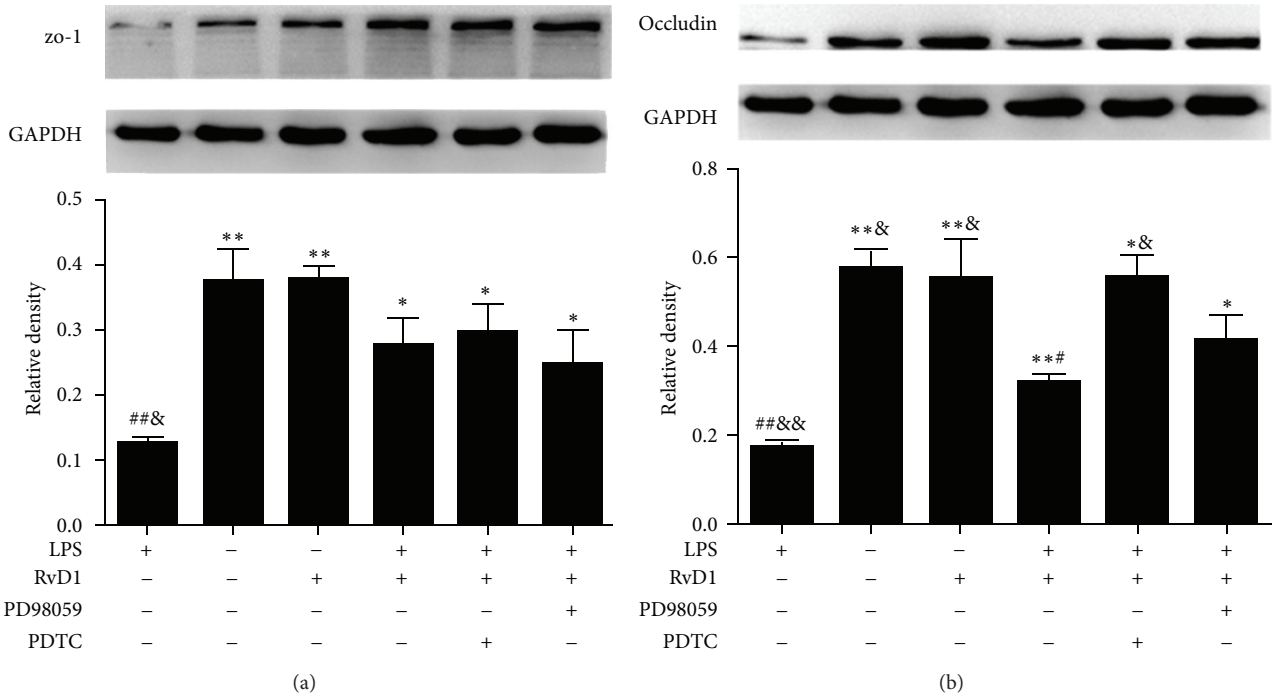

Figure 4: Effects of ERK1/2 and NF-κB inhibitors on the expression of zo-1 and occludin in HUVECs. The protein expression of zo-1 (a) and occludin (b) were detected by western blotting. Densitometric analysis of the protein levels of zo-1 and occludin were shown ($n = 3$). Data was expressed as mean ± s.e.m. $^{**}P < 0.01$, $^{*}P < 0.05$ versus LPS group; $^{\#\#}P < 0.01$, $^{\#}P < 0.05$ versus control group; $^{\&\&}P < 0.01$, $^{\&}P < 0.05$ versus RvD1 + LPS group.

redistribution of occludin and enhanced its expression in endothelial cells via a mechanism that partly involved the IκBα pathway. However, RvD1 did not affect zo-1 through the IκBα pathway, and the mechanism remains to be explored.

As an important regulator in signal transduction pathway, MAPK extracellular signal-regulated kinase (ERK) 1/2 (p44/p42, resp.) can activate many cell types during inflammation [45]. Treatment with LPS results in the loss of TJ integrity and an increase in paracellular permeability in corneal and alveolar epithelial monolayers [46, 47]. The activation of ERK1/2 is also found to be associated with TJ disruption through an H_2O_2-induced endothelial cell monolayer [13]. LPS treatment induces the disruption of epithelial barrier function in epithelial cells through a mechanism involving ERK1/2 phosphorylation [48] and induces the redistribution of occludin and zo-1 from intercellular junctions [18]. Interestingly, pretreatment of cells with RvD1 inhibits the activation of ERK1/2 and IκB in the lung tissues of mice [12]. In view of these findings, we examined whether RvD1 could inhibit LPS-induced ERK1/2 activation and change endothelial permeability by protecting TJ integrity in endothelial cells and whether the changes in TJ protein expression could be reduced by inhibiting ERK1/2 activation. Unexpectedly, our studies showed that there were no differences in ERK1/2 phosphorylation in HUVECs between the experimental groups. In addition, the ERK1/2 inhibitor PD98059 had no effect on zo-1 and occludin protein expression in LPS-induced HUVECs. These results suggested that ERK1/2 signaling was not involved in the protective effect of RvD1 in LPS-induced redistribution of TJ proteins.

In summary, our findings revealed that RvD1 protected against endothelial barrier dysfunction by increasing the proteins expression of occuludin and zo-1 in LPS-induced HUVECs and RvD1 did this via a mechanism that involved the activation of IκBα pathway but not ERK1/2 pathway. Notably, many inflammatory diseases involve changes in TJ protein expression and redistribution. All these were regarded as accelerating the course of inflammatory diseases, and research on tight junction proteins may thus become a new therapeutic strategy for inflammatory diseases.

Abbreviations

ERK: Extracellular-signal regulated kinase
HUVEC: Human umbilical vein endothelial cell
IBD: Inflammatory bowel disease
IFN-γ: Interferon gamma
MDCK: Madin-Darby canine kidney
IκB: Inhibitor of nuclear factor kappa B
MAPKs: Mitogen-activated protein kinases
RvD1: Resolvin D1
siRNA: Small interfering RNA
TJ: Tight junction
TNF-α: Tumor necrosis factor alpha.

Authors' Contribution

Xingcai Zhang and Tinting Wang contributed equally to this work.

Acknowledgment

This study was supported by a Grant from National Natural Science Foundation of China (nos. 81070060 and 30930089).

References

[1] S. M. Dudek and J. G. N. Garcia, "Cytoskeletal regulation of pulmonary vascular permeability," *Journal of Applied Physiology*, vol. 91, no. 4, pp. 1487–1500, 2001.

[2] H. Lum and A. B. Malik, "Mechanisms of increased endothelial permeability," *Canadian Journal of Physiology and Pharmacology*, vol. 74, no. 7, pp. 787–800, 1996.

[3] N. V. Bogatcheva and A. D. Verin, "Reprint of "The role of cytoskeleton in the regulation of vascular endothelial barrier function" [Microvascular Research 76 (2008) 202–207]," *Microvascular Research*, vol. 77, no. 1, pp. 64–69, 2009.

[4] K. Matter and M. S. Balda, "Signalling to and from tight junctions," *Nature Reviews Molecular Cell Biology*, vol. 4, no. 3, pp. 225–236, 2003.

[5] C. M. van Itallie, A. S. Fanning, A. Bridges, and J. M. Anderson, "ZO-1 stabilizes the tight junction solute barrier through coupling to the perijunctional cytoskeleton," *Molecular Biology of the Cell*, vol. 20, no. 17, pp. 3930–3940, 2009.

[6] A. S. Fanning and J. M. Anderson, "Zonula occludens-1 and -2 are cytosolic scaffolds that regulate the assembly of cellular junctions," *Annals of the New York Academy of Sciences*, vol. 1165, pp. 113–120, 2009.

[7] K. Hamada, Y. Shitara, S. Sekine, and T. Horie, "Zonula Occludens-1 alterations and enhanced intestinal permeability in methotrexate-treated rats," *Cancer Chemotherapy and Pharmacology*, vol. 66, no. 6, pp. 1031–1038, 2010.

[8] N. S. Harhaj and D. A. Antonetti, "Regulation of tight junctions and loss of barrier function in pathophysiology," *International Journal of Biochemistry and Cell Biology*, vol. 36, no. 7, pp. 1206–1237, 2004.

[9] S. Hong, K. Gronert, P. R. Devchand, R.-L. Moussignac, and C. N. Serhan, "Novel docosatrienes and 17S-resolvins generated from docosahexaenoic acid in murine brain, human blood, and glial cells: autacoids in anti-inflammation," *Journal of Biological Chemistry*, vol. 278, no. 17, pp. 14677–14687, 2003.

[10] C. N. Serhan, S. Hong, K. Gronert et al., "Resolvins: a family of bioactive products of omega-3 fatty acid transformation circuits initiated by aspirin treatment that counter proinflammation signals," *Journal of Experimental Medicine*, vol. 196, no. 8, pp. 1025–1037, 2002.

[11] N. Chiang, G. Fredman, F. Bäckhed et al., "Infection regulates pro-resolving mediators that lower antibiotic requirements," *Nature*, vol. 484, no. 7395, pp. 524–528, 2012.

[12] B. Wang, X. Gong, J.-Y. Wan et al., "Resolvin D1 protects mice from LPS-induced acute lung injury," *Pulmonary Pharmacology and Therapeutics*, vol. 24, no. 4, pp. 434–441, 2011.

[13] C. G. Kevil, T. Oshima, B. Alexander, L. L. Coe, and J. S. Alexander, "H_2O_2-mediated permeability: role of MAPK and occludin," *The American Journal of Physiology—Cell Physiology*, vol. 279, no. 1, pp. C21–C30, 2000.

[14] D. Li and R. J. Mrsny, "Oncogenic Raf-1 disrupts epithelial tight junctions via downregulation of occludin," *Journal of Cell Biology*, vol. 148, no. 4, pp. 791–800, 2000.

[15] A. Recchiuti, S. Krishnamoorthy, G. Fredman, N. Chiang, and C. N. Serhan, "MicroRNAs in resolution of acute inflammation: identification of novel resolvin D1-miRNA circuits," *The FASEB Journal*, vol. 25, no. 2, pp. 544–560, 2011.

[16] T. H. Kim and J.-S. Bae, "Ecklonia cava extracts inhibit lipopolysaccharide induced inflammatory responses in human endothelial cells," *Food and Chemical Toxicology*, vol. 48, no. 6, pp. 1682–1687, 2010.

[17] A. C. Chin, A. N. Flynn, J. P. Fedwick, and A. G. Buret, "The role of caspase-3 in lipopolysaccharide-mediated disruption of intestinal epithelial tight junctions," *Canadian Journal of Physiology and Pharmacology*, vol. 84, no. 10, pp. 1043–1050, 2006.

[18] P. Sheth, N. Delos Santos, A. Seth, N. F. LaRusso, and R. K. Rao, "Lipopolysaccharide disrupts tight junctions in cholangiocyte monolayers by a c-Src-, TLR_4-, and LBP-dependent mechanism," *The American Journal of Physiology—Gastrointestinal and Liver Physiology*, vol. 293, no. 1, pp. G308–G318, 2007.

[19] G. Fredman and C. N. Serhan, "Specialized proresolving mediator targets for RvE1 and RvD1 in peripheral blood and mechanisms of resolution," *Biochemical Journal*, vol. 437, no. 2, pp. 185–197, 2011.

[20] P. Kumar, Q. Shen, C. D. Pivetti, E. S. Lee, M. H. Wu, and S. Y. Yuan, "Molecular mechanisms of endothelial hyperpermeability: implications in inflammation," *Expert Reviews in Molecular Medicine*, vol. 11, article e19, 2009.

[21] A. E. Medvedev, K. M. Kopydlowski, and S. N. Vogel, "Inhibition of lipopolysaccharide-induced signal transduction in endotoxin-tolerized mouse macrophages: dysregulation of cytokine, chemokine, and Toll-like receptor 2 and 4 gene expression," *Journal of Immunology*, vol. 164, no. 11, pp. 5564–5574, 2000.

[22] R. Settimio, D. F. Clara, F. Franca, S. Francesca, and D. Michele, "Resolvin D1 reduces the immunoinflammatory response of the rat eye following uveitis," *Mediators of Inflammation*, vol. 2012, Article ID 318621, 9 pages, 2012.

[23] Y. Jin, M. Arita, Q. Zhang et al., "Anti-angiogenesis effect of the novel anti-inflammatory and pro-resolving lipid mediators," *Investigative Ophthalmology and Visual Science*, vol. 50, no. 10, pp. 4743–4752, 2009.

[24] G. P. van Nieuw Amerongen, C. M. L. Beckers, I. D. Achekar, S. Zeeman, R. J. P. Musters, and V. W. M. van Hinsbergh, "Involvement of Rho kinase in endothelial barrier maintenance," *Arteriosclerosis, Thrombosis, and Vascular Biology*, vol. 27, no. 11, pp. 2332–2339, 2007.

[25] M. Furuse, T. Hirase, M. Itoh et al., "Occludin: a novel integral membrane protein localizing at tight junctions," *Journal of Cell Biology*, vol. 123, no. 6, pp. 1777–1788, 1993.

[26] R. Al-Sadi, K. Khatib, S. Guo, D. Ye, M. Youssef, and T. Ma, "Occludin regulates macromolecule flux across the intestinal epithelial tight junction barrier," *The American Journal of Physiology—Gastrointestinal and Liver Physiology*, vol. 300, no. 6, pp. G1054–G1064, 2011.

[27] B. T. Hawkins and T. P. Davis, "The blood-brain barrier/neurovascular unit in health and disease," *Pharmacological Reviews*, vol. 57, no. 2, pp. 173–185, 2005.

[28] A. S. L. Yu, K. M. McCarthy, S. A. Francis et al., "Knockdown of occludin expression leads to diverse phenotypic alterations in epithelial cells," *The American Journal of Physiology—Cell Physiology*, vol. 288, no. 6, pp. C1231–C1241, 2005.

[29] M. Saitou, K. Fujimoto, Y. Doi et al., "Occludin-deficient embryonic stem cells can differentiate into polarized epithelial cells bearing tight junctions," *Journal of Cell Biology*, vol. 141, no. 2, pp. 397–408, 1998.

[30] A. S. Fanning, B. J. Jameson, L. A. Jesaitis, and J. M. Anderson, "The tight junction protein ZO-1 establishes a link between the transmembrane protein occludin and the actin cytoskeleton," *Journal of Biological Chemistry*, vol. 273, no. 45, pp. 29745–29753, 1998.

[31] H. A. Edens and C. A. Parkos, "Modulation of epithelial and endothelial paracellular permeability by leukocytes," *Advanced Drug Delivery Reviews*, vol. 41, no. 3, pp. 315–328, 2000.

[32] J.-D. Schulzke and M. Fromm, "Tight junctions: molecular structure meets function," *Annals of the New York Academy of Sciences*, vol. 1165, pp. 1–6, 2009.

[33] S. Krishnamoorthy, A. Recchiuti, N. Chiang et al., "Resolvin D1 binds human phagocytes with evidence for proresolving receptors," *Proceedings of the National Academy of Sciences of the United States of America*, vol. 107, no. 4, pp. 1660–1665, 2010.

[34] P. Fu, A. A. Birukova, J. Xing et al., "Amifostine reduces lung vascular permeability via suppression of inflammatory signalling," *European Respiratory Journal*, vol. 33, no. 3, pp. 612–624, 2009.

[35] M. Ahdieh, T. Vandenbos, and A. Youakim, "Lung epithelial barrier function and wound healing are decreased by IL-4 and IL-13 and enhanced by IFN-γ," *The American Journal of Physiology—Cell Physiology*, vol. 281, no. 6, pp. C2029–C2038, 2001.

[36] T. Oshima, F. S. Laroux, L. L. Coe et al., "Interferon-gamma and interleukin-10 reciprocally regulate endothelial junction integrity and barrier function," *Microvascular Research*, vol. 61, pp. 130–143, 2001.

[37] A. Youakim and M. Ahdieh, "Interferon-γ decreases barrier function in T84 cells by reducing ZO-1 levels and disrupting apical actin," *The American Journal of Physiology—Gastrointestinal and Liver Physiology*, vol. 276, no. 5, pp. G1279–G1288, 1999.

[38] B. D. Levy, "Resolvin D1 and resolvin E1 promote the resolution of allergic airway inflammation via shared and distinct molecular counter-regulatory pathways," *Frontiers in Immunology*, vol. 3, article 390, 2012.

[39] P. A. Baeuerle and D. Baltimore, "Nf-κB: ten years after," *Cell*, vol. 87, no. 1, pp. 13–20, 1996.

[40] S.-Q. Wu and W. C. Aird, "Thrombin, TNF-α, and LPS exert overlapping but nonidentical effects on gene expression in endothelial cells and vascular smooth muscle cells," *The American Journal of Physiology—Heart and Circulatory Physiology*, vol. 289, no. 2, pp. H873–H885, 2005.

[41] S. M. Opal, "The host response to endotoxin, antilipopolysaccharide strategies, and the management of severe sepsis," *International Journal of Medical Microbiology*, vol. 297, no. 5, pp. 365–377, 2007.

[42] T. Y. Ma, G. K. Iwamoto, N. T. Hoa et al., "TNF-α-induced increase in intestinal epithelial tight junction permeability requires NF-κB activation," *The American Journal of Physiology—Gastrointestinal and Liver Physiology*, vol. 286, no. 3, pp. G367–G376, 2004.

[43] S. Gerondakis, R. Grumont, R. Gugasyan et al., "Unravelling the complexities of the NF-κB signalling pathway using mouse knockout and transgenic models," *Oncogene*, vol. 25, no. 51, pp. 6781–6799, 2006.

[44] C. C. Taggart, C. M. Greene, N. G. McElvaney, and S. O'Neill, "Secretory leucoprotease inhibitor prevents lipopolysaccharide-induced IκBα degradation without affecting phosphorylation or ubiquitination," *Journal of Biological Chemistry*, vol. 277, no. 37, pp. 33648–33653, 2002.

[45] J. M. Kyriakis and J. Avruch, "Mammalian mitogen-activated protein kinase signal transduction pathways activated by stress and inflammation," *Physiological Reviews*, vol. 81, no. 2, pp. 807–869, 2001.

[46] X.-J. Yi, Y. Wang, and F.-S. X. Yu, "Corneal epithelial tight junctions and their response to lipopolysaccharide challenge," *Investigative Ophthalmology and Visual Science*, vol. 41, no. 13, pp. 4093–4100, 2000.

[47] H. Eutamene, V. Theodorou, F. Schmidlin et al., "LPS-induced lung inflammation is linked to increased epithelial permeability: role of MLCK," *European Respiratory Journal*, vol. 25, no. 5, pp. 789–796, 2005.

[48] V. B. Serikov, H. Choi, K. Schmiel et al., "Endotoxin induces leukocyte transmigration and changes in permeability of the airway epithelium via protein-kinase C and extracellular regulated kinase activation," *Journal of Endotoxin Research*, vol. 10, no. 1, pp. 55–65, 2004.

Hindawi Publishing Corporation
Oxidative Medicine and Cellular Longevity
Volume 2013, Article ID 859056, 9 pages
http://dx.doi.org/10.1155/2013/859056

Research Article

Transient Limb Ischemia Alters Serum Protein Expression in Healthy Volunteers: Complement C3 and Vitronectin May Be Involved in Organ Protection Induced by Remote Ischemic Preconditioning

Ting Pang,[1] Yang Zhao,[1] Nan-Rong Zhang,[1] San-Qing Jin,[1] and San-Qiang Pan[2]

[1] *Department of Anesthesiology, The Sixth Affiliated Hospital, Sun Yat-sen University, No. 26 Yuancunerheng Road, Guangzhou 510655, China*
[2] *Department of Anatomy, Medical College of Jinan University, No. 601 West Huangpu Avenue, Guangzhou 510632, China*

Correspondence should be addressed to San-Qing Jin; sanqingjin@hotmail.com and San-Qiang Pan; tpsq@jnu.edu.cn

Received 5 September 2013; Accepted 30 September 2013

Academic Editor: Zhengyuan Xia

The protective mechanism underlying remote ischemic preconditioning (RIPC) is unclear. This study aims to verify whether the protein expression profile in the serum could be altered by RIPC and to detect potential protein mediators. Transient limb ischemia consisting of three cycles of 5-min ischemia followed by 5-min reperfusion was performed on sixty healthy volunteers. Serum samples were collected at 30 min before transient limb ischemia and at 1 hour (h), 3 h, 8 h, 24 h, and 48 h after completion of three cycles. Changes in the serum protein profile were analyzed by two-dimensional gel electrophoresis and proteins were identified by MALDI-TOF/TOF mass spectrometry. Fourteen differentially expressed proteins were identified and, respectively, involved in immune system, lipid binding and metabolism, apoptosis, and blood coagulation. Complement C3, vitronectin, and apolipoprotein A-I were further confirmed by western blotting, and the results showed that their contents decreased significantly after transient limb ischemia. It is concluded that transient limb ischemia alters the serum protein expression profile in human being, and that reduction of serum contents of complement C3 and vitronectin may represent an important part of the mechanism whereby RIPC confers its protection.

1. Introduction

Ischemic preconditioning (IPC), induced by exposing tissues to transient nonfetal ischemia prior to a prolonged ischemic insult [1], has been proved as a powerful strategy to attenuate ischemia reperfusion (IR) injury. This concept has been developed into remote ischemia preconditioning (RIPC), whereby transient tissue ischemia in one region or organ leads to subsequent protection in distant tissues or organs subjected to potentially lethal ischemia. Przyklenk and colleagues first showed that brief episodes of ischemia of the circumflex artery protect remote myocardium from subsequent sustained left anterior descending artery occlusion in the dog heart [2]. Furthermore, Kharbanda and colleagues conducted a clinical trial in humans and showed that contralateral forearm ischemic preconditioning induced by three cycles of arm ischemia and reperfusion is associated with diminished IR-induced endothelial injury [3]. From then on, this particular protocol has been shown to attenuate myocardial injury in patients with coronary heart disease [4–7]. Additionally, RIPC has been shown to have an early and late phase of protection [8].

However, the mechanism through which the protective signal is conveyed from the preconditioned limb to the remote organs is unclear, although the neural pathway [8], the humoral pathway [9], and systemic protective response have been proposed. The humoral pathway was suggested by the following studies. Dickson and colleagues showed that coronary effluent obtained from donor hearts subjected to brief preconditioning ischemia could reduce the infarct

Table 1: Healthy volunteers' characteristics*.

Age (years)	22 (1.8)
Male	30 (50%)
Mean arterial pressure (mmHg)	85 (9)
Pulse (bmp†)	75 (12)
Pulse oxygen saturation (%)	99 (1)
Body mass index (Kg/m^2)	20.49 (2.30)

*Data are mean (SD) or counted number (%).
†bmp: beats per minute.

size in isolated buffer-perfused rabbit hearts [10]. A recent study by Shimizu and co-workers demonstrated that transient limb ischemia released unknown circulating factors which induced a potent protection against myocardial IR injury in Langendorff-perfused hearts and isolated cardiomyocytes in the same species, and this cardioprotection was transferable across species [11]. Our recent study found that the transfusion of plasma collected at late phase of RIPC into homogenic rats could improve the systolic blood pressure recovery during the reperfusion, suggesting that cardioprotective effect of transient limb ischemia was transferable via the plasma [12]. Experimental studies have attempted to identify humoral factors. Using proteomic methods, Lang and colleagues failed to identify a humoral mediator with a molecular weight of more than 8 kDa in rats subjected to remote ischemic preconditioning [13]. Serejo and colleagues speculated that thermolabile hydrophobic substances with molecular weights more than 3.5 kDa were cardioprotective factors in the effluent from preconditioned rat hearts [14]. However, most of the prior studies were performed on animals where circulating substances might vary with species and humoral mediators remained unknown.

We designed and conducted this study to investigate whether serum proteins could be altered by transient limb ischemia in human beings and to explore whether there existed any potential protein mediators in the serum that facilitate the protection induced by RIPC. In this study, transient limb ischemia was conducted in healthy volunteers and the approach of comparative proteomics was applied to identify serum proteins before and after transient limb ischemia. Proteins whose expressions were altered after transient limb ischemia were further studied and some of these proteins were validated by western blotting.

2. Materials and Methods

2.1. Subjects. We recruited sixty healthy volunteers and obtained written informed consent from them. Volunteers' characteristics were shown in Table 1. The study protocol was approved by the Ethics Committee of the Sixth Affiliated Hospital of Sun Yat-Sen University.

2.2. Induction of Transient Limb Ischemia. Transient limb ischemia was achieved by three cycles of ischemia and reperfusion, and each cycle consisted of 5-min ischemia followed by 5-min reperfusion of the nondominant arm. Ischemia and reperfusion were induced by a 12 cm-wide blood pressure cuff placed on the nondominant upper arm inflated to 200 mmHg for 5 min and then deflated for 5 min.

2.3. Sample Collection. At 30 min before transient limb ischemia and at 1 h, 3 h, 8 h, 24 h, and 48 h, respectively, after the the completion of three cycles of transient limb ischemia, blood (10 mL) was collected from the contralateral arm into tubes and was processed according to a standard operating procedure. The tubes were labeled and transported to the laboratory on ice within 15 min. The blood was centrifuged at 2500 rpm at 4°C for 10 min. Serum samples of each volunteer at all the time points were then collected, aliquoted, and stored at −80°C. Each serum sample underwent only two freeze/thaw cycles during all the following experimental protocols.

2.4. Two-Dimensional Gel Electrophoresis (2-DE). Samples of 3 volunteers at all the time points were randomly selected from the samples of 60 volunteers to undergo the 2D-gel study. Each serum sample (1 mL) was processed by using reagents provided by the commercial ProteoMiner Protein Enrichment Kits (Bio-Rad) to decrease high-abundance proteins and to enrich low-abundance proteins. After enrichment, serum was purified by ReadyPrep 2D Cleanup Kit (Bio-Rad). Protein concentration was determined by the Bradford assay with the BSA standard (Bio-Rad).

A purified serum sample containing 150 μg protein was diluted into 182 μL with rehydration buffer (7 mol/L Urea, 2 mol/L Thiourea, 2% CHAPS, 1% DTT, and 0.2% Bio-lyte with pH 3–10) and then loaded to an 11-cm immobilized pH gradient (IPG) strip (Bio-Rad) followed by passive rehydration for 16 h. Isoelectric focusing (IEF) was performed at 250 V for 3 h followed by linear increase of 250–7000 V for 3 h, then at 8000 V for 7 h, and finally at 500 V for 30 min in the Bio-Rad PROTEAN IEF cell. IPG strips were equilibrated with reducing equilibration buffer (6 mol/L Urea, 50 mmol/L Tris-HCl pH 8.8, 20% (v/v) glycerol, 2% (w/v) SDS, and 2% (w/v) DTT) for 15 min followed by equilibration with an alkylating equilibration buffer (6 mol/L Urea, 50 mmol/L Tris-HCl pH 8.8, 20% (v/v) glycerol, 1% (w/v) SDS, and 2.5% (w/v) IAA) for 15 min. The strips were then placed in the well of 12% SDS-PAGE gels and sealed with 0.5% (w/v) agarose. Separation of the proteins in the second dimension was performed by 12% SDS polyacrylamide gel electrophoresis. The process began at 120 V for 30 min and continued at 150 V until tracking dye reached the bottom of the gel in a Protean Plus Dodeca cell (Bio-Rad). The gels were then fixed with the fixing solution (10% methanol plus 7% acetic acid in water) and stained with SYPRO-Ruby (Bio-Rad) for 16 h in the dark.

2.5. Protein Identification. Stained gels were scanned by densitometric scanning (Typhoon-9200, Amersham Company, Sweden) and the scanned images were exported into Image Master 2D Elite 5.0 software (Amersham Biosciences, Buckinghamshire, UK) for analysis. Differentially expressed protein spots in the gels, which were the spots expressed more than 1.5-fold differences in expression level as compared

Table 2: Differentially expressed proteins in sera after RIPC compared with that in sera before RIPC.

Spot[a]	Protein name	Accession number[b]	Protein MW (Da)	Protein PI[c]	Sequence coverage[d] (%)	Fold change[e]	Protein score[f]
(i)	*Immune system process*						
1	Complement component 4B	IPI00887154	192627.5	6.89	2	$\downarrow 1.95^{1\,h}$	158
2	Complement C1q subcomponent subunit B	IPI00477992	26704.5	8.83	22	$\downarrow 2.73^{3\,h}$	84
3	Complement C3	IPI00783987	187029.9	6.02	15	$\downarrow 2.23^{1\,h}$	121
4	C4b-binding protein alpha chain	IPI00021727	66989.4	7.15	9	$\downarrow 1.51^{1\,h}$	71
5	Ficolin-3	IPI00419744	31657.4	6.36	18	$\uparrow 1.52^{1\,h}$	107
6	Interalpha-trypsin inhibitor heavy chain H4	IPI00896419	103293	6.51	18	$\uparrow 2.51^{1\,h}$	97
7	Vitronectin	IPI00298971	54271.2	5.55	4	$\downarrow 1.52^{1\,h}$	70
(ii)	*Lipid metabolic process*						
8	Apolipoprotein A-I	IPI00021841	30758.9	5.56	25	$\downarrow 3.85^{1\,h}$	79
9	Apolipoprotein L1	IPI00514475	43946.9	5.6	28	$\uparrow 1.68^{1\,h}$	88
10	Apolipoprotein J	IPI00291262	52461	5.89	20	$\downarrow 1.74^{24\,h}$	219
(iii)	*Apoptosis*						
11	Desmoplakin	IPI00013933	331568.7	6.44	8	$\uparrow 1.62^{48\,h}$	67
12	Gelsolin	IPI00026314	85644.2	5.9	16	$\uparrow 2.21^{1\,h}$	131
(iv)	*Blood coagulation*						
13	Antithrombin-III	IPI00032179	52657.8	6.11	23	$\downarrow 2.01^{1\,h}$	180
14	Heparin cofactor 2	IPI00879573	57034.2	6.41	17	$\uparrow 2.32^{1\,h}$	64

[a]Spot number refers to Figure 1.
[b]Accession number from IPI (International Protein Index) database of matched proteins.
[c]PI refers to isoelectric point.
[d]Percent of number of observed amino acids in sequence length (%).
[e]"↓" means downregulation, and "↑" means upregulation. Superscripts such as "1 h" represented the time point when the fold change reached maximum. The fold change in the table was the maximum change among the different time points.
[f]Combined scores of all observed mass spectra matched to amino acid sequences used for protein identification.

with the samples before transient limb ischemia at any time point after transient limb ischemia, were excised. The excised spots were immediately washed in redistilled water and then washed in 50% (v/v) acetonitrile in 100 mmol/L amine carbonate and then digested with 20 μg/mL trypsin (Roche, Swiss). The extracted peptides were purified by ZipTip pipette tips with μ-C18 Resin (Millipore) and analyzed with tandem time-of-flight 4800 MALDI-TOF/TOF mass spectrometry (Applied Biosystems/MDS Sciex, Toronto, ON, Canada). Protein identification was performed by searching the MS/MS spectra against the international protein index (IPI) database, using a local MASCOT search engine (v2.1, Matrix, London, UK) on a global proteome server (v3.6, Applied Biosystems, Foster City, CA, USA). The database searches were performed using the following parameters: a maximum of 1 missed cleavage, variable modifications of methionine oxidation and cysteine carboxyamidomethylation, and precursor-ion mass tolerance of 0.2 allowed. *Homo sapiens* were selected as the search species. A protein identification was defined when its peptide had confidence interval value more than 95%.

2.6. Western Blotting. Based on their functional relevance and potential significance with regard to IR injury and organ protection, three proteins of complement C3, vitronectin, and apolipoprotein A-I (apoA-I) were selected to undergo western blotting. Original serum samples from all sixty volunteers were analyzed by western blotting to confirm expressions of the three proteins. Protein concentration was determined by the Bradford assay with the BSA standard (Bio-Rad), and then equal amounts of total protein (25 μg) were loaded on 10% PAGE gels with 5% stacking gels. The gels underwent electrophoresis at 60 V for 30 min and 100 V for the duration of the run in running buffer (25 mmol/L Tris, 192 mmol/L glycine). The proteins in the gels were then transferred to polyvinylidene difluoride (PVDF) membranes (Millipore) at 100 V for 100 min in ice-cold transferring buffer (25 mmol/L Tris, 192 mmol/L glycine, 20% (v/v) methanol). After that, PVDF membranes were treated by the MemCode Reversible Protein Stain Kit for PVDF membranes (Pierce, NY) to ensure successful transfer of proteins and to allow for accurate quantitation of protein load. The membranes were blocked in Tris Buffered Saline with Tween (TBS-T; 170 mmol/L NaCl, 50 mmol/L Tris, pH 7.4, 0.1% Tween) containing 5% nonfat milk for 1 h at room temperature. The membranes were then washed in TBS-T three times (15 min for each time) and incubated with antibodies for 10 h to 12 h at 4°C. The dilution ratio of the antibodies for target proteins was: complement C3 1 : 500 (Santa, sc-52629), vitronectin 1 : 500 (R&D, Clone 342603), and apoA-I 1 : 500 (Abcam, ab52945). Membranes were then washed three times (15 min for each time) in TBS-T. The secondary

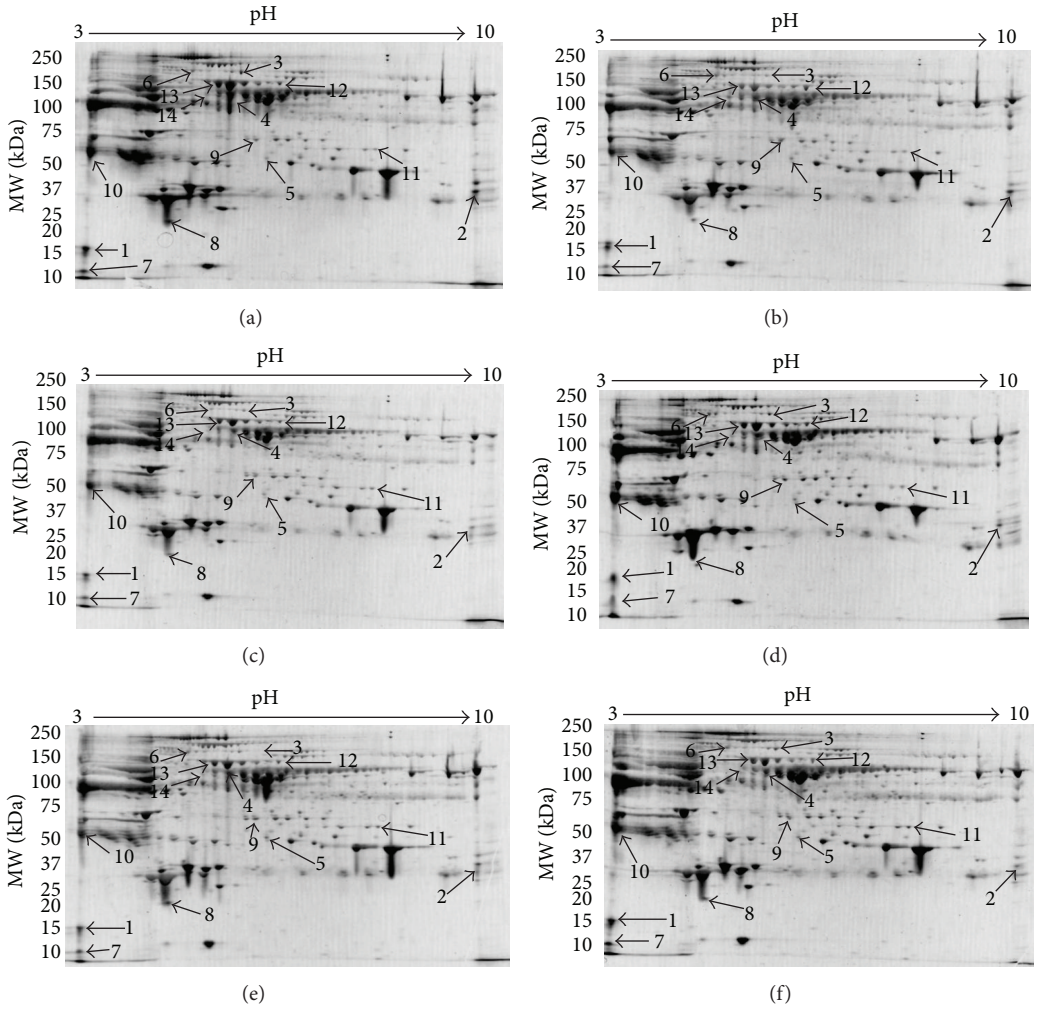

Figure 1: Representative images of SYPRO-Ruby-stained 2-DE gels. Representative images of SYPRO-Ruby-stained 2-DE gels at various time points ((a) before transient limb ischemia, (b) 1 h after transient limb ischemia, (c) 3 h after transient limb ischemia, (d) 8 h after transient limb ischemia, (e) 24 h after transient limb ischemia, and (f) 48 h after transient limb ischemia). The high-abundant proteins such as albumin and immunoglobulins were depleted from serum using the multiple-affinity column, as described in Section 2. Zoomed areas highlight typical spots (arrows) of the fourteen differentially expressed proteins. Changes in these spots' intensity among different time points are clearly visible. The spot numbers refer to proteins summarized in Table 2.

antibody for complement C3 and vitronectin was donkey anti-mouse IgG-HRP 1 : 2000 (Santa, sc-2318) and for apoA-I was donkey anti-rabbit IgG-HRP 1 : 2000 (Santa, sc-2317). Membranes were incubated with secondary antibody for 1 h at 26°C and then washed three times in TBS-T (15 min for each time). Protein blots in the membranes were visualized by enhanced chemiluminescence (ECL) and then exposed to X-ray films (Kodak, USA). Films were scanned into digital images. The primary densities of the band of complement C3, vitronectin at 75 kDa, vitronectin at 65 kDa, and apoA-I were measured by Quantity One 4.62 (Bio-Rad), respectively. Protein expression levels were presented as relative density. The primary band densities at each time point after transient limb ischemia were divided by the band densities before transient limb ischemia (base line) in the same gel. Then relative densities before transient limb ischemia (base) were 1 according to the normalization in all conditions.

2.7. Statistical Analysis. Quantitative data were analyzed with statistical package SPSS 16.0 (Chicago, IL). Data were presented as mean ± standard deviation of the mean. Repeated-measures analysis of variance (RMANOVA) was used for serial measurements. Statistical significances were evaluated at a two-tailed significance level of 0.05. This trial was registered with ClinicalTrials.gov, no. NCT01118000.

3. Results

3.1. Serum Proteomic Profile. Differentially expressed protein spots in the gels were identified as fourteen different proteins by MALDI-TOF/TOF mass spectrometry and database search (Figure 1). A typical MALDIMS spectrum and MS/MS map were shown in Figure 2. The fourteen identified proteins were classified based on gene ontology (GO) annotations (Table 2).

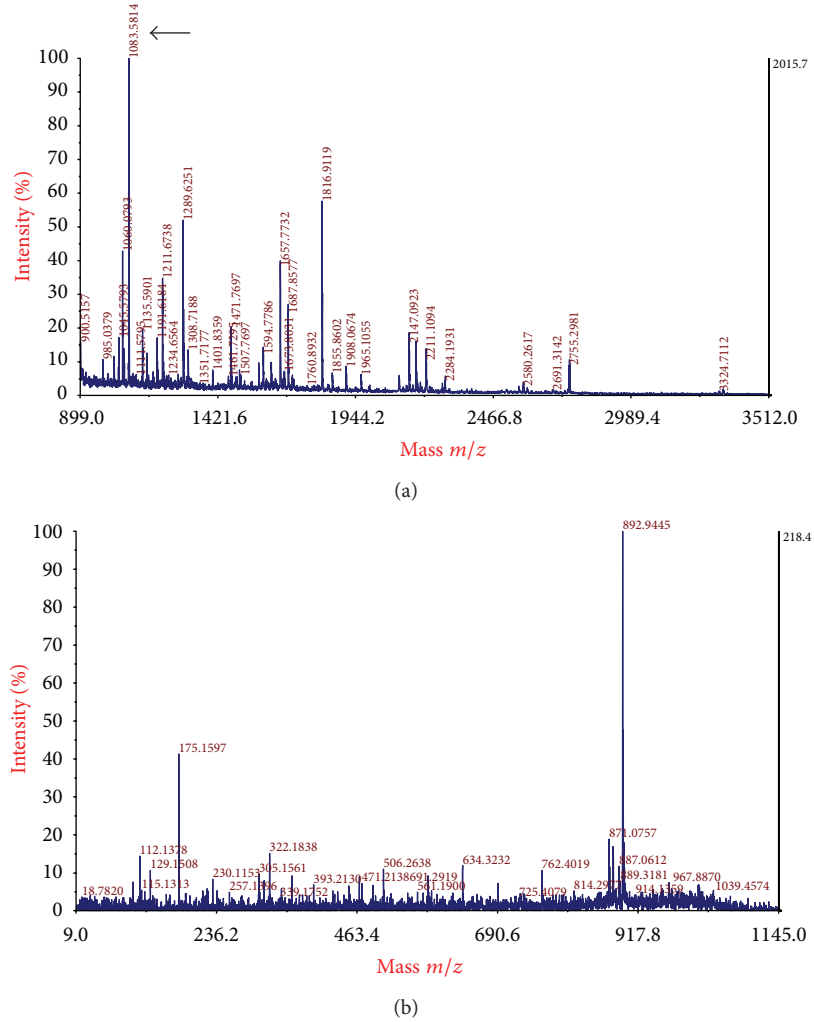

FIGURE 2: Peptide mass fingerprinting spectrum and a typical MS/MS map of complement C3. (a) Peptide mass fingerprinting spectrum of complement C3. The arrow indicates the peptide detected at m/z 1083.5814. (b) A typical MS/MS map of complement C3. The sequence of precursor at m/z 1083.5814 (arrow in (a)) was analyzed in this map.

Among these fourteen proteins, seven proteins were related to immune response processes, including complement component 4B, complement C1q subcomponent subunit B, complement C3, C4b-binding protein alpha chain and ficolin-3 in complement pathway, vitronectin in immune response, and interalpha-trypsin inhibitor heavy chain H4 in acute phase response. Among the altered proteins, ficolin-3 and interalpha-trypsin inhibitor heavy chain H4 were upregulated, while the other proteins were downregulated. Besides, three proteins involved in lipid metabolic process were affected, namely, apoA-I and apolipoprotein J downregulated and apolipoprotein L1 upregulated. These proteins were also related to immune response. Then, two proteins involved in cell apoptosis were all upregulated, including desmoplakin and gelsolin. Finally, two proteins related to blood coagulation were also affected, antithrombin-III downregulated, and heparin cofactor 2 upregulated.

3.2. Changes of Complement C3, Vitronectin, and ApoA-I Validated by Western Blotting Analysis. The contents of the three proteins (complement C3, vitronectin, and apoA-I) in the volunteers' sera ($n = 60$) were decreased after transient limb ischemia. The decrease was significant at most of the time points as compared with the values before transient limb ischemia (Figure 3).

Baseline relative density of complement C3 was defined as 1. The reduction of complement C3 was significant at 1 h (0.84 ± 0.37 at 1 h versus 1; $P = 0.002$), 3 h (0.86 ± 0.54 versus 1; $P = 0.049$), 8 h (0.76 ± 0.48 versus 1; $P = 0.000$), and 24 h (0.78 ± 0.49 versus 1; $P = 0.001$) after transient limb ischemia but not at 48 h (0.88 ± 0.62 versus 1; $P = 0.140$, Figure 3(b)) after transient limb ischemia.

Baseline relative density of vitronectin (75 KDa) was defined as 1. The reduction of vitronectin (75 KDa) was significant at 8 h (0.87 ± 0.36 at 8 h versus 1; $P = 0.013$), 24 h (0.83 ± 0.43 versus 1; $P = 0.004$), and 48 h (0.87 ± 0.40 versus 1; $P = 0.023$) after transient limb ischemia but not at 1 h (0.98 ± 0.24 versus 1; $P = 0.604$) and 3 h (0.96 ± 0.35 versus 1; $P = 0.409$; Figure 3(c)) after transient limb ischemia.

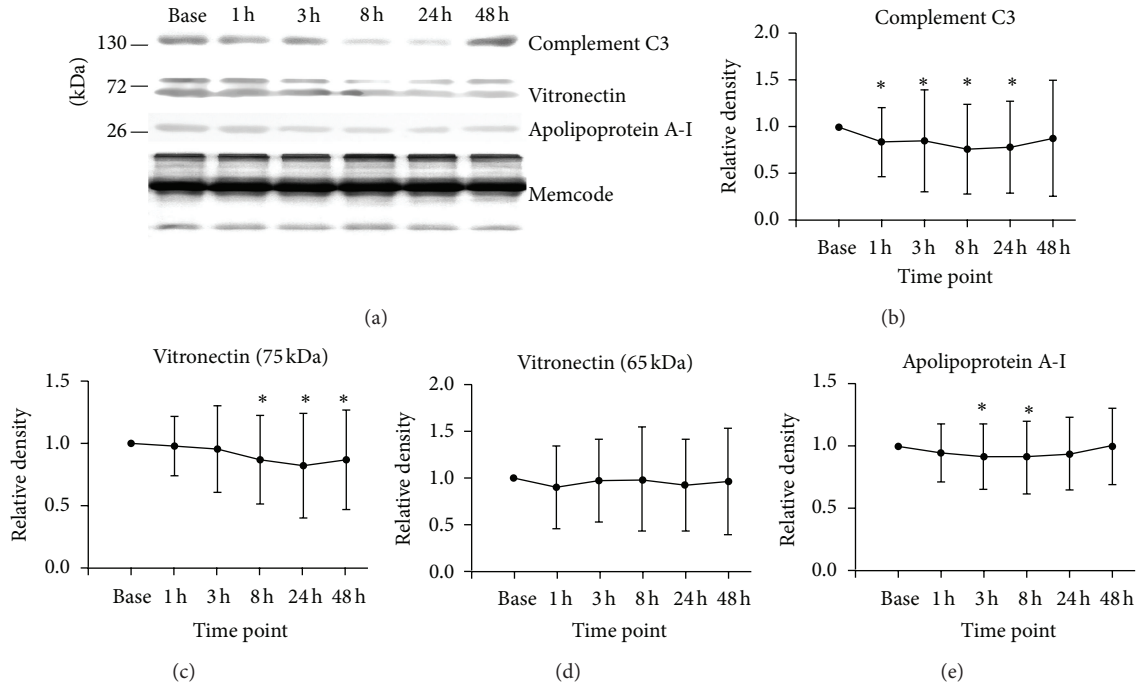

Figure 3: Western blotting data of complement C3, vitronectin, and apoA-I. The results were presented as mean ± SD. Error bars were SD. Repeated-measures analysis of variances was performed to evaluate statistical significance. $^{*}P < 0.05$. (a) Representative western blotting images of serum samples from healthy volunteers obtained prior to transient limb ischemia (base) and at various time points (1 h, 3 h, 8 h, 24 h, and 48 h) thereafter. Memcode was shown to demonstrate equal protein loading. (b) Changes in the expression of complement C3 after transient limb ischemia compared with that before transient limb ischemia ($n = 60$). (c) Changes in the expression of vitronectin at 75 kDa after transient limb ischemia compared with that before transient limb ischemia ($n = 60$). (d) Changes in the expression of vitronectin at 65 kDa after transient limb ischemia compared with that before transient limb ischemia ($n = 60$). (e) Changes in the expression of apoA-I after transient limb ischemia compared with that before transient limb ischemia ($n = 60$).

Baseline relative density of vitronectin (65 KDa) was defined as 1. The reduction of vitronectin (65 KDa) was not significant at 1 h (0.90 ± 0.44 versus 1; $P = 0.123$), 3 h (0.97 ± 0.44 versus 1; $P = 0.646$), 8 h (0.98 ± 0.56 versus 1; $P = 0.789$), 24 h (0.92 ± 0.49 versus 1; $P = 0.261$), and 48 h (0.96 ± 0.56 versus 1; $P = 0.646$) after transient limb ischemia (Figure 3(d)).

Baseline relative density of apoA-I was defined as 1. The reduction of apoA-I was significant at 3 h (0.92 ± 0.26 at 3 h versus 1; $P = 0.016$) and 8 h (0.91 ± 0.29 versus 1; $P = 0.026$) after transient limb ischemia but not at 1 h (0.95 ± 0.23 versus 1; $P = 0.119$), 24 h (0.94 ± 0.29 versus 1; $P = 0.11$) and 48 h (1.00 ± 0.30 versus 1; $P = 0.905$) after transient limb ischemia (Figure 3(e)).

4. Discussion

There were hardly any studies conducted amongst healthy volunteers in order to detect clinically relevant protein mediators that facilitate the protective effects of RIPC. Isolated buffer-perfused animal hearts in vitro and animal models in vivo have been extensively used for investigating the protective effect and mechanism of RIPC. Although these models have been shown to be reproducible and efficient, isolated hearts could not reflect the effects of nervous and circulatory system in the whole body, and animal disease models cannot represent the complex human clinical setting very well. Therefore, conducting a controlled human study is a crucial translational step from bench to bedside. A recent human study by Hepponstall et al. found that the RIPC stimulus modified the plasma protein content in blood, but this study enrolled only five healthy volunteers [15].

In this study, we compared serum proteins profiles after transient limb ischemia with that before transient limb ischemia in healthy volunteers by a proteomic approach and showed that there existed changes of serum proteins induced by transient limb ischemia. The changed proteins were mainly involved in the inflammatory system and also involved in the lipid metabolic system, cell apoptosis, and coagulation system.

In the 2-DE results of our study, we observed that complement component 4B, complement C1q subcomponent subunit B, C4b-binding protein alpha chain, and complement C3 were all decreased after transient limb ischemia.

Furthermore, we confirmed the changes of three proteins of complement C3, vitronectin (75 KDa), and apoA-I after transient limb ischemia by western blotting. The downregulation of complement C3 could persist for one day or perhaps even longer, the content of vitronectin (75 KDa) decreased significantly at 8 h, 24 h, and 48 h after transient limb ischemia, and the content of apoA-I decreased significantly at 3 h and 8 h after transient limb ischemia.

The pathway through which RIPC protects organs is unclear, but three possible mechanisms have been suggested [16]. The neural hypothesis proposed that the remote preconditioned organs could release endogenous substances such as adenosine [17], bradykinin [18], or calcitonin gene-related peptide [19] which activated afferent neural pathway terminating at the heart to confer myocardial protection. On the other hand, the humoral hypothesis thought that these released endogenous substances or some other humoral factors were carried to the heart in the blood stream and recognized specific receptors in the myocardium to activate intracellular pathways of myocardial protection. Finally, RIPC could suppress inflammation and apoptosis, which was called systemic protective response [20]. Our results showed the changes of serum proteins after transient limb ischemia and these proteins mainly involved in inflammatory response, which may support the second and third hypothesis above mentioned.

The complement cascade has been shown to be a key mediator of IR injury [21, 22]. Inhibition of the complement system can improve the outcome of IR injury [23, 24]. In a rabbit model, Tanhehco and co-workers observed that ischemic and chemical preconditioning inhibited the upregulation of complement C1q, C1r, C3, C8, and C9 mRNA expression and the complement C3 and membrane attack complex protein expression caused by IR injury both in vivo and in isolated heart in rabbits [25, 26].

Complement C3 is the central molecule of the complement system, at which the classical, lectin, and alternative pathways converge. Complement C3 is also associated with myocardial infarction, and it is more significant than any other traditional risk factors [27]. We selected complement C3 for further validation by western blotting and showed that the complement C3 expression in human serum significantly decreased from 1 h to 24 h after transient limb ischemia. A study by Zheng and colleagues demonstrated that siRNA solution containing siRNAs targeting tumor necrosis factor α, complement C3, and Fas genes could decrease cardiac IR injury, protect cardiac function, and prolong graft survival in heart transplantation [28]. Mocco and co-workers used mice deficient in selected complement proteins (C1q, C3, and C5) to evaluate which complement subcomponents contribute to cerebral IR injury and demonstrated that only C3−/− mice experienced significant neuroprotection [29].

Vitronectin is a multifunctional glycoprotein present in plasma, extracellular matrix, and blood platelets. It is found in two molecular forms in human blood, which are a single chain (75 kDa) and a clipped form of two chains (65 and 10 kDa) [30]. In our study, we also observed the vitronectin fragment located at ~10 kDa by 2-DE and the vitronectin doublet located at 65~75 kDa by western blotting. Vitronectin has been implicated as a regulator of many diverse physiological processes [31]. Ekmekci and colleagues showed that plasma vitronectin levels in patients with coronary artery diseases were significantly increased and positively correlated with the extent of diseases [32]. Yamani and colleagues observed that myocardial ischemic injury after cardiac transplantation was associated with upregulation of vitronectin receptor (integrinαVβ3) [33]. Using data from a randomized, placebo-controlled trial of abciximab in patients undergoing percutaneous coronary intervention, Derer and co-workers found that serum concentration of vitronectin was an independent risk factor for adverse cardiovascular events [34].

ApoA-I is the major protein of high-density lipoprotein. Besides its role in cholesterol metabolism, it possesses antiatherosclerotic, antioxidant, anti-inflammatory, and antithrombotic activities [35, 36]. A recent study by Shi and Wu showed that apoA-I reduced IR-induced inflammatory responses, decreased renal microscopic damage, and improved renal function [37]. Our results may implicate that apoA-I is not involved in the protective mechanism of RIPC.

This study was designed as a self-control study to confirm whether the composition of serum proteins was changed after transient limb ischemia in human beings. Time points for blood sample collection were selected in consideration of early and late phase of protection induced by RIPC. The early phase lasts for up to 3 h after ischemic preconditioning, whereas the late phase starts at 12–24 h after ischemic preconditioning [8]. Our study suggested that reduction of complement C3 and vitronectin expression may be involved in the mechanism by which preconditioning salvage tissues or organs subsequently subjected to IR, although they are likely to reflect changes induced by the preconditioning mediators. Further study is needed to find by which way these proteins are altered by transient limb ischemia and confirm whether these altered proteins actually protect organs.

It should be noted that it is very complicated to elucidate the mechanism of RIPC. Nevertheless, this study just finds some changes of serum proteins at limited time points which should serve to facilitate future extensive work aimed to elucidate the RIPC protective mechanism.

Conflict of Interests

All authors declared no conflicts of interests.

Authors' Contribution

Ting Pang, Yang Zhao, and Nan-Rong Zhang contributed equally to this study. San-Qing Jin and San-Qiang Pan designed the experiment, and San-Qing Jin supervised the whole process of the study and revised the paper draft. San-Qiang Pan helped analyzing the data. Ting Pang and Yang Zhao did the experiment (including sera collection, 2-DE, and western blotting), analyzed the data, and wrote the paper draft. Nan-Rong Zhang recruited volunteers and performed transient limb ischemia on volunteers. All authors have seen and approved the final version of this paper.

Acknowledgments

The authors thank the Natural Science Foundation from Department of Science and Technology of Guangdong province for its support (no. 07001664). The authors thank Hong-Bin Feng, Yan Zhou, and Dan Hu at Department of Anesthesiology in the Sixth Affiliated Hospital of Sun Yat-Sen

University for recruiting volunteers and collecting blood and Su-Mei Li and Hong-Hai Yuan at Department of Anatomy in Medical College of Jinan University for their assistance in western blotting and protein identification.

References

[1] C. E. Murry, R. B. Jennings, and K. A. Reimer, "Preconditioning with ischemia: a delay of lethal cell injury in ischemic myocardium," *Circulation*, vol. 74, no. 5, pp. 1124–1136, 1986.

[2] K. Przyklenk, B. Bauer, M. Ovize, R. A. Kloner, and P. Whittaker, "Regional ischemic 'preconditioning' protects remote virgin myocardium from subsequent sustained coronary occlusion," *Circulation*, vol. 87, no. 3, pp. 893–899, 1993.

[3] R. K. Kharbanda, U. M. Mortensen, P. A. White et al., "Transient limb ischemia induces remote ischemic preconditioning in vivo," *Circulation*, vol. 106, no. 23, pp. 2881–2883, 2002.

[4] D. J. Hausenloy, P. K. Mwamure, V. Venugopal et al., "Effect of remote ischaemic preconditioning on myocardial injury in patients undergoing coronary artery bypass graft surgery: a randomised controlled trial," *The Lancet*, vol. 370, no. 9587, pp. 575–579, 2007.

[5] S. P. Hoole, P. M. Heck, L. Sharples et al., "Cardiac remote ischemic preconditioning in coronary stenting (CRISP stent) study. A prospective, randomized control trial," *Circulation*, vol. 119, no. 6, pp. 820–827, 2009.

[6] I. Rentoukas, G. Giannopoulos, A. Kaoukis et al., "Cardioprotective role of remote ischemic periconditioning in primary percutaneous coronary intervention. enhancement by opioid action," *JACC: Cardiovascular Interventions*, vol. 3, no. 1, pp. 49–55, 2010.

[7] H. E. Bøtker, R. Kharbanda, M. R. Schmidt et al., "Remote ischaemic conditioning before hospital admission, as a complement to angioplasty, and effect on myocardial salvage in patients with acute myocardial infarction: a randomised trial," *The Lancet*, vol. 375, no. 9716, pp. 727–734, 2010.

[8] S. P. Loukogeorgakis, A. T. Panagiotidou, M. W. Broadhead, A. Donald, J. E. Deanfield, and R. J. MacAllister, "Remote ischemic preconditioning provides early and late protection against endothelial ischemia-reperfusion injury in humans: role of the autonomic nervous system," *Journal of the American College of Cardiology*, vol. 46, no. 3, pp. 450–456, 2005.

[9] E. W. Dickson, C. P. Reinhardt, F. P. Renzi, R. C. Becker, W. A. Porcaro, and S. O. Heard, "Ischemic preconditioning may be transferable via whole blood transfusion: preliminary evidence," *Journal of Thrombosis and Thrombolysis*, vol. 8, no. 2, pp. 123–129, 1999.

[10] E. W. Dickson, M. Lorbar, W. A. Porcaro et al., "Rabbit heart can be "preconditioned" via transfer of coronary effluent," *The American Journal of Physiology—Heart and Circulatory Physiology*, vol. 277, no. 6, pp. H2451–H2457, 1999.

[11] M. Shimizu, M. Tropak, R. J. Diaz et al., "Transient limb ischaemia remotely preconditions through a humoral mechanism acting directly on the myocardium: evidence suggesting cross-species protection," *Clinical Science*, vol. 117, no. 5, pp. 191–200, 2009.

[12] Y. Zhao, Z. N. Zheng, S. Q. Jin, and H. M. Liang, "Effects of plasma collected 48 hours after transient limb ischemia on blood pressure recovery in homogenic rats after myocardial ischemia reperfusion *in vivo*," *Chinese Medical Journal*, vol. 126, no. 15, pp. 2894–2899, 2013.

[13] S. C. Lang, A. Elsässer, C. Scheler et al., "Myocardial preconditioning and remote renal preconditioning—identifying a protective factor using proteomic methods?" *Basic Research in Cardiology*, vol. 101, no. 2, pp. 149–158, 2006.

[14] F. C. Serejo, L. F. Rodrigues Jr., K. C. da Silva Tavares, A. C. C. de Carvalho, and J. H. M. Nascimento, "Cardioprotective properties of humoral factors released from rat hearts subject to ischemic preconditioning," *Journal of Cardiovascular Pharmacology*, vol. 49, no. 4, pp. 214–220, 2007.

[15] M. Hepponstall, V. Ignjatovic, S. Binos et al., "Remote ischemic preconditioning (RIPC) modifies plasma proteome in humans," *PLoS ONE*, vol. 7, no. 11, Article ID e48284, 2012.

[16] D. J. Hausenloy and D. M. Yellon, "Remote ischaemic preconditioning: underlying mechanisms and clinical application," *Cardiovascular Research*, vol. 79, no. 3, pp. 377–386, 2008.

[17] T. J. Pell, G. F. Baxter, D. M. Yellon, and G. M. Drew, "Renal ischemia preconditions myocardium: role of adenosine receptors and ATP-sensitive potassium channels," *The American Journal of Physiology—Heart and Circulatory Physiology*, vol. 275, no. 5, pp. H1542–H1547, 1998.

[18] R. G. Schoemaker and C. L. van Heijningen, "Bradykinin mediates cardiac preconditioning at a distance," *The American Journal of Physiology—Heart and Circulatory Physiology*, vol. 278, no. 5, pp. H1571–H1576, 2000.

[19] Z. L. Tang, W. Dai, Y. J. Li, and H. W. Deng, "Involvement of capsaicin-sensitive sensory nerves in early and delayed cardioprotection induced by a brief ischaemia of the small intestine," *Naunyn-Schmiedeberg's Archives of Pharmacology*, vol. 359, pp. 243–247, 1999.

[20] I. E. Konstantinov, S. Arab, R. K. Kharbanda et al., "The remote ischemic preconditioning stimulus modifies inflammatory gene expression in humans," *Physiological Genomics*, vol. 19, pp. 143–150, 2005.

[21] M. Ikai, M. Itoh, T. Joh, Y. Yokoyama, N. Okada, and H. Okada, "Complement plays an essential role in shock following intestinal ischaemia in rats," *Clinical and Experimental Immunology*, vol. 106, no. 1, pp. 156–159, 1996.

[22] M. Pemberton, G. L. Anderson, V. Vetvicka, D. E. Justus, and G. D. Ross, "Microvascular effects of complement blockade with soluble recombinant CR1 on ischemia/reperfusion injury of skeletal muscle," *The Journal of Immunology*, vol. 150, no. 11, pp. 5104–5113, 1993.

[23] G. A. Toomayan, L. E. Chen, H. X. Jiang et al., "C1-esterase inhibitor and a novel peptide inhibitor improve contractile function in reperfused skeletal muscle," *Microsurgery*, vol. 23, no. 6, pp. 561–567, 2003.

[24] B. de Vries, R. A. Matthijsen, T. G. A. M. Wolfs, A. A. J. H. M. van Bijnen, P. Heeringa, and W. A. Buurman, "Inhibition of complement factor C5 protects against renal ischemia-reperfusion injury: inhibition of late apoptosis and inflammation," *Transplantation*, vol. 75, no. 3, pp. 375–382, 2003.

[25] E. J. Tanhehco, K. Yasojima, P. L. McGeer et al., "Preconditioning reduces tissue complement gene expression in the rabbit isolated heart," *The American Journal of Physiology—Heart and Circulatory Physiology*, vol. 277, no. 6, pp. H2373–H2380, 1999.

[26] E. J. Tanhehco, K. Yasojima, P. L. McGeer, E. G. McGeer, and B. R. Lucchesi, "Preconditioning reduces myocardial complement gene expression in vivo," *The American Journal of Physiology—Heart and Circulatory Physiology*, vol. 279, no. 3, pp. H1157–H1165, 2000.

[27] A. Muscari, G. Massarelli, L. Bastagli et al., "Relationship of serum C3 to fasting insulin, risk factors and previous ischaemic

events in middle-aged men," *European Heart Journal*, vol. 21, no. 13, pp. 1081–1090, 2000.

[28] X. Zheng, D. Lian, A. Wong et al., "Novel small interfering RNA-containing solution protecting donor organs in heart transplantation," *Circulation*, vol. 120, no. 12, pp. 1099–1107, 2009.

[29] J. Mocco, W. J. Mack, A. F. Ducruet et al., "Complement component C3 mediates inflammatory injury following focal cerebral ischemia," *Circulation Research*, vol. 99, no. 2, pp. 209–217, 2006.

[30] D. Seiffert and R. R. Schleef, "Two functionally distinct pools of vitronectin (Vn) in the blood circulation: Identification of a heparin-binding competent population of Vn within platelet α-granules," *Blood*, vol. 88, no. 2, pp. 552–560, 1996.

[31] P. Zhuang, M. N. Blackburn, and C. B. Peterson, "Characterization of the denaturation and renaturation of human plasma vitronectin I. Biophysical characterization of protein unfolding and multimerization," *Journal of Biological Chemistry*, vol. 271, no. 24, pp. 14323–14332, 1996.

[32] H. Ekmekci, H. Sonmez, O. B. Ekmekci, Z. Ozturk, N. Domanic, and E. Kokoglu, "Plasma vitronectin levels in patients with coronary atherosclerosis are increased and correlate with extent of disease," *Journal of Thrombosis and Thrombolysis*, vol. 14, no. 3, pp. 221–225, 2002.

[33] M. H. Yamani, E. M. Tuzcu, R. C. Starling et al., "Myocardial ischemic injury after heart transplantation is associated with upregulation of vitronectin receptor (α(v)β3), activation of the matrix metalloproteinase induction system, and subsequent development of coronary vasculopathy," *Circulation*, vol. 105, no. 16, pp. 1955–1961, 2002.

[34] W. Derer, E. S. Barnathan, E. Safak et al., "Vitronectin concentrations predict risk in patients undergoing coronary stenting," *Circulation: Cardiovascular Interventions*, vol. 2, no. 1, pp. 14–19, 2009.

[35] P. J. Barter, S. Nicholls, K. A. Rye, G. M. Anantharamaiah, M. Navab, and A. M. Fogelman, "Antiinflammatory properties of HDL," *Circulation Research*, vol. 95, no. 8, pp. 764–772, 2004.

[36] C. Mineo, H. Deguchi, J. H. Griffin, and P. W. Shaul, "Endothelial and antithrombotic actions of HDL," *Circulation Research*, vol. 98, no. 11, pp. 1352–1364, 2006.

[37] N. Shi and M. P. Wu, "Apolipoprotein A-I attenuates renal ischemia/reperfusion injury in rats," *Journal of Biomedical Science*, vol. 15, no. 5, pp. 577–583, 2008.

Hindawi Publishing Corporation
Oxidative Medicine and Cellular Longevity
Volume 2013, Article ID 943416, 6 pages
http://dx.doi.org/10.1155/2013/943416

Clinical Study

Aging Might Increase the Incidence of Infection from Permanent Pacemaker Implantation

Yun Lin,[1,2,3] Zhi Zhong Li,[1,2,3] Jingmei Zhang,[1,2,3] Jinrong Zhang,[1,2,3] Qian Fan,[1,2,3] and Jie Du[1,2,3]

[1] *Department of Cardiology, Beijing Anzhen Hospital, Capital Medical University, Beijing 100029, China*
[2] *The Key Laboratory of Remodeling-Related Cardiovascular Diseases, Capital Medical University, Ministry of Education, Beijing 100029, China*
[3] *Beijing Institute of Heart, Lung and Blood Vessel Disease, Beijing 100029, China*

Correspondence should be addressed to Qian Fan; fanqian75@sina.com and Jie Du; jiedubj@126.com

Received 9 August 2013; Accepted 24 September 2013

Academic Editor: Yanfang Chen

Aim. The elderly are the major population receiving the implantation of a permanent pacemaker (PPM). Infection is a devastating complication. The present study is to verify the relationship between age and PPM implantation infection. *Methods*. All patients (162 adult and 292 elder patients) received the implantation of PPM. Subcutaneous tissue samples solution was collected in three time points, the first sample was got at skin incision, and the second sample was got when the PPM had been implanted. And the third sample was got after 0.9% NaCl quick rinse. And the tissue solutions were cultured. If culture results are positive, it is considered as evidence of the presence of bacteria in pocket in operation of PPM implantation. *Results*. The data demonstrated that compared with that in the adult patients, subcutaneous bacterial survival rate was higher significantly in the elderly. *Staphylococcus epidermidis* is the major bacterial strain. The rinse decreased subcutaneous bacterial survival rates in the adult group. *Conclusion*. With the age increasing, PPM implantation might be easier to result in infection. Simple rinse can prevent implantation infection significantly. However, age alleviated the protective effects of rinse. Therefore, we should pay more attention to post implantation infection in the elderly.

1. Introduction

Implantation of a permanent pacemaker (PPM) has been widely accepted and implemented worldwide as the treatment of choice for bradyarrhythmias [1]. Infection in a PPM is a serious complication. It may occur either as a surgical site infection (SSI), occurring within 1 year after implantation, or as late-onset lead endocarditis. Pacemaker implantation rates are on the rise worldwide, and the population of patients living with a PM is growing [2].

Infection is a devastating complication of PPM/ICD use. Rates of infection after system placement have varied considerably, from 0.13% to 19.9%, and antimicrobial therapy alone (without removal of the entire system) is complicated by mortality and frequent infection relapse. Thus, the prevailing opinion is that the optimal management of PPM/ICD infection includes complete removal of the device and leads coupled with antimicrobial therapy. However, this treatment will result in serious hurt to patients [2, 3]. Therefore, the best treatment is to prevent infection instead of surgery and antimicrobial therapy after infection.

The elderly are the major population of PPM implantation [4]. The previous data demonstrated that aging exerted the vital effects on cardiovascular diseases [5, 6]. Then is aging an independent risk factor to PPM implantation? Does aging retard or promote infection after PPM implantation? As to the question, the results from prior studies were contradictory. Some studies indicated that infection rate increased with aging, or there is not a relationship between age and infection rate. Surprisingly, several researches got the inverse results, which demonstrated that infection tend's to occur in the adult [7].

Obviously, most PPM's were implanted in the elderly [4, 7]. Additionally, implantation-induced infection is the most serious complication of this kind of treatment [8, 9].

According to the above confusion, our study was designed to test the following points: (1) the relationship between age and the incidence of infection, (2) the technique to decrease the occurrence of PPM-induced infection, and (3) the effects of age on infection-depressed treatment. It had been well known that implantation infection depends on the bacteria number surviving in the implantation site. Therefore, in the present study, the tissue samples were got from the implantation site, and samples were cultured in vitro. The culture results were used as the markers to evaluate the possibility of infection occurrence.

2. Methods

The clinical trial was carried out in accordance with The Declaration of Helsinki (DoH) of the WMA [10]. The study protocol was approved by the Institutional Ethics Committee of the Beijing Anzhen Hospital-Affiliate of Capital Medical University. After full disclosure of the study's purpose, nature, and inherent risks of participation, all subjects gave written informed consent prior to enrollment.

2.1. Inclusion and Exclusion Criteria of PPM Implantation Patients. All patients who underwent PM (single or dual-chamber) implantation or reoperation with changes in hardware between March 2008 and March 2012 in Beijing Anzhen Hospital were included in the study. As shown in Figure 1, 454 patients were enrolled in the study. Inclusion criteria included (1) sick sinus syndrome (SSS), mean heart rate $\leqslant 40$ with significant clinical symptom; (2) third or second degree type 2 auriculoventricular block; (3) atrial fibrillation with 3 s RR interval and significant clinical symptom, or 5 s RR interval; (4) battery depletion; and (5) patients who signed the informed consent.

Exclusion criteria included (1) patients received antibiotic prior to PPM implantation within 72 h prior to implantation, (2) severe trauma, (3) hemorrhagic diseases, (4) tumor, (5) patients who received dialysis treatment, and (6) patients who received immunodepressant/hormone. According to the above criteria, as shown in Figure 1, 454 patients were enrolled in the study.

2.2. Data Collection Implantation Procedure. Demographic and clinical data were collected from the Beijing Anzhen Hospital medical records. The demographic data consisted of patient age, gender, residence, and payment types. Clinical variables of interest included evidence of presence of high blood pressure (HBP), diabetes, and coronary artery disease. In addition, patient diagnosis, PPM device type, number of implantation were recorded in the study.

The method of implantation was published elsewhere. In addition, antisepsis was performed immediately before surgery; the skin was painted with two solutions, successively: aqueous povidone iodine 10% solution followed by a povidone iodine 7.5% solution. Implantations were performed by the same operators (Yun Lin) under local anaesthesia and conscious sedation. Patients all received the same antibiotic prophylaxis. Clopidogrel therapy was systematically withdrawn 6 days before the implantation and treatment with vitamin K antagonists and heparin was discontinued at least 3 days and 6 h, respectively, before the implantation procedure. All patients had an international normalized ratio (INR) on the day of surgery.

All devices were implanted subcutaneously. Both procedure (skin to skin) and fluoroscopy time were systematically measured by a registered nurse.

2.3. Tissue Samples Collection and Bacterial Culture. Subcutaneous tissue samples solution was collected in three time points, the first sample was got at skin incision, and the second sample was got when the PPM had been implanted. And the third sample was got after saline rinse (0.9% NaCl quick rinse). With a sterile cotton swab dipped in a deep pocket of tissue fluid, cotton tip swab to ensure more than 75% area is infiltration. Within 30 minutes, samples were inoculated in broth. After enrichment, culture was inoculated in sheep blood agar and MacConkey agar to cultivate bacteria growth. The results were then used to determine the presence of bacteria, and for bacterial identification and drug susceptibility testing.

2.4. Saline Rinse and Tissue Solutions Bacterial Culture. In the previous study, we found that there were not significant differences among rinses of iodophors, antibiotic, and saline (30 mL within 2 s). However, the study also indicated, the rinses decreased the positive ratio of bacterial culture. In the present study, we collected the tissue solutions in the deep pockets (the third time point) and compared the positive ratio of bacterial culture between adult and elderly group.

2.5. Statistical Analysis. All values are presented as means ± SEM or ratio. Data were subjected to chi-square analysis and post-hoc Student's t, tests. All statistics were calculated utilizing Graphpad Prism 5.0. P values <0.05 were considered statistically significant.

3. Results

162 adult and 292 elderly PPM implantation patients were enrolled in the clinical trial. Of 454 patients, 12 adult and 21 elderly patients refused participation after enrollment, and 7 elderly patients discontinued participation due to severe situation during operation. Operators forgot to get the tissue solution from 9 adult and 8 old patients. In addition, the sample solutions from 10 adult and 10 old patients were polluted. As shown in Figure 1, data available were got from 131 adult and 262 old patients. Table 1 lists all demographic data, baseline statistics, cardiovascular risk profile, and implanted PPM characters. The major differences between the adult and elderly patient populations involved the incidence of high blood pressure, diabetes, and coronary artery disease.

3.1. Age Increased the Positive Ratio of Bacterial Culture. In the previous study, there is a significant positive relationship between the positive ratio of tissue solution bacterial culture and PPM infection. As shown in Table 2, gender, blood pressure, and coronary artery disease did not increase positive ratio of bacterial culture significantly. Diabetes mellitus

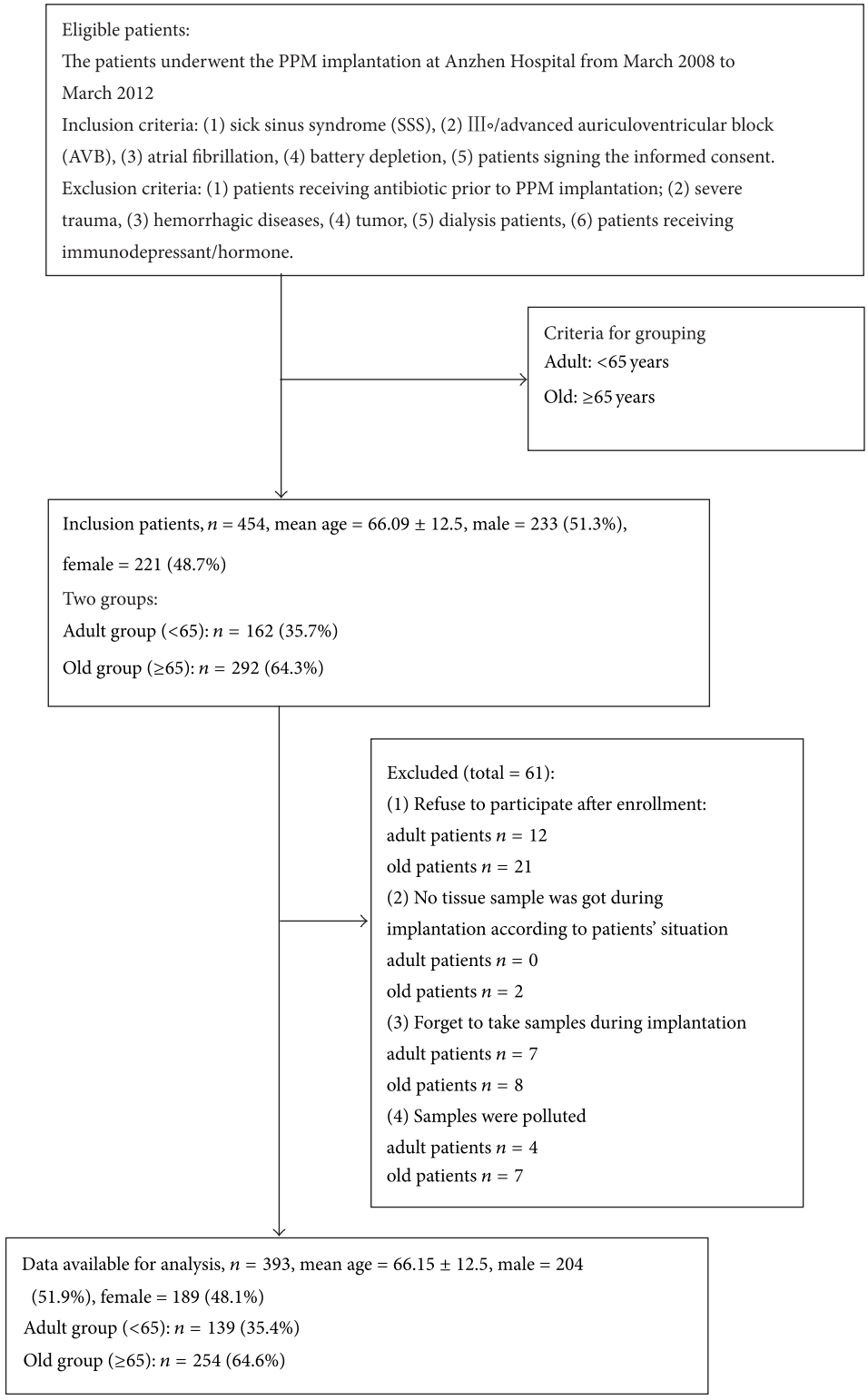

Figure 1

increased the positive ratio of bacterial culture at the first time point, which had been reported in the previous researches. Interestingly, in the present study, aging resulted in the increasing of positive ratio of bacterial culture significantly at two different time points (the fist and third time points). Compared with the past researches, the present study demonstrated that age might be an independent factor of PPM implantation infection. Furthermore, aging resulted in the significant increasing of infection rate after implantation surgery.

Table 1: Baseline characteristics of the study population (mean ± SEM).

	Adult group (n = 131)	Elderly group (n = 262)	χ^2	P
Age (year)	54.3 ± 10.6	73.2 ± 5.24		
Sex, M/F	72/67	137/125	0.046	0.830
Patients residence (Beijing/other places)	111/20	214/48	0.569	0.451
Nonhealth insurance/health insurance	23/108	53/209	0.400	0.527
HBP/total (n/total)	44/131	156/262	23.53	<0.0001
Diabetes (n/total)	18/131	63/262	5.668	0.017
Coronary artery disease (n/total)	22/131	73/262	5.837	0.016
Causes of PPM implantation				
Sick sinus syndrome (SSS)	63 (48.1%)	133 (50.7%)	2.966	0.0850
AVB (III∘/advanced)	34 (26.0%)	33 (12.6 %)	3.866	0.0493
Permanent atrial fibrillation with long RR interval	27 (20.6%)	47 (17.9 %)	0.04981	0.8234
Battery exhausted	15 (11.5%)	40 (15.3%)	1.834	0.1757
Pacemaker types				
Single chamber	30 (22.9%)	47 (17.9%)	1.365	0.243
Dual chamber	101 (77.1%)	215 (82.1%)		
Number of implant				
One	111 (84.7%)	206 (78.6%)		0.284*
≥2	20 (15.3%)	56 (21.4 %)		

HBP: high blood pressure; M: male; F: female.
*Exact probability.

Table 2: The relationship between five factors and positive ratio of sample bacterial culture.

Factors	The first sampling point			The second sampling point			The third sampling point		
	Positive number (positive ratio)	χ^2	P	Positive number (positive ratio)	χ^2	P	Positive number (positive ratio)	χ^2	P
Gender		1.031	0.310		1.157	0.561		0.852	0.356
Male: 204	21 (10.3)			28 (13.7)			18 (8.8)		
Female: 189	22 (11.6)			23 (12.2)			12 (6.3)		
Age		4.057	0.026*		0.501	0.778		4.060	0.045*
<65: 131	8 (7.6)			17 (13.0)			5 (3.8)		
≥65: 262	35 (12.6)			34 (13.0)			25 (9.3)		
BP		2.509	0.113			0.595		0.010	0.919
HBP: 200	26 (13.0)			25 (12.5)			15 (7.5)		
Normal BP: 193	17 (8.8)			26 (13.5)			15 (7.8)		
Blood glucose		0.690	0.408		12.593	0.002		0.309	0.578
Diabetes: 81	11 (13.6)			20 (24.7)			5 (6.2)		
Nondiabetes: 312	32 (10.3)			31 (9.9)			25 (8.0)		
CAD									
CAD: 95	10 (10.5)	0.473	0.492	12 (12.6)	0.330	0.846	9 (9.5)	0.602	0.438
Non-CAD: 298	33 (11.1)			39 (13.1)			21 (7.7)		

* P values <0.05 were considered statistically significant.

3.2. The Construction of Positive Strains in the Different Time Points. In the present study, we tried to investigate which strain is the major source of implantation infection. With the bacterial culture test, we analysed the construction of positive strains in the three different time points. The results were showed in Table 3; compared with the other strain, the most positive culture results were *Staphylococcus epidermidis* (84% in the first, 66.6% in the second, and 50% in the third time point). With the data, the major source of PPM infection might be *Staphylococcus epidermidis*.

Interestingly, within 25 *Staphylococcus epidermidis* positive patients, 4 patients were the adult and 21 patients were the elderly ($P < 0.0001$). Therefore, the old patients might be easier to be infected by *Staphylococcus epidermidis*.

3.3. Aging Alleviated the Protective Effects of Rinse Significantly. Both previous and present studies indicated that rinse might alleviate positive ratio of bacterial culture significantly. Surprisingly, in the present trial, we further found that the protective effects of rinse are significant, but no significant

Table 3: The construction of positive straines in the different time point.

Bacterial strain	The first sampling point		The second sampling point		The third sampling point	
	Positive number	Positive ratio	Positive number	Positive ratio	Positive number	Positive ratio
Staphylococcus epidermidis	36***	83.7	34***	66.7	15**	50.0
Staphylococcus capitis	4	9.3	8	15.7	2	6.7
Staphylococcus haemolyticus	1	2.3	3	5.9	0	0.0
Staphylococcus aureus	0	0	3	5.9	0	0.0
Staphylococcus hominis	0	0	2	3.8	6	20.0
Staphylococcus lentus	0	0	0	0.0	4	13.3
Staphylococcus intermedius	2	4.7	1	2.0	3	10.0
Total	43	100	51	100	30	100

** $P < 0.01$, *** $P < 0.001$ versus the other strain.

Table 4: Aging alleviated the protective effects of rinse.

	Prior to rinse		After rinse		χ^2	P
	Positive number	Positive ratio	Positive number	Positive ratio		
<65 ($n = 131$)	17	13.0	5	3.8	7.145	0.0075*
≥65 ($n = 262$)	34	13.0	25	9.5	1.547	0.2136

* $P < 0.05$ versus post-rinse.

Table 5: Diabetes does not affect the protective effects of rinse in elder patients.

	Prior to rinse		After rinse		χ^2	P
	Positive number	Positive ratio	Positive number	Positive ratio		
Diabetes ($n = 63$)	9	14.3	7	11.1	0.294	>0.05
Nondiabetes ($n = 199$)	25	12.6	18	9.0	1.283	>0.05

differences were found in the elderly between prior to and after rinse. In contrast, there was a significant difference in the adult patients between prior to and after rinse, and rinse alleviated positive ratio of bacterial culture significantly. The results were showed in Table 4. The result further confirms that age might be an independent risk factor to PPM-induced infection. Our further analysis of elderly patients found that the presence of diabetes did not affect the results after rinse. The results were showed in Table 5.

4. Discussion

PPMs are increasingly being used for the prevention and treatment of various cardiac rhythm disturbances. There were 13 million functioning PPMs worldwide in 2000, and the number of PPM placements has continued to increase. In the United States, there was a 42% increase (from 3.26 per 1000 to 4.64 per 1000) in the cardiac device implantation rate among medicare beneficiaries from 1990 to 1999. In China, to date, there is not an exact number to reflect the PPMs implantation rate [11, 12]. However, it is undoubted that PPMs implantation rate is growing greatly. One of the most feared complications of device placement is infection, which can be associated with substantial morbidity and mortality. Infection rates for these devices reportedly vary from 0.7% to 7.0% [8, 9, 11–13] with a resultant 3.1-fold increase in the number of associated hospitalizations in recent years [13, 14]. Mortality rates attributable to infection have ranged from 2.6% to 3.3% [13–16]. Although recent reports have identified several clinical characteristics associated with developing cardiac device-related infection (CDI), there are limited data on outcomes after treatment. Furthermore, most PPMs were implanted in the elderly. What are the clinical characteristics of PPMs infection in the elderly? It still remained unclear. Several novel observations have been made in the present study. Firstly, we found that there might be a significant positive relationship between age and incidence of PPMs-related infection with a clinical trial. More interestingly, the data indicated that rinse decreased the positive ratio of tissue solution culture; however, the effects only occur in the adult. In the elderly, the protective effects of rinse were alleviated significantly. To our knowledge, no similar results had been published.

The factor associated with the greatest increase in infectious risk in previous study was the occurrence of early noninfectious complication (haematoma, pacemaker dysfunction, and displacement of the intracavity lead), requiring reintervention. Klug et al. reported similar results in the PEOPLE study, and repeated procedures were also shown to increase risk of infection in the Danish registry as well as in a recent study of risk factors for device infection. However, to date, seldom researches are involved in the relationship between age and PPMs infection. Some documents indicated that there was not a significant relationship between age and postimplantation infection. Additionally, the research from Johansen et al. demonstrated an inverse relationship between increasing age and the risk of infection, with the rate of

infection being the highest in children and adolescents and declining with age. In present study, the data indicated that age resulted in the significant increasing of tissue culture infection rate. The exact reason that resulted in the above difference is kept unknown. But we found that the present study did not include children and adolescents. In addition, because of the higher cost of ICD and CRT, the implanting number in China is less than that in America/Europe. Therefore, the patients that received ICD/CRT treatments were excluded from the present study. Our finding indicated that age might be an independent risk factor on PMMs implantation infection.

Recently, lots of studies focused on the prevention of PPMs infection. For example, antibiotic is used prior to surgery, which resulted in the cost increasing. The previous works from our lab showed that simple rinse could decrease the infection rate significantly. Furthermore, no significant difference was found between antibiotic and saline rinse. Therefore, 30 mL saline quick rinse will exert an obvious protective effect on implantation-induced infection, which will not increase the cost of treatment. More interestingly, in the present study, we found that age exert is an negative effect on rinse treatment. Aging alleviated the protective effects of rinse.

Rapid growth of the world's geriatric population has heightened awareness of age-related cardiovascular diseases. The elderly are the major population of PPMs implantation. Infection is the most important complication of PPMs implantation. The present study demonstrated that there was the positive relationship between age and PPMs infection. Additionally, we found that saline rinse fail is to alleviate the occurrence of PPM-related infection. The study might be helpful to decrease postimplantation infection in clinical work.

Authors' Contribution

Yun Lin and Zhi Zhong Li contributed equally to this study.

Conflict of Interests

The authors declare that there is no conflict of interests regarding the publication of this paper.

References

[1] A. Catanchin, C. J. Murdock, and E. Athan, "Pacemaker infections: a 10-year experience," *Heart Lung and Circulation*, vol. 16, no. 6, pp. 434–439, 2007.

[2] F. Victor, C. de Place, C. Camus et al., "Pacemaker lead infection: echocardiographic features, management, and outcome," *Heart*, vol. 81, no. 1, pp. 82–87, 1999.

[3] J. G. Martinez, "Pacemaker pocket infection," *Pacing and Clinical Electrophysiology*, vol. 22, no. 4, part 1, pp. 691–692, 1999.

[4] B. Schmidt, M. Brunner, M. Olschewski et al., "Pacemaker therapy in very elderly patients: long-term survival and prognostic parameters," *American Heart Journal*, vol. 146, no. 5, pp. 908–913, 2003.

[5] Q. Fan, M. Chen, X. Fang et al., "Aging might augment reactive oxygen species (ROS) formation and affect reactive nitrogen species (RNS) level after myocardial ischemia/reperfusion in both humans and rats," *Age*, vol. 35, no. 4, pp. 1017–1026, 2012.

[6] M. Liu, P. Zhang, M. Chen et al., "Aging might increase myocardial ischemia / reperfusion-induced apoptosis in humans and rats," *Age*, vol. 34, no. 3, pp. 621–632, 2012.

[7] L. V. Armaganijan, W. D. Toff, J. C. Nielsen et al., "Are elderly patients at increased risk of complications following pacemaker implantation? A meta-analysis of randomized trials," *Pacing and Clinical Electrophysiology*, vol. 35, no. 2, pp. 131–134, 2012.

[8] K. L. Yew, "Infective endocarditis and the pacemaker: cardiac implantable electronic device infection," *The Medical Journal of Malaysia*, vol. 67, no. 6, pp. 618–619, 2012.

[9] E. A. Idelevich, C. A. Pogoda, B. Ballhausen et al., "Pacemaker lead infection and related bacteraemia caused by normal and small colony variant phenotypes of Bacillus licheniformis," *Journal of Medical Microbiology*, vol. 62, part 6, pp. 940–944, 2013.

[10] World Medical Association, "World Medical Association Declaration of Helsinki: ethical principles for medical research involving human subjects," *The Journal of American Medical Association*, 2013.

[11] Y. Hachiro, S. Kikuchi, M. Ito, K. Takahashi, and T. Abe, "Infection of a retained permanent epicardial pacemaker lead," *The Annals of Thoracic Surgery*, vol. 71, no. 6, pp. 2038–2039, 2001.

[12] M. Yamada, S. Takeuchi, Y. Shiojiri et al., "Surgical lead-preserving procedures for pacemaker pocket infection," *The Annals of Thoracic Surgery*, vol. 74, no. 5, pp. 1494–1499, 2002.

[13] A. J. Rastan, N. Doll, T. Walther, and F. W. Mohr, "Pacemaker dependent patients with device infection—a modified approach," *European Journal of Cardio-Thoracic Surgery*, vol. 27, no. 6, pp. 1116–1118, 2005.

[14] E. Bertaglia, F. Zerbo, S. Zardo, D. Barzan, F. Zoppo, and P. Pascotto, "Antibiotic prophylaxis with a single dose of cefazolin during pacemaker implantation: incidence of long-term infective complications," *Pacing and Clinical Electrophysiology*, vol. 29, no. 1, pp. 29–33, 2006.

[15] S. Perl, R. Maier, and N. Watzinger, "A sequel of pacemaker infection," *Clinical Research in Cardiology*, vol. 96, no. 9, pp. 632–633, 2007.

[16] M. R. Sohail, D. Z. Uslan, A. H. Khan et al., "Risk factor analysis of permanent pacemaker infection," *Clinical Infectious Diseases*, vol. 45, no. 2, pp. 166–173, 2007.

Hindawi Publishing Corporation
Oxidative Medicine and Cellular Longevity
Volume 2013, Article ID 329183, 8 pages
http://dx.doi.org/10.1155/2013/329183

Research Article

Acute Hyperglycemia Abolishes Ischemic Preconditioning by Inhibiting Akt Phosphorylation: Normalizing Blood Glucose before Ischemia Restores Ischemic Preconditioning

Zequan Yang,[1,2] Yikui Tian,[1] Yuan Liu,[1] Sara Hennessy,[1] Irving L. Kron,[1] and Brent A. French[2]

[1] *Department of Surgery, University of Virginia Health System, P.O. Box 800709, Charlottesville, VA 22908, USA*
[2] *Department of Biomedical Engineering, University of Virginia Health System, P.O. Box 800759, Charlottesville, VA 22908, USA*

Correspondence should be addressed to Zequan Yang; zy6b@virginia.edu

Received 17 August 2013; Accepted 5 November 2013

Academic Editor: Qian Fan

This study examined the hypothesis that acute hyperglycemia (HG) blocks ischemic preconditioning (IPC) by inhibiting Akt phosphorylation. Brief HG of approximately 400 mg/dL was induced in C57BL/6 mice via intraperitoneal injection of 20% dextrose (2 g/kg). All mice underwent 40 min LAD occlusion and 60 min reperfusion. The IPC protocol was 2 cycles of 5 min ischemia and 5 min reperfusion prior to index ischemia. *Results.* In control mice, infarct size (IF) was 51.7 ± 2.0 (% risk region). Preconditioning reduced IF by 50% to 25.8 ± 3.2 ($P < 0.05$ versus control). In HG mice, IF was significantly exacerbated to 58.1 ± 2.3. However, the effect of IPC completely disappeared in HG mice. Normalization of blood glucose with insulin 5 min before IPC recovered the cardioprotective effect. Administration of CCPA before index ischemia mimicked IPC effect. The cardioprotective effect of CCPA, not its chronotropic effect, completely disappeared in HG mice. Phosphorylation of cardiac tissue Akt before index ischemia was enhanced by IPC or CCPA but was significantly inhibited by HG in both groups. Normalization of glucose with insulin reversed the inhibition of Akt phosphorylation by HG. *Conclusion.* HG abolishes the cardioprotective effect of preconditioning by inhibiting Akt phosphorylation. Normalization of blood glucose with insulin suffices to recover the cardioprotective effect of preconditioning.

1. Introduction

Hyperglycemia is commonly present in the perioperative period in patients undergoing cardiac surgery [1–3]. Hyperglycemia during cardiopulmonary bypass is an independent risk factor for mortality and morbidity in both diabetic and nondiabetic patients [3]. An increasing body of clinical evidence has shown that acute hyperglycemia (or stress hyperglycemia) is independently associated with larger myocardial infarct (MI) size and impaired left ventricular function in both diabetic and nondiabetic patients [4–6]. Animal studies have also shown that the size of MI increases in response to elevations in blood glucose levels [7, 8].

Ischemic preconditioning is a powerful endogenous protective mechanism against myocardial ischemia/reperfusion injury, which is induced by brief episodes of ischemia and reperfusion before the prolonged index myocardial ischemia and reperfusion [9]. However, diabetes mellitus and acute hyperglycemia have been shown to counteract the cardioprotective effects of both ischemic and pharmacological preconditioning in animals and humans [7, 10–12]. The mechanisms underlying the hyperglycemic blockade of preconditioning remain to be defined. Insulin has been used to treat acute or stress hyperglycemia clinically. It is also well known that insulin exerts a salutary preconditioning effect against myocardial ischemia/reperfusion injury [13, 14]. In the setting of hyperglycemia, only a few conflicting results have been reported on the effect of preconditioning-mimetic insulin. Animal studies have reported that the detrimental effects of acute hyperglycemia on the exacerbation of myocardial

infarction or the blockade of ischemic preconditioning are independent of insulin [7, 15]. However, other studies seem to favor the use of insulin to restore the preconditioning effect in hyperglycemic patients or animals [16, 17]. It is now well known that activation of adenosine A_1 receptors (A_1R), either by ischemic preconditioning or by specific agonists, triggers the protective effect against myocardial ischemia/reperfusion injury [18–24]. However, the role of acute hyperglycemia in blocking the A_1R pathway is largely unknown.

The current study employed an *in vivo* mouse model of myocardial ischemia and reperfusion injury to evaluate A_1R signaling and Akt phosphorylation in the hyperglycemic inhibition of ischemic preconditioning, as well as to evaluate the role of insulin in restoring the effect of ischemic preconditioning in mice with acute hyperglycemia.

2. Materials and Methods

This study conformed to the *Guide for the Care and Use of Laboratory Animals* published by the National Institutes of Health (Eighth Edition, revised 2011) and was conducted under protocols approved by the University of Virginia's Institutional Animal Care and Use Committee.

2.1. Agents and Chemicals. Triphenyl tetrazolium chloride (TTC) and 2-chloro-N(6)-cyclopentyladenosine (CCPA) were purchased from Sigma-Aldrich (St. Louis, MO). Phthalo blue was purchased from Heucotech Ltd. (Fairless Hills, PA). Clinical-grade insulin was purchased from Eli Lily (Indianapolis, IN).

2.2. Animals and Experimental Protocol. Seventy-two C57BL/6 mice (9–13 weeks old) were purchased from Jackson Laboratories for use in this study. Three mice died and three mice were excluded due to technical failures in Phthalo blue staining. The rest of the mice, total of 66, were assigned to 8 different groups that underwent 40 minutes of ischemia and 60 minutes of reperfusion as shown in Figure 1. An additional 4 mice/group representing each of these 8 groups were treated similarly and euthanized to provide heart tissue before index ischemia.

Acute hyperglycemia was induced by i.p. injection of 20% dextrose 50 minutes prior to LAD occlusion at a dose of 2 μL/g body weight [8]. Ischemic preconditioning was applied to mice 30 minutes after saline or glucose injection with two cycles of 5 minutes ischemia and 5 minutes reperfusion. In insulin-treated mice, the insulin was injected via external jugular vein 10 minutes before the ischemic preconditioning or before index LAD occlusion (nonpreconditioned mice) at a dose of $0.2–0.4 \times 10^{-3}$ unit/g (0.1 unit/mL, 2–4 μL/g) to normalize blood glucose levels. In CCPA-treated groups, CCPA was administered 20 minutes before index LAD occlusion at a dose of 25 μg/kg via external jugular vein.

2.3. Myocardial Ischemia/Reperfusion Injury and Measurement of Infarct Size. Mice were subjected to 40 minutes of coronary occlusion followed by 60 minutes of reperfusion as detailed previously [8, 25, 26]. Briefly, mice were anesthetized with sodium pentobarbital (100 mg/kg i.p.) and orally intubated. Artificial respiration was maintained with a FiO_2 of 0.80, 100 strokes per minute, and a 0.2 to 0.5-mL stroke volume. The heart was exposed through a left thoracotomy. A 7-0 silk suture was placed around the LAD at a level 1 mm inferior to the left auricle, and a miniature balloon occluder fashioned from microbore Tygon tubing (Small Part Inc., Seattle, WA) was affixed over the LAD. Ischemia and reperfusion were induced by inflating or deflating the balloon, respectively. ECG was monitored perioperatively using PowerLab instrumentation (ADInstruments, Colorado Springs, CO). The mice were euthanized 60 minutes after reperfusion, and the hearts were cannulated through the ascending aorta for perfusion with 3 to 4 mL of 1.0% TTC. The LAD was then reoccluded with the same suture used for coronary occlusion, and 10% Phthalo blue was then perfused to determine risk region (RR). The left ventricle was then cut into 5 to 7 transverse slices that were weighed and digitally photographed to determine infarct size as a percent of RR.

2.4. Western Blot. Total protein was extracted from the indicated experimental groups using RIPA buffer, and protein concentration was determined by BCA protein assay (Thermo Scientific, Rockford, IL). All western blots were performed according to standard procedures. Twenty micrograms of protein were separated by 12% SDS-PAGE. After transfer, nitrocellulose membranes (Bio-Rad, Hercules, CA) were probed with primary antibodies detecting pan-AKT or phospho-AKT S473 (Cell Signaling Technology, Beverly, MA) at a 1 : 1,000 dilution. Secondary antibodies (Promega, Madison, WI) were applied at a 1 : 5,000 dilution in blocking solution (1% milk in TBS-T). Proteins were visualized with enhanced chemiluminescent substrate (Thermo Scientific, Rockford, IL) followed by densitometry analysis using FluorChem 8900 imaging system (Alpha Innotech, Santa Clara, CA).

2.5. Statistical Analysis. All data are presented as mean ± SEM (standard error of the mean). Peri-ischemic heart rate changes were analyzed using repeated measures ANOVA followed by Bonferroni pairwise comparisons. All other data were compared using one-way ANOVA followed by t-test for unpaired data with Bonferroni correction.

3. Results

3.1. Perioperative Heart Rate Changes. Table 1 reports changes in heart rate before, during, and after LAD occlusion. Heart rate increased significantly after LAD occlusion and remained elevated until early reperfusion. There was no significant difference in heart rate between control and treated mice. In mice with ischemic preconditioning, heart rate also increased significantly after LAD occlusion. On the first cycle of reperfusion, up to 40% of all mice developed transient tachycardia with the heart rate reaching from 1000 to 1500 bpm. This lasted a few seconds and spontaneously returned back to baseline. The incidence of tachycardia was not different between any of the preconditioning groups.

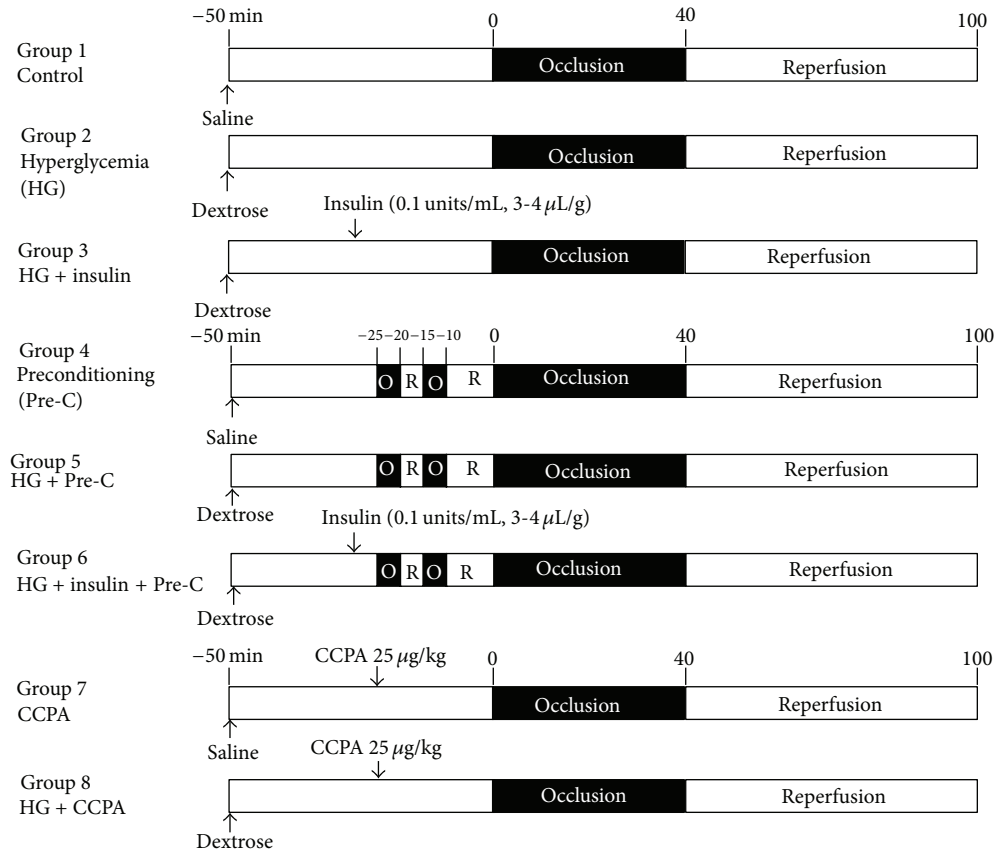

Figure 1: Animal groups and experimental protocols.

Table 1: Blood glucose levels before index LAD occlusion and perioperative heart rates.

Groups	Blood glucose (mg/dL)		Heart rate (beats per minutes)		
	5′ before Pre-C	5′ before occlusion	Before occlusion	During occlusion	Reperfusion
Control		168 ± 27	415 ± 9	484 ± 9$^{\#}$	479 ± 11$^{\#}$
HG		438 ± 51*	432 ± 10	516 ± 14$^{\#}$	521 ± 15$^{\#}$
HG + insulin	467 ± 47$^{\Pi}$	140 ± 12	393 ± 7	483 ± 30$^{\#}$	477 ± 20$^{\#}$
Pre-C		159 ± 32	394 ± 7	455 ± 13$^{\#}$	450 ± 7$^{\#}$
HG + Pre-C		454 ± 12*	401 ± 7	487 ± 17$^{\#}$	511 ± 15$^{\#}$
HG + Pre-C + insulin	407 ± 169$^{\Pi}$	125 ± 7	395 ± 12	492 ± 29$^{\#}$	494 ± 20$^{\#}$

HG: hyperglycemia; Pre-C: ischemic preconditioning.
$^{*}P < 0.05$ versus non-HG groups; $^{\Pi}P < 0.05$ versus 5 min before index LAD occlusion; $^{\#}P < 0.05$ versus before index LAD occlusion.

However, this type of arrhythmia was not seen after the prolonged index LAD occlusion.

3.2. Acute Hyperglycemia and Normalization by Insulin in Mice. Blood glucose levels were monitored with a conventional glucose meter (iTest, Auto Control Med. Inc., Canada) by puncturing the tail vein. A single intraperitoneal bolus injection of 20% dextrose (10 μL/g or 2 g dextrose/kg body weight) achieved transient blood glucose levels between 400 and 500 mg/dL within 20 to 30 minutes (Table 1). Intravenous injection of insulin at a dose of 0.2–0.4 $\times$ 10^{-3} unit/g normalized blood glucose levels to 100–200 mg/dL within 5 min ($P < 0.05$).

3.3. Acute Hyperglycemia Exacerbates Myocardial Ischemia/Reperfusion Injury. Three groups of mice (Figure 1, top 3 groups) underwent 40 min of LAD occlusion followed by 60 min of reperfusion. The mean blood glucose levels before LAD occlusion were 168 ± 27 mg/dL in saline-treated control mice (control group), 438 ± 51 mg/dL in hyperglycemic mice (HG group), and 467 ± 47 mg/dL before insulin injection and 140 ± 12 mg/dL after insulin treatment in HG+insulin-treated mice (HG+insulin group) (see Table 1). There were no statistical differences in risk region (RR, % of LV) among these three groups of mice ($P > 0.05$, left set of columns in Figure 2). The infarct size in control mice was 51.7 ± 2.0 (% of RR). In HG mice, infarct size was significantly exacerbated

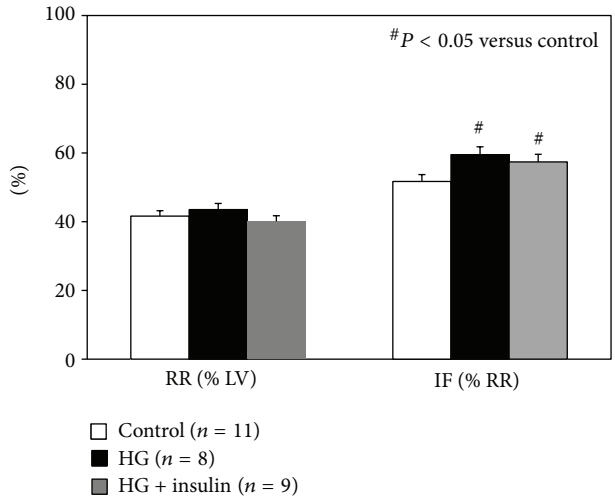

FIGURE 2: Myocardial infarct size after 40 minutes of LAD occlusion and 60 minutes of reperfusion. Acute hyperglycemia exacerbates infarct size. Normalization of blood glucose levels before LAD occlusion failed to counteract the hyperglycemic effect.

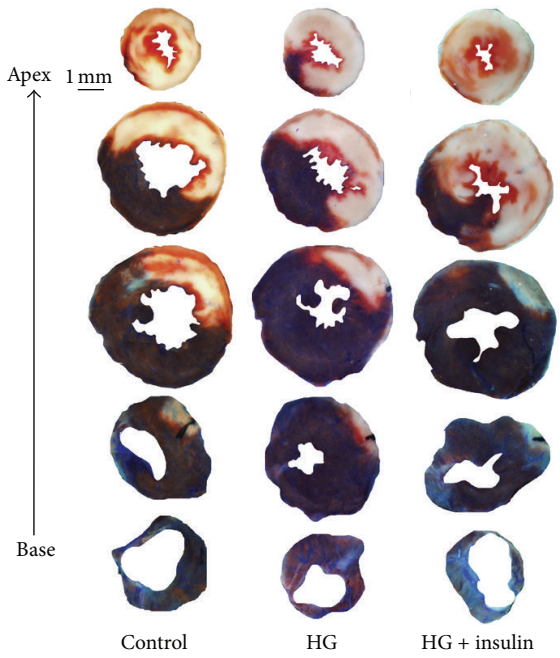

FIGURE 3: TTC and Phthalo blue staining of representative hearts from groups corresponding to Figure 2.

to 59.5 ± 2.3 (a 15% increase, $P < 0.05$ versus control). Infarct size was similarly enhanced both in HG+insulin mice and in HG mice (57.4 ± 2.2, $P < 0.05$ versus control, Figures 2 and 3).

3.4. Acute Hyperglycemia Abrogates the Effect of Ischemic Preconditioning and Insulin Restores It. As shown in Table 1, blood glucose levels before ischemic preconditioning or index ischemia were comparable among euglycemic and

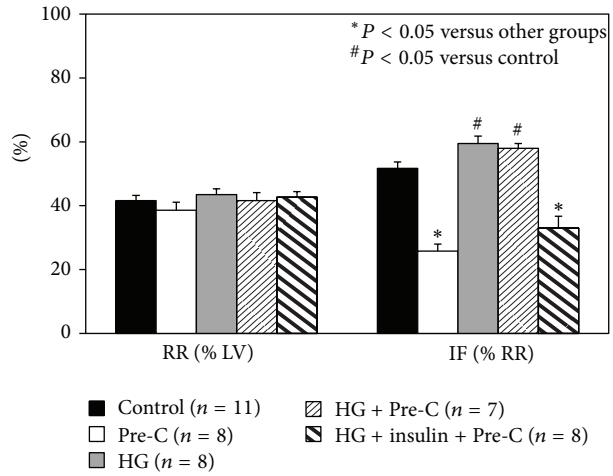

FIGURE 4: The cardioprotective effect of ischemic preconditioning disappears in HG mice, but can be recovered by normalizing blood glucose levels with insulin prior to ischemia.

hyperglycemic groups. Insulin treatment returned glucose levels back to the euglycemic baseline. There were no statistical differences in risk region (RR, % of LV) among groups ($P > 0.05$, left columns in Figure 4). Ischemic preconditioning reduced infarct size to 25.8 ± 3.2% (a 50% reduction, $P < 0.05$ versus control). This infarct-limiting effect completely disappeared in HG+Pre-C mice (58.0 ± 1.5%, P = NS versus HG mice). Normalization of blood glucose with insulin 5 min before the preconditioning procedure served to partially restore the protective effect of preconditioning against myocardial infarction (33.0 ± 3.7%, $P < 0.05$ versus control or HG mice). Hearts from parallel groups of mice were harvested before the index 40 min LAD occlusion. The ratio of phosphorylated Akt relative to total Akt in heart tissue was found to be significantly enhanced in Pre-C mice but significantly inhibited in HG mice and HG+Pre-C mice relative to sham controls. However, normalization of blood glucose with insulin before the preconditioning protocol reversed the inhibitory effect of HG on Akt phosphorylation (Figure 5).

3.5. Acute Hyperglycemia Abrogates the Cardioprotective Effect of Adenosine A_1 Receptor Agonist. CCPA is a selective A_1R agonist and induces a cardioprotective effect if applied before index ischemia. Preliminary dose response studies with CCPT revealed severe bradycardia in euglycemic mice at the dose of 100 μg/kg as well as 50 μg/kg, which compromised survival during ischemia/reperfusion. Moreover, HG mice could not tolerate CCPA at these two doses and died during ischemia. A dose of CCPA at 25 μg/kg was therefore selected for the current study. Although this dose is significantly lower than those reported in the literature for other animal models, significant bradycardia occurred around 30 sec after intravenous injection and then slowly improved. In euglycemic mice, CCPA decreased the heart rate from 413 ± 17 to 310 ± 23 beats/min (a 25% reduction, $P < 0.05$). The heart rate slowly increased back to the baseline before index ischemia. Heart

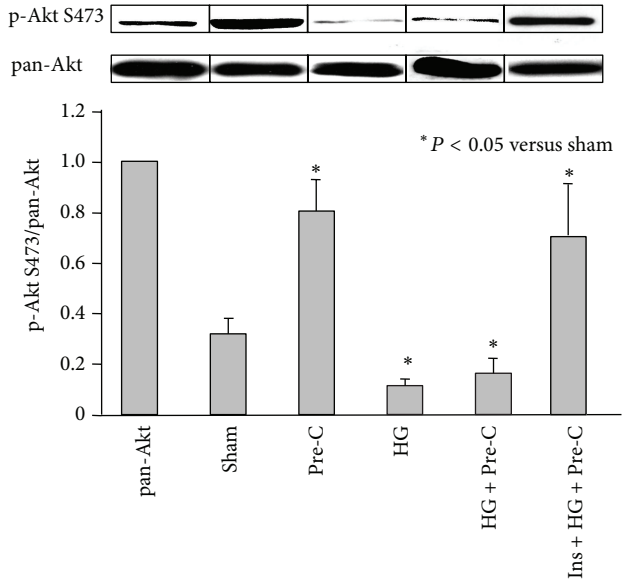

Figure 5: Myocardial phospho-Akt S473 to pan-Akt ratios in the indicated experimental groups. The ratio of phospho-Akt S473 to pan-Akt (the bar graph) was measured by densitometry, where the pan-AKT inputs were normalized to 1.

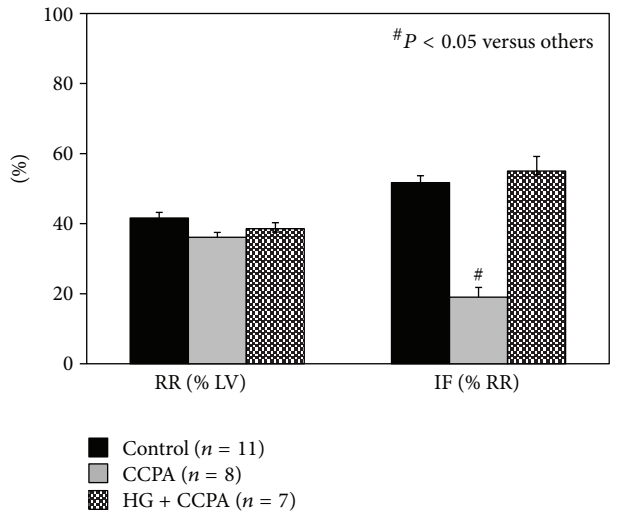

Figure 6: The cardioprotective effect of CCPA mimics the effect of ischemic preconditioning but disappears in HG mice.

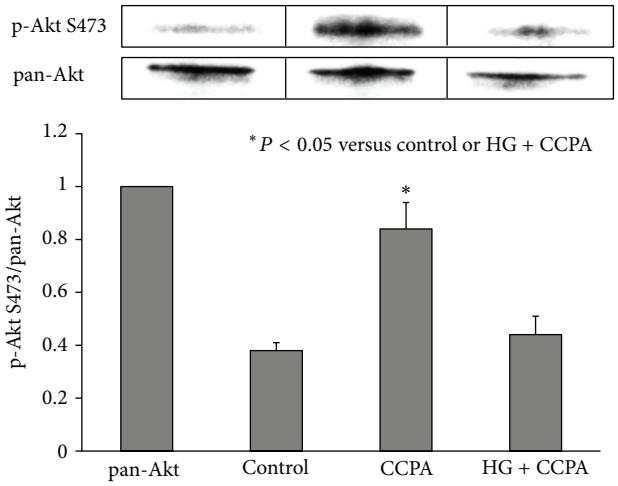

Figure 7: Myocardial phospho-Akt S473 to pan-Akt ratios in mice treated with CCPA.

rate in HG mice at baseline was not different than that in control mice, whereas CCPA decreased heart rate from 401 ± 14 to 258 ± 21 beats/min (a 36% reduction, $P < 0.05$). Heart rate in HG mice increased to 345 ± 15 before index ischemia, which remained significantly lower than that at baseline ($P < 0.05$). Glucose levels before LAD occlusion were 168 ± 27 in control mice, 186 ± 8 in CCPA-treated mice, and 355 ± 23 mg/dL in CCPA-treated HG mice (both $P < 0.05$ versus control). In CCPA-treated mice, infarct size was comparable to that of the Pre-C group (19.0 ± 2.8 versus 25.8 ± 3.2, % of RR) and significantly smaller than that of control mice (19.0 ± 2.8 versus 51.7 ± 2.0, $P < 0.05$). However, the infarct-sparing effect of CCPA disappeared in HG mice (55.0 ± 4.2, P = NS versus control; see Figure 6). Hearts from parallel groups of mice were harvested before the 40 min LAD occlusion. CCPA increased the ratio of phosphorylated to total Akt in heart tissue in euglycemic control mice by over 2-fold ($P < 0.05$) but not in HG mice (Figure 7).

4. Discussion

An increasing body of evidence has shown that acute (or stress) hyperglycemia is an independent predictor of cardiovascular morbidity and mortality [3, 27–29]. Acute or stress hyperglycemia is associated with increased oxidative stress [8, 30–33], inflammation [34–37], and activation of stress-responsive kinase signaling [29, 35]. Infarcts are usually larger in patients with stress or diabetes-related hyperglycemia [4, 5, 29, 38], and animals with acute hyperglycemia sustain markedly larger infarcts following experimental ischemia/reperfusion than do euglycemic controls [7, 8, 10, 11]. Moreover, acute hyperglycemia completely abolishes the cardioprotective effect of ischemic preconditioning, negating a powerful endogenous cardioprotective mechanism and making cardiomyocytes more vulnerable to ischemia/reperfusion injury [7, 9, 10, 39, 40]. Pharmacological preconditioning has been reported to be inhibited by acute hyperglycemia as well [7, 15, 39, 41]. The mechanisms underlying the hyperglycemic blockade of ischemic preconditioning remain unclear. Several lines of evidence point to 3 possible targets on which hyperglycemia may act to abolish the preconditioning effect: (1) increased production of reactive oxygen species [41, 42], (2) inhibition of PI3-Akt pathway [43, 44], and (3) inhibition of K_{ATP} channels [17, 45]. However, MAP kinase appears not to be affected by the acute hyperglycemic event [12, 39].

Hyperglycemia negates the protective effect of ischemic preconditioning and, most importantly, appears to interfere with the salutary effects of insulin [7, 15]. However, other

studies have reported that administration of insulin may restore ischemic or pharmacological preconditioning [16, 17]. Insulin itself is a preconditioning-mimetic and exerts its salutary effect by activating the PI3-Akt pathway [13, 44, 46]. Clinically, aggressive therapy with insulin seems to improve a host of metabolic and physiologic effects associated with acute hyperglycemia and appears to be warranted if euglycemia cannot otherwise be maintained. However, an increasing body of clinical evidence has shown that acute hyperglycemia (or stress hyperglycemia) is independently associated with larger myocardial infarct size and impaired left ventricular function in both DM and nondiabetic patients [4, 5]. The potential of insulin to mitigate against this hyperglycemic effect on myocardial ischemia/reperfusion injury is currently unclear, although clinical trials of glucose-insulin-potassium (GIK) therapy for acute myocardial infarction are certainly relevant. GIK therapy has been shown to improve cardiovascular performance after coronary artery surgery [2]. Moreover, a recent clinical trial on using early intravenous administration of GIK in patients with suspected acute coronary syndromes reported a significant decrease in the composite endpoint of cardiac arrest or in-hospital mortality (4.4% in treated versus 8.7% in placebo group) [47]. Thus while GIK therapy was originally designed to provide balanced metabolic support to ischemic cardiomyocytes, it is possible that the beneficial effects of such a hyperinsulinemic/normoglycemic clamp might also involve the mechanisms investigated in the current study. This study employed a well-established *in vivo* mouse model to explore the role of insulin in treating acute myocardial ischemia/reperfusion injury and in restoring the effects of ischemic preconditioning during acute hyperglycemia.

In the current study, all the mice underwent 40 min LAD occlusion and 60 min reperfusion. The 40 min duration of LAD occlusion was selected to provide maximum sensitivity to both the detrimental effects of acute hyperglycemia and the cardioprotective effects of Pre-C. Longer LAD occlusions would reduce our sensitivity to detect infarct exacerbation due to hyperglycemia, while shorter occlusions would reduce our sensitivity to detect cardioprotection. The selection of 60 min of reperfusion is based on our previous study showing that myocardial infarction in mice attains >95% of its final (24 hr) size within 60 min of reperfusion [48]. Acute hyperglycemia was demonstrated again to exacerbate myocardial infarct size as previously reported in a mouse model with 30 min LAD occlusion and 60 min reperfusion [8]. Normalization of blood glucose levels before the onset of ischemia failed to offset the infarct exacerbation secondary to the brief episode of acute hyperglycemia (Figure 2). Our previous study showed that acute hyperglycemia enhances oxidative stress and exacerbates myocardial infarct size in mice through the activation of NADPH oxidase [8]. Although insulin is cardioprotective via a preconditioning-mimetic effect [13, 44, 46], its salutary effect in the setting of acute hyperglycemia disappeared (Figure 2). The infarct exaggerating effect of acute hyperglycemia was retained even when the blood glucose level was normalized before the onset of ischemia, indicating that once hyperglycemia triggers pro-inflammatory signaling pathway [8], reversal of the hyperglycemia by insulin alone could not block the ongoing signal transduction. Acute hyperglycemia also makes cardiomyocytes vulnerable to injury by inhibiting the phosphorylation of Akt (Figure 5). However, the cardioprotective effect of insulin may be overshadowed by the detrimental effect of hyperglycemia.

In the ischemic preconditioning study, our results supported previous studies showing that acute hyperglycemia completely abolished the effect of ischemic preconditioning against myocardial ischemia/reperfusion injury [7, 9, 10, 39, 40]. Hyperglycemia exerted this effect by inhibiting the phosphorylation of Akt (Figures 4 and 5). To the best of our knowledge, this is the first report to show that the hyperglycemic loss of ischemic preconditioning against myocardial infarction is associated with an inhibition in the phosphorylation of Akt. Contrary to other reports [7, 15], our study showed that normalization of blood glucose before the preconditioning protocol completely recovered the cardioprotective effects of ischemic preconditioning (Figure 4). By normalizing blood glucose, insulin helped to restore the phosphorylation of Akt by ischemic preconditioning. Akt is an important mediator of cell survival and has long been implicated in ischemic preconditioning [49]. Insulin can activate the PI3K-Akt pathway and counteract oxidative stress, likely by increasing NO release [50–52]. The mechanisms underlying hyperglycemic inhibition of Akt phosphorylation, whether direct hyperglycemic effect or indirect, were not investigated in this study. We found that insulin has no direct cardioprotective effect in the setting of acute hyperglycemia but can recover the ischemic preconditioning effect to limit myocardial infarction. This phenomenon further confirmed our conclusion that acute hyperglycemia activates inflammatory responses and on the other hand decreases the internal defense mechanisms in cardiomyocytes.

The effect of hyperglycemia on preconditioning is most likely a direct effect of glucose on cardiomyocytes. Hyperglycemia has no direct effect in blocking adenosine A_1 receptor (A_1R) activation, which is a well-characterized mediator of ischemic preconditioning. Our data shows that acute hyperglycemia blocks ischemic preconditioning by disrupting signaling pathways downstream of A_1R but not A_1R activation itself since hyperglycemia blocked the cardioprotective effect of CCPA (Figures 6 and 7) but not the bradycardia caused by CCPA.

The current study provides indirect evidence to indicate that the inhibition of Akt phosphorylation by acute hyperglycemia is responsible for abolishing the cardioprotective effects of ischemic preconditioning. Nevertheless, these results clearly warrant future investigation into how acute hyperglycemia inhibits the phosphorylation of Akt, as well as the signal transduction pathways lying downstream of Akt. Future studies employing genetically manipulated mice and siRNA-mediated knockdowns are anticipated to further elucidate the effects of acute hyperglycemia on this clinicallyrelevant signal transduction pathway.

In conclusion, the current study clearly demonstrates that acute hyperglycemia exacerbates myocardial ischemia/reperfusion injury and completely abolishes the cardioprotective effect of ischemic preconditioning by inhibiting Akt

phosphorylation. Insulin treatment to normalize blood glucose levels failed to counteract the detrimental effect of hyperglycemia but could nevertheless restore the cardioprotective effects of ischemic preconditioning.

Funding

This study was funded by NIH R01 HL 092305 to Irving L. Kron and Brent A. French.

References

[1] H. L. Lazar, "Hyperglycemia during cardiac surgery," *Journal of Thoracic and Cardiovascular Surgery*, vol. 131, no. 1, pp. 11–13, 2006.

[2] D. W. Quinn, D. Pagano, R. S. Bonser et al., "Improved myocardial protection during coronary artery surgery with glucose-insulin-potassium: a randomized controlled trial," *Journal of Thoracic and Cardiovascular Surgery*, vol. 131, no. 1, pp. 34.e2–42.e2, 2006.

[3] T. Doenst, D. Wijeysundera, K. Karkouti et al., "Hyperglycemia during cardiopulmonary bypass is an independent risk factor for mortality in patients undergoing cardiac surgery," *Journal of Thoracic and Cardiovascular Surgery*, vol. 130, no. 4, pp. 1144.e1–1144.e8, 2005.

[4] M. Ishihara, I. Inoue, T. Kawagoe et al., "Impact of acute hyperglycemia on left ventricular function after reperfusion therapy in patients with a first anterior wall acute myocardial infarction," *American Heart Journal*, vol. 146, no. 4, pp. 674–678, 2003.

[5] R. Marfella, M. Siniscalchi, K. Esposito et al., "Effects of stress hyperglycemia on acute myocardial infarction: role of inflammatory immune process in functional cardiac outcome," *Diabetes Care*, vol. 26, no. 11, pp. 3129–3135, 2003.

[6] N. N. Wahab, E. A. Cowden, N. J. Pearce, M. J. Gardner, H. Merry, and J. L. Cox, "Is blood glucose an independent predictor of mortality in acute myocardial infarction in the thrombolytic era?" *Journal of the American College of Cardiology*, vol. 40, no. 10, pp. 1748–1754, 2002.

[7] J. R. Kersten, W. G. Toller, E. R. Gross, P. S. Pagel, and D. C. Warltier, "Diabetes abolishes ischemic preconditioning: role of glucose, insulin, and osmolality," *American Journal of Physiology—Heart and Circulatory Physiology*, vol. 278, no. 4, pp. H1218–H1224, 2000.

[8] Z. Yang, V. E. Laubach, B. A. French, and I. L. Kron, "Acute hyperglycemia enhances oxidative stress and exacerbates myocardial infarction by activating nicotinamide adenine dinucleotide phosphate oxidase during reperfusion," *Journal of Thoracic and Cardiovascular Surgery*, vol. 137, no. 3, pp. 723–729, 2009.

[9] L. H. Opie, "Preconditioning and metabolic anti-ischaemic agents," *European Heart Journal*, vol. 24, no. 20, pp. 1854–1856, 2003.

[10] J. R. Kersten, "Acute hyperglycemia abolishes ischemic preconditioning *in vivo*," *American Journal of Physiology—Heart and Circulatory Physiology*, vol. 275, no. 2, pp. H721–H725, 1998.

[11] J. R. Kersten, M. W. Montgomery, T. Ghassemi et al., "Diabetes and hyperglycemia impair activation of mitochondrial KATP channels," *American Journal of Physiology—Heart and Circulatory Physiology*, vol. 280, no. 4, pp. H1744–H1750, 2001.

[12] D. Ebel, O. Toma, S. Appler et al., "Ischemic preconditioning phosphorylates mitogen-activated kinases and heat shock protein 27 in the diabetic rat heart," *Hormone and Metabolic Research*, vol. 41, no. 1, pp. 10–15, 2009.

[13] C. J. Zuurbier, "Insulin as ischaemic preconditioning-mimetic," *Acta Physiologica*, vol. 195, no. 2, p. 203, 2009.

[14] C. J. Zuurbier, O. Eerbeek, and A. J. Meijer, "Ischemic preconditioning, insulin, and morphine all cause hexokinase redistribution," *American Journal of Physiology—Heart and Circulatory Physiology*, vol. 289, no. 1, pp. H496–H499, 2005.

[15] D. Ebel, J. Müllenheim, J. Fräßdorf et al., "Effect of acute hyperglycaemia and diabetes mellitus with and without short-term insulin treatment on myocardial ischaemic late preconditioning in the rabbit heart *in vivo*," *Pflugers Archiv European Journal of Physiology*, vol. 446, no. 2, pp. 175–182, 2003.

[16] S. Forlani, F. Tomai, R. De Paulis et al., "Preoperative shift from glibenclamide to insulin is cardioprotective in diabetic patients undergoing coronary artery bypass surgery," *Journal of Cardiovascular Surgery*, vol. 45, no. 2, pp. 117–122, 2004.

[17] H. F. Del Valle, E. C. Lascano, and J. A. Negroni, "Ischemic preconditioning protection against stunning in conscious diabetic sheep: role of glucose, insulin, sarcolemmal and mitochondrial KATP channels," *Cardiovascular Research*, vol. 55, no. 3, pp. 642–659, 2002.

[18] J. D. Mccully, Y. Toyoda, M. Uematsu, R. D. Stewart, and S. Levitsky, "Adenosine-enhanced ischemic preconditioning: adenosine receptor involvement during ischemia and reperfusion," *American Journal of Physiology—Heart and Circulatory Physiology*, vol. 280, no. 2, pp. H591–H602, 2001.

[19] Z.-Q. Zhao, K. Nakanishi, D. S. McGee, P. Tan, and J. Vinten-Johansen, "A1 Receptor mediated myocardial infarct size reduction by endogenous adenosine is exerted primarily during ischaemia," *Cardiovascular Research*, vol. 28, no. 2, pp. 270–279, 1994.

[20] Z. Yang, R. L. J. Cerniway, A. M. Byford, S. S. Berr, B. A. French, and G. Paul Matherne, "Cardiac overexpression of A1-adenosine receptor protects intact mice against myocardial infarction," *American Journal of Physiology—Heart and Circulatory Physiology*, vol. 282, no. 3, pp. H949–H955, 2002.

[21] H. Takano, R. Bolli, R. G. Black Jr. et al., "A1 or A3 adenosine receptors induce late preconditioning against infarction in conscious rabbits by different mechanisms," *Circulation Research*, vol. 88, no. 5, pp. 520–528, 2001.

[22] M. E. Reichelt, A. Shanu, L. Willems et al., "Endogenous adenosine selectively modulates oxidant stress via the A1 receptor in ischemic hearts," *Antioxidants and Redox Signaling*, vol. 11, no. 11, pp. 2641–2650, 2009.

[23] A. R. Lankford, J.-N. Yang, R. Rose'Meyer et al., "Effect of modulating cardiac A1 adenosine receptor expression on protection with ischemic preconditioning," *American Journal of Physiology—Heart and Circulatory Physiology*, vol. 290, no. 4, pp. H1469–H1473, 2006.

[24] E. Giannella, H.-C. Mochmann, and R. Levi, "Ischemic preconditioning prevents the impairment of hypoxic coronary vasodilatation caused by ischemia/reperfusion: role of adenosine A1/A3 and bradykinin B2 receptor activation," *Circulation Research*, vol. 81, no. 3, pp. 415–422, 1997.

[25] Z. Yang, Y.-J. Day, M.-C. Toufektsian et al., "Infarct-sparing effect of A2A-adenosine receptor activation is due primarily to its action on lymphocytes," *Circulation*, vol. 111, no. 17, pp. 2190–2197, 2005.

[26] Z. Yang, Y.-J. Day, M.-C. Toufektsian et al., "Myocardial infarct-sparing effect of adenosine A2A receptor activation is due to its

action on $CD4^+$ T lymphocytes," *Circulation*, vol. 114, no. 19, pp. 2056–2064, 2006.

[27] S. E. Capes, D. Hunt, K. Malmberg, and H. C. Gerstein, "Stress hyperglycaemia and increased risk of death after myocardial infarction in patients with and without diabetes: a systematic overview," *The Lancet*, vol. 355, no. 9206, pp. 773–778, 2000.

[28] M. Ishihara, S. Kojima, T. Sakamoto et al., "Acute hyperglycemia is associated with adverse outcome after acute myocardial infarction in the coronary intervention era," *American Heart Journal*, vol. 150, no. 4, pp. 814–820, 2005.

[29] K. A. Webster, "Stress hyperglycemia and enhanced sensitivity to myocardial infarction," *Current Hypertension Reports*, vol. 10, no. 1, pp. 78–84, 2008.

[30] Y. Hu, G. Block, E. P. Norkus, J. D. Morrow, M. Dietrich, and M. Hudes, "Relations of glycemic index and glycemic load with plasma oxidative stress markers," *American Journal of Clinical Nutrition*, vol. 84, no. 1, pp. 70–76, 2006.

[31] H. Kawano, T. Motoyama, O. Hirashima et al., "Hyperglycemia rapidly suppresses flow-mediated endothelium-dependent vasodilation of brachial artery," *Journal of the American College of Cardiology*, vol. 34, no. 1, pp. 146–154, 1999.

[32] P. Mohanty, W. Hamouda, R. Garg, A. Aljada, H. Ghanim, and P. Dandona, "Glucose challenge stimulates reactive oxygen species (ROS) generation by leucocytes," *Journal of Clinical Endocrinology and Metabolism*, vol. 85, no. 8, pp. 2970–2973, 2000.

[33] M. G. Rosca, T. G. Mustata, M. T. Kinter et al., "Glycation of mitochondrial proteins from diabetic rat kidney is associated with excess superoxide formation," *American Journal of Physiology—Renal Physiology*, vol. 289, no. 2, pp. F420–F430, 2005.

[34] D. Sudic, M. Razmara, M. Forslund, Q. Ji, P. Hjemdahl, and N. Li, "High glucose levels enhance platelet activation: involvement of multiple mechanisms," *British Journal of Haematology*, vol. 133, no. 3, pp. 315–322, 2006.

[35] A. Aljada, J. Friedman, H. Ghanim et al., "Glucose ingestion induces an increase in intranuclear nuclear factor κB, a fall in cellular inhibitor κB, and an increase in tumor necrosis factor α messenger RNA by mononuclear cells in healthy human subjects," *Metabolism*, vol. 55, no. 9, pp. 1177–1185, 2006.

[36] S. Dhindsa, D. Tripathy, P. Mohanty et al., "Differential effects of glucose and alcohol on reactive oxygen species generation and intranuclear nuclear factor-κB in mononuclear cells," *Metabolism*, vol. 53, no. 3, pp. 330–334, 2004.

[37] Y. Iwasaki, M. Kambayashi, M. Asai, M. Yoshida, T. Nigawara, and K. Hashimoto, "High glucose alone, as well as in combination with proinflammatory cytokines, stimulates nuclear factor kappa-B-mediated transcription in hepatocytes *in vitro*," *Journal of Diabetes and its Complications*, vol. 21, no. 1, pp. 56–62, 2007.

[38] S. W. Zarich and R. W. Nesto, "Implications and treatment of acute hyperglycemia in the setting of acute myocardial infarction," *Circulation*, vol. 115, no. 18, pp. e436–e439, 2007.

[39] N. C. Weber, C. Goletz, R. Huhn et al., "Blockade of anaesthetic-induced preconditioning in the hyperglycaemic myocardium. The regulation of different mitogen-activated protein kinases," *European Journal of Pharmacology*, vol. 592, no. 1–3, pp. 48–54, 2008.

[40] M. Ishihara, I. Inoue, T. Kawagoe et al., "Effect of acute hyperglycemia on the ischemic preconditioning effect of prodromal angina pectoris in patients with a first anterior wall acute myocardial infarction," *American Journal of Cardiology*, vol. 92, no. 3, pp. 288–291, 2003.

[41] F. Kehl, J. G. Krolikowski, D. Weihrauch, P. S. Pagel, D. C. Warltier, and J. R. Kersten, "N-acetylcysteine restores isoflurane-induced preconditioning against myocardial infarction during hyperglycemia," *Anesthesiology*, vol. 98, no. 6, pp. 1384–1390, 2003.

[42] F. B. Stentz and A. E. Kitabchi, "Hyperglycemia-induced activation of human T-lymphocytes with de novo emergence of insulin receptors and generation of reactive oxygen species," *Biochemical and Biophysical Research Communications*, vol. 335, no. 2, pp. 491–495, 2005.

[43] S. Matsumoto, S. Cho, S. Tosaka et al., "Pharmacological preconditioning in type 2 diabetic rat hearts: the roles of mitochondrial atp-sensitive potassium channels and the phosphatidylinositol 3-kinase-akt pathway," *Cardiovascular Drugs and Therapy*, vol. 23, no. 4, pp. 263–270, 2009.

[44] A. Tsang, D. J. Hausenloy, M. M. Mocanu, R. D. Carr, and D. M. Yellon, "Preconditioning the diabetic heart: the importance of Akt phosphorylation," *Diabetes*, vol. 54, no. 8, pp. 2360–2364, 2005.

[45] H. F. del Valle, E. C. Lascano, J. A. Negroni, and A. J. Crottogini, "Absence of ischemic preconditioning protection in diabetic sheep hearts: role of sarcolemmal KATP channel dysfunction," *Molecular and Cellular Biochemistry*, vol. 249, no. 1-2, pp. 21–30, 2003.

[46] A. K. Jonassen, M. N. Sack, O. D. Mjøs, and D. M. Yellon, "Myocardial protection by insulin at reperfusion requires early administration and is mediated via Akt and p70s6 kinase cell-survival signaling," *Circulation Research*, vol. 89, no. 12, pp. 1191–1198, 2001.

[47] H. P. Selker, J. R. Beshansky, P. R. Sheehan et al., "Out-of-hospital administration of intravenous glucose-insulin-potassium in patients with suspected acute coronary syndromes: the IMMEDIATE randomized controlled trial," *Journal of the American Medical Association*, vol. 307, pp. 1925–1933, 2012.

[48] Z. Yang, J. Linden, S. S. Berr, I. L. Kron, G. A. Beller, and B. A. French, "Timing of adenosine 2A receptor stimulation relative to reperfusion has differential effects on infarct size and cardiac function as assessed in mice by MRI," *American Journal of Physiology—Heart and Circulatory Physiology*, vol. 295, no. 6, pp. H2328–H2335, 2008.

[49] X. Yang, M. V. Cohen, and J. M. Downey, "Mechanism of cardioprotection by early ischemic preconditioning," *Cardiovascular Drugs and Therapy*, vol. 24, no. 3, pp. 225–234, 2010.

[50] G. Zeng, F. H. Nystrom, L. V. Ravichandran et al., "Roles for insulin receptor, PI3-kinase, and Akt in insulin-signaling pathways related to production of nitric oxide in human vascular endothelial cells," *Circulation*, vol. 101, no. 13, pp. 1539–1545, 2000.

[51] X.-Q. Zeng, C.-M. Zhang, M.-L. Tong et al., "Knockdown of NYGGF4 increases glucose transport in C2C12 mice skeletal myocytes by activation IRS-1/PI3K/AKT insulin pathway," *Journal of Bioenergetics and Biomembranes*, vol. 44, no. 3, pp. 351–355, 2012.

[52] T. Chen, G. Ding, Z. Jin et al., "Insulin ameliorates miR-1-induced injury in H9c2 cells under oxidative stress via Akt activation," *Molecular and Cellular Biochemistry*, vol. 369, pp. 167–174, 2012.

Hindawi Publishing Corporation
Oxidative Medicine and Cellular Longevity
Volume 2013, Article ID 912310, 12 pages
http://dx.doi.org/10.1155/2013/912310

Research Article

N-n-Butyl Haloperidol Iodide Ameliorates Cardiomyocytes Hypoxia/Reoxygenation Injury by Extracellular Calcium-Dependent and -Independent Mechanisms

Yanmei Zhang,[1] Gaoyong Chen,[1] Shuping Zhong,[2] Fuchun Zheng,[3] Fenfei Gao,[1] Yicun Chen,[1] Zhanqin Huang,[1] Wenfeng Cai,[1] Weiqiu Li,[4] Xingping Liu,[1] Yanshan Zheng,[1] Han Xu,[1] and Ganggang Shi[1,5]

[1] *Department of Pharmacology, Shantou University Medical College, 22 Xin Ling Road, Shantou, 515041 Guangdong, China*
[2] *Department of Biochemistry and Molecular Biology, University of Southern California, Los Angeles, CA 90033, USA*
[3] *Department of Pharmacy, The First Affiliated Hospital, Shantou University Medical College, Shantou 515041, Guangdong, China*
[4] *Analytical Cytology Laboratory, Shantou University Medical College, Shantou 515041, Guangdong, China*
[5] *Department of Cardiovascular Diseases, The First Affiliated Hospital, Shantou University Medical College, Shantou 515041, Guangdong, China*

Correspondence should be addressed to Ganggang Shi; ggshi@stu.edu.cn

Received 25 August 2013; Revised 28 September 2013; Accepted 28 September 2013

Academic Editor: Zhengyuan Xia

N-n-butyl haloperidol iodide (F_2) has been shown to antagonize myocardial ischemia/reperfusion injury by blocking calcium channels. This study explores the biological functions of ERK pathway in cardiomyocytes hypoxia/reoxygenation injury and clarifies the mechanisms by which F_2 ameliorates cardiomyocytes hypoxia/reoxygenation injury through the extracellular-calcium-dependent and -independent ERK1/2-related pathways. In extracellularcalcium-containing hypoxia/reoxygenation cardiomyocytes, PKCα and ERK1/2 were activated, Egr-1 protein level and cTnI leakage increased, and cell viability decreased. The ERK1/2 inhibitors suppressed extracellular-calcium-containing-hypoxia/reoxygenation-induced Egr-1 overexpression and cardiomyocytes injury. PKCα inhibitor downregulated extracellularcalcium-containing-hypoxia/reoxygenation-induced increase in p-ERK1/2 and Egr-1 expression. F_2 downregulated hypoxia/reoxygenation-induced elevation of p-PKCα, p-ERK1/2, and Egr-1 expression and inhibited cardiomyocytes damage. The ERK1/2 and PKCα activators antagonized F_2's effects. In extracellular-calcium-free-hypoxia/reoxygenation cardiomyocytes, ERK1/2 was activated, LDH and cTnI leakage increased, and cell viability decreased. F_2 and ERK1/2 inhibitors antagonized extracellular-calcium-free-hypoxia/reoxygenation-induced ERK1/2 activation and suppressed cardiomyocytes damage. The ERK1/2 activator antagonized F_2's above effects. F_2 had no effect on cardiomyocyte cAMP content or PKA and Egr-1 expression. Altogether, ERK activation in extracellular-calcium-containing and extracellular-calcium-free hypoxia/reoxygenation leads to cardiomyocytes damage. F_2 may ameliorate cardiomyocytes hypoxia/reoxygenation injury by regulating the extracellular-calcium-dependent PKCα/ERK1/2/Egr-1 pathway and through the extracellular-calcium-independent ERK1/2 activation independently of the cAMP/PKA pathway or Egr-1 overexpression.

1. Introduction

The phenomenon of exacerbated tissue and organ damage produced by the restoration of blood flow after ischemia is known as ischemia/reperfusion (I/R) injury. Studies have demonstrated that this phenomenon takes place in a variety of tissues and organs such as the brain, heart, liver, lungs, kidneys, gastrointestinal tract, limbs, and skin. Myocardial I/R injury is a pathophysiological phenomenon commonly seen after ischemic heart disease and heart surgery. Reducing and eliminating this damage has become a hot topic in the field.

N-n-Butyl haloperidol iodide (F_2) is a new compound synthesized by our group. A series of previous studies have

shown that F_2 has protective effects on *in vivo* myocardial I/R injury and *in vitro* hypoxia/reoxygenation (H/R) injury models [1–4]. Our studies have shown that the F_2 protection is associated with antagonizing intracellular calcium overload through L-type calcium channels and inhibiting early growth response gene-1 (Egr-1) mRNA and protein overexpression [2, 5–7]. Further analysis has shown that F_2 is able to inhibit Egr-1 expression through suppression of the H/R-induced classical calcium-dependent PKCα translocation/activation. However, it can also activate calcium-independent PKCε translocation/activation to protect cardiomyocytes from sustaining H/R injury [8]. In addition, in cardiac microvascular endothelial cells, which do not have L-type calcium channels, F_2 still has a protective effect against H/R injury [6, 9–11]. These studies indicate that F_2 can protect cells from I/R injury through both calcium-dependent and -independent mechanisms. However, it is not clear which signaling pathways are involved.

The extracellular signal-regulated kinase (ERK1/2) pathway, which has attracted extensive attention in recent years, was the first signal transduction pathway of the MAPK family discovered. It is also the most extensively studied of signal transduction pathway [12]. It is not only involved in the regulation of a variety of cellular physiological functions but also plays an important role in the pathogenesis of a variety of diseases. Numerous studies have shown that the ERK1/2 signaling pathway is closely related to myocardial I/R and H/R injury [13]. Upon I/R or H/R stimulation, ERK1/2 is activated and transducted to the nucleus, phosphorylating serine, and threonine residues of transcription factors and leading to the activation and inactivation of gene transcription and subsequent changes in cell functions [12–14]. Moreover, it was reported that both the Ca^{2+}-dependent and -independent pathways are necessary for elevating active ERK to a level sufficient to affect gene expression [15]. To explore the role of ERK1/2 in I/R and H/R injury, we first observed the change of ERK1/2 activity in cardiomyocytes after H/R in the presence and absence of extracellular calcium. Based on these results, we further investigated whether F_2 protection of cardiomyocytes from H/R injury might take place through its regulation of the calcium-dependent PKCα/ERK1/2/Egr-1 signaling pathway.

Both cAMP and Ca^{2+} are major second messengers. They not only cross-talk by downstream signal molecule but also transduct intracellular signal independently [16]. The cAMP-dependent PKA is the major downstream molecule in the cAMP signaling pathway. The cAMP/PKA activation has been shown to inhibit ERK1/2 activation in Rat-1 cells, NIH/3T3 cells, HEK293 cells, and COS-7 cells [17–19]. In PC12 cells and S49 mouse lymphoma cells, cAMP/PKA acts as an upstream signal to activate ERK1/2 and affect cell function [20, 21]. In cardiomyocytes, the cAMP/PKA signaling pathway is also closely related to ERK1/2. After being activated by isoproterenol, β1AR activates the Gs/AC/cAMP/PKA pathways, consequently activates ERK1/2, and causes myocardial apoptosis [22, 23]. These results suggest that the calcium-independent cAMP/PKA/ERK1/2 pathway may be related to H/R-induced myocardial damage. Therefore, in this study, we focused simultaneously on whether the calcium-independent mechanism of F_2 protection is related to its regulation of the cAMP/PKA/ERK1/2/Egr-1 pathway.

2. Materials and Methods

2.1. Culture of Primary Cardiomyocytes. Adult Sprague-Dawley rats (200–250 g) were obtained from Vital River Laboratory Animal Technology Company (Beijing, China). The research protocol was approved by the Medical Animal Care and Welfare Committee of Shantou University Medical College and performed in compliance with the Guide for the Care and Use of Laboratory Animals (NIH Publication, 1996). Primary cardiomyocytes were cultured as described previously with minor modifications [2]. Briefly, neonatal ventricular cardiomyocytes were isolated from 1- to 4-day-old Sprague-Dawley rats with 0.1% trypsin. The dispersed cells were plated in M-199 medium containing 10% fetal bovine serum for 30 min to remove noncardiomyocytes. Then cardiomyocytes, representing 90–95% of total adhering cells, were cultured in the medium with 0.1 mM 5-bromodeoxyuridine for the first 4 days in an incubator with 5% CO_2 at 37°C. Experiments were performed on day 4 or 5 of the culture.

2.2. Preparation of Reagents and Liquid. F_2 was synthesized in our laboratory. Verapamil was purchased from Shanghai Wellhope Pharmaceuticals (China); ERK inhibitor PD98059 was purchased from Promega (U.S.) and U0126 from Cell Signaling Technology (U.S.); ERK activator EGF was purchased from Pepprotech (U.S.); PKC-α inhibitor Gö6976 was purchased from Plymouth Meeting (U.S.); PKC-α activator PMA, PKA inhibitor H89, and activator Forskolin were purchased from Sigma (U.S.). Anti-p-PKCα, anti-total PKCα, anti-PKA, and chemiluminescence luminol reagents were purchased from Santa Cruz Biotechnology (U.S.); anti-p-ERK1/2, anti-total ERK1/2, and anti-Egr-1 were purchased from Cell Signaling Technology (U.S.); anti-β-actin and horseradish peroxidase-conjugated secondary antibodies were purchased from Wuhan Boster Biotechnology Limited Company (China); all the other chemicals and reagents were purchased from local agencies. Calcium-containing hypoxia solution was composed of the following: 137 mM NaCl, 12 mM KCl, 0.49 mM $MgCl_2 \cdot 6H_2O$, 0.9 mM of $CaCl_2$, 4 mM HEPES, and 20 mM Na lactate. Calcium-free hypoxia solution was composed of the following: 137 mM NaCl, 12 mM KCl, 0.49 mM $MgCl_2 \cdot 6H_2O$, 1 mM EGTA, 4 mM HEPES, and 20 mM Na lactate. The calcium absent reoxygenation solution was normal medium with 2 mM calcium-chelating EGTA added.

2.3. Establishment of Calcium-Containing (Normal Extracellular Calcium) and Calcium-Free (Lacking Extracellular Calcium) H/R Models and Experimental Groups. Cultured cardiomyocytes were randomly grouped (Figure 1). The calcium-containing-H/R model was established as described previously with 2-hour hypoxia instead of 3-hour hypoxia

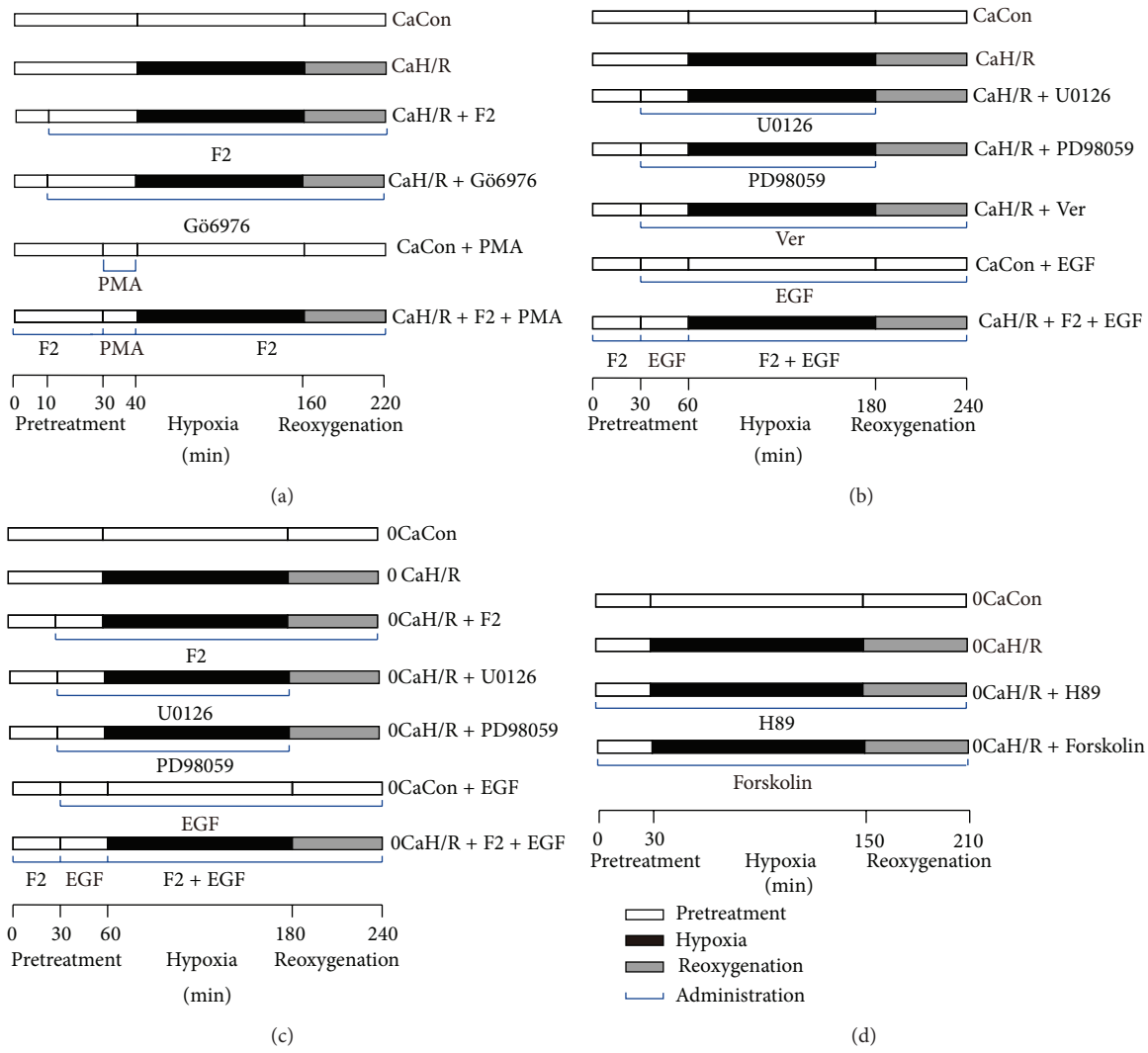

Figure 1: Protocols of experimental grouping and reagent administering. (a) Protocol used to investigate role of ERK1/2 and Egr-1 in extracellular-calcium-containing-H/R injury. (b) Protocol used to investigate role of PKCα/ERK1/2/Egr-1 in extracellular-calcium-containing-H/R injury. (c) Protocol used to investigate role of ERK1/2 and Egr-1 in extracellular-calcium-free-H/R injury. (d) Protocol used to investigate role of cAMP/PKA in extracellular-calcium-free-H/R injury. CaCon, calcium-containing normoxia; CaH/R, calcium-containing H/R; 0CaCon, calcium-free normoxic control; 0CaH/R, calcium-free H/R.

[2]. F_2 (1×10^{-6} mol/L), Ver (2×10^{-6} mol/L), inhibitors (PD98059 (2×10^{-5} mol/L), U0126 (2×10^{-5} mol/L) and Gö6976 (1×10^{-6} mol/L)), and activators (EGF (50 ng/mL) and PMA (1×10^{-7} mol/L)) were given in normal medium (for preincubation), hypoxia solution, and/or reoxygenation medium, respectively. The calcium-containing normoxia (CaCon) group was replenished with fresh medium before the experiment and cultured for 3 hours.

The calcium-free-H/R model was established as before only with calcium-free hypoxia solution substituting for calcium-containing hypoxia solution and calcium-free medium for normal medium. F_2, inhibitors (PD98059, U0126, and H89 (1×10^{-5} mol/L)) and activators (EGF and Forskolin (1×10^{-5} mol/L)) were also given as above. The calcium-free normoxic control (0CaCon) group was replenished with calcium-free medium before the experiment and cultured for 3 hours.

2.4. Western Blot Analysis. Total protein extracts were prepared from cultured cells using cell lysis buffer containing a protease inhibitor cocktail (aprotinin, leupeptin, pepstatin A, and PMSF). Western blot analysis was performed as described previously with some modifications [2]. The protein concentration was determined using a bicinchoninic acid assay (Bio-Rad, Hercules, CA, USA). Equal amounts of total protein were subjected to SDS-PAGE (10%) followed by electrophoretic transfer to nitrocellulose membranes. The nonspecific binding sites on the membrane were blocked with Tris buffer containing 5% nonfat dry milk for 1 hour. Membranes were probed with anti-p-PKCα, anti-total PKCα, anti-p-ERK1/2, anti-total ERK1/2, anti-Egr-1, anti-PKA, and anti-β-actin antibodies (1 : 5000 dilution for anti-β-actin, 1 : 1000 dilution for other antibodies) at 4°C overnight. Blots were then washed three times for 10 min with 20 mM Tris, 150 mM NaCl, and 0.1% Tween 20 (TBST) and incubated

with horseradish peroxidase-conjugated secondary antibodies (1 : 5000) for 1 hour. The detection of immunoreactive bands was performed using Western blotting chemiluminescence luminol reagents. The relative densities of protein bands were quantitated using Gel-pro software of densitometric analysis (Media Cybernetics, USA).

2.5. Measurements of Cardiac Troponin I (cTnI) and Lactate Dehydrogenase (LDH) Levels in Conditioned Medium. The release of cTnI and LDH was detected in conditioned medium after reoxygenation. The levels of cTnI were measured using an ACS 180 Automated Chemiluminescence System (Bayer Corp., U.S.) with a two-site sandwich immunoassay kit (Bayer Corp., U.S.). The levels of LDH in conditioned medium were determined using test kits (Jiancheng Bioengineering Institute, Nanjing, China):

$$\begin{aligned}\text{LDH activity (U/L)} &= \frac{(\text{OD of Assay} - \text{OD of Control})}{(\text{OD of Standard} - \text{OD of Blank})} \\ &\times \text{Standard Concentration}\,(2\,\mu\text{mol/mL}) \\ &\times 1000\,\text{mL}.\end{aligned} \quad (1)$$

2.6. Assessment of Cardiomyocyte Viability by Cell Counting Kit-8 (CCK-8) Colorimetric Assay. The cardiomyocytes were plated at 5×10^4 cells/well in 96 well plates. Then, 4-5 days later, the cells were treated as described previously. 10 μL of CCK-8 solution was added to 100 μL of reoxygenation solution and the cells were incubated for 1 additional hour after reoxygenation. The absorbance was measured by a microplate reader at 450 nm.

Consider

$$\begin{aligned}\text{Cell viability (\%)} &= \frac{(\text{OD of Assay} - \text{OD of Blank})}{(\text{OD of Control} - \text{OD of Blank})} \\ &\times 100\%.\end{aligned} \quad (2)$$

2.7. Levels of cAMP in Cultured Cardiomyocytes. The concentration of cAMP in cultured cardiomyocytes was determined by ELISA using a commercially available kit (Enzo Life Sciences International Inc., Switzerland) according to the manufacturer's instructions. All samples and standards were measured in duplicate. Briefly, cardiomyocytes were treated with 0.1 M HCl for 30 minutes and then harvested. After centrifugation, the supernatant was stored at −30°C for later analysis. Fifty microliters of standards and samples were added to a 96-well plate coated with GxR IgG antibody. Then, cAMP-conjugated alkaline phosphatase and cAMP antibody were added to all wells in sequence. After incubation for 2 hours on a plate shaker at 500 rpm, each well was washed three times with wash buffer and then incubated with substrate solution (p-nitrophenyl phosphate) for 1 hour. The reaction was stopped by addition of the stop solution (trisodium phosphate). The plate was read at 405 nm and the concentration of cAMP was calculated according to the standard curve.

2.8. Statistical Analysis. Data are shown as the mean ± SEM. The significance of differences was determined using one-way ANOVA followed the by Student-Newman-Keuls test. $P < 0.05$ was considered statistically significant.

3. Results

3.1. F_2 Inhibited Calcium-Containing-H/R-Induced ERK1/2 Activation and Consequently Reduced Egr-1 Protein Expression and cTnI Leakage and Improved Cell Viability in Myocardial Cells

3.1.1. Effects of F_2 on Calcium-Containing-H/R-Induced ERK1/2 Activation and Egr-1 Protein Expression. The ratio of p-ERK1/2 density to total ERK1/2 density reflects the degree of ERK activation. The ratio of total ERK density to β-actin density reflects total ERK protein level. The ratio of Egr-1 density to β-actin density reflects Egr-1 protein level. In each experiment, the density ratio in the CaCon group was set as 100% and the density ratio in other groups is here expressed relative to CaCon levels.

As shown in Figure 2, p-ERK1/2 and Egr-1 expression levels were significantly higher in the CaH/R group than in the CaCon group ($P < 0.05$). p-ERK1/2 and Egr-1 expression levels were significantly lower in the CaH/R+F_2 group, CaH/R+U0126 group, CaH/R+PD98059 group, and CaH/R+Ver group than in the CaH/R group ($P < 0.05$). There was no difference in total ERK1/2 protein expression across different groups ($P > 0.05$). EGF was found to antagonize F_2 inhibition of H/R-induced upregulation of p-ERK1/2 and Egr-1 expression but had no discernable effect on total ERK1/2 protein expression. EGF activated ERK1/2 under normoxia but did not affect Egr-1 expression. These results suggest that the ERK1/2 signaling pathway mediated calcium-containing-H/R-induced Egr-1 protein upregulation. F_2 inhibited Egr-1 expression by suppressing the ERK1/2 signaling pathway.

3.1.2. Influence of Inhibition of ERK1/2 Activation on Calcium-Containing-H/R-Induced Leakage of cTnI and Decrease of Cell Viability in Myocardial Cells. cTnI content in cultured cardiomyocyte supernatants was significantly higher and cell viability significantly lower in the CaH/R group than in the CaCon group ($P < 0.05$). F_2, Verapamil, and ERK1/2 inhibitors U0126 and PD98059 significantly reduced cTnI content and improved cell viability ($P < 0.05$). The ERK1/2 activator EGF was found to antagonize F_2's inhibition of cTnI leakage and improvement of cell viability ($P < 0.05$). Under normoxic conditions, EGF had no effect on cTnI content or cell viability (Table 1).

3.1.3. Regulatory Role of F_2 on Calcium-Containing-H/R-Induced Abnormal PKCα/ERK1/2/Egr-1 Pathway. The PKCα inhibitor Gö6976 and activator PMA were used to clarify the effects of F_2 on the PKCα/ERK1/2/Egr-1 signaling pathway. The ratio of p-PKCα density to total PKCα density was used to determine the degree of PKCα activation, and the ratio of total PKCα density to β-actin density was used to determine

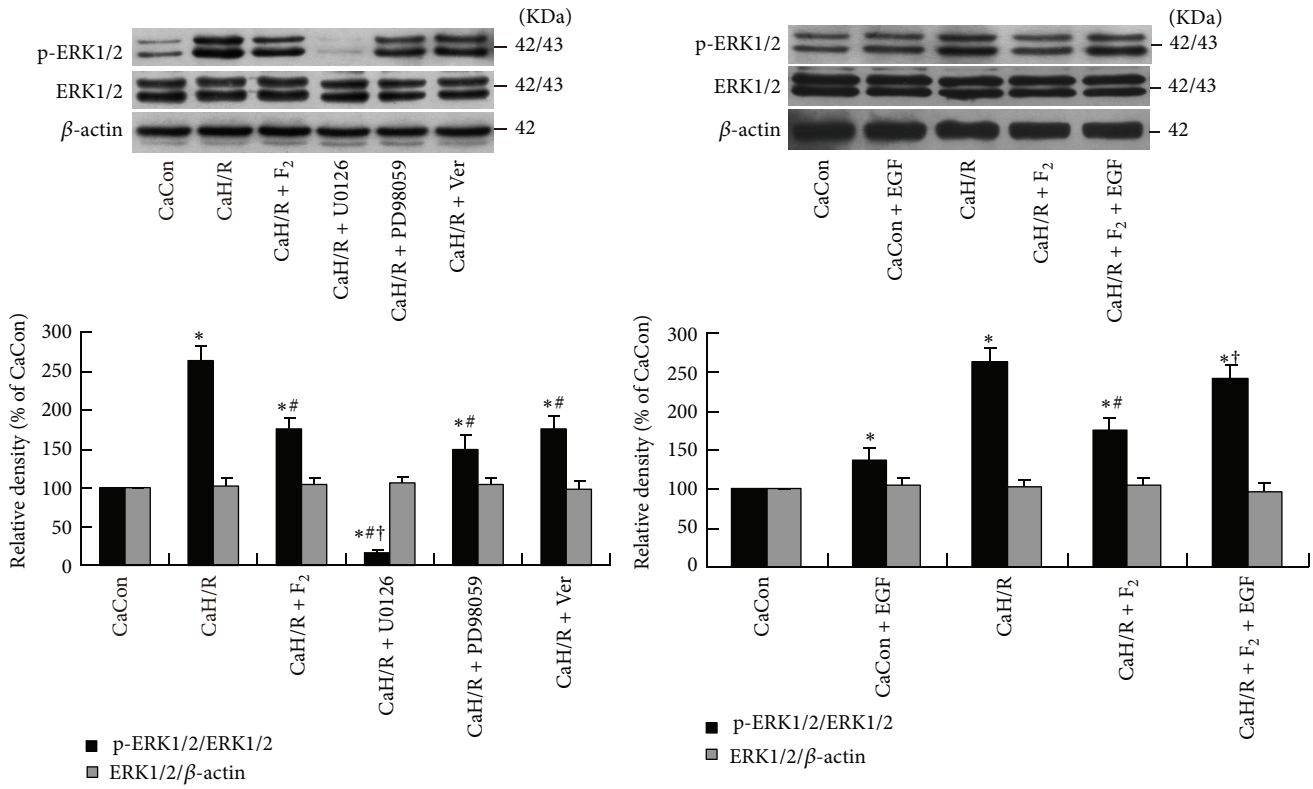

(a)

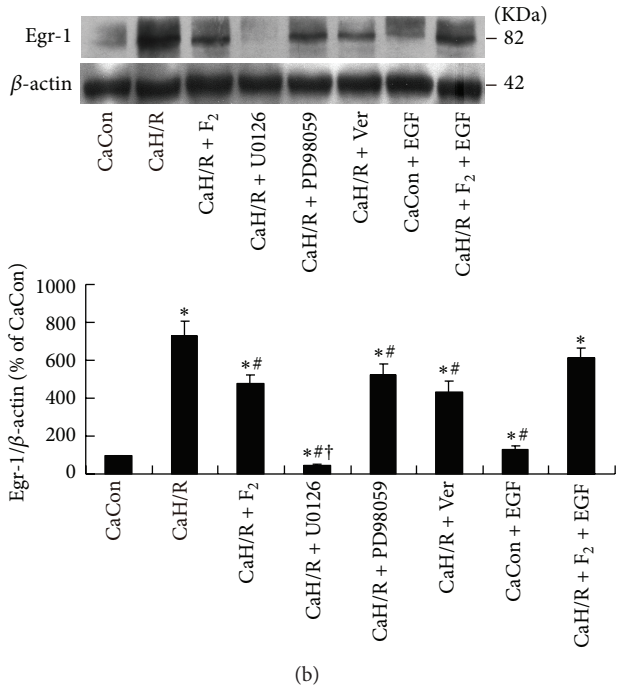

(b)

Figure 2: Effects of F_2, Verapamil, and ERK1/2 inhibitors and activator on p-ERK1/2, total ERK1/2, and Egr-1 expression in extracellular-calcium-containing myocardial H/R by western-blot assay. (a) p-ERK1/2 and total ERK1/2; (b) Egr-1 protein. Quantitative densitometric data were expressed as percentages of the level observed in the CaCon group. All values are expressed as mean ± SEM of at least six individual experiments. $^{*}P < 0.05$ versus CaCon group; $^{\#}P < 0.05$ versus CaH/R group; $^{\dagger}P < 0.05$ versus CaH/R+F_2 group.

Table 1: Effects of F_2, Verapamil, and ERK1/2 inhibitors and activator on cTnI level and cell viability in extracellular-calcium-containing myocardial H/R ($n = 9$).

Group	cTnI (ng/mL)	Survival rate (%)
CaCon	0.22 ± 0.01	100.00
CaH/R	0.61 ± 0.03*	47.51 ± 2.15*
CaH/R + F_2	0.49 ± 0.02$^{*\#}$	64.23 ± 2.78$^{*\#}$
CaH/R + U0126	0.50 ± 0.03$^{*\#}$	63.52 ± 2.46$^{*\#}$
CaH/R + PD98059	0.48 ± 0.02$^{*\#}$	60.40 ± 2.21$^{*\#}$
CaH/R + Ver	0.47 ± 0.02$^{*\#}$	56.85 ± 2.24$^{*\#}$
CaCon + EGF	0.22 ± 0.01$^{\#\dagger}$	93.34 ± 3.91$^{\#\dagger}$
CaH/R + F_2 + EGF	0.59 ± 0.01*†	48.54 ± 3.56*†

F_2, *N*-n-butyl haloperidol iodide; cTnI: cardiac troponin I; H/R: hypoxia/reoxygenation. $^{*}P < 0.05$ versus CaCon group; $^{\#}P < 0.05$ versus CaH/R group; $^{\dagger}P < 0.05$ versus CaH/R + F_2 group.

Table 2: Effects of F_2, and ERK1/2 inhibitors and activator on LDH level, cTnI level, and cell viability in extracellular-calcium-free myocardial H/R ($n = 9$).

Group	LDH (U/mL)	cTnI (ng/mL)	Survival rate (%)
0CaCon	968.65 ± 12.37	0.17 ± 0.01	100.00
0CaH/R	1342.35 ± 15.82*	0.84 ± 0.03*	50.66 ± 1.90*
0CaH/R + F_2	1135.16 ± 22.33$^{*\#}$	0.62 ± 0.04$^{*\#}$	67.38 ± 2.94$^{*\#}$
0CaH/R + U0126	1155.04 ± 24.24$^{*\#}$	0.69 ± 0.03$^{*\#}$	62.81 ± 4.58$^{*\#}$
0CaH/R + PD98059	1261.39 ± 14.20$^{*\#}$	0.53 ± 0.02$^{*\#\dagger}$	57.73 ± 2.71$^{*\#}$
0CaCon + EGF	1019.90 ± 17.16$^{\#\dagger}$	0.17 ± 0.01$^{\#\dagger}$	94.01 ± 4.70$^{\#\dagger}$
0CaH/R + F_2 + EGF	1421.43 ± 17.16*†	0.77 ± 0.05*†	53.17 ± 2.48*†

F_2, *N*-n-butyl haloperidol iodide; LDH: lactate dehydrogenase; cTnI: cardiac troponin I; H/R: hypoxia/reoxygenation. $^{*}P < 0.05$ versus 0CaCon group; $^{\#}P < 0.05$ versus 0CaH/R group; $^{\dagger}P < 0.05$ versus 0CaH/R + F_2 group.

total PKCα protein expression levels. In each experiment, the density ratio in CaCon group was set as 100% and the density ratios in other groups are expressed relative to CaCon group levels (Figure 3).

PKCα activity was significantly higher in the CaH/R group than in the CaCon group ($P < 0.05$). PKCα activity was significantly lower in the CaH/R + F_2 group, CaH/R + Gö6976 group, and CaH/R + Ver group than in the CaH/R group ($P < 0.05$). The PKCα activator PMA was found to antagonize F_2 inhibition of calcium-containing-H/R-induced PKCα activation in cardiomyocytes (Figure 3(a)). p-ERK1/2 (Figure 3(b)) and Egr-1 (Figure 3(c)) showed the same trend as p-PKCα. There were no significant differences in total PKCα or total ERK protein expression ($P > 0.05$). Under normoxia, PMA activated PKCα and ERK1/2 but did not stimulate Egr-1 protein expression. This study showed that F_2 inhibited abnormal calcium-containing-H/R-induced activation of the PKCα/ERK1/2/Egr-1 signal pathway.

3.2. F_2 Protected Cardiomyocytes from Calcium-Free H/R Injury through Inhibition of ERK1/2 Activation

3.2.1. Effects of F_2 on the Calcium-Free-H/R-Induced ERK1/2 and Egr-1 Expression and the Relationship of ERK1/2 with Egr-1. As shown in Figure 4, ERK1/2 activity was significantly higher in the 0CaH/R group than in the 0CaCon group ($P < 0.05$). ERK1/2 activation was significantly lower in the 0CaH/R+F_2 group, 0CaH/R+U0126 group, and 0CaH/R+PD98059 group than in the 0CaH/R group ($P < 0.05$). ERK1/2 agonist EGF was found to antagonize F_2 inhibition of calcium-free-H/R-induced p-ERK1/2 upregulation in cardiomyocytes. No difference in total ERK expression was observed between groups ($P > 0.05$). These results suggested that F_2 could antagonize calcium-free-H/R-induced abnormal activation of ERK1/2 pathway in cardiomyocytes.

No significant changes in Egr-1 protein expression were observed between groups ($P > 0.05$). In the absence of extracellular calcium, H/R was found to activate ERK1/2 but had no effect on Egr-1 protein expression, suggesting that there was no upstream-downstream correlation between ERK1/2 and Egr-1. F_2 had no effect on Egr-1 protein expression in cardiomyocytes under calcium-free H/R injury conditions.

3.2.2. Effects of Inhibition of ERK1/2 Activation on Calcium-Free-H/R-Induced Leakage of LDH and cTnI and Decrease of Cell Viability. LDH and cTnI levels in cultured cardiomyocyte supernatants were significantly higher, and cell viability was significantly lower in the 0CaH/R group than in the 0CaCon group ($P < 0.05$). F_2 and ERK1/2 inhibitors U0126 and PD98059 were found to significantly reduce LDH and cTnI concentration and improve cell viability ($P < 0.05$). The ERK1/2 activator EGF was found to antagonize F_2 inhibition of LDH and cTnI leakage and improvement of cell viability ($P < 0.05$). Under normoxic conditions, EGF was found to have no effect on LDH or cTnI levels or on cell viability (Table 2).

3.2.3. Role of the cAMP/PKA Pathway in F_2 Protection of Cardiomyocyte from Calcium-Free-H/R-Induced Injury. cAMP/PKA is involved in the regulation of myocardial cell function during I/R by acting as an upstream signaling molecule to activate the ERK1/2 signaling pathway [22]. Like Ca^{2+}, cAMP is a transmembrane second messenger. It can be considered a noncalcium second messenger. In this study, we evaluated the effects of F_2 on cAMP levels and PKA protein expression and examined the effects of PKA inhibitor H89 and activator Forskolin on LDH leakage in cardiomyocytes during calcium-free H/R. The density ratio of PKA to β-actin was used to indicate PKA protein expression. The density of PKA in the 0CaCon group was set at 100%, and the density in other groups was calculated relative to these values.

cAMP levels were lower in the 0CaH/R group than in the 0CaCon group, but the difference was not statistically significant ($P > 0.05$). F_2 was found to have no effect on cAMP levels in calcium-free H/R. No significant difference in PKA protein was observed between different groups ($P > 0.05$). LDH levels in cultured cell supernatants were

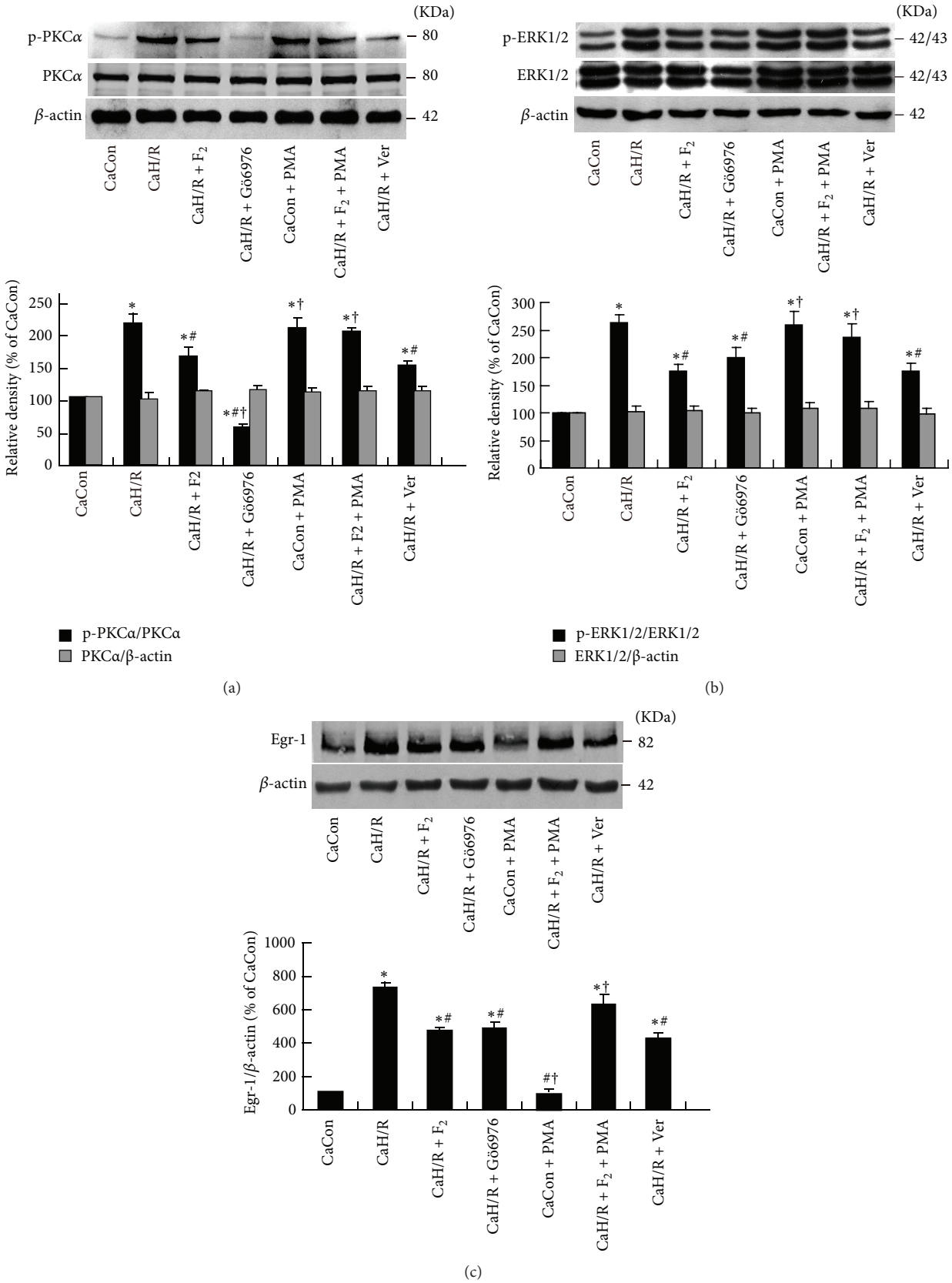

Figure 3: Effects of F_2, Verapamil, and PKCα inhibitor and activator on p-PKCα, total PKCα, p-ERK1/2, total ERK1/2, and Egr-1 expression in extracellular-calcium-containing myocardial H/R by western-blot assay. (a) p-PKCα and total PKCα protein levels; (b) p-ERK1/2 and total ERK1/2 protein levels; (c) Egr-1 protein levels. All values are expressed as mean ± S.E.M. of at least six individual experiments. $^{*}P < 0.05$ versus CaCon group; $^{\#}P < 0.05$ versus CaH/R group; $^{\dagger}P < 0.05$ versus CaH/R+F_2 group.

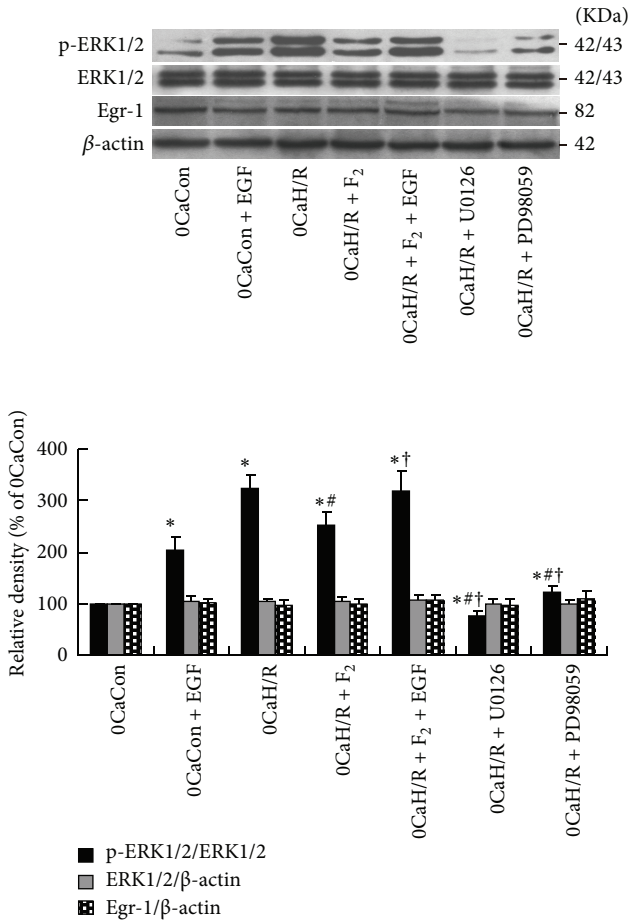

Figure 4: Effects of F_2, ERK1/2 inhibitors, and activator on p-ERK1/2, total ERK1/2, and Egr-1 expression in extracellular-calcium-free myocardial H/R by western-blot assay. All values are expressed as mean ± S.E.M. of at least six individual experiments. $^{*}P < 0.05$ versus 0CaCon group; $^{\#}P < 0.05$ versus 0CaH/R group; $^{\dagger}P < 0.05$ versus 0CaH/R+F_2 group.

significantly higher in the 0CaH/R group than in the 0CaCon group ($P < 0.05$). However, H89 and Forskolin were found to have no effect on LDH levels in cardiomyocytes under calcium-free H/R conditions (Tables 3 and 4 and Figure 5).

4. Discussion

4.1. Effects of ERK1/2 Activation by H/R Stimulation on Cardiomyocyte Damage. The ERK1/2 pathway is an important cell signaling pathway. It can transfer extracellular information into the nuclei and mediate the ultimate cellular reaction. The studies have shown that the ERK1/2 signaling pathway is involved in I/R injury in a variety of tissues and organs, especially in myocardial tissue [13, 24–27]. In this study, we focused on the relationship between myocardial H/R injury and the ERK1/2 signaling pathway. Our results show that H/R stimulation activated ERK1/2 in both the presence and absence of calcium. This was demonstrated by increased levels of p-ERK1/2 and unchanged levels of total ERK. The ERK1/2-specific inhibitors U0126 and PD98059

Table 3: Effects of F_2 on cAMP levels of cardiomyocyte in extracellular-calcium-free H/R ($n = 7$).

Group	cAMP (pmol/mL)
0CaCon	2.82 ± 0.55
0CaH/R	1.60 ± 0.35
0CaH/R + F_2	1.48 ± 0.56

F_2, *N*-n-butyl haloperidol iodide; cAMP: cyclic adenosine monophosphate; H/R: hypoxia/reoxygenation.

Table 4: Effects of PKA inhibitor and activator on LDH leakage of cardiomyocyte in extracellular-calcium-free H/R ($n = 9$).

Group	LDH (U/mL)
0CaCon	952.70 ± 32.02
0CaH/R	1378.33 ± 72.26*
0CaH/R + H89	1389.14 ± 71.65*
0CaH/R + Forskolin	1338.78 ± 51.68*

LDH: lactate dehydrogenase; PKA: protein kinase A; H/R: hypoxia/reoxygenation.* $P < 0.05$ versus 0CaCon group.

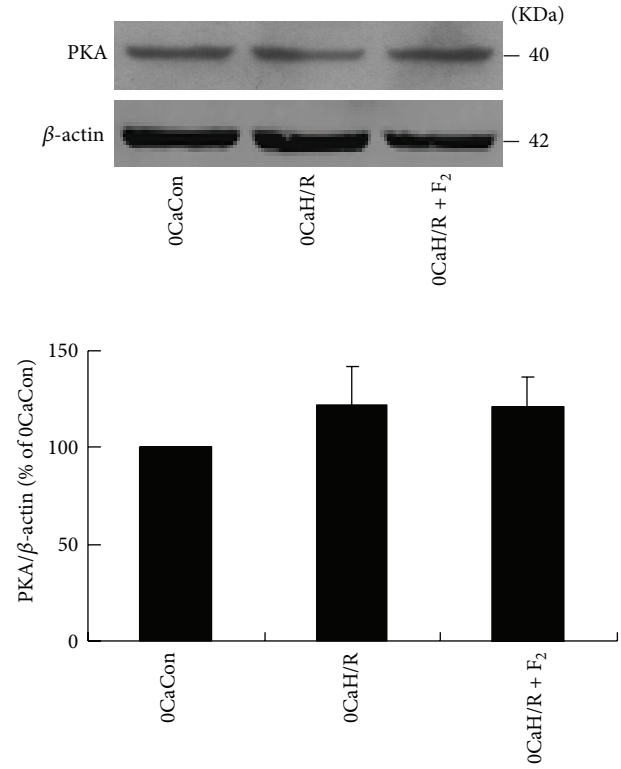

Figure 5: Effects of F_2 on PKA expression in extracellular-calcium-free myocardial H/R by western-blot assay. All values are expressed as the mean ± S.E.M. of at least six individual experiments.

effectively inhibited calcium-containing- and calcium-free-H/R-induced ERK1/2 activation, leading to reduced cell damage, as demonstrated by reduced levels of LDH and cTnI leakage, and improved cell viability. These indicate that ERK1/2 activation caused cardiomyocyte damage in both calcium-containing- and calcium-free-H/R stimulation.

Although studies have suggested that activation of the ERK1/2 pathway may promote cell survival [28, 29], our results have shown that the activation of ERK1/2 signaling pathway led to cell damage under myocardial H/R conditions. This result has been supported by many studies, such as the study conducted by Kang et al., which demonstrated that activated ERK1/2 induced by H/R might be novel drug target in cardiomyocytes [30], and the studies of Tsoporis et al. and Liu et al., where they found that the activation of ERK1/2-p53 signaling pathway caused cardiomyocyte apoptosis after myocardial infarction or administration of anticancer drug doxorubicin [31, 32]. In this way, ERK1/2 has a significant impact on the pathophysiological status of cells, but its role may be different in various cell types and experimental models. We believe that the ERK1/2 may play different roles during different stages of I/R: the activation of ERK1/2 in a very short period of I/R may initiate the endogenous protective processes, such as in ischemic preconditioning, but when accompanied by the extension of I/R processes, ERK1/2 activation may initiate injury signals, leading to cell injury [33, 34].

4.2. Role of Egr-1 Expression Inhibition through the Calcium-Dependent PKCα/ERK1/2/Egr-1 Pathways on F_2 Protection against Myocardial H/R Injury. Our preliminary results showed that blocking L-type calcium channels can inhibit calcium influx and reduce intracellular calcium overload, thereby inhibiting calcium-dependent PKCα activation and subsequent abnormal expression of Egr-1. This is one of the important calcium-dependent mechanisms underlying F_2 protection from H/R-induced myocardial cell injury. However, it is not clear whether ERK mediates signal transduction between PKCα and Egr-1.

We found in one previous study that H/R could induce PKCα translocation from soluble fraction to particulate fraction in cardiomyocytes [8]. In the present study, we also found that H/R could activate PKCα by increasing its phosphorylation. We also observed that the PKCα inhibitor Gő6976 inhibited both p-ERK1/2 and Egr-1 protein overexpression, indicating that PKCα activation has an important impact on ERK1/2 activation and Egr-1 overexpression, which means that both ERK1/2 and Egr-1 are downstream molecules of PKCα signal pathway. Using the ERK1/2 inhibitors U0126 and PD98059, we found ERK1/2 to be an upstream signaling molecule of Egr-1. In the present study, we proved that H/R caused abnormal activation of PKCα/ERK1/2/Egr-1 pathway, leading to a series of cellular injuries.

In this study, p-PKCα, p-ERK1/2, and Egr-1 protein expression decreased after F_2 treatment, but total PKCα and ERK1/2 protein expression did not change, suggesting that F_2 can also inhibit PKCα and ERK1/2 activation in addition to suppressing Egr-1. The PKCα activator PMA can inhibit F_2 downregulation of p-PKCα expression and downregulation of p-ERK1/2 and egr-1 protein expression, suggesting that F_2 inhibition of ERK1/2 and Egr-1 is dependent on its inhibition of PKCα activation. The ERK1/2 activator EGF can inhibit F_2 downregulation of p-ERK1/2 activation and Egr-1 protein expression and F_2 protection of cardiomyocytes (including inhibition of cTnI leakage and improvement of cell viability), suggesting that F_2 protection of cardiomyocytes is dependent on its inhibition of ERK1/2 activation and subsequent downregulation of Egr-1 protein expression. In this way, we proved that F_2 inhibition of ERK1/2 activation is PKCα-dependent and that F_2 inhibition of Egr-1 overexpression is ERK1/2-dependent, suggesting that F_2 protection of cardiomyocytes under H/R conditions takes place through its regulation of the abnormal PKCα/ERK1/2/Egr-1 signaling pathway. In addition, in this study, we used Verapamil as a positive control for the calcium antagonist and found that Verapamil, like F_2, has an effect on p-PKCα, p-ERK1/2, and Egr-1 protein expression and protects cardiomyocytes from a series of H/R injuries. This suggests that both F_2 and Verapamil can regulate the abnormal PKCα/ERK1/2/Egr-1 pathway, which might be initiated through the regulation of calcium. This hypothesis was supported by the fact that PKCα is a calcium-dependent kinase. Under normoxic conditions, Egr-1 expression was low and PMA treatment activated ERK1/2 but did not stimulate Egr-1 protein expression. Similarly, the ERK1/2 activator EGF did not cause Egr-1 protein overexpression or cell damage. These results suggest that the ERK1/2-related cell signaling network is very complicated and the specific intracellular microenvironment at H/R stimulation determines ERK1/2 downstream signaling and its ultimate functions.

4.3. Inhibition of ERK1/2 Activation Is One of the Extracellular Calcium-Independent Mechanisms for F_2 Protection against Myocardial H/R Injury. Intracellular calcium overload is an important cause of I/R injury. Calcium antagonists can antagonize intracellular calcium overload and protect cardiomyocytes from I/R injury. However, Hempel et al. found that Nifedipine had no effect on ischemia-induced intracellular calcium increases in endothelial cells but it could prevent ischemia-induced PKC translocation and ameliorate increased ischemia-induced endothelial cell permeability [35]. A study performed by Eickelberg et al. showed that Amlodipine, Diltiazem, and Verapamil could regulate transcription factor NF-IL6 and NF-κB in an intracellular-calcium-independent manner [36]. These results indicate that calcium antagonists can affect cell function in ways other than blockage of calcium channels and affecting intracellular calcium levels. Our preliminary results also showed that F_2, a new L-type calcium antagonist, can not only activate calcium-independent PKCε through translocation in rat cardiomyocytes at the H/R stimulation and protect cardiomyocytes but also protect rat coronary endothelial cells, which do not have L-type calcium channels, from H/R injury [6, 8–11]. We therefore have reason to speculate that F_2 can protect myocardial cells from H/R injury in an extracellular-calcium-independent manner.

Our results showed that F_2 inhibited calcium-free-H/R-induced ERK1/2 activation, leading to reduced LDH and cTnI leakage, and improved cell viability. The ERK1/2 activator EGF antagonized F_2 inhibition of calcium-free-H/R-induced p-ERK1/2 upregulation and inhibited F_2 protection of cardiomyocytes. These data indicate that in calcium-free H/R,

F_2 can act on ERK1/2 directly or its upstream signal molecule and protect cardiomyocytes from H/R injury. In other words, blocking H/R-induced ERK1/2 pathway activation is an extracellular-calcium-independent mechanism by which F_2 protects cardiomyocytes. Under normoxic conditions, EGF was found to activate ERK1/2 in the presence or absence of calcium but it did not cause cardiomyocyte injury. However, ERK1/2 activation can cause cell injury in H/R, indicating that although ERK1/2 is a key mediator, it still needs other factors to cause cell injury.

In the study of ERK1/2-related pathways, our results showed that cAMP levels was lower in the 0CaH/R group than in the 0CaCon group, but this difference were not statistically significant and PKA levels did not change between the groups. In the 0CaH/R group, LDH leakage increased and the PKA activator Forskolin and inhibitor H89 had no effect on calcium-free-H/R-induced LDH leakage, suggesting that calcium-free-H/R-induced cardiomyocyte injury is not mediated by the cAMP/PKA pathway. We also observed that F_2 had no effect on cAMP concentration or PKA protein expression in calcium-free H/R stimulation, indicating that the extracellular calcium-independent mechanism of F_2 protection against H/R injury in cardiomyocytes is related to ERK1/2, but the upstream signaling molecule is not related to cAMP/PKA.

This study and our previous studies showed that the myocardial protective effects of F_2 are related to the inhibition of I/R- and H/R-induced Egr-1 mRNA and protein overexpression. But the present study showed that calcium-free H/R did not cause Egr-1 protein upregulation and that F_2 had no effect on Egr-1 protein expression in cardiomyocytes in calcium-free H/R. One possible explanation for this is that calcium is involved in the H/R-induced upregulation of Egr-1. We had found that three different types of calcium antagonists, Verapamil, Diltiazem, and Nifedipine, suppressed I/R- and H/R-induced Egr-1 mRNA and protein up-regulation to some extent [7]. Similarly, Lo et al. found that the calcium chelator BAPTA/AM completely inhibited hypoxia-induced Egr-1 overexpression in endothelial cells [37]. We previously observed H/R-induced Egr-1 overexpression and F_2 protection and inhibition of Egr-1 in microvascular endothelial cells [9–11]. These cells lack L-type calcium channels. However, these specific cells were in an environment with calcium. We therefore speculate that H/R may cause extracellular calcium influx and ultimately Egr-1 overexpression due to counter-transportation of calcium by the Na^+/Ca^{2+} exchanger (NCX) or membrane integrity destruction. F_2 exhibited its regulation of Egr-1 expression and protective effect on microvascular endothelial cells through the inhibition of NCX outward currents and the subsequent reduction in calcium influx [38]. In this study, EGTA chelated all extracellular calcium and the intracellular-extracellular calcium gradient disappeared. All means of extracellular calcium influx were eliminated and so calcium-dependent Egr-1 overexpression and F_2's regulation to it became difficult in calcium-free H/R.

Although we observed abnormal ERK/Egr-1 pathway activity in calcium-containing H/R model, ERK1/2 inhibitors and activator had no effect on Egr-1 protein expression in calcium-free H/R. This indicates that ERK activation is a master switch to trigger myocardial H/R injury whether in extracellular calcium-containing or calcium-free H/R, nevertheless, its downstream signaling is also determined by the specific intracellular microenvironment such as intracellular calcium concentration. Thus, in the present study, we found that Egr-1 expression did not change with ERK activation when the influx of calcium was eliminated in calcium-free H/R. This result has been supported by Josefsen et al., who found that Egr-1 expression was dependent on Ca^{2+} influx [39]. Of course, other downstream signaling molecules can be involved and worthy of further study.

5. Conclusions

In summary, in cultured cardiomyocytes, both extracellular-calcium-containing- and extracellular-calcium-free-H/R were found to activate ERK1/2, leading to cell damage. F_2 was found to protect cardiomyocytes against H/R injury by regulating extracellular calcium-dependent abnormal PKCα/ERK1/2/Egr-1 signaling pathway. F_2 was also found to protect cardiomyocytes from H/R injury through extracellular calcium-independent mechanisms, which may be related to its suppression of H/R-induced ERK1/2 activation but are not related to the cAMP/PKA signaling pathway or to Egr-1 protein expression.

Conflict of Interests

The authors declare that there is no conflict of interests.

Acknowledgments

This work was supported by National Natural Science Foundation of China (NSFC) Guangdong Joint Funds (no. U0932005), National Natural Science Foundation of China (no. 81072633), and The Central Government Special Funds Supporting the Development of Local Colleges and Universities.

References

[1] F.-F. Gao, G.-G. Shi, J.-H. Zheng, and B. Liu, "Protective effects on N-n-butyl haloperidol iodide on myocardial ischemia-reperfusion injury in rabbits," *Chinese Journal of Physiology*, vol. 47, no. 2, pp. 61–66, 2004.

[2] Y. Zhang, G. Shi, J. Zheng et al., "The protective effects of N-n-butyl haloperidol iodide on myocardial ischemia-reperfusion injury in rats by inhibiting Egr-1 overexpression," *Cellular Physiology and Biochemistry*, vol. 20, no. 5, pp. 639–648, 2007.

[3] Y.-M. Zhang, G.-G. Shi, Z. Tang et al., "Effects of N-n-butyl haloperidol iodide on myocardial ischemia/reperfusion injury and Egr-1 expression in rat," *Acta Biochimica et Biophysica Sinica*, vol. 38, no. 6, pp. 435–441, 2006.

[4] Z.-Q. Huang, G.-G. Shi, J.-H. Zheng, and B. Liu, "Effects of N-n-butyl haloperidol iodide on rat myocardial ischemia and reperfusion injury and L-type calcium current," *Acta Pharmacologica Sinica*, vol. 24, no. 8, pp. 757–763, 2003.

[5] Y. Zhang, G. Shi, J. Zheng et al., "The protective effect of Egr-1 antisense oligodeoxyribonucleotide on myocardial injury induced by ischemia-reperfusion and hypoxia-reoxygenation," *Cellular Physiology and Biochemistry*, vol. 22, no. 5-6, pp. 645–652, 2008.

[6] Y. Zhou, Y. Zhang, F. Gao et al., "N-n-butyl haloperidol iodide protects cardiac microvascular endothelial cells from hypoxia/reoxygenation injury by down-regulating egr-1 expression," *Cellular Physiology and Biochemistry*, vol. 26, no. 6, pp. 839–848, 2010.

[7] Z. Huang, H. Li, F. Guo et al., "Egr-1, the potential target of calcium channel blockers in cardioprotection with ischemia/reperfusion injury in rats," *Cellular Physiology and Biochemistry*, vol. 24, no. 1-2, pp. 17–24, 2009.

[8] J.-Z. Wang, C.-Y. Cai, Y.-M. Zhang et al., "N-n-Butyl haloperidol iodide protects against hypoxia/reoxygenation-induced cardiomyocyte injury by modulating protein kinase C activity," *Biochemical Pharmacology*, vol. 79, no. 10, pp. 1428–1436, 2010.

[9] T. Matsui, S.-I. Yamagishi, K. Nakamura, and H. Inoue, "Bay w 9798, a dihydropyridine structurally related to nifedipine with no calcium channel-blocking properties, inhibits tumour necrosis factor-α-induced vascular cell adhesion molecule-1 expression in endothelial cells by suppressing reactive oxygen species generation," *Journal of International Medical Research*, vol. 35, no. 6, pp. 886–891, 2007.

[10] S.-I. Yamagishi, K. Nakamura, and T. Matsui, "Role of oxidative stress in the development of vascular injury and its therapeutic intervention by nifedipine," *Current Medicinal Chemistry*, vol. 15, no. 2, pp. 172–177, 2008.

[11] R. Berkels, D. Taubert, A. Rosenkranz, and R. Rösen, "Vascular protective effects of dihydropyridine calcium antagonists. Involvement of endothelial nitric oxide," *Pharmacology*, vol. 69, no. 4, pp. 171–176, 2003.

[12] A. Clerk and P. H. Sugden, "Signaling through the extracellular signal-regulated kinase 1/2 cascade in cardiac myocytes," *Biochemistry and Cell Biology*, vol. 82, no. 6, pp. 603–609, 2004.

[13] D.-Y. Li, L. Tao, H. Liu, T. A. Christopher, B. L. Lopez, and X. L. Ma, "Role of ERK1/2 in the anti-apoptotic and cardioprotective effects of nitric oxide after myocardial ischemia and reperfusion," *Apoptosis*, vol. 11, no. 6, pp. 923–930, 2006.

[14] L. O. Murphy and J. Blenis, "MAPK signal specificity: the right place at the right time," *Trends in Biochemical Sciences*, vol. 31, no. 5, pp. 268–275, 2006.

[15] L. Mao, L. Yang, Q. Tang, S. Samdani, G. Zhang, and J. Q. Wang, "The scaffold protein Homer1b/c links metabotropic glutamate receptor 5 to extracellular signal-regulated protein kinase cascades in neurons," *Journal of Neuroscience*, vol. 25, no. 10, pp. 2741–2752, 2005.

[16] D. C. Andersson, J. Fauconnier, T. Yamada et al., "Mitochondrial production of reactive oxygen species contributes to the β-adrenergic stimulation of mouse cardiomycytes," *Journal of Physiology*, vol. 589, no. 7, pp. 1791–1801, 2011.

[17] S. J. Cook and F. McCormick, "Inhibition by cAMP of Ras-dependent activation of Raf," *Science*, vol. 262, no. 5136, pp. 1069–1072, 1993.

[18] P. Crespo, T. G. Cachero, N. Xu, and J. S. Gutkind, "Dual effect of β-adrenergic receptors on mitogen-activated protein kinase. Evidence for a $\beta\gamma$-dependent activation and a Gα(s)-cAMP-mediated inhibition," *Journal of Biological Chemistry*, vol. 270, no. 42, pp. 25259–25265, 1995.

[19] J. M. Schmitt and P. J. S. Stork, "Cyclic AMP-mediated inhibition of cell growth requires the small G protein Rap1," *Molecular and Cellular Biology*, vol. 21, no. 11, pp. 3671–3683, 2001.

[20] Y. Wan and X.-Y. Huang, "Analysis of the G(s)/mitogen-activated protein kinase pathway in mutant S49 cells," *Journal of Biological Chemistry*, vol. 273, no. 23, pp. 14533–14537, 1998.

[21] M. C. MacNicol and A. M. MacNicol, "Nerve growth factor-stimulated B-Raf catalytic activity is refractory to inhibition by cAMP-dependent protein kinase," *Journal of Biological Chemistry*, vol. 274, no. 19, pp. 13193–13197, 1999.

[22] J. Zheng, H. Shen, Y. Xiong, X. Yang, and J. He, "The β1-adrenergic receptor mediates extracellular signal-regulated kinase activation via Gαs," *Amino Acids*, vol. 38, no. 1, pp. 75–84, 2010.

[23] W.-Z. Zhu, M. Zheng, W. J. Koch, R. J. Lefkowitz, B. K. Kobilka, and R.-P. Xiao, "Dual modulation of cell survival and cell death by β2-adrenergic signaling in adult mouse cardiac myocytes," *Proceedings of the National Academy of Sciences of the United States of America*, vol. 98, no. 4, pp. 1607–1612, 2001.

[24] W.-J. Xing, F.-J. Kong, G.-W. Li et al., "Calcium-sensing receptors induce apoptosis during simulated ischaemia-reperfusion in Buffalo rat liver cells," *Clinical and Experimental Pharmacology and Physiology*, vol. 38, no. 9, pp. 605–612, 2011.

[25] S. Yamamoto, M. Yamane, O. Yoshida et al., "Activations of mitogen-activated protein kinases and regulation of their downstream molecules after rat lung transplantation from donors after cardiac death," *Transplantation Proceedings*, vol. 43, no. 10, pp. 3628–3633, 2011.

[26] H.-P. Tian, B.-S. Huang, J. Zhao, X.-H. Hu, J. Guo, and L.-X. Li, "Non-receptor tyrosine kinase Src is required for ischemia-stimulated neuronal cell proliferation via Raf/ERK/CREB activation in the dentate gyrus," *BMC Neuroscience*, vol. 10, article 139, 2009.

[27] M. Alderliesten, M. De Graauw, J. Oldenampsen et al., "Extracellular signal-regulated kinase activation during renal ischemia/reperfusion mediates focal adhesion dissolution and renal injury," *American Journal of Pathology*, vol. 171, no. 2, pp. 452–462, 2007.

[28] G. Milano, L. K. Von Segesser, S. Morel et al., "Phosphorylation of phosphatidylinositol-3-kinase-protein kinase B and extracellular signal-regulated kinases 1/2 mediate reoxygenation-induced cardioprotection during hypoxia," *Experimental Biology and Medicine*, vol. 235, no. 3, pp. 401–410, 2010.

[29] O. F. Bueno and J. D. Molkentin, "Involvement of extracellular signal-regulated kinases 1/2 in cardiac hypertrophy and cell death," *Circulation Research*, vol. 91, no. 9, pp. 776–781, 2002.

[30] S.-M. Kang, S. Lim, H. Song et al., "Allopurinol modulates reactive oxygen species generation and Ca^{2+} overload in ischemia-reperfused heart and hypoxia-reoxygenated cardiomyocytes," *European Journal of Pharmacology*, vol. 535, no. 1–3, pp. 212–219, 2006.

[31] J. N. Tsoporis, S. Izhar, H. Leong-Poi, J.-F. Desjardins, H. J. Huttunen, and T. G. Parker, "S100B interaction with the receptor for advanced glycation end products (RAGE): a novel receptor-mediated mechanism for myocyte apoptosis postinfarction," *Circulation Research*, vol. 106, no. 1, pp. 93–101, 2010.

[32] J. Liu, W. Mao, B. Ding, and C.-S. Liang, "ERKs/p53 signal transduction pathway is involved in doxorubicin-induced apoptosis in H9c2 cells and cardiomyocytes," *American Journal of Physiology*, vol. 295, no. 5, pp. H1956–H1965, 2008.

[33] X. Yang, M. V. Cohen, and J. M. Downey, "Mechanism of cardioprotection by early ischemic preconditioning," *Cardiovascular Drugs and Therapy*, vol. 24, no. 3, pp. 225–234, 2010.

[34] J.-Z. Juan-Zhang, H.-J. Bian, X.-X. Li et al., "ERK-MAPK signaling opposes rho-kinase to reduce cardiomyocyte apoptosis in heart ischemic preconditioning," *Molecular Medicine*, vol. 16, no. 7-8, pp. 307–315, 2010.

[35] A. Hempel, C. Lindschau, C. Maasch et al., "Calcium antagonists ameliorate ischemia-induced endothelial cell permeability by inhibiting protein kinase C," *Circulation*, vol. 99, no. 19, pp. 2523–2529, 1999.

[36] O. Eickelberg, M. Roth, R. Mussmann et al., "Calcium channel blockers activate the interleukin-6 gene via the transcription factors NF-IL6 and NF-κB in primary human vascular smooth muscle cells," *Circulation*, vol. 99, no. 17, pp. 2276–2282, 1999.

[37] L.-W. Lo, J.-J. Cheng, J.-J. Chiu, B.-S. Wung, Y.-C. Liu, and D. L. Wang, "Endothelial exposure to hypoxia induces Egr-1 expression involving PKCα-mediated Ras/Raf-1/ERK1/2 pathway," *Journal of Cellular Physiology*, vol. 188, no. 3, pp. 304–312, 2001.

[38] Y. Huang, F. Gao, Y. Zhang et al., "N-n-Butyl haloperidol iodide inhibits the augmented Na^+/Ca^{2+} exchanger currents and L-type Ca^{2+} current induced by hypoxia/reoxygenation or H_2O_2 in cardiomyocytes," *Biochemical and Biophysical Research Communications*, vol. 421, no. 1, pp. 86–90, 2012.

[39] K. Josefsen, L. R. Sørensen, K. Buschard, and M. Birkenbach, "Glucose induces early growth response gene (Egr-1) expression in pancreatic beta cells," *Diabetologia*, vol. 42, no. 2, pp. 195–203, 1999.

Hindawi Publishing Corporation
Oxidative Medicine and Cellular Longevity
Volume 2013, Article ID 126083, 6 pages
http://dx.doi.org/10.1155/2013/126083

Research Article

Transient Acidosis during Early Reperfusion Attenuates Myocardium Ischemia Reperfusion Injury via PI3k-Akt-eNOS Signaling Pathway

Xin Qiao,[1,2] Jinjin Xu,[3] Qing-Jun Yang,[4] Yun Du,[1] Shaoqing Lei,[3] Zhi-Hong Liu,[5] Xinwei Liu,[2] and Huimin Liu[3]

[1] *Department of Anesthesiology, Chongqing Zhoushan Hospital, Chongqing 404100, China*
[2] *Department of Anesthesiology, The First Affiliated Hospital of Chongqing Medical University, Chongqing 404100, China*
[3] *Department of Anesthesiology, Renmin Hospital of Wuhan University, Wuhan 430000, China*
[4] *Department of Cardiac Surgery, Chongqing Zhoushan Hospital, Chongqing 404100, China*
[5] *Department of Cardiac Surgery, Sun Yat-sen Cardiovascular Hospital, Shenzhen 515100, China*

Correspondence should be addressed to Huimin Liu; huimin_liu2006@126.com

Received 9 August 2013; Accepted 25 September 2013

Academic Editor: Zhengyuan Xia

In this paper, we concluded that transient acidosis reperfusion conferred cardioprotection against myocardial ischemia reperfusion injury in isolated rat hearts through activating PI3K-Akt-eNOS pathway.

1. Introduction

During myocardial ischemia, tissue pH significantly declines and returns to normal after reperfusion [1]. Recently, studies reported that acidosis (pH < or = 7.0) protected profoundly against cell death during ischemia. However, the quick return from acidotic to normal pH after reperfusion may cause myocytes to lose viability. This worsening of postischemic injury is a "pH paradox" mediated by sudden or quick changes of intracellular pH (pHi) [2]. Normalization of pH after reperfusion initiates reactive oxygen species (ROS) formation and onset of the mitochondrial permeability transition pore (MPTP), which finally leads to cell death in cardiomyocytes, while acidosis can prevent mitochondrial permeability transition pore (MPTP) opening [3]. Therefore, prolongation of transient acidosis during early reperfusion may prevent the myocardium ischemia reperfusion injury.

Ischemic postconditioning, a novel strategy of cardioprotection consisting of the application of brief cycles of ischemia-reflow at the onset of reperfusion, represents a promising approach to protect the myocardium against ischemia and reperfusion injury [4, 5]. And this protection has been related to the activation of phosphatidylinositol 3-kinase-Akt dependent cytoprotective signaling pathway which is part of the reperfusion injury salvage kinase (RISK) that confers cardioprotection when activated at reperfusion [6, 7]. Additionally, Cohen et al. reported that ischemia postconditioning inhibits reoxygenated myocardium to produce reactive oxygen species and prevents MPTP formation by maintaining acidosis during the first 3 minutes of reperfusion [8]. Therefore, we hypothesized that direct acidotic infusion at the onset of reperfusion (acidosis postconditioning) could mimic ischemic postconditioning and induce the delayed recovery of pH and protect myocardium against ischemia reperfusion injury, and this protective effect may be mediated by PI3k-eNOS signaling pathway.

2. Methods

The experimental procedures conformed to the Guide for the Care and Use of Laboratory Animals published by National Institute of Health of the People's Republic of China and approved by the Institutional Animal Ethics Committee.

2.1. Isolated Perfused Rat Heart Preparation. Male Sprague-Dawley rats (450–550 g) were heparinised and then anaesthetized with urethan (700 mg/kg). The hearts were rapidly excised and mounted onto a Langendorff apparatus and perfused with modified Krebs-Henseleit bicarbonate buffer (KHB) that contained (in mM) 115.0 NaCl, 5.0 KCl, 1.2 $MgSO_4$, 1.2 KH_2PO_4, 1.25 $CaCl_2$, 25.0 $NaHCO_3$, and 11.0 Glucose, equilibrated with 95% O_2 and 5% CO_2 to create perfusate pH 7.4, and maintained at 37°C as previously described [8]. Flow rate was initially adjusted to produce a perfusion pressure of 60 mmHg and was held constant thereafter. Then a water-filled latex balloon was inserted into left ventricle (LV) and inflated to obtain an end-diastolic pressure (LVEDP) between 6 and 8 mmHg. A pressure transducer connected to the perfusion line was used to continuously recorde the perfusion pressure.

2.2. Experimental Protocol. Rats were randomly divided into 7 groups ($n = 12$ per group). In control group, hearts were stabilized for 30 min and then subjected to no-flow global ischemia by inflation of the coronary balloon for 30 min followed by 120 min of reperfusion with normal KHB (C group). Postconditioning was achieved by 6 cycles of 15 s reperfusion and 15 s occlusion after no-flow global ischemia (IPO group). In the acidotic reperfusion group, hearts were perfused with KHB adjusted at pH 6.9 for the first 3 min of reperfusion (H^+ group). The acidotic perfusion buffer was adjusted by equilibrating with 80% O_2/20% CO_2 (pH 6.9). To test whether alkali abolished the protection of ischemia postconditioning, hearts were postconditioned with alkalotic buffer which was equilibrated with 100% O_2 (pH 7.8) (IPO + OH^-). In OH^- group, hearts were only reperfused with alkalotic buffer without ischemia postconditioning. Finally, PI3k specific inhibitor wortmannin (100 nmol/L) was added to the acidotic perfused and infused into heart for the first 3 min of reperfusion after ischemia (H^+ + wort group). In wort group, hearts were reperfused with normal KHB cotreatment of wort (100 nmol/L). After the first 3 min of reperfusion with respective treatment, all groups were switched to buffer equilibrated with 5% CO_2. In all hearts, reperfusion lasted for 120 min.

2.3. Infarct Size Measurement. After 120 min of reperfusion, the coronary artery was reoccluded. The hearts were weighed and frozen at −20°C for 20 min and then underwent horizontal long axis slicing at a thickness of 1-2 mm. The slices were incubated for 15 minutes at 37°C in buffered 1% triphenyltetrazolium chloride in order to stain noninfarcted myocardium brick red. Slices were then fixed in 10% formalin for 5 minutes. The infarct size was defined as the ratio of the weight of the necrotic zone to that of the ischemic zone as previously described [9].

2.4. Quantification of Nitric Oxide Release in Isolate Hearts. NO release was measured in the perfusates previously described [10] under ultraviolet/visual spectrometry using an extinction coefficient of 411 nm to 401 nm at ambient temperature. The respective measurements were performed using a double-beam spectrometer (DW2000, SLM-Aminco, USA).

2.5. Western Blot Assay for Akt and eNOS. Frozen heart tissues were homogenized using lysis buffer (20 mmol/L Tris-HCl, PH 7.5, 50 mmol/L 2-mercaptoethanol, 5 mmol/L EGTA, 2 mmol/L EDTA, 1% NP40, 0.1% sodium dodecyl sulfate (SDS), 0.5% deoxycholic acid, 10 mmol/L NaF, 1 mmol/L PMSF, 25 mg/mL leupeptin, and 2 mg/mL aprotinin) for 30 min then sonicated and centrifuged at 12000 g for 20 min at 4°C. Protein concentrations were determined using the Bradford assay (Bio-Rad, USA). Samples containing equal amounts were separated on a 10% SDS-polyacrylamide gel, and then proteins were transferred to PVDF membrane overnight at 4°C. Membranes were blocked with 5% nonfat milk in Tris-buffered saline (TBS)-Tween for 1 hr and were incubated with anti-Akt or anti-eNOS antibodies and GAPDH (Cell Signaling Technology, Beverly, MA) at 1 : 1000 dilution overnight at 4°C. After washing with phosphate buffered saline-Tween (PBST) three times for 30 min, membranes were then incubated with horseradish peroxidase (HRP)-conjugated anti-rabbit IgG at 1 : 2000 dilution for 1 h. Protein bands were developed with enzymatic chemiluminescence, and images were measured by a densitometer with analysis software.

2.6. Measurement of Free 15-F2t-Isoprostane. Free 15-F2t-isoprostane (15-F2t-IsoP), a specific marker of oxidative stress, was measured by using an enzyme-linked immunoassay kit (Cayman chemical, Ann Arbor, MI) as described [11]. Perfusate and homogenized heart tissue (in PBS) were purified using Affinity Sorbent and Affinity Column (Cayman chemical, Ann Arbor, MI) then processed for analysis, according to the protocol provided by the manufacturer. The values of plasma or cardiac free 15-F2t-IsoP were expressed as pg/mL in perfusate or pg/mg protein in cardiac homogenates, respectively.

2.7. Statistical Analysis. Data are presented as means ± standard error of the mean (S.E.M.). Data were analysed by the ANOVA within the same group and between groups. Multiple comparisons of group means were analyzed by Tukey's test. The analysis was performed using statistical software package (GraphPad Prism, San Diego, CA, USA). Significant difference was defined as $P \leq 0.05$.

3. Results

3.1. Cardiac Function. As shown in Table 1, none of the baseline data before ischemia represented statistically significant difference among all groups. In control hearts subjected to 30 min ischemia and 30 min reperfusion, LVEDP was higher and both $+dp/dt_{max}$ and $-dp/dt_{max}$ were lower compared with its baseline data before ischemia. IPO treatment significantly decreased LVEDP and increased $+dp/dt_{max}$ and $-dp/dt_{max}$ at the time of reperfusion (30 min) as compared with the I/R group ($P < 0.05$, versus I/R). When postconditioning was performed with alkalotic perfusate, it was

Table 1: Cardiac function for experimental groups ($n = 10$, $\overline{x} \pm s$).

Group	LVEDP (mmHg)		$+dp/dt_{max}$ (mmHg/s)		$-dp/dt_{max}$ (mmHg/s)	
	Baseline	30 min reperfusion	Baseline	30 min reperfusion	Baseline	30 min reperfusion
Control	5.06 ± 1.02	56.98 ± 9.46	2703 ± 135	2051 ± 81	2637 ± 124	2004 ± 67
IPO	7.25 ± 1.17	43.18 ± 4.62*	2811 ± 116	2297 ± 82*	2798 ± 136	2282 ± 87*
IPO + OH^-	6.16 ± 1.29	48.45 ± 7.15$^{*\#}$	2768 ± 222	2057 ± 246$^{\#}$	2686 ± 149	1996 ± 296$^{\#}$
OH^-	6.52 ± 1.21	56.46 ± 5.29	2759 ± 237	2121 ± 248	2690 ± 240	2101 ± 243
H^+	7.19 ± 0.75	36.34 ± 6.30*	2803 ± 179	2274 ± 135*	2801 ± 171	2250 ± 148*
H^+ + wort	6.55 ± 1.41	51.56 ± 5.43$^{\&}$	2846 ± 148	2199 ± 140$^{\&}$	2802 ± 142	2070 ± 134$^{\&}$
Wort	6.92 ± 1.26	53.55 ± 5.77	2734 ± 187	1913 ± 82	2699 ± 192	1898 ± 78

$^{*}P < 0.05$ or 0.01 versus control group; $^{\#}P < 0.05$, IPO + OH^- versus IPO; $^{\&}P < 0.05$, H^+ + wort versus H^+.

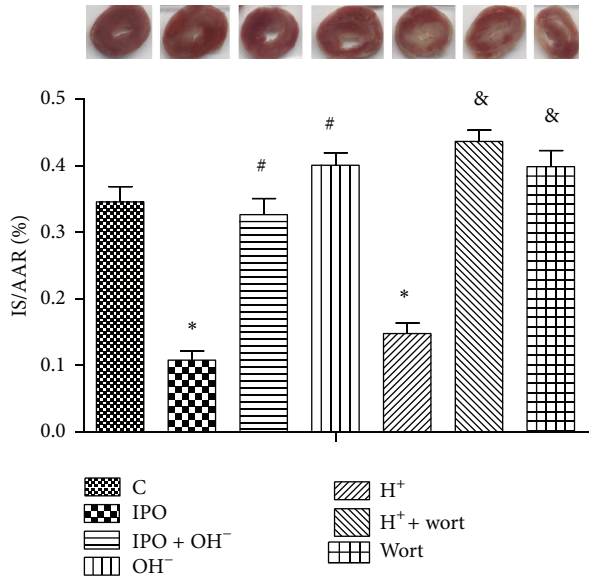

Figure 1: Infarct size expressed as a percentage of risk area. $^{*}P < 0.05$ versus C; $^{\#}P < 0.05$ IPO + OH^- or OH^- versus IPO; $^{\&}P < 0.05$ H^+ + wort or wort versus H^+.

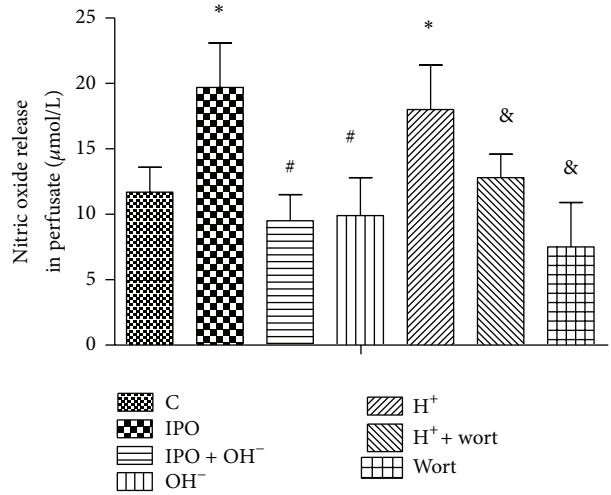

Figure 2: Effects of postconditioning and acidosis perfusate on the nitric oxide release in perfusate. $^{*}P < 0.05$ versus C; $^{\#}P < 0.05$ IPO + OH^- or OH^- versus IPO; $^{\&}P < 0.05$ H^+ + wort or wort versus H^+.

no longer protective. Acidic reperfusion (H^+ group) also improved cardiac function, similar to the effect of postconditioning. However, this protection was reverted by PI3k inhibitor wort ($P < 0.05$) (Table 1) although wortmannin alone in normal KHB perfusate did not significantly alter cardiac function compared with control group ($P > 0.05$).

3.2. Infarct Size. Postconditioning decreased infarct size from 34.6% ± 2.3% of risk zone in control hearts to 10.8% ± 1.4% ($P < 0.01$) (Figure 1). However, this protection was abolished by alkalization perfusate of postconditioning ($P < 0.05$) (Figure 1). However, alkalotic buffer reperfusion alone further increased infarct size compared with control group ($P < 0.05$) (Figure 1). Acidic perfusate (H^+ group) mimicked the protection of postconditioning, which was reverted by PI3k inhibitor wortmannin ($P < 0.05$) (Figure 1) Furthermore, wortmannin alone in normal KHB perfusate increased the infarct size compared with control hearts ($P < 0.05$).

3.3. Nitric Oxide Release. Postconditioning significantly increased nitric oxide release at the time point of reperfusion (30 minutes) compared with that of control group ($P < 0.05$) (Figure 2), which was reverted by alkalized perfusate of postconditioning. Acidotic perfusion buffer also increased the level of nitric oxide, which was blocked by cotreatment of PI3k inhibitor wortmannin. While level of nitric oxide in wort group was even more lower compared with control group ($P < 0.05$), this indicated that the dosage of wortmannin used in this study was enough to inhibit PI3k activation.

3.4. Protein Expression of Akt and eNOS. As shown in Figures 3 and 4, postconditioning induced the phosphorylation of Akt and eNOS protein expression compared with that of control. However, cotreatment with alkalotic perfusate abolished these effects. Acidotic perfusion buffer copied the effect of postconditioning, evidenced as increased phosphorylation of Akt and eNOS protein expression. However, this effect was reverted by cotreatment of PI3k inhibitor wortmannin. Infusion of wortmannin alone also inhibited the phosphorylation of Akt and eNOS expression.

Table 2: Level of perfusate and tissue free *15-F2t-isoprostane*.

	C	IPO	IPO + OH^-	OH^-	H^+	H^+ + wort	Wort
Perfusate (pg/mL)	303.1 ± 15.9	225.7 ± 11.4*	311.5 ± 18.6#	312.5 ± 11.7	235.5 ± 10.6*	308 ± 11.6&	310.3 ± 10.0
Heart tissue (pg/mg protein)	255.3 ± 13.7	208.1 ± 17.1*	262.1 ± 12.1#	270.2 ± 10.3	210.7 ± 12.7*	211.1 ± 13.9&	265.1 ± 153

*$P < 0.05$ or 0.01 versus control group; #$P < 0.05$, IPO + OH^- versus IPO; &$P < 0.05$, H^+ + wort versus H^+.

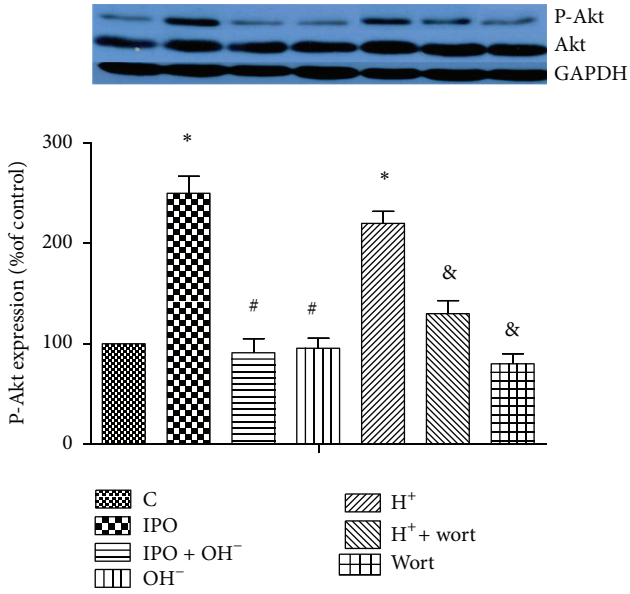

Figure 3: Effects of postconditioning and acidosis perfusate on the activation of Akt in ischemia myocardium. $n = 12$ for each. *$P < 0.05$ versus C; #$P < 0.05$, IPO + OH^- or OH^- versus IPO; &$P < 0.05$, H^+ + wort or wort versus H^+.

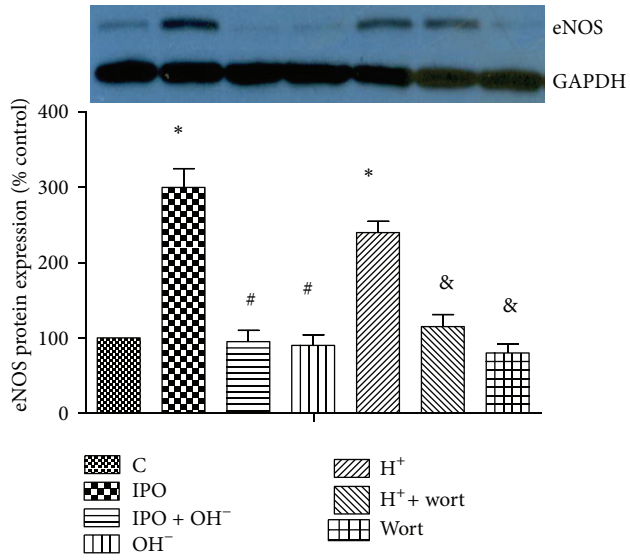

Figure 4: Effects of postconditioning and acidosis perfusate on the protein expression of eNOS. *$P < 0.05$ versus C; #$P < 0.05$, IPO + OH^- or OH^- versus IPO; &$P < 0.05$, H^+ + wort or wort versus H^+.

3.5. Level of Perfusate and Tissue Free 15-F2t-Isoprostane. Compared with the control group, the levels of free 15-F2t-IsoP were significantly decreased in both the perfusate and heart tissues in IPO group ($P < 0.01$ or $P < 0.05$ versus C, Table 2). Postconditioning with alkaline perfusate increased perfusate and heart tissue 15-F2t-IsoP to a level comparable to that in the control ($P < 0.05$, IPO + OH^- versus PO; $P > 0.05$, IPO + OH^- versus control, Table 2). Acidotic perfusion buffer decreased both the perfusate and cardiac tissues of free *15-F2t-isoprostane*, which was reverted by wortmannin. Wortmannin alone did not affect level of both perfusate and tissue free *15-F2t-isoprostane* compared with control group.

4. Discussion

This study demonstrated, in the isolated rat heart, that ischemia postconditioning exerted cardioprotection by delaying pHi recovery, since this effect was abrogated by alkaline perfusate. Acidic perfusion mimicked the cardioprotective effect of postconditioning to limit myocardial infarct size, improve myocardial function, and inhibit ROS production by prolongation of intracellular acidosis during reperfusion. Furthermore, acidic perfusion increased Akt phosphorylation, eNOS expression, and nitric oxide release, which were reverted by cotreatment with the PI3k inhibitor wortmannin. These results suggested that acidic perfusion exerts cardioprotection by activating PI3k-Akt-eNOS signaling pathway during the early reperfusion phase.

Combined action of different transport systems, including Na^+/H^+-exchanger, Na^+/HCO_3^- symport, and H^+-coupled lactate efflux, plays a crucial role in the recovery of pHi during reperfusion. Washout of lactate, H^+, and CO_2 results in normalization of pHi [12]. Therefore, reducing catabolite washout can attenuate transmembrane H^+ gradient and decrease the activity of Na^+/H^+-exchanger and Na^+/HCO_3^- symport. Intracellular low pHi inhibits Ca^{2+}-dependent hypercontracture and opening of MPTP during initial reperfusion which protect the heart from ischemia reperfusion injury. Javier et al. [13] found that acidic reperfusion can prolong intracellular acidosis, but it lasts only for the first 3 minutes of reperfusion. Exceeding this time hearts rapidly restored pHi despite extracellular acidosis. In our study, we performed perfusion with acidic buffer during the first 3 minutes of reperfusion, and our results also found that 3 minutes of acidic perfusion mimicked those protective effects of ischemia postconditioning. However, the underlying mechanism is not well understood.

A variety of studies have demonstrated that postconditioning procedures protect the heart against reperfusion

injury by activating RISK pathways at the time of reperfusion through the phosphorylation of PI3k/Akt pathways. In the current study, we have shown that postconditioning increased activation of PI3k/Akt and limited myocardial infarct size, while infusion of alkaline perfusate abolished the phosphorylation of Akt induced by postconditioning and blunted the cardioprotection of postconditioning, which is consistent with Fujita et al.'s report [14]. Our data further showed that acidic perfusion mimicked the protective effects of ischemia postconditioning, evidenced as decreased infarct size and improved cardiac function, accompanied with increased activation of Akt. However, PI3k inhibitor wortmannin reverted the protection of acidic perfusate and decreased phosphorylation of Akt. These results indicated that acidosis reperfusion protected the myocardium from I/R injury at least in part through the activation of PI3k-Akt pathway.

Furthermore, the activation of PI3k/Akt induced by ischemia postconditioning further activates downstream targets such as endothelial nitric oxide synthase (eNOS) which will induce the release of NO [15–17]. NO can lead to the inhibition of the mitochondrial permeability transition pore opening which may be a key end-effector of cell death and cardioprotection [18, 19]. Studies found that inhibition of NO synthase blunted the infarct size-limiting effects of postconditioning [20]. In the current study, we have shown that acidosis reperfusion increased NO release in the perfusate and enhanced myocardial eNOS protein expression, while infusion of alkaline perfusate reduced the level of NO in perfusate as well as myocardial eNOS protein expression, accompanied with decreased activation of Akt. Besides these, PI3k inhibitor wortmannin reduced NO release and eNOS protein expression, paralleled with decreased phosphorylation of Akt and eNOS. All these results indicated that acidosis induced the activation of PI3k-Akt-eNOS pathway whereby it increased NO release and thus led to the attenuation of ischemia reperfusion injury.

Additionally, restoration of oxygenation during brief reperfusion causes mitochondria to produce ROS which could induce oxidative stress and subsequently lead to the myocardial damage during reperfusion, while acidosis during reperfusion has been reported to attenuate ROS generation [3]. Administration of ROS scavenger alleviated myocardial ischemia reperfusion injury [21, 22]. In our study, we found that acidic perfusate reduced the levels of both perfusate and heart tissue 15-F2t-isoprostane, a specific marker of oxidative stress, similar to the effect of postconditioning. It suggested that acidotic perfusate could inhibit oxidative stress caused by myocardial ischemic reperfusion injury. However, this effect of acidotic perfusate was blocked by cotreatment with the PI3k inhibitor wortmannin. These findings collectively indicate that acidosis attenuated ischemia reperfusion injury partly through activating PI3k signaling pathway to inhibit oxidative stress.

In summary, acidic reperfusion exactly mimics the protection of postconditioning. Acidosis confers cadioprotection by inhibiting ROS production and increasing NO release through activating PI3k-Akt-eNOS pathway.

Authors' Contribution

Xin Qiao, Jinjin Xu, Xinwei Liu, and Huimin Liu contributed equally to this study.

References

[1] M. V. Cohen and J. M. Downey, "Ischemic postconditioning: from receptor to end-effector," *Antioxidants and Redox Signaling*, vol. 14, no. 5, pp. 821–831, 2011.

[2] J. J. Lemasters, J. M. Bond, E. Chacon et al., "The pH paradox in ischemia-reperfusion injury to cardiac myocytes," *EXS*, vol. 76, pp. 99–114, 1996.

[3] M. V. Cohen, X.-M. Yang, and J. M. Downey, "Acidosis, oxygen, and interference with mitochondrial permeability transition pore formation in the early minutes of reperfusion are critical to postconditioning's success," *Basic Research in Cardiology*, vol. 103, no. 5, pp. 464–471, 2008.

[4] Z. Q. Zhao, J. S. Corvera, M. E. Halkos et al., "Inhibition of myocardial injury by ischemic postconditioning during reperfusion:comparision with ischemic preconditioning," *The American Journal of Physiology*, vol. 285, pp. H579–H588, 2003.

[5] C. M. Zhao, X. J. Yang, J. H. Yang et al., "Effect of ischaemic postconditioning on recovery of left ventricular contractile function after acute myocardial infarction," *Journal of International Medical Research*, vol. 40, no. 3, pp. 1082–1088, 2012.

[6] Q. L. Wu, T. Shen, H. Ma, and J. K. Wang, "Sufentanil postconditioning protects the myocardium from ischemia-reperfusion via PI3K/Akt-GSK-3beta pathway," *Journal of Surgical Research*, vol. 178, no. 2, pp. 563–570, 2012.

[7] M. Zhu, J. Feng, E. Lucchinetti et al., "Ischemic postconditioning protects remodeled myocardium via the PI3K-PKB/Akt reperfusion injury salvage kinase pathway," *Cardiovascular Research*, vol. 72, no. 1, pp. 152–162, 2006.

[8] M. V. Cohen, X.-M. Yang, and J. M. Downey, "The pH hypothesis of postconditioning: staccato reperfusion reintroduces oxygen and perpetuates myocardial acidosis," *Circulation*, vol. 115, no. 14, pp. 1895–1903, 2007.

[9] T. Wang, X. Mao, H. Li et al., "N-Acetylcysteine and allopurinol up-regulated the Jak/STAT3 and PI3K/Akt pathways via adiponectin and attenuated myocardial postischemic injury in diabetes," *Free Radical Biology and Medicine*, vol. 63, pp. 291–303, 2013.

[10] D. Hodyc, E. Johnson, A. Skoumalová et al., ".Reactive oxygen species production in the early and later stage of chronic ventilatory hypoxia," *Physiological Research*, vol. 61, no. 2, pp. 145–151, 2012.

[11] J. Xu, S. Lei, Y. Liu et al., "Antioxidant N-acetylcysteine attenuates the reduction of brg1 protein expression in the myocardium of type 1 diabetic rats," *Journal of Diabetes Research*, vol. 2013, Article ID 716219, 8 pages, 2013.

[12] J. I. Vandenberg, J. C. Metcalfe, and A. A. Grace, "Mechanisms of pH(i) recovery after global ischemia in the perfused heart," *Circulation Research*, vol. 72, no. 5, pp. 993–1003, 1993.

[13] I. Javier, B. Ignasi, H. Victor et al., "Effect of acidic reperfusion on prolongation of intracellular acidosis and myocardial salvage," *Cardiovascular Research*, vol. 77, pp. 782–790, 2008.

[14] M. Fujita, H. Asanuma, A. Hirata et al., "Prolonged transient acidosis during early reperfusion contributes to the cardioprotective effects of postconditioning," *The American Journal of Physiology*, vol. 292, no. 4, pp. H2004–H2008, 2007.

[15] B. Ebner, S. A. Lange, T. Eckert et al., "Uncoupled eNOS annihilates neuregulin-1beta-induced cardioprotection: a novel mechanism in pharmacological postconditioning in myocardial infarction," *Molecular and Cellular Biochemistry*, vol. 373, no. 1-2, pp. 115–123, 2013.

[16] S. Sumi, H. Kobayashi, S. Yasuda et al., "Postconditioning effect of granulocyte colony-stimulating factor is mediated through activation of risk pathway and opening of the mitochondrial KATP channels," *The American Journal of Physiology*, vol. 299, no. 4, pp. H1174–H1182, 2010.

[17] A. Tsang, D. J. Hausenloy, M. M. Mocanu, and D. M. Yellon, "Postconditioning: a form of "modified reperfusion" protects the myocardium by activating the phosphatidylinositol 3-kinase-Akt pathway," *Circulation Research*, vol. 95, no. 3, pp. 230–232, 2004.

[18] G. J. Gross, A. Hsu, A. W. Pfeiffer, and K. Nithipatikom, "Roles of endothelial nitric oxide synthase (eNOS) and mitochondrial permeability transition pore (MPTP) in epoxyeicosatrienoic acid (EET)-induced cardioprotection against infarction in intact rat hearts," *Journal of Molecular and Cellular Cardiology*, vol. 59, pp. 20–29, 2013.

[19] H. Ohtani, H. Katoh, T. Tanaka et al., "Effects of nitric oxide on mitochondrial permeability transition pore and thiol-mediated responses in cardiac myocytes," *Nitric Oxide*, vol. 26, no. 2, pp. 95–101, 2012.

[20] X.-M. Yang, J. B. Proctor, L. Cui, T. Krieg, J. M. Downey, and M. V. Cohen, "Multiple, brief coronary occlusions during early reperfusion protect rabbit hearts by targeting cell signaling pathways," *Journal of the American College of Cardiology*, vol. 44, no. 5, pp. 1103–1110, 2004.

[21] P. Pasdois, C. L. Quinlan, A. Rissa et al., "Ouabain protects rat hearts against ischemia-reperfusion injury via pathway involving src kinase, mitoKATP, and ROS," *The American Journal of Physiology*, vol. 292, no. 3, pp. H1470–H1478, 2007.

[22] G. Zhang, Y. S. Master, Y. Wang et al., "Local administration of lactic acid and a low-dose of the free radical scavenger, edaravone, alleviates myocardial reperfusion injury in rats," *Journal of Cardiovascular Pharmacology*, 2013.

Hindawi Publishing Corporation
Oxidative Medicine and Cellular Longevity
Volume 2013, Article ID 529173, 9 pages
http://dx.doi.org/10.1155/2013/529173

Research Article

Protective Effects of Low-Frequency Magnetic Fields on Cardiomyocytes from Ischemia Reperfusion Injury *via* ROS and NO/ONOO$^-$

Sai Ma, Zhengxun Zhang, Fu Yi, Yabin Wang, Xiaotian Zhang, Xiujuan Li, Yuan Yuan, and Feng Cao

Department of Cardiology, Xijing Hospital, Fourth Military Medical University, Xi'an, Shannxi 710032, China

Correspondence should be addressed to Feng Cao; wind8828@gmail.com

Received 8 August 2013; Revised 29 September 2013; Accepted 30 September 2013

Academic Editor: Zhengyuan Xia

Background. Cardiac ischemia reperfusion (I/R) injury is associated with overproduction of reactive oxygen species (ROS). Low frequency pulse magnetic fields (LFMFs) have been reported to decrease ROS generation in endothelial cells. Whether LFMFs could assert protective effects on myocardial from I/R injury *via* ROS regulation remains unclear. *Methods*. To simulate *in vivo* cardiac I/R injury, neonatal rat cardiomyocytes were subjected to hypoxia reoxygenation (H/R) with or without exposure to LFMFs. Cell viability, apoptosis index, ROS generation (including O_2^- and $ONOO^-$), and NO production were measured in control, H/R, and H/R + LFMF groups, respectively. *Results*. H/R injury resulted in cardiomyocytes apoptosis and decreased cell viability, whereas exposure to LFMFs before or after H/R injury significantly inhibited apoptosis and improved cell viability ($P < 0.05$). LFMFs treatment could suppress ROS (including O_2^- and $ONOO^-$) generation induced by H/R injury, combined with decreased NADPH oxidase activity. In addition, LFMFs elevated NO production and enhanced NO/$ONOO^-$ balance in cardiomyocytes, and this protective effect was *via* the phosphorylation of endothelial nitric oxide synthase (eNOS). *Conclusion*. LFMFs could protect myocardium against I/R injury *via* regulating ROS generation and NO/$ONOO^-$ balance. LFMFs treatment might serve as a promising strategy for cardiac I/R injury.

1. Introduction

Acute coronary syndrome, including acute myocardial infarction (AMI), is one of the major causes of morbidity and mortality for patients with coronary heart diseases worldwide [1]. Effective reperfusion therapies like percutaneous coronary intervention (PCI) and coronary artery bypass grafting (GABG) could reduce myocardial ischemia, which in turn minimize myocardial infarction size and improve patients' prognosis [2]. Reperfusion strategies are necessary to resuscitate the ischemic myocardium; however, they may result in paradoxical cardiomyocyte dysfunction and aggravate tissue damage, a process termed as "reperfusion injury" [3]. Thus, an effective strategy to protect heart against ischemia reperfusion (I/R) injury is imperative for successful treatment of coronary heart diseases.

Low-frequency magnetic fields (LFMFs) are considered to be therapeutic and have been started to be applied more and more commonly in medicine. Many studies have demonstrated that LFMFs are capable of affecting a number of physiological and pathological processes. The protective effects of LFMFs on heart tissue against I/R injury have also been widely studied. It is reported that exposure to low-frequency pulsing electromagnetic fields could alleviate cardiac infarction caused by acute permanent ligation of the left anterior descending artery in rats [4]. Kurian et al. also reported that magnetic field preconditioning could enhance cell survival and diminish apoptotic response to simulated I/R injury in H9C2 cells [5]. These results all indicated that LFMFs might play a positive role in cardiac tissue against I/R injury.

In light of these previous studies, our study was designed to investigate whether LFMFs were capable of protecting cardiac tissue from I/R injury and to figure out its underlying mechanism. To simulate *in vivo* cardiac I/R injury,

an *in vitro* cardiomyocyte hypoxia-reoxygenation (H/R) model was established and applied.

2. Methods

2.1. Isolation, Cultivation, and Identification of Cardiomyocytes (CMs). Primary cultures of cardiomyocytes were prepared from 1–3-day-old neonatal Sprague-Dawley rat hearts (purchased from the Animal Centre of Fourth Military Medical University). Briefly, hearts were excised from neonatal rats (1–3 days old) and rinsed into 1–3 mm^2 fragments with phosphate buffered saline (PBS). Then, hearts were minced in PBS and digested in 0.1% collagenase I (Sigma, St. Louis, MO, USA) at 37°C for 5 minutes. Supernatant was collected into 15 mL centrifugal tube with 8 mL medium inside. This process was repeated till the tissue was completely dissolved. The suspensions were pooled and centrifuged at 1,000 rpm for 8 min. Cells were resuspended and subjected to differential attachment at 37°C for 1.5 h to remove fibroblasts. CMs were cultured in high glucose DMEM medium (Hyclone, USA) supplemented with 15% (v/v) fetal calf serum (FCS) and 1% penicillin and streptomycin. The culture medium was replenished every 3 days. Primary cultures of cardiomyocytes were positively identified by cTnI (Abcam, USA) staining. Passage 1 cells were used for further studies.

2.2. Hypoxia/Reoxygenation Condition. Cardiomyocytes cultured for 6 days were used for the treatment of hypoxia/reoxygenation. For hypoxia, the culture media were replaced by modified hypoxia solution (NaCl 98.5 mmol/L, KCl 10 mmol/L, NaH_2PO_4 0.9 mmol/L, $NaHCO_3$ 6.0 mmol/L, $CaCl_2$ 1.8 mmol/L, $MgSO_4$ 1.2 mmol/L, sodium lactate 40 mmol/L, HEPES 20 mmol/L, and pH 6.8), and a constant stream of water-saturated 5% CO_2-95% N_2 was maintained over the cultures for 3 hours. For reoxygenation, the nutrient solution was changed to high glocose DMEM medium supplemented with 15% fetal calf serum under a water-saturated atmosphere of 5% CO_2-95% air for 3 h.

2.3. Application of Low-Frequency Magnetic Fields. Before or after H/R treatment, cardiomyocytes were exposed to low-frequency pulse magnetic fields by MCY-1 Low-Frequency Pulse Magnetic Field Therapeutic Apparatus (Xi'an Century Institute of Measurement and Control Technology, Xi'an, Shaanxi, China). We generated magnetic fields with different amplitudes in a range of 1.5 mT to 6.0 mT and varying sinusoidal currents of 15 Hz or 20 Hz. Eight different parameters of magnetic fields were applied in this experiment: 1.5 mT/15 Hz, 1.5 mT/20 Hz, 3.0 mT/15 Hz, 3.0 mT/20 Hz, 4.5 mT/15 Hz, 4.5 mT/20 Hz, 6.0 mT/15 Hz, and 6.0 mT/20 Hz, respectively. Timing and duration of LFMFs treatment were 1 h, 3 h, and 5 h before or after H/R treatment, respectively. During the experiments, performed in blind manner, the magnetic intensity was monitored by means of a built-in current sensor.

2.4. Evaluation of Different LFMFs Conditions. To determine the best conditions of LFMFs, LFMFs of different parameters were applied to CMs before or after H/R treatment as mentioned above. We measured CMs' viability to evaluate the protective effects of different LFMFs conditions. CMs' viability was evaluated by MTT assay, which is based on the transformation of the tetrazolium salt MTT by active mitochondria to an insoluble formazan salt. Cells were plated in 96-well plates at a density of 5×10^4 cells/mL. MTT was added to each well with a final concentration of 0.5 mg/mL, and the plates were incubated for another 4 h at 37°C. Formazan was quantified spectroscopically at 490 nm by spectrophotometer.

2.5. Assessment of Apoptosis of CMs. Apoptosis index of CMs was detected by terminal deoxynucleotidyl TUNEL assay using a commercial Cell Death Detection Kit (Roche, Penzberg, Germany) according to the manufacturer's instructions. The index of apoptosis was expressed as the proportion of the TUNEL-positive CMs to the total CMs.

2.6. Determination of Oxidative Stress in CMs. NO, $ONOO^-$, and O_2^- were measured to indicate the extent of oxidative stress in CMs. The amount of NO, peroxynitrite ($ONOO^-$) in CMs was detected by a commercial NO and $ONOO^-$ Detection Kit (R&D, USA) according to the manufacturer's instructions. To further demonstrate that the increase of NO production is from eNOS, we used the nonselective inhibitor of eNOS, L-NAME (1 mmol/L, Beyotime Institute of Biotechnology, Nanjing, China), which could suppress NO production *via* deactivating eNOS; then we tested the NO, $ONOO^-$ generation and NO/$ONOO^-$ balance with or without L-NAME under H/R conditions.

Two different methods were used to measure the amount of O_2^- in CMs. In the first method, a ROS Detection Kit (GenMed Scientifics Inc., USA) was used for quantification according to the instructions. The second method is dihydroethidine (DHE) staining under adaption of previously described methods [6]. Briefly, hydroethidine staining was used to detect the in situ formation of superoxide according to the oxidative fluorescent microtopography. Cardiomyocytes were harvested and incubated with DHE (DHE, 1 : 1000 dilution, Beyotime Institute of Biotechnology, Nanjing, China) at 37°C for 30 minutes. Cardiomyocytes without any treatment were considered as negative control. In positive control group, cardiomyocytes were incubated with 100 μM H_2O_2 for 30 min to induce intracellular reactive oxygen species generation. DHE staining was visualized under a confocal microscope (Olympus, Japan). Then, images of cells were analyzed with Image-Pro Plus software version 6.0. The mean fluorescence intensity of each cell and the total cell emission signals per field were calculated for data analysis.

2.7. Quantification of NADPH Oxidase Activity. NADPH oxidase activity was measured by lucigenin-enhanced chemiluminescence with a NADPH oxidase kit (GenMed Scientifics Inc., USA) according to the manufacturer's instructions.

2.8. Western Blot Analysis. Western blot was performed as follows. CMs from each group were cultured and harvested at appropriate time. Cells were washed by PBS and scraped

using lysis buffer. Total proteins were loaded onto an SDS-PAGE gel and transferred electrophoretically to nitrocellulose membranes (Millipore, Billerica, MA, USA). After blocking with 5% skim milk, the membranes then were hybridized at 4°C overnight with the primary antibody, anti-eNOS (1 : 2000; Abcam), anti-eNOS (phospho S1177, 1 : 2000; Abcam), anti-iNOS (1 : 3000; Abcam), and anti-β-actin (1 : 2000; Cell Signaling). The membranes were washed with PBS-Tween and further incubated with secondary antibody, horseradish peroxidase-conjugated goat anti-rabbit IgG (Santa Cruz Biotechnology, CA, USA), at 37°C for 60 minutes. The blots were developed using chemiluminescence reagent kit (Millipore) and visualized with UVP Bio-Imaging Systems. Blot densities were analyzed by Vision Works LS Acquisition and Quantity One Analysis Software.

2.9. Data Analysis. All data were expressed as mean ± SD and were analyzed using one-way ANOVA followed by Tukey's multiple comparison test for post test. A value of $P < 0.05$ was considered to be statistically significant. All statistical tests were performed using GraphPad Prism software version 5.0 (GraphPad Software, San Diego, CA, USA).

3. Results

3.1. Isolation, Cultivation, and Identification of CMs. The cells displayed spontaneous contracting with a beating rate of 120–150 beats/min 72 h after isolation. Light microscopy revealed that the spontaneous beating area was mainly composed of relatively large mononuclear cells, approximately 50 μm in diameter, with fusiform or polygon morphology (Figure 1(a)). For further confirmation of CMs, immunofluorescence staining of troponin I (cTnI) was performed. Figure 1(b) shows positively stained CMs by anti-cTnI. As expected, green fluorescence-labeled cTnI and blue fluorescence-labeled nuclei were observed, indicating the successful isolation and cultivation of CMs.

3.2. LFMFs Increased Cardiomyocyte Viability after H/R Injury. It was indicated in the MTT assay that the survival and proliferation rate of CMs remarkably declined after H/R treatment (Figures 1(a) and 1(b)). Exposure to LFMFs of different parameters and durations attenuated this H/R-induced cell suppression and cell death on different levels. Notably, LFMFs exposure to 4.5 mT/15 Hz, 3 h before or after H/R treatment significantly protected CMs against H/R injuries (Figures 1(a) and 1(b)).

3.3. LFMFs Decreased H/R-Induced Apoptosis in CMs. To investigate the role of LFMFs in H/R-induced apoptosis in CMs, TUNEL assay was performed. H/R treatment significantly increased the percentage of TUNEL-positive cells. Compared with cells treated with H/R, the LFMFs-treated groups showed a significant decline in apoptotic cells, especially under the condition of 4.5 mT/15 Hz and 3 h before or after H/R treatment (Figures 1(e) and 1(f)). These results demonstrated that LFMFs could exert an antiapoptotic effect on H/R-treated CMs.

3.4. LFMFs Exposure Decreased H/R-Induced ROS Production. ROS is known to play an important role in H/R injuries. In our study, O_2^- was considered as a key marker for ROS. To determine whether LFMFs exposure could attenuate H/R-induced ROS production in CMs, O_2^- production was measured. To make surely true superoxide generation from the cells, both negative and positive control DHE staining images were provided in Figures 2(a) and 2(b). As indicated in Figures 2(a) and 2(b), O_2^- production increased significantly in H/R-treated CMs compared with negative control group (0.401 ± 0.116 μmol/L versus 0.267 ± 0.049 μmol/L, $P < 0.05$). LFMFs + H/R groups, 4.5 mT/15 Hz, 3 h before or after H/R treatment, significantly suppressed O_2^- production (0.326 ± 0.055 μmol/L and 0.324 ± 0.056 μmol/L, resp., $P < 0.05$) compared with H/R group (Figures 2(a) and 2(b)).

3.5. LFMFs Exposure Decreased H/R-Induced Cardiac Injury via Regulating ROS Production and NO/ONOO$^-$ Balancing. NO production decreased significantly in H/R-treated CMs compared with control group (5.74 ± 2.26 μmol/L versus 3.15 ± 1.06 μmol/L, $P < 0.05$). LFMFs + H/R group and H/R + LFMFs group robustly increased NO production (4.52 ± 1.9 μmol/L and 4.58 ± 1.6 μmol/L) compared with H/R group ($P < 0.05$) (Figure 3(a)). Nevertheless, LFMFs' effect of NO production was eliminated by L-NAME (nonselective inhibitor of eNOS). As demonstrated in Figure 3(a), compared with H/R + LFMF group, NO production in H/R + LFMF + L-NAME was significantly decreased (2.89 ± 1.54 μmol/L versus 4.52 ± 1.95 μmol/L, $P < 0.05$). However, ONOO$^-$ production displayed an opposite trend. As indicated in Figure 3(b), ONOO$^-$ production increased significantly in H/R-treated CMs compared with control group (27.42 ± 5.74 μmol/L versus 18.12 ± 4.08 μmol/L, $P < 0.05$). LFMF + H/R group and H/R + LFMF group significantly suppressed ONOO$^-$ production (21.67 ± 5.45 μmol/L and 20.85 ± 5.77 μmol/L, resp., $P < 0.05$) compared with H/R group. The ratio of NO to ONOO$^-$ in H/R group was significantly decreased in comparison with that in control group, while this ratio was increased in LFMF + H/R group and H/R + LFMF group compared with that in H/R group. Similarly, LFMFs' effect on increasing the ratio of NO to ONOO$^-$ was reversed by L-NAME ($P < 0.05$).

3.6. LFMFs Exposure Decreased H/R-Induced NADPH Oxidase Activity. To further investigate LFMFs' protective role against H/R injuries in antioxidative stress, NADPH oxidase activity was measured. Comparing with control group, NADPH oxidase activity was significantly increased in H/R group (80.33 ± 7.43 RLU versus 54.03 ± 3.21 RLU, $P < 0.05$). However, NADPH oxidase activity was attenuated under LFMFs treatment (64.35 ± 4.68 RLU and 66.29 ± 7.27 RLU, resp., $P < 0.05$) compared with H/R group (Figure 4(a)).

3.7. LFMFs Protected CMs against H/R Injuries via the Increase of NO Production by the Phosphorylation of eNOS Instead of Inducible Nitric Oxide Synthase (iNOS). Because eNOS and iNOS are both necessary for NO production and antioxidative reaction, we hypothesized that eNOS played an

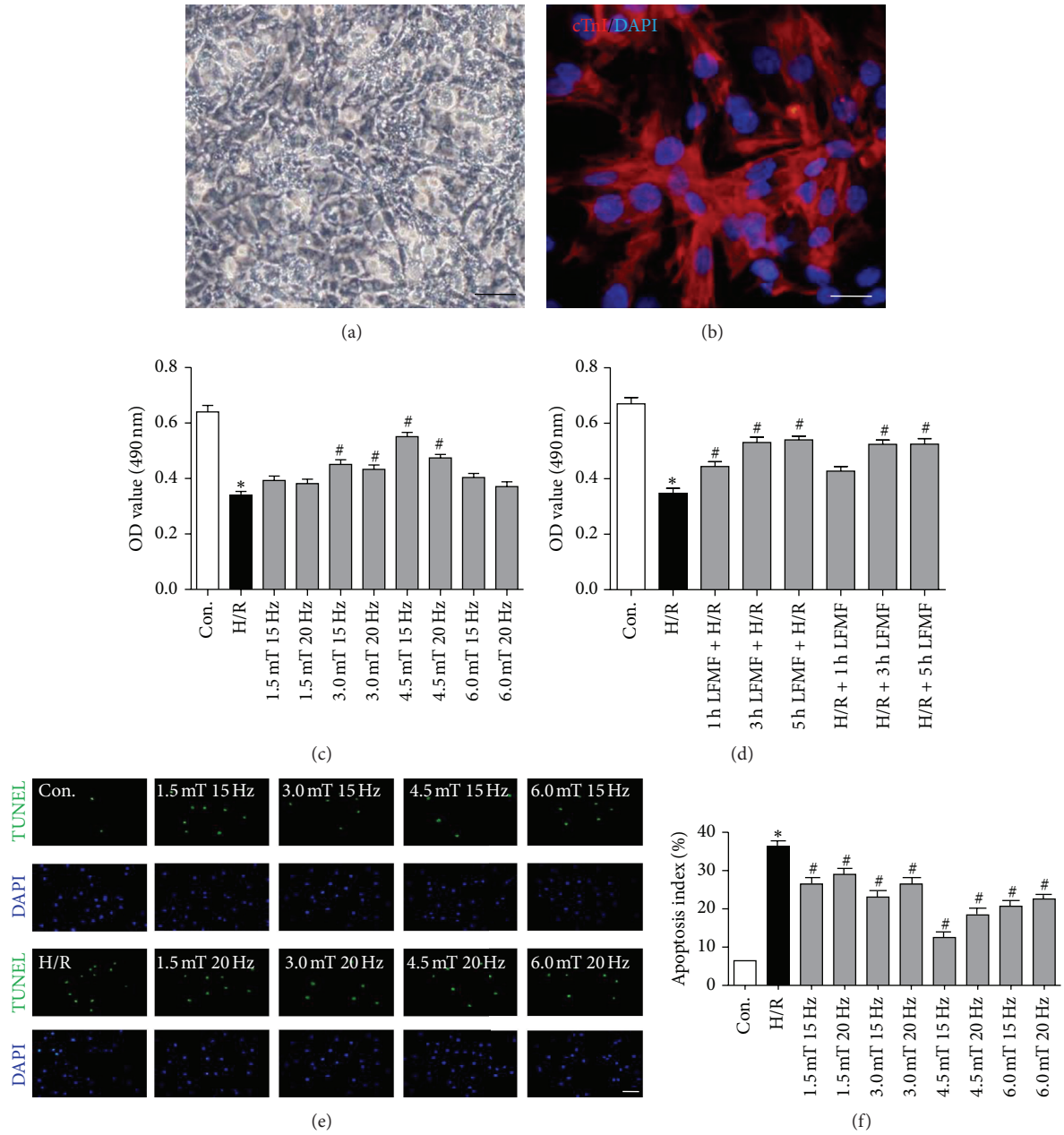

FIGURE 1: Identification of primary cardiomyocytes (CMs) and optimal low-frequency pulse magnetic fields (LFMFs) conditions. (a) Primary CMs by light microscope (scale bar, 100 μm). (b) cTnI staining of primary CMs by immunofluorescence (red, cTnI; blue, DAPI; scale bar, 50 μm). (c), (d) Cell viability measurement by MTT assays under different LFMFs conditions. $^{*}P < 0.05$ versus control group; $^{\#}P < 0.05$ versus H/R group. (e) Representative images of immunostaining for apoptotic cells (green, TUNEL; blue, DAPI; scale bar, 100 μm). (f) Quantification of apoptotic cells by Image-Pro Plus software. $^{*}P < 0.05$ versus control group; $^{\#}P < 0.05$ versus H/R group.

important role in mediating LFMFs' protection against H/R injuries in CMs. To confirm whether iNOS was associated with LFMFs' protective effect, we tested iNOS protein in each group. Western blot results demonstrated that there was no significant difference among control group, H/R group, and H/R + LFMF group (Figure 4(b)). As indicated in the Western blot results (Figure 4(c)), the phosphorylation of eNOS (phosphor S1177) was declined in H/R group compared with control group, and LFMFs treatment increased the phosphorylation of eNOS ($P < 0.05$). However, L-LAME did not affect the phophorylation of eNOS. Quantification analysis of Western blot results further confirmed this hypothesis (Figure 4(c)).

4. Discussion

LFMFs have been reported to suppress apoptosis and enhance cell survival. In the present study, we verified that LFMFs were capable of protecting cardiomyocytes from I/R injury *via* regulating ROS production and NO/ONOO^{-} balance.

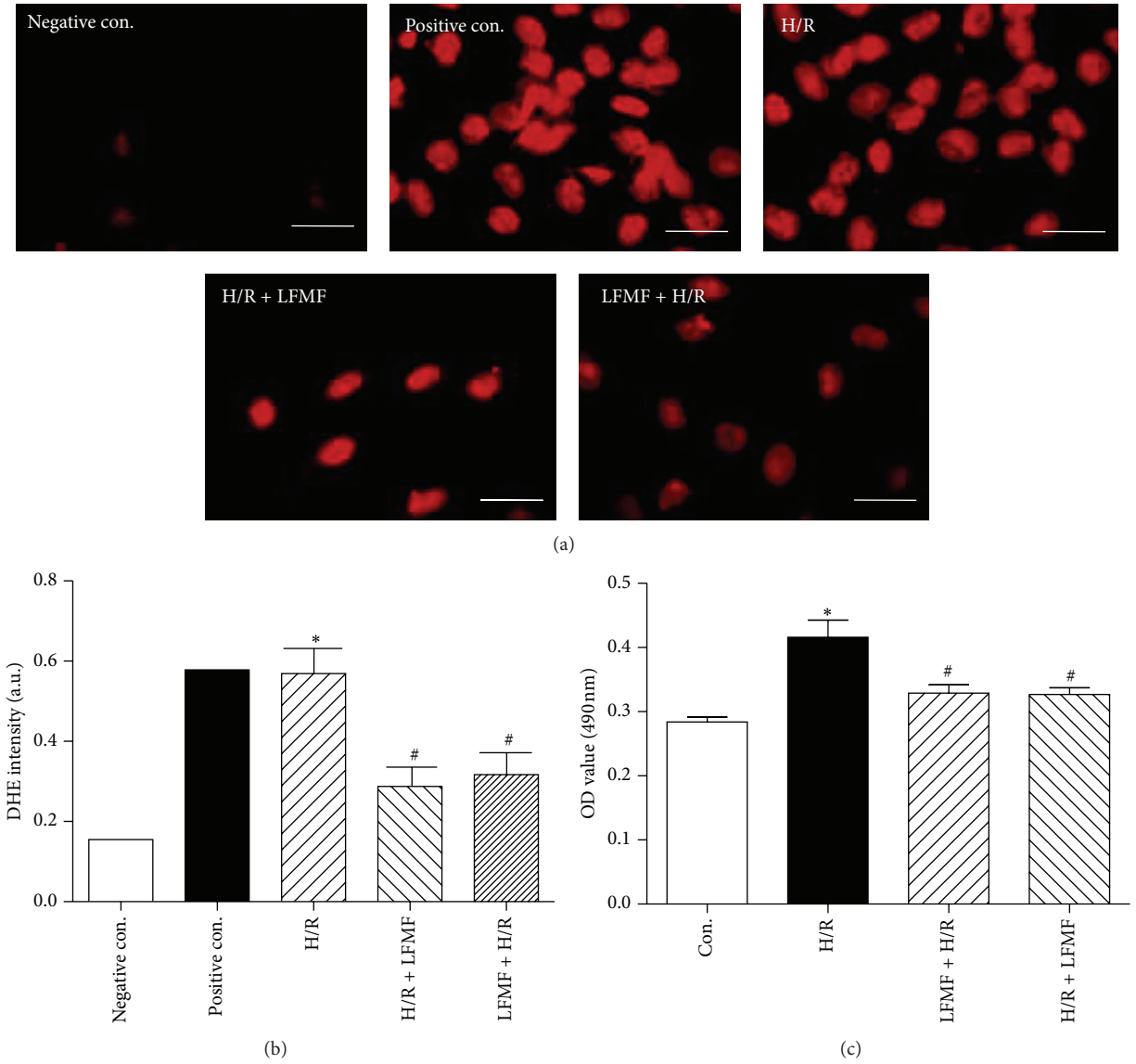

FIGURE 2: O_2^- as an index of ROS generation in CMs. (a) Representative images of dihydroethidine (DHE) staining of CMs (red, DHE; scale bar, 50 μm). (b) The average fluorescence intensity from five fields was summarized. $^*P < 0.05$ versus control group; $^\#P < 0.05$ versus H/R group. (c) O_2^- measurement by commercial ROS Detection Kit. $^*P < 0.05$ versus control group; $^\#P < 0.05$ versus H/R group.

It is recognized that ROS production is elevated by I/R injury and ROS exert crucial effects on I/R injury [7, 8]. ROS, including superoxide radical (O_2^-), hydroxyl radical (OH^-), hydrogen peroxide (H_2O_2), and peroxynitrite ($ONOO^-$), are able to result in cardiomyocytes' oxidative stress. Oxidative stress could mediate I/R injury by bringing about cardiomyocytes' dysfunction and apoptosis [8]. Lines of evidences have shown that oxidative stress is involved in myocardial damage [9] and antioxidative agents are capable of reducing myocardial injury [10]. Our study revealed similar results. In comparison with control group, the generation of ROS in H/R group was significantly increased which was compromised in the LFMFs-treated groups. This result was in accordance with the variation trend of NADPH oxidase activity. The activity of NADPH oxidase in H/R group was significantly increased compared with control group, and LFMFs exposure suppressed NADPH oxidase activity to a certain degree. This suggested that the amount of O_2^- is positively related to the activity of NADPH oxidase.

LFMFs suppressed the production of ROS, thus exerting a protective role in cardiomyocyte against H/R injury. However, the exact mechanism by which LFMFs decreased the generation of ROS remains unknown. Many researchers supposed that mitochondria played a central role in the increase of ROS generation during I/R [11]. Murphy and Steenbergen considered mitochondrial electron transport as one of the primary sources of ROS in I/R injury [7]. Iorio et al. reported that LFMFs with a square waveform of 5 mT amplitude and frequency of 50 Hz could increase energy generation through regulating mitochondrial oxidative phosphorylation [12].

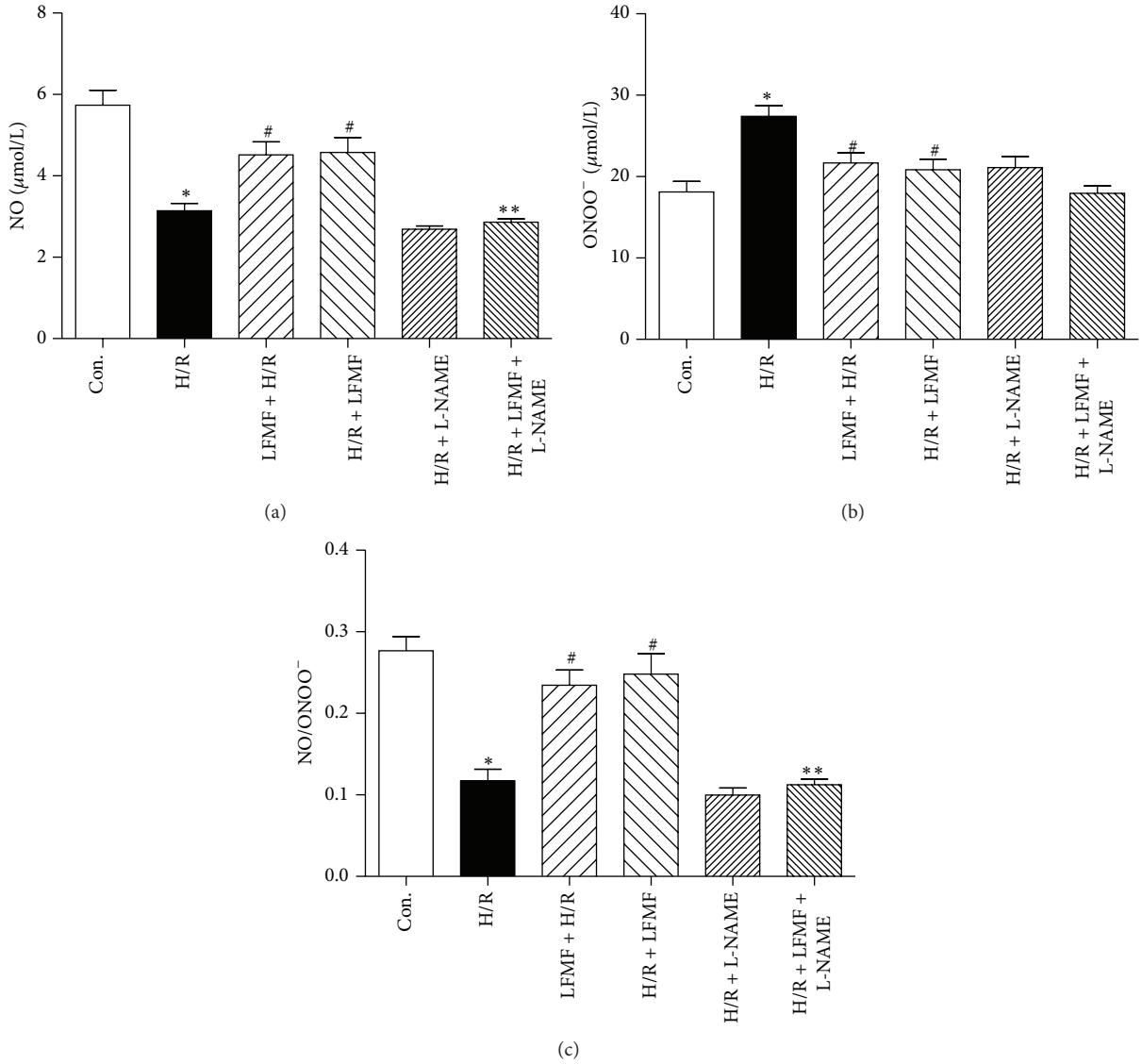

Figure 3: NO, $ONOO^-$ production and NO/$ONOO^-$ balancing in CMs. (a), (b) NO and $ONOO^-$ measurement by commercial NO and $ONOO^-$ Detection Kit. $^*P < 0.05$ versus control group; $^\#P < 0.05$ versus H/R group; $^{**}P < 0.05$ versus H/R + LFMF group. (c) Ratio of NO/$ONOO^-$ as representative of NO/$ONOO^-$ balance. $^*P < 0.05$ control group; $^\#P < 0.05$ versus H/R group; $^{**}P < 0.05$ versus H/R + LFMF group.

It is logical to suppose that LFMFs suppress ROS level in cardiomyocytes through regulating mitochondria function.

In addition to ROS production changes, LFMFs exerted protective effects on cardiomyocytes through upregulating the phosphorylation of eNOS, NO generation and regulating NO/$ONOO^-$ balancing. iNOS and eNOS are important for NO production. In the heart, eNOS is constitutively present enzyme in cardiomyocytes, whereas iNOS is absent in the healthy heart, but its expression is induced by proinflammatory mediators [13]. It is necessary to figure out which is responsible for the increase of NO production under LFMFs treatment. Our data indicated that the expression of iNOS protein did not alter under H/R or LFMFs conditions. This manifested that iNOS activation was not the source of the increased NO production under LFMFs treatment after H/R injury. iNOS is currently considered as a primary source for late-phase toxic NO production after myocardial I/R injury. Wildhirt et al. reported that a significant increase in iNOS activity was observed in myocardial regions 48 h after I/R injury [14]. In our experiment, cardiomyocytes protein was harvested immediately after H/R or LFMFs treatment. That may explain why iNOS expression is not elevated in our study. As was demonstrated in our results, the phosphorylation of eNOS and NO production were the minimum in H/R group, and LFMFs exposure restored phosphorylated eNOS and NO generation to some extent. NO could be generated by eNOS and has been reported to exert beneficial effect on cardiac injuries [15, 16], while $ONOO^-$, as a component of ROS,

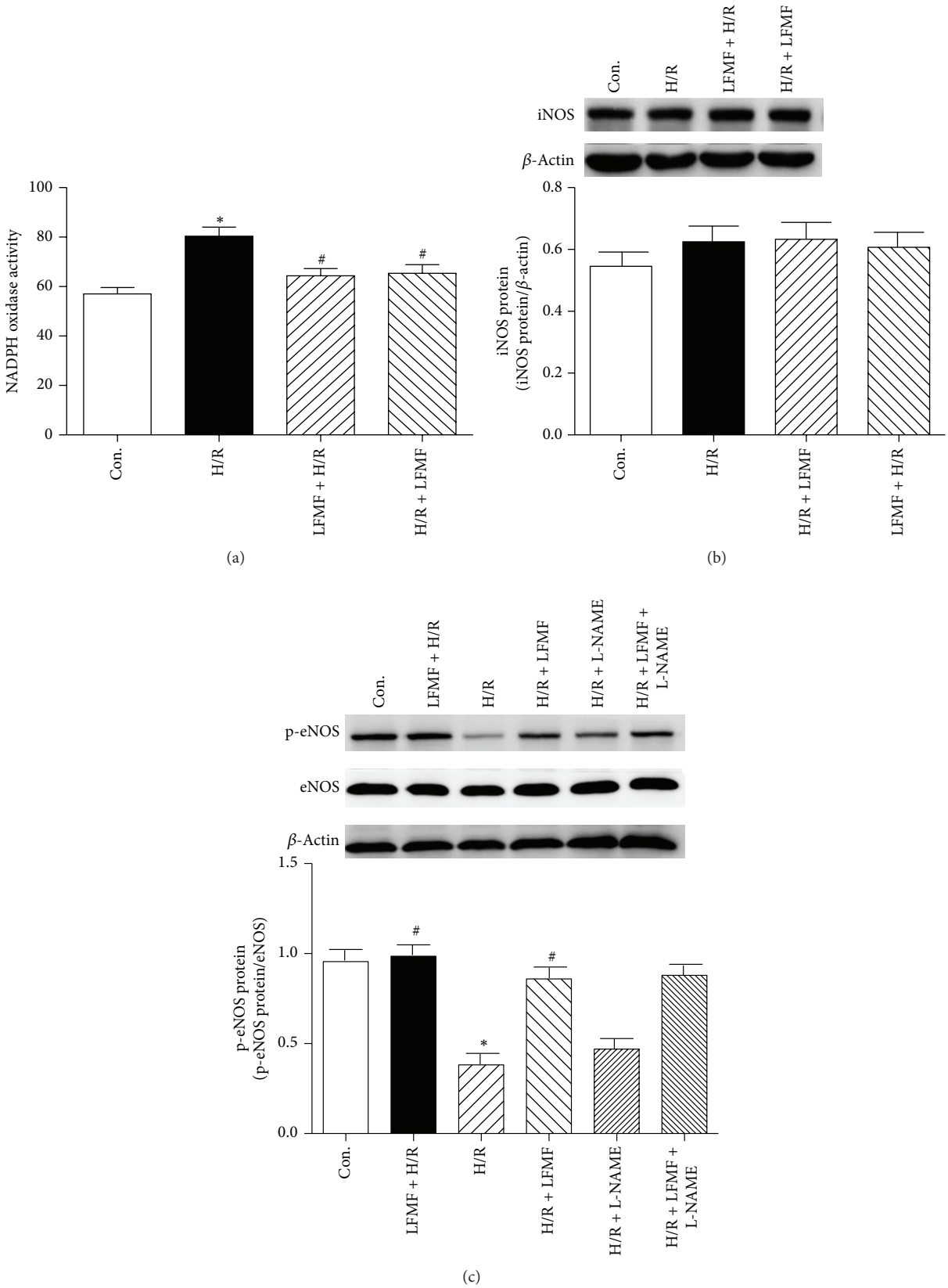

Figure 4: NADPH oxidase activity and phosphorylation of eNOS in CMs. (a) NADPH oxidase activity by commercial NADPH oxidase activity detection kit. $^{*}P < 0.05$ versus control group; $^{\#}P < 0.05$ versus H/R group. (b) Western blot assay for iNOS expression. No significant difference between groups. (c) Western blot assay for phosphorylated eNOS (phospho S1177) and eNOS expression. $^{*}P < 0.05$ versus control group; $^{\#}P < 0.05$ versus H/R group.

has adverse effect on cardiomyocytes viability. The balance of NO/$ONOO^-$ plays an important role in cell function and viability. Heeba reported that stains could restore endothelial function by regulating NO/$ONOO^-$ balancing *in vitro* [17]. Gao et al. reported that phosphorylation of eNOS and the subsequent increase of NO production contributed significantly to the antiapoptotic effect of insulin on myocardial ischemia-reperfusion Sprague-Dawley rats [18]. Our results were in accordance with the studies mentioned above. As was indicated in our study, LFMFs induced the activation of p-eNOS, resulted in NO generation, and decreased $ONOO^-$ production, which shifted the NO/$ONOO^-$ balance towards NO. We also found that L-NAME (nonselective inhibitor of eNOS) could abolish the effects of LFMFs on NO production and NO/$ONOO^-$ balancing. These testified that eNOS modulated NO/$ONOO^-$ balancing, which mediated LFMFs' protective roles in cardiomyocytes. However, iNOS is not involved in LFMFs beneficial effects. Previous studies have reported the favorable effects of LFMFs both *in vivo* and *in vitro*. For example, Yen-Patton et al. demonstrated that pulsed electromagnetic fields could stimulate growth rate of endothelial cells and angiogenesis *in vitro* [19]. However, the effect of LFMFs on organisms and cells remains controversial. Adverse effect of exposure to LFMFs has also been extensively reported. Goraca et al. reported that exposure of rats to ELF-MF (40 Hz, 7 mT, 60 min/day for 2 weeks) resulted in the increase of ROS production in heart tissue and decrease of antioxidant capacity of plasma while exposure to ELF-MF of 40 Hz, 7 mT, 30 min/day for 2 weeks did not alter tissue ROS amount, indicating that the effect of ELF-MF on ROS generation and antioxidative capacity depend on its working time [20]. Emre et al. applied a pulsed square-wave magnetic field at an intensity of 1.5 mT to adult Wistar rats and observed an increase in the levels of oxidative stress indicators and apoptosis in liver samples [21]. Additionally, LFMFs (50 Hz, 1 mT) were also reported to impair cell Ca^+ homeostasis in spermatozoa [22]. These observed conflicting discrepancies of LFMFs effects may be explained by the different exposure conditions, such as intensity, duration, and frequency of magnetic fields. In our study, LFMFs exposure before or after H/R injury both improved cardiomyocytes viability, but the extent of recovery varied depending on different LFMFs parameters.

Our study confirmed the protective role of LFMFs in cardiomyocytes against H/R injury, however; the protective effects of LFMFs were not in liner correlation with the intensity and duration of LFMFs exposure. In our present study, limited parameters of LFMFs were applied. There may be a correspondence between particular parameters of LFMFs exposure and their protective effects. To further explore the optimal conditions of LFMFs, especially in clinical practice, further studies are needed.

In conclusion, our present study provides *in vitro* evidence supporting that LFMFs are capable of protecting myocardium from I/R injury *via* regulating ROS production and NO/$ONOO^-$ balance. This indicates that LFMFs may serve as a promising therapeutic strategy for cardiac I/R injury.

Conflict of Interests

The authors declare that no competing financial interests exist.

Authors' Contribution

Sai Ma, Dong Liang, Zhengxun Zhang, Fu Yi, Yabin Wang, Xiaotian Zhang, and Yuan Yuan performed the research and analysis the data. Sai Ma, Fu Yi, and Yabin Wang wrote the paper. Fu Yi and Feng Cao contributed to initial discussion of and overseeing the project. Sai Ma, Yabin Wang, and Feng Cao edited and reviewed the paper. Sai Ma, Zhengxun Zhang, and Fu Yi contributed equally to this work.

Acknowledgments

This work was supported by the National Nature Science Foundation of China (nos. 81270168, 81090274, 81090270, 81227901, 81000686), (FCao BWS12J037), Innovation Team Development Grant by China Department of Education (2010CXTD01, IRT1053), and the National Basic Research Program of China (2012CB518101).

References

[1] A. S. Go, D. Mozaffarian, V. L. Roger et al., "Executive summary: heart disease and stroke statistics—2013 update: a report from the American Heart Association," *Circulation*, vol. 127, pp. 143–152, 2013.

[2] M. L. Simoons and S. Windecker, "Controversies in cardiovascular medicine: chronic stable coronary artery disease: drugs versus revascularization," *European Heart Journal*, vol. 31, pp. 530–541, 2010.

[3] S. Verma, P. W. M. Fedak, R. D. Weisel et al., "Fundamentals of reperfusion injury for the clinical cardiologist," *Circulation*, vol. 105, no. 20, pp. 2332–2336, 2002.

[4] A. Albertini, P. Zucchini, G. Noera, R. Cadossi, C. Pace Napoleone, and A. Pierangeli, "Protective effect of low frequency low energy pulsing electromagnetic fields on acute experimental myocardial infarcts in rats," *Bioelectromagnetics*, vol. 20, pp. 372–377, 1999.

[5] M. V. Kurian, L. Hamilton, J. Keeven, P. Mehl, and J. M. Mullins, "Enhanced cell survival and diminished apoptotic response to simulated ischemia-reperfusion in H9c2 cells by magnetic field preconditioning," *Apoptosis*, vol. 17, pp. 1182–1196, 2012.

[6] D. Wang, P. Luo, Y. Wang et al., "Glucagon-like peptide-1 protects against cardiac microvascular injury in diabetes via a cAMP/PKA/Rho-dependent mechanism," *Diabetes*, vol. 62, pp. 1697–1708, 2013.

[7] E. Murphy and C. Steenbergen, "Mechanisms underlying acute protection from cardiac ischemia-reperfusion injury," *Physiological Reviews*, vol. 88, no. 2, pp. 581–609, 2008.

[8] K. Raedschelders, D. M. Ansley, and D. D. Y. Chen, "The cellular and molecular origin of reactive oxygen species generation during myocardial ischemia and reperfusion," *Pharmacology and Therapeutics*, vol. 133, no. 2, pp. 230–255, 2012.

[9] R. Ferrari, O. Alfieri, S. Curello et al., "Occurrence of oxidative stress during reperfusion of the human heart," *Circulation*, vol. 81, no. 1, pp. 201–211, 1990.

[10] W. Chan, A. J. Taylor, A. H. Ellims et al., "Effect of iron chelation on myocardial infarct size and oxidative stress in ST-elevation-myocardial infarction," *Circulation*, vol. 5, pp. 270–278, 2012.

[11] R. Quarrie, D. S. Lee, G. Steinbaugh et al., "Ischemic preconditioning preserves mitochondrial membrane potential and limits reactive oxygen species production," *The Journal of Surgical Research*, vol. 178, pp. 8–17, 2012.

[12] R. Iorio, S. Delle Monache, F. Bennato et al., "Involvement of mitochondrial activity in mediating ELF-EMF stimulatory effect on human sperm motility," *Bioelectromagnetics*, vol. 32, no. 1, pp. 15–27, 2011.

[13] S. Umar and A. van der Laarse, "Nitric oxide and nitric oxide synthase isoforms in the normal, hypertrophic, and failing heart," *Molecular and Cellular Biochemistry*, vol. 333, no. 1-2, pp. 191–201, 2010.

[14] S. M. Wildhirt, S. Weismueller, C. Schulze, N. Conrad, A. Kornberg, and B. Reichart, "Inducible nitric oxide synthase activation after ischemia/reperfusion contributes to myocardial dysfunction and extent of infarct size in rabbits: evidence for a late phase of nitric oxide-mediated reperfusion injury," *Cardiovascular Research*, vol. 43, no. 3, pp. 698–711, 1999.

[15] R. Bolli, "Cardioprotective function of inducible nitric oxide synthase and role of nitric oxide in myocardial ischemia and preconditioning: an overview of a decade of research," *Journal of Molecular and Cellular Cardiology*, vol. 33, no. 11, pp. 1897–1918, 2001.

[16] B. I. Jugdutt, "Nitric oxide and cardioprotection during ischemia-reperfusion," *Heart Failure Reviews*, vol. 7, no. 4, pp. 391–405, 2002.

[17] G. Heeba, M. K. A. Hassan, M. Khalifa, and T. Malinski, "Adverse balance of nitric oxide/peroxynitrite in the dysfunctional endothelium can be reversed by statins," *Journal of Cardiovascular Pharmacology*, vol. 50, no. 4, pp. 391–398, 2007.

[18] F. Gao, E. Gao, T.-L. Yue et al., "Nitric oxide mediates the anti-apoptotic effect of insulin in myocardial ischemia-reperfusion: the roles of PI3-kinase, Akt, and endothelial nitric oxide synthase phosphorylation," *Circulation*, vol. 105, no. 12, pp. 1497–1502, 2002.

[19] G. P. A. Yen-Patton, W. F. Patton, D. M. Beer, and B. S. Jacobson, "Endothelial cell response to pulsed electromagnetic fields: stimulation of growth rate and angiogenesis in vitro," *Journal of Cellular Physiology*, vol. 134, no. 1, pp. 37–46, 1988.

[20] A. Goraca, E. Ciejka, and A. Piechota, "Effects of extremely low frequency magnetic field on the parameters of oxidative stress in heart," *Journal of Physiology and Pharmacology*, vol. 61, no. 3, pp. 333–338, 2010.

[21] M. Emre, S. Cetiner, S. Zencir, I. Unlukurt, I. Kahraman, and Z. Topcu, "Oxidative stress and apoptosis in relation to exposure to magnetic field," *Cell Biochemistry and Biophysics*, vol. 59, pp. 71–77, 2011.

[22] N. Bernabò, E. Tettamanti, M. G. Pistilli et al., "Effects of 50 Hz extremely low frequency magnetic field on the morphology and function of boar spermatozoa capacitated in vitro," *Theriogenology*, vol. 67, no. 4, pp. 801–815, 2007.

Hindawi Publishing Corporation
Oxidative Medicine and Cellular Longevity
Volume 2013, Article ID 564902, 8 pages
http://dx.doi.org/10.1155/2013/564902

Research Article

Hyperglycemia-Induced Inhibition of DJ-1 Expression Compromised the Effectiveness of Ischemic Postconditioning Cardioprotection in Rats

Min Liu,[1] Bin Zhou,[2] Zhong-Yuan Xia,[1] Bo Zhao,[1] Shao-Qing Lei,[1] Qing-Jun Yang,[3] Rui Xue,[1] Yan Leng,[1] Jin-Jin Xu,[1] and Zhengyuan Xia[4,5]

[1] *Department of Anesthesiology, Renmin Hospital of Wuhan University, 99 Zi Yang Road, Wuhan, Hubei 430060, China*
[2] *Department of Anesthesiology, The First Affiliated Hospital of University of South China, 69 Chuan Shan Road, Hengyang, Hunan 421001, China*
[3] *Department of Cardiac Surgery, Chongqing Zhongshan Hospital, 312 Zhongshan Road, Chongqing 400013, China*
[4] *Department of Anesthesiology, The University of Hong Kong, Hong Kong*
[5] *Department of Anesthesiology, Affiliated Hospital of Guangdong Medical College, Zhanjiang, Guangdong 524001, China*

Correspondence should be addressed to Zhong-Yuan Xia; xiazhongyuan2005@aliyun.com

Received 29 July 2013; Accepted 15 September 2013

Academic Editor: Qian Fan

Ischemia postconditioning (IpostC) is an effective way to alleviate ischemia and reperfusion injury; however, the protective effects seem to be impaired in candidates with diabetes mellitus. To gain deep insight into this phenomenon, we explored the role of DJ-1, a novel oncogene, that may exhibit powerful antioxidant capacity in postconditioning cardioprotection in a rat model of myocardial ischemia reperfusion injury. Compared with normal group, cardiac DJ-1 was downregulated in diabetes. Larger postischemic infarct size as well as exaggeration of oxidative stress was observed, while IpostC reversed the above changes in normal but not in diabetic rats. DJ-1 was increased after ischemia and postconditioning contributed to a further elevation; however, no alteration of DJ-1 was documented in all subgroups of diabetic rats. Alteration of the cardioprotective PI3K/Akt signaling proteins may be responsible for the ineffectiveness of postconditioning in diabetes. There is a positive correlation relationship between p-Akt and DJ-1 but a negative correlation between infarct size and DJ-1, which may partially explain the interaction of DJ-1 and IpostC cardioprotection. Our result indicates a beneficial role of DJ-1 in myocardial ischemia reperfusion. Downregulation of cardiac DJ-1 may be responsible for the compromised diabetic heart responsiveness to IpostC cardioprotection.

1. Introduction

Ischemic heart disease, one of the major cardiovascular complications, is a leading cause of mortality in diabetic disease. Large evidence showed oxidative stress induced by hyperglycemia was the major mechanism contributing to the development and progression of myocardial infarction in diabetes mellitus (DM) [1]. Reperfusion therapies (coronary artery by-pass grafting, angioplasty, stent placement, or thrombolysis) when applied expeditiously restore coronary flow and limit cardiac dysfunction and infarct size. However, despite this, reperfusion also elicits pathophysiological changes responsible for more tissue injury after restoration of blood flow due to further aggravated oxidative damage [2]. The underlying mechanisms by which oxidative stress exerts adverse effects in myocardial ischemia reperfusion remain incompletely understood. Ischemic postconditioning provides protective effect against ischemia/reperfusion injuries, which is associated with a reduction in reactive oxygen species (ROS) generation, lipid peroxidation, and intracellular and mitochondrial Ca^{2+} overload [3]. Compared with ischemic preconditioning, postconditioning is a more promising approach to cardioprotection due to the difficulty to predict the onset of myocardial ischemia in clinical practice. Clinical data strongly supports an increased susceptibility to myocardial ischemia-reperfusion injury in

patients with diabetes mellitus [4]. The risk of postmyocardial infarction death is increased 2- to 4-fold in diabetic patients compared to those without diabetes [5, 6]. However, postconditioning seems to lose its cardioprotective effect in subjects with diabetes, while the underlying mechanism is largely unknown.

DJ-1, which was initially discovered as a novel oncogene and first reported in 1997 [7], extensively exists in most rodent and human tissues, such as brain, heart, kidney, liver, pancreas, and skeletal muscle [7]. Early studies about DJ-1 also revealed a main dwelling in familial Parkinson' disease. Gratifying, several latest research contributed to a progression in understanding the role of DJ-1 in oxidation and antioxidation. Recently, Jeong et al. [8] demonstrated by immunohistochemical analysis that transduced cell permeable Tat-DJ-1 fusion proteins prevented neuronal cell death in ischemic brain injury. Moreover, Yu et al. [9] found that stable overexpression of DJ-1 attenuated ischemia/reperfusion-induced oxidative stress in H9C2 cells under a hypoxia condition. All these studies suggested that DJ-1 has the antioxidative effect. However, whether or not DJ-1 expression was inhibited in diabetic heart remains unclear. In the present study, we hypothesized that reduction of DJ-1 expression aggravates ischemia reperfusion injury and attenuates the cardioprotective effects of postconditioning in diabetes.

2. Materials and Methods

2.1. Induction of Diabetes and Myocardial Ischemic Model. 108 healthy adult male Sprague-Dawley rats (aged 12 weeks) of SPF level weighing between 250 ± 10 g were obtained from HUNAN SLAC JD Laboratory Animal Co. Ltd. All the animals were randomly divided into 8 groups: normal blank control group, diabetic blank control group, normal rats sham operated (NS group), normal rats subjected to MI/R (NIR group), ischemic postconditioning group (NIPO group), diabetic rats sham operated (DMS group), diabetic rats subjected to MI/R (DMIR group) and ischemic postconditioning group (DMIPO group). After equilibrated to surroundings for three days, diabetes was induced via single intraperitoneal injection of STZ (60 mg/kg, Sigma, St. Louis, MO, USA) dissolved in citrate buffer (0.1 M, pH 4.5), while the normal rats were injected equal volume citrate buffer alone. One week after STZ injection, rats exhibiting hyperglycemia (blood glucose ≥ 16.7 mM) were considered diabetic.

At the end of suffering DM for 12 weeks, the myocardial ischemia-reperfusion injury model was established by the left anterior descending (LAD) coronary artery occlusion. The sham groups (N + S group and DM + S group) that underwent isolation of the LAD without occlusion and the IR groups (both N + IR group and DM + IR group) subjected to 30 min myocardial ischemia and 2 h reperfusion after the LAD had been isolated and occluded while the IPO groups (both N + IPO group and DM + IPO group) were subjected to 3 cycles of 10 s occlusion/10 s reperfusion after myocardial ischemia.

2.2. Determination of Myocardial Infarct Area. The infarction area was measured by Evans blue and 2,3,5-Triphenyltetrazolium chloride (TTC) double staining: after the animals were sacrificed, the ligature around the coronary artery was reoccluded and 2 mL of 0.25% Evens Blue dye was injected into the aorta to map the normally perfused region of the heart. The myocardial area at risk (AAR) for infarction was delineated by the area of myocardium not dyed. The presence of Evans blue was used to identify the area that was not subjected to the ischemia. Rat hearts were rapidly excised and frozen at −20°C and then sliced into 2 mm thick sections perpendicular to the heart base-apex axis using a heart slice chamber. The slices were incubated for 15 min at 37°C in a phosphate-buffered 1% TTC (Sigma-Aldrich, St. Louis, MO) solution to determine infarcted myocardium. The viable tissue was stained red by TTC, while the infarct portion not taking up TTC stain remained pale. Morphometric measurements of the AAR and infarct area (IA) in each slice were performed with a scanner (Epson, v30, Japan) and an image analysis system (Image-Pro plus; Media Cybernetics, Bethesda, MA). The percentage of the infarcted area from the left ventricle (IA/LV) and the area at risk from the left ventricle (AAR/LV) were calculated.

2.3. Biochemical Assays. Myocardial tissue was harvested and immediately homogenized on ice in 9 volumes of ice saline. The myocardial homogenate was centrifuged at 4,000 rpm for 10 min. The activity of Superoxide Dismutase (SOD) and the level of Malondialdehyde (MDA), 15-F_{2t}-Isoprostane (15-F_{2t}), and Total Antioxidant Capacity (T-AOC) in myocardial tissues were measured using SOD (Jiancheng, Nanjing, China), MDA (Jiancheng, Nanjing, China), 15-F_{2t}-Isoprostane (Cayman Chemical Company, USA), and T-AOC (Jiancheng, Nanjing, China) assay kits according to the manufacturer's instructions.

2.4. Western Blot Analysis. Myocardium tissue samples (100 mg) were homogenized in lysis buffer with electric homogenate machine, and then the homogenates were centrifuged at 12,000 rpm for 15 mins at 4°C. After determining with BCA protein assay kit (Beyotime Biotech Inc., Jiangsu, China), the supernatants were used as protein samples. Samples containing equal amounts were separated on a 10% SDS-polyacrylamide gel, and then proteins were transferred to PVDF membrane. After blocked in 5% nonfat-dried milk for 1 h, membranes were incubated with rabbit anti-DJ-1 or anti-PTEN, anti-total Akt, and anti-phospho-Akt monoclonal antibody (1 : 1000 dilution, Cell Signaling Technology, USA) overnight at 4°C. Subsequently, the membranes were washed and incubated with the corresponding fluorescent tags goat anti-rabbit polyclonal IgG (1 : 10000 dilution, LI-COR, USA) for 1 h at room temperature. Open the Odyssey scanner and put the membranes facing down on the designated area for infrared fluorescence detection on the Odyssey Imaging Systems (LI-COR, USA). GADPH was chosen as a loading control to further assure the same volume for all the samples.

2.5. Statistical Analysis. Mean ± SD values were calculated to summarize all outcome measurements. One-way analysis of variance (ANOVA) was used to compare significant differences among the groups, followed by Newman-Keuls

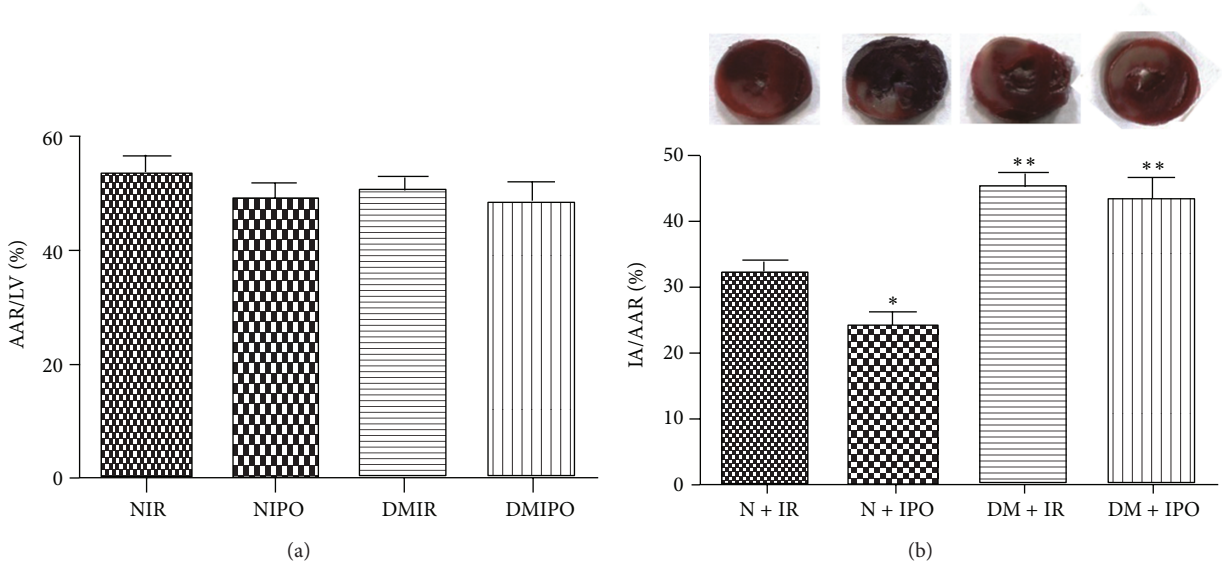

Figure 1: Shown are the area at risk from the left ventricle (AAR/LV) and infarcted area from the area at risk (IA/AAR) in percent means ± SD ($n = 6$ each). The blue-stained areas represent nonischemic tissue, and red stained areas represent the area at risk. Pale areas indicate infarct areas. (a) AAR/LV of normal and diabetic heart suffering from MI/R. There was no significant difference in AAR/LV between the four groups ($P > 0.05$). (b) IA/AAR of normal and diabetic heart which was subjected to MI/R with or without ischemic postconditioning. $^{*}P < 0.05$ & $^{**}P < 0.01$ versus N + IR group; no difference between DM + IR group and DM + IPO group.

Table 1: Changes in body weight and fasting blood glucose of control and diabetic rats before and after 12 weeks of STZ or vehicle injection.

	Normal		Diabetes	
	0 W	12 W	0 W	12 W
Body weight (g)	239.5 ± 7.4	418.7 ± 15.0	235.2 ± 6.7	204.5 ± 7.2***
FBG (mmol/L)	6.6 ± 1.1	7.5 ± 1.6	7.1 ± 1.2	25.7 ± 4.5***

All values are expressed as mean ± SD. $^{***}P < 0.001$ versus normal rats 12 weeks later after STZ injection.

Multiple Comparison Test. A value of $P < 0.05$ was considered to be statistically significant for all the statistical tests.

3. Results

3.1. General Characteristics of STZ-Induced Diabetic Rats. The general characteristics of diabetic compared with age-matched control rats are shown in Table 1. Before STZ induced diabetes, the body weight and fasting blood glucose (FBG) were recorded and no significant evidence was observed between the control and the intervention ($P > 0.05$, Table 1).

During raising animal, we can observe that with a longer duration of diabetes, the diabetic rats were bald and showed polydipsia, polyuria, and weight loss. After feeding for 12 weeks, diabetic rats had remarkably lower body weight and higher blood glucose compared to the age-matched controls with euglycemia and a moderate growth rate at 5–10 g/d in normal group ($P < 0.001$, Table 1).

3.2. The Difference of Myocardial Infarcted Area between Normal and Diabetic Rats. To examine the different effect of cardioprotective postconditioning on the normal and diabetic hearts, myocardial infarcted area was measured. The representative images of AAR and IA from each group were shown in Figure 1. No more significant difference was shown in the size of area at risk (AAR/LV) among the four groups (Figure 1(a)). The infarct size in normal rats remarkably decreased with the protective effect of postconditioning ($P < 0.05$, Figure 1(b)). Interestingly, the diabetic heart shows more extensive infracted area percentage (IA/AAR) than normal heart when it suffers from the same degree of MI/R insult ($P < 0.05$, Figure 1(b)), and the cardioprotective effect of postconditioning was abolished since the infracted area percentage (IA/AAR) in DM + IPO group was similar to DM + IR group. These results provided that diabetic heart was more vulnerable to MI/R, and postconditioning cannot reverse the injury.

3.3. The Difference of Reactive Oxygen Species Level between Normal and Diabetic Rats. Data are shown in Figure 2. Compared with the N + S group, the IR induced injury was manifested by a remarkable decrease in SOD and T-AOC, associate with an increase in MDA and 15-F_{2t}-Isoprostane. The ischemic postconditioning caused a significant reversion of MI/R in normal rats. The diabetic rats got lower activity in SOD and the level of MDA, T-AOC and 15-F_{2t}-Isoprostane in diabetic rats is significantly higher than normal rats. After subject to IR injury the activity of SOD losses mount

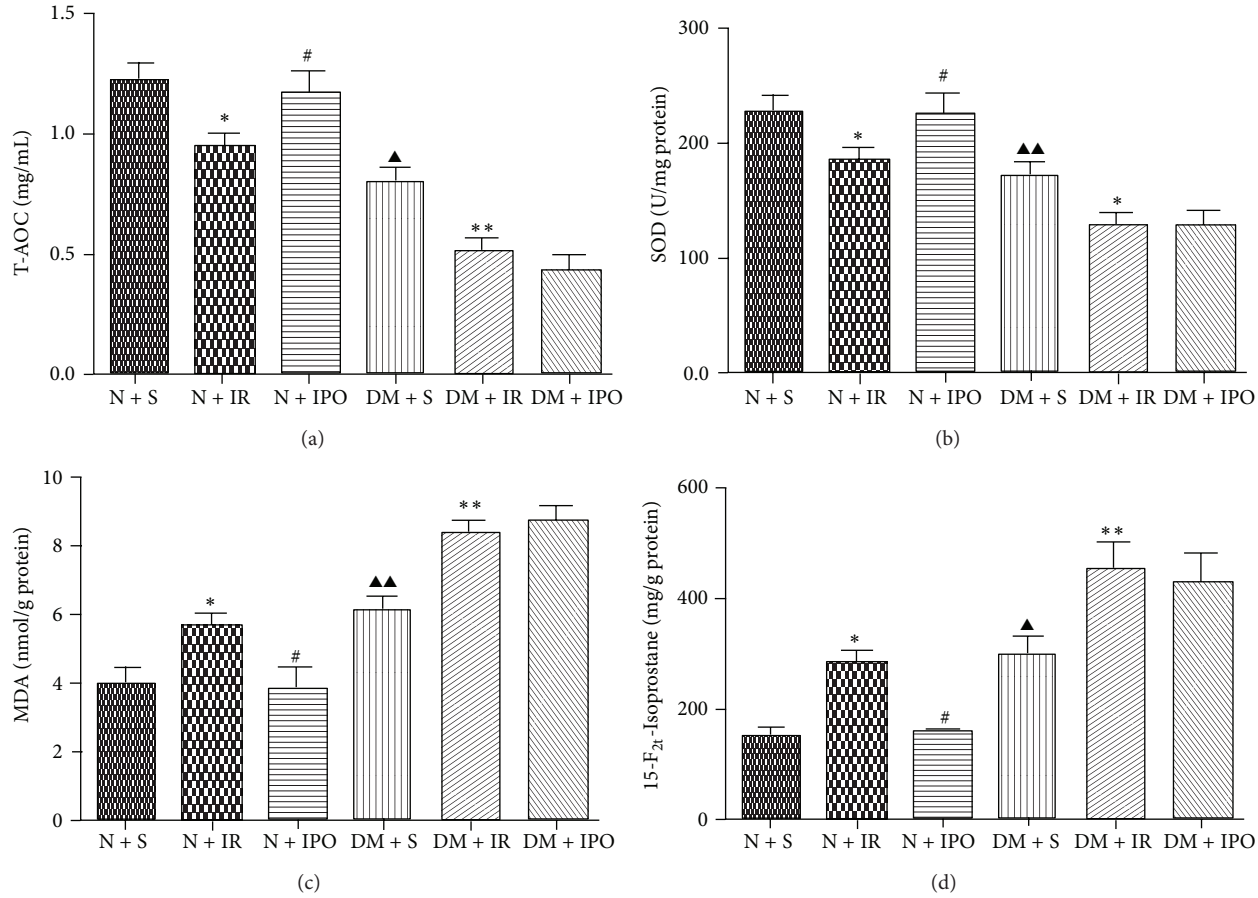

Figure 2: Index of oxidative stress in different groups was analyzed by ANOVA. (a) The level of Total Antioxidant Capacity (T-AOC). (b) The activity of Superoxide Dismutase (SOD). (c) The level of Malondialdehyde (MDA). (d) The level 15-F_{2t}-Isoprostane. Values presented are mean ± SD ($n = 6$ each). $^{\blacktriangle}P < 0.05$ & $^{\blacktriangle\blacktriangle}P < 0.01$ versus N + S group; $^{*}P < 0.05$ & $^{**}P < 0.01$ versus respective sham group $^{\#}P < 0.05$ versus respective IR group.

in diabetic rats. Meanwhile the increasing level of MDA, T-AOC, and 15-F_{2t}-Isoprostane in DM + IR group was aggravated. Unfortunately, ischemic postconditioning cannot restore the MI/R injury in diabetic rats.

3.4. The Difference of DJ-1 Expression between Normal and Diabetic Rats. It has been reported that DJ-1 is an antioxidative protein in ischemic brain injury [8]. To further investigate the different effect of postconditioning on normal and diabetic hearts, we attempted to determine the expression of DJ-1. As shown in Figure 3, the expression of DJ-1 was abolished by diabetes mellitus, when compared with the normal hearts and diabetic hearts, and this difference is not likely to occur by chance ($P < 0.01$).

3.5. Variation of DJ-1 and Related Signal Transduction Molecules in PI3K/Akt Signal Pathway during MI/R and IPost in Normal and Diabetic Rats. Based on the recent studies in other system, DJ-1 may act as antioxidant agents associated with the regulation of PTEN and PI3K/Akt pathways [10], which are considered as important signaling systems involved in cardioprotection; thus, we investigated the expression of DJ-1 and related signal transduction molecules during MI/R and ischemic postconditioning in normal and diabetic rats. As shown in Figure 4(b), expression of DJ-1 in N + IR group was significantly higher than in N + S group ($P < 0.01$), and ischemic postconditioning further amplificated the increment between the N + IR group and N + IPO group ($P < 0.001$). However, when the same strike occurred in diabetic rats, no significant changes were identified in DJ-1 between DM + S group and DM + IR group ($P > 0.05$). In addition, the expression of DJ-1 was abolished by diabetes mellitus during ischemic postconditioning and no significant change was observed between DM + IR group and DM + IPO group ($P > 0.05$). The expression of PTEN was higher during MI/R ($P < 0.01$) and then inhibited when ischemic postconditioning aroused the level of DJ-1 in normal rats ($P < 0.05$). Furthermore, we also observed a high level of expression in MI/R in diabetic heart ($P < 0.001$) and drove the Akt activation at a significantly lower level ($P < 0.05$) due to the dysfunction of DJ-1, even ischemic postconditioning can never reverse (Figures 4(c) and 4(d)). As shown in Figure 4(e), no variation of total Akt was recorded in all groups ($P > 0.05$).

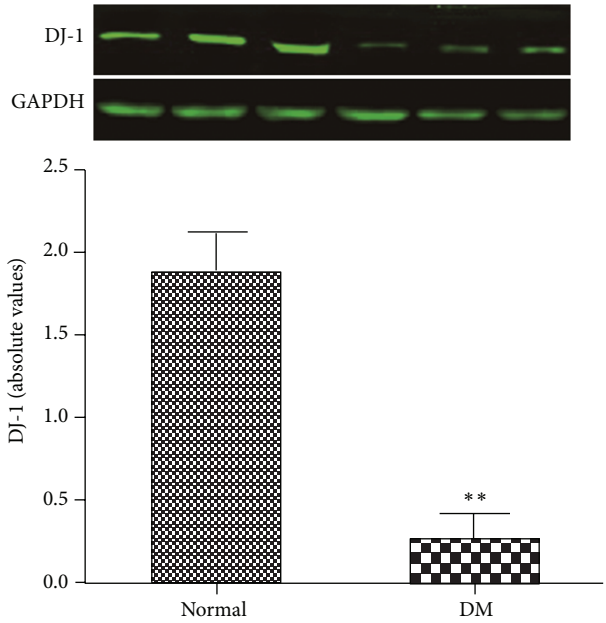

Figure 3: Effects of Diabetes Mellitus on the protein expression of DJ-1. There were three different normal blank control rats (on the left side) and three different diabetic blank control rats (on the right side). All values are expressed as mean ± SD ($n = 6$ each). $^{**}P < 0.01$ versus normal rats.

3.6. The Relationship between DJ-1 and Myocardial Infarcted Area, Phospho-Akt. Group differences in the relationship of DJ-1 expression and the myocardial injury indexes were evaluated with simple linear regression (Figure 5). The expression of DJ-1 was positively correlated with p-Akt with r^2 at 0.6331 ($P < 0.001$), while myocardial infarct size was negatively correlated with DJ-1; the corresponding r^2 was 0.6354 ($P < 0.001$). These results suggest that DJ-1 may be endowed with a salutary role in cardioprotection.

4. Discussion

We present several important observations from our study supporting the beneficial function of DJ-1 in myocardial defense against ROS. First, using *in vivo* models of MI/R, we demonstrated that the effectiveness of ischemic postconditioning as means of myocardial protection may closely related to the level of myocardial DJ-1. Second, to our knowledge, we are the first to report that the cardiac expression of DJ-1 was seriously inhibited in DM condition. Third, unlike the change of DJ-1 expression level in the normal rat, neither the compensatory increase of DJ-1 in response to the MI/R insult nor the protective increment in response to ischemic postconditioning was observed in diabetic condition.

In the present study, ischemic postconditioning reduced myocardial infarction size and oxidative stress level, which was intensely associated with enhanced expression of cardiac DJ-1. Our results are well in line with finding of other researches in kidney and brain [8, 11, 12]. Moreover, Lu et al. have recently demonstrated that hypoxic preconditioning upregulates DJ-1 protein expression in rat heart-derived H9C2 cells which contributes to the cardioprotection against hypoxia/reoxygenation injury [13]. Several lines of evidence suggest that overexpression of DJ-1 may have a crucial role against oxidative stress in ischemia/reperfusion (I/R) models. Regarding the increase in the expression of DJ-1 in normal MI/R group, we conjecture that it may be a compensatory increase during the MI/R injury.

It has been revealed that a reduction of antioxidative capacity in DJ-1 knock-out rats and mice *in vivo* and *in vitro* [14–16]. In our study we also exhibited a decline of T-AOC and SOD together with the increase of MDA and 15-F_{2t} in diabetic rats which may be due to the downregulation of DJ-1. Apart from the direct decreased expression of DJ-1, another possibility that may account for the exacerbation of oxidative stress was the peroxidation inactivation of DJ-1. Meulener and his colleagues [17] demonstrated that human DJ-1 (hDJ-1) rescues flies mutant for DJ-1b, and cysteine residue in the fly DJ-1 (C104) is analogous to C106 in hDJ-1. It has been confirmed in other studies that, the conserved cysteine residue in DJ-1 (Cys106) was both essential for DJ-1 protective function and was sensitive to oxidation [18]. It was supposed that the C104 subunit of DJ-1b was overoxidized in chemical toxin or aged condition, which resulted in the failure of dimerization and inactivation [17], similar to the one occurred in diabetic status in our study. Thus, the oxidative stress was further aggrandized due to the reduced activation of DJ-1 and consequently weakened antioxidative effect.

In the present study, the infarct size and oxidative stress were more extensive in diabetic rat hearts than in normal rats when endured the equivalent extent of ischemic reperfusion insult. The peroxidative inactivation of DJ-1 caused by excessive ROS will facilitate ROS overproduction in diabetes, which may predispose to a hypersensitivity of diabetic myocardium to ischemia and reperfusion in a vicious circle manner.

Despite the emphasis on the impact of the duration of the diabetic state, metabolic disturbance, more extensive lesions (include atherosclerosis and hypertrophied), left ventricle dysfunction on myocardial injury in diabetes [19–22], and a number of studies which were carried out to investigate the myocardial protective signaling disrupted by diabetes have also been advocated [23, 24]. From data presented in the literature, two signal pathways have contributed to myocardial protection, one is Survivor Activating Factor Enhancement (SAFE) pathway and the other is Reperfusion Injury Salvage Kinase (RISK) pathway, which encompasses PI3K/AKT and ERK 1/2. Activation of PI3K/AKT pathway is responsible for protecting the myocardium by regulating essential cellular functions, such as cell migration, cell survival, and modulating several essential biologic processes, such as metabolism [25]. Furthermore, insulin activation of the PI3K/AKT pathway has been shown to delay the time to mitochondrial permeability transition pore (mPTP) opening and reduce ROS level [26]. Therefore, any strategy to activate PI3K/Akt and enlarge the threshold to mPTP opening may provide the protective effect against myocardial ischemia/reperfusion injuries.

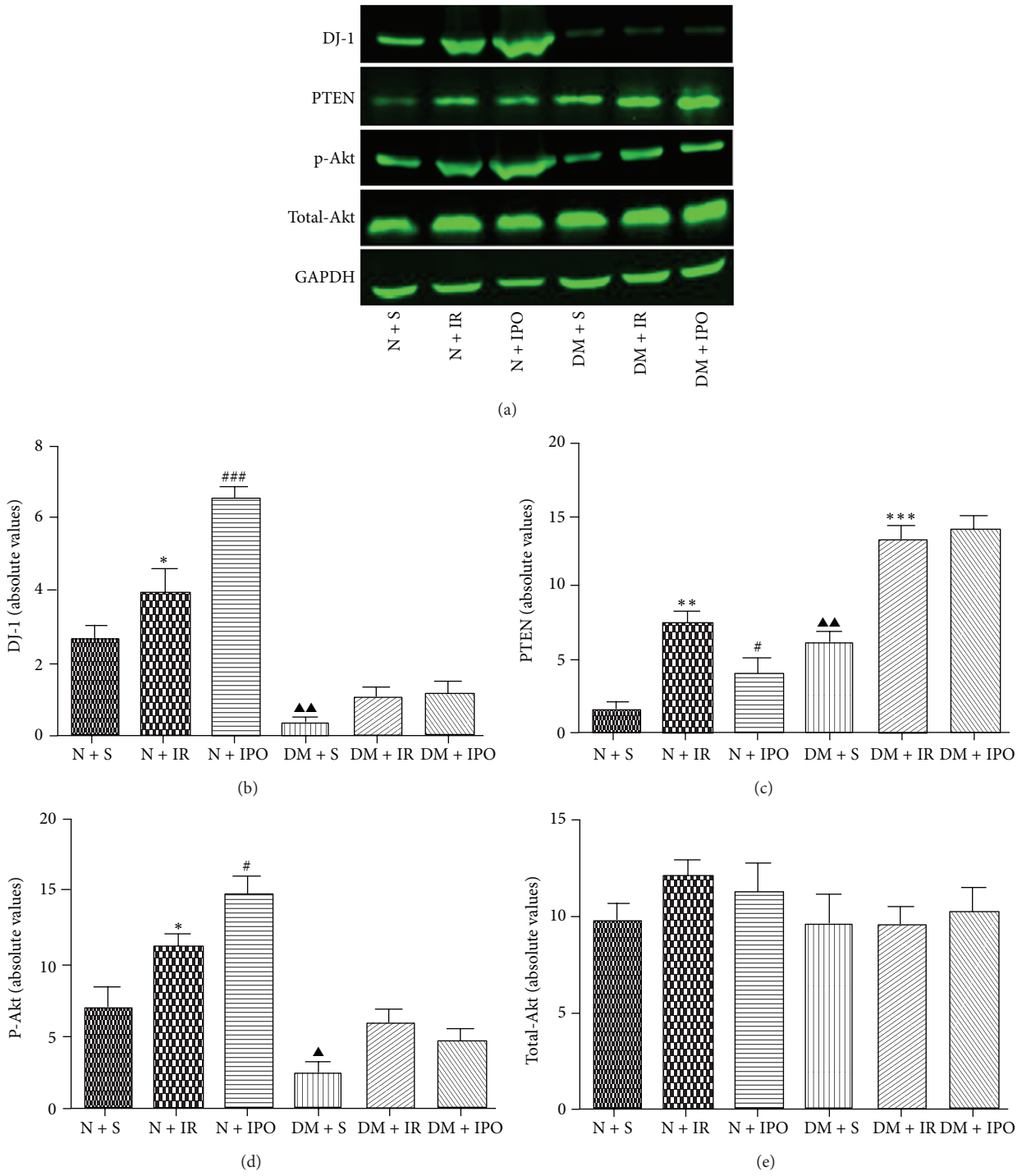

Figure 4: Immunoblot and densitometry analysis of the protein expression of DJ-1, PTEN, phosphorylated, and total Akt in normal and diabetic myocardial tissue. GAPDH was set as a loading control. Data are the mean ± SD ($n = 6$ each). (a) Western blot of DJ-1, PTEN, p-Akt, total Akt, and GAPDH. (b) Statistical analysis of DJ-1 among different groups. (c) Statistical analysis of PTEN among different groups. (d) Statistical analysis of p-Akt among different groups. (e) Statistical analysis of total Akt among different groups. $^{\blacktriangle}P < 0.05$ & $^{\blacktriangle\blacktriangle}P < 0.01$ versus N + S group; $^{*}P < 0.05$ & $^{**}P < 0.01$ & $^{***}P < 0.001$ versus respective sham group; $^{\#}P < 0.05$ versus respective IR group; $^{\#\#\#}P < 0.001$ versus respective IR group.

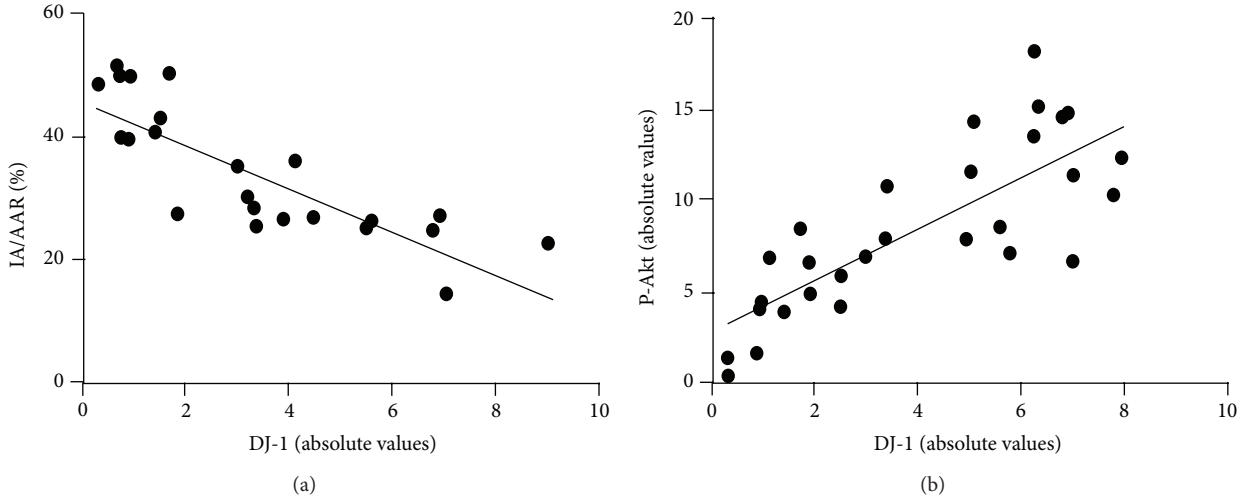

Figure 5: Simple linear regression between DJ-1 and myocardial infarct size together with p-Akt. (a) Linear regression between DJ-1 and IA/AAR. (b) Linear regression between DJ-1 and p-Akt.

Despite that DJ-1 expression would be upregulated under myocardial ischemia and reperfusion injury, it was not enough to resist myocardial insult resulted from ischemia reperfusion, while postconditioning may add to an endogenous activation of the RISK pathway which enhances the antioxidative effects of DJ-1. However, chronic oxidation under DM may attenuate the expression of DJ-1 and the underlying RISK pathway may also be partially inactivated; thus, myocardial DJ-1 could not be stimulated under IR and subsequently the responsiveness to postconditioning could be attenuated or diminished.

Several studies have demonstrated that DJ-1 robustly protects cells from oxidative stress through distinct cellular pathways [27, 28]. In normal rats, ischemic postconditioning can arouse DJ-1 high expression and confer myocardial protection. Base on a series of studies on cancer cells, Kim et al. [10] found that DJ-1 functions in the PI3K/Akt (RISK) pathway as a negative regulator of PTEN. These results are in good agreement with ours. In the normal rats, ischemic postconditioning increased myocardial expression of DJ-1, paralleled with decreased expression of PTEN as well as increased Akt phosphorylation, and protected heart from MI/R, while in diabetic rats, DJ-1 expression was inhibited due to the overoxidation cause by DM. Therefore, ischemic postconditioning cannot reverse the DJ-1 expression in diabetic rats. As a result, the expression of PTEN highly grows unchecked and arrest PI3K/Akt (RISK) pathway functions. These fatal change lead to a reduction in the threshold and triggering mitochondrial permeability transition pore (mPTP) opening in response to Ca^{2+} overload and break the delicate balance between ROS production and scavenging capacity of antioxidant systems. Given the deficiency of agonist and antagonist of DJ-1, a better understanding of the interaction between DJ-1 and ischemia postconditioning protection could only be achieved by simple-linear regression; thus, further silencing and overexpression of DJ-1 via genetic engineering would be needed, which could add to a further comprehension of the underlying mechanism and may provide a promising alternative in the prevention and treatment of cardiovascular disease with DM.

5. Conclusion

With the result of *in vitro* study, we demonstrated the possible correlation between inhibition of DJ-1 induced by hyperglycemia and ineffectiveness of postconditioning in diabetic rats and that PI3K/Akt signal pathway may be one of the major factors involved in the protective effect of DJ-1, which should be further elucidated by *in vivo* studies. Our research revealed a potential curative role of DJ-1 in the treatment of diabetic cardiac complication. Thus, therapeutics aiming at upregulating DJ-1 could be considered as a novel alternative to alleviate the reperfusion injury in diabetic patients with ischemic heart disease.

Conflict of Interests

The authors declare that they have no conflict of interests.

Disclosure

All authors have no financial, personal, or other relationships with other people or organizations that could inappropriately influence the work.

Acknowledgment

This research was supported by the National Natural Science Foundation of China (Grants nos. 81170768 and 81270899).

References

[1] C. D. Filippo, S. Cuzzocrea, F. Rossi, R. Marfella, and M. D'Amico, "Oxidative stress as the leading cause of acute myocardial infarction in diabetics," *Cardiovascular Drug Reviews*, vol. 24, no. 2, pp. 77–87, 2006.

[2] J. W. Hoffman Jr., T. B. Gilbert, R. S. Poston, and E. P. Silldorff, "Myocardial reperfusion injury: etiology, mechanisms, and therapies," *The Journal of Extra-Corporeal Technology*, vol. 36, no. 4, pp. 391–411, 2004.

[3] H. Y. Sun, N. P. Wang, F. Kerendi et al., "Hypoxic postconditioning reduces cardiomyocyte loss by inhibiting ROS generation and intracellular Ca^{2+} overload," *American Journal of Physiology. Heart and Circulatory Physiology*, vol. 288, no. 4, pp. H1900–H1908, 2005.

[4] D. J. Paulson, "The diabetic heart is more sensitive to ischemic injury," *Cardiovascular Research*, vol. 34, no. 1, pp. 104–112, 1997.

[5] US Department of Health and Human Services, Centers for Disease Control Prevention, "National diabetes fact sheet: general information and national estimates on diabetes in the United States," 2007.

[6] J. A. Beckman, F. Paneni, F. Cosentino, and M. A. Creager, "Diabetes and vascular disease pathophysiology, clinical consequences, and medical therapy: part II," *European Heart Journal*, vol. 43, no. 31, pp. 2444–2452, 2013.

[7] D. Nagakubo, T. Taira, H. Kitaura et al., "DJ-1, a novel oncogene which transforms mouse NIH3T3 cells in cooperation with *ras*," *Biochemical and Biophysical Research Communications*, vol. 231, no. 2, pp. 509–513, 1997.

[8] H. J. Jeong, D. W. Kim, M. J. Kim et al., "Protective effects of transduced Tat-DJ-1 protein against oxidative stress and ischemic brain injury," *Experimental and Molecular Medicine*, vol. 44, no. 10, pp. 586–593, 2012.

[9] H. H. Yu, Q. Xu, H. P. Chen et al., "Stable overexpression of DJ-1 protects H9c2 cells against oxidative stress under a hypoxia condition," *Cell Biochemistry and Function* 2013.

[10] R. H. Kim, M. Peters, Y. Jang et al., "DJ-1, a novel regulator of the tumor suppressor PTEN," *Cancer Cell*, vol. 7, no. 3, pp. 263–273, 2005.

[11] S. Cuevas, Y. Zhang, Y. Yang et al., "Role of renal DJ-1 in the pathogenesis of hypertension associated with increased reactive oxygen species production," *Hypertension*, vol. 59, no. 2, pp. 446–452, 2012.

[12] P. Milani, G. Ambrosi, O. Gammoh, F. Blandini, and C. Cereda, "SOD1 and DJ-1 converge at Nrf2 pathway: a clue for antioxidant therapeutic potential in neurodegeneration," *Oxidative Medicine and Cellular Longevity*, vol. 2013, Article ID 836760, 12 pages, 2013.

[13] H. S. Lu, H. P. Chen, S. Wang et al., "Hypoxic preconditioning up-regulates DJ-1 protein expression in rat heart-derived H9c2 cells through the activation of extracellular-regulated kinase 1/2 pathway," *Molecular and Cellular Biochemistry*, vol. 370, no. 1-2, pp. 231–240.

[14] X. Li, F. Arslan, Y. Ren et al., "Metabolic adaptation to a disruption in oxygen supply during myocardial ischemia and reperfusion is underpinned by temporal and quantitative changes in the cardiac proteome," *Journal of Proteome Research*, vol. 11, no. 4, pp. 2331–2346, 2012.

[15] E. Andres-Mateos, C. Perier, L. Zhang et al., "DJ-1 gene deletion reveals that DJ-1 is an atypical peroxiredoxin-like peroxidase," *Proceedings of the National Academy of Sciences of the United States of America*, vol. 104, no. 37, pp. 14807–14812, 2007.

[16] F. Billia, L. Hauck, D. Grothe et al., "Parkinson-susceptibility gene DJ-1/PARK7 protects the murine heart from oxidative damage in vivo," *Proceedings of the National Academy of Sciences of the United States of America*, vol. 110, no. 15, pp. 6085–6090, 2013.

[17] M. C. Meulener, K. Xu, L. Thomson, H. Ischiropoulos, and N. M. Bonini, "Mutational analysis of DJ-1 in Drosophila implicates functional inactivation by oxidative damage and aging," *Proceedings of the National Academy of Sciences of the United States of America*, vol. 103, no. 33, pp. 12517–12522, 2006.

[18] M. A. Wilson, "The role of cysteine oxidation in DJ-1 function and dysfunction," *Antioxidants and Redox Signaling*, vol. 15, no. 1, pp. 111–122, 2011.

[19] T. Ravingerová, A. Adameová, J. Matejíková et al., "Subcellular mechanisms of adaptation in the diabetic myocardium: relevance to ischemic preconditioning in the nondiseased heart," *Experimental and Clinical Cardiology*, vol. 15, no. 4, pp. 68–76, 2010.

[20] G. M. C. Rosano, C. Vitale, and G. Fragasso, "Metabolic therapy for patients with diabetes mellitus and coronary artery disease," *The American Journal of Cardiology*, vol. 98, no. 5, pp. 14–18, 2006.

[21] Z. Xia, K.-H. Kuo, P. R. Nagareddy et al., "N-acetylcysteine attenuates PKCβ2 overexpression and myocardial hypertrophy in streptozotocin-induced diabetic rats," *Cardiovascular Research*, vol. 73, no. 4, pp. 770–782, 2007.

[22] A. N. Mather, A. Crean, N. Abidin et al., "Relationship of dysglycemia to acute myocardial infarct size and cardiovascular outcome as determined by cardiovascular magnetic resonance," *Journal of Cardiovascular Magnetic Resonance*, vol. 12, no. 61, pp. 1–10, 2010.

[23] A. Das, F. N. Salloum, L. Xi, Y. J. Rao, and R. C. Kukreja, "ERK phosphorylation mediates sildenafil-induced myocardial protection against ischemia-reperfusion injury in mice," *American Journal of Physiology. Heart and Circulatory Physiology*, vol. 296, no. 5, pp. H1236–H1243, 2009.

[24] J. Wei, W. Wang, I. Chopra et al., "c-Jun N-terminal kinase (JNK-1) confers protection against brief but not extended ischemia during acute myocardial infarction," *The Journal of Biological Chemistry*, vol. 286, no. 16, pp. 13995–14006, 2011.

[25] A. Eisenreich and U. Rauch, "PI3K Inhibitors in Cardiovascular Disease," *Cardiovascular Therapeutics*, vol. 29, no. 1, pp. 29–36, 2011.

[26] S. M. Davidson, D. Hausenloy, M. R. Duchen, and D. M. Yellon, "Signalling via the reperfusion injury signalling kinase (RISK) pathway links closure of the mitochondrial permeability transition pore to cardioprotection," *The International Journal of Biochemistry & Cell Biology*, vol. 38, no. 3, pp. 414–419, 2006.

[27] E. Giaime, H. Yamaguchi, C. A. Gautier, T. Kitada, and J. Shen, "Loss of DJ-1 does not affect mitochondrial respiration but increases ROS production and mitochondrial permeability transition pore opening," *PLoS One*, vol. 7, no. 7, Article ID 40501, 2012.

[28] J. Y. Im, K. W. Lee, J. M. Woo, E. Junn, and M. M. Mouradian, "DJ-1 induces thioredoxin 1 expression through the Nrf2 pathway," *Human Molecular Genetics*, vol. 21, no. 13, pp. 3013–3024, 2012.

Hindawi Publishing Corporation
Oxidative Medicine and Cellular Longevity
Volume 2013, Article ID 572729, 9 pages
http://dx.doi.org/10.1155/2013/572729

Research Article

Effects of Endothelial Progenitor Cell-Derived Microvesicles on Hypoxia/Reoxygenation-Induced Endothelial Dysfunction and Apoptosis

Jinju Wang,[1] Shuzhen Chen,[1] Xiaotang Ma,[2] Chuanfang Cheng,[3] Xiang Xiao,[1] Ji Chen,[1,2] Shiming Liu,[3] Bin Zhao,[2] and Yanfang Chen[1,2,3]

[1] *Department of Pharmacology & Toxicology, Boonshoft School of Medicine, Wright State University, 3640 Colonel Glenn Highway, Dayton, OH 45435, USA*
[2] *Institute of Neurology, Affiliated Hospital of Guangdong Medical College, Zhanjiang 524001, China*
[3] *Cardiovascular Department, The Second Hospital Affiliated to Guangzhou Medical University, Guangzhou Institute of Cardiovascular Disease, Guangzhou 510000, China*

Correspondence should be addressed to Bin Zhao; zhaobine@vip.tom.com and Yanfang Chen; yanfang.chen@wright.edu

Received 9 August 2013; Accepted 16 September 2013

Academic Editor: Zhengyuan Xia

Oxidative stress-induced endothelial dysfunction plays a key role in ischemia/reperfusion injury. Recent evidence indicates that endothelial progenitor cell-derived microvesicles (EPC-MVs) can promote angiogenesis of endothelial cells (ECs). Here, we investigated the potential effects of EPC-MVs on hypoxia/reoxygenation (H/R) injury in human brain microvascular ECs (hb-ECs). MVs were prepared from EPCs cultured in a serum deprivation (SD) medium (starving stress, sEPC-MVs) or SD medium containing tumor necrosis factor-α (TNFα) (apoptotic stress, aEPC-MVs). H/R injury model of hb-ECs was produced by 6 hr hypoxia (1% O_2) and 24 hr reoxygenation. The H/R hb-ECs were co-cultured with EPC-MVs. Results showed that (1) H/R hb-ECs were dysfunctional and coupled with increased apoptosis and ROS overproduction; (2) under two different conditions, EPCs displayed remarkable difference in caspase 3 and miR126 expression, which were carried by the corresponsive EPC-MVs; (3) functionally, sEPC-MVs had beneficial effects on H/R hb-ECs, whereas aEPC-MVs had detrimental effects; (4) the diverse effects of sEPC-MVs and aEPC-MVs were associated with the changes in miR126 and eNOS expression and were abolished by PI3K inhibitor. In conclusion, sEPCs-MVs and aEPC-MVs are functionally different on hb-EC apoptosis and dysfunction via their carried RNAs associated with ROS production and PI3K/eNOS/NO pathway.

1. Introduction

Reactive oxygen species (ROS) are well known to mediate ischemia/reperfusion (I/R) injury [1]. ROS-induced vascular endothelial cell (EC) injury is the first key step in the pathogenesis of ischemia/reperfusion injury. Therefore, attenuating oxidative stress-induced EC injury could be an important strategy in the management of I/R injury on tissues. Several strategies for inhibiting ROS production or increasing their degradation and scavenging have been attempted and turned out to be less effective [2]. Therefore, novel approaches are greatly demanded for preventing I/R injury.

Endothelial progenitor cells (EPCs) are circulating bone marrow-derived precursors which are able to exert a protective effect in experimental models of hindlimb ischemia [3] and myocardial infarction [4]. Previous studies have shown that EPCs recruited into the kidney could induce tissue repair via secretion of proangiogenic factors [5, 6].

Microvesicles (MVs) are small particles 0.1–1 μm in size, which are shed from the plasma membrane of various cell types [7, 8]. They carry proteins and gene messages (mRNAs and miRNAs). Because of their ability to merge with target cells, MVs can deliver their contents into the cells they communicate with [8–10]. Recent studies have reported that MVs

produced from mesenchymal stem cells and EPCs could exert protective effects in experimental models of acute/chronic kidney injury [11–13]. In addition, another study demonstrates that MVs released from EPCs (EPC-MVs) can trigger angiogenesis by a horizontal transfer of mRNA [14]. Nevertheless, there is little information regarding the effects of EPC-MVs on ECs injured by hypoxia/reoxygenation (H/R).

In this study, we aimed to investigate the potential effects of EPC-MVs on human brain microvascular ECs (hb-ECs) injured by H/R and the underlying mechanisms.

2. Material and Methods

2.1. Culture and Characterization of EPCs. The mononuclear cells (MNCs) isolated from mouse bone marrow were used for EPC culture as previously described [15, 16]. In brief, the cells were counted and plated (1×10^6 cells/well) on fibronectin-coated 24-well plates (BD Bioscience, San Jose, CA) and then grown in endothelial cell basal medium-2 (EBM-2) supplemented with 5% FBS containing EPC growth cytokine cocktail (Lonza, Walkersville, MD). After 3 days, nonadherent cells were removed by washing with PBS. Thereafter, culture medium was changed every 2 days. Cultured cells were characterized by double-positive Di-LDL and Bs-Lectin staining as previously reported [15, 16].

2.2. Preparation of EPC-MVs. EPC-MVs were prepared from EPCs using two different stimulations, starving stress and apoptotic stress, based on previous reports with slight modifications [13, 17]. EPCs were cultured in serum deprivation (SD) medium for 24 hrs for generating starving stress EPC-MVs (sEPC-MVs). For generating apoptotic stress EPC-MVs (aEPC-MVs), EPCs were cultured in SD medium supplemented with 25 ng/mL TNFα (R&D systems, MN) for 24 hrs. MVs collected from EPCs cultured in EBM-2 served as a control (control MVs).

2.3. Characterization and Labeling of EPC-MVs. EPC-MVs were collected from EPC modified culture medium as previously described with slight modification [13]. In brief, EPC culture medium was collected, centrifuged at 2000 g for 20 mins to remove cells and debris, and ultracentrifuged at 120,000 g for 1 hr. The protein concentration of EPC-MV preparations was quantified by the Bradford method (Bio-Rad, Hercules, USA). A concentration of 10 μg/mL EPC-MVs was used for coculture experiments. In selected experiments, EPC-MVs were pretreated with 0.1% Triton-100 for 5 mins, then treated with 200 u/mL RNase (Qiagen, CA) for 90 mins at 37°C, washed, and pelleted by ultracentrifugation. To verify the effect of RNase, the total RNAs of EPC-MVs were extracted using the RNA isolation kit (Ambion, NY), and the RNA concentration was determined using quantitative assay (Thermo Scientific, Nanodrop 2000c, FL). For flow cytometry analysis [18], EPC-MVs were resuspended and incubated for 30 mins at 4°C in the dark with Alexa-488-labeled Annexin V, PE-conjugated VEGFR2, or FITC-conjugated CD34, 5 μL, respectively. Isotype matched (IgG) nonspecific antibodies served as negative controls. All antibodies were purchased from eBioscience (San Diego, CA). After incubation, labeled cells were resuspended with PBS and analyzed under flow cytometry (Accuri C6 flow cytometer, Ann Arbor, MI). For TEM analysis [18], EPC-MVs were fixed with 2% glutaraldehyde and postfixed with 1% osmium (all were purchased from electron microscopy science, Hatfield, PA), then embedded with Spurr resin (Sigma, Louis, MO), and baked at 60°C according to the manufacturer's instruction. Ultrathin sections (60–80 nm) were prepared with MT7000, mounted on 300-mesh copper grids, and stained with uranyl acetate and lead citrate. All samples were examined with an EM 208 (Philips) transmission electron microscope at an accelerating voltage of 70 KV.

EPC-MVs were labeled with PKH26 (Sigma Aldrich, St. Louis, MO) according to the manufacturer's protocol with some modifications [19]. In brief, EPC-MVs were labeled with 2 μM PKH26 dye in PBS for 5 mins at room temperature (RT). An equal volume of FBS was added to stop staining. EPC-MVs were then ultracentrifuged and resuspended with culture medium for coculture experiments.

2.4. H/R Injury Model in Hb-ECs. Hb-ECs were purchased from Cell Systems (Kirkland, WA) and cultured according to the manufacturer's protocol. Briefly, cells were cultured in CSC complete medium containing 10% serum, 2% human recombinant growth factors, and 0.2% antibiotic solution under standard cell culture conditions (5% CO_2, 37°C). All medium and supplement reagents were purchased from Cell Systems. Medium was changed twice a week. Passages 4 to 13 of hb-ECs were used for experiments in this study. For producing an H/R injury model on hb-ECs, hb-ECs were cultured as previously described with slight modifications [20]. Briefly, the hb-ECs were changed with fresh culture medium and cultured for 6 hrs in a hypoxic chamber (1% O_2, 5% CO_2, and 94% N_2; Biospherix hypoxia chamber, NY); cells were then reoxygenated by incubation in a standard 5% CO_2 incubator for 24 hrs. Some cells were harvested for apoptotic assay, western blot, or quantitative real-time PCR (qRT-PCR) analysis. Some plates of cells were pretreated with or without LY294002 (PI3K inhibitor) and then cocultured with sEPC-MVs, aEPC-MVs, RNase treated sEPC-MVs (RNase-sEPC-MVs), or RNase treated aEPC-MVs (RNase-aEPC-MVs). All experiments were repeated four times. At least six plates per experiment were used in each group.

2.5. Coculture Assay of EPC-MVs and Hb-ECs. For coculture experiment between hb-ECs and EPC-MVs [21], the labeled EPC-MVs were resuspended with CSC medium, then added to hb-ECs, and cultured for 2 hrs in an incubator (37°C, 5% CO_2). Cell nuclei were stained with DAPI. The interaction between EPC-MVs and hb-ECs was examined under fluorescence microscope.

2.6. Gene Expression Analysis. MicroRNA 126 (miR126) from EPCs, EPC-MVs, and H/R hb-ECs was extracted by using mirVana miRNA isolation kit (Ambion) following manufacturer's instructions. cDNA was synthesized using miScript reverse transcription kit (QIAGEN). Quantitative real-time PCR was conducted with miR126 specific primers and miScript SYBR Green PCR Kit (QIAGEN) on

a real-time PCR system (Bio-Rad). Small nuclear RNA U6 (U6) was used as an internal control. Relative expression of miR126 was calculated using the $2^{-\Delta\Delta CT}$ method [22].

2.7. Cell Viability Analysis. The cell viability of H/R hb-ECs was examined using methyl thiazolyl tetrazolium (MTT, Invitrogen, NY) method [23]. In brief, cells cultured in 96-well plate were incubated with 10 μL MTT solution (12 mM) for 4 hrs at 37°C, then 100 μL sodium dodecyl sulfate (SDS)-HCl solution was added to each well, and the cells were incubated for another 4 hrs at 37°C. The absorbance of cells was read at 535 nm. The percent of cell viability was defined as the relative absorbance of treated cells versus untreated cells.

2.8. Apoptosis Assay. The apoptosis assay of EPCs and H/R hb-ECs was conducted using FITC Annexin V apoptosis detection kit (BD Biosciences, CA) as previously described [23]. Briefly, cells were washed with PBS, resuspended with 100 μL 1x annexin-binding buffer, incubated with 5 μL FITC-conjugated Annexin V and 5 μL propidium iodide (PI) for 15 mins in the dark, and then analyzed by flow cytometry. The apoptotic cells were defined as Annexin V+/PI− cells. The experiment was repeated four times. At least six plates per experiment were used in each group.

2.9. Tube Formation Assay. The tube formation ability of EPCs and hb-ECs cocultured with EPC-MVs was evaluated using tube formation assay kit (Chemicon) as we previously described [24]. Briefly, ECMatrix solution was thawed on ice overnight, mixed with 10x ECMatrix diluent buffer, and placed in a 96-well tissue culture plate at 37°C for 1 hr to allow the matrix solution to solidify. Then the cells were re-plated (1×10^4 cells/well) onto the surface of the solidified ECMatrix and incubated for 24 hrs at 37°C. Tube formation was evaluated with an inverted light microscope and defined as a tube structure exhibiting a length 4 times its width. Five independent fields were assessed for each well, and the average number of tubes per field (magnification, 200x) was determined.

2.10. Measurement of ROS. Intracellular ROS production was determined by dihydroethidium (DHE) (Sigma) staining followed by flow cytometric analysis. Briefly, cells were incubated with 2 μM DHE solution at 37°C for 2 hrs, washed with PBS twice, trypsinized, and centrifuged. The fluorescence intensity of cells was analyzed by flow cytometry.

2.11. Measurement of NO. The membrane-permeable indicator diaminofluorescein (DAF-FM) diacetate (Invitrogen, Grand Island, NY) was used to assess NO production [16]. Briefly, the hb-ECs were incubated with 2 μM DAF-FM diacetate in serum-free CSC medium at 37°C for 30 mins, washed with PBS twice, then incubated with CSC medium for 20 mins to allow complete de-esterification of the intracellular diacetates. DAF-FM fluorescence was measured using a spectrofluorometer.

2.12. Western Blot Analysis. Proteins from H/R hb-ECs were extracted with lysis buffer. Protein lysates were electrophoresed through SDS-PAGE gel and transferred onto PVDF membranes. The membranes were blocked for 1 hr and incubated with primary antibodies against eNOS (Cell Signaling Technology) and β-actin (Sigma) at 4°C overnight. After washing 3 times, membranes were incubated with horseradish-peroxidase- (HRP-) conjugated IgG (Jackson ImmunoResearch Lab) for 1 hr at RT. Blots were then developed with enhanced chemiluminescence developing solutions and quantified under ImageJ software.

2.13. Enzyme-Linked Immunosorbent Assay. The levels of caspase 3 in EPCs, EPC-MVs, and H/R hb-ECs were measured by enzyme-linked immunosorbent assay (ELISA) [25]. Briefly, cells or EPC-MVs were washed in PBS and their extracts were prepared according to the manufacturer's instructions before being analyzed by ELISA (R&D System, Quantikine).

2.14. Statistical Analysis. All data was expressed as mean ± SEM. Comparison for two groups was examined by Student's t-test. Multiple comparisons were performed by one- or two-way ANOVA. SPSS software version 17.0 was used. For all tests, a value of $P < 0.05$ was considered statistically significant.

3. Results

3.1. The sEPC-MVs and aEPC-MVs Carried the Characters of Their Parent EPCs. As we previously reported [16], EPCs were defined as the cells uptaking Di-LDL and binding with Bs-Lectin (Figure 1(a)). As expected, EPCs in an apoptotic stress condition (SD plus TNFα stimulation) had a significantly higher apoptotic rate than that of EPCs in a starving stress (SD only) or normal culture condition (versus control or SD; $P < 0.05$; $n = 4$/group; Figure 1(b)). Moreover, gene expression of caspase 3 was upregulated, whereas miR126 was down-regulated in EPCs in the SD+TNFα group as compared to control group. In SD group, both caspase 3 and miR126 expressions were higher than those in control (versus control; $P < 0.05$; $n = 4$/group; Figures 1(c)-1(d)).

According to the flow cytometric analysis, both aEPC-MVs and sEPC-MVs positively expressed Annexin V and EPC specific markers (CD34, VEGFR2) (Figure 2(a)). The TEM results showed that there was no difference in morphology between sEPC-MVs and aEPC-MVs (Figure 2(b)). With the digestion of RNase, the total RNAs of both EPC-MVs were significantly decreased (Figure 2(c)). More interestingly, the gene expressions of caspase 3 and miR126 were displayed in the same pattern as that in their parent EPCs. The results showed that caspase 3 was upregulated in aEPC-MVs as compared to that in sEPC-MVs or control, and miR126 was down-regulated in aEPC-MVs as compared to that in sEPC-MVs or control (versus control or sEPC-MVs; $P < 0.05$; $n = 4$/group; Figure 2(d)).

3.2. The Model of H/R Injury in Hb-ECs Was Confirmed by ROS Overproduction, Cell Dysfunction, and Apoptosis. Hb-ECs were exposed to hypoxia (6 hrs) and followed by reoxygenation (24 hrs). As shown in Figure 3(a), MTT assay

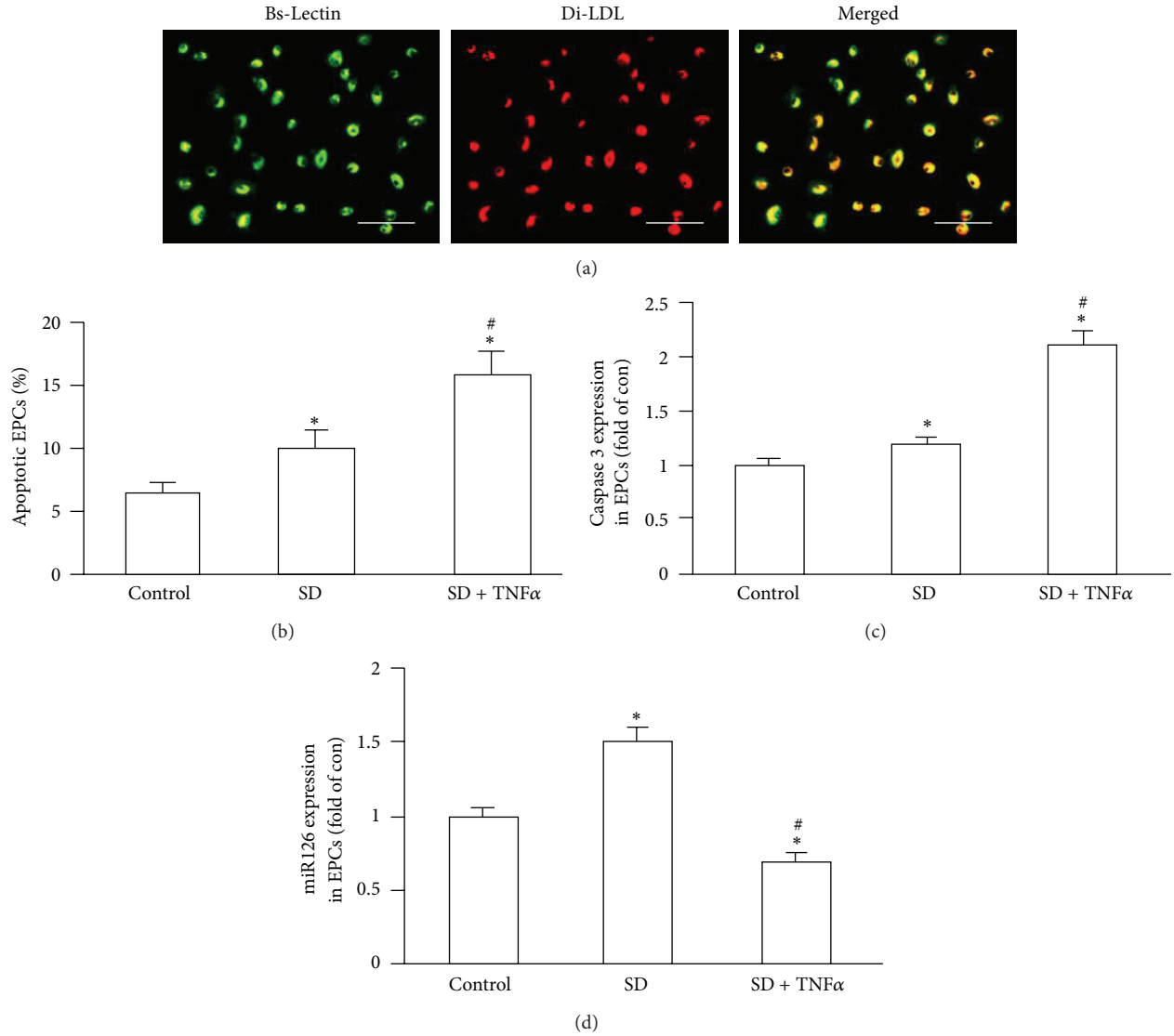

Figure 1: Effects of serum deprivation (SD) alone and SD plus TNFα on EPC apoptosis, caspase 3, and miR126 expression. (a) Representative images showing EPC characterization of Bs-Lectin and Di-LDL double staining. Scale bar: 100 μm. (b) Apoptosis (Annexin V+PI−) of stimulated EPCs. (c) Caspase 3 expression in stimulated EPCs. (d) MiR126 expression in stimulated EPCs. $^{*}P < 0.05$, versus control; $^{\#}P < 0.05$, versus SD; $N = 4$/group.

showed that H/R decreased hb-EC viability (versus control; $P < 0.05$; $n = 4$/group). To confirm this observation, we also performed apoptotic assay and found that H/R hb-ECs had a higher apoptotic rate than those cultured in normoxia condition (versus control; $P < 0.05$; $n = 4$/group; Figure 3(a)). In addition, in H/R hb-ECs, the ROS production was increased, whereas, the NO production was decreased. And tube formation ability of H/R hb-ECs was decreased (versus control; $P < 0.05$; $n = 4$/group; Figures 3(b)-3(c)). These findings indicated the success of H/R injured model on hb-ECs.

3.3. sEPC-MVs Decreased Whereas aEPC-MVs Increased ROS Production and Apoptosis in H/R Hb-ECs via PI3K Pathway. After coculture the hb-ECs with EPC-MVs for 24 hrs, the PKH26 fluorescence was observed in the cytoplasm of hb-ECs, suggesting the EPC-MVs were incorporated into the hb-ECs (Figure 4(a)). Interestingly, the miR126 expression was upregulated in the hb-ECs cocultured with sEPC-MVs and down-regulated in the hb-ECs cocultured with aEPC-MVs as compared to vehicle (versus vehicle; $P < 0.05$, $n = 4$/group; Figure 4(b)). According to flow cytometric analysis (Figures 4(c)-4(d)), sEPC-MVs decreased the apoptosis level and ROS production in H/R hb-ECs (versus vehicle; $P < 0.05$, $n = 4$/group). On the contrary, aEPC-MVs increased the apoptosis level and ROS production in H/R hb-ECs (versus vehicle; $P < 0.05$, $n = 4$/group). As expected, RNase-sEPC-MVs were less effective on decreasing the level of apoptosis and ROS production in H/R hb-ECs. In addition, preincubation of H/R hb-ECs with PI3K inhibitor (LY294002) abolished the aforementioned effects of sEPC-MVs and aEPC-MVs ($P < 0.05$, $n = 4$/group).

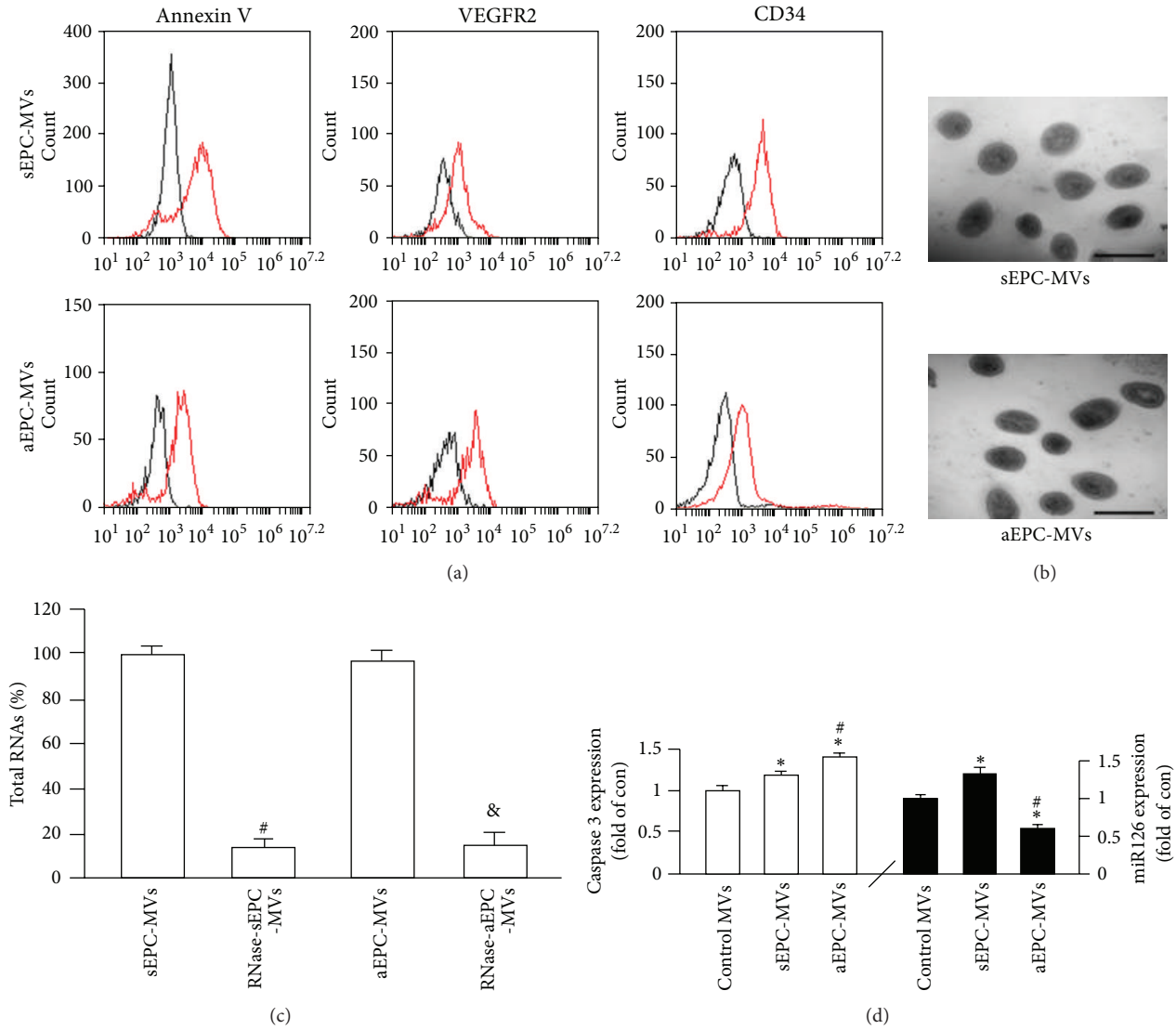

Figure 2: EPC-MV characterization, modification, caspase 3 and miR126 expression. (a) Flow cytometric plots showing Annexin V, CD34 and VEGFR2 expressions (isotype controls: left curves; antibodies: right curves) in EPC-MVs. (b) TEM image showing similar spherical morphology of sEPC-MVs and aEPC-MVs. Scale bar: 500 nm. (c) Summarized data showing effective digestion of EPC-MVs total RNAs by RNase treatment. (d) Caspase 3 and miR126 expression in control MVs (generated from basal condition), sEPC-MVs, and aEPC-MVs. $^{*}P < 0.05$, versus control; $^{\#}P < 0.05$, versus sEPC-MVs; $^{\&}P < 0.05$, versus aEPC-MVs; $N = 4$/group. TEM and transmission electron microscopy.

3.4. sEPC-MVs Increased Whereas aEPC-MVs Decreased eNOS and NO Production in H/R Hb-ECs via PI3K Pathway. As shown in Figures 5(a)-5(b), sEPC-MVs significantly upregulated eNOS and NO expressions in the H/R hb-ECs (versus vehicle, $P < 0.05$, $n = 4$/group). On contrary, aEPC-MVs decreased the eNOS and NO production in H/R hb-ECs (versus vehicle; $P < 0.05$, $n = 4$/group). Again, RNase-sEPC-MVs were less effective on increasing whereas RNase-aEPC-MVs were less effective on decreasing the eNOS and NO production in H/R hb-ECs. Similarly, preincubation of H/R hb-ECs with LY294002 attenuated these effects ($P < 0.05$, $n = 4$/group).

3.5. sEPC-MVs Increased Whereas aEPC-MVs Decreased the Hb-EC Tube Formation Ability in H/R Hb-ECs via PI3K Pathway. As shown in Figure 5(c), the tube formation ability of H/R hb-ECs was increased after coculture with sEPC-MVs, whereas it was decreased after coculture with the aEPC-MVs ($P < 0.05$, $n = 4$/group). Again, preincubation with LY294002 abolished this effect.

4. Discussion

There are three major findings in this study. Firstly, we demonstrated that EPCs stressed with SD (sEPCs) or SD plus

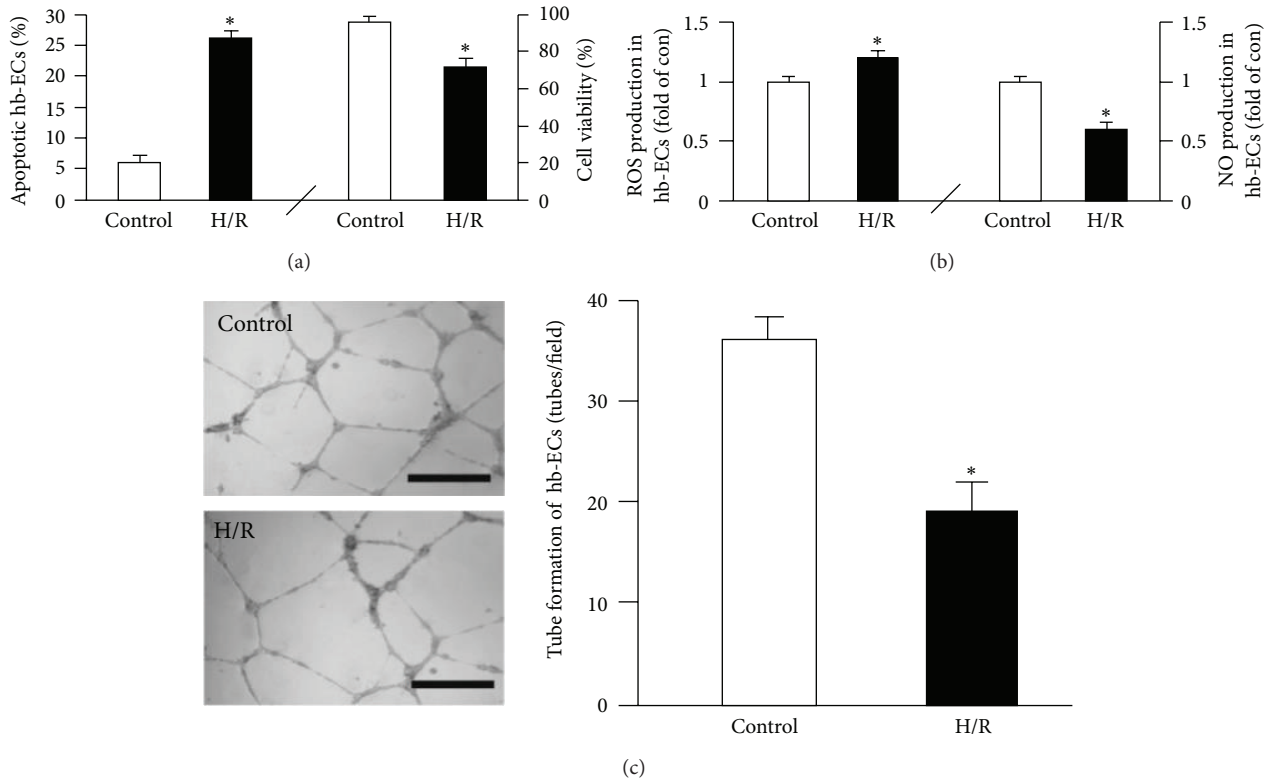

Figure 3: Effects of H/R on hb-EC viability and apoptosis, ROS and NO production, and tube formation. (a) Apoptosis (Annexin V+PI−) and cell viability. (b) ROS and NO production. (c) Tube formation ability. Scale bar: 200 μm. $^{*}P < 0.05$, versus control; $N = 4$/group.

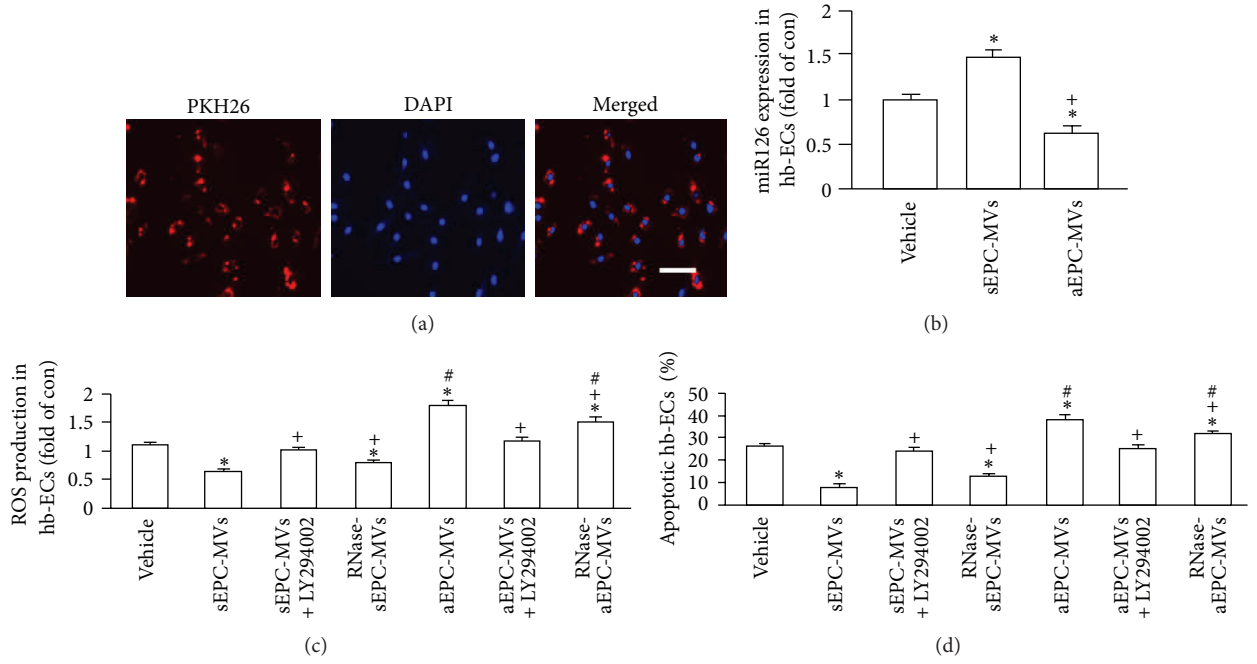

Figure 4: Effects of EPC-MVs on miR126 expression, ROS production, and apoptosis in H/R hb-ECs. (a) Representative images showing the merging of PKH26 labeled EPC-MVs with hb-ECs (red: PKH26; blue: DAPI). Scale bar: 100 μm. (b) miR126 expression in H/R hb-ECs cocultured with aEPC-MVs or sEPC-MVs. (c) ROS production of H/R hb-ECs cocultured with aEPC-MVs or sEPC-MVs. (d) Apoptosis of H/R hb-ECs cocultured with aEPC-MVs or sEPC-MVs. $^{*}P < 0.05$, versus vehicle; $^{+}P < 0.05$, versus sEPC-MVs or aEPC-MVs; $^{\#}P < 0.05$, versus sEPC-MVs or RNase-sEPC-MVs; $N = 4$/group.

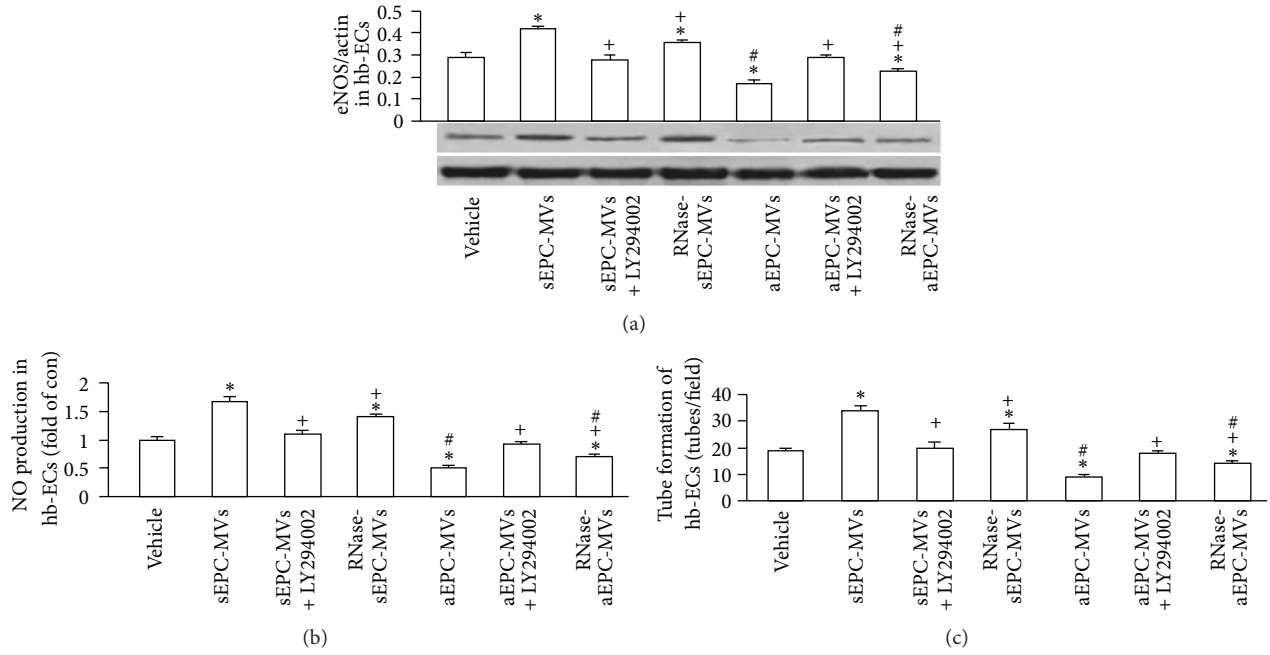

Figure 5: Effects of EPC-MVs on eNOS expression, NO production, and tube formation in H/R hb-ECs. (a) eNOS production of H/R hb-ECs cocultured with aEPC-MVs or sEPC-MVs. (b) NO production of H/R hb-ECs cocultured with aEPC-MVs or sEPC-MVs. (c) Tube formation ability of H/R hb-ECs cocultured with aEPC-MVs or sEPC-MVs. $^{*}P < 0.05$, versus vehicle; $^{+}P < 0.05$, versus sEPC-MVs or aEPC-MVs; $^{\#}P < 0.05$, versus sEPC-MVs or RNase-sEPC-MVs; $N = 4$/group.

TNFα (aEPCs) have different changes regarding cell apoptotic rate and the expression levels of caspase 3 and miR126. Secondly, we identified that the MVs released from sEPCs and aEPCs carry the same characters as their parent cells. Thirdly, we confirmed that EPC-MVs can merge with hb-ECs and sEPC-MVs and aEPC-MVs have different functional roles in H/R-induced hb-ECs injury, which might be dependent on their effects on ROS and NO generation, miR126 expression, and regulation of the PI3K/eNOS/NO pathway.

ROS is well known to be implicated in I/R injury [1]. ROS-induced vascular endothelium injury is a pivotal step in the pathogenesis of I/R injury. Although strategies for inhibiting ROS production or increasing their degradation and scavenging have been attempted, they have turned out to be less effective on the prevention or treatment of I/R injury [2]. Therefore, novel approaches are intensely needed for preventing I/R injury.

MVs are cellular fragments, which have been shown to act as a paracrine mediator as they can merge with target cells for exerting their functions [14]. Several studies have demonstrated that MVs released from mesenchymal stem cells can protect the kidney from I/R injury [11–13]. In this study, we generated MVs from EPCs which underwent SD alone or SD plus TNFα stimulation and examined the effects of both stimuli on EPCs and their released MVs. We found that both apoptosis and caspase 3 expression of EPCs were significantly increased in the SD plus TNFα stimulation group and slightly increased in the SD group. Even more interesting, the miR126, a proangiogenic factor, was upregulated in EPCs stressed by SD and was downregulated in EPCs stressed by SD plus TNFα. These data indicate that EPCs underwent different changes in response to different stimuli.

Next, we examined the morphological and functional characteristics of sEPC-MVs and aEPC-MVs. We found that there was no significant difference in morphology and the expression of parent specific markers between sEPC-MVs and aEPC-MVs as determined by TEM and flow cytometry. But there were differences of caspase 3 and miR126 expression between them. According to the ELISA analysis results, the caspase 3 expression in aEPC-MVs was higher than that in sEPC-MVs. The miR126 expression was lower in aEPC-MVs in comparison to sEPC-MVs as revealed by qRT-PCR assay. These data indicate that both aEPC-MVs and sEPC-MVs carry their parent proteins and genetic materials.

Additionally, our data showed that EPC-MVs can be incorporated by hb-ECs, which suggests that EPC-MVs may have a functional role in hb-ECs. In order to further test the potential effects of EPC-MVs, we constructed an H/R hb-EC injury model, which was characterized by overproduction of ROS, an increase in apoptosis, and decrease in NO production, cell viability, and tube formation ability. In coculture experiments, we found that sEPC-MVs protected hb-ECs from H/R-induced ROS overproduction and apoptosis. Both the eNOS and NO production were increased in the H/R hb-ECs cocultured with sEPC-MVs. Moreover, sEPC-MVs rescued the tube formation disability of H/R hb-ECs. In addition, we also observed that these protective effects of sEPC-MVs were abrogated by PI3 K inhibitor LY294002. These data suggest that sEPC-MVs protect H/R hb-ECs from injury via activating PI3K/eNOS/NO pathway. Contrary

to sEPC-MVs, aEPC-MVs showed deleterious effects on H/R hb-ECs. Our data showed that aEPC-MVs accelerated ROS overproduction and apoptosis, coupled with decreased eNOS expression and NO generation. Meanwhile, the tube formation ability of H/R hb-ECs was also compromised in the aEPC-MVs groups. Likewise, these deleterious effects of aEPC-MVs were also abolished by LY294002. These findings indicate that aEPC-MVs worsen the oxidative stress in H/R hb-ECs via PI3K/eNOS/NO pathway.

Of note, we also found that all the aforementioned effects of EPC-MVs were partially diminished by coculture with RNase-EPC-MVs. Therefore, it is logical to deduce that EPC-MV carried RNAs which participated in the protective or deleterious effects of EPC-MVs. In the present study, we found that the expression of miR126 in H/R hb-ECs was increased in the sEPC-MVs group, whereas it was decreased in the aEPC-MVs group. On contrary, the caspase 3 expression in H/R hb-ECs was decreased in sEPC-MVs group and increased in aEPC-MVs group. These data suggest that miR126 and caspase 3 were delivered to hb-ECs from EPCs via EPC-MVs, which is in agreement with previous studies showing MVs can deliver and transfer their contents to target cells [8–10]. Nevertheless, the detailed mechanisms of their roles need further investigation.

5. Conclusion

Our data demonstrate that sEPCs-MVs and aEPC-MVs are functionally different on H/R-induced apoptosis and dysfunction. These functional roles might rely on the orchestrated mechanisms associated with MV-carried RNAs in control of ROS production and PI3K/eNOS/NO pathway in the target cells. These findings indicate that EPC-MVs could be used as a novel vehicle for treating H/R injury.

Conflict of Interests

The authors declare that there is no conflict of interests regarding the publication of this paper.

Authors' Contribution

Jinju Wang, Shuzhen Chen, and Xiaotang Ma equally contributed to the paper.

Acknowledgments

The authors thank Ms. Michelle Durrant in the Boonshoft School of Medicine, Wright State University, for proofreading the paper. This work was supported by National Heart, Lung, and Blood Institute (HL-098637, Y.C.) and National Natural Science Foundation of China (NSFC, #81270195, #81271214).

References

[1] M. Godinez-Rubi, A. E. Rojas-Mayorquin, and D. Ortuno-Sahagun, "Nitric oxide donors as neuroprotective agents after an ischemic stroke-related inflammatory reaction," *Oxidative Medicine and Cellular Longevity*, vol. 2013, Article ID 297357, 16 pages, 2013.

[2] I. Margaill, M. Plotkine, and D. Lerouet, "Antioxidant strategies in the treatment of stroke," *Free Radical Biology and Medicine*, vol. 39, no. 4, pp. 429–443, 2005.

[3] A. Zampetaki, J. P. Kirton, and Q. Xu, "Vascular repair by endothelial progenitor cells," *Cardiovascular Research*, vol. 78, no. 3, pp. 413–421, 2008.

[4] S. Charwat, M. Gyöngyösi, I. Lang et al., "Role of adult bone marrow stem cells in the repair of ischemic myocardium: current state of the art," *Experimental Hematology*, vol. 36, no. 6, pp. 672–680, 2008.

[5] O. Kwon, S. Miller, N. Li, A. Khan, Z. Kadry, and T. Uemura, "Bone marrow-derived endothelial progenitor cells and endothelial cells may contribute to endothelial repair in the kidney immediately after ischemia-reperfusion," *Journal of Histochemistry and Cytochemistry*, vol. 58, no. 8, pp. 687–694, 2010.

[6] B. Li, A. Cohen, T. E. Hudson, D. Motlagh, D. L. Amrani, and J. S. Duffield, "Mobilized human hematopoietic stem/progenitor cells promote kidney repair after ischemia/reperfusion injury," *Circulation*, vol. 121, no. 20, pp. 2211–2220, 2010.

[7] D. Burger, S. Schock, C. S. Thompson, A. C. Montezano, A. M. Hakim, and R. M. Touyz, "Microparticles: biomarkers and beyond," *Clinical Science*, vol. 124, pp. 423–441, 2013.

[8] S. F. Mause and C. Weber, "Microparticles: protagonists of a novel communication network for intercellular information exchange," *Circulation Research*, vol. 107, no. 9, pp. 1047–1057, 2010.

[9] J. Ratajczak, M. Wysoczynski, F. Hayek, A. Janowska-Wieczorek, and M. Z. Ratajczak, "Membrane-derived microvesicles: important and underappreciated mediators of cell-to-cell communication," *Leukemia*, vol. 20, no. 9, pp. 1487–1495, 2006.

[10] M. E. De Broe, R. J. Wieme, G. N. Logghe, and F. Roels, "Spontaneous shedding of plasma membrane fragments by human cells in vivo and in vitro," *Clinica Chimica Acta*, vol. 81, no. 3, pp. 237–245, 1977.

[11] S. Bruno, C. Grange, M. C. Deregibus et al., "Mesenchymal stem cell-derived microvesicles protect against acute tubular injury," *Journal of the American Society of Nephrology*, vol. 20, no. 5, pp. 1053–1067, 2009.

[12] S. Gatti, S. Bruno, M. C. Deregibus et al., "Microvesicles derived from human adult mesenchymal stem cells protect against ischaemia-reperfusion-induced acute and chronic kidney injury," *Nephrology Dialysis Transplantation*, vol. 26, no. 5, pp. 1474–1483, 2011.

[13] V. Cantaluppi, S. Gatti, D. Medica et al., "Microvesicles derived from endothelial progenitor cells protect the kidney from ischemia-reperfusion injury by microRNA-dependent reprogramming of resident renal cells," *Kidney International*, vol. 82, pp. 412–427, 2012.

[14] M. C. Deregibus, V. Cantaluppi, R. Calogero et al., "Endothelial progenitor cell—derived microvesicles activate an angiogenic program in endothelial cells by a horizontal transfer of mRNA," *Blood*, vol. 110, no. 7, pp. 2440–2448, 2007.

[15] S. Chen, G. Li, W. Zhang et al., "Ischemia-induced brain damage is enhanced in human renin and angiotensinogen double-transgenic mice," *American Journal of Physiology*, vol. 297, no. 5, pp. R1526–R1531, 2009.

[16] J. Chen, X. Xiao, S. Chen et al., "Angiotensin-converting enzyme 2 priming enhances the function of endothelial progenitor cells

and their therapeutic efficacy," *Hypertension*, vol. 61, pp. 681–689, 2013.

[17] Y. Berda-Haddad, S. Robert, P. Salers et al., "Sterile inflammation of endothelial cell-derived apoptotic bodies is mediated by interleukin-1α," *Proceedings of the National Academy of Sciences of the United States of America*, vol. 108, no. 51, pp. 20684–20689, 2011.

[18] J. Wang, S. Chen, C. Zhang et al., "Human endometrial stromal stem cells differentiate into megakaryocytes with the ability to produce functional platelets," *PLoS ONE*, vol. 7, Article ID e44300, 2012.

[19] R. Soleti, E. Lauret, R. Soleti, E. Lauret, R. Andriantsitohaina, and M. M. Carmen, "Internalization and induction of antioxidant messages by microvesicles contribute to the antiapoptotic effects on human endothelial cells," *Free Radical Biology & Medicine*, vol. 53, pp. 2159–2170, 2012.

[20] Y. Ben-Yosef, N. Lahat, S. Shapiro, H. Bitterman, and A. Miller, "Regulation of endothelial matrix metalloproteinase-2 by hypoxia/reoxygenation," *Circulation Research*, vol. 90, no. 7, pp. 784–791, 2002.

[21] T. S. Chen, R. C. Lai, M. M. Lee, A. B. H. Choo, C. N. Lee, and S. K. Lim, "Mesenchymal stem cell secretes microparticles enriched in pre-microRNAs," *Nucleic Acids Research*, vol. 38, no. 1, pp. 215–224, 2009.

[22] H. S. Cheng, N. Sivachandran, A. Lau et al., "MicroRNA-146 represses endothelial activation by inhibiting pro-inflammatory pathways," *EMBO Molecular Medicine*, vol. 5, pp. 1017–1103, 2013.

[23] C. Yang, Y. Wang, H. Liu et al., "Ghrelin protects H9c2 cardiomyocytes from angiotensin II-induced apoptosis through the endoplasmic reticulum stress pathway," *Journal of Cardiovascular Pharmacology*, vol. 59, pp. 465–471, 2012.

[24] J. Chen, S. Chen, Y. Chen et al., "Circulating endothelial progenitor cells and cellular membrane microparticles in db/db diabetic mouse: possible implications in cerebral ischemic damage," *American Journal of Physiology*, vol. 301, no. 1, pp. E62–E71, 2011.

[25] S. C. Wassmer, C. A. Moxon, T. Taylor, G. E. Grau, M. E. Molyneux, and A. G. Craig, "Vascular endothelial cells cultured from patients with cerebral or uncomplicated malaria exhibit differential reactivity to TNF," *Cellular Microbiology*, vol. 13, no. 2, pp. 198–209, 2011.

Hindawi Publishing Corporation
Oxidative Medicine and Cellular Longevity
Volume 2013, Article ID 159864, 11 pages
http://dx.doi.org/10.1155/2013/159864

Research Article

Neuroprotective Effect of Ginkgolide B on Bupivacaine-Induced Apoptosis in SH-SY5Y Cells

Le Li,[1] Qing-guo Zhang,[1] Lu-ying Lai,[1] Xian-jie Wen,[1] Ting Zheng,[1] Chi-wai Cheung,[2] Shu-qin Zhou,[1] and Shi-yuan Xu[1]

[1] *Department of Anesthesiology, Zhujiang Hospital, Southern Medical University, Guangzhou, Guangdong 510282, China*
[2] *Department of Anesthesiology, The University of Hong Kong, Hong Kong*

Correspondence should be addressed to Shu-qin Zhou; 154843189@qq.com and Shi-yuan Xu; xsy111@yeah.net

Received 5 July 2013; Accepted 18 August 2013

Academic Editor: Zhengyuan Xia

Local anesthetics are used routinely and effectively. However, many are also known to activate neurotoxic pathways. We tested the neuroprotective efficacy of ginkgolide B (GB), an active component of Ginkgo biloba, against ROS-mediated neurotoxicity caused by the local anesthetic bupivacaine. SH-SY5Y cells were treated with different concentrations of bupivacaine alone or following preincubation with GB. Pretreatment with GB increased SH-SY5Y cell viability and attenuated intracellular ROS accumulation, apoptosis, mitochondrial dysfunction, and ER stress. GB suppressed bupivacaine-induced mitochondrial depolarization and mitochondria complex I and III inhibition and increased cleaved caspase-3 and Htra2 expression, which was strongly indicative of activation of mitochondria-dependent apoptosis with concomitantly enhanced expressions of Grp78, caspase-12 mRNA, protein, and ER stress. GB also improved ultrastructural changes indicative of mitochondrial and ER damage induced by bupivacaine. These results implicate bupivacaine-induced ROS-dependent mitochondria, ER dysfunction, and apoptosis, which can be attenuated by GB through its antioxidant property.

1. Introduction

Local anesthetics are among the most common clinical drugs and are generally regarded as safe [1, 2]. However, they have also been shown to be neurotoxic even at normal clinical dose [3, 4]. This neurotoxicity is mediated at least in part by activation of apoptotic pathways [5, 6]. In the cauda equina, intrathecally administered local anesthetics induced cell swelling, atrophy, edema, axonal degeneration, and the appearance of myelin ovoids as well as macrophage infiltration [7]. These morphological signs of degeneration indicate that local anesthetics can initiate a complex cascade of direct cytotoxic and ensuing inflammatory responses, although the molecular mechanisms of local anesthetic toxicity are still largely unknown.

Local anesthetics have been shown to induce neural dysfunction and apoptosis *in vitro* [8–11]. For example, bupivacaine may inhibit mitochondrial respiratory complexes I and III, leading to decreased ATP production, collapse of the mitochondrial membrane potential ($\Delta\psi$m), overproduction of reactive oxygen species (ROS), and ultimately liberation of cytochrome c and activation of the caspase-3-dependent apoptosis pathway [10–12]. In fact, ROS accumulation, mitochondrial uncoupling, and depolarization of ψm are among the earliest indicators of apoptosis induced by local anesthetics [13, 14]. In addition to mitochondrial damage, dysfunction of the endoplasmic reticulum (ER) stress has also been implicated in apoptosis. Arai and Nonaka et al. proposed that oxidative stress associated with local anesthetics can induce Ca^{2+} release from intracellular stores, including the rough endoplasmic reticulum (rER) [11, 15]. Loss of intraluminal Ca^{2+} may lead to ER stress [16], further, ROS generation, [17] and activation of ER-dependent apoptosis pathways [18]. Thus, mitochondrial and ER damage associated with ROS overproduction may act synergistically to evoke cell death in response to bupivacaine or other structurally related local anesthetics.

Ginkgo biloba has been used in traditional Chinese medicine for thousands of years. Evidence accumulated over the last decade suggests that concentrated and partially

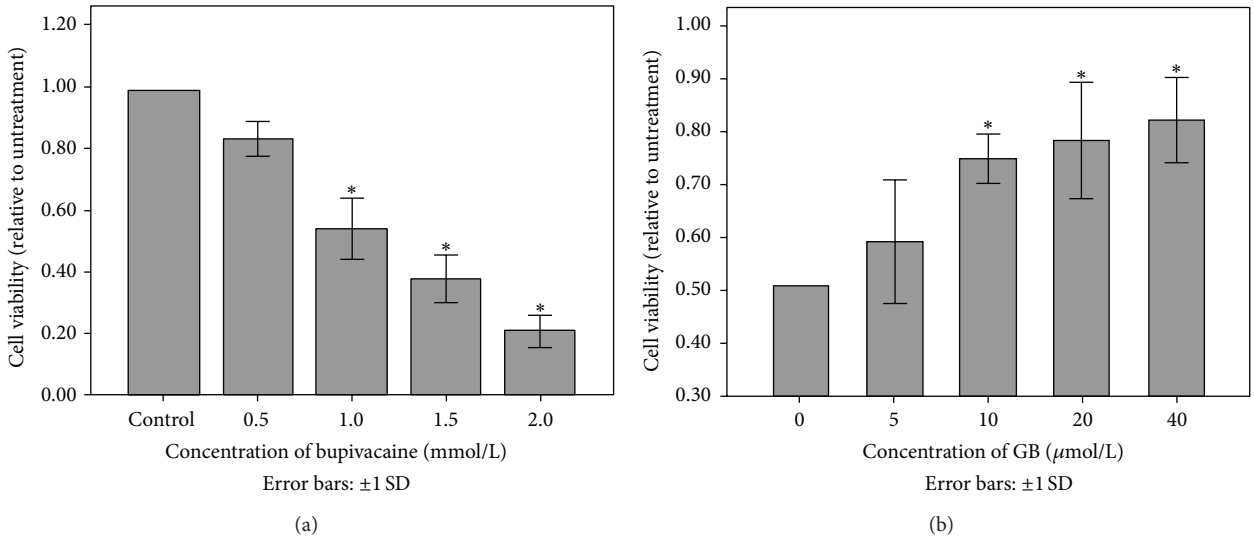

Figure 1: Proliferation effects of bupivacaine on SH-SY5Y cells and GB weakened bupivacaine-induced cell injury in SH-SY5Y cells. (a) Cells were incubated in the presence or absence of various concentrations of bupivacaine for 24 h ($^*P < 0.05$ versus control group). Cell growth was determined by the MTT assay. (b) Cell viability was decreased by treatment with 1 mmol/L bupivacaine for 24 hours. Decreased viability was inhibited by GB pretreatment for 6 hours, except for cells treated with 5 μmol/L GB ($^*P < 0.05$ versus nonpretreated group). Each data point represents the mean ± SD of 6 separate experiments.

purified extracts of Ginkgo biloba leaves may afford protection against certain neurological diseases [19]. Indeed, ginkgolide B (GB), the major active component of Ginkgo biloba extract, has been used to treat degenerative dementia and neurosensory disorders [20]. Even for children, GB is a safe drug without adverse reactions [21]. Furthermore, GB reduced the level of ROS *in vivo*, suggesting that the raw extract contains antioxidants [22]. Therefore, GB may protect neurons against the neurotoxicity of local anesthetics like bupivacaine by reducing oxidative stress.

The principal aims of this study were to examine the molecular mechanisms of bupivacaine toxicity and the neuroprotective efficacy of GB *in vitro*.

2. Materials and Methods

2.1. Materials. The human neuroblastoma cell line SH-SY5Y was purchased from the Shanghai Institutes for Biological Sciences. Bupivacaine hydrochloride (purity 99.9%) was purchased from Sigma (St. Louis, MO, USA). Ginkgolide B (purity ≥ 99.5%) was obtained from the National Institutes for Food and Drug Control and dissolved in dimethyl sulfoxide (DMSO) (KeyGEN, China). Other reagents used included DMEM/F12 medium and fetal bovine serum (Gibco, USA), 5,5′, 6,6′-tetrachloro-1,1′, 3,3′-tetraethyl tetrethyl benzimidalyl carbocyanine iodide (JC-1), 3-(4,5-dimethyl-2-thiazolyl)-2,5-diphenyl-2-tetrazolium bromide (MTT), 2′,7′-dichlorofluorescein diacetate (DCFH-DA), mitochondrial isolation agent and mitochondrial storage solution (all from Beyotime, China), anti-Grp78 and anti-caspase-12 (Abgent, USA), anti-cleaved caspase-3 and anti-HtrA2 (Abcam, UK), anti-GAPDH antibody (Goodhere, China), and Annexin V-FITC and propidium iodide (KeyGEN, China). The cell counting Kit-8 (CCK8) was purchased from Dojindo (Dojindo, Kumamoto, Japan). All reagents were obtained from commercial suppliers and were of standard biochemical quality.

2.2. Cell Culture. Cells of the SH-SY5Y line were cultured in DMEM/F12 medium supplemented with 15% fetal bovine serum, 100 U/mL penicillin, and 100 μg/mL streptomycin and maintained in a humidified 5% CO_2 incubator at 37°C. The media were changed every 2 days.

2.3. MTT Assay. The effect of bupivacaine on the number of viable SH-SY5Y cells was determined by the MTT assay. Cells were seeded onto 96-well plates at 5×10^3 cells/well with 100 μL of culture medium and treated with various concentrations of bupivacaine as indicated below. Treated cells were incubated with 20 μL MTT at 37°C for 4 h, the medium removed, and 150 μL DMSO added to dissolve the formazan crystals produced from MTT by viable cells. The optical density (OD) of the homogenous purple formazan/DMSO solutions was measured using a spectrophotometer (Bio-Tek, USA) at 570 nm.

2.4. CCK-8 Assay. Cells were seeded onto 96-well plates at 5×10^3 cells/well in 100 μL culture medium. In pilot experiments to determine the working range of GB, cultures were pretreated with 5–40 μmol/L GB in new media for 6 h or subjected to a control media change prior to treatment with 1 mmol/L bupivacaine for 24 h (the half-maximal neurotoxic dose according to [23]). After bupivacaine treatment, 10 μL of CCK-8 was added to each well for another 3 h at 37°C. The OD was read at 450 nm using a spectrophotometer.

2.5. Apoptosis Assay by Flow Cytometry. Cells were seeded onto 24-well plates at 5×10^5 cells/well in 500 μL culture

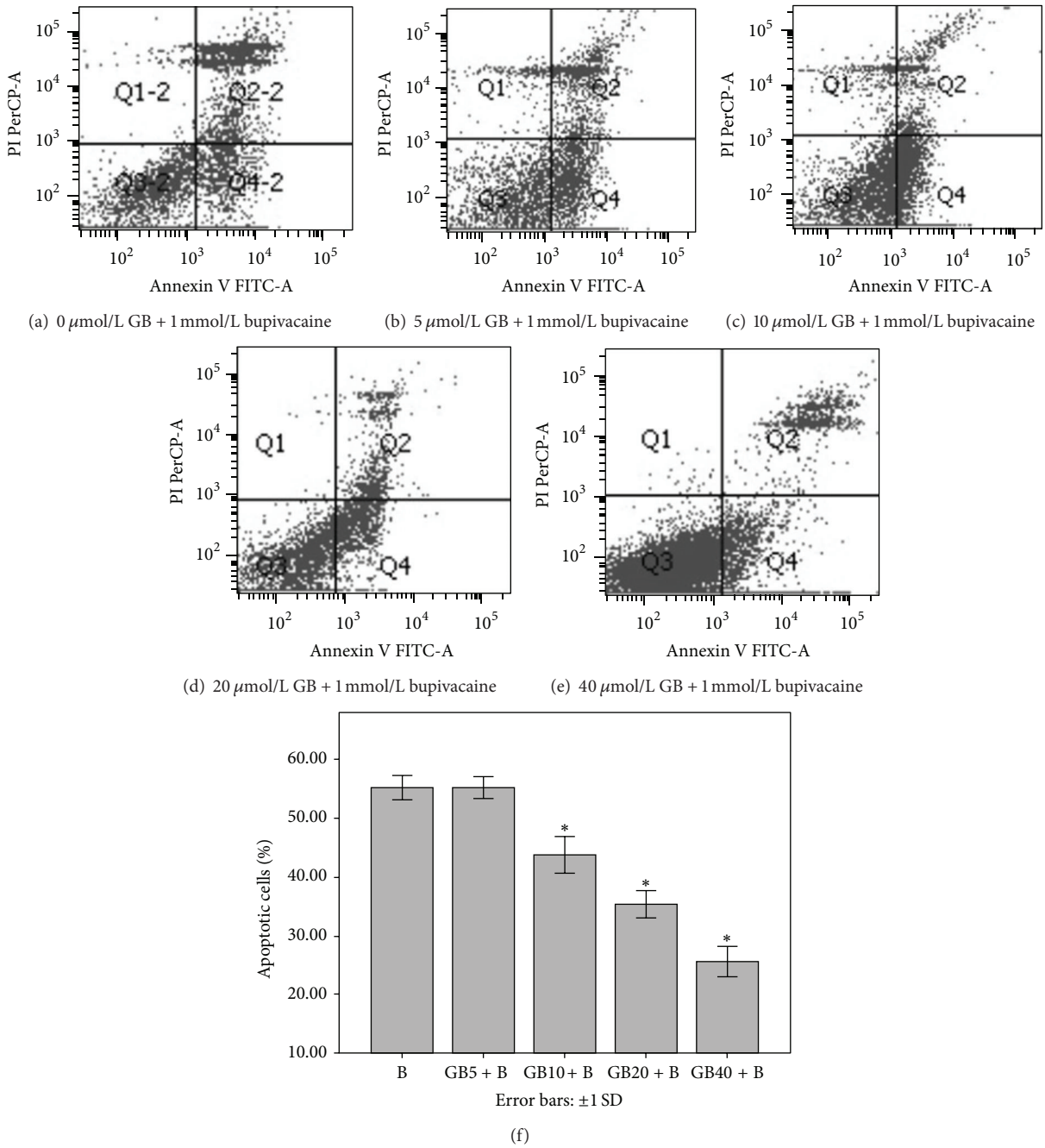

Figure 2: GB pretreatment decreased the number of apoptotic cells induced by bupivacaine. ((a)–(e)) Cells were treated with 0, 5, 10, 20, and 40 μmol/L GB for 6 hours, respectively, prior to treatment with 1 mmol/L bupivacaine for 24 h. (f) Summarized data show apoptotic rate as detected by flow cytometry. Data represented are the mean ± SD of 6 separate experiments ($^*P < 0.05$ versus 0 μmol/L GB).

medium. After control or GB pretreatment and bupivacaine administration as described, the cells were rinsed with PBS, harvested, and resuspended in 500 μL binding buffer. To this cell suspension was added 5 μL Annexin V-FITC (a marker of early apoptosis) and 5 μL propidium iodide (a marker of late apoptosis). After 10 min incubation, cell apoptosis was determined by flow cytometry (BD FACS Calibur, USA).

2.6. Measurement of Reactive Oxygen Species. Cells were seeded onto 24-well plates at 5×10^5 cells/well in 500 μL culture medium and divided into four treatment groups: (i) untreated controls (Con), (ii) cells treated with 1 mmol/L bupivacaine for 24 h (Bup), (iii) cells pretreated with 40 μmol/L GB for 6 h, and (iv) cells treated with 40 μmol/L GB for 6 h prior to 1 mmol/L bupivacaine exposure for 24 h (GB + Bup). Intracellular accumulation of ROS was estimated using the redox-sensitive fluorescent dye DCFH-DA. The cells were incubated with 10 μmol/L DCFH-DA at 37°C during the last 20 min of Con, Bup, GB, or GB + Bup treatment. Treated and DCFH-DA-stained cells were washed 3 times

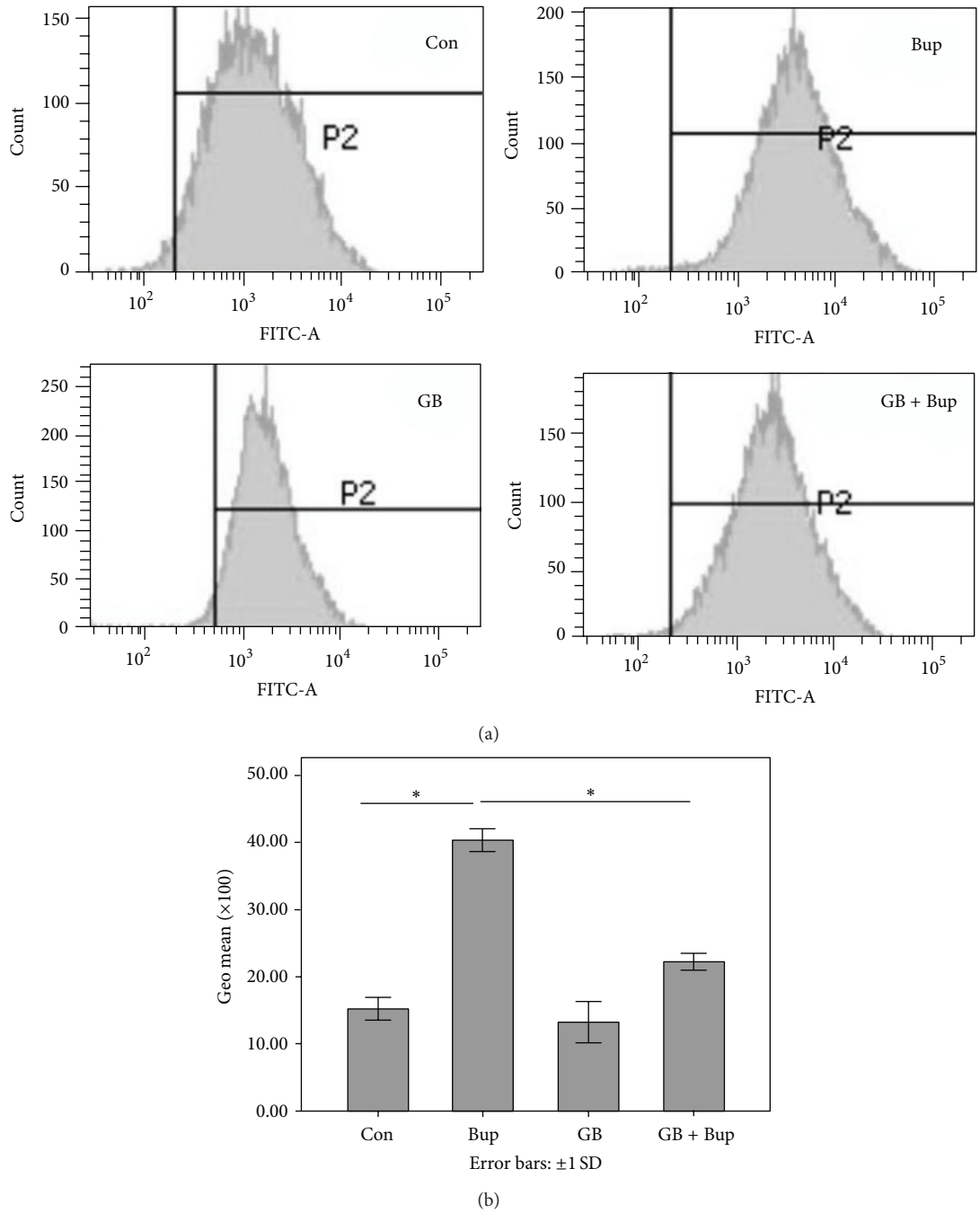

Figure 3: The levels of reactive oxygen species were measured by flow cytometry. GB pretreatment decreased ROS overproduction induced by bupivacaine. Summarized data shows the Geo mean of ROS as detected by flow cytometry. Data represented are mean ± SD of 6 separate experiments ($^*P < 0.01$).

in PBS, harvested, and resuspended in PBS. Fluorescent signal intensity was determined by flow cytometry to estimate relative ROS accumulation.

2.7. Mitochondrial Membrane Potentials Assay. Mitochondrial membrane potential (ψm) depolarization, an early event in the mitochondrial apoptosis cascade, was measured fluorometrically using JC-1. Briefly, cells cultured in 6-well plates and treated as described for the ROS measurement were incubated with JC-1 staining solution (5 μg/mL) at 37°C for 20 min and rinsed twice with PBS. Mitochondrial membrane potential was estimated by measuring the fluorescence ratio of free JC-1 monomers (green) to JC-1 aggregates in mitochondria (red) by dual emission fluorescence microscopy (Nikon ECLIPSE TE2000-u, Japan) and flow cytometry. Mitochondrial depolarization is indicated by an increase in the proportion of cells emitting green fluorescence.

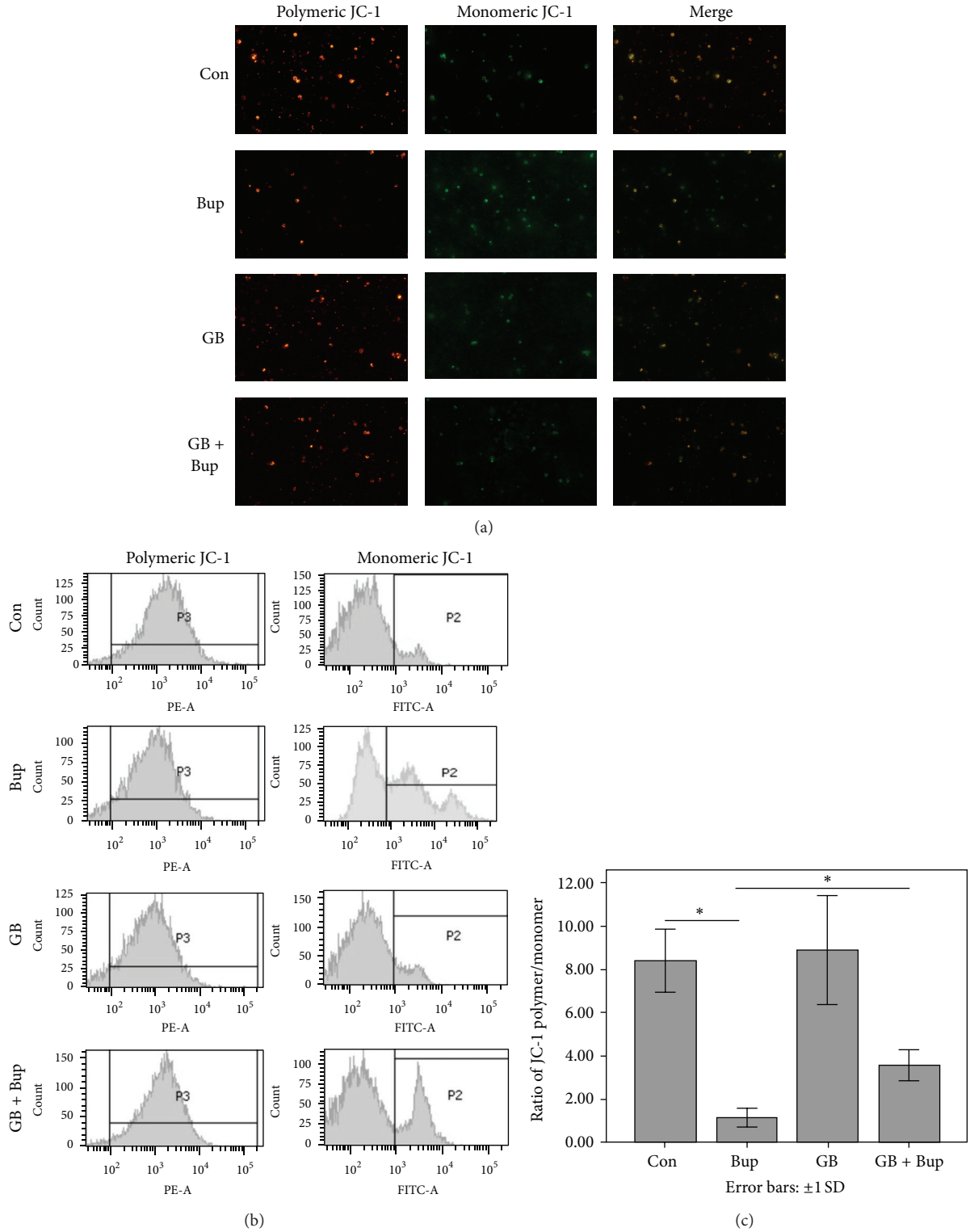

FIGURE 4: GB attenuated the bupivacaine-induced decline of mitochondrial membrane potential ($\Delta\psi$m). SH-SY5Y cells were treated with bupivacaine for 24 hours in the presence or absence of GB. (a) SH-SY5Y cells were observed using fluorescent microscopy. (b) $\Delta\psi$m were detected by flow cytometry (c) $\Delta\psi$m expressed as the ratio of red fluorescence over green fluorescence. Data represented are the mean ± SD of 6 separate experiments ($^*P < 0.01$).

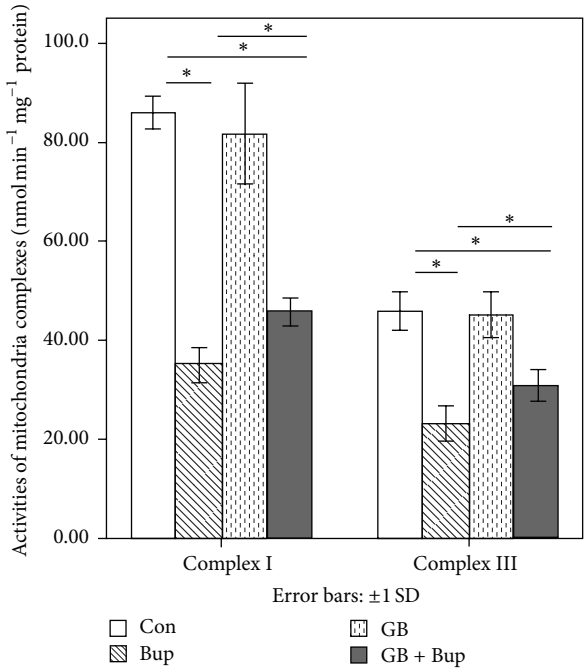

Figure 5: GB attenuated bupivacaine-induced decrease in the activity of mitochondrial complexes I and III. Experiments were repeated 6 times, and the data were presented as the mean ± SD ($^*P < 0.01$).

2.8. Isolation of Mitochondrial. Mitochondria were isolated from SH-SY5Y cells cultured in 6-well plates and treated as described for ROS measurements. After rinsing twice in PBS, cells were harvested, centrifuged at 600 ×g for 5 min at 4°C, and then homogenized in 1 mL mitochondria isolation reagent until 50% of the cells were lysed. Homogenates were centrifuged at 600 ×g for 5 min at 4°C to remove large debris and unlysed cells. The supernatant containing mitochondria then transferred to another centrifuge tube, and mitochondria precipitated by centrifugation at 11,000 ×g for 10 min at 4°C. After centrifugation, the pellet was resuspended in mitochondrial storage solution.

2.9. Measurement of Respiratory Complex I and Complex III Activities. The activities of respiratory chain complexes I and III were determined according to the methods as described by Zhang et al. [24]. All assays were performed at 25°C in a final volume of 1 mL using a spectrophotometer. To release complexes from the mitochondrial membrane, isolated mitochondria were subjected to three freeze-thaw cycles (25°C to −25°C) in hypotonic media (25 mmol/L potassium phosphate, 5 mmol/L $MgCl_2$, pH 7.2) before activity measurements. The enzyme activity was expressed in nanomolars per minute per milligram protein.

2.10. Western Blotting. Cells were incubated as described for the ROS measurements, harvested, and lysed in lysis buffer. After centrifugation, the soluble protein concentration in the supernatant was determined by a BCA Protein Assay Kit (Beyotime, China). Protein samples were separated by sodium dodecyl sulfate-polyacrylamide gel electrophoresis (20 μg/lane), electrotransferred to polyvinylidene difluoride (PVDF) membranes. Membranes were blocked with 5% nonfat dry milk in Tris-buffered saline and then immunoblotted with anti-Grp78 (1 : 500), anti-caspase-12 (1 : 500), anti-cleaved caspase-3 (1 : 500), anti-HtrA2 (1 : 500), or anti-GAPDH antibody (1 : 1000, as the gel loading control) overnight at 4°C. All antibodies were diluted in Tris-HCl-buffered saline containing 5% nonfat dry milk and 0.1% Tween-20. After rinsing, immunolabeled membranes were incubated with horseradish peroxidase (HRP) conjugated anti-rabbit immunoglobulin (1 : 1000) for 1 h. Specific proteins were detected by enhanced chemiluminescence and exposure to X-ray film. Bands were quantified by scanning the films. The expression levels of Grp78, caspase-12, cleaved caspase-3, and HtrA2 protein were normalized to GAPDH.

Table 1: qRT-PCR primers.

Gene	Primers
18srRNA	Forward: 5′-CCT GGA TAC CGC AGC TAG GA-3′
	Reverse: 5′-GCG GCG CAA TAC GAA TGC CCC-3′
GRP78	Forward: 5′-TGC AGC AGG ACA TCA AGT TC-3′
	Reverse: 5′-CGC TGG TCA AAG TCT TCT CC-3′
Caspase-12	Forward: 5′-GGA GAA AGA GAG GCG AAC AT-3′
	Reverse: 5′-CCT GGA TAC CGC AGC TAG GA-3′

2.11. Quantitative Real Time PCR (qRT-PCR). To investigate the effect of bupivacaine on ER stress, we examined Grp78 and caspase-12 mRNA expression levels by qRT-PCR. Total RNA was isolated using an RNA Isolation Kit (Qiagen, USA) according to the manufacturer's instructions. DNase I (TAKARA, Japan) was used to remove DNA from total RNA. cDNA was synthesized using a cDNA Synthesis Kit (Promega, USA), and the Maxima SYBR Green qPCR Master Mix (2X) (Fermentas, USA) was used to quantify gene expression. Conditions for amplification and quantification included initial denaturing (50°C for 2 minutes and 95°C for 10 minutes) followed by 40 cycles of 2 amplification stages (95°C for 15 seconds and 60°C for 1 minute) for primer annealing and elongation. A dissociation stage (95°C for 15 seconds, 60°C for 1 minute, and 95°C for 15 seconds) was added at the end of amplification stage to ensure that a single amplicon was produced and to validate the primer pairs. Reactions were performed in triplicate. Relative expression levels of caspase-12 and Grp78 mRNA were quantified using the 2-ΔΔCT method [25, 26] and 18 srRNA as the normalizing gene. The primers used are listed in Table 1.

2.12. Transmission Electron Microscopy (TEM). Neuroblastoma cells treated as described for the ROS measurements were harvested, washed once with PBS, fixed in 2.5% glutaraldehyde at 4°C for 1 h, postfixed in 1% osmic acid for 30 min, and stained with lead uranium. Cell ultrastructure was observed under a transmission electron microscope (Hitachi-600, Japan).

2.13. Statistical Analysis. All values are expressed as means ± SD. Multiple comparisons between groups were analyzed by

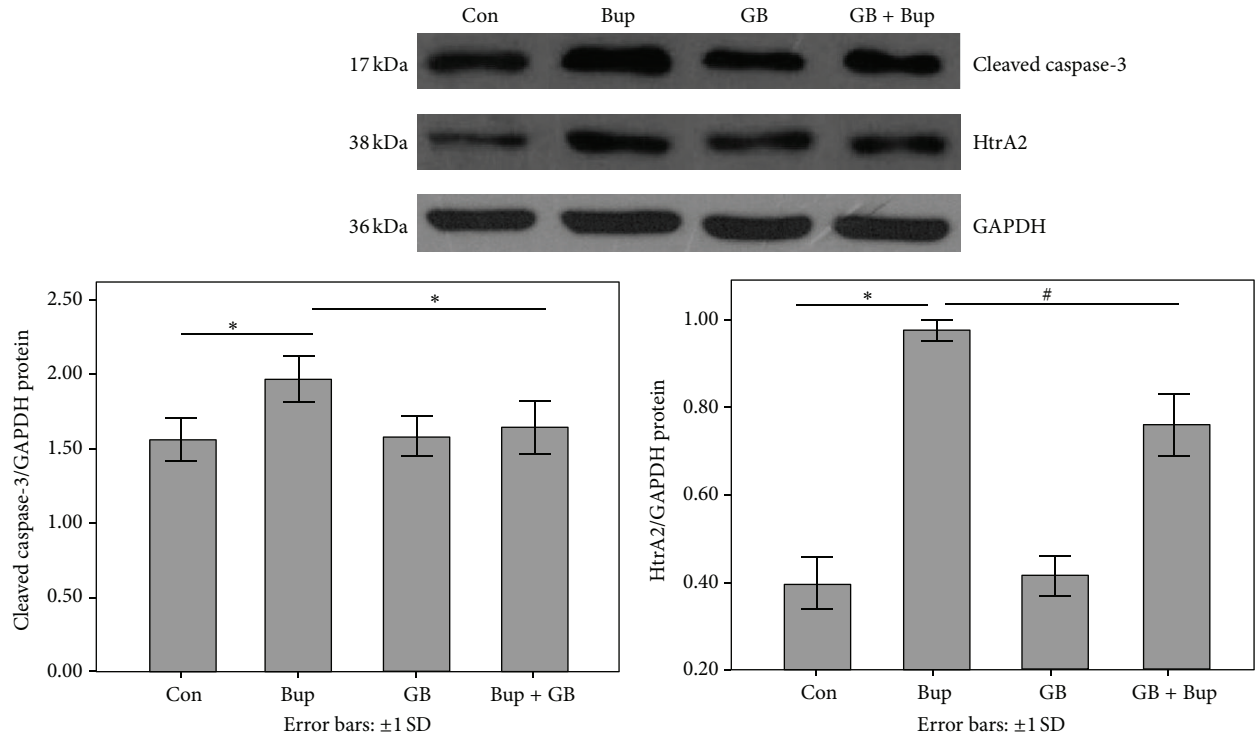

Figure 6: Htra2 induction and cleaved caspase-3 activation were detected by Western blot. Experiments were repeated three times, and the data were presented as mean ± SD ($^{*}P < 0.01$; $^{\#}P < 0.05$).

one-way ANOVA. LSD was performed as post hoc analysis for multiple comparisons between groups. A $P < 0.05$ was considered significant.

3. Results

3.1. Bupivacaine Reduced Cell Viability. The effect of bupivacaine on the viability of SH-SY5Y neuroblastoma cells was first examined using the by MTT assay. Bupivacaine (1, 1.5, 2 mmol/L) significantly reduced viable cell number compared to controls (Figure 1(a)). We then estimated viable cell number at multiple time points during treatment with 1 mmol/L bupivacaine, the LD50 measured in a previous study [23]. Compared to controls, bupivacaine reduced viable cell number at all time points between 24 and 48 h. Thus, bupivacaine reduced SHSY5Y cell proliferation, induced cell death, or both.

3.2. GB Attenuated Cell Toxicity Induced by Bupivacaine. In our pilot experiment, treatment with 5–40 μmol/L GB for 6 h did not affect cell proliferation. The antiproliferative or cytotoxic effect of 1 mmol/L bupivacaine was then compared between GB-pretreated (5–40 μmol/L) and GB-naïve cultures using the CCK-8 assay. Cell counts were higher at all GB doses except at 5 μmol/L, the lowest dose tested (Figure 1(b)). To determine if GB actually protected SHSY5Y cells against bupivacaine-mediated cytotoxicity, apoptosis was examined by flow cytometry.

3.3. GB Attenuated Bupivacaine-Induced SH-SY5Y Cell Apoptosis. Ginkgolide B pretreatment decreased bupivacaine-induced apoptosis as evidenced by reduced Annexin V+/PI− and Annexin V+/PI+ cell numbers (representing early or late apoptosis, resp.) at 40 μmol/L GB (Figure 2). The reduction was similar for both Annexin V+/PI− and Annexin V+/PI+ cell populations, indicating that GB blocked the initiation of apoptosis.

3.4. GB Attenuated ROS Production Induced by Bupivacaine. Treatment with 1 mmol/L bupivacaine increased the intracellular ROS accumulation, indicated by DCFH-DA fluorescence, while GB pretreatment significantly reduced the ROS-dependent fluorescent signal (Figure 3). These results suggest that GB acts to preserve mitochondrial function, elevates endogenous antioxidant capacity, and (or) possesses inherent antioxidant activity.

3.5. GB Inhibited Mitochondrial Depolarization Induced by Bupivacaine. The mitochondrial membrane potential (ψm) is correlated with functional activity, while loss of ψm (depolarization) is indicative of mitochondrial uncoupling and is an early sign of apoptosis. We estimated ψm in SH-SY5Y cells by the shift in JC-1 fluorescence (from red to green). Exposure to 1 mmol/L bupivacaine resulted in ψm dissipation, while GB pretreatment preserved ψm during bupivacaine exposure (Figure 4). These results suggest that GB may prevent apoptosis by preserving mitochondrial function and by preventing activation of mitochondrial-dependent apoptosis.

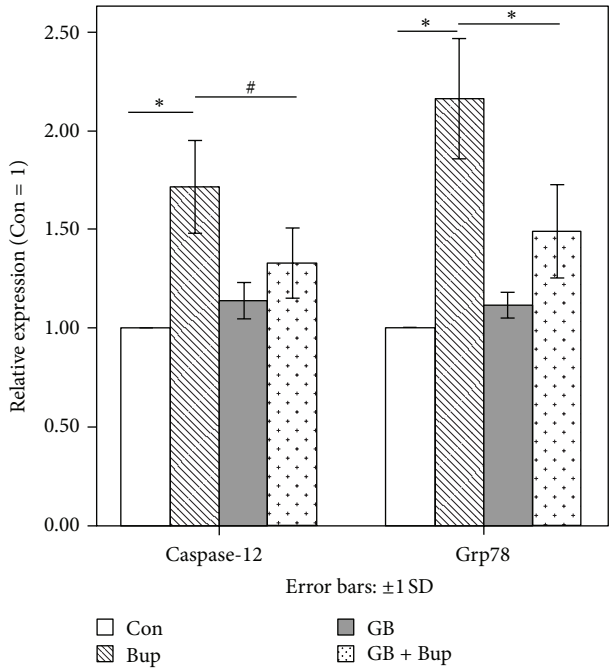

Figure 7: Grp78 and caspase-12 mRNA expression as detected by qRT-PCR. Experiments were repeated three times, and the data were presented as the mean ± SD ($^{*}P < 0.01$, $^{\#}P < 0.05$).

3.6. Preservation of Mitochondrial Respiratory Complex I and III Activity by GB. The activities of mitochondrial complexes I and III were significantly reduced by bupivacaine, suggesting potential loss of oxidative phosphorylation. Again, disruption of mitochondrial function was reversed by GB pretreatment (Figure 5).

3.7. The Level of Cleaved Caspase-3 and HtrA2. Mitochondrial uncoupling and ψm depolarization are associated with a dramatic increase in mitochondrial inner membrane permeability and the release of factors (e.g., cytochrome c and HtrA2) that initiate or regulate apoptotic pathways. Western blots (Figure 6) revealed significantly elevated cleaved (activated) caspase-3 and HtrA2 expression in bupivacaine-treated cultures compared to controls, an effect that was suppressed by GB pretreatment.

3.8. GB Reduced ER Stress Induced by Bupivacaine. Expression of Grp78 and caspase-12 is indicative of ER stress. Quantitative RT-PCR and Western blots revealed enhanced Grp78 and caspase-12 mRNA (Figure 7) and protein expression levels (Figure 8) in BG-naïve bupivacaine-treated cells compared to controls, responses that were reversed by GB pretreatment.

3.9. Morphological Changes of Cells. Normal healthy SH-SY5Y cells were round and regular, with typically shaped ER and mitochondrial membranes in TEM images (Figure 9(a)). After exposure to bupivacaine for 24 h, the ER appeared swollen and degranulated, while mitochondria were swollen with loss of internal membrane structure (Figure 9(b)). Cells treated with 40 μmol/L GB showed a nearly normal ultrastructure (Figure 9(c)), indicating that GB had little endogenous toxicity or physiological effects on ER or mitochondrial function. Cells pretreated with GB prior to bupivacaine exposure resembled controls at the ultrastructural level, with only slight expansion of the ER (Figure 9(d)). This preservation of ER and mitochondrial structure strongly suggests that GB protected SH-SY5Y cells against bupivacaine-induced mitochondrial and ER damage.

4. Discussion

Ginkgolide B (GB), an active component of the traditional medicinal herb Ginkgo biloba, protected SH-SY5Y cells from bupivacaine-induced injury. Pretreatment with 40 μmol/L GB suppressed bupivacaine-induced mitochondrial depolarization, mitochondria complex I and III inhibition, ROS accumulation, ER stress, and apoptosis. These results implicate mitochondrial dysfunction and ER stress in bupivacaine-induced apoptosis and highlight GB as a potential neuroprotectant against bupivacaine toxicity through its antioxidant property.

The therapeutic time window is critical in defining the potential clinical utility of any neuroprotective agent. Ginkgolide B has been shown to exert significant protective effect in cerebral ischemia injury up to 2 h following intravenous administration after reperfusion in rat [27]. In our pilot experiment, pretreatment with 5–40 μmmol/L GB for 2 h, 4 h could not protect SH-SY5Y cells from bupivacaine neurotoxicity, which is different from other people's previous research. Only 6 h duration of pretreatment with GB conferred protective effect; therefore, 6 h treatment protocol was used in our study.

Oxidoredox homeostasis is essential for cellular survival. Overproduction of ROS leads to oxidative stress and plays an important role in the process of apoptosis in many cell types [28], which can be ameliorated by endogenous and exogenous antioxidants. Bupivacaine was shown to induce ROS generation in SH-SY5Y cells [6], while GB reduced ROS levels *in vivo* [22], suggesting that GB may protect against bupivacaine toxicity by suppressing ROS accumulation. Bupivacaine did substantially increase ROS, a major initiator of apoptosis [29], while preincubation with GB suppressed ROS accumulation and many of the biochemical and morphological signs of oxidative stress. To investigate the potential reasons for increased ROS production, we measured the activities of mitochondrial complexes I and III, the main generators of ROS [30]. The activity of both complexes decreased after bupivacaine treatment, while GB pretreatment partially reversed this effect. By preserving oxidative phosphorylation, GB maintained ψm and decreased ROS production associated with mitochondrial uncoupling. Aside from mitochondrial dysfunction, however, ROS may also be generated by calcium-dependent protease activity, nNOS, and acidosis, the contributions of which were not examined and warrant further study as possible mechanisms of bupivacaine toxicity.

Besides energy production via the electron transport chain, mitochondria are responsible for several other important cellular functions, including the initiation and regulation

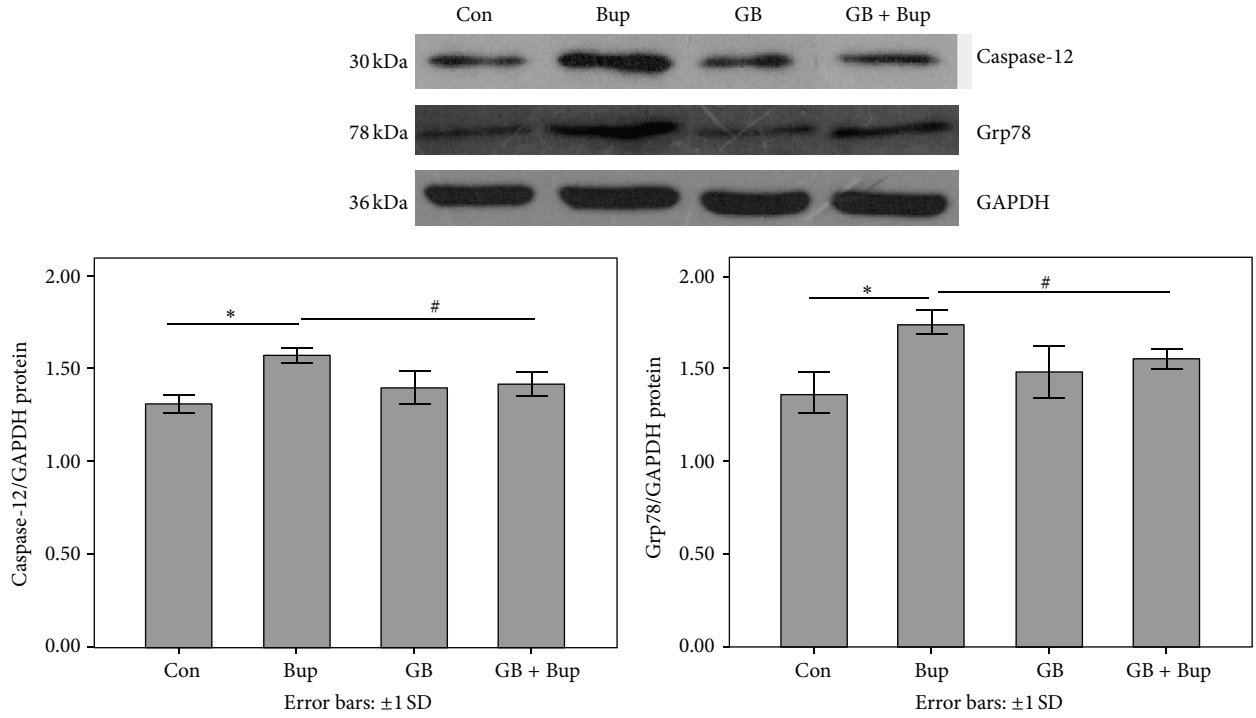

Figure 8: Grp78 and caspase-12 expression representing ER stress as detected by Western blot. Experiments were repeated three times, and the data were presented as the mean ± SD ($^{*}P < 0.01$, $^{\#}P < 0.05$).

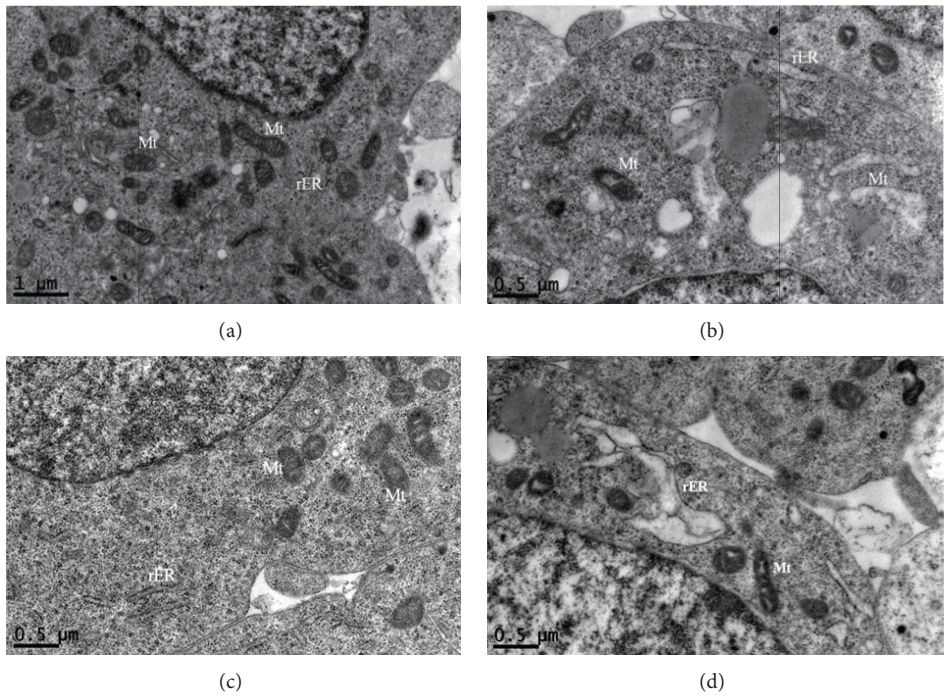

Figure 9: Morphologic changes of SH-SY5Y cells. (a) Cells in the control group retained a normal ultrastructure; (b) cells in the Bup group contained degranulated rER, swollen Mt, and hazy mitochondrial structures; (c) treatment with GB resulted in and showed a nearly normal structure; (d) pretreatment with GB represented slight expansion of ER.

of apoptosis [31]. Local anesthetics may dissipate ψm and activate caspases, leading to apoptotic cell death [6, 32]. In our study, apoptotic cell death induced by bupivacaine was associated with ψm depolarization, and both bupivacaine-induced apoptosis and ψm dissipation were attenuated by GB. The HtrA2 protein is a serine protease that acts as a proapoptotic factor following release from the mitochondrial matrix through large nonselective pores (permeability transition pores, mPTPs) that can be opened by overproduction of ROS [33, 34]. Release of mitochondrial HtrA2 into the cytoplasm was inhibited by the caspase inhibitor z-VAD-fmk [34, 35], suggesting that caspase activation may precede and possibly induce HtrA2 release. Increased cleaved caspase-3 is associated with mitochondria-dependent apoptosis following sustained loss of ψm [36]. Thus, bupivacaine likely induced apoptosis by reducing mitochondria complex activity, leading to overproduction of ROS, collapse of the mitochondrial membrane potential, release of proapoptotic factors from the mitochondrial matrix, and subsequent caspase-3 activation.

ES stress may activate alternate apoptotic pathways or exacerbate mitochondria-dependent apoptosis. The ER is critical for protein synthesis and folding, lipid and sterol synthesis, and calcium homeostasis. Stressors such as hypoxia, glucose deprivation, and calcium depletion from the ER lumen lead to ER dysfunction [37], resulting in cellular calcium dysregulation, protein misfolding and aggregation, and activation of proapoptotic effectors such as caspase-12. Bupivacaine caused ER stress as evidenced by elevated caspase-12 and Grp78 expression, and this stress may have resulted from ROS accumulation as reported by Takahashi et al. [17].

Grp78 is a well-characterized indicator of UPR activation (the unfolded protein response) and a critical protectant against ER stress by preventing protein aggregation [38]. However, when the ER stress is severe or prolonged, the increase in Grp78 is no longer sufficient to prevent apoptosis, and the UPR switches from a cytoprotective to a proapoptotic response involving activation of specific effector proteins such as caspase-12, which is activated only by ER stress-initiated apoptotic pathways [37]. In accordance with previous studies [39, 40], Grp78 expression was upregulated in parallel with caspase-12, indicative of ER stress and ER stress-specific apoptosis. Ginkgolide B inhibited the overexpression of Grp78 and caspase-12, suggesting that suppression of cell death resulted from disruption of both mitochondrial and ER-dependent apoptotic pathways. This conclusion was further corroborated by TEM images showing reduced organelle swelling and maintenance of ER and mitochondrial membrane integrity in cells pretreated with GB prior to bupivacaine.

Some limitations of this study should be noted. First, we examined doses of bupivacaine (1 mmol/L or 0.03%) that are not clinically relevant, as local injections often use 0.25% or 0.5%, although the duration of exposure was greatly prolonged in this study. Second, these *in vitro* results from transformed neuroblastoma cells may not be applicable to neurons *in vivo*. Nonetheless, previous results have demonstrated morphological signs of oxidative stress and apoptosis following local anesthetic administration *in vivo*, and exogenous antioxidants (like GB) have well-established neuroprotective efficacy.

In summary, the current study suggests that bupivacaine elicits ROS production, which in turn triggers mitochondrial depolarization, mitochondria-dependent apoptosis, and ER stress. These pathological responses were reduced or ameliorated by pretreatment with ginkgolide B. These results provide novel insights into the molecular mechanisms underlying the neurotoxicity of bupivacaine and highlight GB as a prototype treatment for the neurotoxicity elicited by this class of local anesthetics.

Acknowledgments

This study was supported by the Grants from the National Natural Science Foundation of China (no. 81271390) and Natural Science Foundation of Guangdong Province, China (no. 2011010004056). All of the authors have no financial relationship with a biotechnology manufacturer, a pharmaceutical company, or other commercial entities with an interest in subject matter or materials discussed in the papers.

References

[1] Y. Auroy, D. Benhamou, L. Bargues et al., "Major complications of regional anesthesia in France: the SOS regional anesthesia hotline service," *Anesthesiology*, vol. 97, no. 5, pp. 1274–1280, 2002.

[2] C. J. Park, S. A. Park, T. G. Yoon, S. J. Lee, K. W. Yum, and H. J. Kim, "Bupivacaine induces apoptosis via ROS in the Schwann cell line," *Journal of Dental Research*, vol. 84, no. 9, pp. 852–857, 2005.

[3] N. M. Gibbs and P. Rodoreda, "Primary anaesthetic deaths in Western Australia from 1985–2008: causationand preventability," *Anaesth Intensive Care*, vol. 41, no. 3, pp. 302–310, 2013.

[4] J. D. Griffiths, N. V. Le, S. Grant, P. Hebbard, and C. Royse, "Symptomatic local anaesthetic toxicity and plasma ropivacaine concentrations after transversus abdominis plane block for Caesarean section," *British Journal of Anaesthesia*, vol. 110, no. 6, pp. 996–1000, 2013.

[5] Z. Tan, S. Dohi, J. Chen, Y. Banno, and Y. Nozawa, "Involvement of the mitogen-activated protein kinase family in tetracaine-induced PC12 cell death," *Anesthesiology*, vol. 96, no. 5, pp. 1191–1201, 2002.

[6] J. Lu, S. Y. Xu, Q. G. Zhang, R. Xu, and H. Y. Lei, "Bupivacaine induces apoptosis via mitochondria and p38 MAPK dependent pathways," *European Journal of Pharmacology*, vol. 657, no. 1–3, pp. 51–58, 2011.

[7] S. Sakura, Y. Kirihara, T. Muguruma, T. Kishimoto, and Y. Saito, "The comparative neurotoxicity of intrathecal lidocaine and bupivacaine in rats," *Anesthesia and Analgesia*, vol. 101, no. 2, pp. 541–547, 2005.

[8] J. W. Russell, K. A. Sullivan, A. J. Windebank, D. N. Herrmann, and E. L. Feldman, "Neurons undergo apoptosis in animal and cell culture models of diabetes," *Neurobiology of Disease*, vol. 6, no. 5, pp. 347–363, 1999.

[9] E. Lelkes, B. R. Unsworth, and P. I. Lelkes, "Reactive oxygen species, apoptosis and altered NGF-induced signaling in PC12 pheochromocytoma cells cultured in elevated glucose: an in vitro cellular model for diabetic neuropathy," *Neurotoxicity Research*, vol. 3, no. 2, pp. 189–203, 2001.

[10] R. Perez-Castro, S. Patel, Z. V. Garavito-Aguilar et al., "Cytotoxicity of local anesthetics in human neuronal cells," *Anesthesia and Analgesia*, vol. 108, no. 3, pp. 997–1007, 2009.

[11] Y. Arai, T. Kondo, K. Tanabe et al., "Enhancement of hyperthermia-induced apoptosis by local anesthetics on human histiocytic lymphoma U937 cells," *Journal of Biological Chemistry*, vol. 277, no. 21, pp. 18986–18993, 2002.

[12] O. Cela, C. Piccoli, R. Scrima et al., "Bupivacaine uncouples the mitochondrial oxidative phosphorylation, inhibits respiratory chain complexes I and III and enhances ROS production: results of a study on cell cultures," *Mitochondrion*, vol. 10, no. 5, pp. 487–496, 2010.

[13] S. Bouderba, M. N. Sanz, C. Sanchez-Martin et al., "Hepatic mitochondrial alterations and increased oxidative stress in nutritional diabetes-prone Psammomys obesus model," *Experimental Diabetes Research*, vol. 2012, Article ID 430176, 8 pages, 2012.

[14] D. B. Zorov, C. R. Filburn, L.-O. Klotz, J. L. Zweier, and S. J. Sollott, "Reactive oxygen species (ROS)-induced ROS release: a new phenomenon accompanying induction of the mitochondrial permeability transition in cardiac myocytes," *Journal of Experimental Medicine*, vol. 192, no. 7, pp. 1001–1014, 2000.

[15] I. Nonaka, A. Takagi, and S. Ishiura, "Pathophysiology of muscle fiber necrosis induced by bupivacaine hydrochloride (Marcaine)," *Acta Neuropathologica*, vol. 60, no. 3-4, pp. 167–174, 1983.

[16] A. Devarajan, V. R. Grijalva, N. Bourquard et al., "Macrophage paraoxonase 2 regulates calcium homeostasis and cell survival under endoplasmic reticulum stress conditions and is sufficient to prevent the development of aggravated atherosclerosis in paraoxonase 2 deficiency/apoE(−/−) mice on a Western diet," *Molecular Genetics and Metabolism*, vol. 107, pp. 416–427, 2012.

[17] S. Takahashi, Y. Izawa, and N. Suzuki, "Astroglial pentose phosphate pathway rates in response to high-glucose environments," *ASN Neuro*, vol. 4, no. 2, pp. 71–88, 2012.

[18] W. Abbas, K. A. Khan, M. K. Tripathy et al., "Inhibition of ER stress-mediated apoptosis in macrophages by nuclear-cytoplasmic relocalization of eEF1A by the HIV-1 Nef protein," *Cell Death & Disease*, vol. 3, p. e368, 2012.

[19] C. Zhang, X. Tian, Y. Luo, and X. Meng, "Ginkgolide B attenuates ethanol-induced neurotoxicity through regulating NADPH oxidases," *Toxicology*, vol. 287, no. 1–3, pp. 124–130, 2011.

[20] K. M. Maclennan, C. L. Darlington, and P. F. Smith, "The CNS effects of Ginkgo biloba extracts and ginkgolide B," *Progress in Neurobiology*, vol. 67, no. 3, pp. 235–257, 2002.

[21] M. Esposito and M. Carotenuto, "Ginkgolide B complex efficacy for brief prophylaxis of migraine in school-aged children: an open-label study," *Neurological Sciences*, vol. 32, no. 1, pp. 79–81, 2011.

[22] M. Huang, Y. Qian, T. Guan, L. Huang, X. Tang, and Y. Li, "Different neuroprotective responses of Ginkgolide B and bilobalide, the two Ginkgo components, in ischemic rats with hyperglycemia," *European Journal of Pharmacology*, vol. 677, no. 1–3, pp. 71–76, 2012.

[23] R. Werdehausen, S. Fazeli, S. Braun et al., "Apoptosis induction by different local anaesthetics in a neuroblastoma cell line," *British Journal of Anaesthesia*, vol. 103, no. 5, pp. 711–718, 2009.

[24] S. Zhang, J. Fu, and Z. Zhou, "In vitro effect of manganese chloride exposure on reactive oxygen species generation and respiratory chain complexes activities of mitochondria isolated from rat brain," *Toxicology in Vitro*, vol. 18, no. 1, pp. 71–77, 2004.

[25] T. D. Schmittgen and K. J. Livak, "Analyzing real-time PCR data by the comparative CT method," *Nature Protocols*, vol. 3, no. 6, pp. 1101–1108, 2008.

[26] K. J. Livak and T. D. Schmittgen, "Analysis of relative gene expression data using real-time quantitative PCR and the 2-ΔΔCT method," *Methods*, vol. 25, no. 4, pp. 402–408, 2001.

[27] W. Fang, Y. Deng, Y. Li et al., "Blood brain barrier permeability and therapeutic time window of Ginkgolide B in ischemia-reperfusion injury," *European Journal of Pharmaceutical Sciences*, vol. 39, no. 1–3, pp. 8–14, 2010.

[28] B. Brodská and A. Holoubek, "Generation of reactive oxygen species during apoptosis induced by DNA-damaging agents and/or histone deacetylase inhibitors," *Oxidative Medicine and Cellular Longevity*, vol. 2011, Article ID 253529, 7 pages, 2011.

[29] N. Zamzami, P. Marchetti, M. Castedo et al., "Sequential reduction of mitochondrial transmembrane potential and generation of reactive oxygen species in early programmed cell death," *Journal of Experimental Medicine*, vol. 182, no. 2, pp. 367–377, 1995.

[30] T. A. Young, C. C. Cunningham, and S. M. Bailey, "Reactive oxygen species production by the mitochondrial respiratory chain in isolated rat hepatocytes and liver mitochondria: studies using myxothiazol," *Archives of Biochemistry and Biophysics*, vol. 405, no. 1, pp. 65–72, 2002.

[31] G. Nagy, A. Koncz, D. Fernandez, and A. Perl, "Nitric oxide, mitochondrial hyperpolarization, and T cell activation," *Free Radical Biology and Medicine*, vol. 42, no. 11, pp. 1625–1631, 2007.

[32] M. E. Johnson, C. B. Uhl, K.-H. Spittler, H. Wang, and G. J. Gores, "Mitochondrial injury and caspase activation by the local anesthetic lidocaine," *Anesthesiology*, vol. 101, no. 5, pp. 1184–1194, 2004.

[33] P. Bernardi, A. Krauskopf, E. Basso et al., "The mitochondrial permeability transition from in vitro artifact to disease target," *FEBS Journal*, vol. 273, no. 10, pp. 2077–2099, 2006.

[34] D. Arnoult, B. Gaume, M. Karbowski, J. C. Sharpe, F. Cecconi, and R. J. Youle, "Mitochondrial release of AIF and EndoG requires caspase activation downstream of Bax/Bak-mediated permeabilization," *The EMBO Journal*, vol. 22, no. 17, pp. 4385–4399, 2003.

[35] M. Zoratti, I. Szabò, and U. de Marchi, "Mitochondrial permeability transitions: how many doors to the house?" *Biochimica et Biophysica Acta*, vol. 1706, no. 1-2, pp. 40–52, 2005.

[36] N. J. Waterhouse, K. A. Sedelies, V. R. Sutton et al., "Functional dissociation of $\Delta\psi$m and cytochrome c release defines the contribution of mitochondria upstream of caspase activation during granzyme B-induced apoptosis," *Cell Death and Differentiation*, vol. 13, no. 4, pp. 607–618, 2006.

[37] M. Schröder and R. J. Kaufman, "The mammalian unfolded protein response," *Annual Review of Biochemistry*, vol. 74, pp. 739–789, 2005.

[38] M. Boyce and J. Yuan, "Cellular response to endoplasmic reticulum stress: a matter of life or death," *Cell Death and Differentiation*, vol. 13, no. 3, pp. 363–373, 2006.

[39] A. Takada, T. Miki, A. Kuno et al., "Role of ER Stress in ventricular contractile dysfunction in type 2 diabetes," *PLoS One*, vol. 7, no. 6, Article ID e39893, 2012.

[40] E. Araki, S. Oyadomari, and M. Mori, "Endoplasmic reticulum stress and diabetes mellitus," *Internal Medicine*, vol. 42, no. 1, pp. 7–14, 2003.